COMISION NACIONAL DE ENERGIA ATOMICA
PRESIDENCIA DE LA NACION

PROYECTO MULTINACIONAL DE TECNOLOGIA DE MATERIALES

(Programa Regional de Desarrollo Cientifico y Tecnológico - OEA)

RECUPERACION Y RECRISTALIZACION DURANTE DEFORMACIONES A ALTAS TEMPERATURAS

J.J JONAS

Mc Gill University - Montreal - Canadá

Buenos Aires - Argentina

1981

COMISION NACIONAL DE ENERGIA ATOMICA
PRESIDENCIA DE LA NACION

PROYECTO MULTINACIONAL DE TECNOLOGIA DE MATERIALES

(Programa Regional de Desarrollo Cientifico y Tecnológico - OEA)

RECUPERACION Y RECRISTALIZACION DURANTE DEFORMACIONES A ALTAS TEMPERATURAS

J.J JONAS

Mc Gill University - Montreal - Canadá

Buenos Aires - Argentina

1981

CHAPITRE VII

RECOVERY AND RECRYSTALLIZATION DURING HIGH TEMPERATURE DEFORMATION

J.J. JONAS

Department of Mining and Metallurgical Engineering. Me Gill University, Montréal – Canada

and

H.J. Mc QUEEN

Department of Mechanical Engineering, Concordia University, Montréal – Canada

Résumé

Restauration et recristallisation au cours de la déformation à haute température

Les différents types de sous-structures formées au cours de la restauration dynamique à hautes températures sont analysées en détail. Les effets de changements de vitesse de déformation, de température et de concentration de soluté sont discutés. L'influence de la formation de la sous-structure sur la contrainte d'écoulement à haute température est examinée et les caractéristiques de l'écoulement plastique à haute et moyenne températures sont comparées. Les courbes d'écoulement obtenues au cours de la recrystallisation dynamique sont présentées et analysées par comparaison avec les courbes obtenues au cours de la restauration dynamique. Les facteurs qui affectent la déformation critique pour la recristallisation dynamique sont présentés et les changements de microstructures qui suivent le début de la recristallisation sont décrits. L'influence de la restauration dynamique et de la recristallisation dynamique sur la ductilité est discutée. Un intérêt particulier est porté sur les trois causes principales d'adoucissement qui apparaissent *après* la déformation à chaud ou durant les intervalles entre des déformations à chaud : restauration statique, recristallisation statique and recristallisation metadynamique. Enfin, les effets des sous-structures de déformation résultante sur les propriétés mécaniques à la température ambiante sont présentées et analysées.

Abstract

The substructures formed when dynamic recovery is occurring at high temperatures are considered in detail. The effects of changes in strain rate, temperature and solute concentration are discussed. The influence of substructure formation on the high temperature flow curve is examined and the characteristics of room temperature and elevated temperature flow are compared. Flow curves obtained under conditions of dynamic recrystallization are presented and contrasted to recovery flow curves. The factors affecting the critical strain for dynamic recrystallization are introduced and the microstructural changes following the initiation of recrystallization are described. The influence of the processes of dynamic recovery and dynamic recrystallization on ductility is discussed. Some attention is given to the three principal softening processes occurring *after* hot working, or between intervals of high temperature deformation : i.e. to static recovery, static recrystallization and metadynamic recrystallization. Finally, the effect of retained deformation substructures on the mechanical properties at room temperature is presented and analyzed.

VII.1. – Introduction

Almost all metals, excluding some castings and sintered parts, are hot worked during processing into a final product. Most of these hot-worked materials go into service in the as-deformed state in the form of products such as steel plate and skelp and aluminum extrusions. The remainder is cold-worked in a further series of operations. Whether as an intermediate or as a final product, the properties of such hot deformed materials are markedly influenced by the characteristics of the microstructure that is produced by the working process. It is the main purpose of the present article to consider the microstructural changes

* "Treatise on Materials Science and Technology, Vol. 6 : Plastic Deformation of Materials" (Edited by R.J. Arsenault) pp. 394-490. Academic Press, New York, 1975.

occurring both during and after hot working and to describe the influence of these changes on the mechanical properties of the worked material.

VII.1.1. – Static and Dynamic Restoration Processes

Recovery and recrystallization have traditionally been considered as mechanisms of restoration through which *cold-worked* metal returns partially or completely to its condition prior to working. These mechanisms generally operate when a metal is annealed at a high temperature for a period of time. In this respect, the term "high temperature" is of course relative; it depends upon the individual metal being heated and is best expressed in terms of homologous temperature, that is as a fraction of the absolute temperature of melting. A high homologous temperature in relation to annealing is anything over about one-half.

Annealing is usually carried out in the absence of stress or strain, in which case the recovery or recrystallization that occurs in termed static. However, recovery and recrystallization can also take place under stress and during concurrent straining, i.e. under conditions of high temperature deformation. In such an event, they

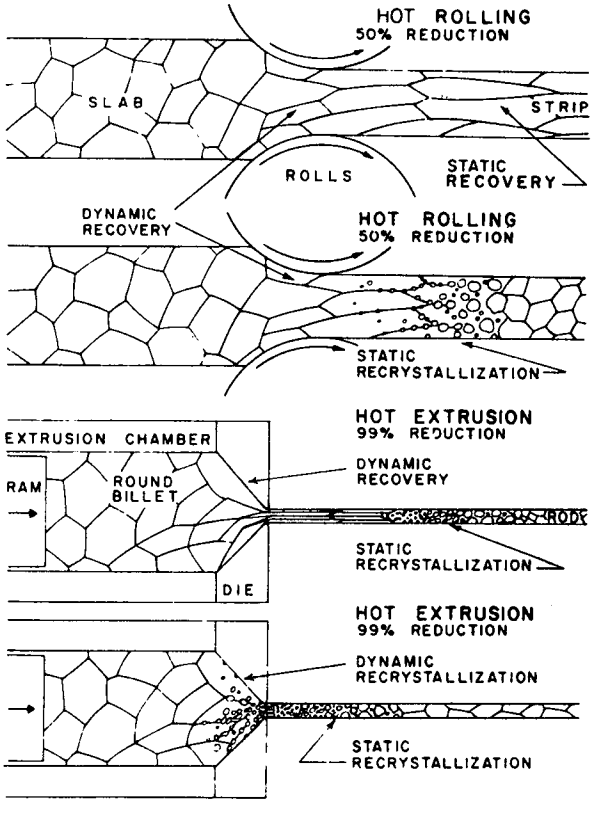

Fig. VII.1 - In a commercial hot-working operation in which the strain is low, as in rolling, the grains soften during deformation by dynamic recovery. In metals of high stacking fault energy, static recovery takes place during cooling, whereas in metals of low stacking fault energy, static recrystallization readily occurs as well. In operations producing high strains, such as extrusion, metals of high stacking fault energy undergo dynamic recovery followed by static recovery and static recrystallization ; on the other hand, metals of low stacking fault energy undergo both dynamic recovery and recrystallization followed by static recovery and recrystallization.

are distinguished from the respective static processes by the terms dynamic recovery and dynamic recrystallization. Schematic representations of some of the combinations of the dynamic and static softening processes occurring in hot working are shown in Fig. VII.1. Since dynamic recovery and dynamic recrystallization have been observed to take place under both hot working and creep conditions, there often is considerable similarity between the microstructures produced by these two modes of deformation. Consequently, it will be useful to take note of some of the observations made in creep studies where these are relevant to our examination of hot-worked structures. The similarities and differences between loading in the creep and hot-working modes will therefore be considered briefly before attention is given to the microstructural processes themselves.

VII.1.2 – Comparison of Creep and Hot-Working Modes of Deformation

Under creep conditions, a sample of metal is deformed under a constant or nearly constant stress, and the strain rate is the dependent variable. The stresses are considerably lower than the yield stress in a standard tensile test at the temperature in question, and the strain rates accordingly lie in the range $10^{-10} - 10^{-3}$ sec^{-1}. In practice, creep also occurs under conditions of stress relaxation; that is, in a sample of metal held at a constant value of total (elastic plus plastic) strain. Here the stress gradually diminishes as the elastic strain is replaced by plastic flow ; however, the plastic deformation is limited to that required to relieve the elastic strain, and is therefore only of the order of 0.1 %.

The strain rate under creep conditions is largely controlled by dynamic recovery processes. Between intervals of creep deformation, static recovery also plays an important role if the temperature is maintained. By contrast, the possibility of dynamic recrystallization, which can lead to strain rate increases of up to an order of magnitude, is generally prevented by the alloying elements present in commercial alloys. These alloy additions also prevent static recrystallisation from occurring between intervals of loading.

In hot-working practice, a sample of heated metal is deformed into the required shape at a rate defined by the process machinery. This usually involves a strain rate – time profile which is umque to the process. Although it also takes places at elevated temperatures, the hot-working operation can be distinguished from the process of creep by three factors. First, in the case of hot working, the strain rate profile is an arbitrary one, and is therefore the independent variable, with the developed stress as the dependent variable (in creep, the converse applies). Furthermore, hot-working tests and operations are conducted in the much higher strain rate range of $10^{-3} - 10^{3}$ sec^{-1}, so that the developed stresses are considerably higher than the stresses which will produce creep at the same temperature. Finally it should be noted that, whereas softening under creep conditions is usually restricted to the static and dynamic *recovery* processes, all four of the principal softening processes operate under hot-working conditions.

VII.2. – Static Recovery and Recrystallization after Cold Working

VII.2.1 – Static Recovery of Cold-Worked Substructures

Before turning to a detailed examination of the four principal restoration processes associated with high temperature deformation, it will be useful to review briefly some of the relevant features of static recovery and static recrystallization as they occur after low temperature deformation. When a cold-worked metal is held at any homologous temperature T_H above about 0.1, some recovery always occurs. The mechanisms of recovery operating in the region of $0.1 < T_H < 0.3$, however, are restricted to the motion of point defects and are not therefore of concern here, inasmuch as they lead to changes in physical rather than mechanical properties (Cahn, 1965). Changes in mechanical properties, on the other hand, require the motion and rearrangement of dislocations, and it is the latter process which we will be referring to when the term static recovery is used.

In worked metals of high stacking fault energy, a cell structure forms during deformation (Fig. VII.2) (Leslie *et al.*, 1963; Swann, 1963). When straining is interrupted, static recovery can gradually lead to considerable softening (e.g. to a 40 % decrease in residual strain hardening), and, if the strain has not exceeded the so-called critical strain for recrystallization, may even be the only restoration process that operates (Perryman, 1956). There is almost

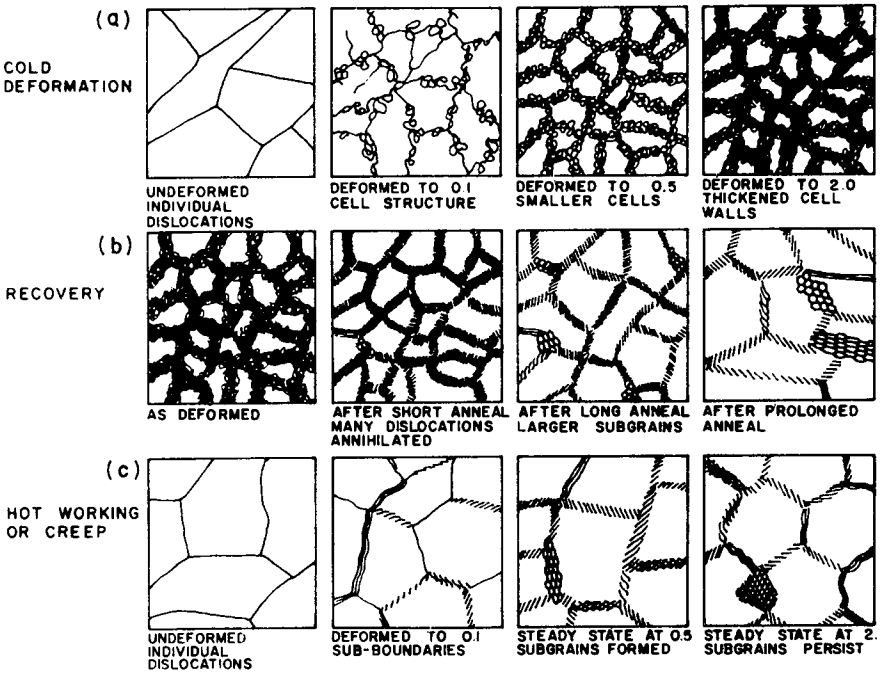

Fig. VII.2 a) During cold deformation, a cellular substructure develops as the strain increases ; by about 0.5 the cells reach their limiting size and thereafter the cell walls become much more dense. b) Recovery during annealing commences with the annihilation of dislocations in the cell walls which turn into subboundaries. As recovery continues, the subgrains grow in diameter and the overall dislocation density decreases. c) In hot working, subgrains develop in the strain hardening stage and reach an equilibrium size which is maintained during steady state flow.

no motion of grain boundaries during recovery, so that there is little observable change in the microstructure of the elongated grains produced by working. In worked metals of low stacking fault energy, the dislocations are present in planar arrays of high energy, which constitute a strong driving force for recrystallization, so that recrystallization is likely to proceed before recovery progresses significantly (Chan, 1965; Byrne, 1965).

The process of static recovery involves the following sequential changes in the dislocation cell structure (Fig. VII.2). In the rapid phase, called polygonization, the dislocations within the cells are attracted into the cell walls and the redundant dislocations in the cell walls annihilate each other, leaving neat dislocation networks separating the polygonal crystallites (Leslie *et al.*, 1963; Vandermeer and Gordon, 1963). Eventually the subgrains grow larger as the shared subboundary between neighboring subgrains is unraveled, and the individual dislocations move away, becoming incorporated in other boundaries or annihilated (Hu, 1963; Weissmann *et al.*, 1963). By such a mechanism of growth, a cluster of subgrains becomes a recrystallization nucleus, preparing the scene for the next stage of softening. These changes can be observed by optical techniques, such as polarized light microscopy and etch pitting, by X-ray diffraction methods involving the splitting of Laue arcs into discrete spots, and by transmission electron microscopy through the direct observation of dislocations.

The softening associated with recovery can be attributed to the gradual loss of the dislocations which were

generated and became entangled during working. The movement of an individual dislocation occurs in response to the long range internal stress fields of the other dislocations. However, the motion of the dislocations is also opposed by various short range barriers, which are overcome by thermal activation. The thermally activated mechanisms of importance at high temperatures are climb and cross-slip, as well as the unpinning of attractive junctions (Kivilahti *et al.*, 1974; Sastry *et al.*, 1974). Since the overall activation energy for recovery is in many cases lower than that for recrystallization, the observation of recovery as a separate process is favored by the use of lower temperatures, for which the incubation times for recrystallization can be fairly long.

From a practical point of view, the effect of alloying on the operation of the recovery mechanisms is of considerable importance (Byrne, 1965; Cahn, 1965). Although many aspects of these mechanisms are still unclear, it appears that solute addition can hamper climb through the binding energies that tie vacancies to solute atoms. In a similar way, solute additions usually permit the dislocations to extend into partials separated by a ribbon of stacking fault. The extension of the dislocations makes climb and cross-slip more difficult and renders network nodes more resistant to unpinning, thus hindering the recovery or growth of the dislocation network. The presence of precipitates, in turn, can stabilize networks of subboundary dislocations and in this way retard recovery (Leslie *et al.*, 1963; Humphreys and Martin, 1968). Because of their industrial interest, these are matters to which we will return below, when we consider static recovery after high temperature deformation.

VII.2.2 – Static Recrystallization after Cold Working

After static recovery has proceeded to some degree, a further and larger decrease in strength occurs, which is indicative of static recrystallization. It is attributable to the formation and growth of new grains which have much lower dislocation densities ($\sim 10^{10}$ m^{-2}) than the worked grains they replace ($\sim 10^{16}$ m^{-2}) (Byrne, 1965; Cahn, 1965). Several mechanisms of nucleation have been proposed based on observations of different metals after various strains (Fig. VII.3). The subgrain coalescence mechanism has already been briefly described above. It occurs in metals of high stacking fault energy, and leads to the establishment of regions of low internal dislocation content surrounded by boundaries of high misorientation capable of migrating (Bourelier and Montuelle, 1968). In metals of low stacking fault energy, the concentration of dislocations in the tangles formed by straining is higher, and the cell walls appear to develop high misorientations, and therefore become capable of migrating directly upon annealing (Bailey, 1963).

The occurrence of the subgrain coalescence mechanism is favored by the application of relatively large prestrains. When the amount of prior straining is reduced (to less than about 0.4), an alternative mechanism, that of grain boundary bulging, takes place in many metals. This process entails the bulging out of a short segment of an existing high angle boundary to produce a roughly spherical volume, relatively free of dislocations, which then acts as a nucleus and is free to grow (Bailey, 1963).

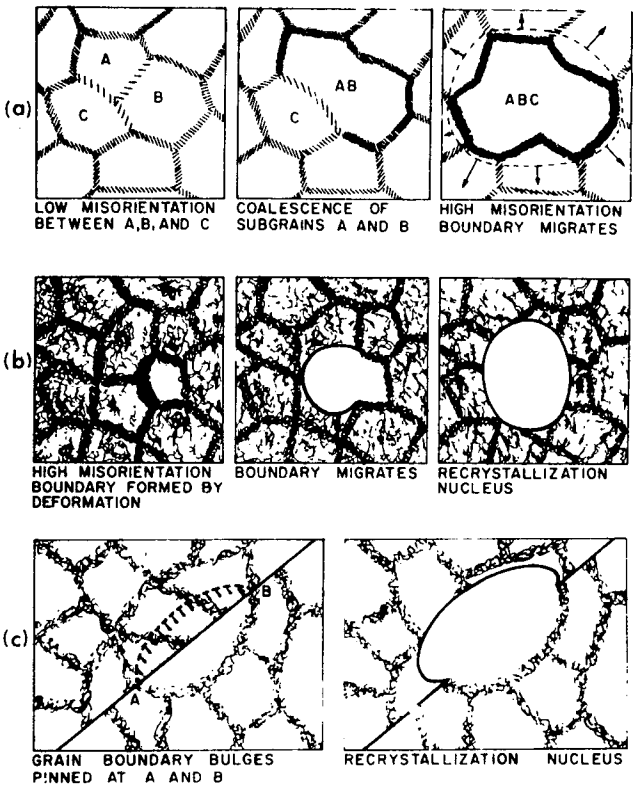

Fig. VII.3 – The mechanism of nucleation of recrystallized grains depends upon the metal and the strain. a) In metals of high stacking fault energy, cells such as A, B, and C, coalesce into one crystallite to form a nucleus. This occurs as a result of the dislocations between the cells moving to surrounding subboundaries and increasing their misorientation until they can migrate freely. b) In metals of lower stacking fault energy, straining creates localized high densities of dislocations which transform into high angle boundaries upon annealing. c) When the strain is low, so that the dislocation density varies from grain to grain, an existing boundary anchored by the substructure in one grain may bulge out into a region of higher density.

Once nuclei are formed, they grow into the deformed material by the migration of their boundaries. The driving force for migration is provided by the difference in dislocation density between the interior of a nucleus and the surrounding worked metal. The driving force continuously decreases because of two factors. On the one hand, the dislocation density in the worked area diminishes with time as a result of recovery (Vandermeer and Gordon, 1963). On the other hand, the most heavily deformed regions, containing the highest densities of dislocations, tend to undergo recrystallization first. The process of recrystallization is considered complete when all of the worked regions have become absorbed, and the growing nuclei impinge upon each other. As in the case of static recovery, the rate of static recrystallization is strongly affected by the presence of impurities, either in solution or as fine particles; however, here it is the result of their effect on the rate of migration of the boundaries.

Both nucleation and growth are thermally activated processes and consequently their rates increase rapidly as the temperature is increased. Nevertheless, the grain size at the end of recrystallization depends primarily on the density of nuclei, and hence on the initial degree of deformation within the crystals. The severity of deformation depends in turn on the amount, rate, and temperature

of prior straining. The rate of recrystallization also increases with the severity of straining because of the increasing density of nucleation sites and the higher driving force.

VII.3 – Dynamic Recovery at Elevated Temperatures

VII.3.1 – The Flow Curve at High Temperatures

When a recrystallized metal is loaded at constant nominal strain rate, the flow curve that results can be divided into three distinct stages (Luton and Jonas, 1970). The first stage is that of microstrain deformation, which is the interval during which the plastic strain rate in the sample increases from zero to the approximate strain rate of the test (Fig. VII.4). During this interval, the state of stress in the material rises rapidly, although not quite as steeply as it does at conventional temperatures. Typical loading slopes during initial loading range from E/50 at high temperatures and low strain rates to E/5 at relatively low temperatures and high strain rates* (Immarigeon, 1974). The loading slopes are not in general comparable with the modulus because of the plastic strain produced during the loading interval prior to macroscopic flow.

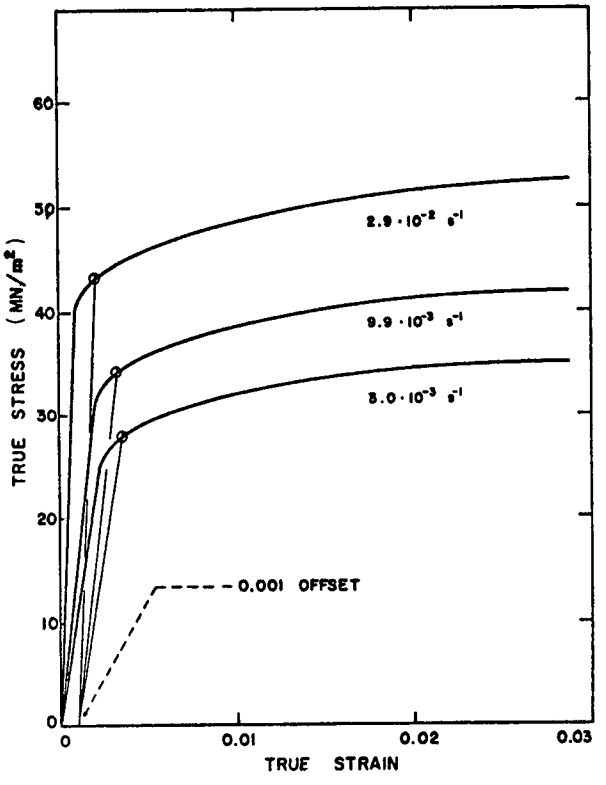

Fig. VII.4 - Three typical stress-strain curves determined at 775° C (0.5 T_m) for a Zr -0.7 % Sn alloy and plotted on an expanded strain scale. The transition from microstrain flow to generalized yielding can be seen, as well as the offset method used to establish the yield stress (Luton and Jonas, 1972a).

* E represents the value of Young's modulus at the temperature of the test.

This strain arises from the operation of the thermally activated mechanisms that are rate controlling in this temperature range, and therefore increases with a high temperature and a low rate of loading. When the rate of loading is low and the temperature is high, the amount of microstrain deformation is about 1 %; by contrast, at higher loading rates and lower temperatures, it is only a few tenths of a percent.

The end of the microstrain interval is signified by a decrease in the slope of the loading curve of about an order of magnitude. Yield drops are not, in general, observed, and the "yield" stress is defined instead in terms of a plastic strain offset of 0.1 or 0.2 %. The region of the yield stress marks the beginning of work hardening and, as before, the slopes are temperature and rate sensitive. Typical values range from E/500 at high temperatures and low strain rates to E/100 at low temperatures and high strain rates (Immarigeon, 1974).

During this second stage of deformation, the work hardening rate gradually decreases, until finally, in the third or steady state region, the net rate of work hardening is zero (Fig. VII.5). The steady state regime in hot working is characterized, as is secondary creep, by the constancy of the three parameters: stress, temperature, and strain rate.

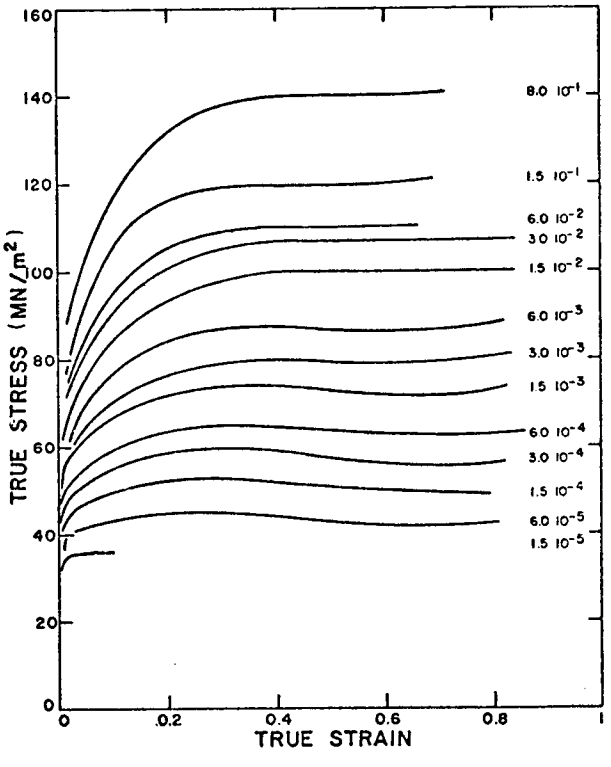

Fig. VII.5 – Typical true stress-true strain curves for Armco iron, illustrating the strain rate dependence of the flow stress at 700° C (0.54 T_m) (Immarigeon and Jonas, 1974).

It should be noted that the simple shape of flow curve illustrated in Fig. VII.5 pertains to the case where the flow rate is limited by dynamic recovery processes alone. In practice, the flow curve may drop as a result of the operation of other mechanisms. Examples of such processes are dynamic recrystallization, which will be considered below

in more detail, adiabatic heating, precipitate coarsening, modification of "hard" textures, and superplastic flow (Jonas and Luton, 1976). More rarely, the flow stress may rise as a result of precipitation or of the elimination of "soft" textures.

VII.3.2 – Microstructural Development during Plastic Flow

It will now be of interest to consider the microstructural changes that accompany the three stages of flow depicted in Fig. VII.5. Although little electron microscopy has been carried out to date on samples deformed to the vicinity of the yield strain, the limited evidence available (D.J. Abson and J.J. Jonas, unpublished work, McGill University, Montreal, Canada, 1974) suggests that some dislocation multiplication takes place during the micro-strain interval, and that the dislocation density increases from about $10^{10} - 10^{11}$ m^{-2} in annealed, polycrystalline samples to $10^{11} - 10^{12}$ m^{-2} at the commencement of macroscopic flow. The dislocation density continues to increase with strain after "yielding", albeit at a slower rate, and attains a value in the neighborhood of $10^{14} - 10^{15}$ m^{-2} in the steady state region.

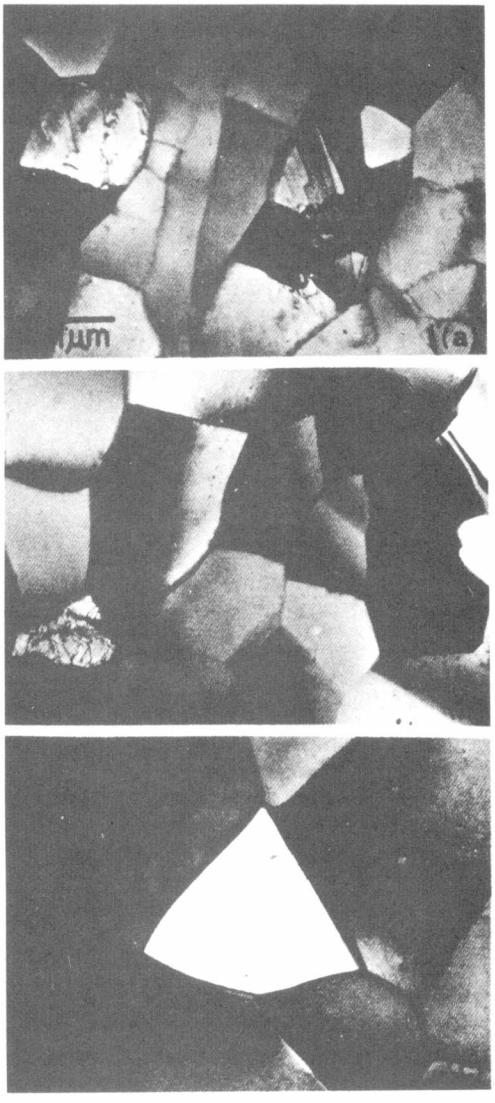

Fig. VII.6 – Substructures produced in commercial purity aluminum by extrusion at a mean strain rate of 1 sec^{-1} and an extrusion ratio of 40 : 1 ($\epsilon = 3.7$). a) 250° C (0.56 T_m). b) 350° C (0.67 T_m). c) 450° C (0.77 T_m) x 8000. Transmission electron micrographs of longitudinal sections (Wong *et al.*, 1967).

During the phase of positive strain hardening, the dislocations become entangled and begin to form a cellular structure. By the time the steady state regime is attained, the dislocations have arranged themselves into subgrains whose perfection, dimensions, and misorientation depend on the metal, and on the strain rate and temperature of deformation (Fig. VII.6) (Jonas *et al.*, 1969). The main features of the substructure, i.e. the dislocation density between dislocation walls, the average spacing between them, and the misorientation across them, do not change during the course of steady state deformation (Jonas *et al.*, 1968a). This condition of essentially constant dislocation density, which is necessary for the absence of strain hardening, results from the attainment of dynamic equilibrium between the rates of dislocation generation and annihilation.

The generation rate is a function of the strain rate and the associated effective stress*, but is relatively independent

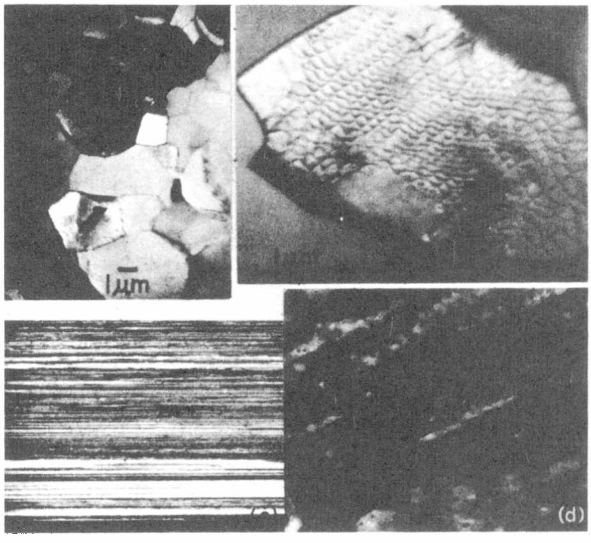

Fig. VII.7 – a) Substructure of commercial purity aluminum extruded at 445° C (0.76 T_m) and a strain rate of 1.2 sec^{-1}. The subgrains are equiaxed despite extension of the sample to a true strain of 3.7 (3900 % elongation) x 2000 (McQueen *et al.*, 1967). b) Some of the subboundaries produced by hot working are simple, low energy arrays like this twist boundary. Extrusion was carried out at 250° C (0.56 T_m) and a strain rate of 1.2 sec^{-1} x 40,000 (Jonas *et al.*, 1968a). c) The fibrous appearance of the grains in a sample of commercial purity aluminum rolled to a reduction of 96 % (2400 % elongation) in 15 passes in the temperature range 525-300° C (0.85-0.62 T_m) x 10 (Vaughan, 1968). d) The formation of subgrains has resulted in an irregular or scalloped grain boundary in this sample of aluminum extruded at 420° C (0.74 T_m) and 0,1 sec^{-1} to a strain of 2.3 (900 % elongation) x 100 (Demianczuk, 1967).

---

* The effective stress σ^* is the local value of the net stress acting at a dislocation. It is related to the applied or developed stress σ by the relation $\sigma^* = \sigma - \sigma_i$, where σ_i is the local value of the internal stress associated with the presence of other dislocations, or of grain boundaries or precipitates.

of strain. The rate of annihilation, on the other hand, depends on the dislocation density, and on the ease of operation of the recovery mechanisms, such a climb, cross-slip, and node unpinning. Thus the gradual elimination of strain hardening comes about through the increase in dislocation density with strain, which leads to continual increases in the annihilation rate until this matches the generation rate.

An additional interesting feature of steady state deformation is particularly worthy of note; the subgrains appear equiaxed even at large strains (Figs. VII 7a and b), whereas the grains deform in conformity with the outward change in shape of the object (Fig. VII 7c). This cannot be explained solely by migration of the subboundaries, since not all of them are capable of migration and since it has been shown that such migration contributes only 6-10 % of the strain (Exell and Warrington, 1972). Another contributing process is repolygonization, that is the repeated unraveling of the subboundaries and the subsequent reformation of new subboundaries at locations which keep their average spacing and dislocation density constant (McQueen *et al.*, 1967). The stable subgrain size depends in turn on the equilibrium dislocation density (Holt, 1970), which is established by the balance between generation rate and annihilation rate. Holt demonstrated that a uniform distribution of dislocations, when allowed some mobility, will form "clusters". The wavelength of clustering, which is in effect the cell wall spacing, will be proportional to the mean dislocation spacing, $l = \rho^{-1/2}$. This result is based on the condition that the stress level at a dislocation in a wall due to a dislocation in an adjacent wall is a small fixed fraction of the stress level due to a nearest-neighbor

Fig. VII.8 – The effects of temperature and strain rate are shown in these electron micrographs (all x 5000) of commercial purity aluminum which has been compressed to a strain of 0.7 (50 % reduction). The first series is compressed at a strain rate of about 11 sec^{-1} at temperatures of a) 20° C (0.36 T_m), b) 200° C (0.50 T_m) c) 400° C (0.72 T_m), d) 500° C (0.82 T_m). The second series is compressed at 400° C (0.72 T_m) at rates of approximately e) 200 sec^{-1}, f) 12 sec^{-1}, g) 1.4 sec^{-1}, and h) 0.1 sec^{-1} (McQueen and Hockett, 1970)

dislocation. In addition, when the subboundary dislocation density is higher, the long range stress field of an individual dislocation in the boundary is neutralized to a greater degree. As a result, the higher the subboundary density, the shorter the distance over which the stress field of the boundary as a whole has an influence, and the smaller is the equilibrium subgrain size.

In concluding this section, the reader is reminded that the process of dynamic recovery as it occurs during hot working cannot be considered as equivalent to the superposition of static recovery and cold working. The concurrence of straining and recovery prevents the high dislocations densities of cold working from ever developing. In fact, the small subgrains produced by hot working cannot be synthesized by cold working and annealing because of the intervention of recrystallization. The marked effectiveness of an applied stress in accelerating recovery at high temperatures was originally observed in a phenomenon called stress annealing (Wood and Suiter, 1951); this matter will be considered later with the deformation of metal initially containing a worked substructure.

VII.3.3 – Effect of Strain Rate and Temperature on the Substructure

The higher the temperature of deformation and the lower the strain rate, the larger are the subgrains that are formed during high temperature deformation (Bird *et al.*, 1969). As they increase in size, the subgrains contain fewer dislocations and have boundaries in which there are less dislocations arranged in more orderly arrays (Fig. VII.8). These substructural variations reflect the diminution in the equilibrium dislocation density arising from the increase in temperature and decrease in strain rate through their effects on the generation and annihilation rates. The generation rate decreases because the effective stress decreases with strain rate decrease and with temperature increase. The annihilation rate, on the other hand, does not decrease as much with a decrease in strain rate because it is not as sensitive to a stress decrease as the generation rate. Furthermore, increases in temperature tend to increase the recovery rate, thereby offsetting in part the effect of a decrease in stress.

The onset of steady state deformation is also rate sensitive and occurs at strains varying from about 0.1 at high temperatures and low strain rates to 0.5 or more at relatively low temperatures and high strain rates. This increase in strain arises because both the decrease in temperature as well as the increase in strain rate decrease the number of recovery events per unit strain. The amount of generation per unit strain, on the other hand, actually increases with strain rate and with temperature decrease.

The dependence of mean subgrain diameter d on temperature T and strain rate $\dot{\epsilon}$ is illustrated in Fig. VII.9 and is described by the relation

$$d^{-1} = a + b \log Z \qquad (1)$$

Here a and b are empirical constants and the temperature-corrected strain rate Z is given by

$$Z = \dot{\epsilon} \exp (Q/RT) \qquad (2)$$

where Q is the experimental activation energy associated with the temperature dependence of the flow stress and R is the universal gas constant.

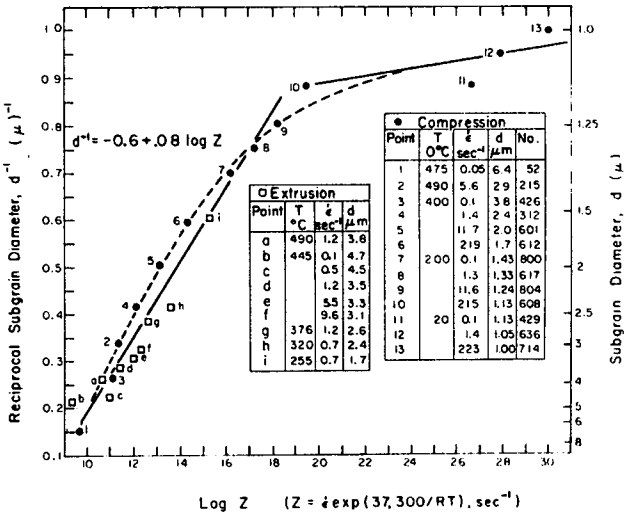

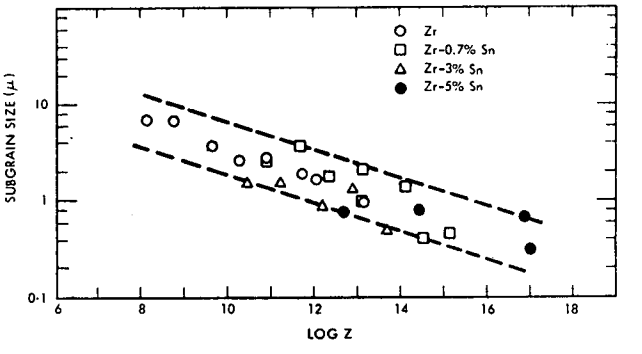

Fig. VII.9 – The subgrain diameter increases as the temperature-compensated strain rate Z decreases (i.e. temperature increases). a) Commercial purity aluminum extruded to a strain of 3.7 or compressed to a strain of 0.7. Points 11, 12 and 13 are not on the fitted line since they correspond to cold-worked materials (McQueen and Hockett, 1970). b) This dependence also holds for α-zirconium and zirconium-tin alloys. The experimental activation energy used to calculate Z for each alloy increases with tin content, yet the sizes fall in a single band, indicating that there are compensating decreases in diameter associated with the increases in activation energy (Abson and Jonas, 1972).

VII.3.4 – The Flow Stress at High Temperatures

In the room temperature region, it is common to express σ as

$$\sigma = \sigma_0 + \alpha \mu b \sqrt{\rho} \qquad (3)$$

Here σ_0 is a friction stress, which may or may not be rate dependent, α is a geometrical constant, μ is the shear modulus, b the Burgers vector, and ρ the dislocation density. A similar relation appears to hold at high temperatures (Luton and Jonas, 1970), as given by

$$\sigma = \sigma^* + \sigma_t \qquad (4)$$

Here σ^*, known as the effective stress, is the reversible component of the flow stress, changes in which are concurrent with changes in temperature or strain rate. The term σ_i refers to the "irreversible" or structural component of the flow stress, also known as the internal stress. Changes in σ_i do not follow immediately on changes in strain rate or temperature, but are associated with structural modifications, and therefore either with strain or with the effects of annealing.

VII.3.4.1 – The Yield Stress at High Temperatures

It was pointed out earlier that at yielding, the dislocation density is about three orders of magnitude below that attained during steady state flow. Setting

$$\sigma_i = \alpha \mu b \sqrt{\rho} \tag{5}$$

it can be seen that the internal stress at yielding is in the neighborhood of 3 % of the internal stress present under steady state conditions. As a first approximation, we can therefore write that

$$\sigma_y \simeq \sigma^* \tag{6}$$

where σ_y is the yield stress.

The yield stress of alpha zirconium is shown as a function of strain rate and temperature in Fig. VII.10. It is evident that σ_y (and therefore σ^*) is strongly temperature and rate sensitive, unlike the "friction" stress commonly observed in the room temperature range. Qualitatively similar dependences on temperature and strain rate have been reported for yielding in bcc materials by Immarigeon (1974) and in fcc materials by Petkovic (1975).

The mechanism controlling yielding at high temperatures has not been established with certainty but has been suggested to be the thermally activated unpinning of dislocation nodes (Sastry *et al.*, 1974). This conclusion was supported by the following common features of high temperature yield data: (a) the relatively large experimental activation volumes, (b) the stress dependent nature of the experimental activation energies, (c) the rapid increase in certain alloys of experimental activation energy with solute concentration, and (d) the absence, at yielding, of a well-developed substructure or of subgrains, and therefore the inapplicability of the secondary creep models based on the presence of a steady state substructure

The node unpinning model for yielding involves a zero-stress activation energy of about 0.4 μb^3 in high stacking

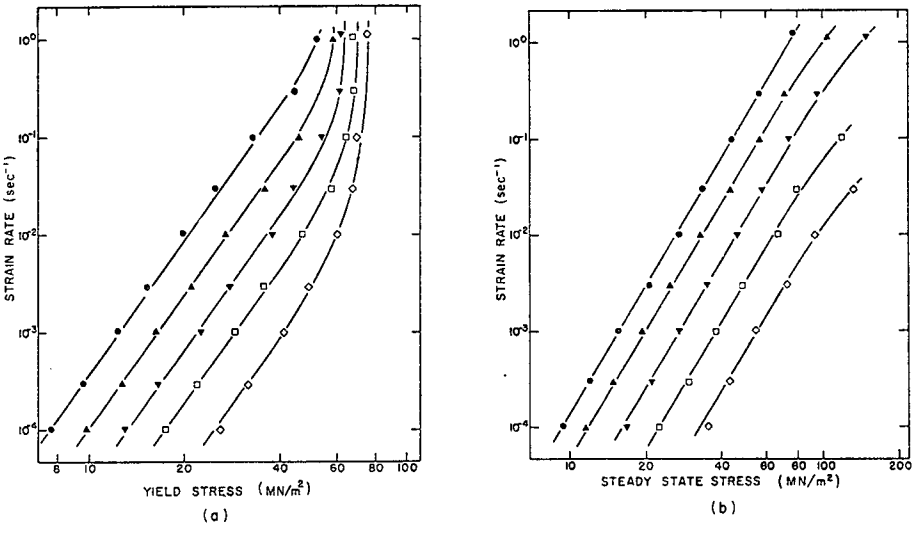

Fig. VII.10 The strain rate dependence of a) the yield stress and b) the steady state flow stress of α-zirconium plotted in the manner of creep data. The temperature range lies between 0.44 T_m and 0.63 T_m. The straight line fits at the higher temperatures and lower strain rates exhibit a power law exponent of 4.6 for the yield stress and 4.4 for the steady state stress (Luton and Jonas, 1972b). ◇, 625° C ; □, 675° C ; ▼, 725° C ; ▲, 775° C ; ●, 825° C.

fault energy metals. This value is somewhat higher than the activation energy for self-diffusion; it increases with decreasing stacking fault energy to as much as 0.5 to 0.7 μb^3.

VII.3.4.2 – The Steady State Stress

The steady state flow stresses σ_s observed in alpha zirconium are also shown in Fig. VII.10. It is clear from the diagram that the temperature and rate dependence of σ_s is closely similar to that of σ_y. When a creep power law*, e.g.

$$\dot{\epsilon} = A \sigma_s^n \exp(-Q/RT) \tag{7}$$

is fitted to these data, stress exponents of 4.6 and 4.4

* Here $\dot{\epsilon}$ is strain rate, A and n are empirical constants, Q is an experimental activation energy, and R is the gas constant.

and activation energies of 226 and 234 kJ/mol are obtained for σ_y and σ_s, respectively. It is of interest that the ratio σ_y/σ_s for alpha zirconium, as well as for a series of Zr–Sn alloys (Luton and Jonas, 1972b), is in the range 0.7 to 0.85. For bcc alpha iron and silicon iron, σ_y/σ_s has been reported to vary from 0.5 to 0.9 (Immarigeon, 1974), and for fcc copper and gamma iron to range from 0.4 to 0.7 (Petkovic, 1975).

The broad similarity in the temperature and rate dependences of σ_y and σ_s in many materials leads to an interesting speculation. The activation parameters associated with σ_y, and therefore with σ^*, are characteristic of the rate controlling glide process, which may for example be node unpinning or the breakup of attractive junctions, as suggested above. The temperature and rate dependence of σ_s, on the other hand, will depend on the combined dependences of the glide mechanism and of the internal stress σ_i. The stable value of σ_i is, however, determined by the detailed nature of the dynamic recovery processes that are operating at high temperatures. The conclusion can therefore be drawn that the similarity in the behavior of σ_y and σ_s implies that the glide obstacles and the obstacles to recovery have similar features and may even involve the same rate controlling events.

It is of interest to note that, if the high temperature glide obstacle is the breakup of attractive junctions, and if these junctions remain stable, as expected, at intermediate temperatures, then the considerable difference between the amount of work hardening attainable at room temperature ($\sigma_i/E \propto b/\sqrt{\rho} \simeq 3 \times 10^{-2}$) and that attainable at high temperatures ($\sigma_i/E \propto b/\sqrt{\rho} \simeq 3 \times 10^{-3}$) is readily explained.

VII.3.4.3 – The Transition to Athermal Flow

The similarities in the temperature and rate dependences of σ_y and σ_s have already been noted above. When the dissimilarities indicated in Fig. VII.10 are also taken into account, a clearer picture emerges of the differences between ambient and elevated temperature deformation. In Fig. VII.11, the σ_y and σ_s values of Fig. VII.10 are collected and compared as functions of the temperature-corrected strain rate. The small difference in experimental activation energy for the two types of flow is neglected for this purpose. It can be seen from the figure that as the temperature is decreased or the strain rate is increased, the yield stress becomes progressively less sensitive to temperature and strain rate, until the deformation is virtually athermal. It can also be seen from Fig. VII.11 that at low temperatures and high strain rates, steady state flow becomes increasingly difficult to attain, because of the progressive inhibition of the recovery processes that accompanies the transition to athermal flow. At sufficiently low temperatures and high strain rates, i.e. well within the athermal range, steady state flow cannot be attained at all.

The transition to athermal flow is considered further in Fig. VII.12 in which the three regimes of flow stress–

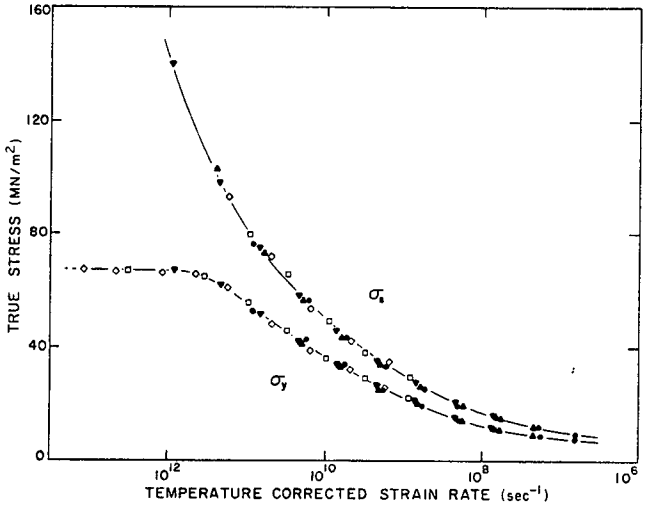

Fig. VII.11 The data of Fig. VII.10 collected and plotted in terms of temperature-corrected strain rate Z. As the temperature is reduced (leftward motion on the diagram), the yield stress σ_y stops increasing and reaches a limiting (athermal) value. By contrast, the steady state flow stress σ_s increases rapidly as the athermal flow regime is approached.

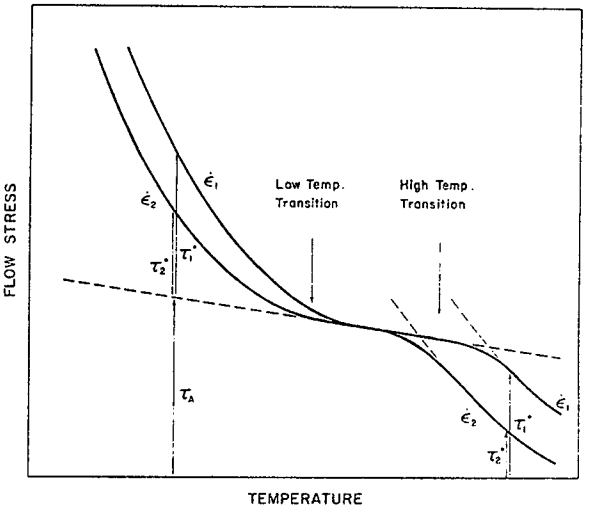

Fig. VII.12 Schematic representation of the athermal flow regime and its relation to the low and high temperature thermally activated regions. The transition between athermal and high temperature thermally activated flow is seen to be rate sensitive. The low yield stresses observed at high temperatures signify that the obstacles to athermal flow are bypassed or inoperative at elevated temperatures (Jonas, 1973).

temperature dependence are compared. The figure demonstrates that, in each region, it is the lower of the two flow stresses, thermal or athermal, which is operative, so that the transition under consideration is likely to involve alternative mechanisms, which do not operate at all outside their respective temperature and strain rate ranges. Thus the athermal mechanism is unlikely to be controlled by obstacles such as solute or impurity atoms, which must also be present and active at high temperatures. It is more probable instead that the athermal stress corresponds to the stress required for the dislocations to bow out between the nodes by a Frank-Read or Orowan mechanism (Heritier *et al.*, 1974).

VII.3.5 — Substructure and Flow Stress

In many investigations carried out under both creep and hot-working conditions, it has been observed that there is a unique relationship between the scale of the substructure and the flow stress once steady state flow is achieved. The relationship, which is illustrated in Fig. VII.13, is as follows:

$$\sigma_s = K_1 d^{-1} \tag{8}$$

Here K_1 is an empirical constant. This relation can be given a physical interpretation in terms of Eq (4) above:

$$\sigma_s = \sigma^* + \sigma_i \tag{4}$$

First is must be recalled that, at yielding, $\sigma^* \sim \sigma_y$. If σ^* remains approximately constant with strain (Immarigeon, 1974), and setting

$$\sigma_i = K_2 d^{-1} \tag{9}$$

where K_2 is the subboundary strengthening coefficient*, we can write that

$$\sigma_s = \sigma_y + K_2 d^{-1} \tag{10}$$

But σ_y in most materials is an approximately constant fraction $f < 1$ of σ, i.e. $\sigma_y \simeq f\sigma_s$. Thus

$$\sigma_s \simeq K_2 d^{-1}/(1-f) \tag{11}$$

and we see that the empirical constant $K_1 \simeq K_2/1-f)$.

In the above, it has been assumed that the internal stress σ_i is uniquely related to the subboundary density $3/d$, as suggested by Abson and Jonas (1970). This could arise through a causal relationship in which the subboundaries are the principal source of internal stress at high temperatures. Alternatively, the dislocations within the subgrains ρ_s could be directly responsible for the internal stress, as given by Eq.(5):

$$\sigma_i = \alpha\mu b\sqrt{\rho_s} \tag{12}$$

In this event, the empirical correlation (7) takes its physical base from Eq.(5) through a relation of the type introduced by Holt (1970) and discussed above. From the evidence available to date (e.g., Cuddy, 1970), it has not yet been

---

* The term $K_2 d^{-1}$ will be considered in more detail below in the section on the strengthening effect of subboundaries at room temperature.

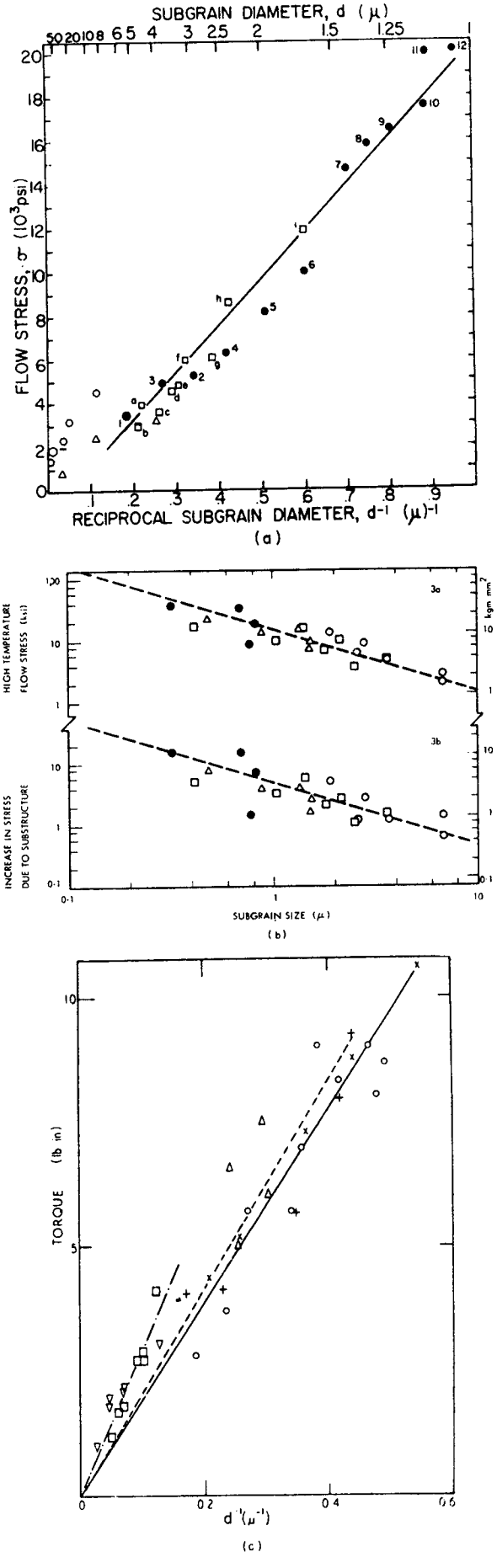

Fig. VII.13 — The correlation between steady state flow stress and mean subgrain diameter for a variety of deformation conditions and metals. a) Commercial purity aluminum (fcc) deformed to a variety of strains from 0.7 to 3.7 within the steady state regime (McQueen and Hockett, 1970). •, Compression ; □, extrusion (McQueen, *et al.*, 1967) ; Δ, creep (Wood and Rachinger, 1949) ; ○,hot torsion (Farag. *et al.*, 1968). b) Subgrain size versus both flow stress and internal stress in α-zirconium and zirconium-tin alloys (hcp). The alloy data points are shifted toward decreasing subgrain size and increasing flow stress (Abson and Jonas, 1972). ○, Zr ; □, Zr–0.7 % Sn : Δ, Zr–3 % Sn • Zr–5 % Sn. c) The torque for steady state flow is related to the subgrain size for bcc iron and its alloys with Ni and Cr (Redfern and Sellars. 1968). x ——— ○, S102 iron, alloy 2, 0.62 % Cr : + — — — Δ, alloy 7, 2.29 % Ni, alloy 9, 3.05 % Ni ; ▽ – . – □. alloy 3, 12.9 % Cr, alloy 4, 14.0 % Cr.

possible to determine whether the principal source of the internal stress (i.e. of work hardening at high temperatures) is the subboundary structure directly on the one hand or the dislocation network within the subgrains on the other.

VII.3.6 – Substructure Formation in Pure Metals

Since dynamic recovery involves the occurrence of climb, cross-slip, and node unpinning, it takes place more readily in metals which have higher stacking fault energies. However, comparisons must be made at a common homologous temperature, so that the fluctuations which promote thermal activation will be of similar magnitude in each metal. Such a comparison is made in terms of the substructures produced by hot working in Figs. VII.14a, b, and c for the fcc metals. It can be seen from the figure that aluminum in which dynamic recovery proceeds with ease, contains subgrains which are well formed, and in which the subboundaries are simple arrays (Jonas *et al.*, 1969). Nickel and copper, on the other hand, with their much lower stacking fault energies, have very tangled substructures (Drube and Stüwe, 1967). It will be seen later that, at higher strains, these high dislocation densities lead to dynamic recrystallization.

In the bcc metals, stacking fault energies are relatively high, so that crossglide, climb, and node unpinning are not unduly difficult, and the facility for dynamic recovery approaches that of aluminum (Rossard, 1960; Jonas *et al.*, 1968b; Glover and Sellars, 1973). Not unexpectedly then, the deformation microstructures of the ferritic irons (Fig. VII.14e) and of aluminum are more closely

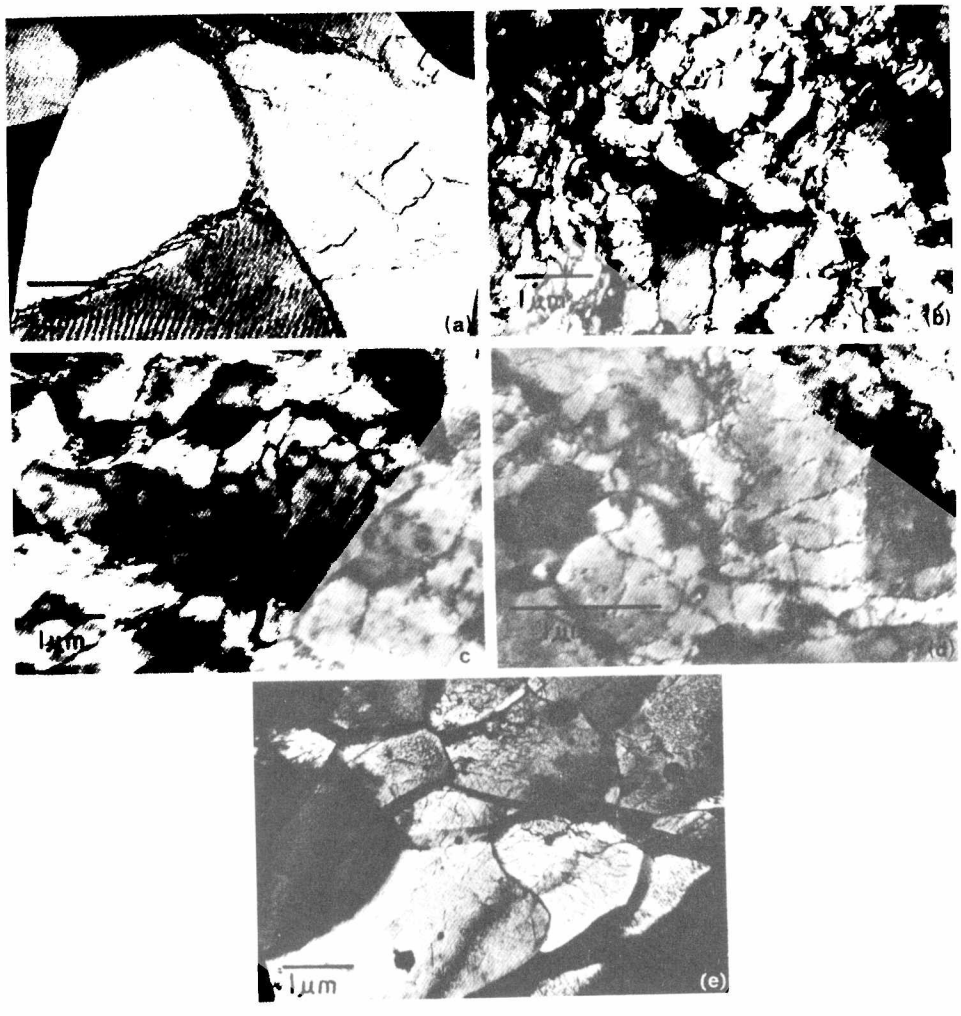

Fig. VII.14 – Transmission electron micrographs of substructures resulting from hot working : a) through d) are for fcc metals rolled to 90 % reduction ($\epsilon = 2.3$) in one pass, at an average strain rate of 20 sec^{-1}, and an exit temperature of 0.65 T_m. a) Aluminum, 340 C. x 10.000. b) Nickel, 840 C. x 10.000. c) Copper, 600. C. x 10.000. d) 70/30 brass, 600 C. x 20.000 (McQueen, 1968). e) The substructure of Armco iron deformed at 675 C (0.52 T_m) and 10^{-1} sec^{-1} closely resembles that of aluminum, x 9000 (Immarigeon and Jonas, 1971).

similar than those of aluminum and of fcc metals and alloys with low stacking fault energies.

Subgrains also form in hexagonal close packed metals during high temperature deformation and have been observed in zinc (Hardwick and Tegart, 1961), beryllium (Webster *et al.*, 1973), and zirconium. The subgrains in zirconium are similar to those in aluminum in size and perfection (Fig. VII.15a).

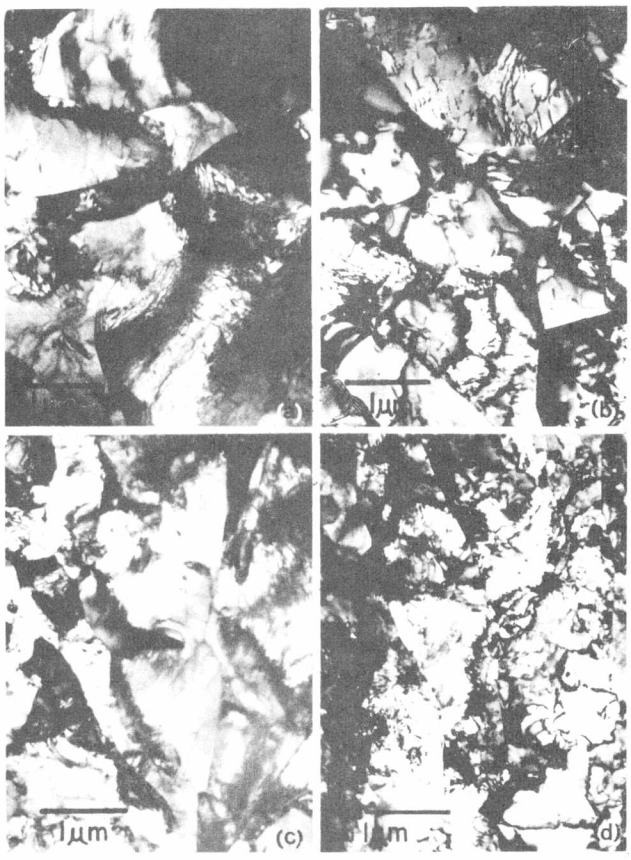

Fig. VII.15 – Electron micrographs of commercial purity α-zirconium and zirconium-tin alloys deformed into the steady state regime at 675° C (0.44 T_m) at a strain rate of 3×10^{-2} sec^{-1} x 11,000. a) Zr. b) Zr–0.7 % Sn. c) Zr–3 % Sn. d) Zr–5 % Sn. The subgrains become smaller and the density of dislocations becomes greater as the tin content increases (Abson and Jonas, 1972).

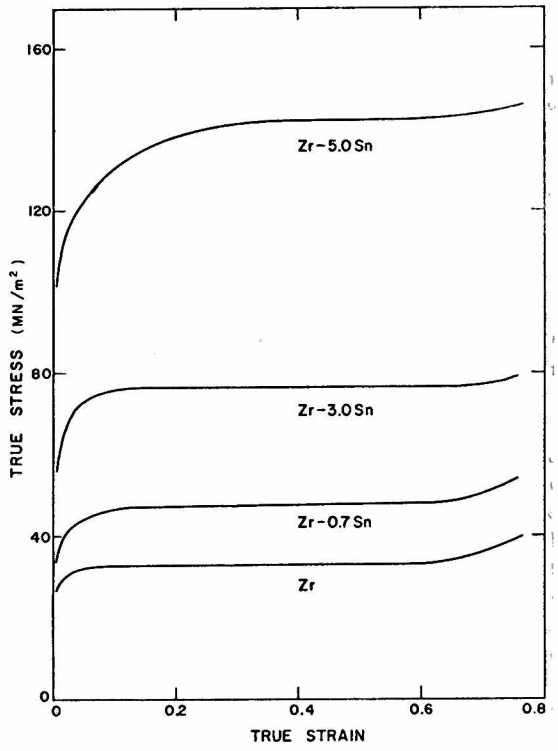

Fig. VII.16 – The strengthening effect of solute addition is shown in this group of stress-strain curves for Zr and three of its alloys with tin. The temperature is 775° C (0.5 T_m) and the strain rate 10^{-2} sec^{-1} (Luton and Jonas, 1972b).

VII.3.7 – Effect of Solute Addition

When solute elements are present in the range 1-20% by weight, both the flow stress and the resistance to creep increase by up to an order of magnitude (Fig. VII.16). The increase in yield and steady state stress with concentration diminishes as the temperature is raised, although the increases relative to those of the pure metal remain approximately constant. This is illustrated in Fig. VII.17, from which it can be seen that the yield and steady state flow strengths of binary solid solutions are temperature and rate sensitive, as are those of a pure metal (Luton and Jonas, 1972b). The increase in flow stress of solid solution alloys is sufficiently great that considerably more force and energy is required to deform these materials in industrial hot working (Sabroff *et al.*, 1968; Sellars and Tegart, 1972). For the same reason, alloys developed specifically for creep resistant service are based on solid solutions which are further strengthened by means of precipitation.

The effect of solid solution alloying on the microstructures produced by working are rather diverse and require the individual discussion of each alloy system. In general, solute addition lowers the stacking fault energy, which makes dynamic recovery more difficult. This is observed in brass, which does not form a well-defined subgrain structure under conditions of temperature and strain rate for which it is found in copper (Fig. VII.14d). Similarly, in Zr-Sn alloys, the addition of up to 5 % tin reduces the stacking fault energy from 240 to 60 mJ/m^2 and also increases the fault width from about 2.5 to 10*b* (Sastry *et al.*, 1974). Consequently, the equilibrium subgrain size produced in these alloys at the same temperature and strain rate decreases from about 3.5 to 0.7 μm as the tin concentration in increased (Fig. VII.15).

In the Al-Mg system, on the other hand, while the strength increases with greater concentration of Mg, the size of the subgrains also increases for tests at the same temperature and strain rate (Fig. VII.18). The latter observation can be reconciled with the increased amount of work hardening in the alloys if the internal stress does not depend directly on subboundary density, as has been suggested above, but increases with $\sqrt{\rho}$ instead. A further alternative, that the internal stress contribution of the subboundaries is strongly dependent on the dislocation structure of the boundary itself, and that this changes with alloying, is also possible. In the austenitic stainless steels, a well developed substructure forms, one which is more "recovered" than that of copper under equivalent conditions, suggesting that the stacking fault energy is higher than in copper at these temperatures (Garofalo *et al.*, 1963; Buhler *et al.*, 1970). It is not possible to compare the stainless substructures with those formed in unalloyed austenite, since the substructures in the latter material are lost during the phase transformation produced by cooling. When the nickel-base superalloys

are worked in the single phase condition, a recovered substructure is produced which is apparently as well defined and orderly as that observed in nickel (Fulop and McQueen, 1972).

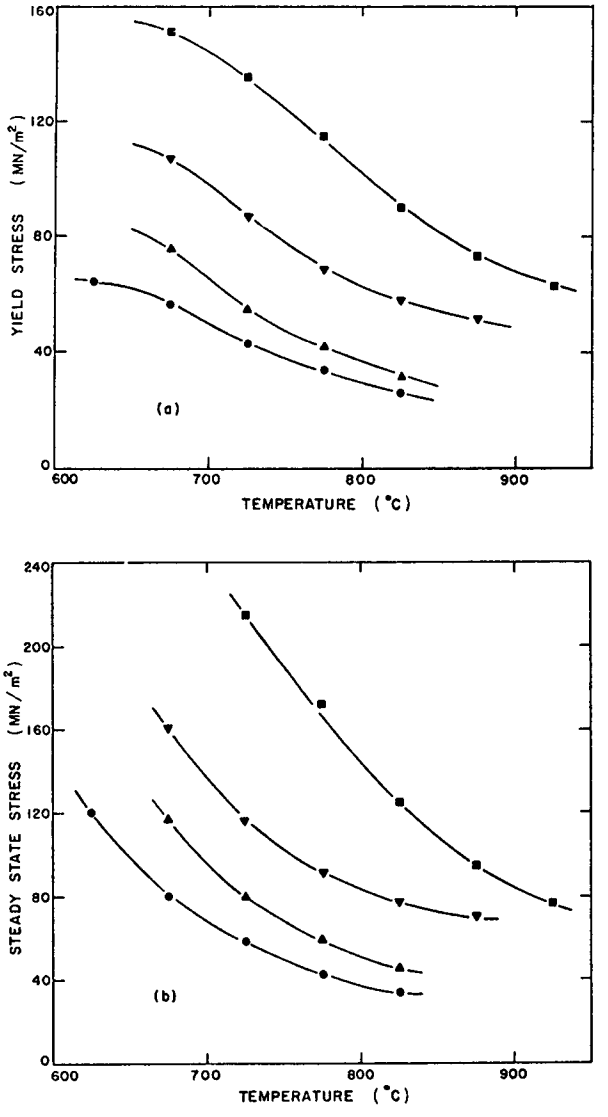

Fig. VII.17 The temperature dependence of the flow stress for alpha zirconium and three of its alloys with tin. For deformation at 3×10^{-2} sec^{-1}, the yield stresses appear in a) and the steady state stress data in b) (Luton and Jonas, 1972b) ●, Zr ; ▲, Zr–0.7Sn ; ▼, Zr–3.0Sn ; ■, Zr–5.0Sn.

In bcc alloys, additions of chromium or nickel increase the flow stress of the alloy (Redfern and Sellars, 1968). In iron-silicon alloys, the addition of silicon produces strengthening from about 600 to 800°C (Immarigeon and Jonas, 1974). Above 800°C, however, the addition of silicon leads to weakening, a phenomenon known as solute softening in the low temperature range. This has been attributed to the increase in the density of mobile dislocations associated with silicon addition, which overrides the increase in node stability. The solution of the above elements in iron does not markedly affect the scale of the substructure under given conditions of temperature and strain rate (Jonas *et al.*, 1968b). The steady state flow stress for a given subgrain size is greater for the alloys than for pure iron (Fig. VII 13c). As in the case of the Al-Mg alloys, these observations suggest that the subboundaries are not the primary source of internal stress in these materials. Finally, it should be noted that the addition of Si or particularly of Cr stabilizes the α phase and extends the working range to higher temperatures.

A special application of alloying and hot working is the ausforming process in which the objective is the transformation of austenite to martensite immediately after hot working so that the dislocation structure is carried into the martensite. Alloying of the austenite creates a bay in the isothermal transformation curves in which the working can be carried out and rapid quenching achieved (Schmatz *et al.*, 1963; Irani and Taylor, 1968).

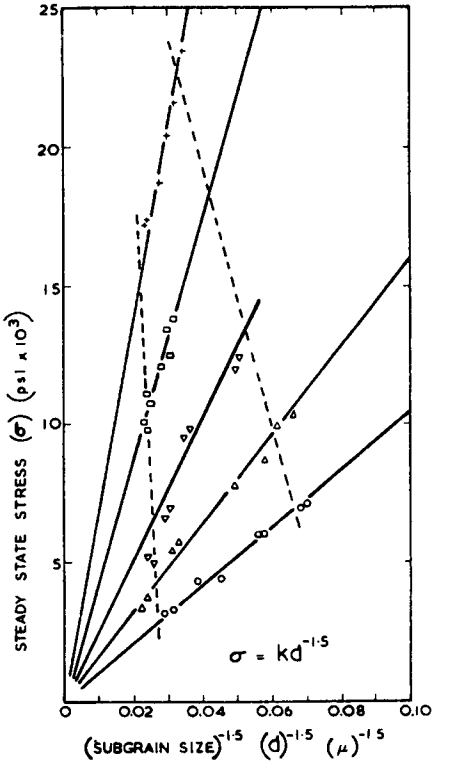

Fig. VII.18 The effect of magnesium concentration and subgrain size on the steady state flow stress of Al-Mg alloys. Samples were deformed in torsion between 400° C and 550° C at a strain rate of 2 sec^{-1}. Since the data points for each alloy follow the same sequence of temperatures, it can be seen that for a given temperature the subgrain size increases with Mg concentration (Cotner and Tegart, 1969). ○, S.P. Al ; Δ, Al–1/3 % Mg ; ▽, Al–1 % Mg ; □, Al –2 % Mg ; +, Al–5 % Mg.

VII.3.8 – Dynamic Recovery in Two-Phase Alloys

The simplest two-phase materials are those in which the second phase is present as roughly spherical particles which are relatively hard at the temperature of deformation. In situations where the particles are not cut by the dislocations and are relatively stable, they serve as obstacles which help initially to build up the substructure and finally to stabilize it. This effect has been observed at strains not exceeding two in many systems: e.g. Al with

Al_2O_3 particles, Ni with ThO_2 particles (Clauer and Wilcox, 1967), Ni-base superalloy with γ' precipitate (Oblak and Owczarski, 1972), ferrite with carbide precipitates, and austenite with NbC particles (Le Bon *et al.*, 1973) or other carbides (Garofalo *et al.*, 1961). Under these conditions, the subgrain diameter may be reduced to the order of the interparticle spacing, which leads to an increase in flow stress. The presence of precipitates can prevent the formation of a subgrain structure altogether if the spacing is small enough, or if, as a result of their shearing, they induce the formation of matrix superdislocations, which cannot leave their slip planes. Furthermore, by preventing grain boundary migration, the particles can shift the initiation of dynamic recrystallization to higher strains, which can be useful in controlled rolling (Irvine *et al.*, 1970; Tegart, 1971). It appears that the presence of NbC in austenite can completely inhibit dynamic recrystallization at moderate temperatures, although this may actually be caused by the inhibiting effect of the particles on subgrain formation, and therefore on the nucleation of new grains (Petkovic, 1975).

If the elements comprising the second phase are soluble in the matrix, even to a very limited degree, it can coalesce during deformation into fewer and larger particles. In hot working this can cause a significant decrease in flow stress over a strain increment of 1 or 2 (Fig. VII.19). Coalescence proceeds more rapidly at higher temperatures and higher strain rates. At higher temperatures and lower strain rates, the second phase particles are coarser when steady state flow is finally achieved. This phenomenon has been observed in pearlitic-ferritic steels (Sherby *et al.*, 1969) and in eutectoid steel; for example, at 700°C (1292°F), a degree of spheroidization which would take 660 hr of annealing takes place in 210 sec of deformation at 0.016 sec^{-1} (Chojnowski and Tegart, 1968). The diffusional process producing the spheroidization is considered to be accelerated by the hot-work subboundaries which provide paths for pipe diffusion, which is considerably more rapid than lattice diffusion under the same conditions. Another example of this effect is found in the warm working of bainite. Here spheroidization of the acicular particles increases the ductility considerably without loss in overall strength because of the strengthening contribution of the substructure introduced. In Waspalloy, the Ni_3 (TiAl) particles appear to coalesce during straining, giving rise to stress-strain curves similar to those for eutectoid steel.

If precipitation occurs *during* high temperature deformation, it causes the flow stress to increase or the creep rate to decrease. The presence of a dislocation substructure during precipitation assures a uniform distribution of precipitate in most cases. For example, when the thermo-

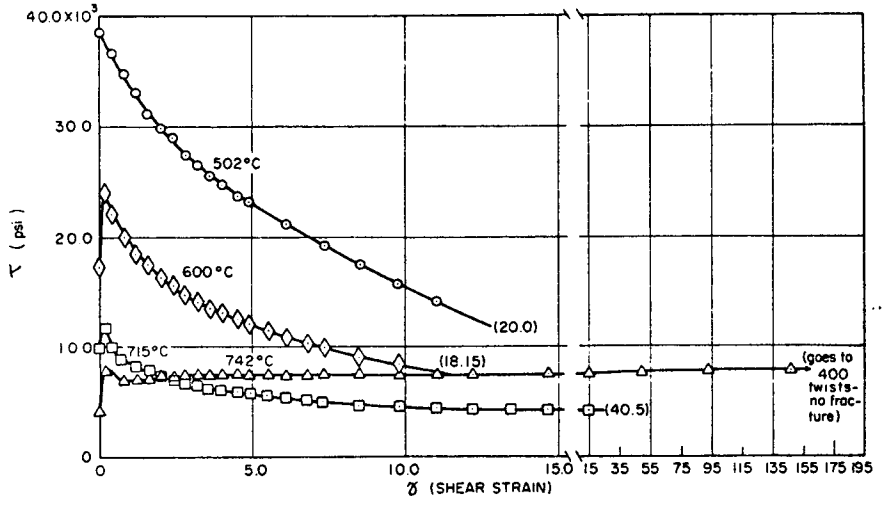

Fig. VII.19 — Torsional stress-strain curves for an alloy of pure iron and 0.8 % carbon. At 502°C (0.43 T_m) and 715°C (0.56 T_m), the microstructure at the beginning of the test is completely pearlitic. In the course of deformation, the carbide spheroidizes, giving rise to a continuous decrease in flow stress. The figures in parentheses indicate the number of twists to failure (Robbins *et al.*, 1967). $\dot{\gamma} = 4.1\ \%\ sec^{-1}$.

mechanical working of a nickel-base superalloy is designed to permit precipitation during working, the resultant properties are better than those obtained when precipitation precedes or follows working (Oblak and Owczarski, 1972). This phenomenon is also exploited in the isoforming process, in which austenite is deformed as it is transforming to ferrite and carbide (Irani and Taylor, 1968). In this case, the precipitated carbides are nucleated on dislocations in the ferrite and the particles grow as spheres. Ultimately the carbide particles serve to stabilize and strengthen the substructure.

VII.3.9 — The Ease of Dynamic Recovery and Its Effect on Ductility

In hot working as well as in creep, the most common cause of fracture is the formation of grain boundary cracks (Tegart, 1968). The cracks are nucleated as a result of grain boundary sliding and are propagated by the tensile stresses generated during the working operation. In creep studies, it has been observed that as the stress and the strain rate are increased, the sites for crack initiation change from grain boundary ledges to the triple junctions. In hot work-

ing, because the flow stress is much higher than in creep, and because less time is available for grain boundary sliding and the diffusional growth of pores, the nucleation sites are almost entirely limited to grain boundary junctions.

The formation of subgrains in metals displaying a susceptibility to dynamic recovery results in the scalloping of the grain boundaries, which diminishes intergranular sliding (Fig. VII 7d). Furthermore, such materials have fairly low flow stresses and flow readily at triple junctions to relieve stress concentrations and thus diminish the initiation of W cracks. Both of these effects contribute to the high ductility observed in aluminum, α-iron, and α-iron-chromium alloys. In such metals, the ductility usually increases with temperature because the accommodation processes are more sensitive to temperature than those promoting crack nucleation (Gittins, 1970). However, in metals such as nickel and the nickel-base superalloys, in which the rate of recovery is relatively low, the ductility *decreases* with temperature in the lower part of the high temperature range (where dynamic recrystallization does not intervene) because of increases in the amount of grain boundary sliding (Shapiro and Dieter, 1971; White and Rossard, 1968).

A reduction in ductility with increasing temperature can also arise as a result of phase changes. For example, fcc austenitic iron above the transformation temperature is less ductile than bcc ferritic iron below the transformation temperature because of the higher yield stress of the austenite, as well as its lower capacity for recovery (Reynolds and Tegart, 1962). Similarly, at a given temperature in the range 900-1200°C, the ductility of the Fe-Cr-Ni alloys is higher for the high recovery rate δ-ferrite structure (bcc) than for the low recovery rate γ-austenite structure (fcc).

In general, solid solution alloying tends to reduce ductility (Luton and Tegart, 1969) and the effect becomes more pronounced with increasing concentration (Fig. VII.20). This is partly because the smaller subgrains formed in these materials are not as effective in producing scalloping of the grain boundaries, so that grain boundary sliding is not impeded to the same extent. The scalloping is also reduced by the retarding effect solutes exert on grain boundary migration. In addition, the decreased ease of dynamic recovery raises the flow stress considerably, which is instrumental in nucleating and opening up the cracks.

The presence of precipitate particles, e.g. carbides in ferritic steel, usually reduces the ductility (Fig. VII.21).

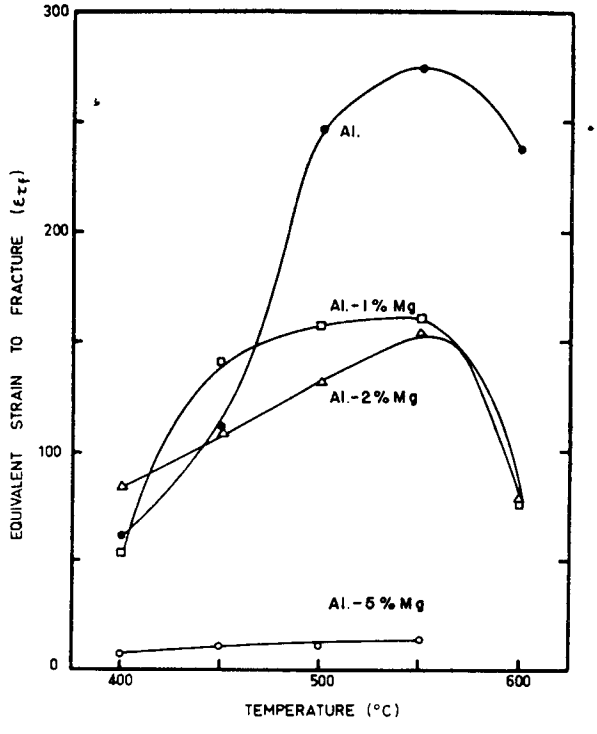

Fig. VII.20 – Increasing the amount of magnesium in solid solution decreases the ductility of Al-Mg alloys; at 5 % Mg. the ductility is severely reduced over the entire temperature range. The deformation rate employed in these hot torsion tests was 2.3 sec^{-1} (after Cotner and Tegart, 1969).

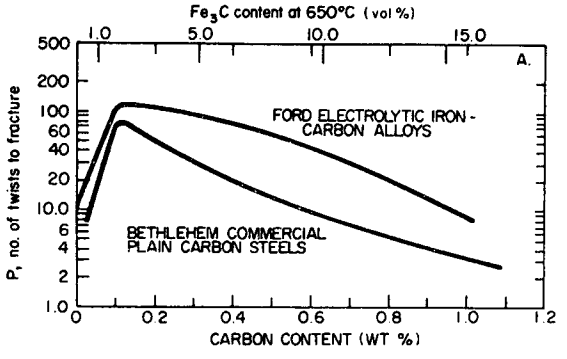

Fig. VII.21 – The influence of carbon on the ductility of bcc iron tested in torsion at 0.03 sec^{-1} and 650°C (0.5 T_m). The ductility initially increases as a result of the decrease in concentration of oxide inclusions. At higher carbon content, the ductility decreases as the volume fraction of carbide increases (Robbins *et al.*, 1967).

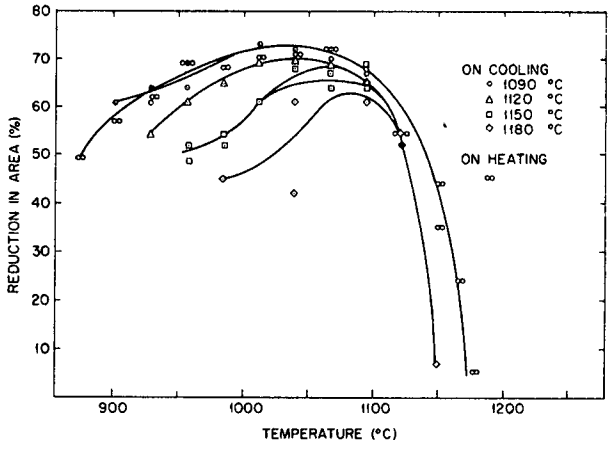

Fig. VII.22 – The ductility of a nickel-base superalloy (Inconel 718) increases with temperature on heating from room temperature as a result of enhanced dynamic recrystallization. The ductility drops rapidly at high temperatures as the solvus temperature is approached. The ductility decrease resulting from cooling from a high preheating temperature, such as 1150 or 1180°C, is due to the increase in size of precipitate particles. The yield stress diminishes with temperature and is unaffected by the preheating temperature. The tests were carried out in tension and a crosshead speed of 5 in./sec was used (Bailey, 1969).

However, the size and distribution of the particles are very important. Fine discrete precipitates uniformly distributed on the grain boundaries improve the ductility by impeding sliding (Cremisio *et al.*, 1969). Particles larger than 10μ or semicontinuous films of precipitate that are harder or more brittle than the matrix are very damaging, since they help to initiate wedge cracks and prevent boundary migration (Gittins *et al.*, 1972). The overheating of certain alloys before hot working can also give rise to poor ductility because of the increase in size of the precipitate particles which form on the grain boundaries (Fig. VII.22).

A ductility reduction is also observed when the second phase is a metallic one and is present in much larger volume fractions. Examples are γ in α-iron (Robbins *et al.*, 1967) or in δ-iron and β-phase in Ti alloys (Reynolds, 1968). The magnitude of this effect depends upon the volume fractions of the two phases, on their relative ductilities, and on the softening mechanisms operating within the phases. The effect is typified by the Fe-Ni-Cr alloys, in which the fcc γ and bcc δphases coexist at high temperatures. If the δ phase is taken as the reference matrix, then, as the proportion of the harder γ-phase is gradually increased, the ductility understandably decreases (Fig. VII.23). The effect is more marked, however, if the proportion of δ (which softens by dynamic recovery) is increased in a γ matrix (which softens by dynamic recrystallization). In this case the addition of a ductile phase to a less ductile one *decreases* the ductility ! A possible explanation of this phenomenon is that the presence of the second phase inhibits dynamic recrystallization in the γ by restricting grain boundary mobility. It is interesting to note that, despite the presence of a ductility minimum, the strength follows approximately the law of mixtures, with the alloy gradually softening as the volume of the softer phase is increased.

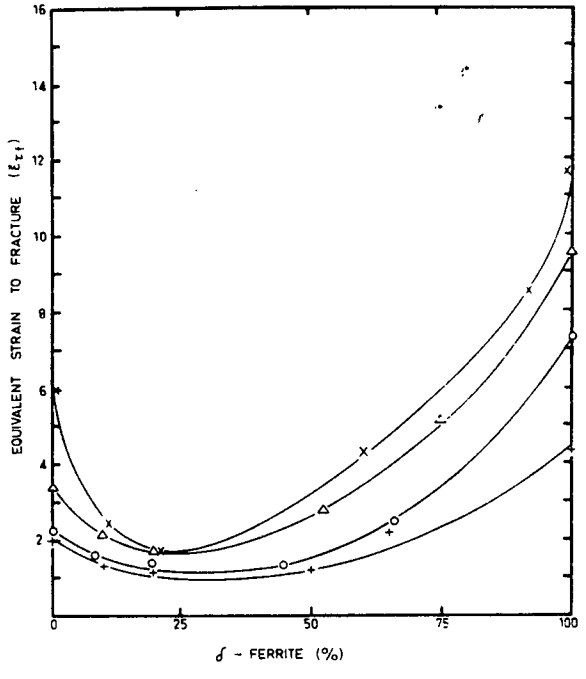

Fig. VII.23 – The effect on ductility of the relative volume fractions of bcc δ-ferrite (which undergoes dynamic recovery) and of fcc austenite (which softens by dynamic recrystallization). The torsion tests were conducted at a strain rate of 0.02 sec^{-1} (Müller, 1967). x, 1200°C; Δ, 1100°C; ○, 1000°C; +, 900°C.

Similarly, in Cu-Ni-Zn-Mn alloys at 800°C, the duplex alloy of 72 % bcc α-phase is more ductile than that of 71 % fcc α-phase (Ward and Helliwell, 1970). One can therefore conclude that the ductile bcc phases (which soften by dynamic recovery, and in which grain boundary migration is not essential) have their ductility reduced less than the harder fcc phases which soften by dynamic recrystallization. An exception to this generalization occurs when the two phases are uniformly distributed as fine grains of diameter 3 μ or less. In this case, the material becomes superplastic, but only at strain rates that span the division between creep and hot working, as discussed in more detail by T.H. Alden (1975).

In commercial alloys which contain inclusions, the fracture mechanism involves the linking up of voids nucleated at the inclusions. In such cases the ductility decreases with inclusion content, and this effect completely overshadows the alloying effects already described (Sellars and Tegart, 1972).

VII.3.10 – Effect of Prior Substructure on Subgrain Formation

In the previous sections, it was assumed that the starting material for a particular cycle of working was fully annealed. However, in many hot-working operations, such as rolling or forging, successive operations are performed on materials containing substructures inherited from previous cycles of deformation. The only common exceptions are extrusion and planetary hot rolling. It will therefore be of interest to consider the effect on the processes of dynamic recovery, and in particular on that of subgrain formation, of the presence of the substructures produced in earlier treatments.

This subject is, unfortunately, rather complex because of(1) the variety of substructures from which a given test may start, (2) differences in behavior associated with the relative strength of the initial substructure and the final equilibrium substructure at steady state, and (3) the diversity of experimental procedures employed in such tests. For simplicity, consideration will first be given to cases where deformation is initiated with a softer substructure than the stable one. In a later section, we will consider commencement with a stronger substructure. One phenomenon is common to the two types of experiment; the final equilibrium substructure is dependent only on the deformation conditions, regardless of the initial substructure, provided recrystallization or failure does not intervene (Bird *et al.*, 1969; Jonas and McQueen, 1973). However, when the starting structure is a denser one than the final equilibrium substructure, the probability of recrystallization intervening during deformation under given conditions is much greater than for a nondeformed starting material.

VII.3.10.1 – Initial Substructure Weaker Than the Stable Substructure

In this case, the starting material contains relatively large subgrains with low wall densities. As straining proceeds, the wall density increases and intermediate subboundaries begin to form. Since the final subgrains must be equiaxed and an integral number is unlikely to fit into an initial subgrain, considerable adjustment is required to reach

the final structure. In constant strain rate tests, the initial yield stress is higher than that of a recrystallized specimen, and in constant stress creep, the creep rate is initially less than that of recrystallized material. Considerable strain is required to produce the equilibrium substructure and the flow stress (or strain rate) may reach its steady state value before the gross features of the substructure do. The strain required for such evolution may be greater than that for recrystallized metal to attain steady state flow for the given conditions of deformation. The following results for α-iron may be taken as an example: when the strain rate is increased by a factor of 100, the initial flow stress is less than that of annealed material deformed to the same total strain entirely at the higher strain rate (Fig. VII.24). A strain of about 0.2 to 0.3 is required at the new strain rate for the flow stress and the substructure to reach their normal steady state values (Fig. VII. 25).

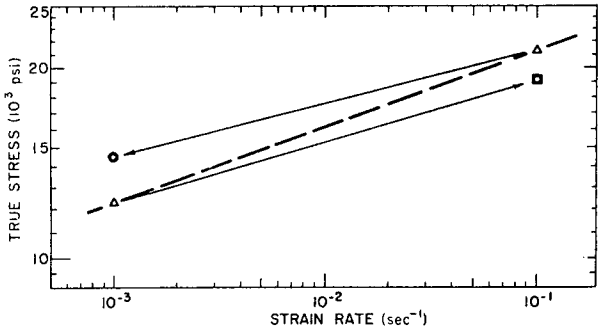

Fig. VII.24 -- Probable range of flow stresses developed in industrial processes in which marked strain rate variations occur. The broken line represents the steady state flow stresses measured in tests on Armco iron at 675°C (0.54 T_m). The upper arrow indicates the decrease in flow stress from 10^{-1} to 10^{-3} sec^{-1}. The lower arrow indicates the increase in flow stress when the strain rate is rapidly increased from 10^{-3} to 10^{-1} sec^{-1}. The final flow stress is less than that in a continuous test at the higher strain rate. The actual increase is only 63 %of the increase expected on the basis of continuous tests at constant strain rate (Immarigeon and Jonas 1971).

Changes of the above nature can arise in creep service when the stress is raised either as a singular event or as a cyclic variation. Rapid changes in temperature or strain rate are also used in experiments to determine the activation energy or activation volume at constant structure. In industrial hot working, inherited substructures can play a role in a variety of processing schedules, some examples of which will now be considered.

a) *Multipass Deformation at Constant Temperature and Strain Rate.* Here the metal is held at a constant temperature for some interval between passes in the same mill. During the interval, the metal can either be held in a furnace or can simply be cooling back to the temperature through the loss of heat of the previous partially adiabatic deformation. During the interval, the metal undergoes static recovery, so that its yield stress is lower than at the end of the previous pass. If the interval is not too long, there is little change in subgrain size, although the density of dislocations in the subboundaries has decreased. If the strain of a particular pass is insufficient for the attainment of steady state flow, then the cumulative strain of several passes may produce the equilibrium structure.

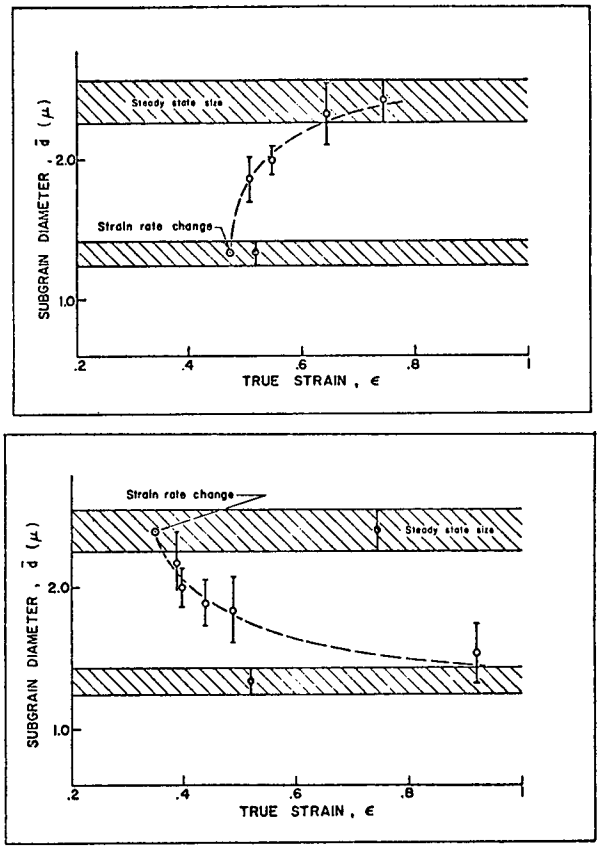

Fig. VII.25 -- Variation in subgrain size during transient deformation in Armco iron at 675°C (0.54 T_m). The substructural changes were initiated by a rapid change in strain rate at the strains indicated. Upper figure: strain rate decrease from 10^{-1} to 10^{-3} sec^{-1}. Lower figure: Strain rate increase from 10^{-3} to 10^{-1} sec^{-1}. It can be seen that the substructural modifications associated with hardening take place over greater strains than those associated with softening between the same limits (Immarigeon and Jonas, 1971).

b) *Interrupted Deformation at Falling Temperatures or Increasing Strain Rates.* Here the metal is cooler at each stage of deformation in either rolling or forging. Alternatively, each pass is at a higher strain rate, as in a continuous mill, where the sheet or shape is speeded up by the deformation it undergoes in each stand. In this case, neglecting the effect of static recovery, each cycle of deformation is performed on metal with a softer (more highly recovered) substructure than would normally develop under the conditions of that working operation. If the strain in each pass is less than the strain required to transform the initial structure into the steady state one, the final flow stress in that pass may be considerably less than that of initially recrystallized metal (Vaughan, 1968). In aluminum, for example, a controlled series of 14 deformations was carried out, each of $\epsilon = 0.8$, separated by 30 sec intervals, with temperatures decreasing from 600 to 400°C (Farag *et al.*, 1968). This treatment resulted in a final flow stress that was 25 % lower than that pertaining to metal deformed continuously at 400 °C. Increasing the number of stages and reducing the strain per pass had little effect. However, doubling the time interval, which allowed more static recovery to take place, gave a final flow stress only 15 % less than that for isothermal deformation at 400°C. A similar but simpler schedule is shown in Fig. VII.26.

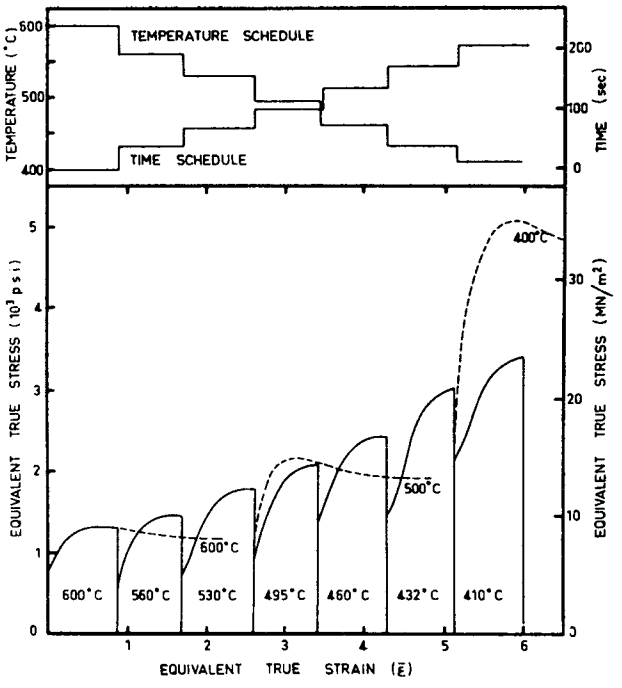

Fig. VII.26 - The upper portion of the diagram shows the temperature-time schedule of a series of torsion tests on superpurity aluminum conducted at a strain rate of 2.3 sec^{-1}. On the temperature curve, a horizontal segment indicates the temperature of a stage of deformation and a vertical segment the cooling between stages. On the time graph, an almost horizontal segment indicates the short time elapsed during a stage of deformation, and a vertical segment indicates the delay between stages. In the lower graph, the solid lines indicate the flow stresses recorded, whereas the broken lines are for continuous isothermal tests at the temperatures noted. The slight decrease in steady state flow stress results from adiabatic heating (Farag *et al.*, 1968).

c) *Continuous Deformation at Continuously Falling Temperatures or Rising Strain Rates.* This case arises in certain forming operations, such as extrusion or rolling, in which the strain rate rises rapidly as the metal passes into and partially through the deformation zone, and then rapidly falls to zero as the metal moves out of the zone (Jonas and McQueen, 1973). In forging, the strain rates vary in a more complex manner as the hammer is decelerated and as different portions of the billet come into contact with the die. Although the temperature can increase due to adiabatic heating, in many forming operations it decreases as heat is lost to the tooling and to the atmosphere. When the temperature is continuously dropping or the strain rate rising, the flow curve is lower than that calculated from isothermal isostrain rate data (Fig. VII.27). This is because, at each strain, the metal contains a softer substructure, inherited from the prior strain increment, than the stable one pertaining to the current temperature and strain rate. For example, in iron (Fig. VII.28), deformation under continuous cooling required a stress up to 30 % less than that expected from isothermal testing. Similarly, a 50 % upset at a constant velocity, which involves a doubling of the true strain rate, required an average flow stress 6 % lower than that for

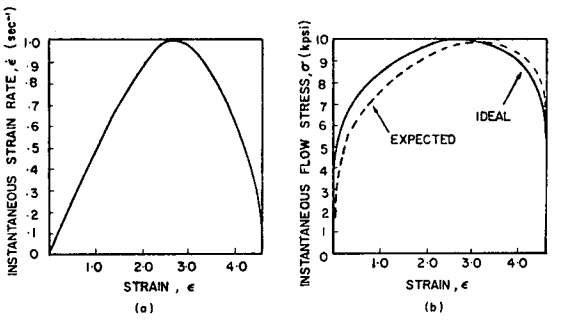

Fig. VII.27 – (a) Strain rate profile as a function of strain for a 100: 1 extrusion die and a ram speed of 6 x 10^{-3} in/sec. (b) Flow stress profiles for material flowing through the strain rate profile of (a). The full line is the ideal profile based on constant strain rate steady state data for α-Zr at 850°C. The broken line is the expected profile after the deformation history is taken into account. The area under the broken curve is the actual work done and is greater or less than the ideal area depending on whether the peak strain rate is attained early or late along the profile (Jonas and McQueen, 1973).

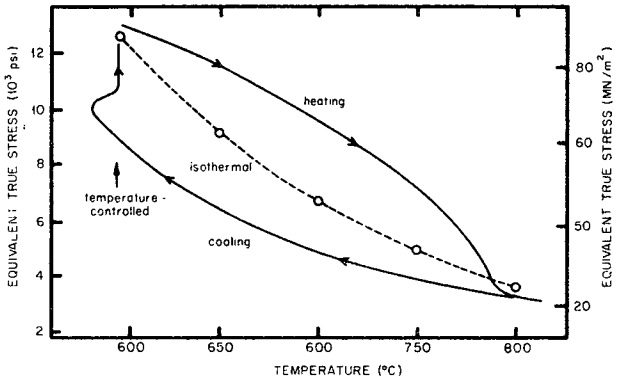

Fig. VII.28 - The flow stresses measured during continuous heating or continuous cooling are compared to the flow stresses measured in a series of isothermal tests. The material was vacuum melted bcc iron, the strain rate in the torsion tests was 1.5 x 10^{-3} sec^{-1}, and the rate of heating or cooling was about 50 ° C/sec. (Glover, 1969).

reduction at the mean of the true strain rate* (Loizou and Sims, 1953).

VII.3.10.2 – Initial Structure Stronger Than Stable Substructure

In this case, the initial structure has a finer cell size with more tangled boundaries than the equilibrium substructure. Thus as deformation progresses, the dislocation density diminishes, some subboundaries disappear, and equiaxed subgrains of the stable size and wall density form. During the transition, there is an increase in creep rate in a constant stress test and a decrease in flow stress in a constant strain rate test. The latter is often referred to as work softening. Substructural softening in α-iron has

---

* When the strain rate during a hot-working operation varies by a substantial factor, the appropriate mean strain rate to use for flow stress correlations is $[\bar{\dot{\varepsilon}}^m]^{1/m}$, where m is the rate sensitivity of the flow stress (Jonas and Chandra, 1971).

been observed to require a greater strain, 0.45 compared to 0.25, than the substructural hardening described earlier (Fig. VII-25).

Industrially, the conversion of fine to coarser substructures occurs when multipass deformations are carried out at increasing temperatures or decreasing strain rates. This situation can arise when, with rapid forming, adiabatic deformation heats up the metal. This gives rise to higher flow curves if the strains applied are small (less than 30 %), so that the stable configuration is not reached. Such a result is in opposition to the lower flow curves observed when the initial structure is softer than the stable one. When straining is continuous, with increasing temperature or decreasing strain rate, an augmented flow stress is again observed, which is in contrast to the effect of continuously dropping the temperature or increasing the strain rate (Fig. VII.27). Since most forming processes have a strain-time profile with a rising rate followed by a falling rate, such operations can be expected to lead to finer substructures than indicated by the final strain rate. Similar effects arise when adiabatic heating raises the finishing temperature above the entrance temperature.

The introduction of a fine substructure has been tried as a means of increasing creep resistance. Cold work, while giving a great initial improvement, almost always results in dynamic or static recrystallization, with a resulting diminution of creep resistance. Success has been attained by using substructures produced by static recovery after cold straining to the order of 10 %, or by prior creep at a higher stress. Such treatments are mainly of scientific interest since they are difficult to carry out industrially and do not offer as much benefit as raising the creep resistance through alloying. A more practical alternative is the production of a suitable substructure by hot working and, when possible, its stabilization by precipitation. This method, which will be described later, is a means of further increasing the rupture life of creep-resistant alloys.

Stress Recovery. When a cold-worked metal is an annealed under stress, the rate of recovery increases considerably, and recrystallization can be delayed or even prevented (Auld *et al.*, 1957; Thornton and Cahn, 1961). This can arise in industrial processes such as continuous annealing, in which the traveling strip is under tension because of its weight and for purposes of materials handling. The application of external stress, which produces a form of creep, assists the dislocations to move through the crystal and increases the opportunity for annihilation to occur. It is most effective in metals such as aluminum which normally recover, but has been observed to occur in copper as well.

VII.3.11 – High Temperature Dynamic Recovery and Stage III Deformation

Before concluding this section, we consider it advisable to distinguish between the sense of dynamic recovery as we have discussed it above and the more common meaning of the term associated with ambient temperature deformation. The latter is concerned with the declining rate of strain hardening in the stage III deformation of fcc single crystals at homologous temperatures below one-half. In both cases, the softening process involves the rearrangement of dislocations in the course of deformation. Furthermore, in both types, the facility of different metals for recovery increases with their stacking fault energy. On the other hand, true steady state flow, with an equilibrium substructure of constant dislocation density, does not occur in stage III deformation. Instead, although the cell size usually remains constant, the wall dislocation density increases, leading to an increase in flow stress (Kuhlmann-Wilsdorf, 1966). The reason for this difference stems from the limitation of the stage III recovery mechanisms to cross-slip. By contrast, at elevated temperatures, other mechanisms are activated, such as dislocation climb and node unpinning. As a result of the availability of these additional processes at high temperatures, the accumulation of dislocations to the high concentrations associated with cold working does not occur. The dislocation density levels out instead at much reduced values, leading to the relatively low flow stresses normally associated with high temperature deformation.

As the temperature of working is raised, stage III dynamic recovery merges into the type of dynamic recovery found in hot working. Concurrently, at a given strain, the subgrain size and perfection gradually increase and the flow stress decreases. This continuous decline in flow stress and increase in ductility is employed in the warm working of steels at temperatures between 100°C and the lower end of the hot-working range. In this range, the surface does not become oxidized, and lubricated polished dies can be used (Reynolds and Tegart, 1962; Keegan, 1967).

VII.4 – Dynamic Recrystallization

VII.4.1 – The Flow Curve

The flow curve under conditions of dynamic recovery has already been described. In that case, all the softening processes involved single dislocations, which are annihilated in individual events. We now turn to the contrasting situation where dislocations are annihilated in large numbers through the migration of a high angle boundary. By this means, the lattice in which they reside is destroyed and replaced by a new and substantially perfect one in one integral operation.

The occurrence of dynamic recrystallization modifies the appearance of the flow curves produced at constant strain rate so that they no longer have the simple shape shown in Fig. VII.5 above. At high strain rates in the hot-working range, the flow stress rises to a maximum at the peak strain e_p. Thereupon, as a result of dynamic recrystallization, it diminishes to a value intermediate between the yield stress and the maximum or peak stress (Fig. VII.29a). At lower strain rates in the hot-working range, the softening produced by dynamic recrystallization is followed by renewed hardening and a cyclic flow curve of approximately constant period but declining amplitude is traced out instead (Fig. VII.29a) (Sellars and Tegart, 1966a). The effect of decreasing the strain rate on the shape of torsional flow curves is shown in more detail in Fig. VII.30a. Here it can be seen that, at strain rates of more than 10^{-1} sec^{-1} in γ-iron, softening by recrys-

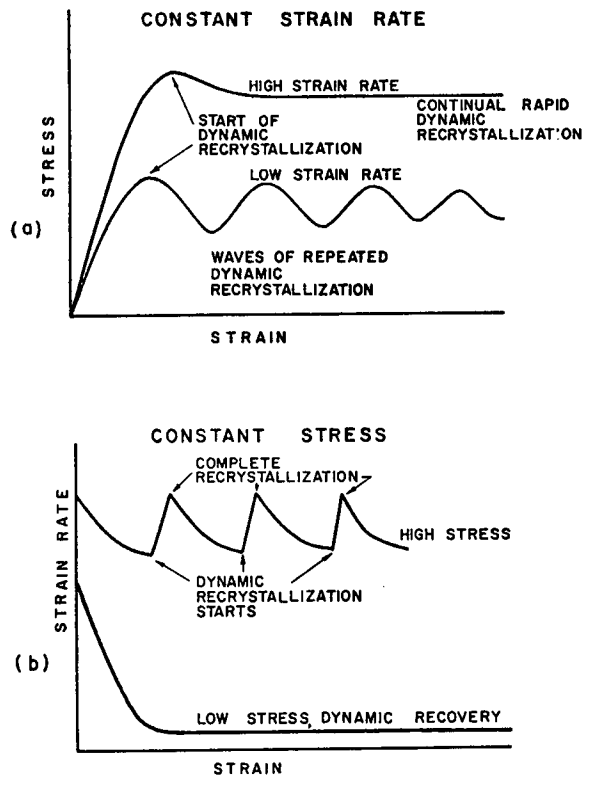

Fig. VII.29 – Dynamic recrystallization during creep and hot working is common in metals such as lead and copper in which the rate of dynamic recovery is limited. (a) Hot working at a slow rate leads to a cyclic stress-strain curve caused by waves of recrystallization. At high strain rates, recrystallization starts at higher strains, causing the drop in stress after the peak. However, before recrystallization is complete, the oldest of the new grains deform enough to start recrystallizing again. In this way, new nuclei are continually forming throughout the material. Since these nuclei are soft, they keep the average flow stress low. Up to the peak, softening occurs by means of dynamic recovery processes. Nevertheless, after the initiation of dynamic recrystallization, dynamic recovery continues to take place in each new grain until it once again recrystallizes. (b) At low creep stresses, the amount of dynamic recovery is sufficient to keep the dislocation density below critical levels. At high stresses, the substructure becomes so dense that recrystallization nuclei form and grow rapidly to engulf the whole specimen. The specimen then begins to creep at high rates as it did initially.

tallization, once initiated, is continuous. By contrast when strain rates of less than 10^{-1} sec^{-1} are used, the softening is periodic, with intervening cycles of hardening.

In a constant stress or creep test, the advent of dynamic recrystallization appears as a rapid increase in strain rate, which terminates the otherwise normal stage of primary creep, usually before steady state deformation has been attained (Fig. VII.29b). After the acceleration, a new stage of primary creep commences, which is also likely to terminate in dynamic recrystallization. This phenomenological cycle may be repeated several times (Fig. VII.30b). In general, it occurs only at high stresses in the creep range, when these are present at temperatures above 0.7 T_m (Richardson *et al.*, 1966).

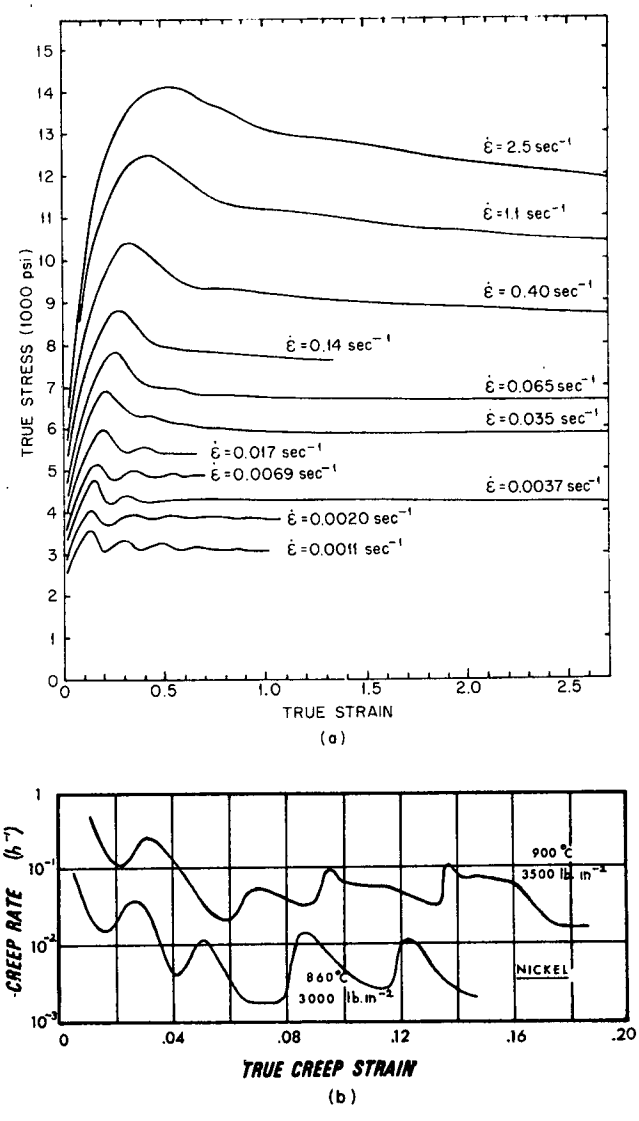

Fig. VII.30 – (a) Flow curves of a plain 0.25% C steel in the austenitic state (fcc) at 1100° C (0.76 T_m), illustrating the strong influence of strain rate. At the higher strain rates, they exhibit the typical shape for dynamic recrystallization: strain hardening to a peak stress followed by work softening to a steady state level. The work softening is caused by the start of dynamic recrystallization and the stable flow results from continuous dynamic recrystallization. At low strain rates, the flow curve is periodic due to recurrent cycles of recrystallization (Rossard, 1960). (b) Creep curves for nickel under constant stress in compression at 860° C(0.65 T_m) and 900°C (0.72 T_m). The sudden increases in strain rate mark the initiation of cycles of dynamic recrystallization (Hardwick *et al.*, 1961).

VII.4.2 – Microstructural Changes Associated with Dynamic Recrystallisation

In the metals which undergo dynamic recrystallization, a dislocation substructure develops in the initial stage of deformation which is rather poorly recovered; i.e. the cells have relatively smaller size and more tangled walls compared to the metals described previously, which undergo a high degree of recovery. At lower strain rates, the evidence indicates that nucleation occurs by bulging

of an existing grain boundary (Luton and Sellars, 1969). Although scalloped boundaries are also observed in the high dynamic recovery metals, nucleation does not occur. The structural features peculiar to low recovery metals that account for the nucleation of dynamic recrystallization are: (1) the greater effectiveness with which a grain boundary is pinned by the highly tangled cell walls, and (2) the greater difference in strain energy between the region within the bulge and that in front of it. It should be noted that dynamic recrystallization has also been observed in lead single crystals undergoing creep, specimens to which the grain boundary bulge mechanism of nucleation clearly does not apply (Hirst, 1940). In this case, the nuclei were observed to form in slip bands, presumably by a nucleation mechanism similar to that described below for high strain rates.

At high strain rates, on the other hand, a fine tangled cellular structure is developed throughout all the grains, which does not leave grain boundary segments long enough to bulge. There is evidence that, with increasing strain, some tangles build up to high misorientations, giving rise to nuclei throughout each grain (McQueen and Bergerson, 1972). The density of nuclei is probably higher near grain boundaries because the strain is higher there as a result of accommodation to plastic anisotropy. By the time steady state flow is attained, new small equiaxed grains have replaced the original grains (Fig. VII.31). Throughout the steady state region, the grains remain constant in size and equiaxed in shape (Rossard, 1960).

Since straining of the material continues during nucleation and growth, the new grains are deformed as they grow. When the strain rate is low, the gradient of strain energy from the center of the recrystallized grain to the rapidly advancing boundary is low, and the region behind the boundary is relatively free of dislocations. As a result, the driving force due to the difference in dislocation density on opposite sides of the boundary, and hence the rate of migration, is not reduced appreciably by the continuing deformation. In this way, recrystallization proceeds to completion, with the center of each grain in a deformed state, so that the material is not as soft as statically recrystallized metal of the same grain size. Once recrystallization is complete, the dislocation density builds up again, raising the flow stress (or decreasing the strain rate in creep) until recrystallization is again nucleated.

In the case of high strain rate deformation, the gradient of deformation from center to boundary of a recrystallized grain is high, and so there is a considerable dislocation density just behind the advancing boundary. By diminishing the driving force, the rate of migration is reduced relative to that in static recrystallization. Before recrystallization is complete, the dislocation densities at the centers of the recrystallizing grains have increased sufficiently that another cycle of nucleation occurs and new grains begin to grow again (Fig. VII.32a). Thus, at any instant, there is a distribution of regions with different degrees of deformation, from zero to a value just higher than the peak strain (Fig. VII 32b and c). It is this distribution of dislocation substructures which maintains the average flow stress at a value intermediate between the yield stress of statically annealed material and the peak stress.

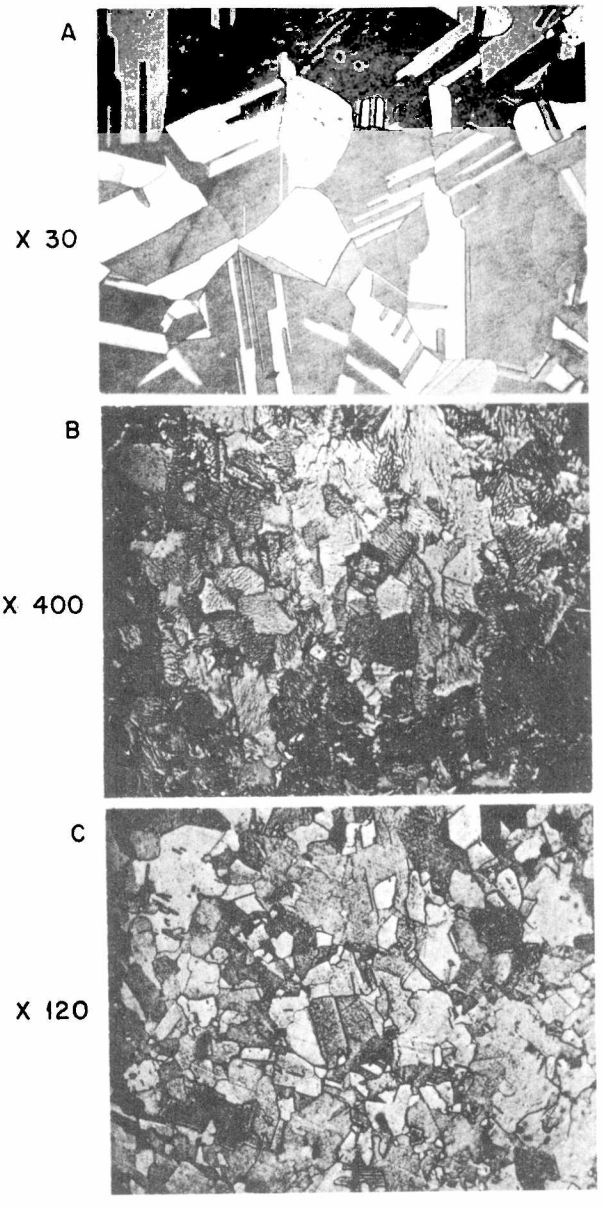

Fig. VII.31 – Micrographs of selected copper torsion specimens: (a) The initial large grains. x 30. (b) The very small dynamically recrystallized grains present after deformation into the steady state flow region at 800°C (0.8 T_m) and 5.6 sec^{-1}, rapidly quenched. x 400. (c) The small statically recrystallized grains in metal deformed as in (b) but cooled less rapidly, x 120 (McQueen and Bergerson, 1972).

VII.4.3 – Critical Strains for Nucleation and Completion of Recrystallization

As already illustrated above, the start of recrystallization is quite marked on stress–strain curves, as it is on strain rate–time curves. The critical strain ϵ_c for the start of recrystallization is actually slightly less than the peak strain ϵ_p because, while the first nuclei are softening the material locally, the remaining material continues to get stronger. The difference between the two strains is even greater at higher strain rates. According to Rossard (1973), who has

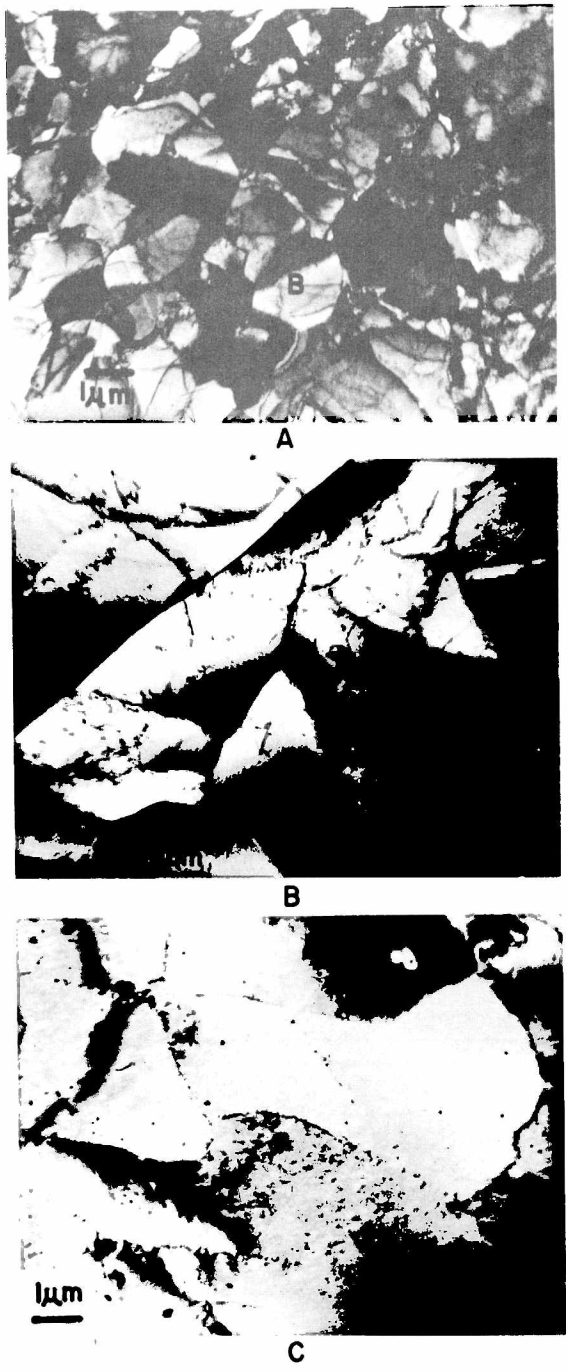

Fig. VII.32 – Substructures in specimens of copper that have dynamically recrystallized during high temperature deformation to a strain of about 30: (a) Two recrystallization nuclei A and B, surrounded by a heavily deformed region, 800°C (0.8 T_m), 11.6 sec^{-1}. (b) Region of high dislocation density. (c) Region of low dislocation density in material deformed at 950°C (0.9 T_m) and 3.7 sec^{-1}. x 5000 (McQueen and Bergerson, 1972).

carried out extensive studies of this phenomenon, ϵ_c is given by the approximate relation:

$$\epsilon_c \simeq 5\,\epsilon_p/6 \simeq 0.83\,\epsilon_p \qquad (13)$$

It should be noted that the critical strain for dynamic recrystallization may not in fact be attained for a variety of reasons. For example, the material could continue to strain harden, developing higher and higher flow stresses, until failure occurs. In such an instance it can be concluded that true hot-working conditions do not apply. If, on the other hand, the operation of dynamic recovery processes alone leads to a high enough dislocation annihilation rate, the nucleation of recrystallization can be avoided entirely. This is the description that applies to bcc iron at low temperatures and high strain rates (Glover and Sellars, 1973), to aluminum over the entire hot-working range, and to most alloys in creep service.

By means of metallographic examination, it has been established that the progress of recrystallization follows the normal S-curve of volume recrystallized-versus-log time which, in constant strain rate tests, is the same as volume recrystallized-versus-log strain. For explaining some features of dynamic recrystallization, ϵ_x has been defined as the strain from the point of nucleation to that where the volume percent of material recrystallized is x. For convenience, the strain for "complete" recrystallization, ϵ_r, has been defined as the strain for 95% recrystallization.

VII.4.4 – Effect of Strain Rate and Temperature on ϵ_c and ϵ_r

In general, the critical strain ϵ_c for recrystallization increases with increasing strain rate and decreasing temperature (Luton and Sellars, 1969). [This does not, however, apply at very low strain rates, where the critical strain seems to increase with decreasing strain rate (Fig. VII.33)].

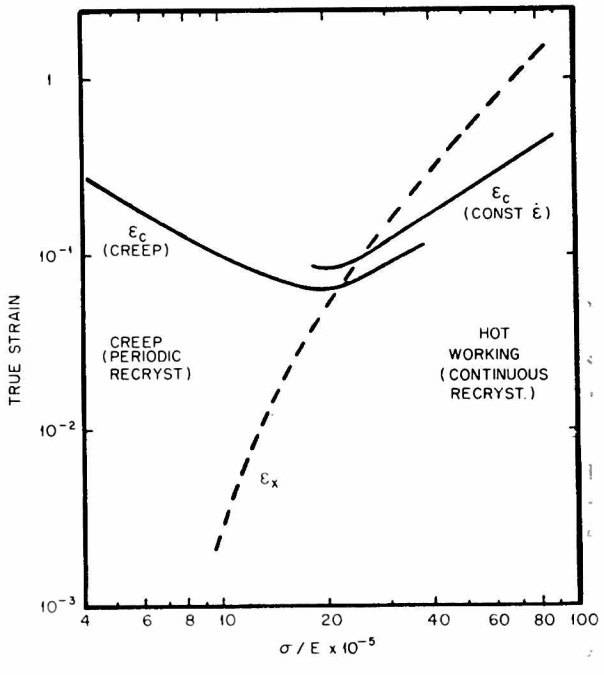

Fig. VII.33 – Stress dependence of ϵ_c, the critical strain for the onset of recrystallization, and of ϵ_x, the strain occurring during the time for a large fraction of the volume to recrystallize. The strain scale is that for pure Ni at 935°C (0.7 T_m). At low stresses, where ϵ_c is greater than ϵ_x, the flow curve is periodic. However, at high stresses, where ϵ_c is less than ϵ_x, dynamic recrystallization is continuous (Sellars, 1971).

The increase in ϵ_c with temperature-corrected strain rate Z (Fig. VII.34a) signifies that, at higher Z, the subboundary density is higher before recrystallization is nucleated. The increase in ϵ_c with decrease in temperature is attributable to the decreased rate of recovery, and therefore of nucleation, at lower temperatures. When the strain rate is increased at constant temperature, there is actually a decrease in the time required for recrystallization to begin, although the decrease is insufficient to offset the increase in strain rate, leading to the net increase in critical strain (Sah *et al.*, 1969).

The strain for completion of recrystallization ϵ_r also increases with temperature-corrected strain rate Z for reasons similar to those described for ϵ_c above (Fig. VII.34b). In addition, there is a reduction in driving force with increased strain rate resulting from deformation behind the advancing boundary. This reduction is more marked at higher strain rates than at low, so that the rate of increase of ϵ_r with strain rate is much greater than that of ϵ_c.

Periodic and Continuous Recrystallization

In the first detailed paper on dynamic recrystallization, Luton and Sellars (1969) showed that the different dependences of ϵ_c and ϵ_r on strain rate and temperature described above lead to the periodic cycles of recrystallization at low

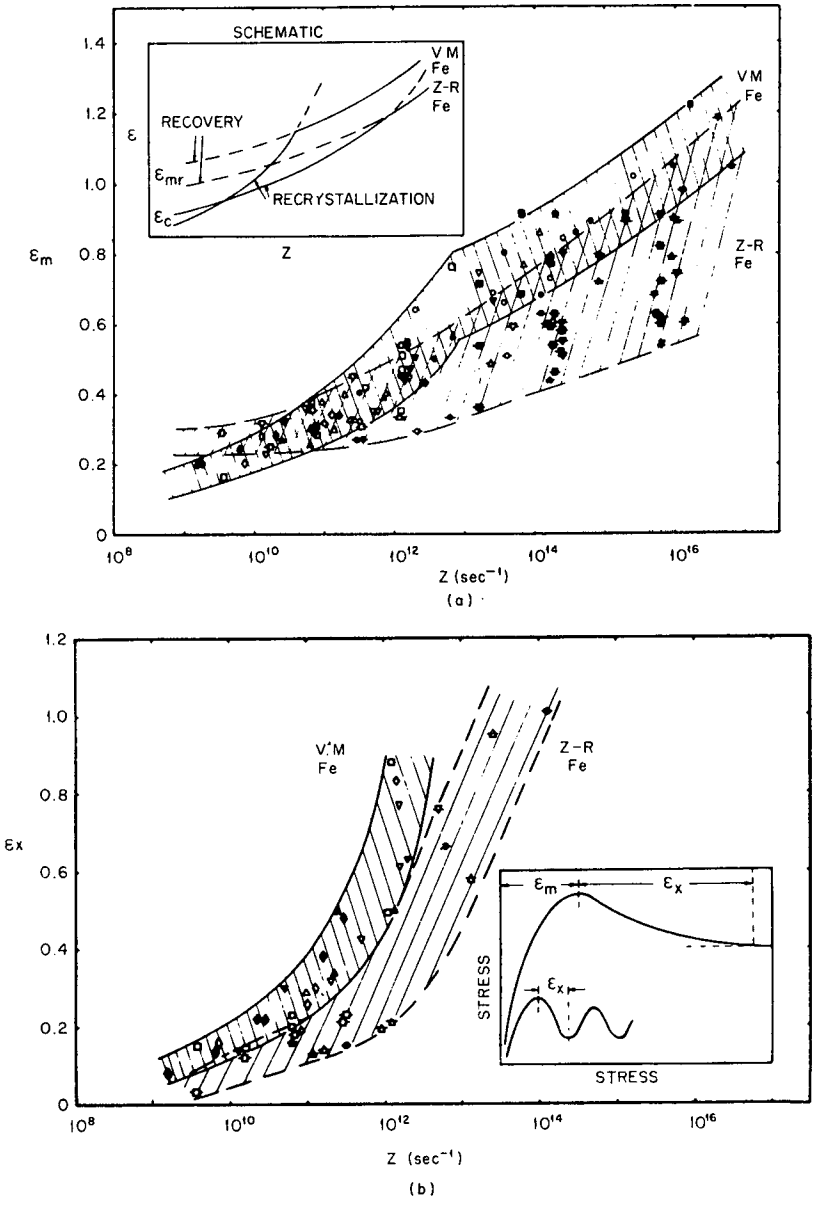

Fig. VII.34 - (a) Dependence on Z of ϵ_m, the strain to the initial peak in flow stress or to the onset of steady state flow when no initial peak is observed. The insert shows a schematic interpretation of the data in terms of ϵ_{mr}, the strain to the onset of steady state flow if recovery is the only softening process, and of ϵ_c, the critical strain for the onset of dynamic recrystallization. It is seen that dynamic recrystallization is favored by low Z, i.e. low $\dot{\epsilon}$ and high T. The materials here and in (b) are vacuum melted and zone refined iron for which Q is 281 kJ/mol. (b) Dependence on Z of the strain ϵ_x for the completion of recrystallization. The manner of measuring ϵ_x is indicated in the insert (Glover and Sellars, 1973).

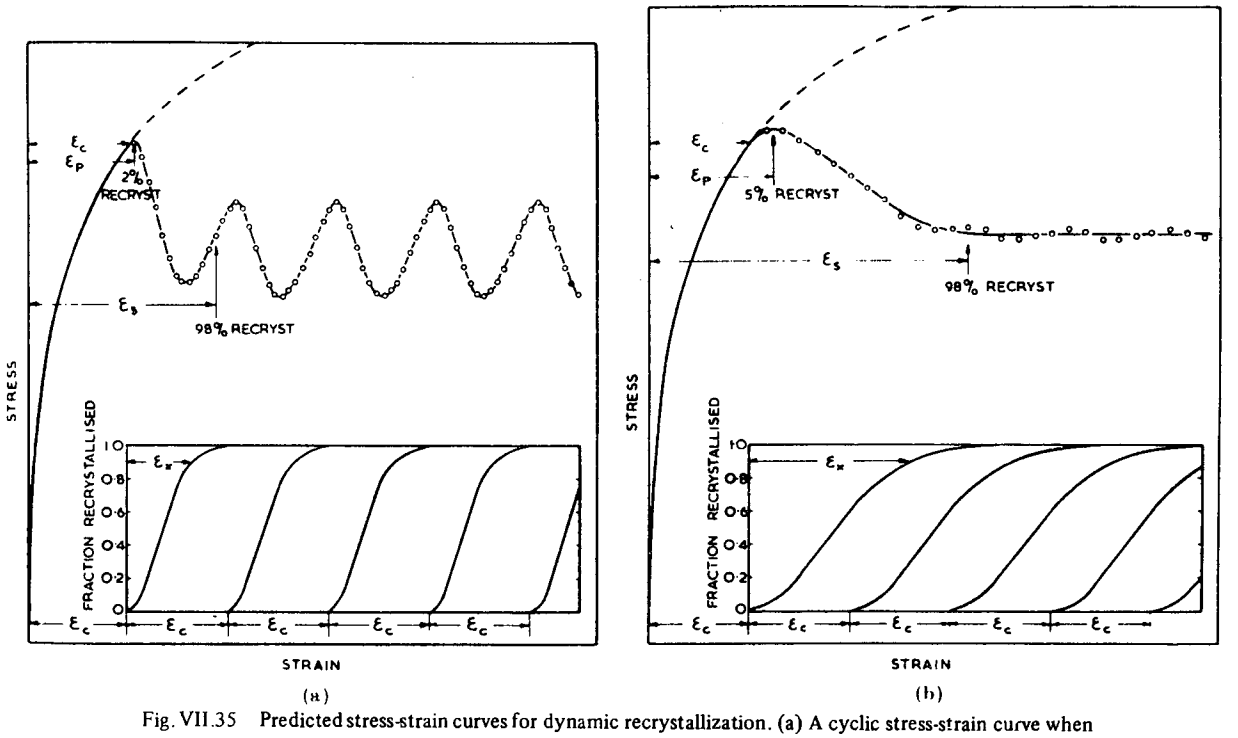

Fig. VII.35 Predicted stress-strain curves for dynamic recrystallization. (a) A cyclic stress-strain curve when the critical strain to initiate recrystallization $\epsilon_c > \epsilon_x$, the strain occurring in the time for a large fraction of recrystallization. (b) A steady state curve for the condition when $\epsilon_c < \epsilon_x$. The strain for completion of the first cycle ϵ_s equals the sum, $\epsilon_c + \epsilon_x$ (Luton and Sellars, 1969).

strain rates, and to the overlapping and continuous cycles of recrystallization at high strain rates illustrated in Figs. VII.29a and VII.30a.

The periodicity arises because, at low strain rates, ϵ_r is much less than ϵ_c (Fig. VII.35). Thus, once recrystallization starts, it is completed long before the regions which first recrystallized can work harden and nucleate a second time. At high strain rates, ϵ_r is much greater than ϵ_c, so that before recrystallization is complete, the regions which first recrystallized reach the critical strain for a second nucleation (Fig. VII.35). In this way, more than one cycle of recrystallization may be taking place in the metal at the same time, each cycle of which is at a different stage of the recrystallization process. The result is an equilibrium distribution of regions having different strains between zero and ϵ_c, giving rise to a constant average flow stress.

The size of the dynamically recrystallized grains decreases as the temperature-corrected strain rate Z increases, because the associated increase in subgrain density gives rise to a higher density of nuclei (Fig. VII.36). There are also more cycles of recrystallization present simultaneously at higher values of Z. It follows from this that there is also a relationship of grain size to steady state flow stress which will be presented in the next section.

VII.4.5 – Relationship of Flow Stress to Structure

The grain structure of dynamically recrystallized material affects the high temperature flow stress in two distinct ways. In the first place, the *volume fraction* that has recently recrystallized determines the degree to which the flow stress approaches that of statically recrystallized material on the one hand or that of fully work-hardened

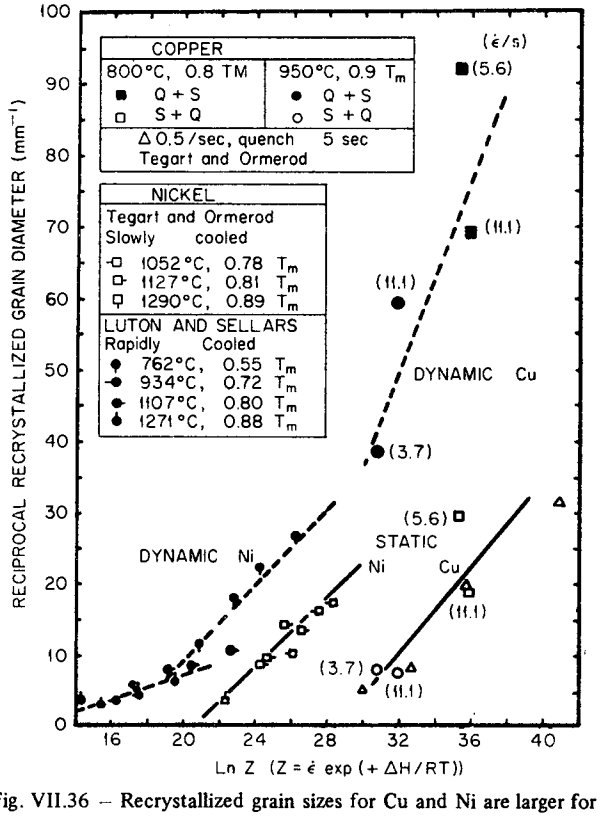

Fig. VII.36 – Recrystallized grain sizes for Cu and Ni are larger for higher temperatures and lower rates of deformation (McQueen and Bergerson, 1972; W.J. McG. Tegart and H. Ormerod, unpublished work, University of Sheffield, England, 1971; Luton and Sellars, 1969). The statically recrystallized grains, which form during cooling, are larger than the dynamically recrystallized grains, even though cooling occurs within seconds. In the calculation of Z, the values of activation energy Q used for Cu and Ni were 302 and 234 kJ/mole.

material on the other. Secondly, the grain *size* itself can influence the high temperature flow stress when the grain boundaries act so as to impede the propagation of slip throughout the material.

The relationship between volume fraction recrystallized per increment of strain and the flow stress was first analyzed in detail by Luton and Sellars (1969). They showed that the volume recrystallized during each strain increment after the critical can be calculated from a knowledge of ϵ_c and ϵ_r (Fig. VII.35). Thus at any strain, the distribution of progressively deformed volumes and hence of progressively increased strengths can be summed to give the average flow stress. This assumes of course that all regions are undergoing the same strain, which is not unreasonable since they are quite small and are uniformly dispersed.

By this technique of calculation, it is possible to simulate, for low strain rates, cyclic stress–strain curves with the correct period, amplitude, and shape. At high strain rates, by taking into consideration the presence of more than one cycle of recrystallization, it is possible to derive a stress–strain curve with the same work-softening characteristics and approximately the same steady state flow stress as observed experimentally. Furthermore, according to the analysis, the calculated curves change from the cyclic to the steady state shape as ϵ_r becomes greater than ϵ_c at approximately the value of Z at which the experimental curves change character (Sah *et al.*, 1969; Glover and Sellars, 1973).

It should be noted that the steady state flow stress which results from dynamic recrystallization is considerably less than that which would result if only dynamic recovery operated in these metals. This reduction in flow stress can only be exploited industrially if the strain exceeds the peak strain for the conditions of deformation in effect; this can be fairly high at industrial forming rates. Nevertheless, dynamic recrystallization generally takes place in the low recovery metals, as long as the deformation is continuous, as in extrusion, or if it accumulates, as in a hot strip mill when there is no static recrystallization between stands.

With regard to the effect of grain size on the high temperature flow stress, the situation is not quite as clear. As was stated earlier, the dynamically recrystallized grain size does not vary with strain during steady state deformation. Under most conditions, a relationship between steady state flow stress σ_s and grain size d_g of the following form is observed (Fig. VII.37).

$$\sigma_s = M d_g^{-q} \qquad (14)$$

Here M is an empirical constant and q has been observed to be 0.71 in zone refined α-iron (Glover and Sellars, 1973), 0.75 in Ni and Ni-Fe alloys (Luton and Sellars, 1969), and 0.75, 1.0, and 1.0 in Cu-Al alloys, Cu, and Ni, respectively (Tegart, 1968).

Despite the form of Eq. (14), however, the flow stress σ_s is unlikely to be causally related to the grain size d_g; rather d_g is probably linked to the magnitude of the induced stress σ_s. This arises because the subgrain size d formed by the dynamic recovery processes that are taking place (see Sections VII.3.3 and VII.3.5) is causally related to the strain rate and temperature, and therefore to the flow stress σ_s and the amount of work hardening σ_i by Eqs. (8) and (9):

$$\sigma_s = K_1 d^{-1} \qquad (8)$$

$$\sigma_i = K_2 d^{2} \qquad (9)$$

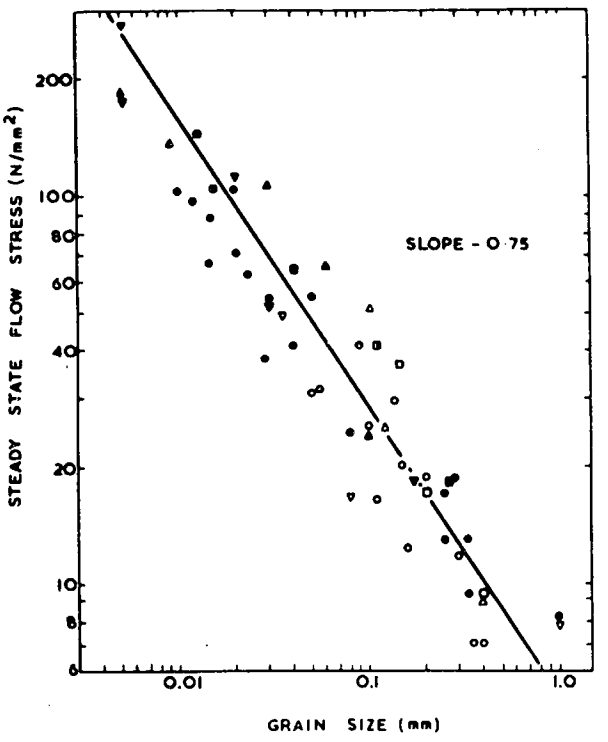

Fig. VII-37 Correlation between the steady state flow stress and the recrystallized grain size for the copper-aluminum alloys of Fig.VII.40. The data for all alloys fall on the same curve. This indicates that the pure metal and the alloy have the same grain size when the steady state flow stresses are the same; for the latter to be in effect, the alloys must be deformed at a higher temperature or a lower strain rate. In a similar way, when the pure metal and the alloy are deformed at the same temperature and rate, the alloy has a higher stress and a finer grain size (Bromley and Sellars, 1973).

Now the dynamically recrystallized grain size will in general be related to the nucleus density and therefore to the volume density of subgrains present within the material. Under these conditions, the recrystallized grain size d_g is approximately proportional to the subgrain size d (Luton and Sellars, 1969), so that σ_s can be correlated with d_g as well as with d; i.e

$$\sigma_s \simeq K_3 d_g^{-1} \qquad (15)$$

$$\sigma_i \simeq K_4 d_g^{-1} \qquad (16)$$

It should be noted that Eqs.(15) and (16) are *correlations* rather than causal relationships in view of the additional hardening contributions of both the subboundaries and the dislocations contained within the subgrains. This point can be seen more clearly if the steady state flow stress is written as

$$\sigma_s = \sigma^* + \alpha\mu b\sqrt{\rho_s} + K_2 d^{-1} + K_5 d_g^{-1/2} \qquad (17)$$

Here σ^* is the effective stress, Eqs.(4) and (6), the term $\alpha\mu b\sqrt{\rho_s}$ represents the hardening contribution of the dislocations, Eq.(12), $K_2 d^{-1}$ that of the subboundaries, Eq.(9), and $K_5 d_g^{-1/2}$ the Hall-Petch strengthening contri-

bution of the grain boundaries*. Bearing in mind that $\sqrt{\rho_s} \propto 1/d$ (Section VII.3.5), we can write

$$\sigma_s = \sigma^* + K_6 d^{-1} + K_5 d_g^{-1/2} \qquad (18)$$

and, given the dependence referred to above that $d_g \propto d$, σ_s is given by

$$\sigma_s \simeq \sigma^* + K_7 d_g^{-1} + K_5 d_g^{-1/2} \qquad (19)$$

The experimental values of q in Eq. (14), which are closer to 1 than to 1/2, thus indicate that the component of substructure strengthening ($K_7 d_g^{-1}$) is generally greater than the Hall-Petch contribution of the grain boundaries ($K_5 d_g^{-1/2}$), and that Eq. (14) is therefore more likely to reflect the link between flow stress and nucleus density than that between grain size and resistance to flow.

VII.4.6 – Characteristics of Different Metals and Alloys

The metals which exhibit dynamic recrystallization are generally those that undergo a relatively low degree of dynamic recovery during high temperature deformation. This is because separation of the partial dislocations make climb, crossglide, and node detachment difficult. The low rate of dynamic recovery gives rise in turn to a dense dislocation substructure which promotes nucleation. This effect is found in fcc metals of low and moderate stacking fault energy, notably nickel (Shapiro and Dieter, 1971), cobalt (Jacquerie and Habraken, 1968), copper, and austenitic Fe (Keane *et al.*, 1968).

The capacity for dynamic recrystallization also depends on the ease of migration of the grain boundaries, which increases as the purity of the metal is improved. Thus dynamic recrystallization has been observed in vacuum melted and zone refined α-iron, but not in iron of standard purity or in steels (Glover and Sellars, 1973). Even in the former materials, dynamic recrystallization occurs only when the temperature-corrected strain rate remains below a certain value, which is higher for the more purified metal.

Effect of Alloying.

In solid solution alloys, the addition of solute tends to diminish the ability of the metal to recover, thus increasing the tendency to dynamic recrystallization; however, the solute may also hinder the migration of boundaries, slowing the rate of dynamic recrystallization. Some typical flow curves in copper alloys, which soften by dynamic recrystallization, are shown in Fig. VII.39. It can be seen that the rate of work hardening diminishes with strain, through the operation of dynamic recovery processes, until strains of 0.15 to 0.20 are reached. In relatively pure

* The validity of the Hall-Petch relation at high temperatures has not been conclusively established. However, aside from the fine grain sizes associated with superplastic behavior and with the appreciable weakening attributable to grain boundary sliding, there is clear evidence that, for grain sizes above about 20 μ, the high temperature yield strength increases with decreasing grain size (Fink *et al.*, 1955; P.J. Wray, private communication, 1974). Although the exact form of the dependence was not determined in these investigations, in copper at 600°C, the strengthening component has been reported to follow the Hall-Petch relation (Fig. 38), and this is the view that is adopted here.

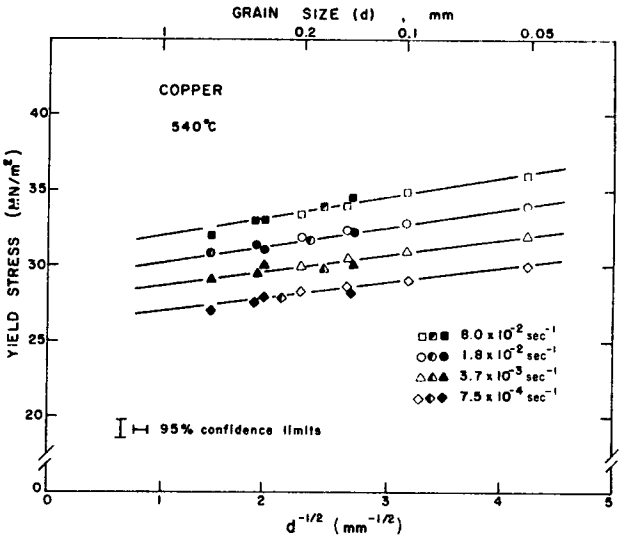

Fig. VII.38 – Effect of grain size on the high temperature yield stress of tough pitch copper. Testing was done in compression and the different grain sizes were produced by prestraining to a constant strain of 0.4 at various strain rates and temperatures. The yield stress can be seen to be rate sensitive; the slopes of the fitted lines increase perceptibly with strain rate, indicating a slight dependence of the Hall-Petch boundary strength coefficient on strain rate (Petkovic, 1975).

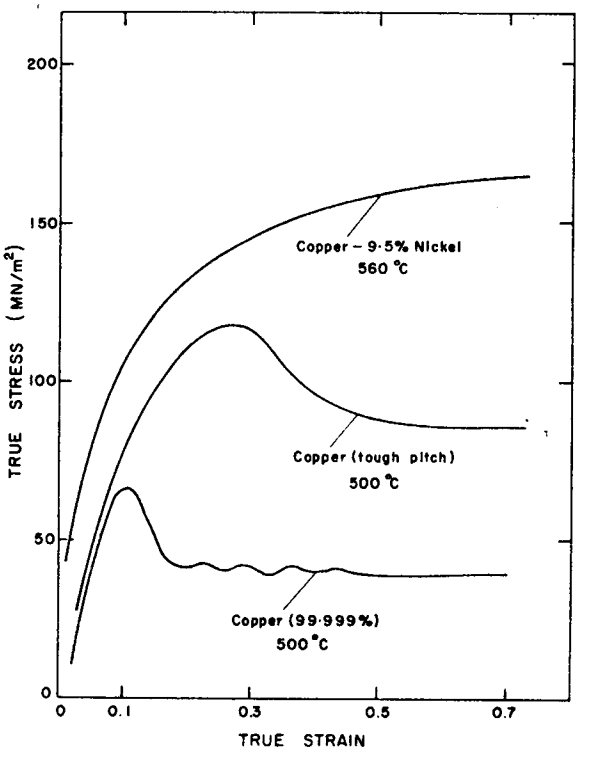

Fig. VII.39 – Compression flow curves in three cuprous materials. Strain rate 1.8×10^{-2} sec^{-1}. In pure copper at 500°C, dynamic recrystallization begins after a strain of about 0.1 and is complete in strains of about 0.05 or less. In tough pitch copper (0.05% O), the peak strain doubles to about 0.2 and the recrystallization strain increases even more sharply to about 0.3. This can be attributed to the effect of a dispersion of Cu_2O particles. In the Cu-Ni alloy, the net rate of work hardening is increased appreciably by the addition of Ni, and the critical strain for recrystallization is greater than the strain limit imposed by the testing method (Petkovic, 1975).

copper, when recrystallization is initiated, the flow stress drops rapidly and then levels out after a further strain of about 0.05. In copper containing 0.05 % oxygen, numerous particles of Cu_2O are present, which impede the motion of grain boundaries, with the result that the softening associated with dynamic recrystallization is retarded, and an increased strain of 0.3 is required to attain stable flow. An even greater difference can be discerned in the flow curve for the Cu-Ni alloy. Here the addition of 9.5 % Ni has considerably diminished the rate of dynamic recovery, and the rate of work hardening is higher than in the other two materials. The addition of Ni has also affected the processes of nucleus formation and of grain boundary migration so that, by the time the end of the test and a strain of 0.7 have been attained, softening by dynamic recrystallization has still not become fully developed.

Dynamic recrystallization has been observed in brass (Sunter and Burman, 1972), monel (Rhines and Wray, 1961), nickel-base superalloys (Fulop and McQueen, 1972), and austenites of plain carbon, low alloy, stainless, and tool steels (Rossard, 1960). In these metals, the general effect of alloying is an augmentation of strength and a retardation of dynamic recrystallization so that, at temperatures low in the hot-working range, it does not occur, giving rise to a severe ductility minimum. On the other hand, in alloys of copper in which the aluminum content varies between 1 and 8 %, there is little reduction in ductility in the range 0.55-0.9 T_m. While the steady state flow stress does increase with aluminum content up to 4 % Al, it is almost unchanged if the concentration is increased further to 8 % Al (Fig. VII.40). In these alloys,

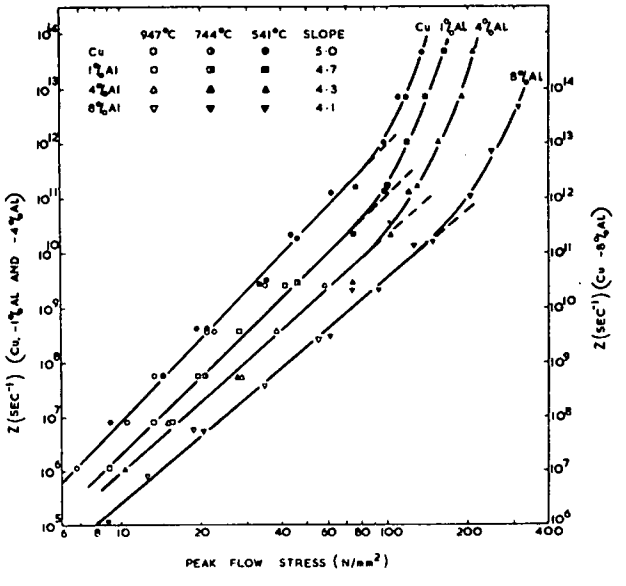

Fig. VII.40 – The peak stress in Cu alloys increases with increase in strain rate and decrease in temperature. The peak stress also increases with the concentration of aluminum, which is known to lower the stacking fault energy at room temperature. However, the peak stresses for the 4 % and 8 % Al alloys are almost the same (note difference in vertical scales). The same activation energy (Q = 200 kJ/mole) was used for all the alloys (Bromley and Sellars, 1973).

the presence of solute appears to have little effect on the relationship between the high temperature flow stress and the dynamically recrystallized grain size (Fig. VII.37). However, information is lacking in regard to differences in substructure in the pure metal and the alloy at the same grain size.

In Ni-Fe alloys, as the iron concentration is increased to 20 %, the stresses at the peak and in the steady state region gradually increase (Fig. VII-41). Although the

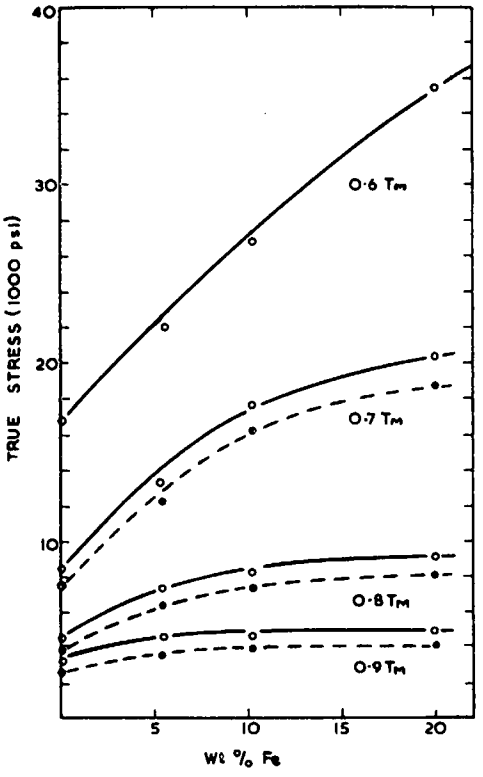

Fig. VII.41 – The influence of the addition of Fe to Ni on the peak flow stress (open points) and steady state flow stress (filled points) at constant strain rate, $\dot{\epsilon} = 7.7 \times 10^{-2}$ sec^{-1} (Luton and Sellars, 1969).

absolute magnitude of the solute strengthening component decreases with increasing temperature, the degree of strengthening relative to unalloyed material remains approximately constant. The activation energy of deformation increases with iron content from 234 kJ/mole for pure Ni to 298 for 5 % Fe, 330 for 10 % Fe, and 393 for 20 % Fe. In Eq. (14), the constant M decreases from 1.45 to 0.82 ksi/$mm^{3/4}$ for 20 % Fe, indicating that, for a given flow stress, the grain size of the alloy is lower as the Fe concentration in increased, because the dissolved iron increases the probability of nucleation and decreases the rate of boundary migration. The lack of increase in flow stress with decrease in grain size supports the view described earlier that the internal stress component of the flow stress is associated mainly with the dislocation substructure.

In Fe-C alloys, an increase in carbon concentration and associated alloying elements raises the activation energy from 322 to 460 kJ/mole (Rossard, 1960). The flow stress, however, can increase or decrease somewhat with the concentration of additional elements, perhaps for reasons similar to those mentioned above (Section VII.3.7) with respect to the effect of silicon addition to α-iron. The flow stress for Fe–18 % Cr–8 % Ni has been reported to be 50 % higher than for a plain carbon steel and again the activation energy is higher in the alloyed material

(450 kJ/mole). The addition of Cr, Mo, or W increases the flow stress still further (Gueussier and Castro, 1958).

The presence of dispersed second phase particles tends to stabilize the substructure and prevent or restrain grain boundary migration. Such inhibition or retardation of dynamic recrystallization has been observed in austenite containing NbC (Le Bon *et al.*, 1973) and in Udimet 700 with γ' precipitate (Oblak and Owczarski, 1972). The coalescence of second phases during high temperature deformation has already been described in Section VII.3.8 above ; at present there is insufficient evidence to say whether or not dynamic recrystallization occurs in alloys which exhibit this behavior and in which the matrix recovers poorly.

VII.4.7 – Dynamic Recrystallization and Ductility

In constant strain rate tests, the metals which undergo limited dynamic recovery have a minimum in ductility in a temperature zone near the lower limit of the hot-working range. This effect has been observed principally in nickel and its alloys (Figs. VII.42 and VII.43). The cause of the phenomenon has been clarified from an examination of the mode of fracture.

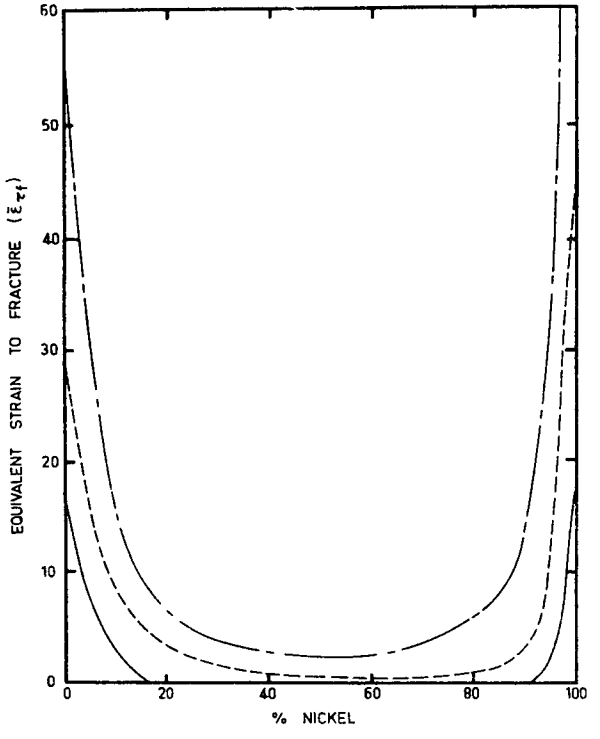

Fig. VII.42 – The effect of solid solution alloying on the ductility of copper-nickel alloys. It can be seen that increasing the temperature greatly improves the ductility in dilute alloys, but only marginally improves the concentrated alloys, in which dynamic recrystallization does not take place before fracture (Sellars and Tegart, 1966b). —, 0,6 T_m ; - - - . 0.7 T_m ; - · -, 0.8 T_m.

At temperatures below the decline, the fracture mode is similar to that at room temperature and the ductility is somewhat higher. As the test temperature is increased to that of the minimum, more and more grain boundary cracking is observed and the fracture becomes entirely inter-

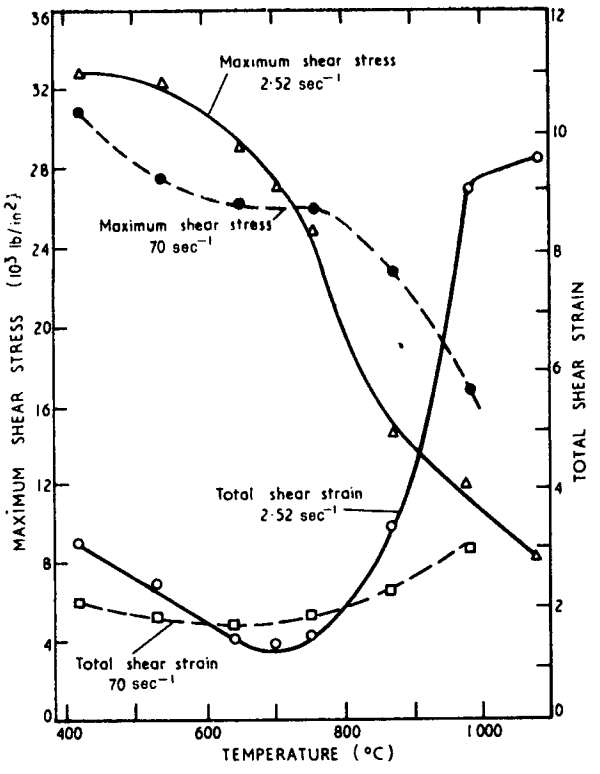

Fig. VII.43 – The effect of temperature and strain rate on the ductility and peak stress for Inconel 600. The minimum in ductility results from the widespread occurrence of grain boundary cracking; the rapid rise in ductility at higher temperatures for a strain rate of 2.52 sec^{-1} is the result of dynamic recrystallization. At a strain rate of 70 sec^{-1}, dynamic recrystallization is delayed to greater critical strains and thus does not have an opportunity to improve the ductility in the temperature range of the tests (Dieter *et al.*, 1968).

crystalline (White and Rossard, 1968). This arises because metals which undergo little dynamic recovery have high yield stresses and high work-hardening rates. The resultant high flow stresses at finite strains prevent the accommodation, by lattice deformation, of the stress concentrations developed at triple points by grain boundary sliding. As the temperature is increased beyond that of the minimum, more and more dynamic recrystallization is observed (Bailey, 1969). The introduction of new grains isolates the cracks already formed from the grain boundaries, thus inhibiting their propagation (Fig. VII.44). Thus, in hot working, the initiation of dynamic recrystallization leads to a considerable increase in ductility. It is also valuable to point out that in multipass operations, static recrystallization between passes has a similar effect in increasing ductility (White and Rossard, 1968).

As the strain rate is increased, the minimum in ductility tends to move to higher deformation temperatures (Rhines and Wray, 1961). However, the increase in strain rate also reduces the fraction of the strain attributable to grain boundary sliding relative to the overall lattice strain, so that the minimum becomes less noticeable (Fig. VII.43).

The metals which exhibit a ductility minimum in hot working usually exhibit severe grain boundary cracking in creep. Dynamic recrystallization, if it occurred, would increase their ductility, but the improvement would not be as great as at hot-working strain rates. In part this is because, at creep strain rates, where dynamic recrystal-

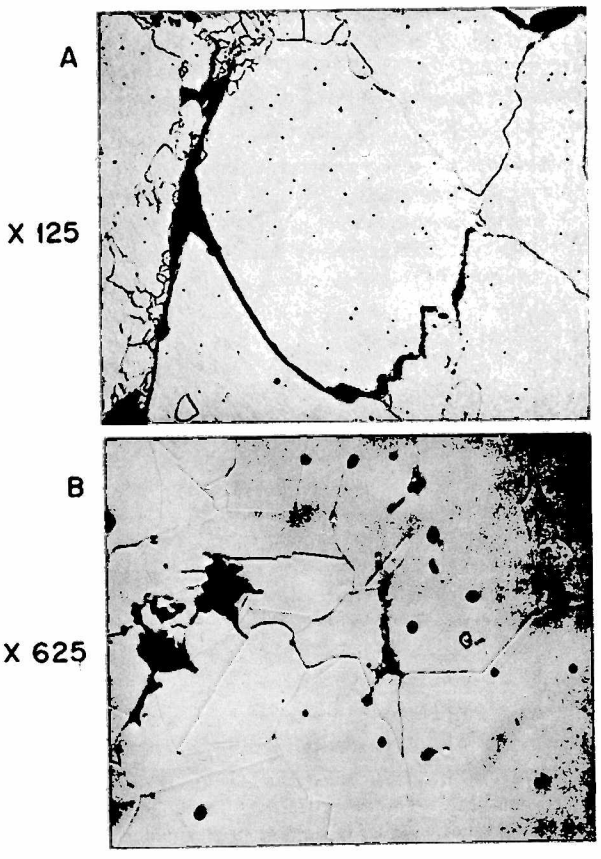

Fig. VII.44 – Grain boundary cracking in Ni-5 % Fe deformed at a strain rate of 2×10^{-3} sec^{-1}. (a) At 760°C (0.6 T_m), which is near the ductility minimum, the cracks have propagated extensively by the time a strain of 0.35 is reached. x 125. (b) At 934°C (0.7 T_m), dynamic recrystallization (as evidenced by the finer grain size) has prevented propagation even at a strain of 1.6 x 625 (Luton and Tegart, 1969).

lization tends to occur in distinct cycles, there is considerable opportunity for the cracks to grow in the part of the cycle in which recrystallization is not taking place. To some extent, the improvement in ductility that can be brought about by the operation of dynamic recrystallization is only of academic interest in creep service because the desirable increase in ductility would be outweighed by the undesirable increase in the average creep rate.

VII.4.8 – Effect of Interruption or of Continuous Variation in the Conditions of Deformation

As discussed in Section VII.3.10, many industrial operations consists of a series of passes with intervening delays. Furthermore, in the course of any single forming operation, there is usually a continuous change in strain rate and temperature (Figs. VII.26, VII.27, and VII.28). While Section VII.3.10 dealt with the structures produced by prior dynamic or static recovery, this section will discuss the effect arising from prior dynamic or static recrystallization. To be of interest, the latter must not be complete, for it is only in the partially recrystallized condition that the effect of further deformation differs from that described so far in this section. A more complete description of static recovery and recrystallization following dynamic recrystallization will be presented in Section VII.5.

Since a dynamically recrystallizing material contains a substructure, interruption of a test or operation generally leads to partial static recrystallization. On interruption, the most severely strained regions recrystallize first, so that the flow stress in a subsequent limited strain cycle is less than for steady state flow (Bromley and Sellars, 1973). As some worked grains are retained, which recrystallize with little strain upon resumption of deformation, the strain to the peak stress, as well as the height of the peak, is reduced. If complete recrystallization takes place during an interruption, then the flow curve in the next strain cycle resembles that of the previous cycle.

In tests at continuously increasing strain rates or decreasing temperatures, the flow stress is lower than that observed in isothermal, isostrain-rate tests. This is similar to the situation described earlier under conditions of dynamic recovery, and for essentially the same reasons. The dynamically recrystallizing material contains a substructure characteristic of the temperature and strain rate of deformation. If the former is augmented and the latter reduced, further deformation is imposed on an inherited substructure which is softer than the equilibrium structure for the new conditions of deformation (Fig. VII.45).

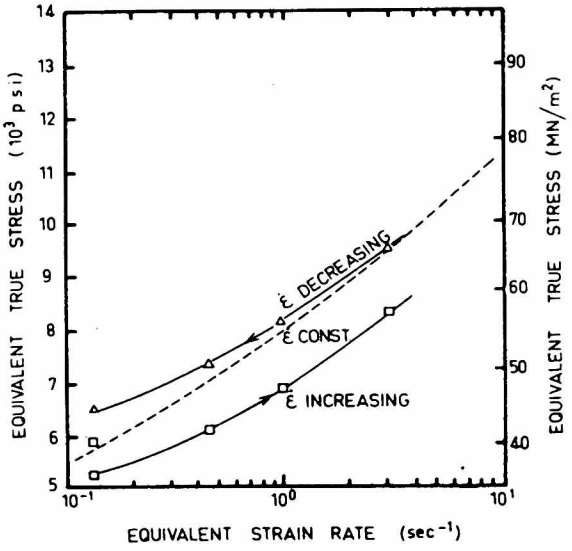

Fig. VII.45 – The flow stresses measured during two series of deformations, one with decreasing strain rate and the other with increasing strain rate, are compared to the flow stresses measured in individual isostrain rate tests. The points plotted represent the flow stress attained after a strain of 0.9 in each stage. Since the specimens were maintained at 750°C throughout all experiments, the delays of 10 sec between stages permitted some static recovery and recrystallization to occur. The flow stress upon inheritance of a softer microstructure is less than the normal steady state stress, which in turn is less than that upon inheritance of a stronger structure (Bromley, 1969).

VII.5 – Static Recovery and Recrystallization after Hot Working

VII.5.1 – Static Recovery

In Sections VII.3 and VII.4 above, we were primarily concerned with the softening processes occurring *during*

high temperature deformation, i.e. with dynamic recovery and recrystallization. We turn our attention now to the static softening processes, i.e. those taking place *after*

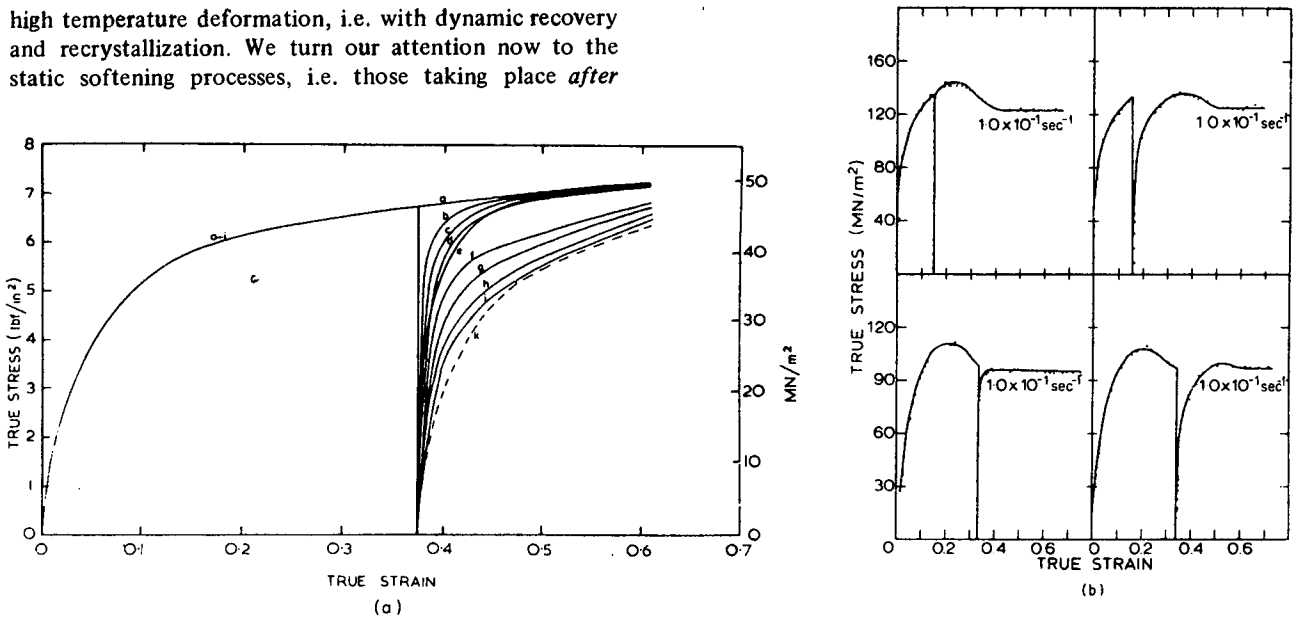

Fig. VII-46 – Interrupted stress-strain curves for a material undergoing (a) dynamic recovery and (b) dynamic recrystallization. (a) Commercial purity aluminum tested at 410°C (0.74 T_m) and 2.7 sec^{-1}. The delay time on interruption ranged from 1.8 to 4100 sec. For comparison, the broken curve k is a trace of the initial loading curve (Evans and Dunstan, 1971). Curve and delay time (sec): b, 1.8; c, 2.5; d, 3.95; e, 8.5; f, 405; g, 490; h. 1314; i, 4100. a, Single deformation test; k, initial portion of curve a. (b) The upper curves, which are for a 0.42 % C steel, have an interruption strain of 0.14 in the dynamic recovery region. Both tests were conducted at 870°C (0.65 T_m) and the delay time was 0.5 sec for the left-hand curve and 17 sec for the right-hand curve. The lower curves, for a 0.68 % C steel deformed at 915°C (0.78 T_m), were strained to 0.33 in the dynamic recrystallization region. The test on the left was for a delay time of 0.5 sec, and that on the right for a delay time of 10.5 sec. All samples were austenitized at 960°C (Djaic and Jonas, 1972).

deformation is complete or between intervals of hot working. As before, these processes can be conveniently divided into two distinct categories: (a) the recovery processes, which involve the annihilation of dislocations in individual events, and (b) the recrystallization processes, in which dislocations are simultaneously eliminated in large numbers as a result of the motion of high angle boundaries. Each of these topics can be further subdivided according to whether the prior dynamic softening occurred solely by recovery or whether dynamic recrystallization was involved as well. This further distinction is particularly relevant to our discussion of recrystallization below, which will therefore be separated into two parts.

VII.5.1.1 – The Critical Strain For Static Recrystallization

The critical strain for static recrystallization is generally of the order of 10 %. If the critical strain is exceeded, an incubation period must elapse before recrystallization proceeds. The length of this incubation period depends on temperature and on the amount and nature of the prior strain, as will be described in more detail below. Of interest in the present context is that, if the critical strain is exceeded, softening by static recovery can only take place during the incubation period prior to recrystallization. Furthermore, if the critical strain for recrystallization is not reached, the recovery process does not lead to full softening, but saturates at a softening level well below 100 %; i.e. *full softening cannot be produced by recovery processes alone.*

The existence of a critical strain for full softening, and of a saturation limit to the effect of recovery, are readily revealed by the technique of interrupted compression testing. According to this method, individual samples are deformed at a constant strain rate, and then, at a selected strain, they are unloaded and held for increasing delay times before they are reloaded at the original strain rate. Examples of such interrupted tests are given in Fig. VII.46. In this type of work, the fractional softening that takes place can be evaluated in terms of the quotient:

$$\frac{\text{flow stress on interruption} - \text{reloading yield stress}}{\text{flow stress on interruption} - \text{original yield stress}}$$

Four such tests, executed on samples of low carbon steel, are shown in Fig. VII.47. Here it can be seen that at 746°C, which is in the $\alpha + \gamma$ region, strains of 2.5 % and 9 % do not lead to recrystallization within 10^4 sec (Fig. VII.47b). When accumulated strains of 15 % (10 % + 5 %) and 30 % (15 % + 15 %) are imposed at a temperature of 677°C, on the other hand, recrystallization begins in less than 100 sec and is virtually complete at the end of the test (Fig. VII.47a).

The existence of a critical strain is shown more clearly in Fig. VII.48. In these experiments, conducted on a 0.68 % C plain carbon steel, a prestrain of 5.5 % (curve a) was followed by a recovery cycle lasting some 100 sec. As softening did not go to completion, it can be concluded that the critical strain exceeded 5.5 %. From curve *b* it can be seen that, after an interruption strain of 9.8 %, softening by recovery was complete after about 100 sec ; after a further delay of about 6000 sec, recrystallization began and proceeded to completion in a further 10^6 sec. The critical strain for this material, at 780° C, is thus between 5.5 and 9.8 %.

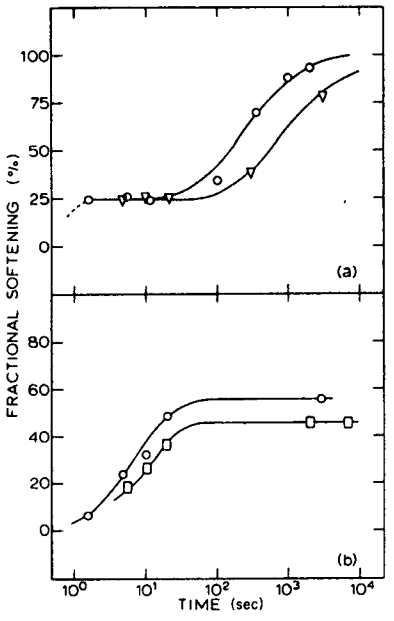

Fig. VII-47 – Effect of temperature and interruption strain on the rate of softening of a 0.14 %C steel. Tests in (a) were conducted at 677°C (0.54 T_m) on α-phase material. ○, ϵ = 0.15 + 0.15, $\dot{\epsilon}$ = 0.1 sec^{-1} ; ▽ , ϵ = 0.10 + 0.05, $\dot{\epsilon}$ = 0.05 sec^{-1}. (b) Tests were conducted at 746°C (0.57 T_m) on a mixture of α + γ phases. □, ϵ = 0.025, $\dot{\epsilon}$ = 0.03 sec^{-1}; ○, ϵ = 0.09, $\dot{\epsilon}$ = 0.075 sec^{-1}. The upper curves exhibit recrystallization after an incubation period, whereas the lower curves are for strains which have not exceeded the critical (Djaic and Jonas, 1972).

The softening curves of Fig. VII.48 reveal that, for the particular steel chosen, the maximum relative softening that can be produced by static recovery alone is about 40 %. This compares with softening levels of about 40 %, 50 %, and 50 % produced by recovery alone in aluminum (Evans and Dunstan, 1971), tough pitch copper (Petkovic, 1975), and in niobium-modified steels (Petkovic *et al.*, 1975).

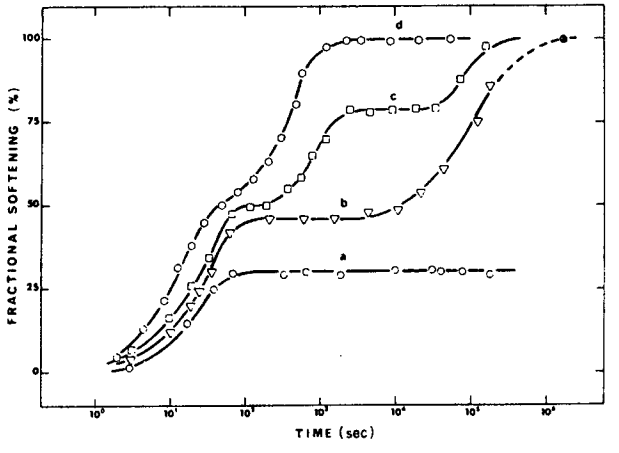

Fig. VII.48 – Effect of strain on the static softening of a 0.68 % C steel at 780°C (0.58 T_m). $\dot{\epsilon}$ = 1.3 x 10^{-3} sec^{-1}. The following interruption strains were used. Curve a, 0.055; curve b, 0.098; curve c, 0.24; curve d, 0.41. The final point in curve b was obtained by heating the sample to 915°C during the interruption. The first plateau in each curve indicates the completion of static recovery. The second plateau in c indicates the termination of metadynamic recrystallization (Djaic and Jonas, 1973).

VII.5.1.2 – The Effect of Temperature. Strain Rate, and Strain on the Rate of Recovery.

The main experimental variables affecting the recovery rate are the temperature, strain, strain rate, and composition. The influence of temperature is illustrated in Fig. VII.49a for a medium-carbon steel. The recovery

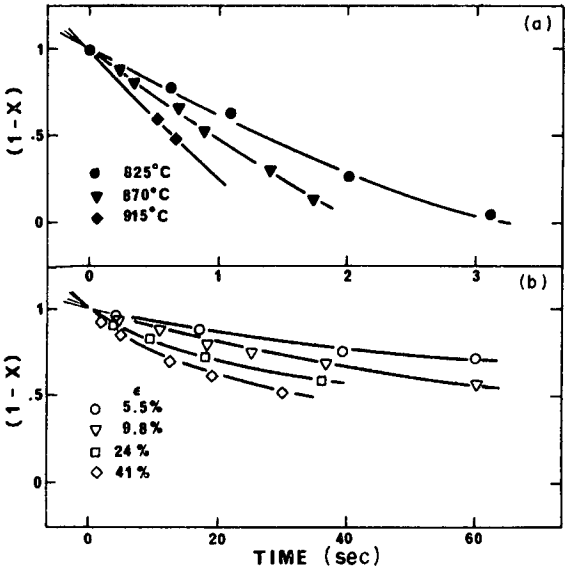

Fig. VII.49 – (a) Effect of temperature (0.61 – 0.67 T_m) on the rate of static recovery in a 0.42 % C plain carbon steel. The results were obtained by interrupted compression testing after an interruption strain of 0.14, $\dot{\epsilon}$ = 1 x 10^{-1} sec^{-1}. X represents the fractional softening, i.e. relative reduction in yield stress with time, and 1 – X is the residual strain hardening. (b) Effect of interruption strain on the rate of static recovery in a 0.68 % C plain carbon steel at 780°C (0.58 T_m). $\dot{\epsilon}$ = 1.3 x 10^{-3} sec^{-1}. The increases in softening rate at strains of 0.24 and 0.41 include a component of concurrent softening by metadynamic recrystallization (Petkovic *et al.*, 1975).

curves all represent softening cycles occurring after a prestrain of 14 % ; i.e. following interruption strains below the critical. The effect of temperature on the recovery rate is evident, but is not particularly marked, in part because the amount of stored energy driving the recovery process decreases as the deformation temperature is increased. It is less than the effect of temperature on the recrystallization rate, as will be shown in more detail below. It is also apparent that the rate of recovery decreases with time, indicating that the stored energy or driving force is progressively reduced by the operation of the recovery process. Because the driving force for recovery is generally different at different deformation temperatures, it is difficult to determine the activation energy associated with static recovery after high temperature deformation.

In general, increases in strain lead to increases in the recovery rate until steady state flow is achieved. This can be attributed to the attendant increase in dislocation density, and therefore driving force, with strain until equilibrium is reached. The effect upon the recovery rate of increasing the driving force is shown in Fig. VII 49b. These curves were constructed from the recovery or initial restoration portions of the softening curves of Fig. VII.48. It can be seen that the recovery rate increases continuously

with the amount of interruption strain, up to a prestrain of 41 %. These prestrains were selected to be : curve a) below the critical strain ; curve b) above the critical strain for static recrystallization, but below that for dynamic recrystallization ; curve c) just beyond the peak of the flow curve, and therefore just beyond the critical strain for dynamic recrystallization ; curve d) close to the steady state region, i.e. that of continuous dynamic recrystallization. It appears that when a strain cycle is interrupted in the dynamic recrystallization range, the grain boundaries continue to move. i.e. recrystallization continues, without requiring an incubation period. This special kind of softening has been termed metadynamic or post-dynamic recrystallization (Djaic and Jonas, 1972, 1973) and will be discussed again later. For the moment, it is sufficient to note that part of the increase in apparent recovery rate from curve *c* to curve *d* can be attributed to the simultaneous occurrence of metadynamic recrystallization.

A further effect of driving force is shown in Fig. VII.50a. Here two different strain rates, differing by an

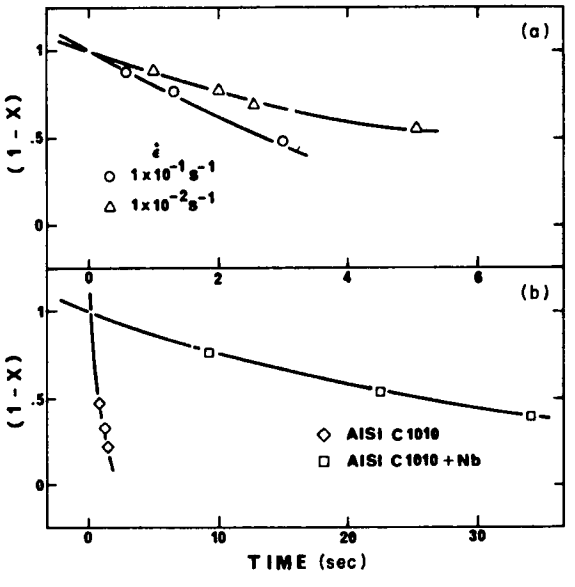

Fig. VII-50 - (a) Effect of strain rate on the rate of static recovery in a 0.42 % C plain carbon steel at 825°C (0.61 T_m), ϵ = 14 %. The increased rate of recovery that follows the higher testing strain rate is attributable to the higher dislocation density and therefore the higher stored energy that is produced under these conditions. 1 - X represents the residual strain hardening as determined by yield stress measurements made by interrupted compression testing. This steel and the samples referred to in Fig. VII.49 were austenitized at 960°C. (b) Effect of Nb addition on the rate of static recovery in a low carbon steel at 930°C (0.68 T_m), $\dot{\epsilon} = 8 \times 10^{-2}$ sec^{-1}, ϵ = 25 %. The plain carbon steel was austenitized at 960°C and the Nb-modified steel at 1150°C. The very large decrease in recovery rate that follows on the addition of Nb appears to play a large part in the retardation of recrystallization in such steels. It is not clear whether the reduction in rate is due to the effect of Nb in solution or as a precipitate (Petkovic *et al.*, 1975).

order of magnitude, were employed to produce the prestrain. As in the previous case, it can be seen that, at a fixed temperature, the recovery rate increases with stored energy. i.e. with the prior deformation rate.

VII.5.1.3 – Effect of Alloying.

It is evident from the discussion above that after high temperature deformation, static recovery begins as soon as the force is removed. That is, no delay period is required for softening to be initiated. In general, the factors that increase the rate of static recovery (e.g. increases in temperature, prestrain, and strain rate), decrease the incubation time, i.e. the time available for recovery before recrystallization begins. However, when comparing different metals, an increase in stacking fault energy increases the rate of static recovery and can also increase the incubation time. The latter can be attributed to the decrease in worked dislocation density that is associated with stacking fault energy increase, or to changes in the nucleation mechanism (McQueen, 1968).

The addition of some solutes, as has already been noted above, decreases the stacking fault energy and therefore decreases the rate of dynamic recovery and increases the net work hardening rate. In a similar way, solute addition can decrease the rate of static recovery and concurrently increase the incubation time. From a practical point of view, because solute addition makes dynamic recovery more difficult, and therefore increases the flow stress at a fixed temperature, higher temperatures are frequently used to work alloys (and low stacking fault energy metals). It is the higher working temperature and the attendant diminished incubation time that makes the observation of static recovery rare or difficult in these materials.

An example of the effect of alloy addition is illustrated in Fig. VII.50b. Here we see that the presence of 0.07 % Nb has an enormous effect on the rate of static recovery in plain carbon steel. It is not yet clear whether the retardation of recovery is due to a solute effect (i.e. to large decreases in stacking fault energy) or to the effect of the precipitation of NbC particles on the dislocation network. Whatever the cause, it is clear that the retardation of static *recrystallization* in carbon steels is attributable, in a large measure, to the retardation of *recovery* caused by niobium addition.

VII.5.2 – Static Recrystallization.

The occurrence of static recovery, which certainly always takes place, is difficult to observe and to study because its progress is not readily followed by means of optical metallography. More dramatic, from the microstructural point of view, is the occurrence of static recrystallization, and as a result, it has been reported and described more frequently in the literature (Fig. VII.51). A good example of the results obtained by metallographic means is displayed in Fig. VII.52. From Fig. VII.52a, the effect of temperature on the incubation time can clearly be seen. In these experiments, the interruption flow stress, and therefore the driving force, was maintained approximately constant by suitably varying the strain rate of each series of test. Had the strain rate been held constant, the softening curves would have been closer together in time. The effect of temperature on the *rate* of recrystallization cannot be seen as readily because of the use of the log scale for time ; it is, however, apparent that an increase in temperature

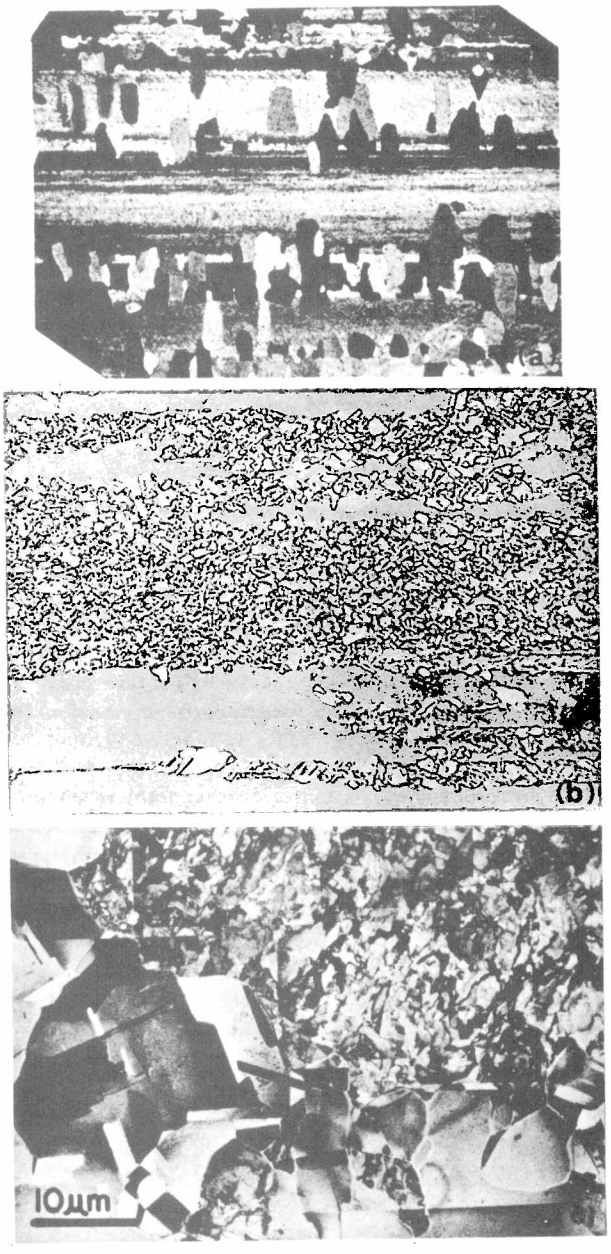

Fig. VII.51 – Static recrystallization is usually clearly followed using optical microscopy by measuring the volume fraction of equiaxed grains and elongated deformed grains. (a) Aluminum extruded to a strain of 3.7 at 450°C (0.77 T_m) and slowly cooled. x 25 (Jonas *et al.*, 1968a). (b) Copper rolled to a strain of 2.3 at 600°C (0.65 T_m) and quenched in 3 sec. x 35. (c) Copper rolled as in (b). x 1300. Electron microscopy reveals that the statically recrystallized grains contain no dislocation substructure. This microstructure should be compared with that of the dynamically recrystallized metal in Fig. VII.32 (McQueen, 1968).

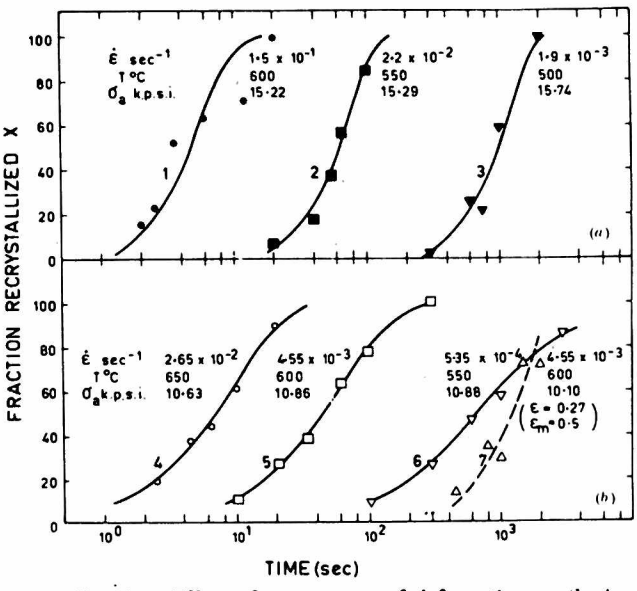

Fig. VII-52 – Effect of temperature of deformation on the isothermal static recrystallization of zone refined iron. (a) The fraction recrystallized after dynamic recovery for specimens deformed to the same flow stress at three different combinations of temperature and strain rate. (b) The fraction metadynamically recrystallized after deformation to the same steady state flow stress at three different combinations of temperature and strain rate. The dashed curve is for static recrystallization after deformation to same stress level before the peak; it should be compared with the middle solid curve. The homologous temperatures of deformation are 0.51 (650°C), 0.49 (600°C), 0.46 (550°C), and 0.43 (500°C) (Glover and Sellars, 1972).

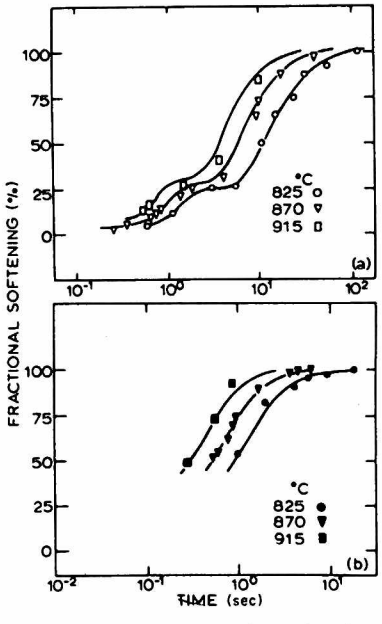

Fig. VII-53 – The effect of temperature of deformation on the isothermal recrystallization rate for specimens deformed at the same strain rate. (a) The strain of interruption, 0.14 lies within the dynamic recovery region. (b) The strain of interruption, 0.35, lies within the dynamic recrystallization region (Djaic and Jonas, 1972).

of 50° C leads to a decrease in recrystallization time of about an order of magnitude and therefore to an approximate order of magnitude increase in recrystallization rate.

The effect of temperature at constant strain rate is evident from the results reproduced in Fig. VII.53. Here the interruption flow stress was not held constant and so the softening curves are closer together. In addition, it should be noted that Fig. VII.53 was determined on *fcc* γ-iron and that the samples were deformed in compression. By contrast, Fig. VII.52 represents results on *bcc* α-iron which were produced by torsion testing, a deformation mode leading to a different flow pattern, and a less homogeneous one than compression testing.

The accelerating effect on the recrystallization rate of raising the temperature while holding the strain rate constant has been reported by numerous workers (Sellars and Tegart, 1966b ; Buhler *et al.*, 1970) (see Fig. VII.36). In a modification of this type of test, Schey (1957) heated or cooled a series of specimens to a single holding temperature after deformation. He observed that the time for complete recrystallization *increased* with the deformation temperature (i.e. the recrystallization rate *decreased* with increasing temperature). The recrystallized grain size also increased with deformation temperature, confirming the strong influence of subgrain size and driving force on the processes of nucleation and growth.

VII.5.2.1 – Effect of Strain Rate and Strain on Recrystallization.

Increasing the strain rate of deformation decreases the incubation time and increases the rate of subsequent recrystallization for the reasons described above. An example is given in Fig. VII.54, for the case of a niobium-

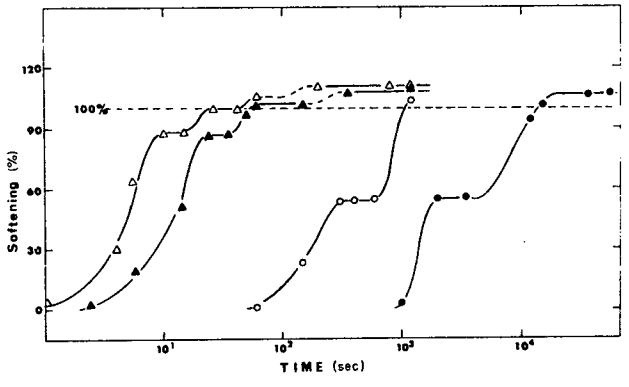

Fig. VII-54 – The effect of strain rate and interruption strain on the isothermal recrystallization of a C1010 steel containing 0.07 %Nb. The low strain interruption was in the dynamic recovery region, whereas the high strain interruption was in the dynamic recrystallization region. The softening exceeded 100 %as a result of changes in the nature of the NbC precipitate. The samples were austenitized at 1150°C and tested at 1040°C (0.73 T_m) (Petkovic, 1975). Strain and strain rate (sec^{-1}) : Δ, 0.25, 8 x 10^{-2}; ▲, 0.25, 8 x 10^{-3}; ○, 0.1, 8 x 10^{-2}; ●, 0.1, 8 x 10^{-3}.

modified steel. It should be noted, however, that in materials like the niobium steels, in which particle precipitation takes place, decreasing the strain rate can permit more precipitation to take place during deformation. Thus part of the retardation associated with the strain rate decrease may be attributed to the retarding effect of the increased particle density on the softening processes. Finer grains are produced by deformation at higher strain rates (and lower temperatures) because of the reduced subgrain sizes formed by dynamic recovery at lower values of temperature-corrected strain rate, Z. An example of this effect is given in Fig. VII.55, in which the correlation is plotted against stress instead of Z.

The influence of the amount of prior strain on the rate of recrystallization and on the recrystallized grain size has also been noted by numerous investigators. The work of English and Backofen (1964), for example, was carried out on bcc silicon iron, whereas that of Wusatowski (1966) and Buhler *et al.* (1970) was conduc-

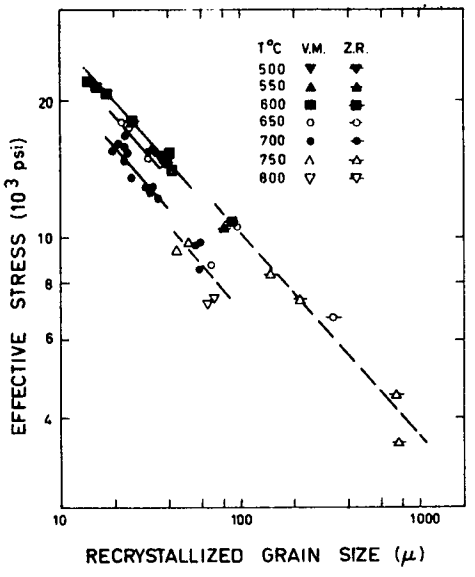

Fig. VII-55 – Correlation between steady state flow stress and statically recrystallized grain size in vacuum melted and zone refined iron (Glover and Sellars, 1972). Solid lines, dynamic recovery; dashed lines, dynamic recrystallization.

ted on fcc austenitic stainless steel. Similar results were also obtained on plain carbon steels in the austenite range by Gueussier and Castro (1958) and by Weiss *et al.* (1972).

Some of the data reported recently by four groups of workers are collected and illustrated in Fig. VII.56. Here it can be seen that the time for 50 % softening by recrystallization decreases by as much as two orders of magnitude with increasing strain, finally leveling out when the steady state regime of flow is attained. For deformations between the critical strains for static and dynamic recrystallization, the increase in rate is attributable directly to the increased driving force. At larger strains, however, part of the increase in rate is attributable to the displacement of classical static recrystallization, which requires an incubation time, by metadynamic or post-dynamic recrystallization, which does not (Djaic and Jonas, 1972).

The increase in recrystallization rate with strain is accompanied by a decrease in recrystallized grain size. Once again the grain size becomes independent of strain when steady state flow has been reached (Fig. VII.57). The preferred sites for nucleation of static recrystallization are heavily deformed regions near grain and twin boundaries.

VII.5.2.2 – Effect of Alloying Elements on Recrystallization.

In many metals, the rate of recrystallization can be reduced by the addition of suitable solutes (e.g. Fe in Ni ; Luton and Sellars, 1969). An increase in solute concentration can also lead to finer recrystallized grain sizes. There are several reasons why this trend is observed. One is the drag effect of impurity atoms on moving grain boundaries ; another is the increase in the density of possible nucleation sites caused by impurity addition. An increase in solute concentration can also affect recrystallization indirectly through its influence on the preceding recovery processes.

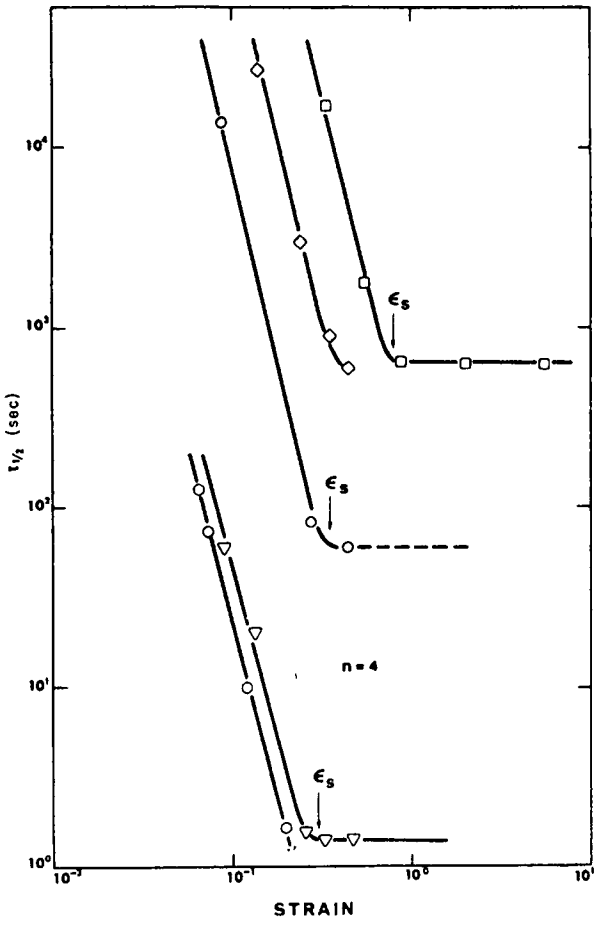

Fig. VII.56 – The effect of strain on the time for 50 % softening for several ferrous alloys in both the ferritic and austenitic conditions. The driving force for recrystallization increases with strain up to the steady state region in which the substructure remains dynamically stable. The symbols and references from top to bottom are: □, Vacuum melted iron at 650°C (Glover and Sellars, 1972); ◇, Fe-4% Si at 812°C (English and Backofen, 1964); ○, 0.68 % C steel at 780°C (Djaic and Jonas, 1973); ▽, 0.68 % C steel at 915°C (Djaic and Jonas, 1973); ⬡, 0.055 % C, 0.46 % Mn steel at 900°C (Morrison, 1972).

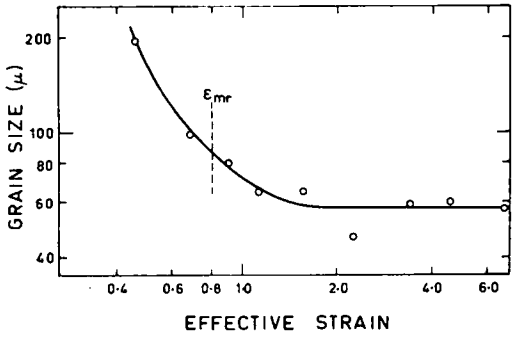

Fig. VII.57 – Effect of strain upon the statically recrystallized grain size in vacuum melted iron after deformation at 650°C (0.53 T_m) and a strain rate of 3.8 x 10^{-2} sec^{-1}. Once the equilibrium dynamic recovery structure for steady state flow, ϵ_{mr}, is well established, the recrystallized grain size becomes independent of strain (Glover and Sellars, 1972).

The latter effect is illustrated in Fig. VII.58, in which two low carbon steels containing Nb are compared with three unmodified plain carbon steels. It can be seen that

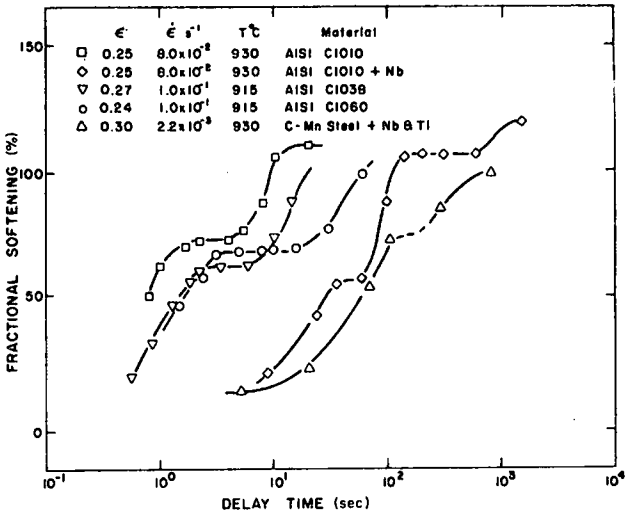

Fig. VII.58 – Effect to Nb addition on the recovery and recrystallization rates of plain carbon steels at about 0.68 T_m. These results were obtained by interrupted compression testing and show that the addition of Nb decreases the softening rate of such steels by more than an order of magnitude in time (Petkovic, *et al.*, 1975). The data for the final alloy (0.17 % C, 1.25 % Mn) in the diagram are from Weiss *et al.* (19[illegible]2).

substantial softening by recrystallization takes at least an order of magnitude longer in the niobium steels than in the unmodified steels. However, it should be noted that the presence of niobium leads to a similar retardation in the rate of static recovery (see also Fig. VII.54), suggesting that the effect of solute addition on the recovery rate, and particularly on the nucleation rate or incubation time, is the rate limiting one. In solid solution alloys such as stainless steel (Sokolkov and Surkov, 1963 ; Irvine *et al.*, 1969), the rate of static recrystallization is retarded to such a degree that it is possible to retain the hot-worked substructures by rapid cooling.

VII.5.3 – Metadynamic Recrystallization

It is not generally recognized that there are three distinct softening processes taking place after high temperature deformation. The two that we have already discussed are closely related to their counterparts occurring after room temperature deformation, and are therefore familiar processes. We turn now to a type of static recrystallization which does not have a parallel in the annealing of cold-worked materials, i.e. to metadynamic or post-dynamic recrystallization.

When high temperature deformation is halted during dynamic recrystallization, many nuclei are already present within the material, and some of the grain boundaries are migrating and sweeping regions free of dislocations. These boundaries can continue to migrate and the nuclei to grow without any classical incubation period being required. The softening process which results from the continued growth of these nuclei is known as metadynamic recrystallization. As this type of recrystallization does not require a nucleation interval, it proceeds very rapidly upon the termination of deformation. Nevertheless, nucleation for static recrystallization can still take place in regions which do not contain dynamic nuclei.

The interrelation between the three static softening processes depends on the prior or interruption strain and is depicted schematically in Fig. VII.59. Here we see

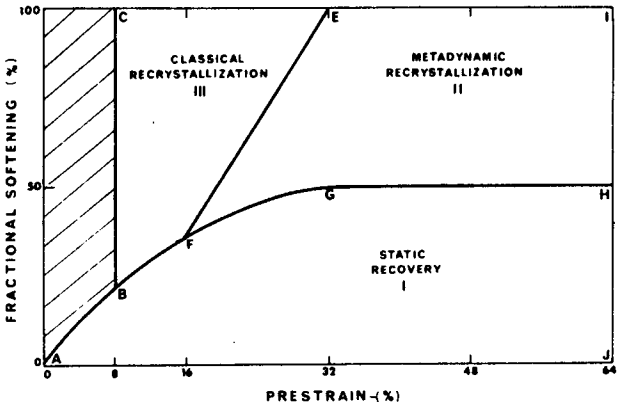

Fig. VII.59 – Schematic representation of the interrelation between the three static softening mechanisms and of their dependence on strain for a material which dynamically recrystallizes. The proportions of softening attributable to each mechanism are also shown. The sequence of static restoration processes at each strain is read vertically upwards. B represents the critical strain for static recrystallization, F the peak strain, and G the strain for the onset of steady state flow (Djaic and Jonas, 1973).

that for deformations below the critical strain for static recrystallization, the only possible restoration process is static recovery. For strains which are larger, but still below the peak strain, ϵ_p, static recovery is followed, after a suitable interval, by static recrystallization. For strains greater than the peak but less than the steady state strain, there is a period of concurrent static recovery and metadynamic recrystallization, followed by a diminished cycle of static recrystallization similar to that prior to the peak, but with a shorter completion time (Fig. VII.48). Finally, once within the steady state range, static recrystallization is superceded entirely, and only metadynamic recrystallization takes place, with some concurrent static recovery.

Metadynamically recrystallized grains are shown in Fig. VII.31, where they may be compared with the dynamically recrystallized grains from which they formed during cooling. At these relatively high temperatures of deformation, the dynamic grains are smaller (Fig. VII.36) because the continuing deformation generates further nuclei. At relatively low temperatures, on the other hand, the metadynamic grains are finer because potential nuclei are rendered ineffective by continued deformation (Sandstrom and Lagneborg, 1975).

The data in Fig. VII.55 indicate that the relationship between the statically recrystallized grain size and the high temperature flow stress is little affected by the dynamic softening process that precedes recrystallization. This is somewhat surprising since the dynamically recovered substructure is uniform, whereas the substructure in the dynamically recrystallized material is highly nonuniform, containing regions of both high and low dislocation density. The explanation may lie in the opposing effects of the low density regions on the one hand, which should promote a coarse grain size, and the small size of the dynamically recrystallized grains on the other, which would tend to favor a fine grain size. Furthermore, as has been shown for the case of dynamic recovery (Fig. VII.56), metals which undergo dynamic recrystallization exhibit a decrease in the statically recrystallized grain size with increase in strain, but only until steady state flow is reached (Petkovic, 1975).

The practical importance of metadynamic recrystallization arises from the absence of any prior incubation time, with the result that it is about an order of magnitude more rapid than classical recrystallization. Allowances must therefore be made for the structural and mechanical changes associated with metadynamic recrystallization if dynamic recrystallization is taking place within a material prior to the cessation of deformation.

VII.6 – The Effect of High Temperature Deformation on the Room Temperature Mechanical Properties.

VII.6.1 – The Effect of Deformation Substructure on Mechanical Properties.

We have been considering above the two main categories of dynamic softening process and the three types of static softening process. We turn now to the substructures produced by dynamic recovery (with or without concurrent dynamic recrystallization) and to the effect these can have on the mechanical properties of the materials in which they are found. In order to have an effect, the dynamic recovery substructures must of course be retained after deformation, which requires a suitable rate of cooling. The rate of cooling, in turn, must be high enough to prevent the occurrence of both classical and metadynamic recrystallization. From our earlier discussions of these mechanisms, it is therefore clear that the prospects for substructure strengthening are greater in the dynamic recovery than in the dynamic recrystallization metals.

It has been observed by numerous workers that, in the presence of a hot-work substructure, the room temperature yield strength, σ_{RT}, is given by a relationship of the form :

$$\sigma_{RT} = \sigma_A + N d^{-p} \qquad (20)$$

Here σ_A is the yield strength of coarse grained material in the absence of subboundaries, N is a constant, and d is the mean subgrain size. The exponent p has been reported to be about 1 in Al (Hockett and McQueen, 1970), Armco iron, Fe–3 % Si, Zr, and Zr–Sn alloys (Fig. VII.60). An equation of similar form, but with different values of p, has been reported for strength correlations carried out by means of hardness testing (e.g., Redfern and Sellars, 1968). It should be noted, however, that the conversion factor for hardness to yield strength is not a linear one (Abson and Jonas, 1970), so that it is more difficult to give a physical interpretation to hardness/subgrain size correlations. The relation between some of the subgrain sizes in Fig. VII.60 and the conditions of working required to produce them is illustrated in Fig. VII.61.

VII.6.2 – A Modified Hall-Petch Relation for Substructure Strengthening.

Equation (20) above differs from the conventional

Hall-Petch relation for grain boundaries :

$$\sigma_{RT} = \sigma_0 + k\, d_g^{-1/2} \qquad (21)$$

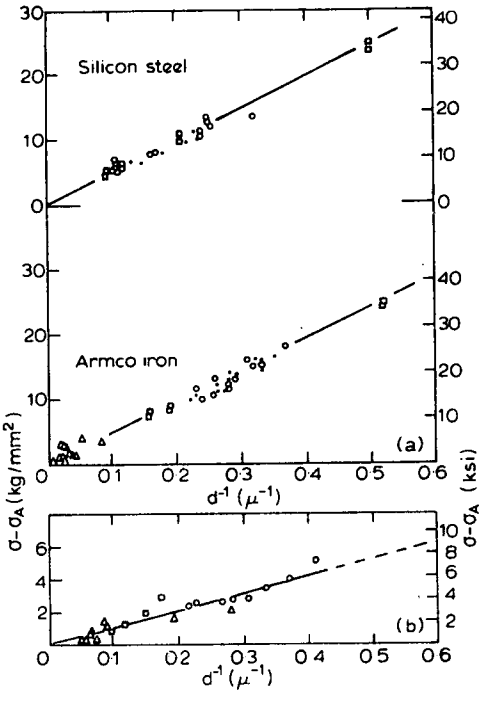

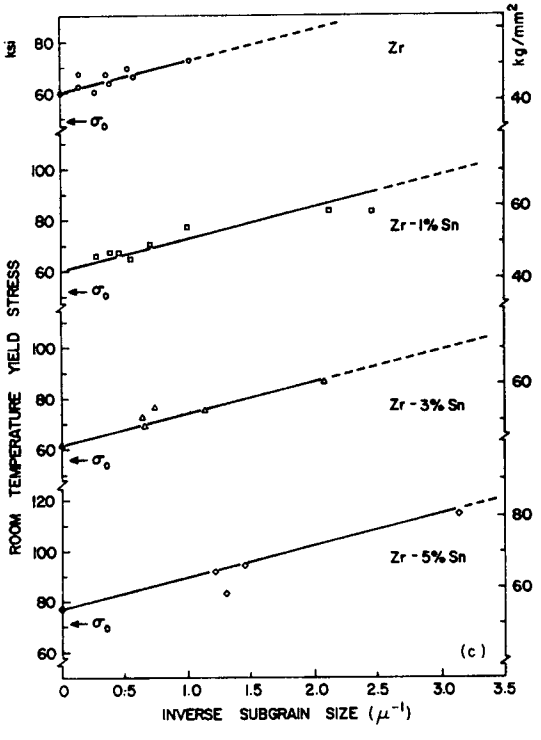

Fig. VII.60 – The increase in yield stress attributable to the presence of a deformation substructure plotted against inverse subgrain size or subboundary density. The annealed yield strength of substructure free material is represented by σ_A. It can be seen that subgrains in the size range 1 - 10μ lead to strength increases of about (a) 30,000 psi in Armco iron and silicon steel (○, Uvira, 1967; Δ, Warrington, 1963; □, Kosik, 1970), (b) 7000 psi in commercial purity aluminum (□, Cotner and Tegart, 1969; ○, McQueen *et al.*, 1967; Δ, after Ball, 1957) (Kosik *et al.*, 1971), and (c) 20,000 psi in a series of Zr-Sn alloys (Abson and Jonas, 1972).

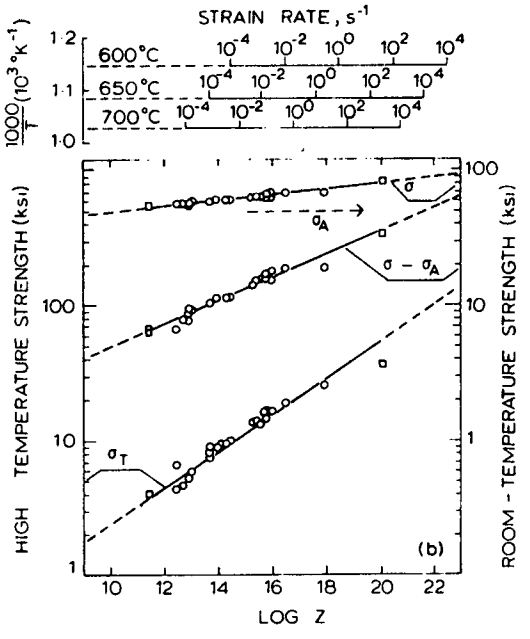

Fig. VII.61 – The room temperature strength σ and strength increment $\sigma - \sigma_A$ and the high temperature steady state flow stress σ_T plotted against the logarithm of the temperature-compensated strain rate Z ($\doteq \dot{\varepsilon} \exp Q/RT$) for the silicon steel of Fig. VII.60a. An activation energy of Q = 335 kJ/mole was used to prepare the diagram, which also indicates the combinations of working temperature and strain rate required to produce the substructure strengthening component $\sigma - \sigma_A$, ○, Uvira, 1967 ; □, Kosik, 1970 (Kosik *et al.*, 1971).

principally in that p is equal to 1 instead of 1/2. Here σ_0 is the yield strength of a single crystal of similar purity and k is the grain boundary strength coefficient. The difference between the two equations is largely attributable to the decrease in subboundary strength and increase in subgrain size that are both associated with deformation at lower values of temperature-corrected strain rate.

The effect of the variation in subboundary strength with the conditions of deformation is shown in Fig. VII.62. For reference purposes, Eq. (21) for grains is plotted on the top left-hand side of Fig. VII.62b. Below this line are plotted similar relations for subgrains having boundary strengths 10, 30, 50 and 70 % as high as the grain boundary strength. Recalling now that subboundary thickness and strength increase as subgrain size decreases (Section VII.3.3), it can be seen that the scatter band of strength data can be expected to pass from the region of low subboundary strength $k_{sb} \simeq 0.1\, k$, at large subgrain sizes, to that of high subboundary strength, $k_{sb} \simeq 0.7\, k$, at small subgrain sizes (Fig. VII 62.a). The resultant curvature in the σ_{RT} vs $d^{-1/2}$ plot is equivalent to a straight line fit on a σ_{RT} vs d^{-1} plot.

The variation in subboundary strength coefficient k_{sb} with subgrain size d takes the form (Abson and Jonas, 1970) ;

$$k_{sb} = N\, d^{-m} \qquad (22)$$

where $m \simeq 1/2$, so that the Hall-Petch relation for subgrains can be expressed as

$$\sigma_{RT} = \sigma_0 + k_{sb}\, d^{-1/2} \qquad (23)$$

$$= \sigma_0 + N d^{-(m+1/2)}$$

$$\simeq \sigma_A + N d^{-p} \qquad (20)$$

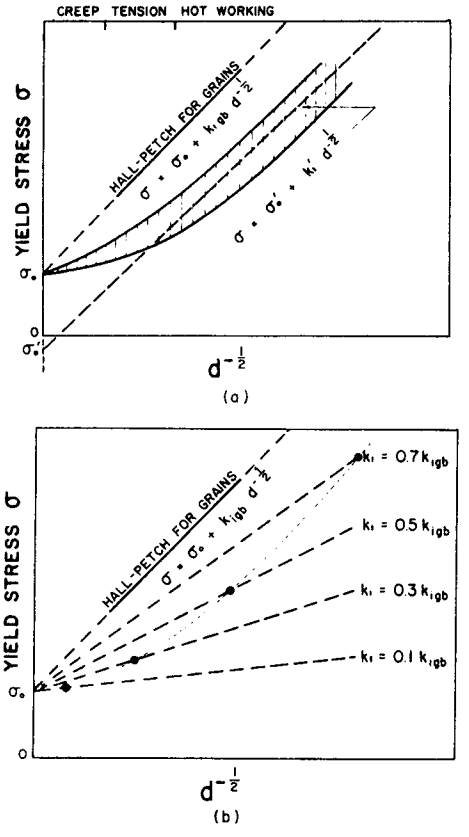

Fig. VII.62 a) Schematic diagram showing the available room temperature data for Al and Fe containing subgrain boundaries. A negative intercept can be seen to result from the fitting of a straight line to part of the scatter band ; the similarity in the values of k_1, the grain boundary strength coefficient, and k'_1, the apparent subboundary strength coefficient, can also be seen. b) The data in a) are represented as the locus of points with a varying true Hall-Petch slope k_1 and a constant friction stress σ_0. (After Abson and Jonas, 1970).

VII.6.3 — Industrial Significance of Substructure Strengthening.

The strengthening due to a hot-work substructure is of industrial importance in the production of nonheat-treatable aluminum and Al-Mg alloy sheet and extruded shapes. In the press heat treatment of alloys 6061, 6063. 7005, and 7039, the preheating and working serve as the solution treatment, and the quenched-in dislocations lead to substructure strengthening on the one hand, and to increases in precipitation strengthening on the other (Ashton, 1969). In steels, the partially recovered substructures produced during warm working close to the lower limit of the hot-working range are responsible for increases in the final strength of such forgings. This process is applied particularly to low carbon steels, and also to austenitic stainless steels and to superalloys (Reynolds and Tegart, 1962 ; Keegan, 1967). In ausforming, the substructure developed during the deformation of metastable austenite is retained during the martensite transformation to strengthen the tempered martensite by improving the dispersion of the temper carbides (Johari and Thomas, 1965 ; Schmatz *et al.*, 1963).

Retained hot-work substructures can also impart improved creep resistance. For example, by quenching in the substructure, creep life can be extended by a factor of 5 in simple metals, stainless steels, and nickel-base superalloys. This must be followed by a low temperature anneal to permit precipitation on the dislocation network and its subsequent stabilization (Ivanova and Gordienko, 1968). After this treatment, the service temperature must be limited so as to prevent recrystallization, which causes the loss of the improved properties. In a similar way, Udimet 700 can be given a thermomechanical treatment by means of which working is carried out in steps, with the precipitation of γ' occurring both between and during the deformation. This results in a strong stable substructure, which leads to much greater creep resistance at lower temperatures. If the temperature is raised to 760° C, however, the creep resistance is reduced to that of the normal heat treated material (Kear *et al.*, 1972).

VII.6.4 — Dynamic Recrystallization and Substructure Strengthening.

If a hot-worked material which is recrystallizing dynamically is rapidly quenched, it is possible to retain the dislocation substructure on cooling to room temperature. Furthermore, by preventing metadynamic recrystallization, the dynamic grain size is also preserved. This can be coarser or finer depending on the deformation and holding conditions. The room temperature hardness increases with increase in the temperature compensated strain rate of hot forming (Fig. VII.63) since that yields a finer substructure and grain size. Moreover, it can be seen that the hardness of dynamically recrystallized metal is intermediate between the hardness of hot-rolled dynamically recovered metal (points identified as hot rolled and unrecrystallized in Fig. VII.63) and that of statically recrystallized metal. Furthermore, it can be seen

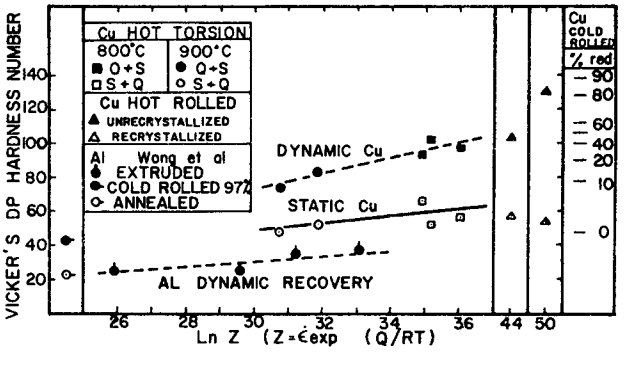

Fig. VII.63 — The effect of temperature compensated strain rate during hot torsion on the room temperature properties of dynamically and metadynamically recrystallized copper. For comparison the hardnesses pertaining to the following treatments are included : dynamically recovered aluminum (Wong *et al.*, 1967), hot rolled copper, both dynamically recovered and statically recrystallized, and cold rolled copper (McQueen and Bergerson, 1972).

that the hot-worked material has a hardness similar to that found in material cold-worked 10 to 50 %. Structures such as these are, unfortunately, unstable at elevated service temperatures.

In copper-aluminum alloys, the room temperature hardness has been observed to vary inversely with the square root of the dynamically recrystallized grain size (Fig. VII.64). The broken line in the diagram shows the

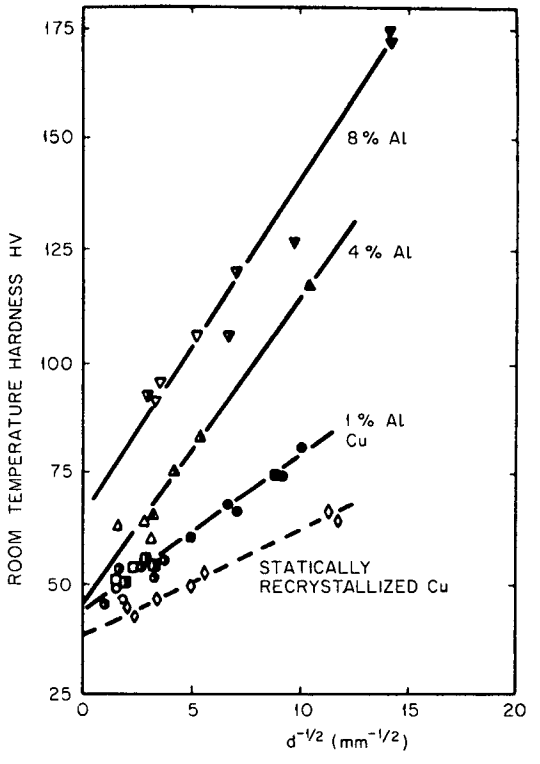

Fig. VII.64 – The dependence of the room temperature hardness on the dynamically recrystallized grain size follows a Hall-Petch type of relationship. The increase in substructure density with decrease in grain size is responsible for the slope for the dynamically recrystallized copper being higher than that for statically recrystallized copper (Bromley and Sellars, 1973).

Hall-Petch relation applicable to substructure-free copper. Comparison of the first full plot, for Cu and Cu-1 % Al, with that for the statically recrystallized material, shows that, for the same grain size, the dynamically recrystallized samples are stronger. This is to be expected from the presence of the subgrains in the latter material. It is also of interest to note that the slope or boundary strength coefficient is about 1 1/2 times higher for the dynamically than for the statically recrystallized samples. This can be attributed to the higher exponent applicable to subgrains [Eq. (20)] than to grains, and to the consequent more rapid increase in subboundary density than grain boundary density that accompanies a decrease in grain size.

VII.6.5 – Static Recrystallization and Controlled Rolling

In many hot-working operations, recrystallization takes place before the product can be cooled to room temperature. Such recrystallization eliminates the substructure and removes that source of strengthening. While this would not be beneficial if the product were to be put into service without further processing, it is useful if the metal is to undergo cold deformation. Thus, even if the substructure is not to be retained, the cooling rate following working is important in controlling grain size for both strength and uniformity of cold deformation.

The effects of hot working and of the rate of cooling on the characteristics of recrystallization are utilized in the process known as controlled rolling, which is applied mainly to steels (Irvine *et al.*, 1970; Tegart, 1971). The objective is a fine, uniform ferrite grain size which has a high yield strength and a low transition temperature, and which is produced by rapid transformation from fine grained austenite (Fig. VII.65). The latter is produced

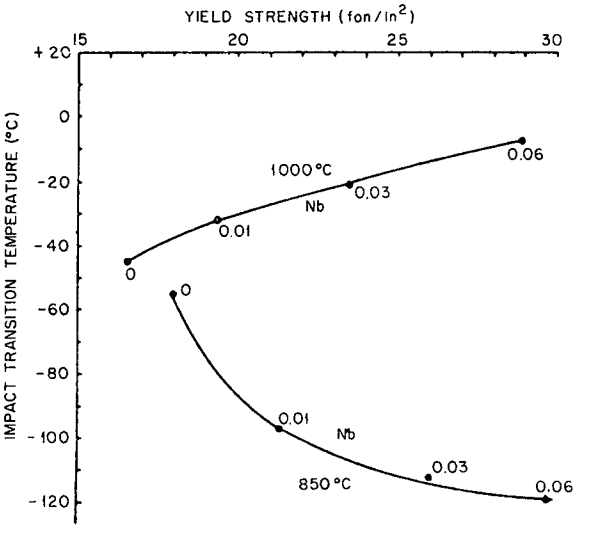

Fig, VII.65 – The effect of niobium addition on the room temperature yield strength and impact transition temperature of a 0.04 % C, 6.5 % Mn steel. The improvement resulting from a lower rolling temperature is also shown (Jones and Rothwell, 1968).

by static recrystallization from austenite which has been deformed up to 50 % at a finishing temperature low enough so that there is very little grain growth during run-out from the rolling mill. If the total strain in the relevant passes is much greater than 50 %, there is a strong possibility that the austenite will recrystallize dynamically during deformation. However, there is also the possibility that the slab or billet will recrystallize statically while cooling to the proper finishing temperature before undergoing the final passes. Such a softening cycle can coarsen the final grain size or lead to undesirable mixed grain sizes. To slow down the recrystallization of the austenite so that the process is easier to control, small amounts of Nb are added to the steel. This has the further advantage that higher strains can be attained without dynamic recrystallization, thus increasing the number of nuclei (Jones and Rothwell, 1968). In the case where NbC inhibits static recrystallization, the elongated austenite grains give rise to ferrite grains approximately equal to their shortest dimension since nucleation is mainly at the boundaries.

A detailed review of the principles of controlled rolling is clearly beyond the limits of the present chapter. It

should, however, be apparent that an understanding of the factors affecting controlled rolling requires some insight into the dynamic and static softening processes which have been described above.

VII.7 – Summary

When metals are deformed under both hot working and creep conditions, strain hardening is counterbalanced by the concurrent softening processes of dynamic recovery and recrystallization. During dynamic recovery, mechanisms such as cross-slip, climb, and node unpinning permit the dislocations to unravel from hardening networks and annihilate each other. During dynamic recrystallization, new grains nucleate and grow; they deform as they grow, however, with the result that recrystallization takes place again and again. During dynamic recrystallization, dynamic recovery is occurring in both the old and the new grains. The characteristics of the two dynamic softening mechanisms are summarized and compared below.

A. The capacity of a metal for dynamic recovery diminishes with decrease in stacking fault energy as the dislocations become more extended. Dynamic recrystallization occurs in a metal if the degree of dynamic recovery is insufficient to maintain the substructure density below the critical level for nucleation. The characteristics of different metals and alloys are summarized in Table I.

TABLE I

Restoration Processes in Deformed Metals

<table>
<tr><th rowspan="3">Metals</th><th rowspan="3">Cold-worked structure</th><th colspan="3">High temperature softening process</th></tr>
<tr><th>During annealing</th><th>During deformation</th><th>During holding</th></tr>
<tr><th>Static</th><th>Dynamic</th><th>Static</th></tr>
<tr><td>Al
α-Fe
Ferritic alloys
Bcc refractory metals
Zr alloys
Hcp metals</td><td>Well developed cell structure</td><td>Recovery followed by recrystallization (nucleation by coalescence at high strains)</td><td>Recovery even to high strains</td><td>Recovery
Recrystallization relatively slow, easily prevented by cooling after working</td></tr>
<tr><td rowspan="4">Ni
Ni-base superalloys
γ-Fe
Austenitic alloys
Cu
Brass</td><td rowspan="4">Cell structure alters gradually to uniform distribution of dislocations with decrease in stacking fault energy</td><td rowspan="4">Limited recovery followed by recrystallization (nucleation by g.b. bulging or from high local concentration of dislocations</td><td colspan="2">Hot working at small strains
Creep at normal strain rates</td></tr>
<tr><td>Recovery:</td><td>Recovery; followed by rapid static recrystallization</td></tr>
<tr><td colspan="2">Hot working at large strains</td></tr>
<tr><td>Recovery and Recrystallization:</td><td>Recovery and Metadynamic recrystallization followed by static recrystallization</td></tr>
</table>

B. Both dynamic processes lead to flow curves with steady state regions. With dynamic recrystallization, however, the steady state flow stress is reached only after passing through a maximum; recrystallization is initiated at this point, producing softening with further strain. At low values of temperature-corrected strain rate, dynamic recrystallization leads to periodic flow curves.

C. When dynamic recovery is taking place, the grains become elongated in the direction of flow; meanwhile, the substructure undergoes a process called repolygonization,which keeps it dimensionally stable and equiaxed. Under conditions of dynamic recrystallization, new grains continually replace the most work-hardened ones, maintaining a fine equiaxed grain structure, with a distribution of degrees of deformation.

D. Increases in the temperature and decreases in the strain rate of deformation result in larger, more perfect, subgrains or grains during dynamic recovery or recrystallization, respectively.

E. Decreases in temperature and increases in strain rate increase the strains for the nucleation and for the completion of recrystallization. As the latter becomes greater than the former, the periodic cycles of softening begin to overlap, and recrystallization becomes continuous.

F. The yield stress under hot-working conditions is highly sensitive to strain rate and temperature. In this respect, it differs from the essentially athermal yields observed at intermediate temperatures. The strain rate and temperature dependence of the steady state stress is similar to that of the yield stress, indicating that similar mechanisms are rate controlling.

G. The steady state stresses observed at high temperatures are about twice the yield stresses. The increase in flow stress after yielding can be attributed to an increase in internal stress, which is in turn proportional to both the subboundary density and the square root of the dislocation density.

H. The subgrain size developed under conditions of both dynamic recovery and recrystallization is inversely related to the steady state stress. The similar correlation between dynamically recrystallized grain size and flow stress arises from the dependence of nucleus density on subgrain density.

I. The ductility is increased many times over that at room temperature by the occurrence of either high temperature dynamic recovery or recrystallization. A high level of dynamic recovery reduces intergranular cracking through the formation of bulges in the grain boundaries which restrict sliding. The lower flow stresses brought about by enhanced dynamic recovery also permit easier accomodation at triple points, reducing crack nucleation. When dynamic recrystallization occurs, it prevents the propagation of intergranular cracks by continually displacing the grain boundaries from the ends of the cracks.

J. Solute additions usually retard dynamic recovery, especially if they cause further extension of the dislocations. This is turn tends to increase the stored energy, and therefore to promote dynamic recrystallization. However solute atoms also retard nucleation and slow down grain boundary migration; as a result, higher deformation temperatures are required for the attainment of steady state flow. In many alloys, the occurrence of

grain boundary sliding without concurrent dynamic recrystallization, at intermediate temperatures, leads to unimpeded grain boundary cracking with consequent reduction in ductility.

K. The presence of fine second phase particles usually stabilizes the substructure, thus raising the steady state flow stress and delaying dynamic recrystallization. Larger second phase particles frequently cause a considerable decrease in ductility in metals that recrystallize dynamically in so far as they pin the grain boundaries, permitting the propagation of intergranular cracks.

L. The presence of a dynamically recovered or dynamically recrystallized structure at the commencement of a further stage of deformation can have a considerable effect on further flow. The inherited structure may lead to initially higher or lower flow stresses depending on whether it is harder or softer than the equilibrium structure for the new stage of deformation. Nevertheless, at high strains, the equilibrium structure and flow stress are independent of the initial structure.

M. As soon as deformation is completed or interrupted, static recovery and recrystallization take place, following the dynamic softening processes. A high degree of dynamic recovery delays and may prevent static recrystallization. Dynamic recrystallization provides nuclei for metadynamic (post-dynamic) recrystallization, which as a result does not have an incubation period and takes place concurrently with static recovery. The rates of all three static softening processes increase with the temperature, strain rate, and strain of the prior deformation.

N. The substructures produced by dynamic recovery and recrystallization, when retained to room temperature, lead to yield stresses higher than those of annealed materials. The yield strength of worked metals is proportional to the inverse subgrain size and to the inverse square root of the grain size.

While a general description of the dynamic softening processes has been presented in this chapter, for brevity, many details have been omitted. For those who wish to examine the experimental evidence in greater depth, the following reviews are recommended: Stüwe and Drube (1967), Tegart (1968), Jonas *et al.* (1969), Sellars and Tegart (1972), Fulop and McQueen (1972) (Ni-base superalloys), McElroy and Szkopiak (1972), Jonas and McQueen (1973), and Rossard (1973).

Those interested in experimental techniques should refer to the following publications: Rossard and Blain (1962), Henning and Boulger (1964), Nicholson (1964), Rossard (1968), Young and Sherby (1969), Weiss *et al.* (1970), and McQueen and Jonas (1971).

Acknowledgments

The authors wish to thank Atomic Energy of Canada Limited, the National Research Council of Canada, and the Defence Research Board of Canada for the financial support of many of the investigation described in this chapter.

References

ABSON D.J. and JONAS J.J. – *Metal. Sci. J.*, 1970, 4, 24-28.

ABSON D.J. and JONAS J.J. – *J. Nucl. Mater.*, 1972, 42, 73-85.

ALDEN T.H. – "Treatise on Materials Science and Technology, Vol. 6: Plastic Deformation of Materials" (R.J. Arsenault, ed.), pp. 225-266. Academic Press, New York, 1975.

ASHTON R.F. – *J. Metals*, 1969, 22, No. 9, 35-38.

AULD J.H., GARROD R.I., and THOMSON T.R. – *Acta Met.*, 1957, 5, 741-746.

BAILEY J.E. – *In* "Electron Microscopy and Strength of Crystals" (G. Thomas and J. Washburn, eds.), pp. 535-574. Wiley (Interscience), New York, 1963.

BAILEY R.E. – "Microstructural Examination of Waspaloy and Al-718 Gleeble Hot Workability Test Specimens", Rep. SP-69-9. Allegheny Ludlum Steel Research Center, Brackenridge, Pennsylvania, 1969.

BALL C.J. – *Phil. Mag.*, 1957, 2, 1011-1017.

BIRD J.E., MUKHERJEE A.K. and DORN J.E. – *In* "Quantitative Relation Between Properties and Microstructure" (D.G. Brandon and A. Rosen, eds), pp. 255-342. Isr. Program Sci. Transl., Jerusalem, 1969.

BOURELIER F. and MONTUELLE J. – *Mém. Sci. Rev. Mét.*, 1968, 65, 65-76.

BROMLEY R. – Ph. D. Thesis, Sheffield University, Sheffield, England, 1969.

BROMLEY R., and SELLARS C.M. – *Proc. Int. Conf. Strength Metals Alloys, 3rd*, Vol. 1, pp. 380-385. 1973.

BUHLER H., BOBBERT D., and ROSE A. – *Stahl Eisen*, 1970, 90, 21-28.

BYRNE J.G. – "Recovery, Recrystallization and Grain Growth." Macmillan, New York, 1965.

CAHN R.W. – *In* "Physical Metallurgy" (R.W. Cahn, ed.), pp. 925-987. Wiley, New York, 1965.

CHOJNOWSKI E.A., and TEGART W.J. McG. – *Metal Sci. J.*, 1968, 2, 14-18.

CLAUER A.H., and WILCOX B.A. – *Metal Sci. J.*, 1967, 1, 86-90.

COTNER J.R., and TEGART W.J. McG. – *J. Inst. Metals*, 1969, 97, 73-79.

CREMISIO R.C., BUTLER, H.M., and RADAVICH J.F. – *J. Metals*, 1969, 21, No. 11, 55-61.

CUDDY L.J. – *Met. Trans.*, 1970, 1, 395-401.

DEMIANCZUK D.W. – M. Eng. Thesis, McGill University, Montreal, Canada. 1967.

DIETER G.E., MULLIN J.V., and SHAPIRO E. – "Deformation Under Hot Working Conditions", pp. 7-13. Iron Steel Inst., London, 1968.

DJAIC R.A.P., and JONAS, J.J. – *J. Iron Steel Inst.*, 1972, 210, 256-261.

DJAIC R.A.P., and JONAS J.J. – *Met. Trans.*, 1973, 4, 621-624.

DRUBE B., and STÜWE H.P. – *Z. Metalk.*, 1967, 58, 799-804.

ENGLISH A.T., and BACKOFEN W.A. – *Trans. AIME*, 1964, 230, 396-407.

EVANS R.W., and DUNSTAN G.R. – *J. Inst. Metals*, 1971, 99, 4-14.

EXELL S.F., and WARRINGTON D.H. – *Phil. Mag.*, 1972, [8] 26, 1121-1136.

FARAG M.M., SELLARS C.M., and TEGART W.J. McG. – "Deformation Under Hot Working Conditions", pp. 60-67, Iron Steel Inst., London, 1968.

FINK K., LUEG W., and BURGER G. *Arch. Eisenhuettenw.*, 1955, 26, 665-688.

FULOP S., and McQUEEN H.J. – "Superalloys: Processing", pp. H1-H21. Metals and Ceramics Information Center, Columbus, Ohio, 1972.

GAROFALO F., von GEMMINGEN F., and DOMIS W.F. – *ASM (Amer. Soc. Metals) Trans. Quart.*, 1961, 54, 430-443.

GAROFALO F., RICHMOND C., DOMIS W.F., and von GEMMINGEN F. – *Joint Int. Conf. Creep*, 1963, pp. 131-139.

GITTINS A – "Fracture of Metals Under Hot Working Conditions", MRL 29/1. BHP Melbourne Res. Lab., Australia, 1970.

GITTINS A., HINTON L.G., and TEGART W.J. McG. – "Ductility of Steels in Hot Working", MRL S3/10. BHP Melbourne Res. Lab., Australia, 1972.

GLOVER G. – Ph. D. Thesis, Sheffield University, Sheffield, England, 1969.

GLOVER G., and SELLARS C.M. – *Met. Trans.*, 1972, 3, 2271-2280.

GLOVER G., and SELLARS C.M. – *Met. Trans.*, 1973, 4, 765-755.

GUEUSSIER A., and CASTRO R. – *Rev. Mét. (Paris)*, 1958, 55, 1023-1040.

HARDWICK D., and TEGART W.J. McG. – *J. Inst. Metals*, 1961, 90, 17-20.

HARDWICK D., SELLARS C.M., and TEGART, WJ. McG. – *J. Inst. Metals*, 1961, 90, 21-22.

HENNING H.J., and BOULGER F.W. – "Mechanical Working of Steel," Vol. 1, pp. 107-125. Gordon & Breach, New York, 1964.

HERITIER B., LUTON M.J. and JONAS J.J. – *Metal Sci.*, 1974, 8, 41-48.

HIRST H. – *Proc. Australas. Inst. Min. Met.*, 1940, 120, 777-806.

HOCKETT J.E., and McQUEEN H.J. – *Proc. Int. Conf. Strength Metals Alloys, 2nd, 1970* pp. 991-995. 1970.

HOLT D.L. – *J. Appl. Phys.*, 1970, 41, 3197-3201.

HU H. – *In* "Recovery and Recrystallization of Metals" (L. Himmel, ed.), pp. 311-378. Wiley (Interscience), New York, 1963.

HUMPHREYS F.J., and MARTIN J.W. – *Phil. Mag.*, 1968, [8], 17, 365-380

IMMARIGEON J.-P.A. – Ph. D. Thesis, McGill University, Montreal, Canada, 1974.

IMMARIGEON J.-P.A., and JONAS J.J. – *Acta Met.*, 1971, 19, 1053-1061.

IMMARIGEON J.-P.A., and JONAS J.J. – *Acta Met.*, 1974, 22, 1235-1247.

IRANI J.J., and TAYLOR P.R. – "Deformation Under Hot Working Conditions", pp. 83-96. Iron Steel Inst., London, 1968.

IRVINE K.J., GLADMAN T., and PICKERING F.B. – *J. Iron Steel Inst.*, 1969, 207, 1017-1028.

IRVINE K.J., GLADMAN T., ORR J., and PICKERING F.B. – *J. Iron Steel Inst.*, 1970, 208, 717-726.

IVANOVA V.S., and GORDIENKO L.K. – "New Ways of Increasing the Strength of Metals", pp. 13-35. Iron Steel Inst., London, 1968.

JACQUERIE J.M., and HABRAKEN L. – *Cobalt*, 1968, 38, 13-19.

JOHARI O. and THOMAS G. – *ASM (Amer. Soc. Metals) Trans. Quart.* 1965, 58, 563-578.

JONAS J.J. – *J. Sci. Ind. Res.*, 1973, 32, 528-535.

JONAS J.J. and CHANDRA T. – "Metal Forming : Interrelation Between Theory and Practice", pp. 115-129. Plenum, New York, 1971.

JONAS J.J. and LUTON M.J. – "Advances in Deformation Processing", Sagamore Conference 21st, 1974, Syracuse University Press (in press). 1976.

JONAS J.J. and McQUEEN H.J. – *Trans. Soc. Mfr. Eng.*, 1973, 2, 209-233.

JONAS J.J., McQUEEN H.J. and WONG W.A. – "Deformation Under Hot Working Conditions", pp. 49-59, Iron Steel Inst., London, 1968a.

JONAS J.J., AXELRAD D.R. and UVIRA J.L. – *Trans. Jap. Inst. Metals*, 1968b, 9, Suppl., 257-267.

JONAS J.J., SELLARS C.M., and TEGART W.J. McG – *Met. Rev.*, 1969, 14, 1-24.

JONES J.D. and ROTHWELL A.B. – "Deformation Under Hot Working Conditions", pp. 78-82. Iron Steel Inst., London, 1968.

KEANE D.M., SELLARS C.M. and TEGART W.J. McG – "Deformation Under Hot Working Conditions", pp. 21-28. Iron Steel Inst., London, 1968.

KEAR B.H., OBLAK J.M. and OWCZARSKI W.A. – *J. Metals*, 1972, 24, N° 6, 25-32.

KEEGAN J.W. – *Metal Progr.*, 1967, 92, N° 2, 31-33.

KIVILAHTI J.K., LINDROOS V.K. and LEHTINEN B. – *In* "High Voltage Electron Microscopy" (P.R. Swann *et al.*, eds.), p. 195. Academic Press, New York, 1974.

KOSIK O. – M. Eng. Thesis, McGill University, Montreal, Canada, 1970.

KOSIK O., ABSON D.J. and JONAS J.J. – *J. Iron Steel Inst.*, 1971, 209, 624-671.

KUHLMANN-WILSDORF D. – *In* "Work Hardening" (J.P. Hirth and J. Weertman, eds.), pp. 97-139. Gordon & Breach, New York, 1966.

LE BON A., ROFES-VERNIS J. and ROSSARD C. – *Mém. Sci. Rev. Mét.*, 1973, 70, 577-588.

LESLIE W.C., MICHALAK J.T. and AUL F.W. – *In* "Iron and its Dilute Solid Solutions" (C.W. Spencer and F.E. Werner, eds.), pp. 119-216. Wiley (Interscience), New York, 1963.

LOIZOU N. and SIMS R.B. – *J. Mech. Phys. Solids*, 1953, 1, 234-243.

LUTON M.J. and JONAS J.J. – *Proc. Int. Conf. Strength Metals Alloys, 2nd, 1970*, pp. 1100-1105.

LUTON M.J. and JONAS J.J. – *Can. Met. Quart.*, 1972a, 11, 79-90.

LUTON M.J. and JONAS J.J. *Proc. Inter-Amer. Conf. Mater. Technol., 3rd*, 1972b, pp. 910-917.

LUTON M.J. and SELLARS C.M. – *Acta Met.*, 1969, 17, 1033-1043.

LUTON M.J. and TEGART W.J. McG – *Metal Sci. J.*, 1969, **3**, 142-146.

McELROY R.J. and SZKOPIAK Z.C. – *Int. Met. Rev.*, 1972, **17**, 175-202.

McQUEEN H.J. *Trans. Jap. Inst. Metals*, 1968, 9, Suppl., 170-177.

McQUEEN H.J. and BERGERSON S. – *Metal Sci. J.*, 1972, 6, 25-29.

McQUEEN H.J. and HOCKETT J.E. – *Met. Trans.*, 1970, **1**, 2997-3004.

McQUEEN H.J. and JONAS J.J. – "Metal Forming : Interrelation Between Theory and Practice", pp. 393-428. Plenum, New York, 1971.

McQUEEN H.J., WONG W.A. and JONAS J.J. – *Can. J. Phys.*, 1967, 45, 1225-1235.

MORRISON W.B. – *J. Iron Steel Inst.*, 1972, **210**, 618-623.

MÜLLER T.L.F. – Ph. D Thesis, Sheffield University, Sheffield, England, 1967.

NICHOLSON A. – *Iron Steel (London)*, 1964, 37, 290-294 and 363-367.

OBLAK J.M. and OWCZARSKI W.A. – *Met. Trans.*, 1972, 3, 617-626.

PERRYMAN E.C.W. – "Creep and Recovery", pp. 111-145. Amer. Soc. Metals, Metals Park, Ohio, 1956.

PETKOVIC R.A. – Ph.D. Thesis, McGill University, Montreal, Canada, 1975.

PETKOVIC R.A., LUTON M.J. and JONAS J.J. – *Can. Met. Quart.*, 1975, 14, 137-145.

REDFERN G.A. and SELLARS C.M. – "Deformation Under Hot Working Conditions", pp. 29-37. Iron Steel Inst., London, 1968.

REYNOLDS K.A. – "Deformation Under Hot Working Conditions", pp. 107-116. Iron Steel Inst., London, 1968.

REYNOLDS R.A. and TEGART W.J. McG – *J. Iron Steel Inst.*, 1962, **200**, 1044-1059.

RHINES F.N. and WRAY P.J. – *ASM (Amer. Soc. Metals) Trans. Quart.*, 1961, **54**, 117-128.

RICHARDSON G.J., SELLARS C.M. and TEGART W.J. McG., *Acta Met.*, 1966, **14**, 1225-1236.

ROBBINS J.L., SHEPARD O.G., and SHERBY O.D. – *ASM (Amer. Soc. Metals) Trans. Quart.*, 1967, **60**, 205-216.

ROSSARD C. – *Métaux*, 1960, 35, 102-115, 140-153, and 190 205.

ROSSARD C. – *Rev. Mét.*, 1968, **65**, 181-193.

ROSSARD C. – *Proc. Int. Conf. Strength Metals Alloys, 3rd, 1973*, Vol. II, pp. 175-203, 1973.

ROSSARD C. and BLAIN P. – "Flat Rolled Products", Vol. III, pp. 3-28. Gordon & Breach, New York, 1963.

SABROFF A.M., BOULGER F.W. and HENNING H.J. – "Forging Materials and Practice". Van Nostrand-Reinhold, Princeton, New Jersey, 1968.

SAH J.P., RICHARDSON G.J. and SELLARS C.M. – *J. Aust. Inst. Metals*, 1969, **15**, 292-297.

SANDSTROM R. and LAGNEBORG R. – *Scripta Met.*, 1975, 9, 59-65 ; *Acta Met* ; 1975, 23, 387-398.

SASTRY D.H., LUTON M.J. and JONAS J.J. – *Phil. Mag.*, 1974, [8] 30, 115-127.

SCHEY J. – *Acta Tech. (Budapest)*, 1957, **16**, 131-152.

SCHMATZ D.J., SCHALLER F.W. and ZACKAY V.F. "The Relation Between the Structure and Mechanical Properties of Metals", pp. 613-645. HM Stationery Office, London, 1963.

SELLARS C.M. – *J. Sheffield Univ. Met. Soc.*, 1969, 8, 43-47.

SELLARS C.M. and TEGART W.J. McG – *Acta Met.*, **14**, 1136-1138.

SELLARS C.M. and TEGART W.J. McG – *Mém. Sci. Rev. Mét.* 1966b, 63, 731-746.

SELLARS C.M. and TEGART W.J. McG – *Int. Met. Rev.*, 1972, 17, 1-24.

SHAPIRO E. and DIETER G.E. – *Met. Trans.*, 1971, 2, 1385-1391.

SHERBY O.D., HARRIGAN M.J., CHAMAGNE L. and SAUVE C. – *ASM (Amer. Soc. Metals) Trans. Quart.*, 1969, **62**, 575-580.

SOKOLKOV Ye. N. and SURKOV Yu P. – *Phys. Metals Metallogr. (USSR)*, 1963, 16, N° 6, 107-109.

STUWE H.P. and DRUBE B. – *Z. Metallk.*, 1967, **58**, 499-506.

SUNTER B.J. and BURMAN N.M. – *J. Aust. Inst. Metals*, 1972, **17**, N° 2, 91-100.

SWANN P.R. – *In* "Electron Microscopy and Strength of Crystals" (G. Thomas and J. Washburn. eds.), pp. 131-182. Wiley (Interscience), New York, 1963.

TEGART W.J. McG. – "Ductility" pp. 133-177. Amer. Soc. Metals, Metals Park, Ohio., 1968.

TEGART W.J. McG *Metals Aust.*, 1971, 3, N°, 1, 3-8.

THORNTON P.H. and CAHN R.W. – *J. Inst. Metals*, 1961, **89**, 455-463.

UVIRA J.L. – Ph.D. Thesis, McGill University, Montreal, Canada, 1967.

VANDERMEER R.A. and GORDON P. – In "Recovery and Recrystallization of Metals" (L. Himmel. ed.), pp. 211-240. Wiley (Interscience), New York, 1963.

VAUGHAN T.B. – "Deformation Under Hot Working Conditions", pp. 68-78. Iron Steel Inst., London, 1968.

WARD D.M. and HELLIWELL B.J. – *J. Inst. Metals*, 1970, **98**, 199-203.

WARRINGTON D H. – J. Iron Steel Inst., 1963, **201**, 610-613.

WEBSTER D., CROOKS D.D. and VIDOZ A.E. – *Met. Trans.*, 1973, 4, 2841-2847.

WEISS B., GROTKE G.E. and STICKLER R. – *Weld. Res., Suppl.*, 1970, **35**, 471s-487s.

WEISS H., GITTINS A., BROWN G.G. and TEGART W.J. McG – "Recrystallization of Steel in the Austenite Range", MRL 41/1. BHP Melbourne Research Lab., Australia, 1972.

WEISSMANN S., IMURA T. and HOSOKAWA N. – *In* "Recovery and Recrystallization of Metals" (L. Himmel, ed.). pp. 241-267. Wiley (Interscience), New York, 1963.

WHITE F.E. and ROSSARD C. – "Deformation Under Hot Working Conditions", pp. 14-20. Iron Steel Inst., London, 1968.

WONG W.A. McQUEEN H.J. and JONAS J.J. – *J. Inst. Metals*, 1967, **95**, 129-137.

WOOD W.A. and RACHINGER W.A. – *J. Inst. Metals*, 1949, **76**, 237-253.

WOOD W.A. and SUITER J.W. – *J. Inst. Metals*, 1951, **80**, 501-506.

WUSATOWSKI R. *J. Iron Steel Inst.*, 1966, **204**, 727-736.

YOUNG C.M. and SHERBY O.D. – "Simulation of Hot Forming Operations by Means of Hot Torsion", AFML-TR-69-294, Stanford University, Palo Alto, California, 1969.

STRENGTHENING EFFECT OF HOT-WORK SUBGRAINS AT ROOM TEMPERATURE

O. KOŠÍK, D. J. ABSON, and J. J. JONAS

Most hot-worked materials are produced for service at ambient temperatures and more than 50% of these, in the case of the ferrous metals, are fabricated or used in the hot-finished condition. It is therefore of interest to examine the room-temperature strength of hot-deformed metals and to correlate this with the scale of the hot-work substructure, and with the hot-working parameters. Most metals soften by dynamic recovery when deformed at homologous temperatures greater than 0·5. In these, in contrast to room-temperature behaviour, a more or less equiaxed substructure is present at large strains. After working, the deformation-induced substructure can be preserved by rapid cooling, or by suitable alloy additions to retard recrystallization, and the room-temperature strength of the metal can then be measured. In the laboratory investigations carried out to date, due to the limited size of the experimental samples, such strength measurements have taken the form of hardness determinations. The data obtained have usually been fitted to an equation of the Hall–Petch type, viz.,

$$H=H_0+k'd^{-\frac{1}{2}} \quad \ldots\ldots(1)$$

where H and d are the measured strength and subgrain size respectively, and H_0 and k' are empirical constants. By considering data over a wide range of subgrain sizes and converting the available hardness data to equivalent flow stresses, Abson and Jonas[1] showed that a relationship of the form

$$\sigma=\sigma_0+kd^{-m} \quad \ldots\ldots(2)$$

applied. Here σ is the yield strength, σ_0 is the Hall–Petch friction stress and is $\sim M$ times τ_0, the critical resolved shear stress for multiple slip, (M is the Taylor orientation factor), and k and m are constants. From available hardness data, the approximate value given for m was 3/4. It is the purpose of the present paper to evaluate more accurately, by means of *compression* rather than *hardness* testing, the extent of room-temperature strengthening that can be attributed to a deformation-induced substructure. It is also proposed to extend the equation to include the influence of grain size, and to evaluate m more precisely for Armco iron, silicon steel, and aluminium. Correlations between the room-temperature strength and high-temperature deformation parameters will also be examined.

EXPERIMENTAL PROCEDURE

Room-temperature compression testing

The availability of samples of known subgrain size which were relatively small imposed limitations on the geometry of the samples used for room-temperature testing. Cylindrical specimens, 2·5 – 5·0 mm in diameter were machined from hot-compressed Armco iron and silicon steel which had been used in a previous investigation.[2] A height to diameter ratio of 1·5 was chosen as a compromise between the large value required to minimize the effects of friction and the small value required for mechanical stability. The same geometry, and a diameter of 5·0 mm, was used for aluminium samples machined from the 6·3 mm diameter extruded bar produced in an earlier investigation.[3] Compositions of the materials are given in Table I. The guide lines laid down in ASTM specification E–9–67 were followed in preparing the specimens.[5] An aerosol

 Manuscript received 23 October 1970. Mr Košík is at VUMA, Research Institute for Mechanization and Automation, Nové Mesto Nad Váhom, Czechoslovakia. Dr Abson is with Westinghouse Electric Corporation, Wright-Patterson AFB, Dayton, Ohio, USA. Dr Jonas is with the Department of Metallurgical Engineering, McGill University, Montreal, Canada.

Room-temperature compression tests were carried out on samples of Armco iron, silicon steel, and aluminium containing subgrains in the size range 2 – 10 μm. Hot-compression tests were also performed in order to extend the subgrain size range of the available materials. The yield data were analysed according to the modified Hall–Petch relation: $\sigma=\sigma_0+KD^{-\frac{1}{2}}+kd^{-m}$.
Here, σ_0 and $KD^{-\frac{1}{2}}$ are the usual Hall–Petch terms and kd^{-m} is the strength increment due to the presence of a hot-work substructure. The exponent m was observed to be $\sim$1 for the three materials. The strength increment attributable to the presence of the subgrains was observed to be proportional to a power of the temperature-compensated strain rate of their formation. Thus a simple correlation exists between the high-temperature deformation conditions and the room-temperature strength. Maximum strengths observed were 35, 39, and 9·7 kg/mm² (50000, 84000, and 13800 lb/in²) for the three materials, respectively, at subgrain sizes of $\sim$2 μm. The significance of these results to industrial hot-working practice is considered briefly. Comparison of the flow stress at 7·4% strain with the hardness values permitted evaluation of the Tabor hardness: flow-stress ratio. The hardness: yield strength ratio was also determined, anomalously high values being found, in each case, for the annealed material.

669.12–175.4: 539.4/.5

3757

TABLE I Chemical composition wt-% of the material tested

Element	Armco iron[4]	Silicon steel[4]	Aluminium[8]
Fe	balance	balance	0·21
C	0·03	0·03	..
P	0·005	0·008	..
S	0·01	0·02	..
Mn	0·26	0·39	..
Si	0·15	2·70	0·06
Cu	0·13	0·07	..
Cr	0·01	0·02	..
Ni	0·05	0·05	..
Al	..	0·06	balance
N	0·007	0·01	..

TABLE II Specimen preparation procedure

Operetion		Armco iron	Silicon steel
Turning	Diameter, in	0·294	
Facing	Length, in	0·468	
Grooving of the faces	Spacing between grooves, in	0·02	
	Depth of grooves, in	0·003	
Preannealing	Temperature, °C	950	1100
	Time, h	7	2
	Cooling	air quench	air quench
Straining	$\dot{\epsilon}$	0·038	
Strain annealing	Temperature, °C	850	1020
	Time, h	100	10
	Cooling	50°C/h	air quench

form of teflon spray lubricant* was applied to the ends of the specimens to reduce friction.

Room-temperature compression testing was carried out on an Instron testing machine; the variable-speed control was used so that, for the different specimen heights, an initial strain rate of 1×10^{-3} s^{-1} was obtained. Deformation was continued to ~8% strain, and the specimen contraction was measured by means of a linear variable differential transformer (LVDT) mounted within the compression head and adjacent to the specimen. The Instron chart was driven by the output from the LVDT, with a sensitivity of 1in/10 μm in of specimen contraction. The output from the load cell was connected to the recorder pen so that load-contraction curves were plotted directly. From the chart, the 0·2% proof stress and the flow stress at 7·4† engineering strain were evaluated. In addition to the tests carried out on hot-deformed material, annealed samples, i.e. samples free of substructure, were tested in compression. These tests provided a datum from which the influence of substructure on strength could be evaluated.

High-temperature compression testing

In order to extend the available range of subgrain sizes for the Armco iron and silicon steel, further samples were prepared at the extremes of strain rate and temperature. Substructure-free cylinders were first prepared by strain annealing which produced grain sizes of ~0·1 mm and 0·5 mm in the Armco iron and silicon steel respectively. The specimen geometry and preparation are described in Table II. The specimens were annealed in an argon atmosphere. The straining, by compression, was carried out in the room-temperature Instron, barrelling being prevented by using a piece of 0·05 mm thick teflon tape at each end of the specimen. Substructure-free aluminium was produced by annealing the extruded material for 4 h at 600°C followed by cooling at 50°C h^{-1}

The high-temperature compression tests were carried out in another Instron modified to produce constant true strain rates.[6] A Hewlett–Packard high-speed, two-pen recorder was used to monitor the load and contraction at the highest strain rate. The specimens were compressed in an argon atmosphere and were quenched within ~2 s of the removal of the load. Samples of both the Armco iron and the silicon steel were deformed at 600° and 850°C. The glass lubricants for use at these two temperatures had the following compositions[4]: 20%B_2O_3 and 80%PbO; and 5%SiO_2, 10%B_2O_3, 50%PbO, and 25% window glass, respectively. The parameters relating to the hot deformation are given in Table III, together with the resulting subgrain sizes.

Specimen preparation for subgrain size measurement

Both optical and electron microscopy were used for the determination of subgrain size for Armco iron and silicon steel. In preparation for optical microscopy, electrolytic polishing was carried out in a stainless-steel dish, which acted as the cathode. The electrolyte consisted of 7 ml water, 133 ml glacial acetic acid and 25 g chromium trioxide, and was cooled to 18°–20°C. The specimen was rotated at 100 rev/min, 6 mm above the bottom of the dish.[24] A voltage of 30–50 V gave a current density of 1·5–2·0 A cm^{-2} for Armco iron, while a voltage of 20–25 V gave a current density of 0·2–0·3 A cm^{-2} for silicon steel. After 5 min, the Armco iron was already etched and was removed, washed, and dried. After 1–2 min, the voltage applied to the silicon-steel specimen was decreased to 10 V and etching continued for 1/2–1 min. Optical examination was carried out in a Vickers 55 metallograph.

In preparing specimens for electron microscopy, slices 0·6–0·8 mm thick were cut, by spark machining, parallel to the compression axis. The thickness was reduced to 0·2–0·3 mm by grinding. Final thinning was carried out in a solution devised by Packwood[7] consisting of 5% of HF (46%), 80% of H_2O_2 (30%), and 15% H_2O by volume. Slices were held in platinum-tipped tweezers and were moved continuously in the solution. When a hole appeared, a piece of adjacent metal was carefully cut out with a scalpel, rinsed in ethanol and dried between filter paper. Specimens were examined and photographed in a Philips EM300 electron microscope operating at 100 kV.

The subgrain size was determined as the square root of the average subgrain area by counting the number of subgrains,

*'Fluoroglide' manufactured by Chemplast Inc., Wayne, N.J., USA

†a contraction of 7·4% is equivalent to a true strain in compression of −0·0769; the equivalent engineering strain, in tension, is 8%, and this is the value used by Tabor in relating hardness and flow stress, as discussed later

TABLE III Experimental conditions of hot compression and the mean subgrain sizes produced

Material	Temperature, °C	ϵ	$\dot{\epsilon}$, s^{-1}	Delay, s	log Z	Activation energy,[4] cal/mole	σ, ksi	Measured values of d TEM μm	optical μm
Armco iron	600	0·4	1·11	2	18·2	66000	49·5	1·9	..
	850	0·2	$1·8\times10^{-3}$	2	11·0		5·1	..	5·4
	850	0·15	$7·4\times10^{-5}$	2	10·1		4·6	..	6·2
Silicon steel	600	0·4	1·11	2	19·4	80000	36·5	2·0	..
	850	0·2	$3·7\times10^{-3}$	2	12·7		5·4*	..	4·8
	850	0·15	$7·4\times10^{-5}$	2	11·0		4·0	..	10·2

*interpolated from data of Uvira[4]

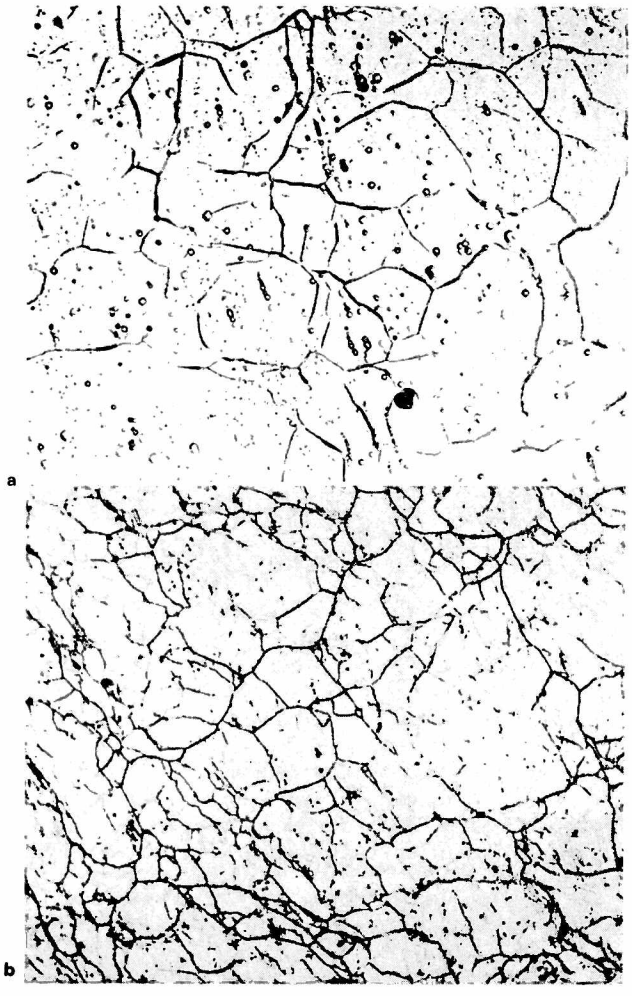

a Armco iron ×300; *b* silicon steel ×450

1 Optical micrographs of material deformed at 850°C at a constant true strain of $7{\cdot}4\times10^{-5}$ s^{-1}; strain=0.15

(a) lying wholly, and those (b) lying partly, within a rectangle of known area, A. A correction factor of unity was added to the formula given by Jeffries,[8] as recommended by Saltykov.[9] The subgrain size, d, is then given as a function of magnification X by the formula

$$d=\frac{1}{X}\sqrt{\frac{A}{a+0{\cdot}5b+1}} \quad \ldots\ldots(3)$$

RESULTS

Microstructural observations and subgrain-size measurements

The subgrain sizes of a large number of the specimens had previously been determined in studies of Armco iron and silicon steel,[2] and aluminium.[3] Hence, measurements were made only on those samples which were hot deformed in the present study. The subgrain sizes determined in the present work are listed in Table III. Typical optical microstructures are shown in Fig.1*a* and *b* for Armco iron and silicon steel, respectively. Figure 2 shows, in a typical electron micrograph, the more or less equiaxed substructure observed in Armco iron; the microstructure of the silicon steel appeared to be almost identical.

Room-temperature strength/subgrain size correlations

The measurement of the yield strength, σ_A, of all three materials in the annealed condition simplified the correlation of strength and subgrain size considerably. The influence of the deformation-induced substructure was measured by subtracting σ_A from the measured room-temperature yield stress, σ. The empirical relationship employed was

$$\sigma-\sigma_A=kd^{-m} \quad \ldots\ldots(4)$$

where k and m are constants. This form permitted the determination of m as the slope of log–log graphs, Fig.3. The values of m, and the standard errors, determined by regression analysis of the data obtained in the present study are $1{\cdot}03\pm0{\cdot}05$ for Armco iron, $0{\cdot}98\pm0{\cdot}03$ for silicon steel, and $1{\cdot}12\pm$

2 Electron micrograph of Armco iron deformed at 600°C at a constant true strain rate of 1·11 s^{-1}; strain=0·4 ×18500

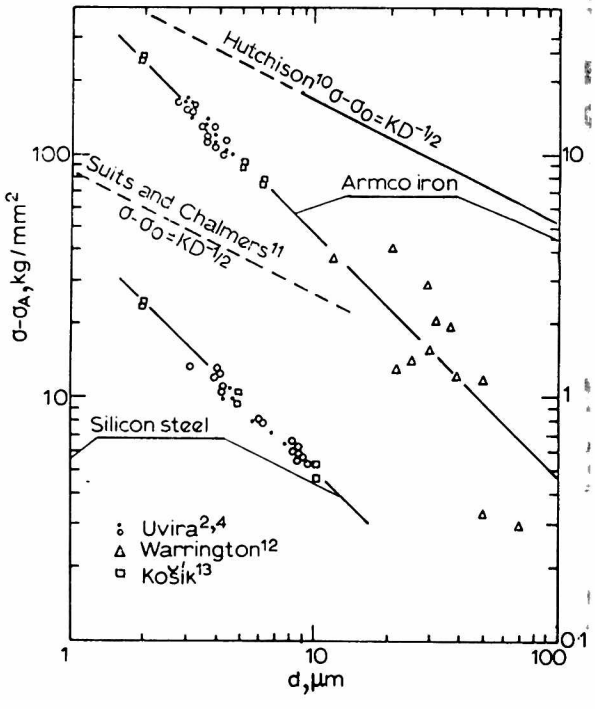

lines representing the true Hall–Petch equation for grains are also shown

3 Room-temperature strength increment due to substructure formation as a function of subgrain size for Armco iron and silicon steel

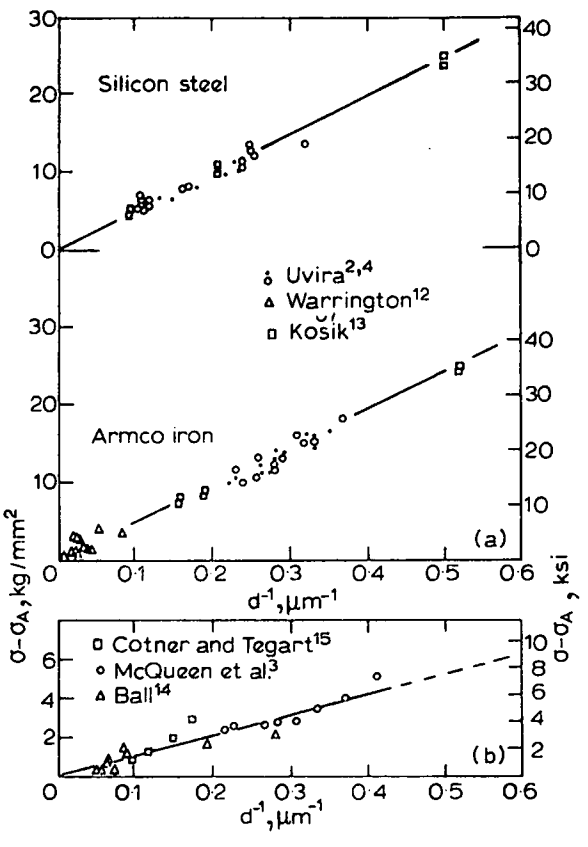

a Armco iron and silicon steel; *b* aluminium

4 Room-temperature strength increment as a function of subgrain size

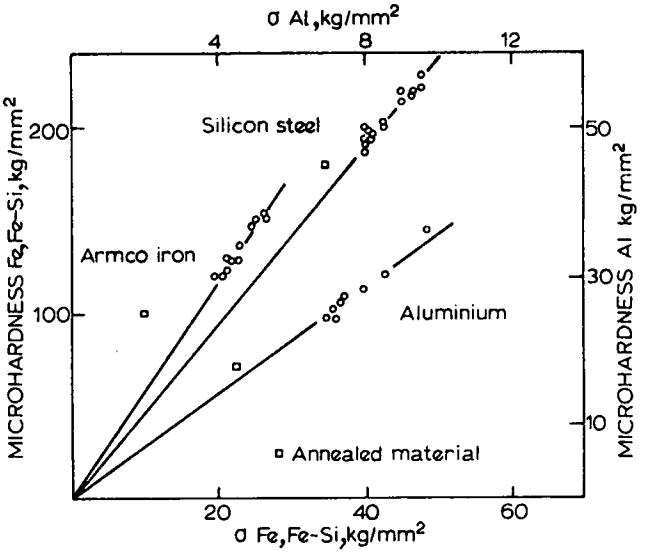

5 Microhardness v. 0.2% yield stress for Armco iron, silicon steel, and aluminium

0·16 for aluminium. The data for the three materials are shown in Fig.4, plotted against d^{-1}. Data obtained in high-temperature tensile tests by Warrington[12] have been added to Figs.3 and 4*a*; the value of σ_A was estimated from the Hall–Petch terms $\sigma_0(\simeq M\tau_0)+KD^{-\frac{1}{2}}$. Estimates of these terms were also made for the aluminium used by other investigators; these data have been incorporated into Fig.4*b*. The estimated components of σ_A, together with the values measured on the materials used in the present investigation, are shown in Table IV.

Hardness/flow-stress correlations

Although not a major part of the investigation, it is of interest to compare the present yield-stress and flow-stress results with the microhardness results obtained in the earlier investigations.[4,17] The yield strength and hardness results are presented in Fig.5. From this graph, the ratios of microhardness to yield strength were found to be 5·9, 4·8, and 3·6 for the Armco iron, silicon steel, and aluminium, respectively. The latter value was used to convert the hardness data of Cotner and Tegart[15] to equivalent yield stress for inclusion in Fig.4*b*. Anomalously high values of 10, 5·2, and 3·9 were obtained for the annealed materials; the anomaly is attributable to the initially high rate of work hardening of an annealed material.[1] Ratios of the microhardness to flow stress at 7·4% strain were also evaluated, Fig.6, for comparison with the values obtained by Tabor[18] of 2·9–3·0. Values obtained in the present study were 3·5, 3·1, and 2·5 for Armco iron, silicon steel, and aluminium, respectively.

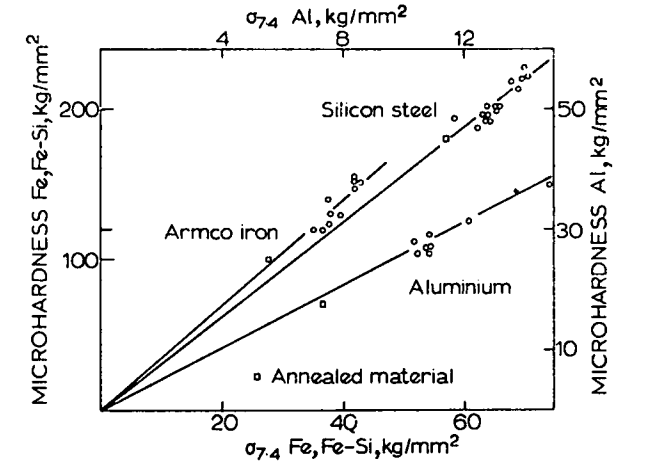

6 Microhardness v. flow stress at 7·4% engineering strain for Armco iron, silicon steel, and aluminium

TABLE IV Mechanical property data for silicon steel, Armco iron, and aluminium

Material	Purity	Reference	σ_0, kg/mm²	Grain size D, μm	K, kg/mm$^{3/2}$	$KD^{-1/2}$, kg/mm²	$\sigma_{0.2}$[19], kg/mm²
Fe–Si	Fe–2·7%Si 0·03%C 0·01%N	2	30·6	500	..	..	34·6
Armco iron	Fe–0·03%C 0·007%N	2	5·4	100	..	..	10·0
	99·97	12	5·4	1 000	1·67[10]	1·67	..
Aluminium	99·7	3	1·1	150	..	..	4·5
	99·994	14	0·31	200	0·36[16]	0·75	..
	99·86	15	1·1	15–30	0·36[16]	2·8	..

DISCUSSION

Practical implications of the present results

The linear relationship established between $\sigma - \sigma_A$ and d^{-m} in the log–log graphs, Fig.3, confirms the strong dependence of the flow stress on subgrain size, as proposed in an earlier paper.[1] The value of $m \simeq 1$ is substantially larger than previously suggested*. For all three materials, m is somewhat greater than $\frac{1}{2}$, so that the validity of equation (4), or the alternative formulation

$$\sigma = \sigma_0 + KD^{-\frac{1}{2}} + kd^{-m} \quad \ldots\ldots\ldots\ldots\ldots\ldots\ldots\ldots\ldots\ldots (5)$$

is established. Note that, particularly as d approaches D, care should be exercised in the experimental determination of the sub-boundary density so as to distinguish it from the total boundary density, as discussed elsewhere.[19]

The determination of the value of m allows the data to be plotted on standard graph paper as $\sigma - \sigma_A$ v. d^{-m}. On either this type of graph, or on a log–log plot, extrapolation outside the experimental range is permissible only to a limited degree. Such an extrapolation would suggest that the introduction of 1 μm subgrains into the materials used in this investigation should give yield strengths. of 56, 83, and 21·5 kg/mm^2 (80000, 118000, and 31000 lb/in^2) respectively for Armco iron, silicon steel and aluminium. The highest strengths found in the present study were 35, 59, and 9·7 kg/mm^2 (50000, 84000, and 13800 lb/in^2), corresponding to subgrain sizes of 1·9, 2·0, and 2·5 μm respectively for the three materials. The contribution of the deformation-induced substructure amounted to ~71, 41, and 54% of the yield stress, respectively. The use of fine-grained starting material instead of the coarse-grained metal used in the present study would decrease the proportion of strength contributed by the substructure, but could give rise to a substantial increase in the total yield stress, due to a true Hall–Petch effect, as implied in equation (5). Still higher room-temperature strengths could be produced by hot deforming at higher values of Z, the temperature-compensated strain rate. This could be achieved, for the ferrous materials, by warm working (at ~600°C) at strain rates greater than ~1/s^{-1}. The resulting elongation of the grains would be equivalent to grain refinement, and the strength increment attributable to this may be significant. It is appreciated also that adiabatic heating may lead to appreciable temperature increases in material being deformed at high strain rates, making the attainment of very high Z conditions more difficult.

It is of interest to note that the relationship between $\sigma - \sigma_A$ and d, referred to above, is similar to that between the high-temperature flow-stress σ_T and d, viz., $\sigma_T = K'd^{-q}$, where $q \simeq 1{\cdot}5$ for most metals.[20] This suggests that a simple correlation of the room-temperature strength and the high-temperature deformation conditions may be possible. From the equations

$$\sigma - \sigma_A = k\,d^{-m},\ \sigma_T = K'd^{-1{\cdot}5},\ \dot{\epsilon} = A'\sigma_T^n \exp(-Q/RT)$$

and

$$Z = \dot{\epsilon}\exp(Q/RT)$$

both $\sigma - \sigma_A$ and σ_T can be shown to be related to powers of Z. (Here k, m, K', A', Q, and R are constants.) This indicates that the logarithms of $(\sigma - \sigma_A)$ and Z on the one hand and σ_T and Z on the other are linearly related. In Fig.7, straight lines are fitted to these two linear relationships. It should be noted that, on the basis of the above relations, log σ and log Z are *not* linearly related, although the departure from linearity is not significant over the present experimental range. In view of the greater utility for predictive purposes of a linear relationship, a straight line is drawn through the σ/Z data points in Fig.7. The incorporation of the high-temperature flow stress σ_T on the same graph permits the estimation of the force required for hot deformation. The beneficial effects of warm rolling on room-temperature strength have already been investigated on a laboratory scale for some low- and medium-carbon steels. It is found, however, that an increase

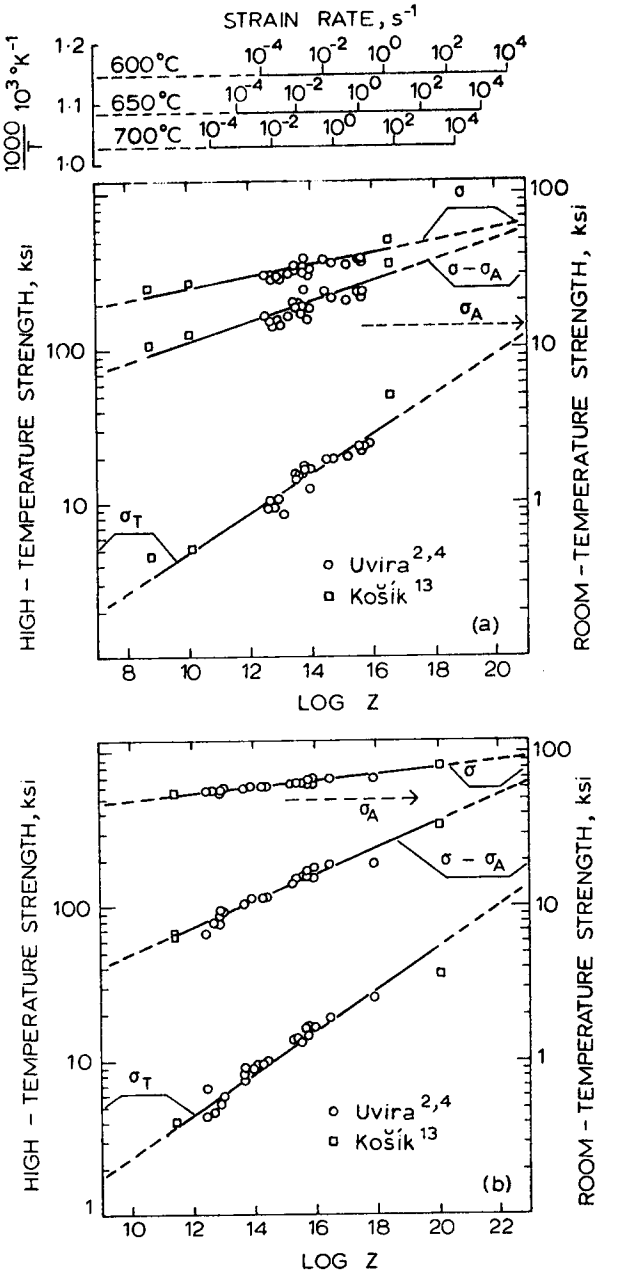

a Armco iron, Q=66 kcal mole^{-1} (ref.4); *b* silicon steel, Q=80 kcal mole (ref.4)

7 The room-temperature strength, σ, and strength increment, $\sigma - \sigma_A$,[13] and the high-temperature steady-state flow stress, σ_T,[4] plotted against the logarithm of the temperature-compensated strain rate, $Z(=\dot{\epsilon}\exp(Q/RT))$; typical warm working temperatures, T, and a range of strain rates, $\dot{\epsilon}$, are also shown

*It should be noted that, in the graphs presented previously, $m = \frac{1}{4}$ was used. The difference in the exponent is attributable to two causes. First, in the present work σ_A is used as a datum from which the substructure strengthening is measured, not σ_0 as in the previous treatment. Second, the ratio of hardness to yield stress for the annealed material was previously assumed to be twice the equivalent ratio for substructure strengthened material; from the present experiments, it is found that the value of this factor is not 2, but 1·8, 1·1, and 1·1 for Armco iron, silicon steel, and aluminium, respectively.

in strength is accompanied by some loss of ductility in the low-carbon steels.[21]

The present findings support the view advanced by Robbins and co-workers[22] that the final reductions of ferrous materials should be in the high-temperature ferritic region, i.e. below the γ–α transition temperature. It should be recalled that the strength and ductility of α-iron worked at 760° – 860°C is similar to that of γ-iron in the range 950°–1050°C.[22] Thus, delaying the final pass in a hot-rolling sequence to allow cooling by about 200°C results in only minor changes in the hot-rolling load. However, the expected increase in room-temperature strength in Armco iron is ~15000 lb/in² (log $Z=13$, Fig.7*a*) if recrystallization during cooling is prevented. Similar considerations should apply to steels and other ferrous materials warm rolled below the A_3 temperature.

Comparison with the true Hall–Petch relationship and with theory

In the previously proposed modified Hall–Petch relationship it was suggested that an increase in sub-boundary strength with decrease in subgrain size was responsible for the negative exponent of d having a value greater than $\frac{1}{2}$. The increase in strength was attributed to an increase in the sub-boundary misorientation, and in the redundant dislocation content of the sub-boundaries.[1] It was also suggested that the range of the local or true Hall–Petch slopes applicable to data in the hot-working range obtainable from a σ v. $d^{-\frac{1}{2}}$ plot, was from 0·3 to 0·7 of that of the grain-boundary data. In the present study, the ranges of the true Hall–Petch slopes * expressed as fractions of the grain-boundary values were 0·4 – 0·7; 0·2 – 0·4; and 0·5 – 0·7 for Armco iron, silicon steel, and aluminium, respectively. According to a theory of Li,[23] the local value of the true Hall–Petch slope K should be proportional to the square root of the sub-boundary misorientation, $\theta^{\frac{1}{2}}$. Thus, the misorientation would be expected to change by factors of 2·9, 4·4, and 2·3 for the three materials respectively, according to the ranges of values for K given above. These ranges are probably greater than the actual changes in misorientation through the range of subgrain sizes studied. Thus, it is reasonable to ascribe at least a part of the increase in K to an increase in redundant dislocation content as d decreases.

It is of interest to note that, on the log–log graphs of Fig.3, a line representing Hall–Petch data for grain boundaries has a slope of $-\frac{1}{2}$. Such a line must intersect the lines drawn through the present experimental data. It is found that the intersection occurs at subgrain sizes $<1\,\mu$m. Thus, the introduction of hot-work substructures by warm rolling at high strain rates may be expected to give strength increments comparable with those obtained by grain refinement in the submicron range.

CONCLUSIONS

1. The preservation, by rapid cooling, of a substructure produced at high temperatures has been found to give appreciable room-temperature strengthening in Armco iron, silicon steel, and aluminium. The strength, σ, varies linearly with the inverse subgrain size, $1/d$, and can be represented by the equation

$$\sigma = \sigma_0 + KD^{-\frac{1}{2}} + kd^{-1}$$

where K and k are constants. Here σ_0 is the Hall–Petch 'friction stress' and D is the grain size. The above equation, which has been substantiated for $D>>d$, permits the correlation of data over a wide range of subgrain sizes. Furthermore, an approximately linear relation between log σ and log Z permits the correlation of room-temperature strength with the high-temperature deformation conditions.

2. At least part of the increase in sub-boundary strength, as the subgrain size decreases, is attributable to an increase in the redundant dislocation content of the sub-boundaries.

3. The maximum strengths observed were 35, 59, and 9·7 kg/mm² (50000, 84000, and 13800 lb/in²) in Armco iron, silicon steel, and aluminium, at subgrain sizes of 1·9, 2·0, and 2·5 μm respectively. The strength increments attributable to the substructure were ~25 kg/mm² (35000 lb/in²) for the ferrous materials and ~6 kg/mm² (8500 lb/in²) for the aluminium.

4. Ratios of hardness to yield strength were evaluated. For Armco iron, silicon steel, and aluminium the values were 5·5, 4·8, and 3·6 respectively. Higher values (10·0, 5·2, and 3·9) were observed for the annealed material, due to the higher initial rate of work hardening. Ratios determined from the hardness and the flow stress at 7·4% strain in compression were 3·5, 3·1, and 2·5 respectively. These values differ somewhat from those quoted by Tabor of 2·9 – 3·0.

ACKNOWLEDGMENTS

The authors are indebted to Atomic Energy of Canada Ltd and the National Research Council of Canada for financial support. Helpful discussions with J. -P. A. Immarigeon, M. J. Luton, H. J. McQueen, and J. L. Uvira are gratefully acknowledged. The authors wish to express their appreciation to to M. J. Luton for assistance with the high-temperature compression tests.

REFERENCES

1. D. J. ABSON and J. J. JONAS: *Met. Sci. J.*, 1970, **4**, 24.
2. J. J. JONAS *et al.*: *Trans. Japan Inst. Met.*, 1968, **9**, 257.
3. H. J. MCQUEEN *et al.*: *Can. J. Phys.*, 1967, **45**, 1225.
4. J. L. UVIRA: Ph. D. thesis, 1967, McGill University, Montreal.
5. 'Standard methods of compression testing of metallic materials at room temperature', ASTM Standards E9–67.
6. M. J. LUTON and J. J. JONAS: *Can. Met.Q.*, 1971, **10**, in press.
7. R. PACKWOOD: private communication quoted in ref. 4.
8. 'Estimating the average grain size of metals', ASTM Standards E112–63.
9. S. A. SALTYKOV: 'Stereometric Metallography', 1958, Moscow, Metallurgizdat.
10. M. M. HUTCHISON: *Phil. Mag.*, 1963, **8**, 121.
11. J. C. SUITS and B. CHALMERS: *Acta Met.*, 1961, **9**, 854.
12. D. H. WARRINGTON: *JISI*, 1963, **201**, 610.
13. O. KOŠÍK: M.Eng. Thesis, 1970, McGill University, Montreal.
14. C. J. BALL: *Phil. Mag.*, 1957, **2**, 1011.
15. J. R. COTNER and W. J. MCG.TEGART: *J. Inst. Met.*, 1969, **97**, 73.
16. R. P. CARREKER and W. R. HIBBARD: *Trans. AIME*, 1957, **209**, 1157.
17. W. A. WONG *et al.*: *J. Inst. Met.*, 1967, **95**, 129.
18. D. TABOR: 'The hardness of metals'; 1951, Oxford, Clarendon Press.
19. D. J. ABSON and J. J. JONAS: *J. Nuclear Mat.*, 1971, **28**, in press.
20. J. J. JONAS *et al.*: *Met. Rev.*, 1969, **14**, 1.
21. J. L. UVIRA *et al.*: Paper presented at the Canadian conference of metallurgists, Hamilton, Ontario, August 1970.
22. J. L. ROBBINS *et al.*: *JISI*, 1961, **199**, 176.
23. J. C. M. LI: *Trans. Met. Soc. AIME*, 1963, **227**, 239.
24. C. E. MORRIS: *Met. Prog.*, 1949, **56**, 696.

*The *true* Hall–Petch slope K appropriate to materials containing subgrains of size d can be determined from a log $(\sigma-\sigma_A)$ v. log d plot of slope $m\simeq1$ as follows. A line of slope $-\frac{1}{2}$ is drawn through the data points at the chosen value of d and is extrapolated to d equals unity in the appropriate units. The ordinate at that point is equal to K.

THE TRANSITION FROM MULTIPLE TO SINGLE PEAK RECRYSTALLIZATION DURING HIGH TEMPERATURE DEFORMATION

J.J. JONAS and T. SAKAI*

Department of Metallurgical Engineering
McGill University, 3450 University St.,
Montreal, Canada, H3A 2A7

Résumé: Les modèles de Steinemann, de Luton et Sellars, et de Sah, Richardson et Sellars, décrivant la transition de la recristallisation périodique à la recristallisation continue, sont passés en revue et critiqués. Il est ainsi montré que le critère fondé sur l'égalité entre la déformation au maximum de contrainte et la déformation pendant la recristallisation ($\varepsilon_p = \varepsilon_x$) ne s'applique pas dans le cas de déformation homogène comme la traction et la compression. En effet, ce critère s'appuyait sur des données expérimentales de torsion, ce qui conduisait à des courbes contrainte - déformation déformées et erronées à cause des gradients de déformation et de vitesse de déformation existant dans les échantillons. Les récents résultats de Sakaï et ses co-auteurs au Japon sont également décrits ici. Ceux-ci ont montré que l'existence d'un seul ou de plusieurs maxima de contrainte est liée respectivement à l'*affinage* et au *grossissement* des grains. Pendant le *grossissement*, les oscillations s'arrêtent quand la taille de grain stable est obtenue. Après un seul pic de contrainte, l'adoucissement prend fin quand l'*affinage* des grains aboutit à un équilibre ou une structure stable.

La relation entre la taille de grain à l'état stable D_s et la vitesse de déformation corrigée par la température Z est décrite, ainsi que la relation entre la vitesse corrigée critique Z_c d'une part et la taille de grain initiale D_o d'autre part. Nous avons démontré que la correspondance entre ces deux relations aboutit à un critère simple, fondé sur la considération des tailles de grain, permettant la distinction entre les comportements à un seul ou à plusieurs pics. Le comportement à un pic se rencontre quand $D_o > 2D_s$, alors que la condition inverse $D_o < 2D_s$ conduit à plusieurs maxima. La contre expérience qui a permis de vérifier ce critère est décrite également.

Enfin, un modèle simple, reposant sur la considération de densité de germes de recristallisation, permet d'expliquer les deux types de comportement. D'après ce modèle, la recristallisation est synchronisée à travers le matériau (et la courbe est alors cyclique) s'il y a une grande densité de germes potentiels dans chaque nouveau grain. Ceci est valable pour les matériaux ayant au départ une structure à grains *fins* et aboutit à une faible variation $\Delta\varepsilon_c$ de la déformation nécessaire à la germination. Dans les matériaux ayant une structure initiale à *gros* grains, il y a, par opposition, très peu de germes potentiels. Une très grande variation de l'orientation des grains et de la désorientation des joints de grain provoque un étalement des valeurs de la déformation nécessaire à la germination. De ce fait, la recristallisation n'est ni synchronisée ni homogène dans l'espace, et l'on obtient qu'une valeur moyenne de la contrainte, ce que empêche l'étude du phénomène local. La condition limite de l'obtention d'un étalement dans les valeurs de la déformation est $\Delta\varepsilon_c = \varepsilon_c$, où ε_c est la déformation nécessaire à la germination dans les parties les plus favorisées du matériau.

Summary: The models of Steinemann, of Luton and Sellars, and of Sah, Richardson and Sellars for the transition from periodic to 'continuous' recrystallization are reviewed critically. It is shown that the transition criterion founded on the equivalence of the peak and recrystallization strains ($\varepsilon_p = \varepsilon_x$) does not apply to homogeneous modes of deformation such as tension or compression. This is because the previous condition was based on torsion test data, and these lead to distorted (and misleading) derived flow curves because of the strain and strain rate gradients present in solid bars. The recent results of Sakai and co-workers in Japan are also reviewed. These authors showed that single and multiple peak behaviour are associated with grain refinement and grain coarsening, respectively. During grain coarsening, the oscillations cease when the final, stable grain size is attained; following a single flow stress maximum, flow softening comes to an end when grain refinement finally leads to the equilibrium or steady state grain structure.

The dependence of twice the stable grain size ($2D_s$) on the temperature-corrected strain rate Z is described, as is that of the transition value of Z, Z_c, on the initial grain size

---

*On leave from the University of Electro-Communications, Tokyo, Japan.

D_o. It is shown that the correspondence between these two relations, first pointed out by Sakai and co-workers, permits the use of a simple criterion based on grain size considerations for distinguishing between single and multiple peak behaviour. The former occurs when $D_o > 2D_s$, whereas the latter is observed under the converse condition, $D_o < 2D_s$. A critical experiment is described which was carried out to test this criterion.

Finally, a simple model is proposed, expressed in terms of the relative nucleus density, to provide a rational basis for the two types of flow. According to this view, the occurrence of recrystallization is synchronized throughout the material (and the flow curve is therefore cyclic), when there is a *high density* of potential nuclei within a given new grain. This condition is met in initially fine-grained materials and leads to a limited spread $\Delta\varepsilon_c$ in the nucleation strain. In initially coarse-grained materials, there is by contrast a *scarcity* of potential nuclei within a given new grain. As a result of the wide variation in grain orientations and boundary misorientations, the nucleation strain also has a wide spread; thus the progress of recrystallization is highly unsynchronized and spatially inhomogeneous, and only an average flow curve, which obscures the local behaviour, is observed. The critical condition for the spread in the nucleation strain is $\Delta\varepsilon_c = \varepsilon_c$, where ε_c is the nucleation strain in the most favoured regions of the material.

1. INTRODUCTION

The subject of dynamic recrystallization has a considerable history, reaching back to 1939, when its occurrence was first reported during the creep of Pb (1). During the twenty years that followed, most of the observations were made on metals under creep conditions (2-9), although a particularly detailed study was also carried out on ice (10) under conditions of compressive loading. More recently, several geologic materials have been examined (11-14), with a view to explaining the behaviour of 'galloping glaciers' (11) and of some of the minerals in the earth's crust (12-14). The first detailed investigation of metallic behaviour under constant strain rate conditions was published by Rossard and Blain in 1959 (15), and led to a much closer examination of the phenomena associated with dynamic recrystallization.

Rossard and Blain showed clearly that, as the strain rate of testing is increased, or the experimental temperature is decreased (see Fig. 1), the flow curves change their character from the 'periodic' form associated with cyclic recrystallization to the 'single peak' type of curve attributed to 'continuous* recrystallization'. In an elegant and now classical paper (17), Luton and Sellars suggested that the transition from 'periodic' to 'continuous' behaviour is associated with the different strain rate and temperature dependences of the critical strain to *initiate* recrystallization ε_p and the strain for the *completion* of recrystallization ε_x (see Fig. 2). On the basis of their results concerning the torsion testing of Ni, they showed that when $\varepsilon_p > \varepsilon_x$, i.e. at low strain rates and high temperatures, recrystallization is cyclic, and conversely when $\varepsilon_p < \varepsilon_x$, i.e. at relatively high strain rates and low temperatures, recrystallization is continuous. The Luton and Sellars model of 1969 was subsequently improved by Sah, Richardson and Sellars in 1973 (18). Since the pioneering work of Rossard and Blain and of Sellars and co-workers, several theoretical papers have been published dealing, from a more microscopic point of view, with the nucleation and growth of new dynamic grains (22-25).

During the period that the 'European school' of dynamic recrystallization was being established, an independent (and in some ways opposing) interpretation of the phenomenon was being developed in Japan. This was based on some painstaking experiments carried out by Sakai and co-workers (26-29), and led to the notion that the transition from periodic to single peak recrystallization depended sensitively on *grain size considerations* and could be effected at a fixed temperature and strain rate simply by varying the initial grain size (26-28). According to this view, when the initial grain size is *finer* than the equilibrium dynamic grain size, recrystallization will be periodic; conversely, when the starting grain structure is *coarser* than the equilibrium one, only a single flow stress peak will be observed (27,28).

---

*Although the expression 'continuous recrystallization' has been used in each of references 10, 15, 17 and 18 (as well as by later workers), it can lead to confusion with respect to the type of 'continuous recrystallization' which is also known as 'recrystallization in situ' (19,20). In the balance of this review, we will therefore employ, where possible, alternative terms to refer to this phenomenon.

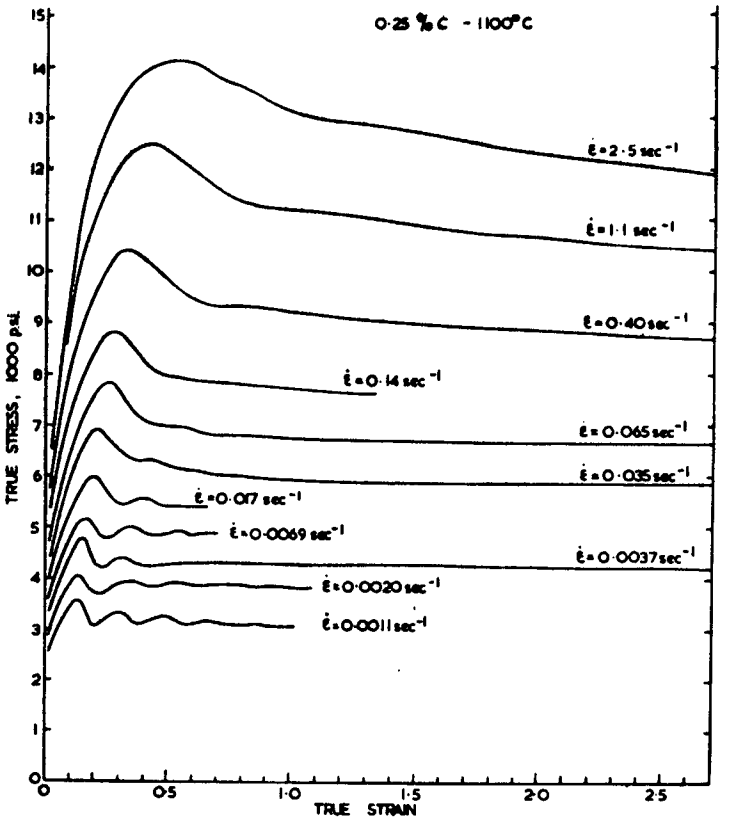

Fig. 1a Influence of strain rate on the flow curves derived from hot torsion data at 1100°C for 0.25% C steel (after Rossard and Blain (15)).

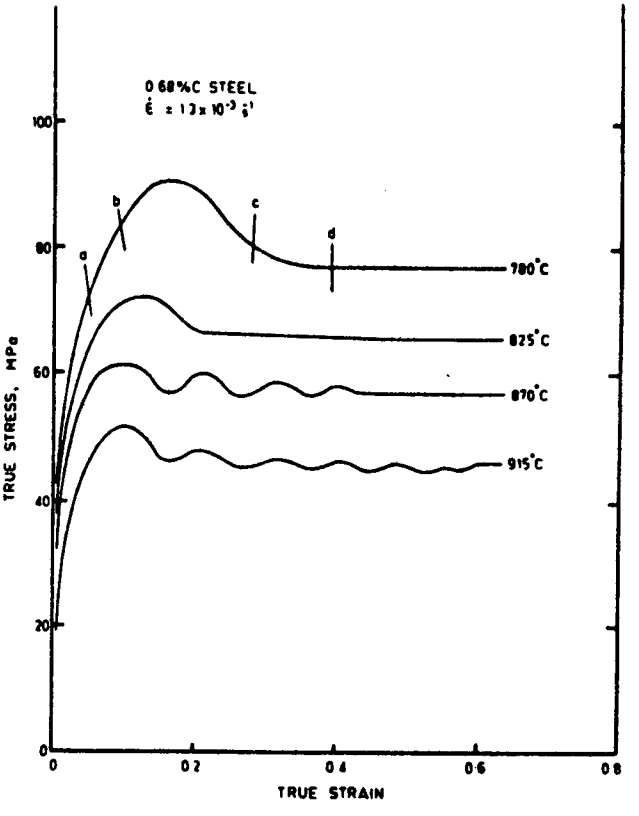

Fig. 1b Effect of temperature on the flow curves determined in axisymmetric compression on a 0.68% C steel at a strain rate of 1.3×10^{-3} s^{-1} (after Petkovic et al (16)).

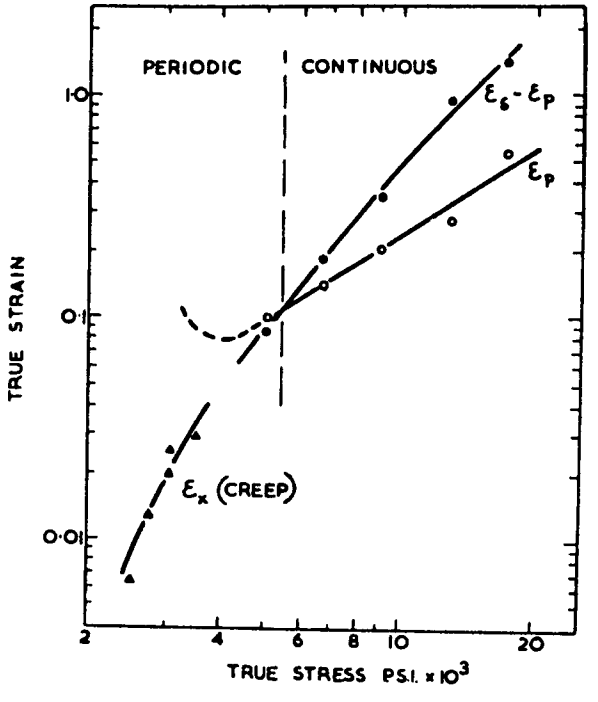

Fig. 2 Stress dependence of the strain to peak flow stress ($\varepsilon_p \cong \varepsilon_c$) and of the additional strain to the start of steady state flow ($\varepsilon_x \cong \varepsilon_s - \varepsilon_p$) for pure nickel at 934°C. Values of ε_x also calculated from data for time of recrystallization during creep of high purity nickel (21) (after Luton and Sellars (17)).

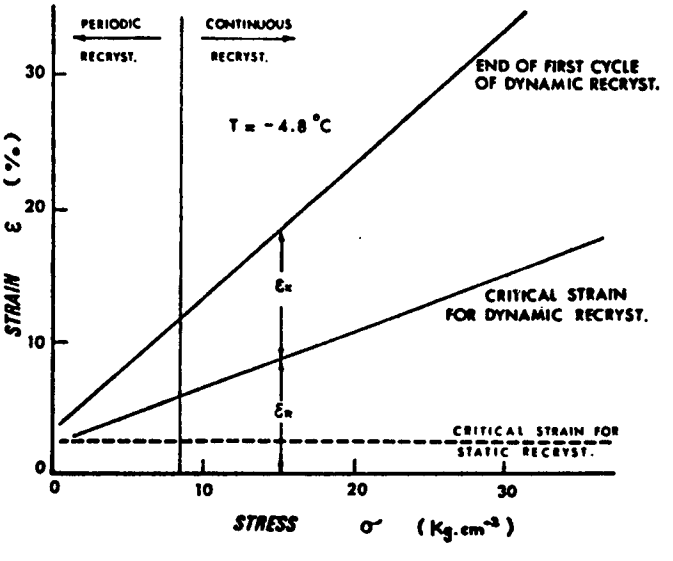

Fig. 3 A critical stress separates the regions of periodic and continuous recrystallization when ice is deformed in compression creep. Both the critical strain for the initiation of dynamic recrystallization ε_R and the strain required for the completion of recrystallization ε_x increase almost linearly with stress (after Steinemann (10)).

As the investigations of Sakai and co-workers have been published exclusively in the Japanese literature, they are not well-known to western researchers. One of the objectives of this review will therefore be to outline the principal features of the Sakai interpretation and to make some modifications to it on the basis of the most up-to-date data available. In addition, the model of Sellars and co-workers will be reassessed in the light of the extensive experimental results produced recently both in Japan (26-32) and in Canada (16, 33-39). Finally, as there is an element of conflict between the 'Japanese' and 'British' models for the transition between the two types of flow, an attempt will be made to reconcile these two approaches to the subject.

2. THE TRANSITION RESULTS OF STEINEMANN

From a historical point of view, it is relevant to record that Steinemann (10) was the first to point out (in 1958) that periodic recrystallization occurred at low, and 'continuous' or 'sustained' recrystallization at high stress levels (see Fig. 3). He also defined clearly the 'incubation' strain for the initiation of recrystallization (ε_R in Fig. 3) as well as the 'growth' strain ε_x. Steinemann's experiments were carried out on polycrystalline ice compressed between two heavy glass or metal plates and analyzed microstructurally by means of crossed polarizers. With the aid of this technique, he was able to follow the progress of dynamic recrystallization very closely, and the method has since been applied to the study of recrystallization during indirect extrusion (40).

The results of his extensive tests, carried out at -1.9, -4.8 and -11.5°C, showed that ε_R and ε_x both decreased as the temperature was increased (as did the critical strain for static recrystallization). His observations also indicated that ε_x was generally about 1.25 ε_R for periodic recrystallization, and that the $\varepsilon_x/\varepsilon_R$ ratio increased with stress to considerably higher values during 'sustained' recrystallization. (Note that ε_R was determined from *microstructural* observations and is therefore always less than ε_p.) When further cycles of recrystallization occurred, the subsequent nucleation strain ε_R (measured from the beginning of growth ε_c, i.e. from $\varepsilon_x = 0$) was usually less than the growth strain ε_x. Steinemann also studied the meta-dynamic recrystallization process closely (he called the latter 'postkinematic' and the former 'parakinematic'). For both types of behaviour he reported that the resulting grain size decreased as the applied stress was increased (the dynamic size was always finer), and that the time exponent in the usual equations describing the progress of recrystallization fell in the range 1 to 2.

It is of interest that glaciers are formed from compacted snow crystals and thus have a relatively fine initial grain size. As a result of gradual grain growth on the one hand and of dynamic recrystallization on the other, grain coarsening generally takes place, usually over a period of years. This can lead, as explained at greater length below, to a transition from flow involving periodic increases in strain rate ('galloping glaciers') to one in which the velocity remains fairly constant.

3. THE MODEL OF LUTON AND SELLARS

The results of the computer simulation of dynamic recrystallization carried out by Luton and Sellars (17) are reproduced for ready reference in Fig. 4. Two observations are of particular relevance to the discussion that will follow.

(a) Because $\varepsilon_c > \varepsilon_x$, all of the material in Fig. 4a obeys a single softening law; i.e. the nucleation of *all* new grains occurs at $\varepsilon_c \cong \varepsilon_p$, and the growth of these grains is restricted to the interval ε_x. No further nucleation events take place during ε_x and growth is substantially over before recrystallization can once more be initiated.

(b) Because $\varepsilon_c < \varepsilon_x$, the material in Fig. 4b can be divided into several 'volume fractions'. Supposing here for simplicity that dynamic recrystallization is initiated at ε_c in *all* the grains,* it is apparent that, before recrystallization is complete, the regions which first recrystallized reach the critical strain for a second nucleation. In this way, more than one cycle of recrystallization is taking place in the metal at the same time, each cycle of which is at a different stage of the recrystallization process. During steady state flow, there is an

*The case where the nucleation strain ε_c is different in different volume fractions of the material will be considered later.

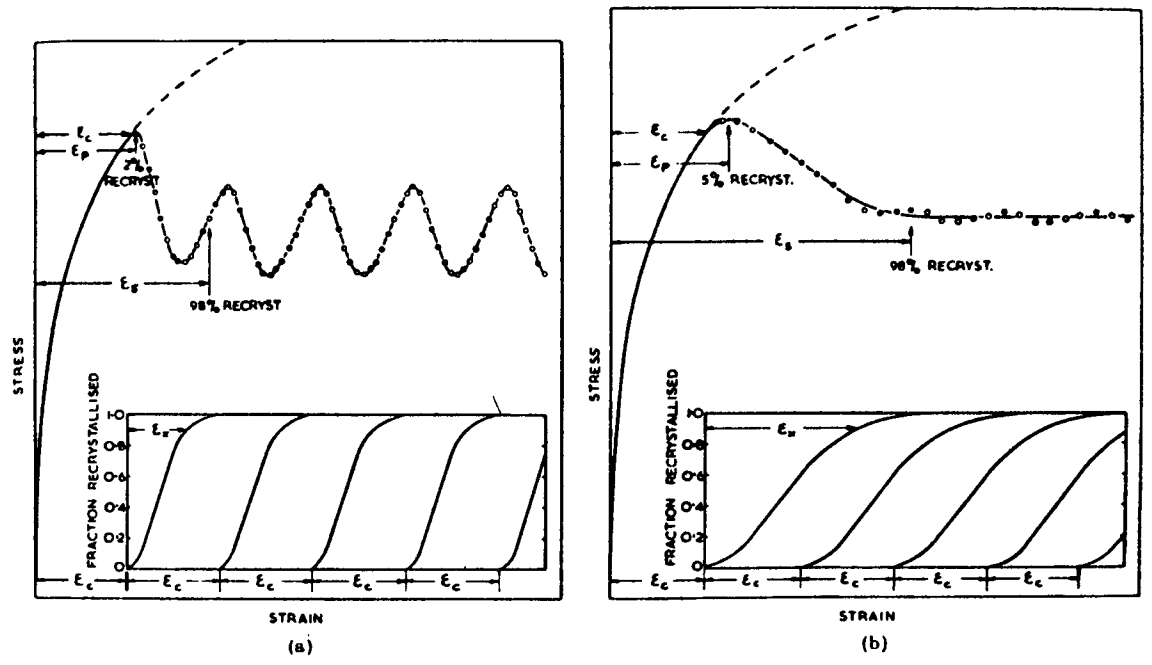

Fig. 4 Predicted stress-strain curves for dynamic recrystallization. (a) A cyclic flow curve when the critical strain to initiate recrystallization $\varepsilon_c > \varepsilon_x$, the strain occurring in the time for a large fraction of recrystallization. (b) A steady state curve for the condition when $\varepsilon_c < \varepsilon_x$. (Luton and Sellars (17)).

equilibrium distribution of regions having different strains between zero and ε_c, giving rise to a constant average flow stress (three such concurrent cycles are depicted in Fig. 4b). This 'inhomogeneous' situation is in sharp contrast to the 'homogeneous' behaviour of Fig. 4a.

Although it represented a significant advance when published in 1969, the Luton and Sellars model was acknowledged to have a number of limitations. Foremost was the fact that, consistent with observation (a) above, the alternate cycles of work hardening and recrystallization succeed each other indefinitely, whereas experimentally, they generally die out after from about two to eight cycles. Three further limitations that have been mentioned in the literature are that: (i) the steady state flow stress predicted by the model depends only on ε_c (and not, as could be expected, on ε_x as well) (18); (ii) the predicted peak and steady state strains are about a factor of two too high (18); and (iii) the predicted steady state flow stresses are lower than the experimental ones (41). Some further problems are discussed by Sellars in Ref. 42.

4. THE MODEL OF SAH, RICHARDSON AND SELLARS

In order to overcome some of the above problems, a more complex model was proposed by Sah et al. (18) in 1973. Their concepts are illustrated in schematic form in Fig. 5. The flow curves resulting from the application of this model are presented in Fig. 6. The important features of the modified model are the following.

(a) The critical strain ε_c' for the second and subsequent cycles of recrystallization can be significantly smaller than the initial critical strain ε_c (Fig. 5a).

(b) The recrystallization strain ε_x associated with a particular volume fraction of the material is considerably smaller (see Fig. 6) than the macroscopic 'recrystallization strain' ε_x (defined as the steady state strain ε_s minus the peak strain ε_p). The normalized recrystallization behaviour of the volume fraction ΔX_1 when it undergoes its second cycle of recrystallization, is shown as a broken curve in Fig. 5b.

(c) Each volume fraction undergoing a second cycle of recrystallization in Fig. 5b (e.g. ΔX_1, ΔX_2, ΔX_3, etc.) is divided into *two* separate volume fractions during the third cycle of recrystallization (a similar subdivision occurs in going from the third to the fourth, the fourth to the fifth cycles, etc.)

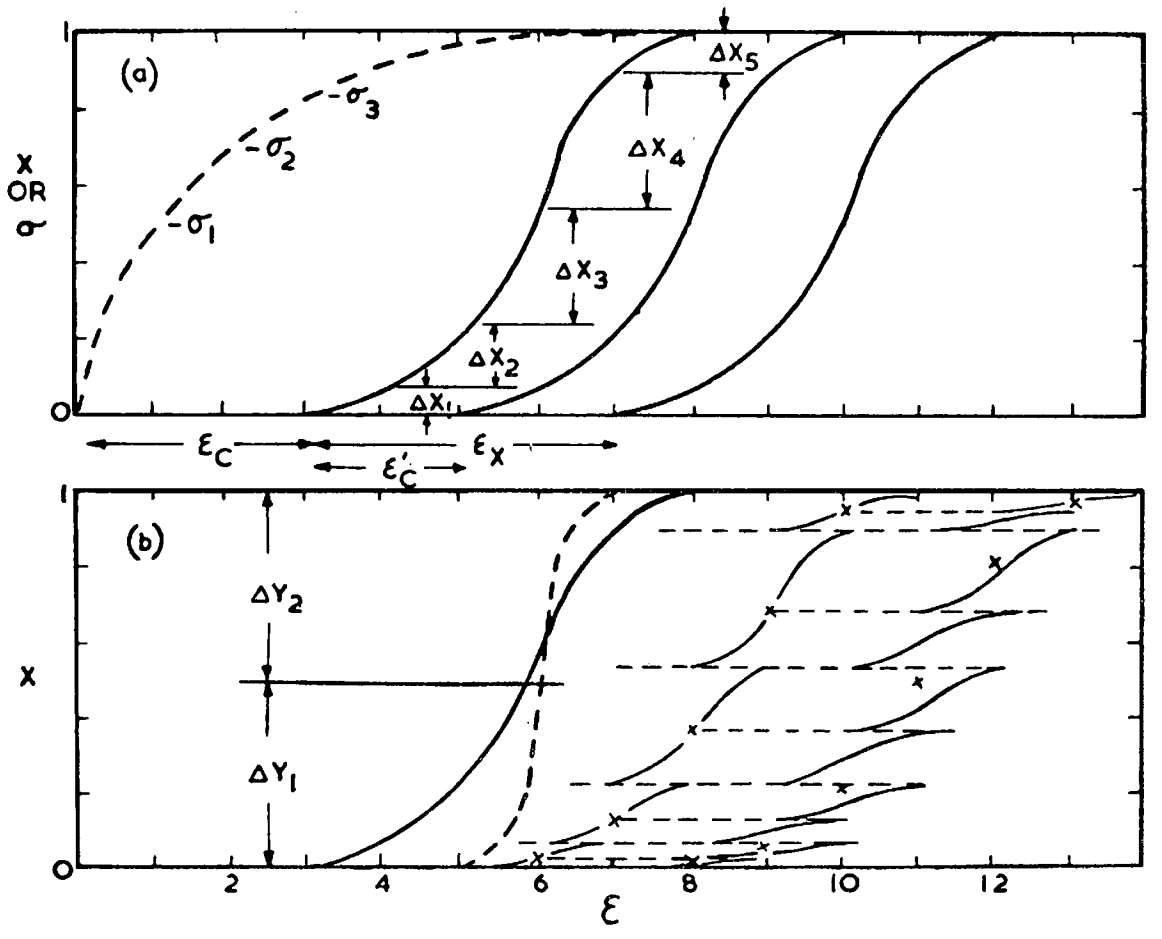

Fig. 5 Schematic diagram showing the dynamic recrystallization kinetics assumed (a) by the model of Luton and Sellars (17) and (b) by the modified model for the effect of recrystallization on flow stress (Sah, Richardson and Sellars (18)). The form of the flow curve expected in the absence of recrystallization is shown in (a).

Feature (b) is responsible for the single peak behaviour of the flow curves d/f, c/e, b/f and a/e of Fig. 6. (It was not employed for the periodic flow curves f/f and e/e.) Feature (c) is responsible for the gradual damping out of the oscillations in curves f/f and e/e. These two features were not given a physical basis in references 18 and 42, but can be given the following interpretation:

(i) The subdivision of the macroscopic recrystallization strain ε_x into numerous smaller entities ε_{x1} corresponds to the recognition that, in a single peak experiment, different volume fractions of the material are at different stages of the recrystallization process at a given instant of time.

(ii) The continuous subdivision of the individual volume fractions after each cycle is a recognition of the progressive 'desynchronization' of the recrystallization process that takes place during a given torsion experiment.

These two aspects of dynamic recrystallization behaviour will be examined in greater detail later in the present review after some new experimental evidence has been presented and analysed.

5. DOES THE TORSION-BASED LUTON AND SELLARS MODEL APPLY TO TENSION AND COMPRESSION?

The model of Luton and Sellars was deduced from the results of torsion experiments carried out on commercial purity nickel and three nickel-iron alloys. It is also consistent with the torsion data of Rossard and Blain (15) presented in Fig. 1a, which were obtained on a 0.25% C steel deformed in the austenite phase (see Fig. 7a). However, it is of interest that the model may not be applicable (without further modification) to other modes of

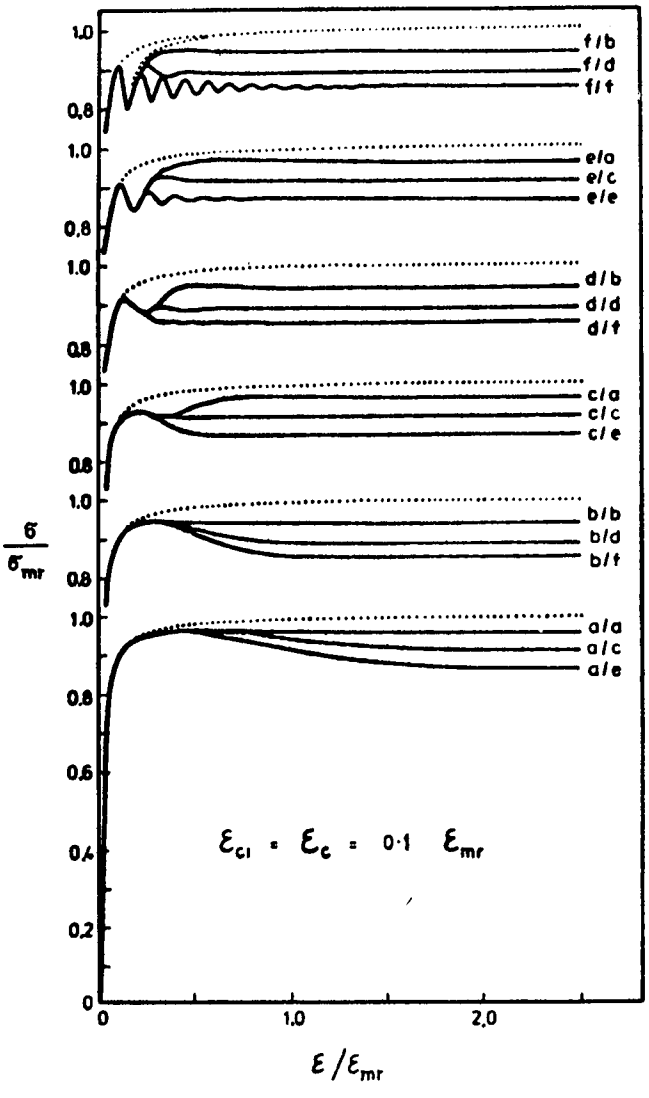

Fig. 6 Calculated form of the flow curves for dynamic recrystallization when ε_c for the first and ε_{c1} for the subsequent cycles are equal, but the rates of recrystallization differ (as represented by ε_x for the first and ε_{x1} for the subsequent cycles). Here the letters a/e, etc. indicate the values of ε_x and ε_{x1}, respectively, and are as follows: (a) $16\varepsilon_c$; (b) $8\varepsilon_c$; (c) $4\varepsilon_c$; (d) $2\varepsilon_c$; (e) ε_c; (f) $\varepsilon_c/2$. The dotted curves are expected in the absence of recrystallization. ε_{mr} is the strain required to attain 0.99 of the saturation stress σ_{mr} in the absence of recrystallization (Sellars (42)).

testing or of deformation such as tension or compression. An example is given in Fig. 7b, in which are presented the peak and recrystallization strains, ε_p and ε_x respectively, determined by Sakui, Sakai and Takeishi (26,28) on a 0.16% C steel. It can be seen that, unlike the behaviour displayed by the torsion results, the ε_p and ε_x curves do *not* intersect in this case. A similar lack of intersection is observed in the ε_p and ε_x data of Petkovic (16,43), which were determined in compression on a 0.68% C steel (Fig. 7c). It should be noted that when ε_p and ε_x are measured in tension or compression, they are *less* than the corresponding torsion values associated with the same peak stress. It is particularly relevant to the present discussion that the ratio ε_p (torsion)/ε_p (tension or compression) is considerably smaller than the ratio ε_x (torsion)/ε_x (tension or compression).

As these differences between the characteristics of torsion and axisymmetric flow curves are of considerable importance with regard to the conclusions of the present review, some of the possible factors responsible for the ε_p and ε_x discrepancies will be introduced at this point. Then, after the presentation of some metallographic evidence concerning grain size changes during dynamic recrystallization, an alternative model will be introduced and discussed.

6. WHY DO THE PEAK AND RECRYSTALLIZATION STRAINS DETERMINED IN TORSION DIFFER FROM THOSE DERIVED FROM TENSION OR COMPRESSION DATA?

In this section, we present two different features of torsion testing which affect the flow curves deduced from torque/twist data, and which can therefore lead to discrepancies when torsion-based flow curves are compared with those determined by more conventional techniques. The first feature involves the radial gradient in strain and strain rate which is inherent in the testing of solid bars, as a result of which ε_p and ε_x are different in each concentric cylindrical layer in the torsion bar. The effect of the spread in these two characteristic strains is illustrated in Fig. 8a. For this diagram, the simulated torsion curves were calculated on the assumptions that, (i) at a given equivalent strain rate, the rates of work hardening are equal in tension and torsion, and (ii) that the differences in the textures developed are not significant. (These assumptions are not, strictly speaking, accurate, as will be demonstrated below when Fig. 8b is discussed.)

It is evident from Fig. 8a that ε_p in torsion is *greater* than the corresponding tension value, even under the artificial condition that the same basic flow curves apply to the two

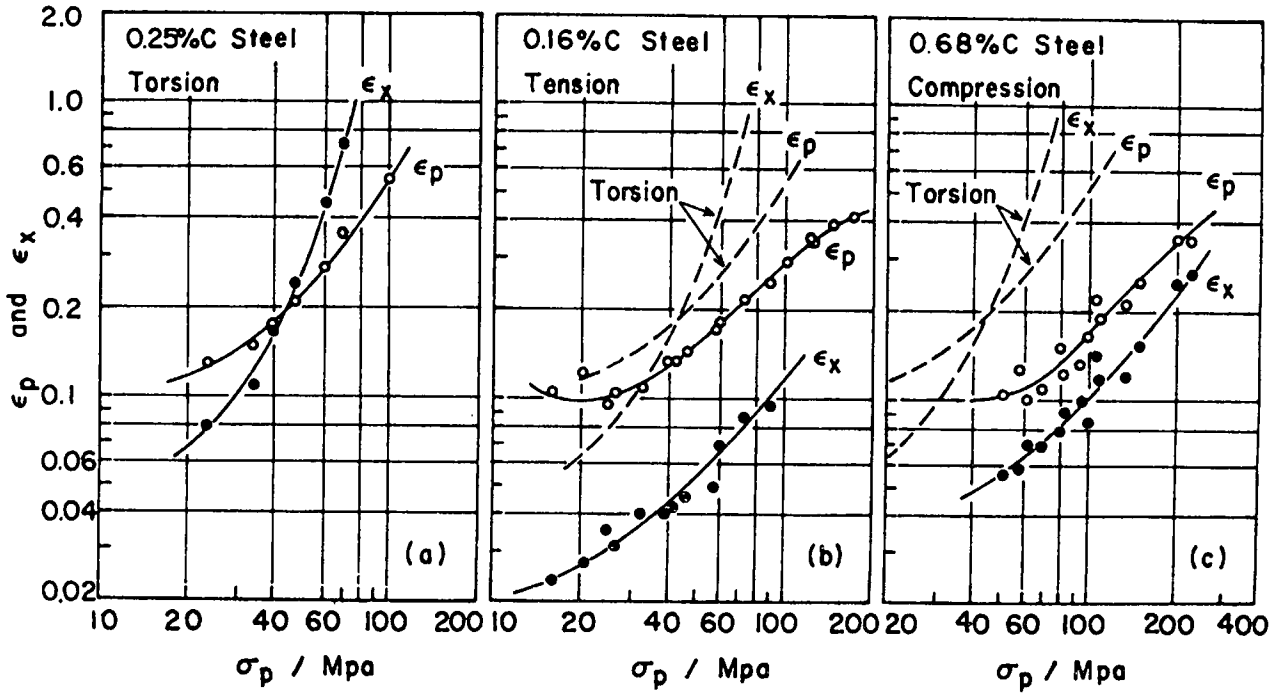

Fig. 7 Dependence of ε_p and ε_x on the peak stress σ_p. (a) Determined from the *torsion* flow curves of Fig. 1a (note intersection). (b) Determined from the *tension* data of Sakui et al. (26,28). Note that ε_p and ε_x do not intersect in this case. (c) Determined from the axisymmetric *compression* data of Petkovic (16,43). Again the ε_p and ε_x curves do not intersect.

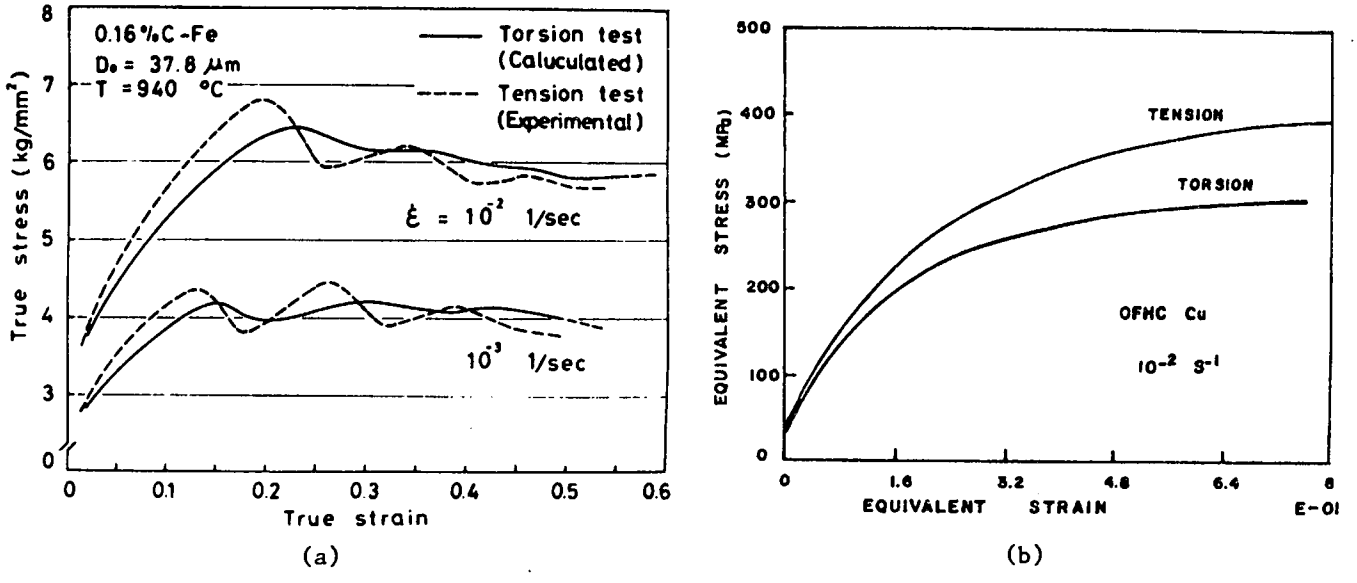

Fig. 8 (a) Comparison of *actual* true stress-true strain curves determined in tension with *calculated* torsion curves. The latter were derived from tensile data determined at the strain rate appropriate to each cylindrical 'shell' in the simulated torsion bar. The torque contributions of the individual shells were then summed and the effective stress-effective strain curves were deduced by the method of Fields and Backofen (38,44). (b) Comparison of the *actual* flow curves determined in tension and in torsion at the same effective strain rate (38). The torsion flow curve was derived by the differential method of Canova et al. (38) from experiments on ten solid bar samples of increasing radius.

testing modes. This arises from the non-linear dependence of ε_p on $\dot{\varepsilon}$, which, when combined with the *linear* dependence of ε and $\dot{\varepsilon}$ on radius in the concentric shells of the torsion bar, means that each layer attains the peak stress condition at a different *time*. Bearing in mind that the strain rate and peak stress are related by the approximate relation

$$\dot{\varepsilon} = A\,\sigma_p^{\,n} \qquad (1)$$

where $n \cong 6$, and that, from Figs. 7b and 7c,

$$\varepsilon_p \propto \sigma_p \qquad (2)$$

over much of the diagram, it can be seen that:

$$\varepsilon_p \propto \dot{\varepsilon}^{1/n} \qquad (3)$$

where $1/n \cong 1/6 < 1$. It is a consequence of relation (3) (and of the linear ε and $\dot{\varepsilon}$ distribution) that, when the outermost shell attains ε_p, the underlying layers will not yet have reached their peak strains, passing through this condition successively in an inwards direction. As a result, the torque passes through *its* maximum later (in time) than does the stress in the outermost layer. When the torque is converted into equivalent stress (e.g. by the method of Fields and Backofen (44)), the retardation of ε_p (with respect to tension) illustrated in Fig. 8a is produced.

A similar argument applies to ε_x, with a further complication (37). In the analysis described above, all the layers began the experiment in the fully annealed or recrystallized condition, i.e. their metallurgical structures were 'synchronized' at the beginning of the test. This simple picture does not apply to ε_x, however, because the zero time base or datum for ε_x is ε_p, and this is different in each layer, as indicated by Equation (3). As explained in more detail in reference (37), the net result is that there are *two* components of retardation in the torsion-based values of ε_x:

(i) one is because, given a dependence of the form

$$\varepsilon_x \propto \dot{\varepsilon}^{q} \qquad (4)$$

where $q < 1$, each layer in the torsion bar below the outermost one takes a progressively longer time in going from the ε_p to the $\varepsilon_s = \varepsilon_p + \varepsilon_x$ condition;

(ii) the second arises from the 'desynchronization' of the time base for ε_x.

It is of interest that the desynchronization of ε_p and ε_x in the various layers increases with each cycle of recrystallization (37). As a result, at the same level of flow stress, the oscillations die out fairly rapidly in torsion (e.g. at 7000 psi in Fig. 1a), but not in compression (e.g. at 50 MPa in Fig. 1b). A second effect of the increasing desynchronization is that the ratio ε_p (torsion)/ε_p (tension or compression) increases with each successive cycle (see Fig. 8a), as does the ratio ε_x (torsion)/ε_x (tension or compression).

7. EFFECT OF TESTING MODE ON THE RATE OF WORK HARDENING AND ON THE NATURE OF THE TEXTURE DEVELOPED

The *simulated* torsion flow curves of Fig. 8a were based on the premise that the basic shear stress/shear strain curves applicable to the active slip planes are identical in torsion and in tension, and on the further assumption that the differences in the textures developed can be neglected. Both of these approximations can affect the relative ease of nucleation of recrystallization as well as the growth rate of the recrystallizing grains. The extent to which the apparent rate of work hardening is different in tension and torsion is illustrated in Fig. 8b. In this case the method of Fields and Backofen (which is not rigorously valid for materials in which dynamic recovery is occurring (38)), was not used, and the torque/twist data were decomposed instead by the more general method of Canova et al. (38).

It can be seen that the flow stress at small strains (e.g. up to 0.16) is about 7-10% higher in tension than in torsion. This can be attributed to the difference in the mean Taylor factors applicable to randomly oriented grains in these two modes of testing (38), as a result of which the equivalent stress in torsion is 6.5% lower than in tension *when the critical resolved shear stresses are the same along both sets of slip planes.*

At larger strains (i.e. beyond 0.16), the discrepancy increases, as both work hardening and texture differences develop and make their individual contributions. This is because, on the one hand, the FCC torsion texture leads to a *decrease* in the mean Taylor factor, whereas the FCC tension texture leads to an *increase* (38). In addition, the combinations of slip systems which are active in axisymmetric tension and torsion (and in axisymmetric compression and torsion) are different (38,45,46), so that the dislocation distributions and misorientations developed can be expected to be differentiated as well. The detailed influence of these work hardening and texture discrepancies has not been evaluated as yet, but is likely to cause the divergence between the high temperature flow curves in torsion and tension to be *greater* than depicted in the idealized case of Fig. 8a above.

It is inherent in the arguments reviewed above that the critical condition $\varepsilon_p = \varepsilon_x$ proposed on the basis of torsion experiments is unlikely to apply to tensile and compressive deformation in general (or, by extension, to rolling and extrusion). Nevertheless, as the process of dynamic recrystallization can play an important role in both grain refinement during control rolling (47), and texture development (48), an attempt will now be made to present an alternative model for the transition from multiple to single peak behaviour.

8. THE CRITICAL ZENER-HOLLOMON PARAMETER ASSOCIATED WITH THE TRANSITION FROM PERIODIC TO SINGLE PEAK BEHAVIOUR

The metallographic evidence relating to grain size changes during dynamic recrystallization produced by Sakai and co-workers in Japan (26-29,32) has led to the proposal of a new transition model based primarily on grain size considerations. Before describing their results, however, it will be useful to define the critical value of the temperature-corrected strain rate Z_c associated with the transition. The definition is based on the dependence (see Fig. 9) of the flow stress increment $\Delta\sigma_H$ associated with the second cycle of work hardening on temperature and strain rate. From this diagram it is apparent that, as long as dynamic recrystallization is occurring, the stress drop $\Delta\sigma_s$ produced by the annihilation of dislocations increases continuously with Z and does not attain a critical value. By contrast,

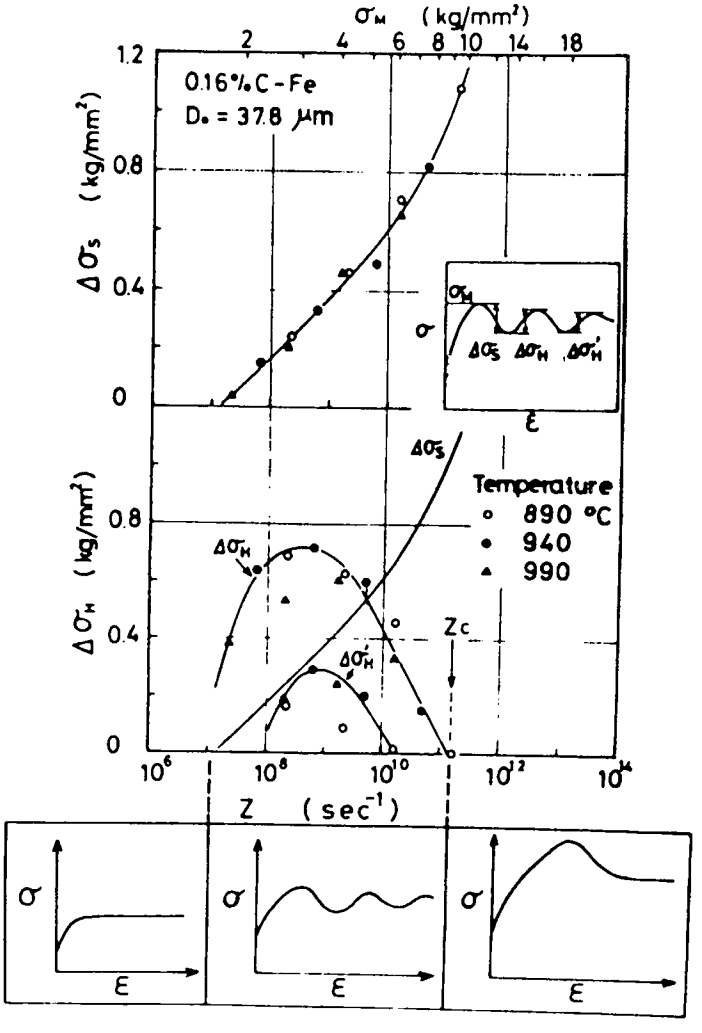

Fig. 9 Dependence of the stress drop $\Delta\sigma_s$, second cycle work hardening increment $\Delta\sigma_H$ and third cycle work hardening increment $\Delta\sigma_H'$ on temperature corrected strain rate Z. The critical value Z_c is defined as the temperature-corrected strain rate at which $\Delta\sigma_H$ goes to zero. (This figure is a modified version of the one presented earlier in refs. 27 and 28.) In the construction of Fig. 9, as well as of Fig. 14 below, a value of Q = 286 kJ/mole was used. Note also that σ_M on the upper axis refers to the maximum or peak stress.

when single peak behaviour is observed, the hardening increments associated with the second and later cycles of recrystallization vanish by definition. (In practice, there can be a *suggestion* of a second peak in 'single peak' flow curves (see Fig. 16 below), so that $\Delta\sigma_H$ may not vanish completely. Nevertheless, there is a sharp break in the dependence of $\Delta\sigma_H$ on Z which permits the definition of Z_c at least by extrapolation, as shown in Fig. 9.)

9. EVOLUTION OF AUSTENITE GRAIN STRUCTURE DURING HIGH STRAIN RATE TENSILE TESTING

In most methods of high temperature testing, it is difficult to follow the changes in austenite grain structure because of the high quench rate required in low carbon, plain carbon steels. Even when no phase change occurs, as in nickel (32) or copper (33), a fast quench is essential because of the rapid progress of metadynamic recrystallization (33) after straining is interrupted. In order to reduce the quench time to a minimum, Sakai and co-workers (26,28) constructed two specialized variable strain rate tensile machines which operate in a vacuum and which are resistance heated. At the end of each experiment, a H_2 gas quench is initiated, which enables a cooling rate of about 2500°C/s to be attained (28).

The results obtained with this equipment at 940°C on a 0.16% C steel tested in tension at 1.48×10^{-1} s^{-1} are presented in Fig. 10. The original (ε=0) austenite grain size in this experiment was 32 μm. Separate samples were quenched at strains of 0.18, 0.25, 0.44 and 0.59 (indicated as a, b, c and d, respectively on the flow curve). It is evident from the microstructures observed that grain *refinement* took place. Once steady state flow was established, an equilibrium grain size was produced, which will be considered in more detail below.

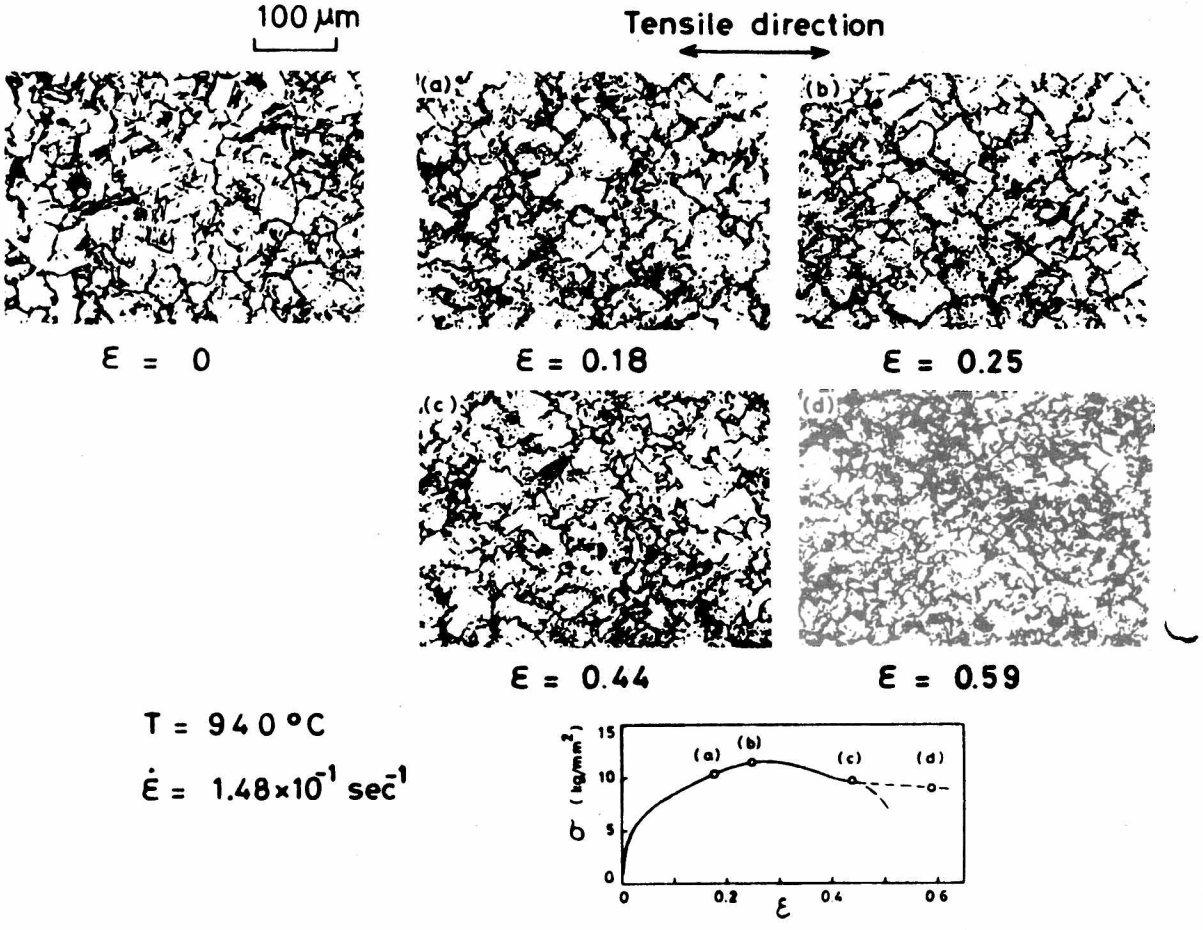

Fig. 10 Evolution of the austenite grain structure with strain in a 0.16% C steel tested in tension at 1.48×10^{-1} s^{-1}. Samples were rapid quenched using H_2 gas. Note the progressive grain *refinement* with strain (26,28).

10. EVOLUTION OF AUSTENITE GRAIN STRUCTURE DURING LOW STRAIN RATE TENSILE TESTING

The evolution of the austenite grain size at a relatively low strain rate of testing (2.6×10^{-4} s^{-1}) contrasts sharply with that shown in Fig. 10 above for the 'high' strain rate case, and is displayed in Fig. 11. In this experiment, the initial grain size was also 32 μm (illustrated at ε=0 in Fig. 10), and the micrographs pertaining to the following strains: a 0.06; b 0.09; c 0.15; d 0.22 and e 0.42, are reproduced in Fig. 11. It is apparent from this diagram that considerable grain *coarsening* took place during the experiment, which continued over three periods of recrystallization.

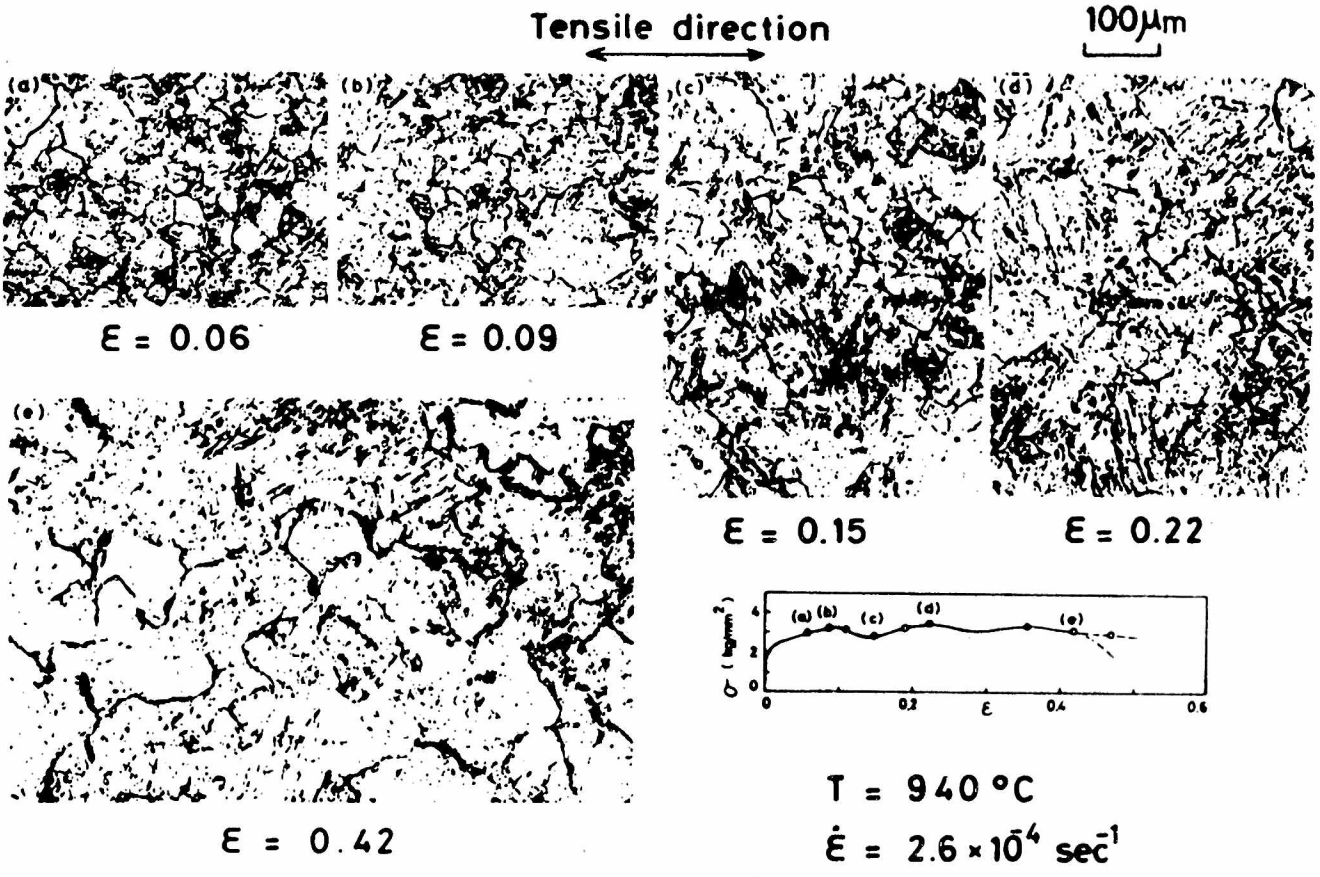

Fig. 11 Evolution of the austenite grain structure with strain in a 0.16% C steel tested in tension at 2.6 x 10^{-4} s^{-1}. Samples were rapid quenched with H_2 gas. Note the progressive grain *coarsening* with strain (26,28).

The grain size changes established from the micrographs of Figs. 10 and 11 are presented in graphical form in Fig. 12, in which the strains at which the peak stresses were observed are also indicated. The results of two further experiments, conducted at 2.0 x 10^{-3} and 2.0 x 10^{-2} s^{-1}, are included for completeness. It is clear from these data that, when grain *coarsening* takes place, multiple peak behaviour can be expected. The data also suggest that when grain *refinement* leads to at least a halving of the initial grain size, only a single peak is observed. It is of particular interest that a single 'cycle' of recrystallization (i.e. a total strain of $\varepsilon_s = \varepsilon_p + \varepsilon_x$) is sufficient to produce the final equilibrium grain size at the highest strain rate (1.48 x 10^{-1} s^{-1}). By contrast, at the lower strain rates, two or more cycles of recrystallization (i.e. two or more sets of $\varepsilon_p + \varepsilon_x$) are required before a stable grain structure is introduced, and the cycles continue until the equilibrium microstructure is attained. The physical processes likely to be responsible for such divergent behaviour will be described below, but first, consideration must be given to the dependence of the equilibrium dynamic recrystallization grain size on Z, i.e. on temperature and strain rate.

11. DEPENDENCE OF THE DYNAMIC STEADY STATE GRAIN SIZE ON TEMPERATURE AND STRAIN RATE

In order to verify that a single peak curve is associated with grain refinement, a further experiment was carried out at 940°C (26,28), but at a strain rate of 18 s^{-1} (see Fig. 13). In this case, because of the high rate, it was not possible to deform the samples into the fully developed steady state region. The steady state data displayed in Fig. 13 confirmed that single peak behaviour resulted from grain refinement, and also enabled the authors to determine the dependence of the equilibrium grain size D_s on Z (see Fig. 14a). In this diagram, the critical value of Z_c established in Fig. 9 for an initial grain size of 38 μm is also identified. As can be seen, the original grain size D_o is about 1.8 times the equilibrium grain size D_s at the critical strain rate/temperature combination. Thus it

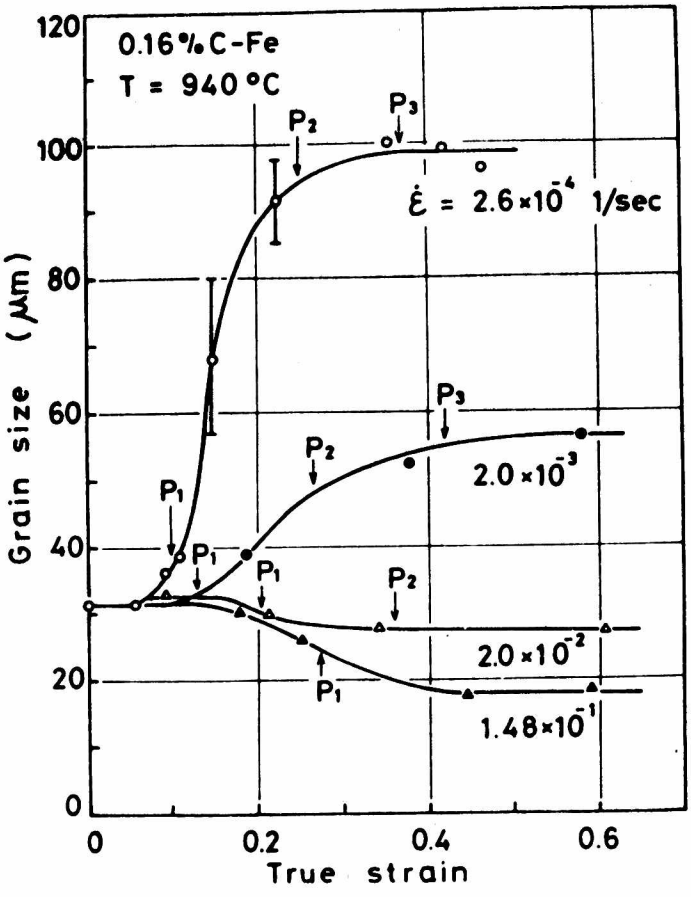

Fig. 12 Effect of strain and strain rate on the mean grain size of a 0.16% C steel deformed in tension at 940°C. P_i identifies the strain at the ith flow stress peak. Note that *multiple peaks* are observed during grain *coarsening* (and when grain refinement produces less than a 2:1 reduction in grain size). Conversely, a *single peak* is observed when the grain *refinement* ratio is about 2:1 (26,28).

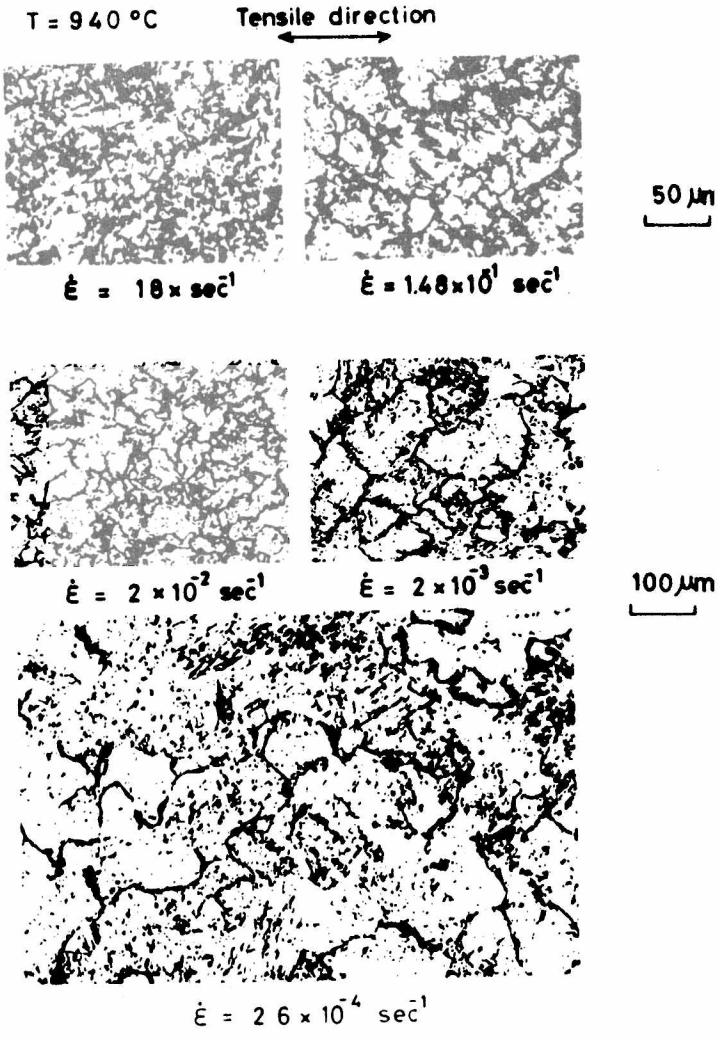

Fig. 13 Dependence of the steady-state austenite grain size on testing strain rate in a 0.16% C steel deformed in tension at 940°C and H_2 quenched. The original mean grain size was about 32 μm; grain *refinement* took place at the three highest and grain *coarsening* at the two lowest strain rates (26,28).

appears that single peak behaviour occurs when grain refinement produces at least a 2:1 reduction in grain size (which corresponds to nearly an order of magnitude reduction in grain volume).

The Z-D_s relationship of Fig. 14a is reproduced as a broken line in Fig. 14b for comparison with the Z_c vs. D_o data determined by Sakai and co-workers (26-28). These researchers showed that Z_c depended on D_o, an observation that had not been reported by earlier investigators. It can be seen that the two dependences are nearly parallel, although they do not overlap. Also displayed is the Z vs. $2D_s$ relation suggested by the remark above that the transition from multiple to single peak behaviour corresponds approximately to a 2:1 reduction in grain diameter. The latter two curves nearly overlap (full congruence occurs for the Z vs. $1.8D_s$ curve, but the Z-$2D_s$ relation is selected here for simplicity), a coincidence which permits the two flow domains to be distinguished as shown in Fig. 15.

12. A GRAIN-SIZE-BASED CRITICAL CONDITION FOR DYNAMIC RECRYSTALLIZATION

In Fig. 15, the Z_c-D_o and Z-$2D_s$ relations are plotted as a single curve for simplicity. According to this illustration, at a given initial grain size (e.g. D_{o1}), stress oscillations

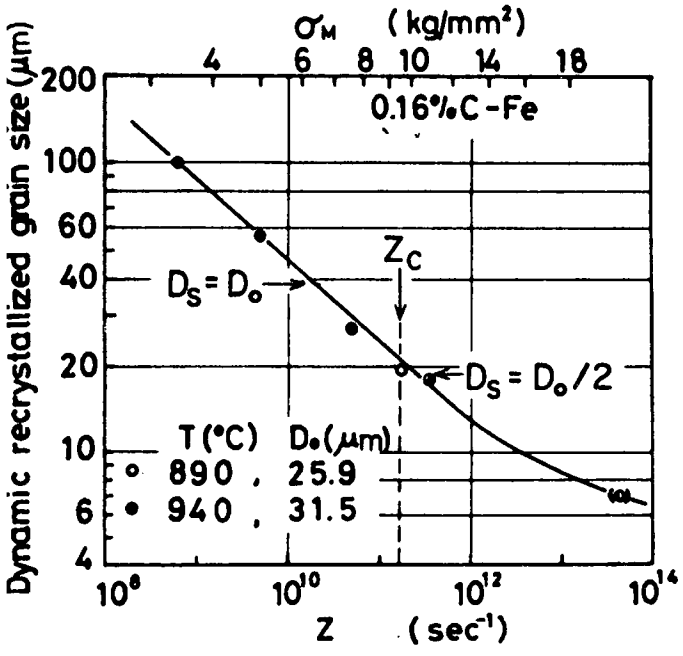

Fig. 14a Dependence of the steady-state austenite grain size D_S on testing strain rate (depicted in the micrographs of Fig. 13) and on temperature. Note that the critical Z_C associated with an initial grain size D_O = 38 μm (established in Fig. 9) is located between the Z values corresponding to $D_S = D_O$ and $D_S = D_O/2$, and more precisely, at a value D_O = 1.8 D_S (after Sakui et al. (26,28)).

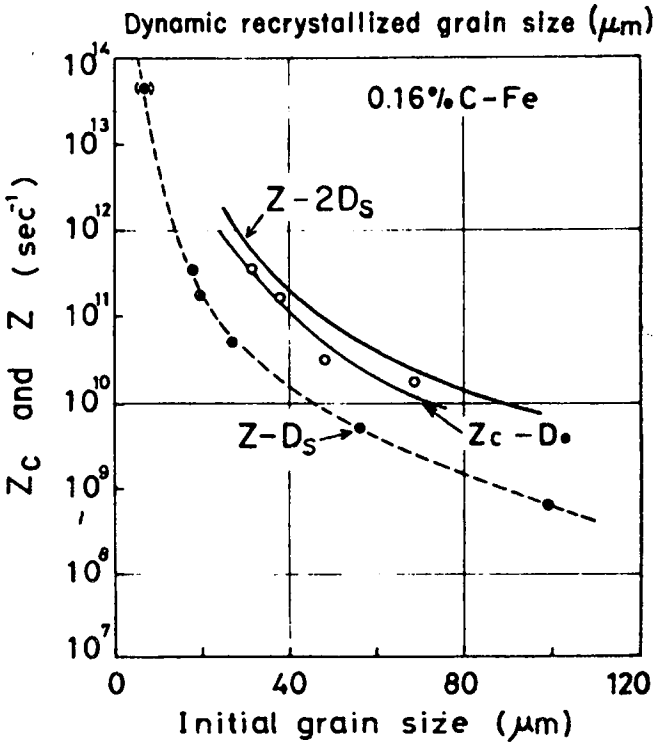

Fig. 14b Dependence of the critical Z_C on initial austenite grain size D_O in 0.16% C steel (from data of Sakui et al. (27,28)). The broken line is the Z-D_S relationship determined in Figs. 13 and 14a. Note that the Z-$2D_S$ (continuous line) and Z_C-D_O relations are nearly coincident.

occur when a combination of a relatively low testing strain rate and high temperature (e.g. Z_1) is used. Each cycle of recrystallization then produces *grain coarsening*, until the stable grain size D_S pertaining to Z_1 is attained. Conversely, if a combination of a relatively high testing strain rate and low temperature (as represented by Z_2) is used, a single peak is observed and *grain refinement* occurs. In this region (crosshatched in Fig. 15), flow softening continues to take place until the grain size declines to the value D_S appropriate to Z_2.

When testing is carried out at a fixed temperature and strain rate (e.g. at Z_1), this model predicts that *both* types of behaviour can be observed. Thus when the initial grain size D_{O1} is finer than the D_S corresponding to Z_1, multiple peaks and grain coarsening are called for, persisting until D_S is attained. Alternatively, when the initial grain size D_{O2} is greater than the D_S appropriate to Z_1, a single flow stress peak and grain refinement are predicted, the latter continuing until D_S and a steady state of flow are achieved.

13. A CRITICAL TEST OF THE GRAIN-SIZE-BASED CRITERION

The discussion concerning the horizontal line at Z_1 in Fig. 15 suggests the possibility of carrying out a critical experiment to test the predictions of the analysis described above. Such a test was performed by Dr. M.G. Akben of McGill University and her results are presented in Fig. 16 for examination. These experiments were carried out in axisymmetric compression at 900°C at a strain rate of 1.4×10^{-3} s^{-1} (i.e. at a fixed value of Z) on a 0.06% C - 1.43% Mn steel. For this material and testing condition, D_S and $2D_S$ are approximately 75 and 150 μm respectively (26-28,43). In order to produce a range of starting grain sizes, austenitization was performed at a series of five temperatures up to 1260°C, leading to gamma grain sizes of about 60, 90, 150, 270 and 375 μm. It is apparent from Fig. 16 that

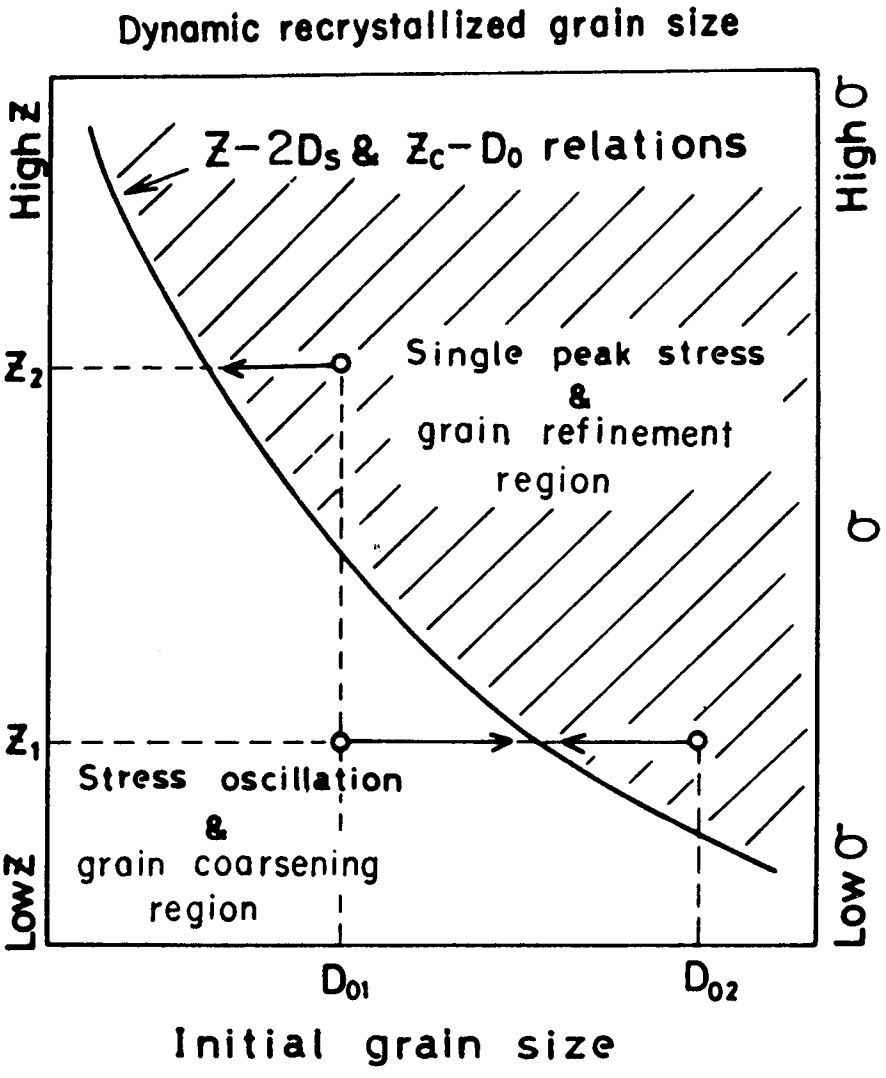

Fig. 15 The curve describing the $Z-2D_s$ and Z_c-D_o relations distinguishes the single peak from the multiple peak region. When testing is carried out at a fixed temperature and strain rate (fixed Z), grain coarsening and repeated stress oscillations occur as long as each successive $D_o < 2D_s$ (e.g. at D_{o1} and Z_1). Conversely, when $D_o > 2D_s$, there is grain refinement and a single stress peak (e.g. at D_{o2} and Z_1). When a fixed initial grain size is used (e.g. D_{o1}), stress oscillations and grain coarsening are associated with $Z < Z_c$ (e.g. $Z_1 < Z_c$), and a single stress peak and grain refinement with $Z > Z_c$ (e.g. $Z_2 > Z_c$).

when $D_o < 2D_s$, i.e. for the 60 and 90 μm material, multiple stress peaks are induced, a total of four stress maxima being observed at the strain limit of 1.0 pertaining to the experiment. The amplitude of the oscillations is also seen to decrease with strain, as each successive wave of grain coarsening brings the mean grain size closer to D_s. (Unlike the experiments of Fig. 11, the evolution of grain size was not verified in this case.)

For the 150, 270 and 375 μm materials, a single marked flow stress peak is observed, after which grain refinement occurred. This type of behaviour corresponds to the industrial situation where relatively high reheating temperatures are used, leading to high values of D_o, and then rolling is performed at lower temperatures and fairly high strain rates, a combination which corresponds to a much smaller stable grain size D_s. The present analysis suggests that, if the periodic type of behaviour is required for a particular application, it could be produced by arranging for the reheated grain size to be fine, and for the deformation conditions to correspond to a similar value of D_s.

Although there is a relatively clear difference between the so-called 'periodic' behaviour of the fine-grained materials and the near absence of oscillations in the

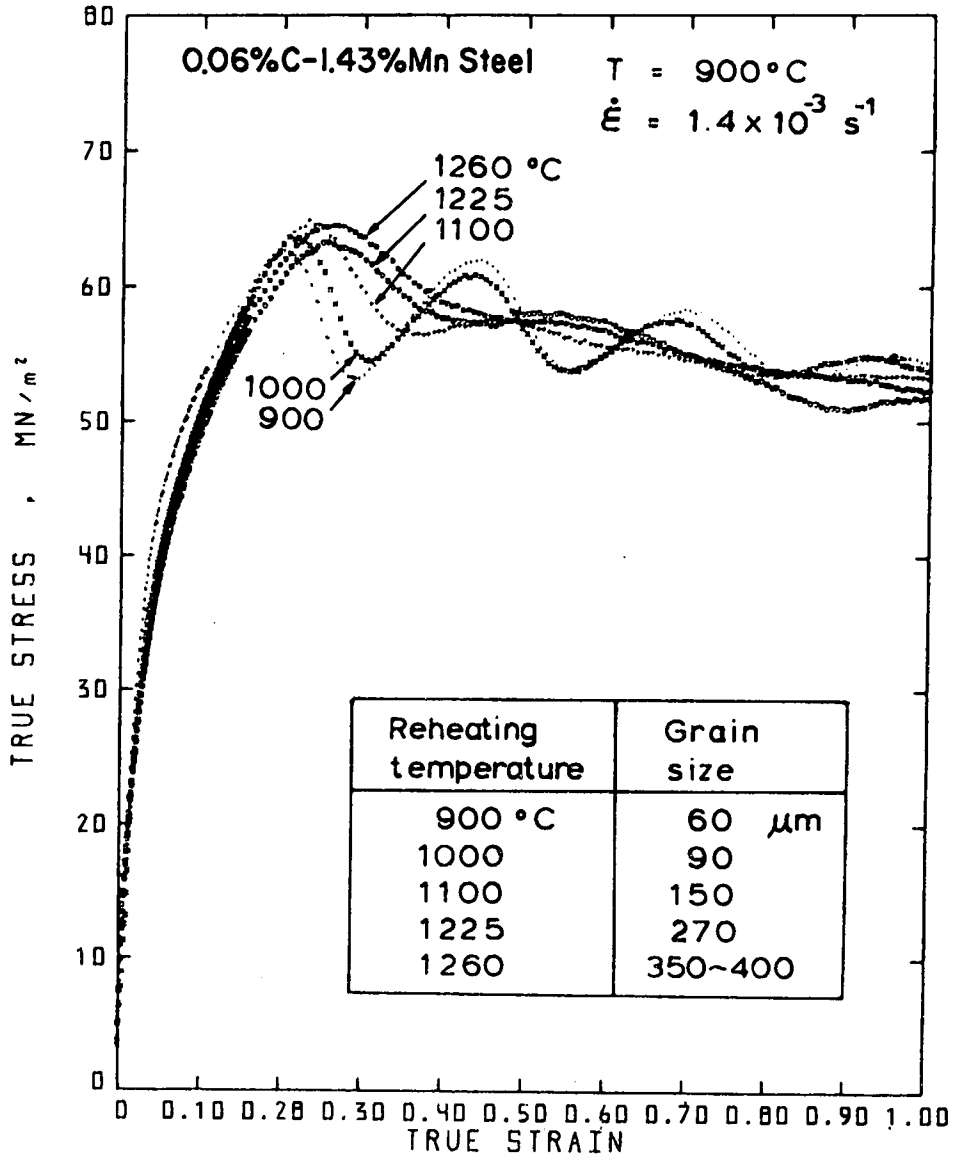

Fig. 16 Critical experiment designed to test the model of Fig. 15. A 0.06% C - 1.43% Mn steel was austenitized at a series of temperatures ranging from 900 to 1260°C selected to produce initial austenite grain sizes of 60 to 375 μm, respectively (see inset). Testing was carried out in axisymmetric compression at 900°C and 1.4 x 10^{-3} s^{-1}, for which $2D_s \cong$ 150 μm. Cyclic σ/ε behaviour was observed when $D_o < 2D_s$; by contrast, single peak behaviour was obtained when $D_o > 2D_s$ (Akben (49)).

coarse-grained specimens, a slight second peak can be detected in the flow curves of the latter materials. The magnitude of the stress increase ($\Delta\sigma_H$ in Fig. 9) in this case decreases with an increase in the initial grain size. A possible explanation of this phenomenon will be introduced below. It is also apparent that the peak strain increases with grain size, as reported by Sah et al. (50), as well as by other authors (27,28,51).

14. EXTENT OF SUPPORT FOR THE PROPOSED GRAIN-SIZE-BASED CRITERION FROM THE RESULTS OF OTHER WORKERS

The effect of initial grain size on the peak strain ε_p was reported fairly early on in the study of dynamic recrystallization (50). However, Sah et al. (50) did not consider in detail the effect of starting grain size on ε_x and did not carry out a systematic investigation of the effect of D_o on the transition between the two types of flow behaviour. In their 1974 paper on the recrystallization of nickel (50), they describe the stress/strain

properties of material of 140, 350 and 400 μm initial grain size when deformed in torsion. It is of interest that at 1000°C and a rotation rate of 0.05 rpm, the 140 μm sample displayed a *multiple peak* flow curve, whereas deformation of the 350 and 490 μm specimens led to *single peak* curves (see Fig. 1b of their paper). From Fig. 10 of their work, in which the D_S vs. σ_S relation is given, where σ_S is the steady state stress, an estimate can be made of D_S under the experimental conditions of Fig. 1b. This leads to a value of 120 μm, so that $2D_S$ = 240 μm, and the critical condition proposed in this review is respected (even when straining is performed by torsion!).

Further support for the present criterion is obtained from the research of Ouchi and Okita (30). They investigated the recrystallization behaviour of six steels, including a 0.10% C - 1.50% Mn and a 0.12% C - 1.32% Mn - 0.13% Mo - 0.017% Ti steel, which were deformed in compression at 1000°C and 1100°C. Three mean strain rates were applied, 5.0×10^{-4}, 2.1×10^{-3} and 10.3 s^{-1}. They prepared samples with five initial grain sizes ranging from 29 to 350 μm, and also determined the relation between D_S and σ_S, the steady state flow stress. It is evident from their data that the $D_O = 2D_S$ condition gives a good fit to the transition in the flow behaviour, although two of the eighteen cases they looked at closely are borderline in that the Z condition for the first case, which was judged to evidence single peak behaviour, fell just over the boundary in the multiple peak zone, and the Z condition for the second case fell just within the single peak zone, although multiple peaks were displayed.

More recently, in an investigation of the dynamic recrystallization behaviour of eight steels, Akasaka et al. (31) also found that the transition from a periodic to a single peak curve was associated with the initial grain size of the material. Although an exact determination of the critical condition was not made, their data are consistent with a transition in the initial grain size range $D_S \leq D_O \leq 2D_S$.

15. A POSSIBLE RATIONALIZATION FOR THE GRAIN SIZE CRITERION BASED ON NUCLEUS DENSITY CONSIDERATIONS

It was demonstrated above that single peak flow behaviour is associated with grain refinement and multiple peak behaviour with grain coarsening. On the basis of the results of Sakai and co-workers (26-29,32), it was shown that the critical condition corresponds to a grain refinement ratio of about 2:1, i.e. where the initial grain size is twice the stable dynamic grain size. This conclusion is well supported by the literature results just cited. It now remains to consider a possible physical basis for these characteristics, and for this purpose, the reader is referred to Table I. In this comparison, we will consider how the flow curves can change with initial grain size (see Fig. 16). At constant Z, the flow stresses, and therefore the stored energies promoting recrystallization, are approximately equal. The analysis is based on three hypotheses. The first and second are that nucleation is restricted to the original grain boundaries, and that the nucleus density is therefore inversely proportional to the specific grain boundary area, $1/D_O$. Thirdly, for simplicity, it is assumed that a nucleus, once formed, grows at a rate which is independent of its location within the material, i.e. of the orientation of the grain being consumed.

On this basis, in a fine-grained material (one in which $D_O < 2D_S$), the nucleus density N_O will be *greater* than half the steady state or equilibrium density N_S (see Table I). By contrast, the nucleus density in a coarse-grained material ($D_O > 2D_S$) will be *less* than half the steady state density N_S. This difference in nucleus density can have a large effect on the local value of the nucleation strain ε_c, as shown schematically in Table I. The two diagrams in the table illustrate the difference in the number of D_O grain boundaries associated with an individual D_S (i.e. eventual) grain in the two cases of interest. In the initially fine-grained material, there are *many* D_O boundaries, and therefore many potential nucleation sites within every future grain. As a result, it can be hypothesized that by the time the nucleation strain ε_c is attained in the most favoured regions, even in the less favoured regions there will not be a scarcity of potential sites, so that the spread in the nucleation strain, $\Delta\varepsilon_c$, will be *small* in this case. This condition can be expressed quantitatively as $\Delta\varepsilon_c < \varepsilon_c$. Qualitatively it signifies that the whole of the material is at about the *same* stage of the recrystallization process, i.e. it is in synchronism, at a given time. According to this model, several recrystallization cycles are needed to attain D_S because, at fine D_O, the nucleus density is actually too high, so that too fine an intermediate grain size, D_S', is produced. The number of cycles thus depends on the disparity between D_O and D_S.

The conditions in the coarse-grained material stand in sharp contrast to the above, particularly with regard to the nucleus density. Here there is only *one part* of a single

Table I

Comparison of Nucleus Densities for Dynamic Recrystallization in Initially Fine-Grained and Initially Coarse-Grained Materials

Material	Fine initial grain	Coarse initial grain
Grain size	$D_o < 2D_s$	$D_o > 2D_s$
Experimental Result	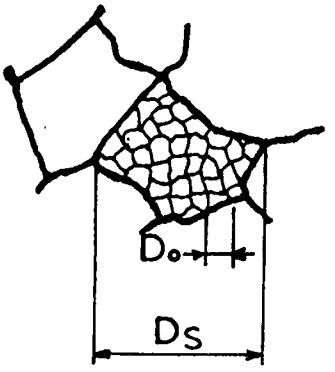 $D_o < D_s' < - - - - - - - - < D_s$ Recrystallized grain size increases with strain	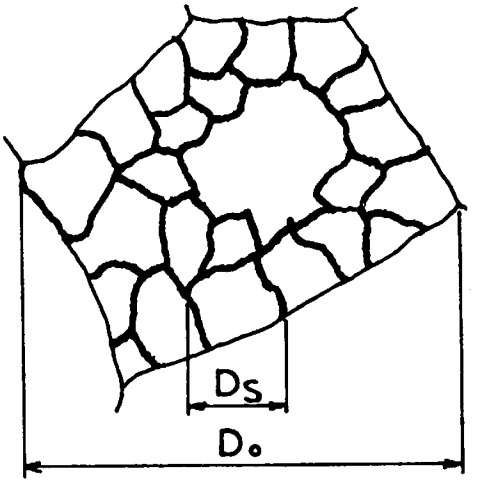 Necklace like nucleation New grains constant in size
Nucleus density	$N_o > 1/2\ N_s$	$N_o < 1/2\ N_s$
$\Delta\varepsilon_c$	Small	Large
Critical Condition	$\Delta\varepsilon_c(i) < \varepsilon_c(i+1)$	$\Delta\varepsilon_c(i) > \varepsilon_c(i+1)$
Assumptions	1. Nucleation sites are generally at the grain boundaries. 2. Nucleus density is inversely proportional to the grain boundary area per unit volume ($N \propto 1/D_o$). 3. Growth rate uniform throughout the material.	
Definitions	D_o: Initial grain size; D_s: Equilibrium dynamic recrystallization grain size. N_o: Initial nucleus density; N_s: Equilibrium nucleus density. $\varepsilon_c(i+1)$: Nucleation strain of (i+1)-st cycle of recrystallization. $\Delta\varepsilon_c(i)$: Spread of nucleation strain of i-th cycle of recrystallization.	

D_o boundary (and therefore a real scarcity of potential nucleation sites) associated with a particular future grain. Because of the wide range of grain orientations and grain boundary misorientations present in typical materials, the nucleation strain ε_c pertaining to a group of new grains can be expected to vary widely. A wide spread in ε_c is also associated with the nucleation of successive generations of 'necklace' grains. Thus $\Delta\varepsilon_c$ will be *large* and can even exceed ε_c, the nucleation strain associated with the most favoured region (or first generation). In this case, $\Delta\varepsilon_c > \varepsilon_c$, and the different volume fractions of the sample will be at *different* stages of the recrystallization process, i.e. recrystallization will be very heterogeneous (as in necklace formation (50,51)), and asynchronized at a particular moment. According to this view, flow softening will occur until both the least favourably oriented regions, as well as the grain interiors, have participated in the recrystallization process. Because of the great scarcity of potential nucleus sites, once again D_s may not be attained in one complete cycle of recrystallization (i.e. where the entire volume fraction has been involved), and a faint second cycle will sometimes be observed.

16. EFFECT OF THE RELATIVE SPREAD IN THE NUCLEATION STRAIN ON THE SHAPE OF THE FLOW CURVE

The degree of 'synchronism' or 'asynchronism' during dynamic recrystallization undoubtedly has an effect on the shape of the flow curve. This is illustrated schematically in Fig. 17, in which the usual S-curves associated with the progress of recrystallization are represented, for simplicity, by the lines tangent to their steepest portions. Thus, when $\Delta\varepsilon_c$ is small and the material is in synchronism, both flow softening and work hardening will be occurring concurrently throughout the material, leading to clearly discernible stress oscillations. With each cycle of recrystallization and of grain coarsening, $\Delta\varepsilon_c$ will increase for the reasons outlined above, until $\Delta\varepsilon_c = \varepsilon_c$ and recrystallization is completely asynchronous.

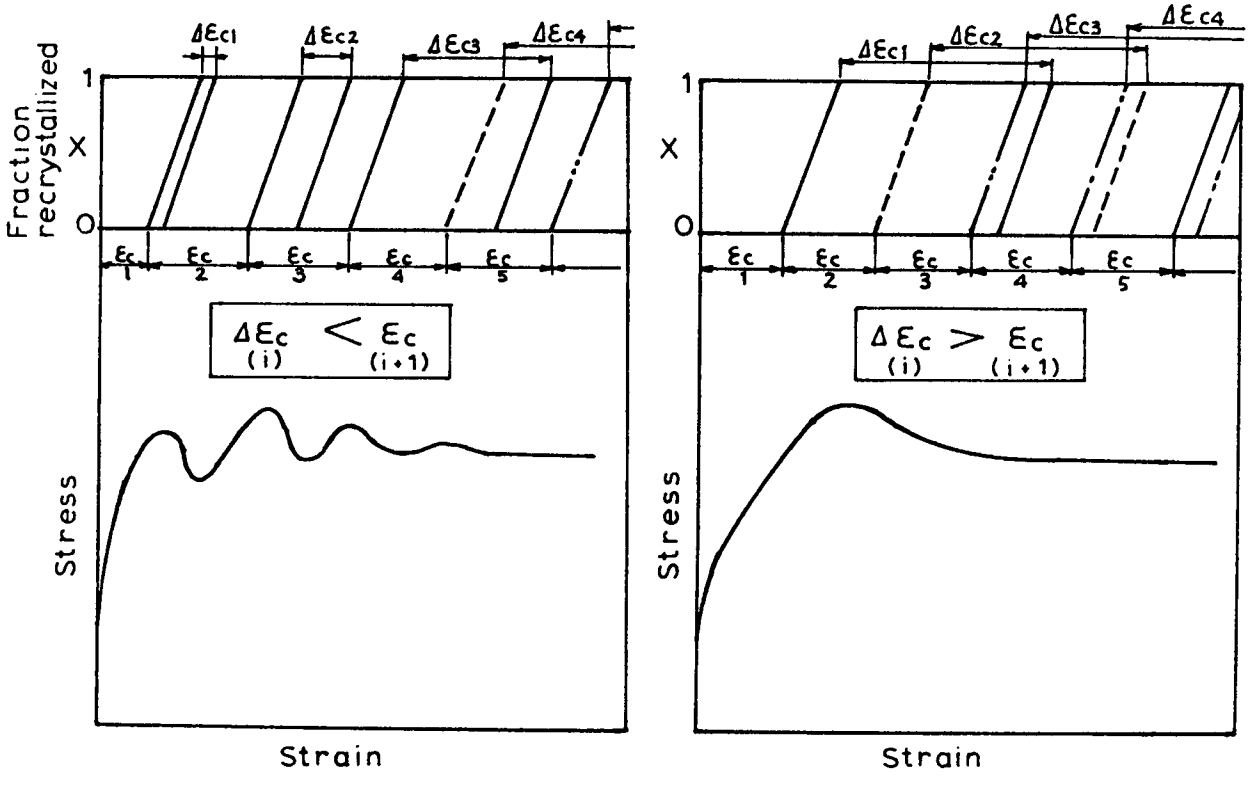

Fig. 17 Expected effect of the relative spread in the nucleation strain $\Delta\varepsilon_c/\varepsilon_c$ on the shape of the flow curve. (a) When $\Delta\varepsilon_c/\varepsilon_c$ is small (i.e. when recrystallization is nucleated approximately concurrently throughout the material, as in fine-grained specimens), distinct cycles of softening and hardening can be seen. These are gradually damped out because $\Delta\varepsilon_c$ increases as grain coarsening takes place (see Table I). (b) When $\Delta\varepsilon_c/\varepsilon_c$ is large (i.e. when there is a considerable spread in the nucleation strain in different volume fractions of the material, as in coarse-grained specimens), only a single cycle of flow softening occurs, which persists until the equilibrium grain size D_s is established.

The asynchronism attained at large strains in the initially fine-grained material is present in the coarse-grained material ab initio. As each volume fraction of the specimen is at a different stage of recrystallization, the local softening and hardening processes overlap and only a single macroscopic flow stress peak is observed.

It should be remarked parenthetically that the more rapid damping of the torsion rather than the compression flow curves in Figs. 1a and b, respectively (e.g. at a peak stress level of about 50 MPa ≅ 7000 psi), can be attributed directly to the higher degree of asynchronization inherent in the torsion test, which has already been discussed above in connection with the contributions of the individual cylindrical shells to the overall torque.

Finally, it should be added that, although the present analysis seems to be well-founded from a metallographic point of view, its applicability to a wide range of FCC materials, including systems involving static and dynamic precipitation, remains to be demonstrated. Experiments should also be carried out to determine the detailed influence of the dislocation substructure on the spread in the nucleation strain $\Delta\varepsilon_c$, and computer simulations should be performed using the nucleus density criterion to assess the predictive accuracy of the present transition model.

17. THE RELATION BETWEEN THE CRITICAL STRAIN AND CRITICAL GRAIN SIZE CRITERIA

It remains to consider the possible relation between a transition criterion based on critical strains, and the present one expressed in terms of the difference between the initial and stable grain sizes (and between the initial and stable nucleus densities). The former are useful because ε_p and ε_x, for example, are readily determined from the strains at maximum stress and at the attainment of steady state flow ε_s (or at the mean stress under cyclic conditions, see Fig. 4). Although it was shown above in Fig. 7 that the $\varepsilon_p = \varepsilon_x$ condition is not satisfied in tension or compression (and a physical explanation was given in Fig. 8 for the effect of the strain and strain rate gradients present in torsion on the *apparent* values of ε_p and ε_x), it nevertheless remains possible that some *modified* form of the critical strain model could apply in homogeneous deformation. This possibility will now be examined briefly.

For this purpose, we make the simplifying assumption that, under *single peak* conditions, the minimum strain at which new nuclei appear, ε_c, is about one half the macroscopic peak strain ε_p, so that $\varepsilon_p = 2\varepsilon_c$. (The *exact* value of the multiplier is not critical.) We also distinguish between the *macroscopic* 'recrystallization strain' ε_x given by $\varepsilon_x = \varepsilon_s - \varepsilon_p$, and the *local* 'recrystallization strain' ε_x^*. The latter is the strain during which new grains form in any particular volume fraction of the material; e.g. in the first 'string' of the necklace. If we now state that steady state flow begins when the innermost string in the necklace is fully recrystallized, i.e. when the *entire volume* of the material has undergone at least one cycle of recrystallization, we can write that

$$\varepsilon_x = \varepsilon_s - \varepsilon_p = (\varepsilon_c + \Delta\varepsilon_c + \varepsilon_x^*) - 2\varepsilon_c = \Delta\varepsilon_c + (\varepsilon_x^* - \varepsilon_c) \qquad (5)$$

Here the steady state strain $\varepsilon_s = \varepsilon_c + \Delta\varepsilon_c + \varepsilon_x^*$ (see Fig. 17), and $\varepsilon_p = 2\varepsilon_c$, as suggested above. If we return to the inequality between the minimum nucleation strain ε_c and the spread in the nucleation strain $\Delta\varepsilon_c$ suggested earlier (Table I and Fig. 17), i.e. to $\varepsilon_c < \Delta\varepsilon_c$, this is equivalent, from relation (5) above, to $\varepsilon_x^* < (\Delta\varepsilon_c + \varepsilon_x^* - \varepsilon_c)$ or to $\varepsilon_x^* < \varepsilon_x$. Now setting $\varepsilon_c \cong \varepsilon_x^*$, the above condition can be written as

$$\varepsilon_c < \varepsilon_x \qquad (6)$$

Note that the essential difference between relation (6) and that of Fig. 17 is the replacement of the spread in the nucleation strain $\Delta\varepsilon_c$ by the macroscopic 'recrystallization strain' ε_x.

Turning now to the case of *multiple peak* flow, under these conditions, $\varepsilon_p \cong \varepsilon_c$, so that the condition $\varepsilon_p > \varepsilon_x$ can be written as

$$\varepsilon_c > \varepsilon_x \qquad (7)$$

instead. Thus it appears from the present considerations that the criterion

$$\varepsilon_c = \varepsilon_x \qquad (8)$$

might be a valid one for distinguishing between periodic and single peak recrystallization in homogeneous flow. It is, however, a type of 'hybrid' criterion (unlike the Sellars relation) in that the *mechanical* quantity ε_x is measured directly from the flow curve, whereas the *microstructural* term ε_c can only be determined metallographically. It remains to be added that the quantity ε_x measured in the *multiple peak* range of behaviour is indeed equivalent to ε_x^*, the local recrystallization strain, because of the *synchronization* of recrystallization throughout the material that applies in this range. By contrast, the quantity ε_x measured in the *single peak* domain, precisely because of the *asynchronization* that prevails, corresponds to several overlapping growth periods, and is therefore more closely related to the term $\Delta\varepsilon_c$, as can be seen from Equation (5).

18. CONCLUSIONS

1. The criterion for the transition from multiple to single peak behaviour during dynamic recrystallization based on the equivalence of the peak and recrystallization strains ($\varepsilon_p = \varepsilon_x$) does not apply to homogeneous modes of deformation such as tension or compression. This is because the condition $\varepsilon_p = \varepsilon_x$ was derived from torsion test data on solid bars, and such data lead to distorted (and physically misleading) flow curves because of the manner in which the elemental cylindrical shells contribute to the macroscopic couple. In particular, because of the specific non-linear dependence of peak strain on strain rate, the peak strain is attained first in the outer region of a torsion bar, so that the 'overall' or macroscopic peak strain normally determined in torsion is always larger than that obtained from compression or tension experiments. This effect is compounded for the recrystallization strain ε_x, because the latter is based on the steady state strain ε_s, which includes a retarding component from both ε_p and ε_x. As a result, the recrystallization strain ε_x determined in torsion differs from that measured in tension or compression by a greater amount than does ε_p. The net effect is that the ε_p and ε_x curves do not in general intersect in tension or compression testing.

2. *Single peak* behaviour is associated with *grain refinement*, and the flow softening that follows the stress maximum comes to an end when refinement has affected the entire volume of the material, leading to the stable grain size D_s. Conversely, *oscillations* in the flow curve are related to *grain coarsening*; the oscillations cease when the successive waves of coarsening finally produce the equilibrium grain size.

3. The dependence of twice the stable grain size ($2D_s$) on temperature-corrected strain rate Z parallels that of the transition parameter Z_c on initial grain size D_o. This correspondence is responsible for the transition criterion $D_o = 2D_s$, according to which single peak behaviour is observed when $D_o > 2D_s$, and stress oscillations when $D_o < 2D_s$.

4. Multiple stress peaks are observed as long as recrystallization is taking place synchronously throughout the material. This occurs when there is a high density of potential nuclei within a future new grain, a condition which is respected in initially fine-grained materials, as a result of which there is only a limited spread $\Delta\varepsilon_c$ in the nucleation strain. With each wave of grain coarsening, the spread in the nucleation strain increases, until, when $\Delta\varepsilon_c = \varepsilon_c$ (the nucleation strain in the most favoured regions), the oscillations cease.

5. Single stress peaks are observed in initially coarse-grained materials because of the relative scarcity of potential nuclei within a given new grain. The wide variation in grain orientations and in grain boundary misorientations, as well as the occurrence of necklace nucleation, lead to a large spread $\Delta\varepsilon_c$ in the nucleation strain, leading to the condition $\Delta\varepsilon_c > \varepsilon_c$. As a result, the progress of recrystallization is spatially inhomogeneous and highly unsynchronized, and the mean flow stress obscures the local cycles of work hardening and recrystallization.

19. ACKNOWLEDGEMENTS

The authors wish to thank Dr. Melek G. Akben for performing the critical experiment described in the second half of the paper and Dr. C.M. Sellars of the University of Sheffield, England, for a stimulating correspondence concerning the grain size criterion. They are also indebted to the following ministries and agencies for the financial support of the research described in this review: the Natural Sciences and Engineering Research Council of Canada, the Department of Energy, Mines and Resources, Canada, and the Quebec Ministry of Education (JJJ); the Ministry of Education of Japan and the Hot Deformation Committee of the Iron and Steel Institute of Japan (TS). One of the authors (TS) acknowledges with gratitude the granting of a period of sabbatical leave by the University of Electro-communications, Tokyo, and the receipt of a travelling fellowship from the Ministry of Education of Japan.

20. REFERENCES

1. J.N. GREENWOOD and H.K. WORNER, J. Inst. Metals, 1939, 64, 135.
2. E.N. da C. ANDRADE, Nature, 1948, 162, 410; J. Iron Steel Inst., 1952, 171, 217.
3. L.M.T. HOPKIN and C.J. THWAITES, J. Inst. Metals, 1953-54, 82, 181.
4. R.C. GIFKINS, J. Inst. Metals, 1957-58, 86, 15; 1958-59, 87, 255.
5. H. HIRST, Proc. Australian Inst. Min. Met., 1940, 118, (N.S.), 101; 1941, 121, (N.S.), 29.
6. W.D. JENKINS, T.G. DIGGES and C.R. JOHNSON, J. Research Nat. Bur. Stand., 1954, 53, 329.
7. P. FELTHAM and J.D. MEAKIN, Acta Met., 1959, 7, 614.
8. P. FELTHAM, Proc. Phys. Soc., 1953, 66, 865.
9. D. HARDWICK, C.M. SELLARS and W.J. McG. TEGART, J. Inst. Metals, 1961-62, 90, 21.
10. S. STEINEMANN, Beiträge Geol. Schweiz (Hydrologie), 1958, 10, 1.
11. J.J. JONAS and F. MÜLLER, Can. J. Earth Sciences, 1969, 6, 963.
12. S. WHITE, Phil. Trans. R. Soc. Lond., 1976, A283, 69.
13. J-C.C. MERCIER, D.A. ANDERSON and N.L. CARTER, Pure Appl. Geophys., 1977, 115, 199.
14. R.J. TWISS, Pure Appl. Geophys., 1977, 115, 227.
15. C. ROSSARD and P. BLAIN, Mém. Sci. Rev. Mét., 1959, 56, 285.
16. R.A. PETKOVIC, M.J. LUTON and J.J. JONAS, Can. Met. Quart., 1975, 14, 137.
17. M.J. LUTON and C.M. SELLARS, Acta Met., 1969, 17, 1033.
18. J.P. SAH, G.J. RICHARDSON and C.M. SELLARS, Indian J. Technology, 1973, 11, 445.
19. E. HORNBOGEN and U. KÖSTER, 'Recrystallization of Metallic Materials', 2nd Edition, ed. by F. Haessner, Riederer-Verlag, Stuttgart, 1978, p. 159.
20. R. LOMBRY, C. ROSSARD and B.J. THOMAS, 'Les Traitements Thermomécaniques: Aspects Théoriques et Applications', 24éme Colloque de Métallurgie, INSTN (Saclay), June 1981, in press.
21. C.M. SELLARS and W.J. McG. TEGART, discussion in 'Deformation Under Hot Working Conditions', Special Report No. 108, Iron Steel Inst., London, 1968, p. 43.
22. R. SANDSTRÖM and R. LAGNEBORG, Acta Met., 1975, 23, 387.
23. W. ROBERTS and B. AHLBLOM, Acta Met., 1978, 26, 801.
24. H.P. STÜWE and B. ORTNER, Metal Sci., 1974, 8, 161.
25. R. SANDSTRÖM and R. LAGNEBORG, Scripta Met., 1975, 9, 59.
26. S. SAKUI, T. SAKAI and K. TAKEISHI, Tetsu-to-Hagane, 1976, 62, 856.
27. S. SAKUI and T. SAKAI, Tetsu-to-Hagane, 1977, 63, 285.
28. S. SAKUI, T. SAKAI and K. TAKEISHI, Trans. Iron Steel Inst. Japan, 1977, 17, 718.
29. T. SAKAI, Hot Deformation and Fracture, ed. by I. Tamura, Iron Steel Inst. Japan, Tokyo, 1981, p. 34.
30. C. OUCHI and T. OKITA, Tetsu-to-Hagane, 1976, 62, S208.
31. K. AKASAKA, M. MAKI and I. TAMURA, Tetsu-to-Hagane, 1981, 67, S639.
32. T. SAKAI, M. OHASHI and J.J. JONAS, to be published.
33. R.A. PETKOVIC, M.J. LUTON and J.J. JONAS, Acta Met., 1979, 27, 1633.
34. M.G. AKBEN, I. WEISS and J.J. JONAS, Acta Met., 1981, 29, 111.
35. J.P. MICHEL and J.J. JONAS, Acta Met., 1981, 29, 513.
36. I. WEISS, J.J. JONAS and G.E. RUDDLE, Proc. ASM Symposium on 'Process Modeling Tools', Cleveland, Oct., 1980, ASM, in press.
37. T. SAKAI and J.J. JONAS, to be published.
38. G.R. CANOVA, S. SHRIVASTAVA, J.J. JONAS and C. G'SELL, Proc. ASTM Symposium 'Formability-2000', 1980, Chicago, ASTM, Philadelphia, PA, in press.
39. B. BACROIX, M.G. AKBEN and J.J. JONAS, Proc., Int. Conf. on the Thermomechanical Processing of Microalloyed Austenite, Aug., 1981, AIME, Pittsburg, in press.
40. T. CHANDRA and J.J. JONAS, Met. Trans., 1970, 1, 2079.
41. G. GLOVER and C.M. SELLARS, Met. Trans., 1973, 4, 765.
42. C.M. SELLARS, Metalurgia I. Odlewnictwo (Metallurgy and Foundry (Poland)), 1979, 5, 377.
43. R.A. PETKOVIC, Masters thesis, McGill University, Canada, 1971.
44. D.S. FIELDS JR. and W.A. BACKOFEN, Proceedings, ASTM, 1957, 57, 1259.
45. U.F. KOCKS and G.R. CANOVA, 2nd Risø Int. Symp. on Metallurgy and Materials Science, Risø, Denmark, Sept. 1981, in press.
46. G.R. CANOVA, J.J. JONAS and U.F. KOCKS, to be published.
47. I. KOZASU, C. OUCHI, T. SAMPEI and T. OKITA, 'Microalloying 75', Union Carbide Corp., New York, 1975, p. 100.
48. E.L. BROWN and A.J. DeARDO, Met. Trans., 1981, 12A, 39.
49. M.G. AKBEN, McGill University, Montreal, unpublished research.
50. J.P. SAH, G.J. RICHARDSON and C.M. SELLARS, Met. Sci., 1974, 8, 325.
51. W. ROBERTS, H. BODEN and B. AHLBLOM, Met. Sci., 1979, 13, 195.

Acta Metallurgica, Vol. 27, pp. 1633 to 1648

0001-6160/79/1001-1633$02.00/0

RECOVERY AND RECRYSTALLIZATION OF POLYCRYSTALLINE COPPER AFTER HOT WORKING

R. A. PETKOVIC
Exxon Research & Engineering Company, Linden, NJ 07036, U.S.A.

M. J. LUTON
Columbia University, New York, NY 10027, U.S.A.

and

J. J. JONAS
McGill University, Montreal, Canada, H3A 2A7

(*Received* 28 *September* 1978; *in revised form* 12 *March* 1979)

Abstract—The restoration processes that take place during the isothermal annealing of hot worked copper, in the temperature range 450–540°C, have been studied in detail. The annealing response was monitored by means of an interrupted compression technique and by quantitative metallography. The study firmly establishes the existence of three distinct mechanisms of static restoration, namely recovery, classical recrystallization and metadynamic recrystallization. The presence of the third process requires the occurrence of dynamic recrystallization during the prior hot working strain. The relative importance of the contribution of each of the three mechanisms to static annealing is shown to be highly sensitive to the degree of prestrain. There exists a critical strain (~12%) below which no recrystallization occurs during the anneal, and recovery is the only restoration process. At higher strains, both recovery and recrystallization take place, and operate sequentially, because the latter mechanism requires a high degree of substructural rearrangement before it can be initiated. Once the material is worked beyond the critical strain for dynamic recrystallization (~22%) static restoration proceeds by the operation of metadynamic recrystallization as well as recovery and classical recrystallization. The former process is shown to commence immediately on the cessation of straining, as it requires no induction period for the formation of new grain nuclei. Instead, the nuclei are formed during the prior deformation so that recrystallization proceeds by growth from these centers, until all such sites are exhausted. For all conditions considered in the present work, it was found that the grains produced by both types of static recrystallization were smaller than those produced by dynamic recrystallization. It is argued that potential nuclei that are destroyed by work hardening on continued deformation, become critical when straining ceases, thereby increasing the nucleus density and producing a finer grain size.

Résumé—Nous avons étudié en détail la restauration isotherme du cuivre entre 450 et 540°C, après une déformation à chaud. Nous suivions la réponse au recuit par interruption de la compression et métallographie quantitative. Cette étude établit fermement l'existence de trois mécanismes distincts de restauration statique, à savoir la restauration proprement dite et les recristallisations classique et métadynamique. La présence du troisième phénoméne nécessite une recristallisation dynamique au cours de la déformation à chaud préalable. Nous montrons que l'importance relative de la contribution de chacun de ces trois mécanismes au recuit statique est trés sensible au taux de prédéformation. Il existe un écrouissage critique (~12%) au-dessous duquel il ne se produit pas de recristallisation au cours du recuit, mais seulement une restauration. Pour des déformations plus fortes, restauration et recristallisation agissent l'une après l'autre, car ce dernier mécanisme ne peut débuter qu'après un réarrangement important de la sous-structure. Lorsque le matériau est déformé au-delà de la déformation critique pour la recristallisation dynamique (~22%) la restauration statique se produit et met en jeu la recristallisation métadynamique, ainsi que la restauration et la recristallisation classique. La restauration, qui ne nécessite pas de période d'induction pour la formation de nouveaux germes de grains, commence dis que cesse la déformation. Les germes étant formés au cours de la prédéformation, la recristallisation se produit par croissance à partir de ces germes, jusqu'à épuisement de ceux-ci. Pour les conditions étudiées dans ce travail, les grains produits par les deux types de recristallisation statique étaient plus petits que ceux produits par recristallisation dynamique. Nous montrons que les germes potentiels, qui sont détruits par l'écrouissage au cours de la déformation continue, deviennent critiques lorsqu'on arrête la déformation; il acroissent ainsi la densité de germes, ce qui conduit à une plus petite taille des grains.

Zusammenfassung—Die während des isothermen Ausheilens von warmverformtem Kupfer im Temperaturbereich von 450–540°C ablaufenden Ausheilprozesse wurden ausführlich untersucht. Das Ausheilverhalten wurde mit einem diskontinuierlichen Kompressionsverfahren und mit quantitativer Metallografie verfolgt. Die Untersuchung zeigt klar, daß drei unterschiedliche Mechanismen statischen Ausheilens auftreten, nämlich Erholung, klassische Rekristallisation und metadynamische Rekristallisation. Vorbedingung für das Auftreten des dritten Prozesses ist dynamische Rekristallisation während der vorherge-

henden Warmverformung. Der Beitrag jedes der drei Mechanismen zum statischen Ausheilen hängt sehr empfindlich vom Grad der Vorverformung ab. Es existiert eine kritische Dehnung (~12%), unterhalb der keine Rekristallisation während des Ausheilens auftritt; es tritt dann nur Erholung auf. Bei höheren Dehnungen laufen sowohl Erholung als auch Rekristallisation ab, und zwar sequentiell, da Rekristallisation vor dem Einsetzen ein hohes Maß an substruktureller Umordnung erfordert. Ist das Material bis über die kritische Dehnung für dynamische Rekristallisation (~22%) verformt, dann verläuft das statische Ausheilen über metadynamische Rekristallisation, wie auch über Erholung und klassische Rekristallisation. Es wird gezeigt, daß metadynamische Rekristallisation sofort nach Beendigung der Verformung einsetzt, da hierfür keine Wartezeit für die Bildung neuer Kornkeime erforderlich ist. Stattdessen werden Keime während der vorhergehenden Verformung gebildet, so daß die Rekristallisation durch Wachstum aus diesen Zentren heraus abläuft, bis alle solche Zentren aufgebraucht sind. Bei allen in dieser Arbeit betrachteten Bedingungen waren die durch beide Arten statischer Rekristallisation erzeugten Körner kleiner als die durch dynamische Rekristallisation erzeugten Körner. Dieses Ergebnis läßt sich damit erklären, daß potentielle Keime, die durch die Verfestigung bei kontinuierlicher Verformung zerstört wurden, kritisch werden bei Beendigung der Verformung. Dadurch wird die Anzahldichte der Keime vergrößert, welches zu kleineren Körnern führt.

1. INTRODUCTION

The stimulus for the present study arose from results obtained concerning the softening behavior of a series of plain carbon steels [1–3]. These results were interpreted in terms of a model in which the interaction of the recovery and recrystallization processes was deduced entirely on the basis of mechanical observations. A microstructural confirmation of this model was not possible, unfortunately, because a detailed metallographic analysis of the austenite structures developed was prevented by the products of γ/α transformation.

The aim of the present work was, consequently, to investigate the interaction of recovery and recrystallization in a material in which no phase change is involved, and therefore to judge the validity, or the extent of validity, of the previous model. For this purpose, electrolytic tough pitch (ETP) copper† was selected as the model material, and various methods of etch pitting and quantitative metallography were developed and employed which enabled the inter-relation between the various softening mechanisms to be analyzed in detail. A further feature of the method was that it permitted the kinetics of the individual restoration processes to be determined as well; these will be described in a separate publication.

2. EXPERIMENTAL PROCEDURE

The method of intermediate unloading employed in the present study, in which the softening taking place during the unloading interval is measured, has been described in detail elsewhere [1–3], and will therefore be reviewed only briefly here. The method is based on the principle that the initial flow stress at high temperatures is a sensitive measure of the microstructural state of the material. Samples are loaded at a constant true strain rate, in compression, to some prescribed strain and unloaded. After a given time interval the samples are reloaded at the same strain rate as before. The initial flow stress measured on reloading is taken as an indication of the amount of isothermal softening that has occurred during the annealing period. The degree of softening, X, is given by the expression

$$X = (\sigma_m - \sigma_r)/(\sigma_m - \sigma_0)$$

where σ_m is the flow stress immediately before unloading and σ_0 and σ_r are the initial flow stresses recorded during prestraining and reloading, respectively.

2.1 *Specimen preparation*

Compression samples were machined from cold drawn bar into right cylinders 11.4 mm in height and 7.6 mm in diameter. The end faces of the specimens were grooved [4, 5], in order to retain the glass lubricants used to obtain uniform axisymmetric compression at elevated temperatures [5–11]. In order to minimize differences in the initial microstructure, all specimens were strained 2% in compression, annealed for 16 h at 900°C and then quenched. The resulting mean linear intercept grain size was 0.56 mm.

2.2 *Mechanical testing procedures*

The mechanical tests were carried out on an Instron testing machine modified for constant true strain rate compression at elevated temperatures, incorporating an automated test control and data acquisition system [12]. All tests were conducted in an atmosphere of high purity argon.

Two series of tests were performed in the present study. The first series consisted of intermediate unloading tests conducted at the following combinations of temperature and strain rate: 450°C and $1.8 \times 10^{-3}\,s^{-1}$; 500°C and $1.8 \times 10^{-2}\,s^{-1}$; and 540°C and $8 \times 10^{-2}\,s^{-1}$. By this means the flow stresses developed were comparable at all strains for the three temperatures. Seven levels of prestrain were chosen, namely 0.05, 0.10, 0.15, 0.18, 0.30, 0.40, 0.52; in this way static softening could be studied in dynamically recovered or in dynamically recovered and recrystallized microstructures. The second series of experiments was carried out for a single test temperature and strain rate, 500°C at $1.8 \times 10^{-2}\,s^{-1}$. Specimens were prestrained 0.05, 0.10, 0.15 and 0.40 and

† Chemical composition in wt%: Pb, 0.09; Ni, <0.05; O_2, 0.015; Ag, 0.005; As, <0.0003.

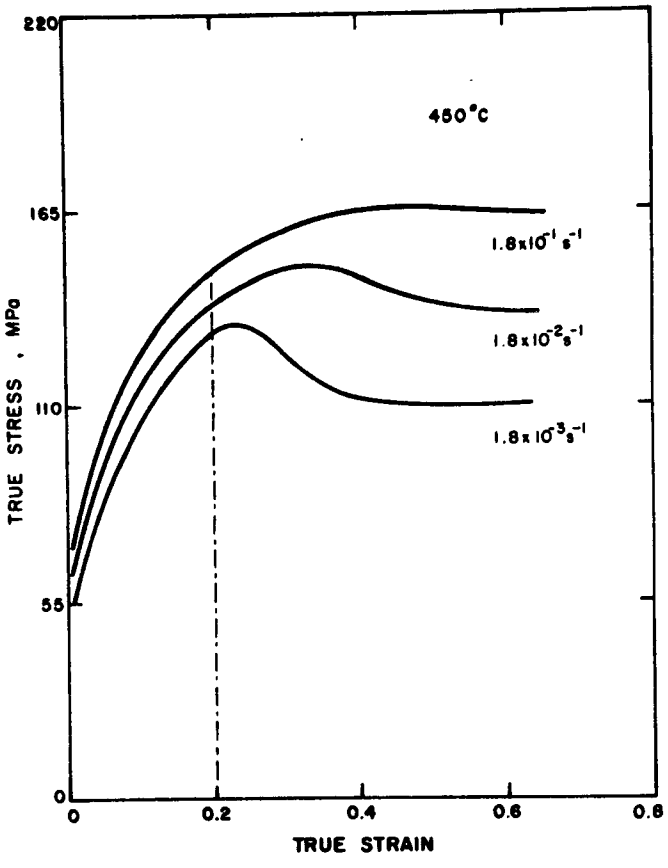

Fig. 1. Strain rate dependence of the flow curves of polycrystalline copper at 450°C.

quenched after different delay times. Two sections were cut transversely to the compression axis on each of these samples. One section was taken close to the mid-height and the other near one of the ends. This procedure was adopted in order to minimize the effect of strain localization on measurements of the grain structures.

The sections were ground and electropolished and etched sufficiently to clearly delineate the grain boundaries.† In excess of 400 individual grain intercept measurements were made on each sample to determine the distribution of grain intercept lengths.

3. EXPERIMENTAL RESULTS

A typical set of stress–strain curves obtained in compression at 450°C is shown in Fig. 1. Polycrystalline copper strained in the present temperature range exhibits stress–strain curves of this character, indicating that recrystallization occurs during deformation [13, 14]. Hot compression tests performed on samples at 540 and 500°C at 8×10^{-2} and $1.8 \times 10^{-2}\,s^{-1}$, respectively, produced curves identical in shape and stress level to that established at $1.8 \times 10^{-3}\,s^{-1}$ and 450°C. Under these three sets of testing conditions the flow stresses are comparable at any given strain. Consequently, the microstructures developed under each of the test conditions can be considered to be a function of strain only [15, 16].

A set of stress–strain curves determined, at $1.8 \times 10^{-2}\,s^{-1}$ and 500°C, using the technique of intermediate unloading, is shown in Fig. 2. Several samples were prestrained to a strain of 0.3 and rapidly and completely unloaded. After a short delay, the flow stress on restraining rises rapidly to a level comparable to the stress developed just prior to unloading. Long delay times, on the other hand, produce a profound drop in the initial flow stress on reloading and the stress–strain behavior approaches that of the material during prestraining. In all cases, the initial flow stresses during the prestrain and reload cycles were defined by expanding the strain scales and taking the 0.001 offset stresses.

3.1 *Effect of strain*

The results of earlier studies on plain carbon and microalloyed austenite have indicated that, after hot working, static softening proceeds by the sequential

† Electropolishing: 133 ml glacial acetic acid, 25 g chromium trioxide, 7 ml H_2O at 8.5 V and 18°C. Etching: 65 ml concentrated H_2SO_4, 16 g potassium dichromate, 3 g sodium chloride, 800 ml H_2O.

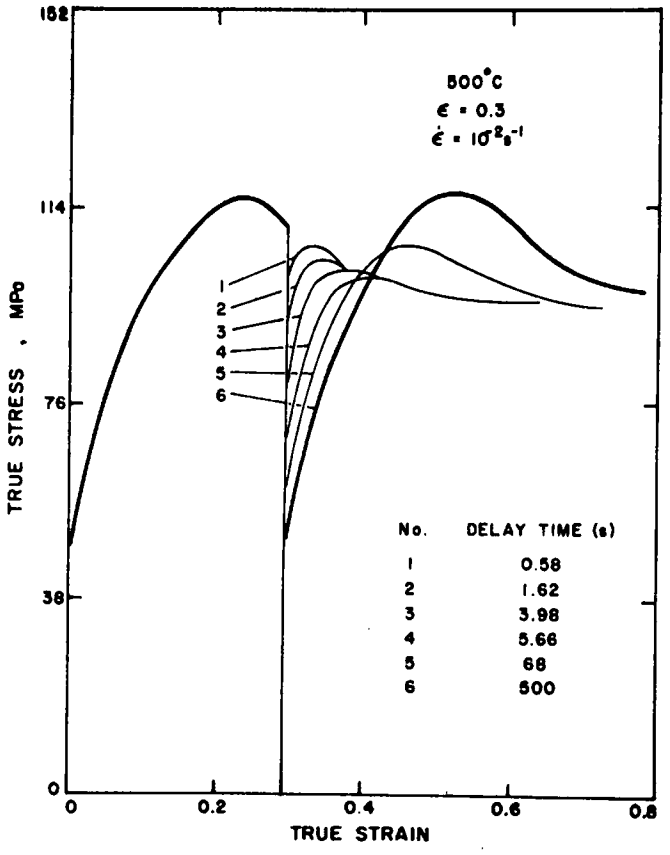

Fig. 2. Effect of increasing delay time on the interrupted flow curves of polycrystalline copper at 500°C.

operation of up to three distinct processes [1–3]. The relative importance of each of these processes depends critically on the prior hot working strain. This effect is illustrated in Fig. 3, where softening curves are displayed. These tests were carried out at 500°C at a strain rate of $1.8 \times 10^{-2}\,s^{-1}$ and the samples were held at the testing temperature after seven different amounts of prestrain. The location of the interruption strains was chosen to be before the peak flow stress for conditions (a–d), and after the peak flow stress for conditions (e–g).

For small amounts of prior strain [curves (a and b)], that is at a strain considerably less than that required to reach the maximum in flow stress, only one stage of softening is observed. This first cycle of softening has been attributed to static recovery [1–3], and is completed in about 1000 s [curve (a)] or 500 s [curve (b)]. By this time, 40–50% of the work hardening introduced during prestraining is removed. The statically recovered structure is clearly very stable, since recovery saturates at these levels, no further softening occurring even after 15 h. These results also imply that a strain of 0.10 is less than the critical strain for static recrystallization.

When the amount of prestrain is increased to 0.15 [curve (c)] or 0.18 [curve (d)], the first cycle of softening is completed after 50 and 20 s, respectively, as indicated by the inflection in the softening curves. Evidently, the rate of recovery increases with the amount of prestrain. This arises because of the higher driving forces associated with the greater dislocation densities present at interruption. The second stage of softening, observed in curves (c and d), is associated with static recrystallization [1–3]; this conclusion will be fully justified below. Furthermore, since all four strains were below that required to reach the peak of the uninterrupted stress–strain curve, we may conclude that dynamic recrystallization did not take place during prestraining. Consequently, the behavior exhibited by the material [curves (a–d)] is characteristic of static softening that is initiated in a dynamically recovered structure.

The next three curves represent strains selected to be: between the peak and steady state strains, curve (e) and well into the steady state regime, curves (f and g). Curve (e) typifies the softening response of material in which dynamic recrystallization has just begun and is not yet fully developed. Curve (g), on the other hand, is representative of the progress of softening in material in which dynamic recrystallization is fully developed. It should be noted that in curves (e–g), the amount of softening produced by

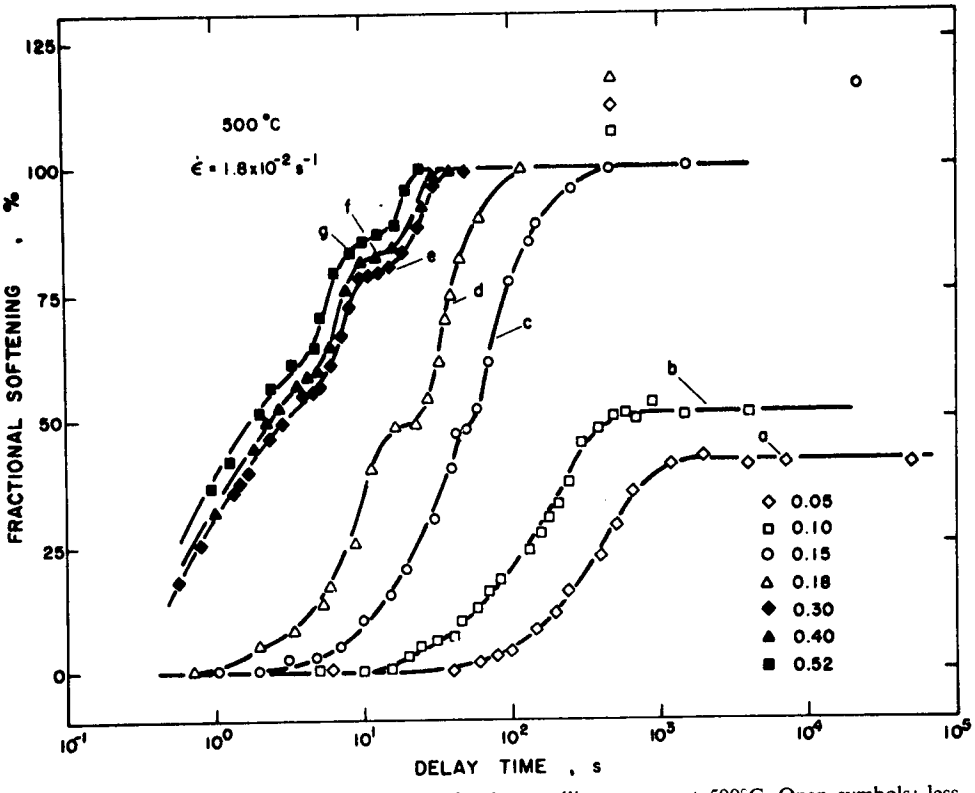

Fig. 3. Effect of strain on the static softening of polycrystalline copper at 500°C. Open symbols: less than peak strain (dynamic recovery). Closed symbols: greater than peak strain (dynamic recrystallization).

static recovery is difficult to identify because metadynamic recrystallization occurs concurrently [1–3]. The latter process consists of the continued growth of dynamic recrystallization nuclei after the deformation is stopped.

The first softening arrest can be attributed in the present case to the completion of metadynamic recrystallization and the second to the saturation of static recovery.† The *length* of the second arrest (see also Figs. 4 and 5) can in turn be associated with the incubation period required for the initiation of classical recrystallization. This is considered to take place during the continued operation of metadynamic recrystallization and static recovery, but in regions of the sample that are not swept clear of dislocation substructure by the metadynamic process.

3.2 *Effect of temperature*

As stated earlier, interrupted tests were also conducted at 450 and 540°C. The strain rates were selected so that the flow stresses developed at interruption, for all three temperatures, were approximately equal. The softening curves obtained at 450 and 540°C are shown in Figs. 4 and 5 respectively. The curves exhibit the same generally sigmoidal form, with intermediate inflection plateaus, as the curves determined at 500°C. For prestrains of 0.05 and 0.10 at 450°C and 0.05 at 540°C, softening does not go to completion, but saturates at 42, 50 and 42% respectively. No further softening is observed under these conditions, even after delays of up to 10^5 s, indicating that the critical strain for static recrystallization was not reached during prestraining. A prestrain of 0.15, at both temperatures, leads to two cycles of softening, separated by an intermediate plateau. It can be seen that the rates of recovery and recrystallization are both strongly temperature dependent. The duration of the softening arrest decreases with increasing temperature, indicating that the activation energy for static recrystallization is higher than the one for static recovery.

The softening curves determined for a prestrain of 0.40, at 450 and 540°C, relate to material which is recrystallizing dynamically at the point at which the deformation is stopped. Because of the rapid progress of softening at 540°C under these conditions, the earliest part of the curve could not be established. Nevertheless, in both curves obtained after 0.40 prestrain, two softening arrests are evident.

3.3 *Metallography*

A metallographic examination of the grain structures developed during the isothermal annealing, at

† This will be demonstrated in Fig. 11 and is also supported by the detailed analysis of the kinetics of the three processes [17].

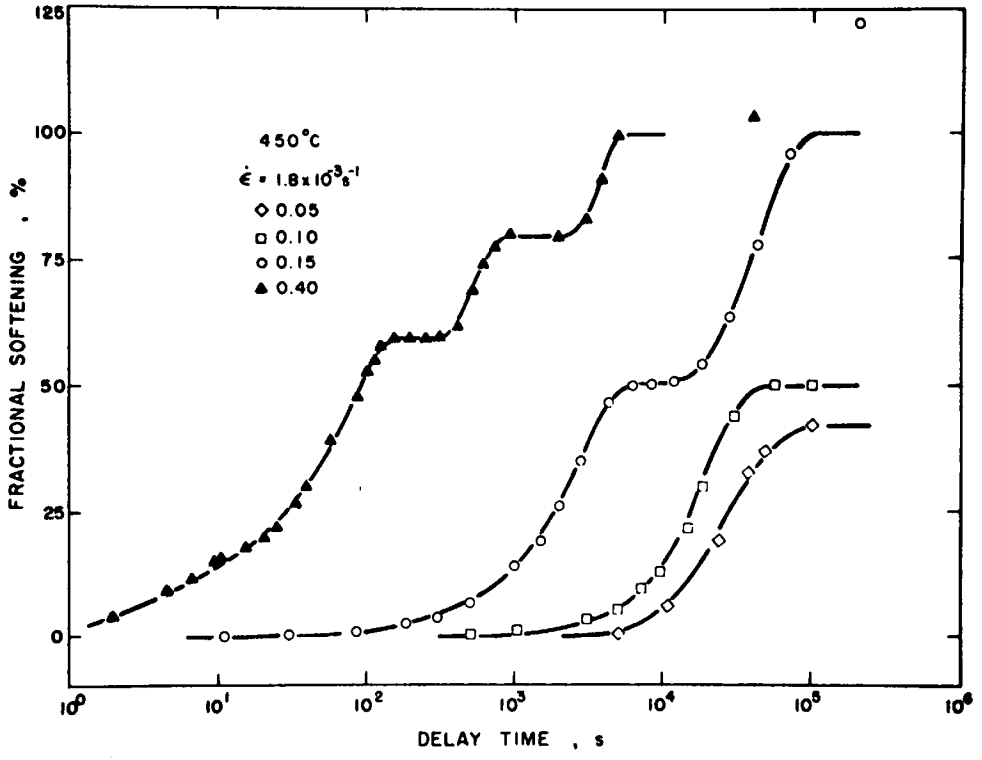

Fig. 4. Effect of strain on static softening at 450°C. (Symbols as in Fig. 3.)

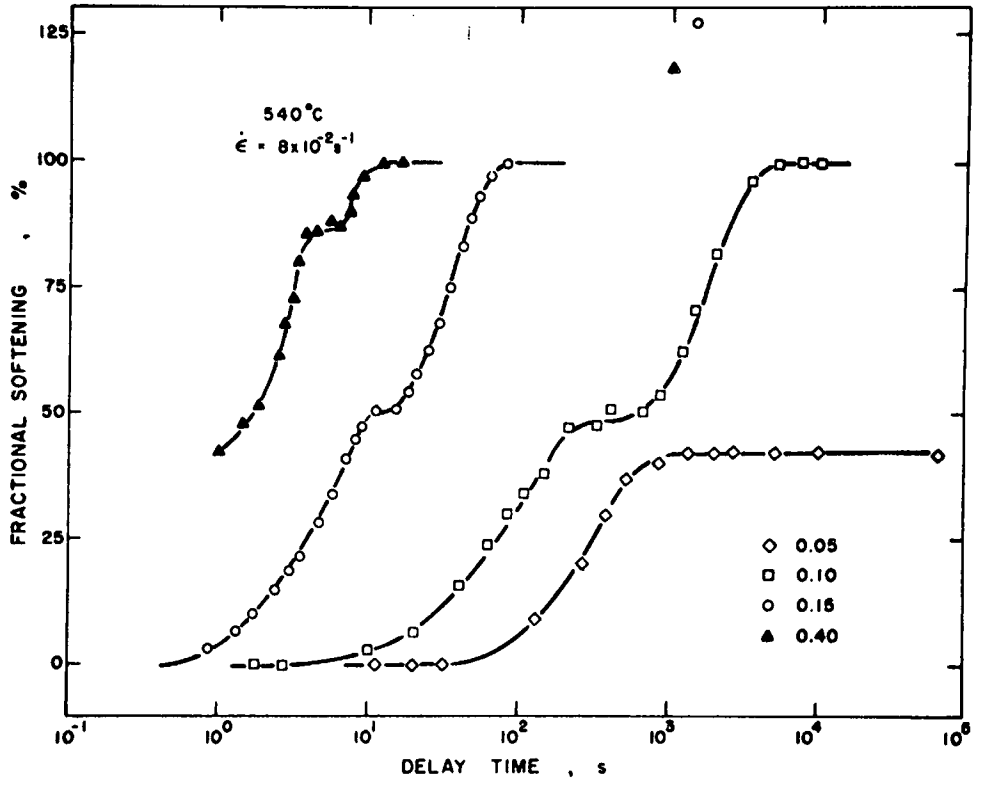

Fig. 5. Effect of strain on the static softening at 540°C. (Symbols as in Fig. 3.)

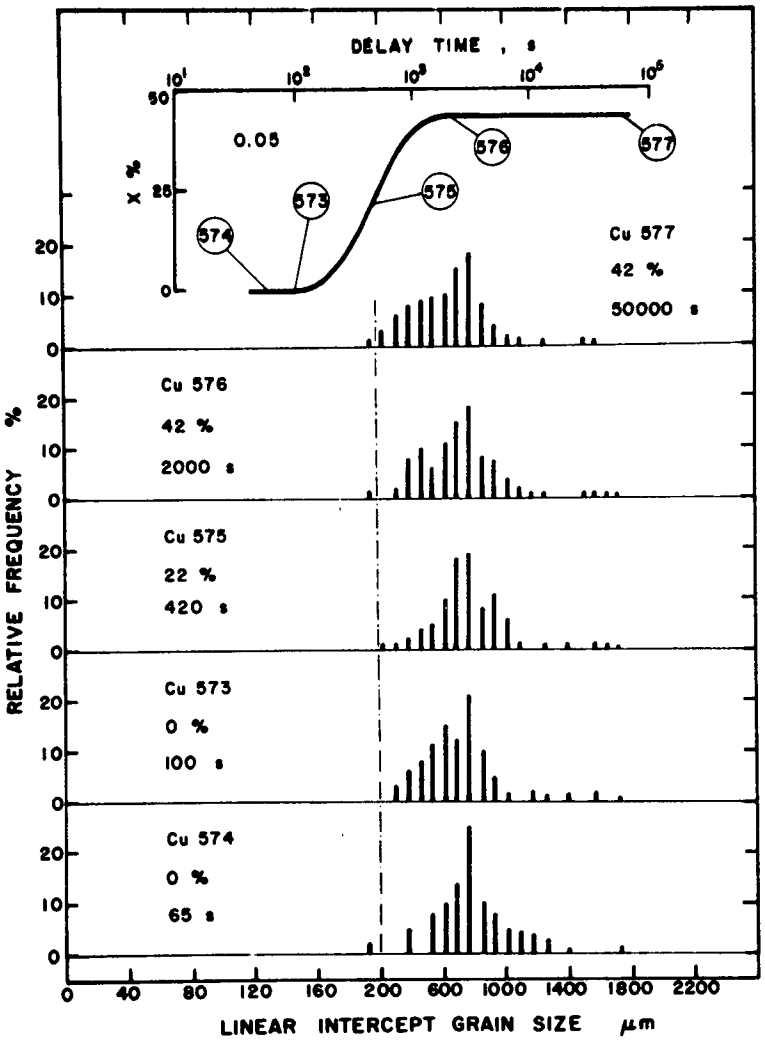

Fig. 6. Discontinuous frequency distribution of grain size in copper held at 500°C after 0.05 prestrain.

500°C, of the hot compressed copper was carried out. The softening curves suggested that grains derived from two distinct types of recrystallization should be present in the samples that had undergone high degrees of prestrain. In view of this, it was decided that simple point counting techniques would not yield sufficient information to allow the grains produced by the two processes to be distinguished. Instead, up to 500 individual grain intercepts were measured at random over the prepared surfaces. The intercept lengths were then subdivided into 8 μm size intervals between 0 and 200 μm, and 80 μm intervals between 200 and 2000 μm; and the relative frequency of the intercepts within each interval was also computed. The separation of the population into two size groups with a cut-off at 200 μm was based on the observation that 99% of the intercepts measured in undeformed samples fell in the upper group.

The data obtained, from samples quenched after delays between 65.5 and 50,000 s following prestraining to 0.05, are shown in Fig. 6. The softening curve determined by interrupted mechanical testing for the same prestrain [curve (a), Fig. 3], is displayed at the top of the figure. The points indicated on the softening curve represent the experimental conditions to which the corresponding intercept distribution applies. It is evident from this figure that the intercept class corresponding to the mode as well as the width of the distribution is relatively unchanged by increasing the delay time. The mean linear intercept grain size established from the individual measurements is constant to within $\pm 6\%$. Furthermore, the mean linear intercept grain size of these samples is equal to that of the undeformed samples, i.e. prior to prestraining.

Similar conclusions can be drawn from the linear intercept distribution established for a prestrain of 0.10, illustrated in Fig. 7. Here the prestraining conditions and the delay times correspond to those used to develop curve (b) in Fig. 3. These findings are in

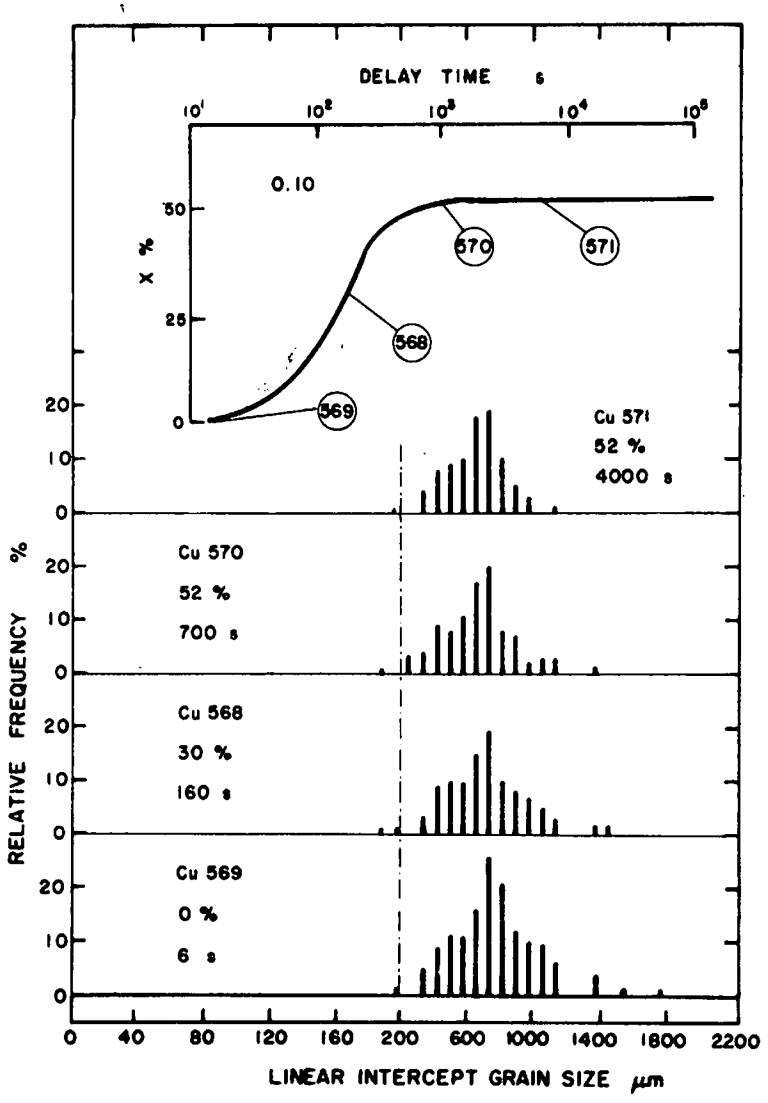

Fig. 7. Grain size distribution at 500°C after prestrain of 0.10.

agreement with the hypothesis that a hot working strain in excess of 0.10 is required at 500°C and $1.8 \times 10^{-2}\,s^{-1}$ to initiate static recrystallization. The grain size and intercept distribution is then unchanged with delay time, since softening occurs only by static recovery.

By contrast, Fig. 8 represents the distribution of grain sizes obtained in samples given a prestrain of 0.15. The static softening curve determined for this condition [curve (c), Fig. 3] indicates that two softening processes occur; these were tentatively identified as static recovery and static recrystallization. It is evident from the lowest grain intercept distribution that no significant change took place within the first second of annealing in either the modal class or the distribution width, i.e. the distribution is similar to that of the undeformed material. However, after 36 s, a new intercept distribution starts to appear centered on a mean size of 90 μm. After longer delay times, this new distribution grows at the expense of those grouped about the original grain size. Finally, after 500 s, the entire population of intercept lengths is grouped about a new mean grain size of 90 μm. It is of interest to note that, on delaying for a further 3 h, an additional 190 μm grouping begins to develop. This latter effect is taken as evidence for grain growth, and the associated further softening can be attributed, not to a reduction in dislocation density within the grains, but rather to the increase in grain size [18].

From Fig. 8, it can be seen that the newly recrystallized grains increase in number but do not grow, so that their mean size does not change appreciably with time. This result suggests that nucleation is occurring *inhomogeneously*, i.e. that different regions of the material have similar nucleation densities, but very different incubation times. An example of this type of inhomogeneous distribution of new grains is presented in Fig. 9(a), from which it can be seen that

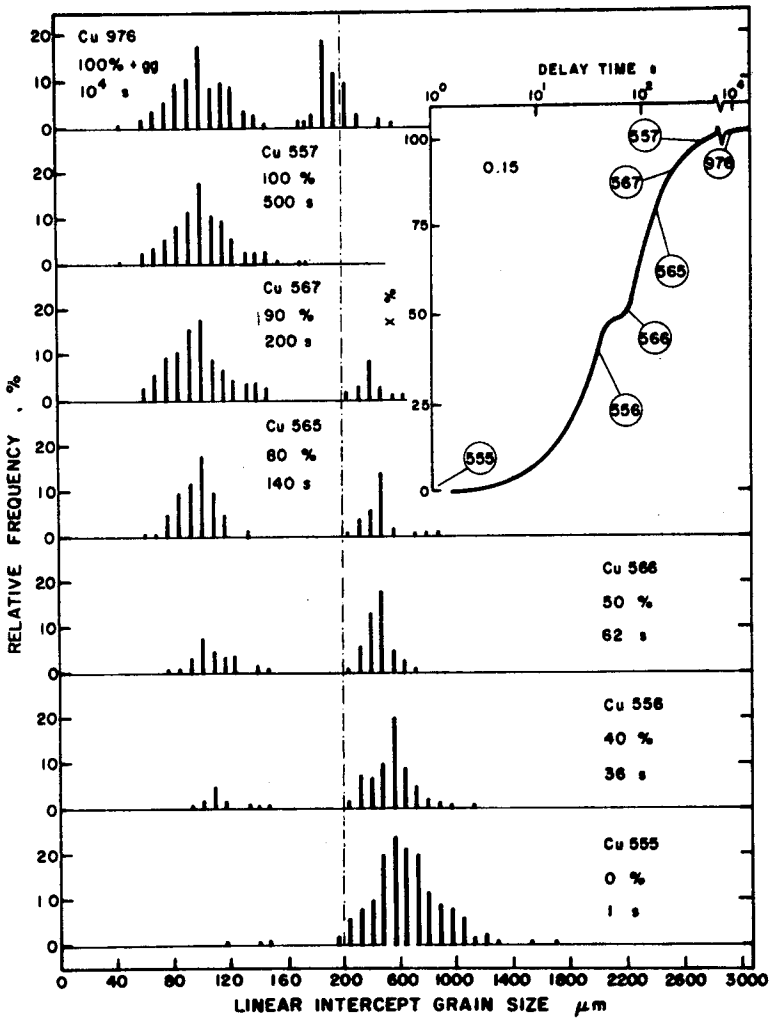

Fig. 8. Grain size distribution at 500°C after prestrain of 0.15.

the new grains are clustered together, and that other regions remain unrecrystallized. Such an observation is typical for materials deformed lightly at high temperatures [19–21] and may be related simply to the significantly lower dislocation densities present after such prestrains than are produced at ambient temperatures. It should be added that the bimodal distribution observed after annealing for 10^4 s suggests that abnormal grain growth is occurring. The micrograph taken from sample Cu 976 and shown in Fig. 9(b), clearly indicates the occurrence of secondary recrystallization.

The distribution curves determined for samples strained beyond the peak in the flow curve to a strain of 0.4 are illustrated in Fig. 10. All these samples had undergone dynamic recrystallization during the prestraining interval. In the sample that was quenched after the shortest delay interval of 0.9 s two groupings of intercept lengths are apparent. The longer lengths are gathered about a mean size of 170 μm; this is smaller than the original size of 560 μm. It is evident from the distributions observed after longer delay times, that the number of these larger grains decreases with increasing time. This grouping of intercept lengths is therefore associated with the dynamically recrystallized grains formed during prior straining. The number of grains within the second group, formed about a mean size of 40 μm, increases as the delay time increases. These latter grains are consequently associated with the static recrystallization process. Since 30% of the intercepts lie within this group after only 1 s of delay, it can be concluded that these grains are formed by metadynamic recrystallization.

As the delay time is increased, the dynamically recrystallized grains are gradually replaced by the metadynamic ones. However, after 6 s the short intercept distribution starts to be skewed towards longer lengths, and after 6–12 s, a third discrete distribution starts to appear, grouped about a mean of 80 μm. Once this group appears the number of intercepts associated with the metadynamically recrystallized

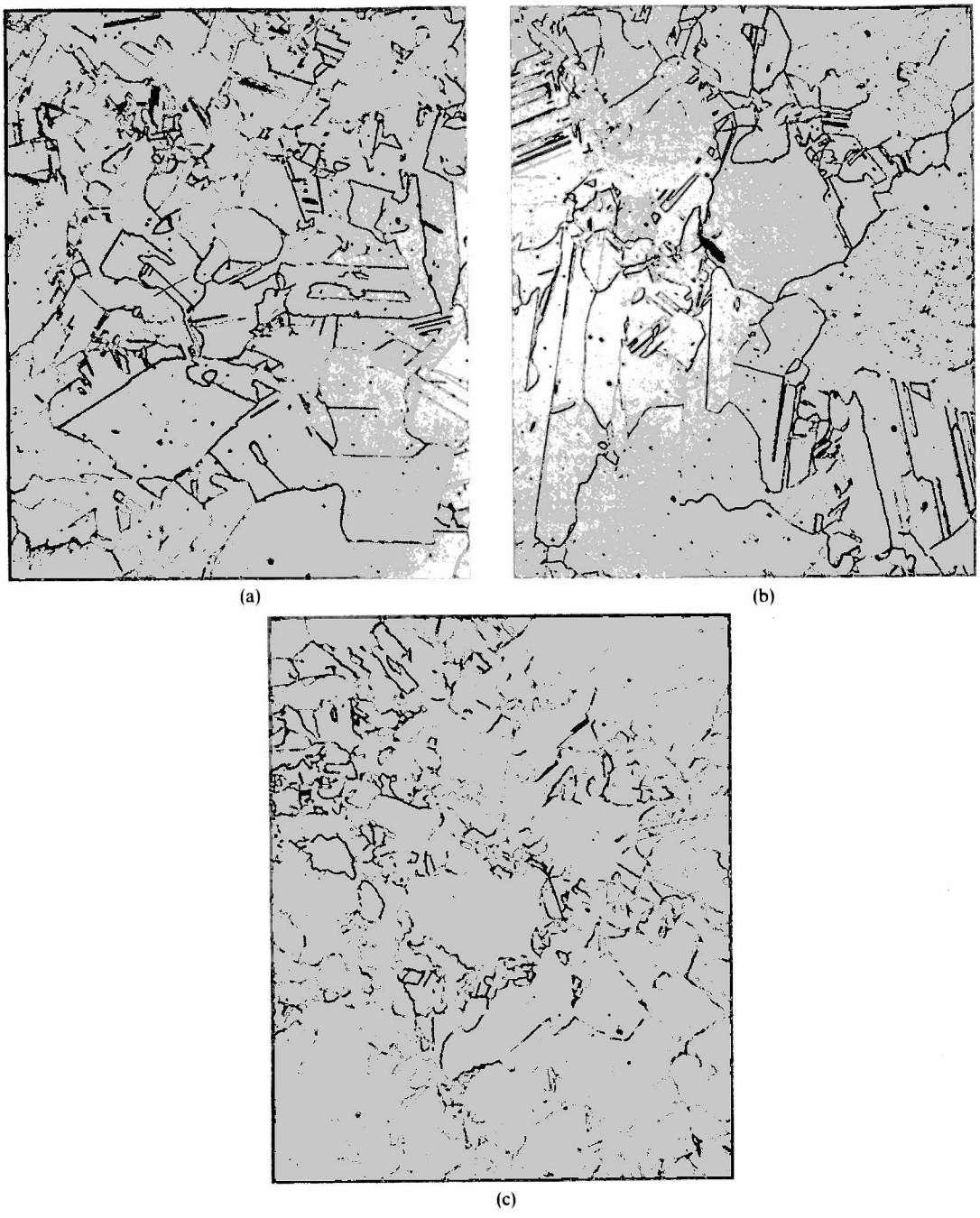

Fig. 9. Optical microstructures observed in samples prestrained at 500°C and $1.8 \times 10^{-2}\,s^{-1}$. (a) Isothermally annealed for 62 s after a prestrain of 0.15 (Cu 566) × 75. Note the packets of new fine grains in a matrix of large unrecrystallized material. (b) Isothermally annealed for 10^4 s after a prestrain of 0.15 (Cu 976) × 50. The micrograph shows evidence of abnormal grain growth where the large grains consume the fine recrystallized material. (c) Isothermally annealed for 3.6 s after a prestrain of 0.40 (Cu 564) × 150. The metadynamic grains, the fine material, form preferentially at the boundaries of the dynamically formed grains.

grains does not increase with further holding. Instead, the decrease in the number of dynamically formed grain intercepts is compensated by the increase in the number of intercepts associated with the third grouping. In terms of the present analysis, the grains with a mean size of 80 μm are considered to be formed by classical static recrystallization. The number of intercepts within this grouping continues to increase at the expense of the dynamically recrystallized ones, until the latter are almost completely consumed after a delay of 90 s, which corresponds to full softening.

The grain size distributions, illustrated in Fig. 10,

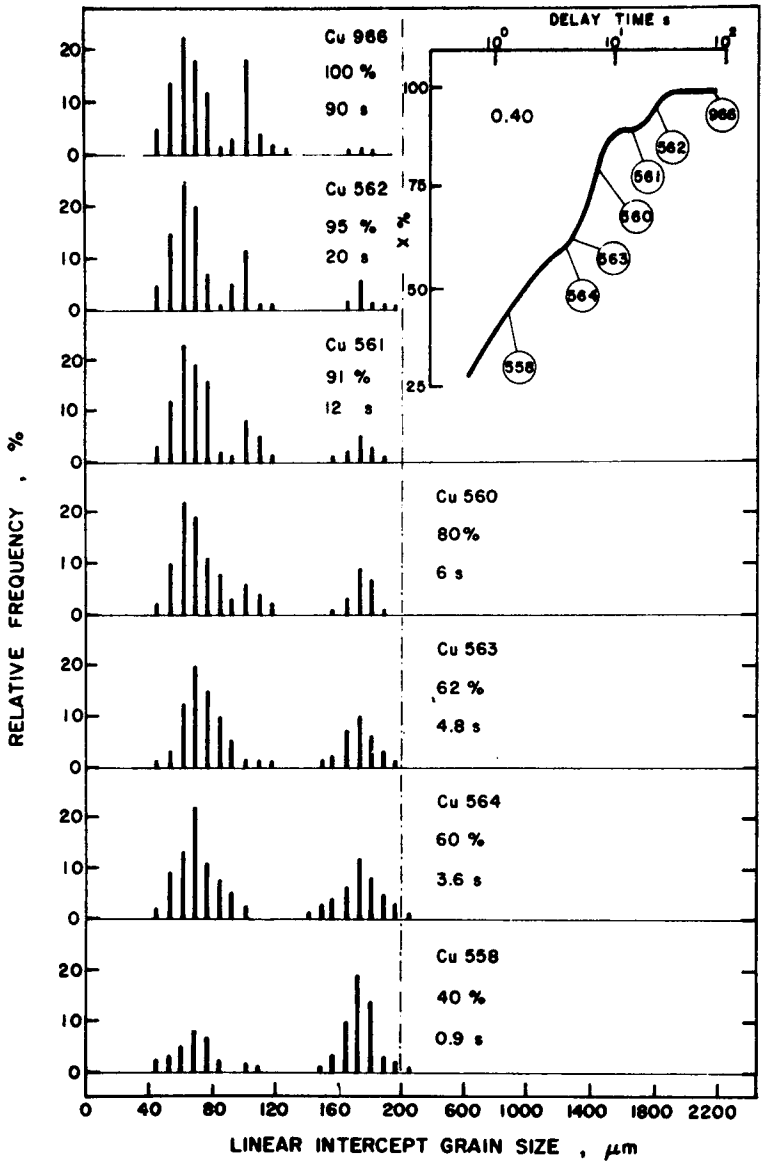

Fig. 10. Grain size distribution at 500°C after prestrain of 0.4.

show no growth in the mean size of grains associated with the two populations present at short times. Furthermore, it is evident that the metadynamic process does not go to completion. Instead, the balance of the structure recrystallizes independently at a larger size. It is evident from Fig. 9(c) that the metadynamic grains tend to develop in a few clusters that are scattered throughout the dynamically formed population. This observation suggests that, like the classical recrystallization nuclei, the metadynamic ones are dispersed inhomogeneously. Once the nuclei have all grown, impingement occurs within the clusters, so that the process of metadynamic recrystallization can only continue at the surface of the cluster at a much reduced rate. Ultimately, classical recrystallization takes place in the unrecrystallized material so that metadynamic recrystallization is prevented from consuming the unrecrystallized material.

3.4 *Calculation of volume fraction recrystallized*

The grain size distributions described in Figs. 6–8 and 10 lend themselves to the determination of the volume fraction recrystallized. For this purpose it is assumed that the size distribution of the unrecrystallized material is unchanged during prestraining up to the strain ϵ_{CD} required to initiate dynamic recrystallization. The intercept length range corresponding to the unrecrystallized material is apparent from the short time distributions of Figs. 6 and 7. It can be assumed, for the present purposes, that grains falling into size classes greater than 200 μm belong to the unrecrystallized population, while smaller intercepts

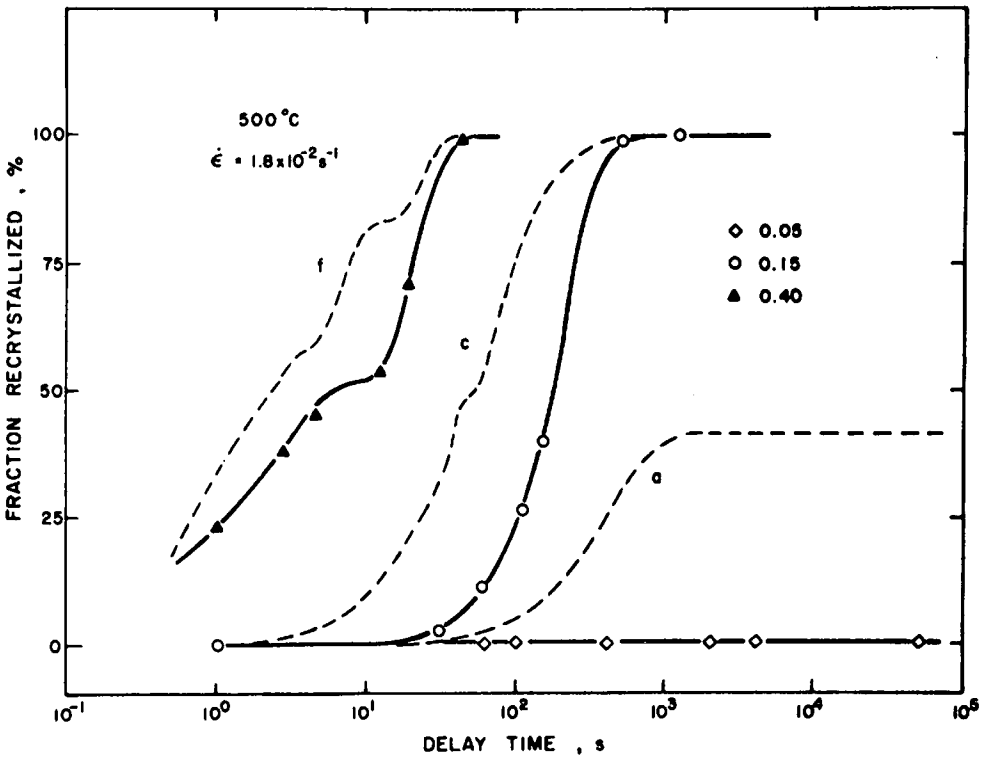

Fig. 11. Comparison of the softening curves obtained mechanically (broken lines) and the recrystallization curves obtained by quantitative metallography (full lines) at 500°C after prestraining at $1.8 \times 10^{-2} s^{-1}$.

are derived from the new grains. The volume fraction recrystallized is then calculated from the linear fraction $L_L (= V_v)$ of the latter group.

The dependence of the volume fraction of recrystallized material on delay time for samples prestrained 0.05, 0.15 and 0.40 at 500°C is presented in Fig. 11 (solid curves). For comparison purposes, the corresponding softening curves taken from Fig. 3 are plotted on the same axes. The softening curve (a) corresponding to 0.05 prestrain shows a maximum softening of 40% after a delay time of 1000 s. Under such conditions, however, no change in grain distribution was observed and consequently the volume fraction recrystallized remains zero for all delay times. After 0.15 prestrain, recrystallization is first observed after about a 40 s delay by which time the fraction recrystallized is 5%. At the same time, the corresponding mechanical softening curve shows 40% softening [broken curve (c)]. This observation indicates that recrystallization has already begun before the softening attributable to recovery is complete. The inflection plateau in the softening curve can be seen to arise from the gradual diminution of softening by recovery as this process becomes saturated. Finally the mechanical softening curve approaches that obtained by quantitative metallography, as recrystallization goes to completion.

In the case of the recrystallization data obtained on samples that were prestrained to 0.40, two intercept distributions were already evident, even after a delay as short as 1 s. The distribution associated with the larger intercepts, grouped about a mean size of 170 μm has been attributed to dynamic recrystallization. In this case 130 μm was selected as the cut-off; shorter lengths were considered to arise from the static recrystallization processes.

It is evident from Fig. 10 that the dynamically recrystallized grains are gradually consumed as more metadynamic grains are formed. Reference to Fig. 11, however, shows that more softening occurs than is indicated by the recrystallization data. This difference is once more attributable to static recovery, which goes to completion in about 10 s. Here the recovery is considered to take place in dynamically recrystallized grains which have not yet undergone either metadynamic or classical recrystallization.

In contrast to the data obtained after 0.15 prestrain, the 0.4 prestrain *recrystallization* data show an inflection plateau and the *mechanical* tests show two arrests. The second mechanical arrest has already been attributed to the saturation of recovery. After the first mechanical arrest (i.e. the metallographic arrest), a third distinct intercept size grouping starts to appear in Fig. 10. This group can be associated with the formation of classically recrystallized grains within the dynamically recrystallized matrix. Figure 11

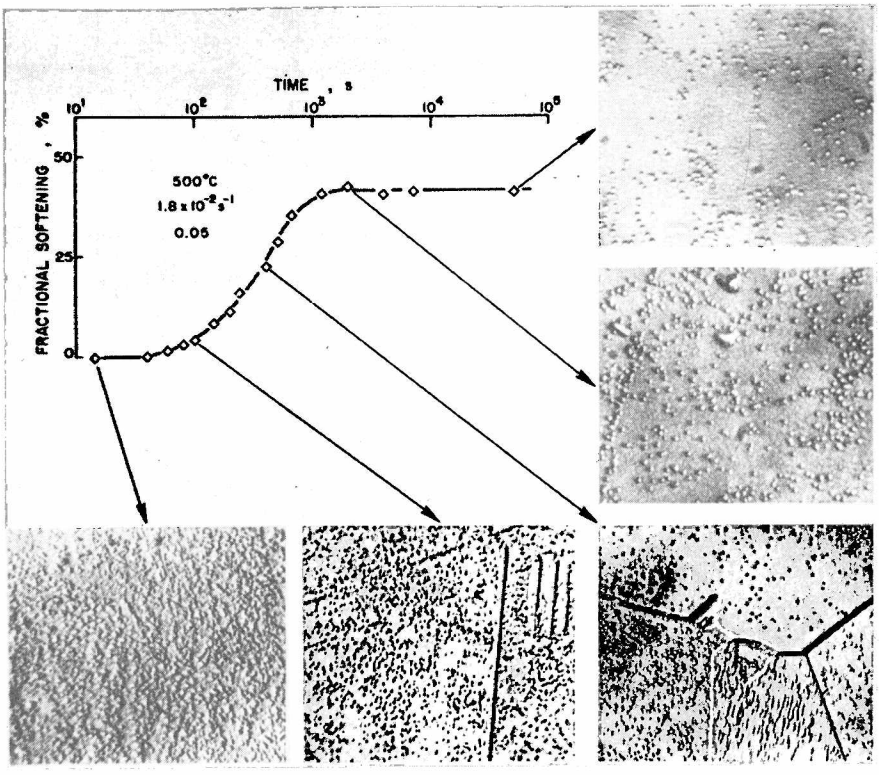

Fig. 12. Dislocation structure as revealed by etch-pitting after 0.05 prestrain at 500°C. ×900.

indicates that the process of metadynamic recrystallization goes to saturation in the vicinity of the first arrest, and that continued recrystallization after the arrest occurs primarily by growth in the volume fraction of the grains within the third, intermediate, group.

4. DISCUSSION

The results of the present investigation clearly establish that up to three distinct cycles of softening can take place after an interval of hot working. The processes responsible for such static restoration are recovery, recrystallization and metadynamic recrystallization, which can occur sequentially or concurrently. The metadynamic (or post-dynamic) recrystallization process was first introduced to explain the presence of three softening cycles after the prior dynamic recrystallization of austenite [1–3]. The present data confirm the existence of this distinctly separate type of recrystallization. The process is envisioned as arising from the continued growth of recrystallization nuclei that were formed dynamically, and can, therefore, only take place in materials that are undergoing dynamic recrystallization during the prior straining intervals.

An interesting feature of the present work is the result that after prestrains less than some critical value, softening takes place by recovery alone. Furthermore, the fractional softening attributable to recovery saturates at some 40–50%; that is, as much as half the flow stress increase introduced during working is removed. Similar results were obtained by Evans and Dunston [22] in high purity aluminum, although they measured the degree of restoration in a somewhat different manner.

The value of the critical strain ϵ_{CR}, below which no recrystallization ensues, appears to be relatively independent of temperature; that is, $0.10 < \epsilon_{CR} < 0.15$ for all three temperatures. Since the experiments were designed to ensure that the flow stress at a given prestrain is the same for all temperatures, the result is similar to that observed after cold working; that is, that a minimum dislocation density and lattice curvature are required before the material is able to recrystallize on subsequent annealing.

At strains in excess of ϵ_{CR} recovery goes almost to completion before the onset of recrystallization, so that the two processes always appear to operate sequentially. A question that arises is why recrystallization only takes place after a certain amount of strain energy is removed by recovery.

The events that accompany recovery can be monitored by observation of the changes in etch pit density. Representative micrographs obtained using the technique of Gupta and Strutt [23] on samples strained 0.05 at 500°C are shown in Fig. 12.† It can

† Specimens were electropolished using the same techniques as for general metallography and then etched with a solution containing: 1 ml bromine, 15 ml glacial acetic acid, 25 ml HCl, 90 ml water and 130 ml methanol.

be seen that, in samples quenched within 10 s of the removal of the stress, a high concentration of dislocations is present. The area density, of $4 \times 10^{10}\,m^{-2}$, is likely to be unreliable because many overlapping pits were observed, and not all of the dislocations present are expected to produce pits [24]. After holding for 100 s, the average pit density appears to decrease to some extent. This decrease is accompanied by a tendency towards a more orderly arrangement of the pits and therefore a decrease in the stored energy of the configuration. It is evident that this trend is continued as the holding time is increased to 1000 s and beyond. The observations, although qualitative in nature, suggest that the recovery of stress is accompanied at first by changes in network density and then, later, by changes in the thickness of the sub-boundaries arising from a reduction in the redundant dislocation content [25]. These two stages of the recovery process are discussed in more detail in reference [17].

4.1 *Effect of concurrent deformation on nucleus formation*

As a contrast to the static recrystallization that occurs after working to low strains ($\epsilon_{CR} < \epsilon < \epsilon_{CD}$), metadynamic recrystallization requires no induction period after the cessation of deformation. The rapid inception of this type of recrystallization is indicative of the postulate that the nuclei are formed during prior deformation. Furthermore, the process becomes exhausted when all the nuclei thus formed have become new grains.

The question that naturally comes to mind is the following: how can the nuclei formed during deformation lead to smaller grain sizes when recrystallization follows straining than do the same nuclei when the deformation is not interrupted? There seems to be two possible explanations for the observation that a higher nucleus density is produced by *interrupted* straining than by the *continuation* of straining. One is the hypothesis that, under continued deformation, the mean strain energy difference across an embryo (sub-critical nucleus) boundary is *less* (because of concurrent work hardening on both sides of the moving boundary) than when the deformation is interrupted. In the latter case, a completely dislocation-free region is formed behind the moving boundary, and this region can be expected to have a lower internal stress level due to the action of long range stress fields. This concept is in keeping with the model for dynamic recrystallization nucleus formation proposed by Sandstrom and Lagneborg [26]. An alternative explanation is that the *act of unloading*, which leads to the reverse motion of dislocations, gives the latter a greater degree of freedom for nucleus formation than continued forward straining. Clearly further work is required to clarify this important point.

4.2 *Comparison of the present results with observations regarding the hot working of steels*

One of the motivations for the present work was the aim of interpreting the various softening plateaus observed during the static annealing of hot worked carbon [1–3] and HSLA [27–29] steels. It is of interest in this connection that Rossard determined the dependence of austenite grain size on holding time after hot working in some of these materials [30]. He deformed his samples in the temperature range 900–1000°C and applied prestrains of 1.0 at $4\,s^{-1}$. According to his observations, based on a quench time of about 0.01 s, the austenite grain size was about 5 μm in the HSLA steel and in the range 10–15 μm in the plain carbon steel. These levels increased rapidly with holding time to about 10–15 μm for the HSLA steel and 30–50 μm for the plain carbon steel after about 100 s of holding. On the basis of the rapid quench, Rossard assumed that the 5 μm HSLA grain sizes were produced by *dynamic* recrystallization (10–15 μm in the plain carbon steel), and the 10–15 μm HSLA grain sizes by *metadynamic* recrystallization (20–50 μm in the plain carbon steel). Thus he concluded that metadynamic recrystallization leads to a *coarser* grain structure than does dynamic recrystallization.

By contrast, the present results indicate that metadynamic recrystallization leads to *finer* grain structures than do either of the other two types of recrystallization. The resolution of this discrepancy affects, not only the applicability of the model proposed above, but also has practical implications in metal processing. A possible explanation of the conflict between the two sets of results is the following. The steel results [30] were carried out at significantly higher homologous temperatures, strains and strain rates than the current work. Thus the kinetics of both metadynamic and classical recrystallization are likely to be much more rapid that observed here [27]. Accordingly, the HSLA grain size of 5 μm determined after the rapid quench may not be the result of the dynamic, but rather of the metadynamic process. In a similar way, the HSLA grain size of 10–15 μm after 100 s, may represent the influence of classical rather than that of metadynamic recrystallization.

The rapidity of metadynamic recrystallization in austenite under processing conditions may indeed make the determination of the dynamic grain size a difficult task. In order to prove or disprove the rationalization advanced above, and to shed more light generally on the applicability of the current results to the processing of micro-alloyed steels, the necessity for studies involving the frequency distribution of austenite grain size and its dependence on time, strain and temperature is clearly evident.

5. SUMMARY

Interrupted hot compression experiments were carried out on polycrystalline copper at temperatures and strain rates of 450°C and $1.8 \times 10^{-3}\,s^{-1}$; 500°C and $1.8 \times 10^{-2}\,s^{-1}$; and 540°C and $8 \times 10^{-2}\,s^{-1}$. The response of the material to isothermal annealing was

studied by this means at seven levels of prestrain between 0.05 and 0.4. These were selected so as to distinguish between the annealing behavior of dynamically recovered and of dynamically recovered and recrystallized matrices. In addition, the progress of static recrystallization was followed by the quantitative metallography of samples quenched following isothermal annealing and the same strain intervals at 500°C.

The results obtained clearly establish the existence of three distinct mechanisms of static restoration following hot working. These are recovery, classical recrystallization, and metadynamic recrystallization. The second type of recrystallization was postulated earlier [1–3] to explain the softening behavior of hot worked plain carbon and microalloyed austenite. The present metallographic results confirm the occurrence of the postulated process of metadynamic recrystallization in a material that has undergone dynamic recrystallization.

In the temperature and strain rate regime studied, there is a critical strain ($\simeq 12\%$) below which no static recrystallization ensues during subsequent annealing. At strains inferior to this amount, softening occurs by recovery alone, and 40–50% of the flow stress increase due to work hardening can be removed in this way. At higher strains, a period of static recovery is followed by complete recrystallization. It is of interest that the recovery cycle is likely to be associated with the anelastic, i.e. recoverable, portion of the nonelastic strain. Thus, on reloading, the flow curve rejoins the interrupted flow curve after a brief transient during which the anelastic strain is reintroduced.

When working is carried out to strains that are large enough to induce dynamic recrystallization during the prestrain (>20–30%), metadynamic recrystallization occurs in addition to recovery and classical recrystallization. Metadynamic recrystallization only takes place in a material that is conditioned by dynamic recrystallization. The occurrence of this process is distinguished from classical recrystallization by the fact that no induction period for nucleation is required. The nuclei are formed during the prestrain and, as a result, metadynamic recrystallization proceeds immediately after (and even during) the unloading of the specimen. Metadynamic recrystallization is, therefore, viewed as occurring by the continued growth of a fixed number of nuclei and continues until all such centers are exhausted. It was found that, for the deformation conditions under consideration, the mean size of grains formed by both types of static recrystallization are smaller than those due to dynamic recrystallization. The metadynamic ones were the smallest; being about one third the size of those generated during the deformation (i.e. 70 μm compared with 170 μm). The production of these different grain sizes, which result from the growth of nuclei from the same population, can be attributed to the selective destruction of potential nuclei during deformation. According to this view, a larger number of potential nuclei reach criticality when the straining is stopped, so that the resulting recrystallized grain size is smaller.

Acknowledgements—The authors are indebted to the National Research Council of Canada for financial support and to Prof. D. H. Sastry for his encouragement, help and stimulating discussions.

REFERENCES

1. R. A. Petkovic-Djaic and J. J. Jonas, *J. Iron Steel Inst.* **210,** 256 (1972).
2. R. A. Petkovic-Djaic and J. J. Jonas, *Metall. Trans.* **4,** 621 (1973).
3. R. A. Petkovic, M. J. Luton and J. J. Jonas, *Can. metall. Quart.* **14,** 137 (1975).
4. A. T. English and W. A. Backofen, *Trans. TMS-AIME* **230,** 396 (1964).
5. M. J. Luton and J. J. Jonas, *Can. metall. Quart.* **11,** 79 (1972).
6. J. F. Alder and V. A. Phillips, *J. inst. Metals* **83,** 80 (1954–1955).
7. P. M. Cook, *Proc. Conf. Properties of Mat. at High Rates of Strain*, p. 86. Inst. Mech. Engrs, London (1957).
8. J. E. Hockett, *Proc. ASTM* **59,** 1305 (1959).
9. J. E. Hockett, *High Speed Testing, Vol. VI, The Rheology of Solids*, p. 205. Interscience, New York (1967).
10. J. E. Hockett, *TMS-AIME* **239,** 969 (1967).
11. D. V. Wilson and G. W. Rowe, *J. Inst. Metals* **95,** 25 (1967).
12. M. J. Luton, J-P. A. Immarigeon and J. J. Jonas, *J. Phys. E, Sci. Instr.* **7,** 862 (1974).
13. M. J. Luton and C. M. Sellars, *Acta metall.* **17,** 1033 (1969).
14. W. Roberts and B. Ahlblom, *Acta metall.* **26,** 801 (1978).
15. J. J. Jonas, C. M. Sellars and W. J. McG. Tegart, *Metall. Rev.* **14,** 1 (1969).
16. H. J. McQueen and J. J. Jonas, Recovery and recrystallization during high temperature deformation, in *Plastic Deformation of Materials* (edited by R. J. Arsenault), pp. 393–493. Academic Press, New York (1975).
17. M. J. Luton, R. A. Petkovic and J. J. Jonas, *Acta metall.* (submitted.)
18. R. A. Petkovic, M. J. Luton and J. J. Jonas, *Metal Sci.* To be published.
19. J. P. Sah, G. J. Richardson and C. M. Sellars, *Metal Sci.* **8,** 325 (1974).
20. G. Glover and C. M. Sellars, *Metall. Trans.* **3,** 2271 (1972); *Metall. Trans.* **4,** 755 (1973).
21. C. M. Sellars, *Phil. Trans. R. Soc. (London)* A **288,** 147 (1978).
22. R. W. Evans and G. R. Dunston, *J. Inst. Metals* **99,** 4 (1971).
23. V. P. Gupta and P. R. Strutt, *Can. J. Phys.* **45,** 2113 (1967).
24. J. E. Bird, A. K. Mukherjee and J. E. Dorn, in *Quantitative Relation Between Properties and Microstructure* (edited by D. G. Brandon and A. Rosen), p. 255. Israel Univ. Press, Jersalem (1969).
25. L. G. Fritzemeier and M. J. Luton, unpublished research, Columbia University (1979).
26. R. Sandstrom and R. Lagneborg, *Scripta metall.* **9,** 59 (1975); *Acta metall.* **23,** 387 (1975).

27. R. A. Petkovic, M. J. Luton and J. J. Jonas, in *Hot Deformation of Austenite* (edited by J. Ballance), pp. 68–85. AIME, New York (1977).
28. T. Greday and M. Lamberigts, in *Microalloying 1975*, pp. 145–148. Washington, D.C. (1975).
29. L. J. Habraken, M. Lamberigts and T. Greday, in *Hot Deformation of Austenite* (edited by J. Ballance), pp. 286–315. AIME, New York (1977).
30. C. Rossard, *Proc. 3rd Int. Conf. on Strength of Metals and Alloys, Cambridge, England*, Vol. 2, pp. 175–203 (1973).

Acta Metallurgica, Vol. 28, pp. 729 to 743

0001-6160/80/0601-0729$02.00/0

KINETICS OF RECOVERY AND RECRYSTALLIZATION IN POLYCRYSTALLINE COPPER

M. J. LUTON
Columbia University, New York, NY 10027

R. A. PETKOVIC
Exxon Research & Engineering Co., Linden, NJ 07036 U.S.A.

and

J. J. JONAS
McGill University, Montreal, H3A-2A7, Canada

(*Received* 28 *September* 1979; *in revised for* 25 *October* 1979)

Abstract—The kinetics of the restoration processes that take place during the isothermal annealing of polycrystalline copper have been analyzed with the aid of a three component model for softening. The data describing the overall softening were obtained by the method of interrupted hot compression and these were supplemented by a quantitative metallographic study of the recrystallized structures. Prestraining was performed at rates between 1.8×10^{-3} and $8 \times 10^{-2}\,s^{-1}$, in the temperature range 450 to 540°C, and to true strains between 0.05 and 0.4. The temperature-corrected strain rate was the same for all temperatures.

The three components of softening are identified as static recovery, classical recrystallization and metadynamic recrystallization. The paper describes the procedures used to separate the individual components of softening from the total restoration curve. It is shown that the softening due to the two recrystallization processes is faithfully described by an expression of the form

$$x = 1 - \exp(-kt^n)$$

where x is the fraction of the process complete at a given time t, k is a rate constant and n a constant characteristic of the process. The time exponents for classical and metadynamic recrystallization are independent of the amount of prestrain and temperature, and are equal to 2.2 and 1.0 respectively. The static recovery process is shown to be comprised of two sequential mechanisms, the first of which leads to a considerably smaller degree of dislocation annihilation than the second. The first mechanism appears to be primarily anelastic and probably involves the reverse motion of network dislocations from the forward (dynamic recovery) to the backward (static recovery) obstacles. The second mechanism leads to a decrease in the sub-boundary dislocation density as well as in internal stress, but does not reduce the "hardness state" as much as it effects the yield stress.

Résumé—Nous avons analysé la cinétique de la restauration au cours du revenu isotherme de polycristaux de cuivre, à l'aide d'un modéle de l'adoucissement à trois composantes. Nous avons obtenu les données concernant l'adoucissement par la méthode de la compression à chaud interrompue et par une étude métallographique complémentaire des structures recristallisées. La prédéformation était effectuée à une vitesse comprise entre $1{,}8 \times 10^{-3}$ et $8 \times 10^{-2}\,s^{-1}$, à une température comprise entre 450 et 540°C, les déformations vraies étant comprises entre 0,05 et 0,4. Les vitesses de déformation corrigées en température étaient les mêmes pour toutes les températures.

Les trois composantes de l'adoucissement sont constituées par la restauration statique, et les recristallisations classique et dynamique. Nous présentons dans cet article les méthodes qui permettent de séparer les composantes individuelles de l'adcucissement à partir des courbes de globales restauration. Nous montrons qu l'adoucissement provenant des deux processus de recristallisation est bien représenté par une expression de la forme

$$x = 1 - \exp(-kt^n)$$

où x est le taux d'avancement du processus à un instant t donné, k est une constante de vitesse et n une constante caractéristique du phénomène. Les exposants du temps pour les recristallisations classique et métadynamique sont indépendants du taux de prédéformation et de la température; ils sont égaux respectivement à 2,2 et 1,0. La restauration statique est constituée de deux mécanismes séquentiels, le premier conduisant beaucoup moins que le second à une annihilation des dislocations. Le premier mécanisme est essentiellement anélastique; il met probablement en jeu le mouvement inverse de réseaux de dislocations, depuis les obstacles à l'avancement (restauration dynamique) jusqu'aux obstacles au recul (restauration statique). Le second mécanisme produit une diminution de la densité de dislocations dans les sous-joints et une diminution des contraintes internes; il n'abaisse pas l'"état de dureté" autant qu'il affecte la limite élastique.

Zusammenfassung—Die Kinetik des während des isothermen Ausheilens von polykristallinem Kupfers ablaufenden Ausheilprozesses wurde mit einem dreikomponentigen Entfestigungsmodell analysiert. Die Daten des Entfestigungsverhaltens wurden mittels der unterbrochenen Heißpressung erhalten; diese wurden ergänzt mit quantitativen metallografischen Studien der rekristallisierten Struktur. Die Vorverformung wurde ausgeführt mit Geschwindigkeiten zwischen $1{,}8 \cdot 10^{-3}$ und $8 \cdot 10^{-2}\,s^{-1}$ im Temperatur-

bereich 450 bis 540°C bis zu wahren Dehnungen von 0,05 bis 0,4. Die temperaturkorrigierte Verformungsgeschwindigkeit war dieselbe für alle Temperaturen.

Die drei Komponenten der Entfestigung sind statische Erholung, klassische und metadynamische Rekristallisation. In dieser Arbeit werden die Verfahren beschrieben, mit denen die einzelnen Erholungskomponenten aus der Summenerholungskurve isoliert wurden. Es wird gezeigt, daß die von den beiden Rekristallisationsporzessen herrührende Entfestigung mit einem Ausdruck der Form

$$x = 1 - \exp(-kt^n)$$

genau beschrieben werden kann; x ist der Bruchteil des abgelaufenen Prozesses bei gegebener Zeit t, k ist die Ratenkonstante und n ist eine den Prozess charakterisierende Konstante. Die Zeitkonstanten der klassischen (=2,2) und metadynamischen (=1,0) Rekristallisation hängen von dem Vorverformungsgrad und von der Temperatur nicht ab. Es wird gezeigt, daß der klassische Erholungsprozess aus zwei sequentiellen Mechanismen besteht. Der erste führt zu einer beträchtlich geringeren Versetzungsannihilation als der zweite. Der erste Mechanismus scheint vorwiegend anelastisch zu sein und besteht wahrscheinlich in der Rückwärtsbewegung von Netzwerkversetzungen von den 'Vorwärts'-(dynamische Erholung) zu den 'Rückwärts'-(statische Erholung) Hindemissen. Der zweite Mechanismus führt zu einer Abnahme in der Versetzungsdichte in den Subkorngrenzen und in den inneren Spannungen, er verringert den 'Härtezustand' jedoch nicht so sehr wie die Fließspannung.

1. INTRODUCTION

In a recent paper [1], the present authors reported results concerning the isothermal annealing of polycrystalline copper after hot working. On the basis of metallographic evidence, the paper established that annealing proceeds by the operation of up to three distinct restoration processes: namely, static recovery, classical recrystallization, and metadynamic recrystallization. It is the purpose of the present paper to examine these results in more detail in order to extract information regarding the kinetics of the individual processes. Such kinetics can be useful for the calculation of roll torque and separating force, and for the design of both rolling equipment and roll schedules.

Several studies [1–4] have shown that the relative contributions made by each of the three restoration processes depend critically on the strain introduced during the prior hot working interval. After low prestrains, e.g. less than 10%, annealing proceeds by recovery alone. When recovery is complete, as much as 40–50% of the flow stress increase due to work hardening is removed. Such recovered microstructures are evidently highly stable, as no further change in flow stress is observed after appreciable holding times. When a critical value of hot working strain is exceeded, e.g. more than 10% but less than 15%, isothermal annealing proceeds in two stages, with an interval of static recovery followed in turn by classical recrystallization. Once again, as much as 40–50% of the net work hardening is removed by recovery, but in this case recrystallization leads to *complete* softening, so that the final flow stress corresponds approximately to that of the undeformed material. If the critical strain for dynamic recrystallization is exceeded during the prestrain, e.g. 25%, then both dynamic recovery and recrystallization are in progress when the deformation is stopped. Under these circumstances, isothermal annealing occurs by the operation of metadynamic recrystallization, as well as by static recovery and classical recrystallization.

In the earlier paper [1], data concerning the progress of annealing and the contributions to softening of each of the three mechanisms were determined by means of both a mechanical technique and by quantitative metallography. The more complete results were those of the mechanical method. These data will now be used for the evaluation of the kinetics of the individual processes which, in turn, will shed light, not only on the nature of these mechanisms, but also on the interactions between them.

2. EXPERIMENTAL METHOD AND RESULTS

2.1 Scheme of analysis

The empirical parameters that can be used to describe the kinetics of softening after hot deformation are not well defined. This is because the concurrent operation of up to three distinct processes precludes the direct application of a single equation of the form proposed by Avrami [5, 6]. This type of equation is restricted to a single overall process consisting of two mechanisms such as nucleation and growth. Such a conclusion is supported by the detailed metallographic study of the recrystallization of copper published by Schweizer and Form [7], as well as the work described previously [1]. The difficulty can be resolved, however, if a way is found to separate the macroscopic softening observed into the three components attributable to each of the individual processes. Empirical relationships can then be fitted to the *individual* softening processes, and these can be used to evaluate the strain and temperature dependence of the mechanisms involved. Thus the analysis of complex restoration curves, such as those considered here, depends on the development of a reliable means of separating the individual softening components. This was possible in the present investigation because the softening information from the mechanical tests was supplemented by sufficient quantitative metallographic data [1] to allow this separation to be made.

Examination of the softening curves presented in Figs, 3, 4 and 5 of Reference [1] reveals that each

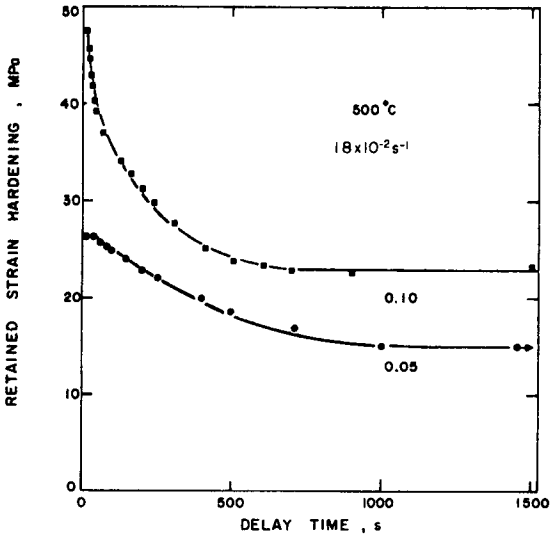

Fig. 1. The progress of static recovery in polycrystalline copper after straining at 500°C and $\dot{\epsilon} = 1.8 \times 10^{-2}\,s^{-1}$ to prestrains of 0.05 and 0.10.

sector of the curves has a characteristic sigmoidal form when plotted semi-logarithmically. This is typical of solid state reactions involving phase transformations. A suitable choice for the integrated form of the rate equation is then:

$$x = 1 - \exp(-kt^n) \tag{1}$$

where x is the volume fraction of material that has completed the process, k is the rate constant and n is the time exponent. This expression is simply the general form of the Johnson-Mehl equation, which was originally proposed for the formation of pearlite from austenite [8], but also adequately describes recrystallization [9–11].

The sigmoidal semi-logarithmic *recovery* curves generally observed after high temperature deformation [1–4] are similar in most respects to those for recovery after cold working [12–15]. They differ, however, in that a short, yet distinct, *delay time* or *incubation period* occurs prior to the mechanism which reduces the yield stress, see Fig. 1†. In view of the occurrence of a delay period it is convenient to fit the recovery data with an *empirical relation* of the form of equation (1) above, with $n > 1$. The *physical* significance of such a fit and the information that it provides about the present type of recovery mechanism will be considered in detail below, but first, the various components of softening will be separated and the empirical kinetics appropriate to each process will be described in turn.

2.2 Empirical recovery kinetics

Data for copper deformed at 500°C and $1.8 \times 10^{-2}\,s^{-1}$ and interrupted at strains of 0.05 and 0.10 are used to illustrate the progress of recovery in Fig. 1. It is evident from the figure that, for a given prestrain, the retained work hardening decreases to an asymptotic level which depends on the prior strain, that is on the value of the stress at the beginning of the annealing period. For the analysis of recovery, it is useful to define an expression for the fractional recovery in which full recovery is represented by the asymptotic stress σ_∞. When only recovery is taking place, the fractional softening is given by

$$X^r = \frac{\sigma_m - \sigma_r}{\sigma_m - \sigma_0} \tag{2}$$

where σ_m is the flow stress immediately before unloading and σ_0 and σ_r are the initial flow stresses recorded during prestraining and reloading, respectively. The superscript r is used here to denote the softening fraction attributable to recovery only‡. It follows that the fractional softening at the completion of recovery X^r_∞, is given by

$$X^r_\infty = \frac{\sigma_m - \sigma_\infty}{\sigma_m - \sigma_0} \tag{3}$$

and the degree of recovery x^r by

$$x^r = \frac{X^r}{X^r_\infty} = \frac{\sigma_m - \sigma_r}{\sigma_m - \sigma_\infty} \tag{4}$$

The experimental quantities X^r and X^r_∞ can be substituted into equation (1) to yield a form of the integrated rate equation in terms of the softening fraction, viz.

$$X^r = X^r_\infty [1 - \exp(-k^r t^n)] \tag{5}$$

The value of the time exponent n in equation (5) can be determined by plotting log ln $[X^r_\infty/(X^r_\infty - X^r)]$ against log t. The data obtained for polycrystalline copper at 450, 500 and 540°C under conditions where only static recovery is taking place are presented in this way in Fig. 2.

It should be noted that the slopes of the curves appear to be independent of strain and temperature and exhibit a constant value of 1.33. This empirical expression represents the present recovery data, with the attendant delay period, more faithfully than the hyperbolic law ($x = a - \ln t$) commonly used with data for recovery after cold working [12–16]. The rate constant k^r for each prestraining condition *that led to recovery only* was obtained from plots of ln $[X^r_\infty/(X^r_\infty - X^r)]$ versus $t^{1.33}$, as shown in Fig. 3. It is evident that k^r increases rapidly with both strain and temperature and thereby reflects the displacement of the recovery portions of the softening curves, presented in Ref [1], to shorter times as the prestrain and temperature are increased.

† It should be noted that delay periods were observed in all the present recovery experiments. The duration of these intervals was typically about 1.5 orders of magnitude shorter than the time for complete recovery, so they are de-emphasized in plots like those of Fig. 1.

‡ Note that with respect to the term X^r in Equation (2), r is a *superscript* and not an exponent. Similar remarks apply to X^r_∞ in equation (3), x^r in equation (4) and k^r in equation (5).

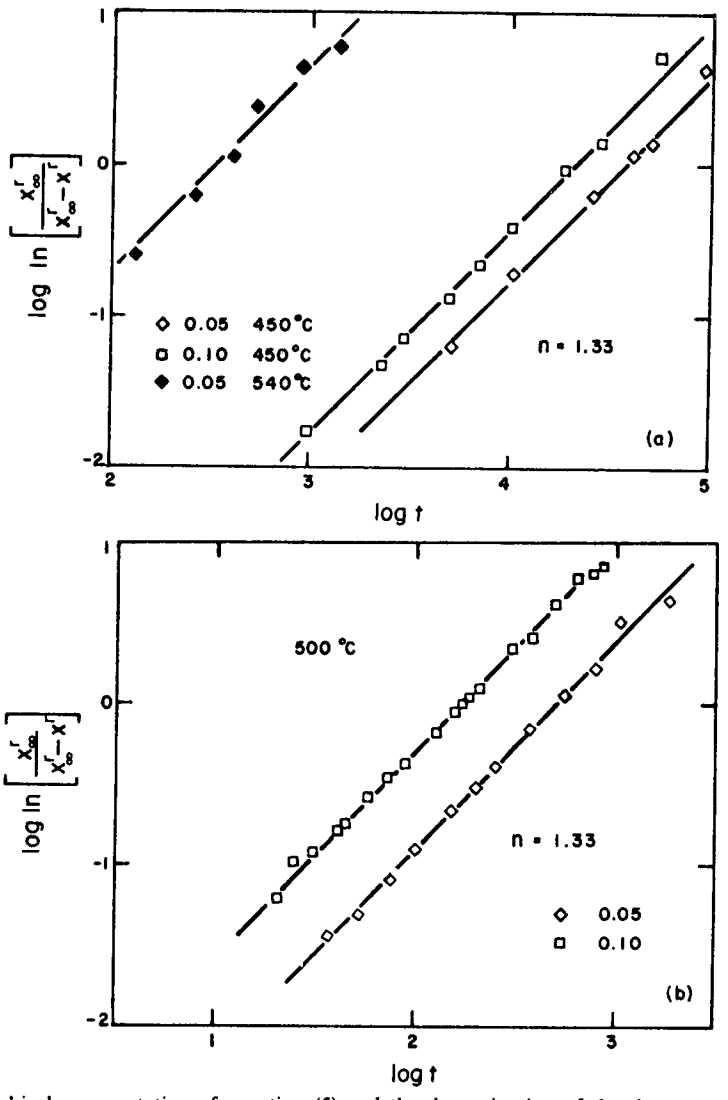

Fig. 2. Graphical representation of equation (5) and the determination of the time exponent n where recovery is the sole restoration process. (a) 450 and 540°C, (b) 500°C.

2.3 Kinetics of recovery and recrystallization

It was shown above that an empirical rate equation of the form of equation (1) adequately fits the recovery curves under conditions where recovery is the *only* static softening process. However, equation (1) is normally used to describe the kinetics of recrystallization. By and large, in studies of recrystallization after cold or hot working, the progress of recrystallization is followed by metallographic means, so that it is unnecessary to consider the influence of prior or concurrent recovery. When the structural changes are followed by *mechanical* means on the other hand, as in the present case, the recovery component of softening must be included in any overall rate equation. Furthermore, when dynamic recrystallization occurs during prestraining, the softening component due to metadynamic recrystallization must be included as well. Since the detailed mechanisms of these processes differ, the empirical constants in the component rate equations must differ also.

The overall softening produced when the three restoration processes occur together will in general be given by the sum of the individual components, i.e.

$$X = X^r + X^R + X^M \tag{6}$$

where the superscripts R and M refer to classical recrystallization and metadynamic recrystallization respectively. When the overall softening has gone to completion, all processes saturate, so that, in general†:

† Note that if the final grain size after recrystallization is complete is *coarser* than the original grain size (particularly if significant grain growth has occurred [1]), then $X_\infty > 1$. Similarly if the initial and prestrain conditions lead to grain refinement and a component of Hall Petch strengthening [17], then $X_\infty < 1$. More precisely, $X_\infty \simeq 1$ only if the initial and recrystallized grain sizes are about equal (and if the yield strengths are unaffected by aging or precipitation reactions).

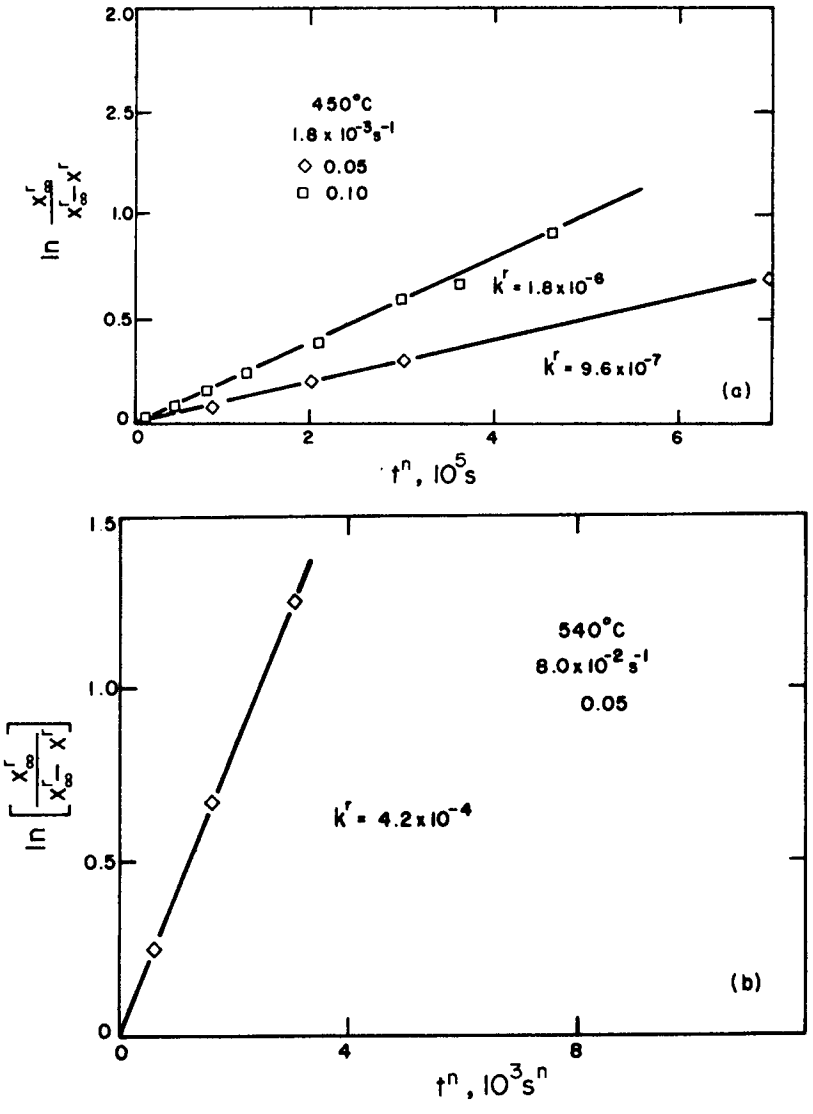

Fig. 3. Graphical determination of the rate constant k^r for the data presented in Fig. 2a above.

$$X_\infty = X^r_\infty + X^R_\infty + X^M_\infty = 1. \quad (7)$$

In section 2.2 above it was established that, when recovery occurs alone, X^r is described by equation (5). We assume here that

$$X^R = X^R_\infty [1 - \exp(-k^R t^p)] \quad (8)$$

and

$$X^M = X^M_\infty [1 - \exp(-k^M t^q)] \quad (9)$$

where k^R and k^M are the rate constants and p and q are the time exponents appropriate to the two processes.‡ These quantities can, in principle, be evaluated in the same manner as k^r and n. All that remains is to obtain suitable estimates of X^R_∞ and X^M_∞. For this it is necessary to rely on the metallographic data [1].

2.4 *Rate constants for recovery and classical recrystallization*

The present results indicate that recovery and classical recrystallization operate sequentially at first and then concurrently after prestrains of 0.15 and 0.18. Under such circumstances, X^M is always zero and $X = X^r + X^R$.

The largely sequential operation of the two processes facilitates the separation of the two softening components, which was carried out as follows. Bearing in mind the recovery saturation results described above and in Ref [1] for the case where recovery is the *sole* restoration process, the maximum softening due solely to recovery *when it is accompanied by recrystallization* was first set equal to 50%. In fractional softening terms, $X^r_\infty \simeq X^R_\infty \simeq 0.5$. The validity of this assumption was then checked in the following way.

† Note that with respect to the terms X^R, k^R, X^M and k^M in equations (8) and (9), R and M are *superscripts* and not exponents.

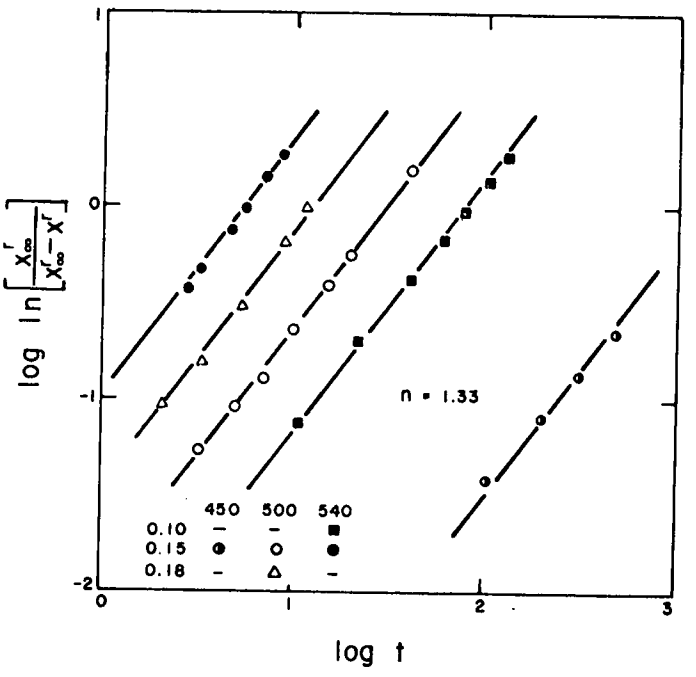

Fig. 4. Components of softening due to recovery separated from the two stage restoration curves plotted according to equation (5).

The metallographic examination of samples prestrained 0.15 at 500°C revealed that recrystallization begins only after a delay time of 30 s. The corresponding softening curve indicated the presence of a single inflection at 50% softening after about 40 s of delay.

Since the recovery process is complete or almost complete prior to the commencement of recrystallization, in the interval up to 50%, we can set $X^r = X$. The kinetics of recovery can then be evaluated as in Section 2.2 above. The curves representing the recovery kinetics calculated in this way for prestrains of 0.10 at 540°C, 0.15 at 450, 500 and 540°C and 0.18 at 500°C are shown in Fig. 4. It is evident that the data are well represented by a series of straight lines with a

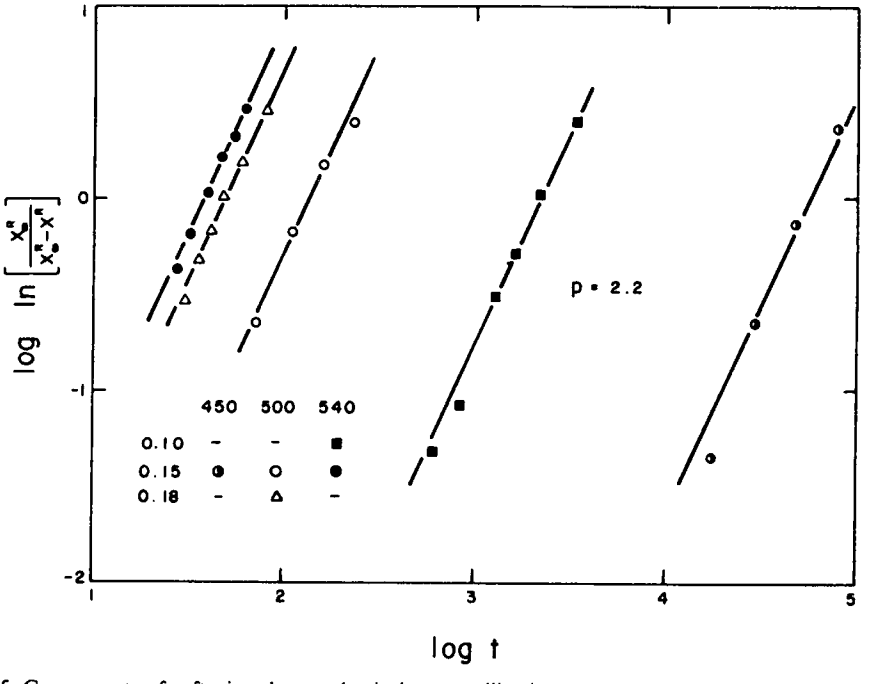

Fig. 5. Components of softening due to classical recrystallization separated from the same restoration curves as Fig. 4 and plotted according to equation (8).

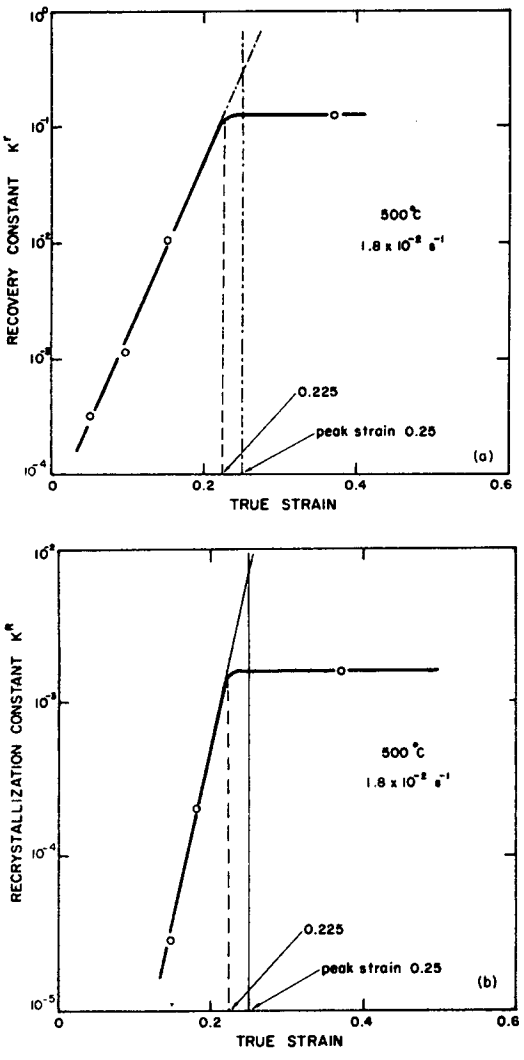

Fig. 6. The strain dependence of the rate constants. (a) recovery constants, k^r. (b) recrystallization constants, k^R.

slope n of 1.33, in good agreement with the 'recovery only' analysis of Fig. 2. Thus the values of the 'rate constant' k^r were determined in the same manner as before.

Once the values of the constants in equation (5) are known, X^r can be calculated for any value of t, and X^R can be extracted by difference from the experimental data, with the aid of equation (6). The fractional softening calculated in this way for the same experimental conditions as Fig. 4 is displayed in Fig. 5. Here the slopes of the curves p have a value of 2.2, which is apparently independent of strain and temperature. By contrast, the rate constant k^R, like that for recovery, is strongly dependent on strain and temperature, see Fig. 6.

It should be added that the good fit to the recrystallization kinetics obtained by assuming that $X^r_\infty = 0.5$ was not entirely fortuitous. Calculations were also made for $X^r_\infty = 0.40$ and $X^r_\infty = 0.60$, and these led to dependences which were decidedly inferior to those of Fig. 5. This is a point which will be taken up in more detail in the Discussion.

2.5 Rate constants for recovery, classical and metadynamic recrystallization

When all three processes operate together, the estimation of X^r_∞, X^R_∞ and X^M_∞ is less straightforward, because metadynamic recrystallization and recovery occur concurrently to a considerable degree. However, examination of the grain size distributions (Fig. 10 of Ref [1]) shows that after 3.8 s (which corresponds to the end of the first cycle of mechanical softening), 36% of the volume has recrystallized statically. This is attributable solely to metadynamic recrystallization, so that X^M_∞ is equal to 0.36. The balance of the material ultimately recovers and then recrystallizes in the classical manner, also contributing to the overall softening.

In order to estimate the individual saturation levels attributable to recovery and classical recrystallization, it was necessary to first assume that the time exponents n and p remain unchanged when dynamic recrystallization occurs during the prestrain, and second that the rate constants k^r and k^R for recovery and classical recrystallization can be represented by the expressions

$$k^r = Ae^{B\epsilon} \tag{10}$$

and

$$k^R = Ce^{D\epsilon} \tag{11}$$

Here ϵ is the value of the prestrain and A, B, C and D are empirical constants, see Fig. 6. We note, however, that in a material that undergoes dynamic recrystallization, the stored energy reaches a maximum at or near the peak of the flow curve. It is therefore reasonable to assume that the rate constants for recovery and classical recrystallization will also reach a maximum at some critical value of strain. For example, Rossard *et al.* [18] have suggested that dynamic recrystallization begins when the strain reaches a value of 0.83 ϵ_p, where ϵ_p is the strain to the peak flow stress.

In order to evaluate X^r_∞ and X^R_∞ and therefore to separate the softening components, tentative values of k^r and k^R were chosen with the aid of equations (10) and (11) for prestrains between 0.7 ϵ_p and ϵ_p. Then an iterative procedure was used in which X^r_∞ and X^R_∞ as well as k^r and k^R were varied [19]. The criterion of best fit was that the component of softening $X^M = 1 - X^r - X^R$ should be well represented by equation (9) at all values of t. This procedure yielded $X^r_\infty = 0.40$ and $X^R_\infty = 0.24$ as well as k^r and k^R values corresponding to a prestrain of 0.9 ϵ_p (i.e. 0.225).

The curves representing the individual softening components for a prestrain of 0.4 at 500°C are plotted in the manner of Fig. 2 in Fig. 7. The slope of the curve for the metadynamic recrystallization component was found to be approximately equal to 1 and the rate constant k^M took a value of 1.5.

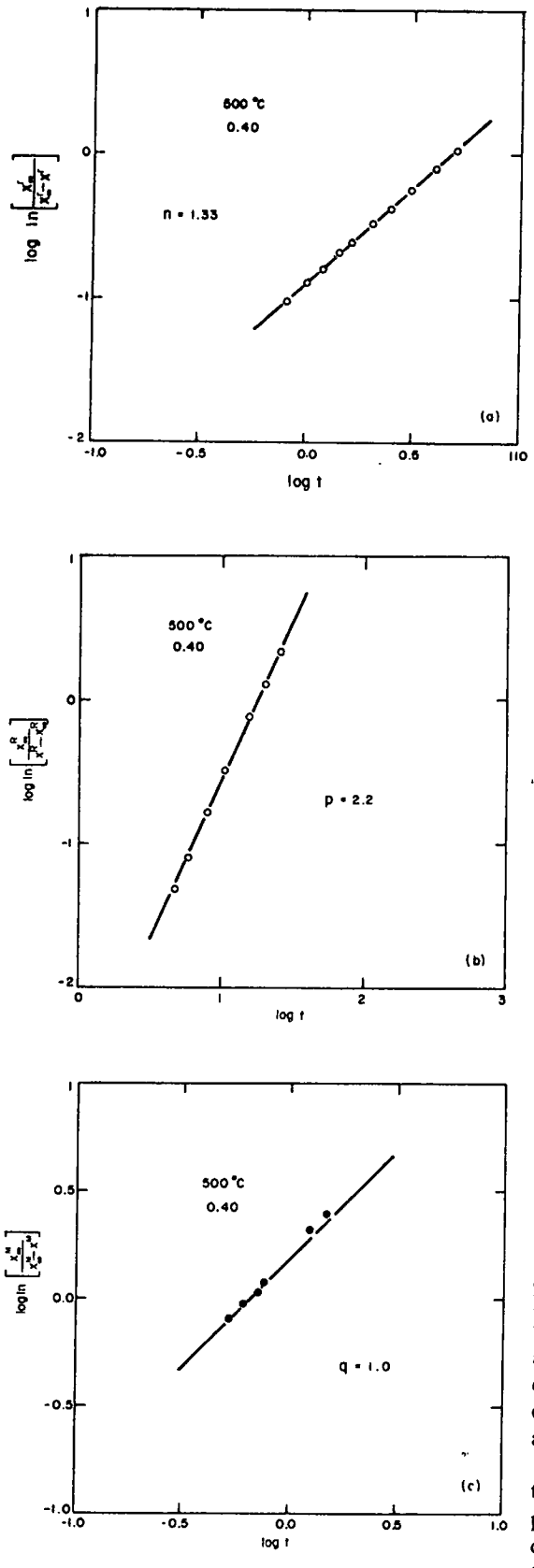

Fig. 7. Graphical determination of the time exponents for (a) recovery $-n$, (b) classical recrystallization $-p$. (c) metadynamic recrystallization $-q$.

2.6 *Comparison of empirical restoration kinetics with metallographic and mechanical softening data*

When static recovery is the only restoration process operative in the delay interval, the material response is governed by equation (5). This behavior is represented in Fig. 8 by the solid line which is based on the empirical constants determined above and listed in Table 1. The individual data points are the softening measurements obtained from the mechanical technique. The agreement is good, but not particularly significant, as only a single softening process was being considered. When recovery and classical recrystallization both contribute to the overall restoration, the total softening at any given time is the sum of the contributions from the two processes, both governed by relations of the form of equation (5). The empirical relations are plotted individually as continuous lines in Fig. 9 for prestrains of 0.15 and 0.18. In addition the sum of the two softening components is plotted (as a full line) for comparison with the original data points. It is evident that the two component model (based on a combination of mechanical *and* metallographic data) faithfully describes the observed behavior (which is entirely mechanically based).

It is of interest that the curves of Fig. 9 indicate that the recovery and recrystallization processes are not completely sequential. Instead, recovery is only 80–90% complete when 10% recrystallization has already taken place. This observation is consistent with the metallographic work described in Ref. [1]. Furthermore, recovery is complete by the time that 50–60% of the material is recrystallized. To this extent, recovery and recrystallization are *concurrent* processes, and recovery in the unrecrystallized material ahead of the advancing boundaries can be expected to influence the rate of recrystallization.

The case where all three static restoration processes contribute to softening is shown in Fig. 10. The individual softening curves are plotted as solid lines derived from equations (5), (8) and (9) with the appropriate constants from Table 1. Once more the sum of the three individual components, representing the overall softening X, is plotted as a full line along with the original data points. It is evident that the coupled rate expression (based on mechanical *and* metallographic data) describes the mechanical softening behavior very well. The good fit depends, of course, on the numerous assumptions already outlined above, and so the values of the rate and other constants can only be regarded as tentative. They do, however, establish that the three-component softening model is a consistent one.

It is evident from Fig. 10 that metadynamic recrystallization occurs very rapidly and is about 50% complete before any significant amount of static recovery occurs. Furthermore, this process is finished before there is any softening contribution from classical recrystallization. Once more the recovery process is about 90% complete before even 10% of the classical

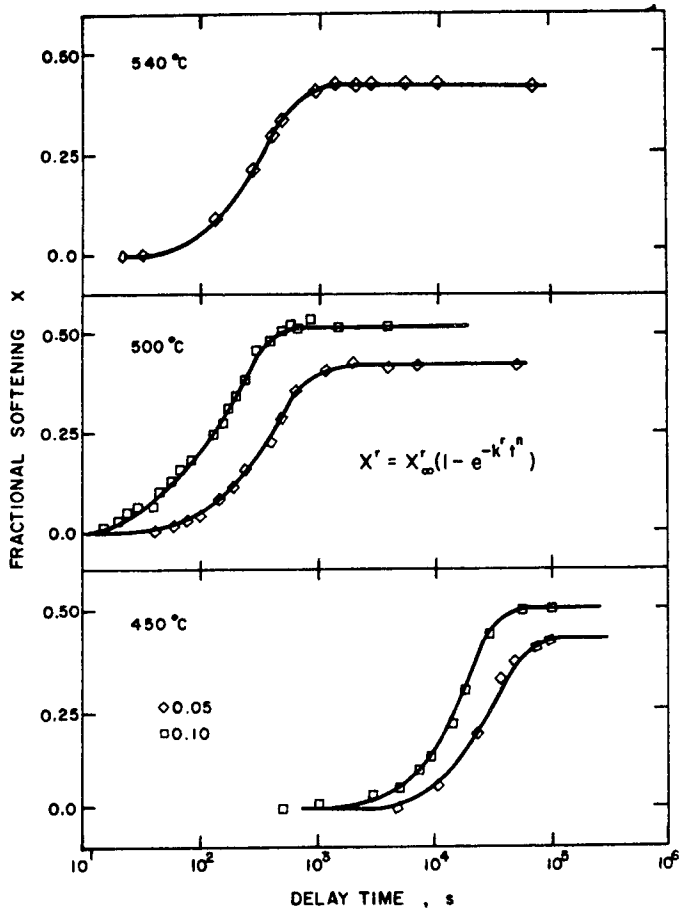

Fig. 8. Fit of equation (5) to experimental data points for static recovery.

recrystallization has taken place, but softening by recovery continues until only 12% of the material remains unrecrystallized.

3. DISCUSSION

3.1 Classical recovery kinetics and the incubation time

We now turn to consider the physical significance of a relationship of the form of equation (5) as applied to static recovery after hot working. The classical experiments on the recovery of cold work show that the rate of change of initial flow stress varies inversely with time (12–16). In most cases where an extended range of data is available it is seen that the rate 'constant' changes with time, or stress [12, 14, 15]. This has been taken by some to imply that the activation energy for the process increases as recovery proceeds [14, 20], and by others to indicate the sequential operation of two processes [15].

Table 1. Empirical constants for equations (5), (8) and (9) obtained from the softening data

Temp {°C} (1)	Strain rate {s^{-1}} (2)	Prestrain (3)	Recovery k^r (4)	n (5)	X^r_∞ (6)	Classical recrystallization k^R (7)	p (8)	X^R_∞ (9)	Metadynamic recrystallization k^M (10)	q (11)	X^M_∞ (12)
450	1.8×10^{-3}	0.05	9.6×10^{-7}	1.3	0.42	—	—	—	—	—	—
		0.10	1.8×10^{-6}	1.3	0.50	—	—	—	—	—	—
		0.15	3.1×10^{-5}	1.3	0.50	5.4×10^{-11}	2.2	0.50			
500	1.8×10^{-2}	0.05	3.2×10^{-4}	1.3	0.42	—	—	—	—	—	—
		0.10	1.1×10^{-3}	1.3	0.50	—	—	—	—	—	—
		0.15	1.1×10^{-2}	1.3	0.50	2.7×10^{-5}	2.2	0.50	—	—	—
		0.18	3.0×10^{-2}	1.3	0.50	2.0×10^{-4}	2.2	0.50	—	—	—
		0.40	1.2×10^{-1}	1.3	0.40	1.6×10^{-3}	2.2	0.24	1.50	1.0	0.36
540	8×10^{-2}	0.05	1.2×10^{-4}	1.3	0.42	—	—	—	—	—	—
		0.10	2.4×10^{-3}	1.3	0.50	5.4×10^{-8}	2.2	0.50	—	—	—
		0.15	1.2×10^{-1}	1.3	0.50	3.0×10^{-4}	2.2	0.50	—	—	—

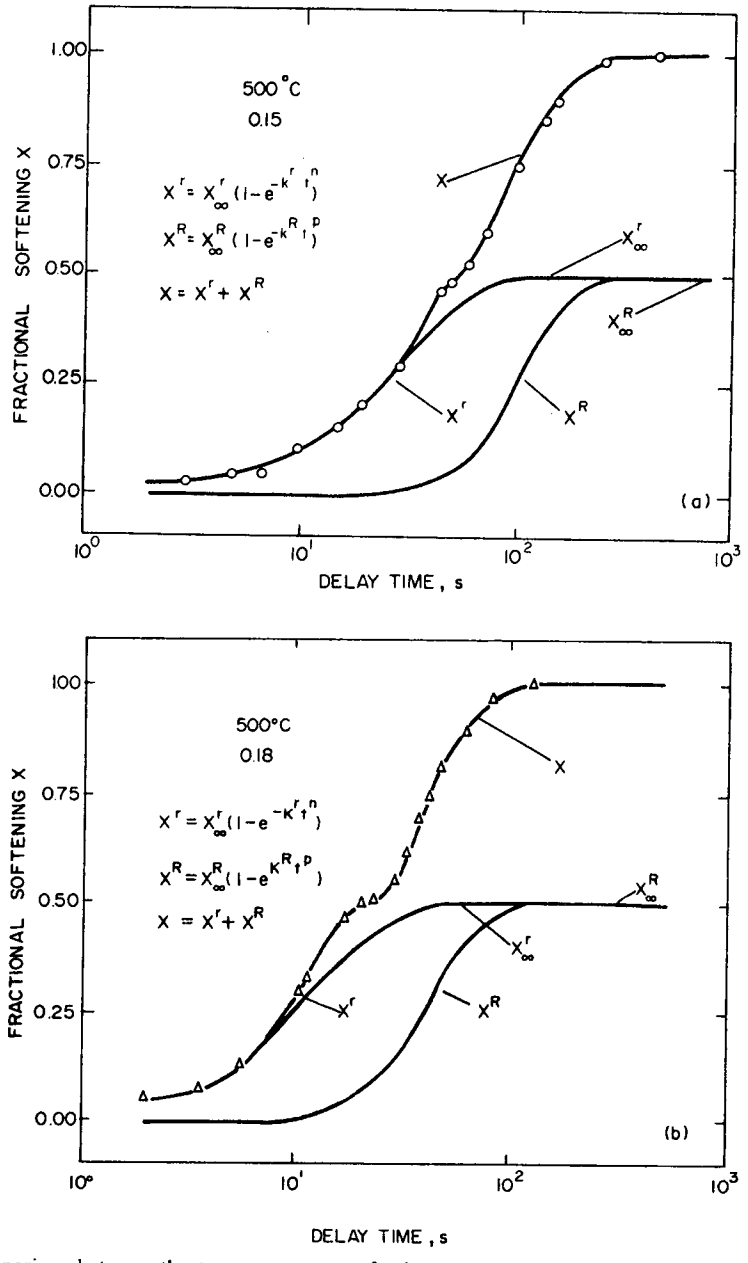

Fig. 9. Comparison between the two-component softening curves based on equations (5) and (8) and experimental data obtained at 500°C.

Consideration of the dislocation processes that produce recovery of flow stress has lead to the conclusion [20, 21] that the appropriate rate equation has the form,

$$\frac{d\sigma}{dt} = -k\sigma^m \qquad (12)$$

where m takes values between 1 and 3†. The present recovery data, like those obtained after cold working [13–15], show that the recovery rate goes to zero at stress levels in excess of the initial flow stress for the fully annealed material. It appears reasonable, therefore, to take $(\sigma_r - \sigma_\infty)$ as the driving force for recovery in equation (12). Thus equation (12) can be rewritten as,

$$\frac{d\sigma_r}{dt} = k(\sigma_r - \sigma_\infty)^m \qquad (13)$$

Integration of equation (13) with $m \neq 1$ leads to a power relationship between the annealing time and the fractional recovery. When $m = 1$, on the other

† When the range of stress is small or m is large, a power and exponential function, as implied by the inverse time dependence of the recovery rate, can be considered equivalent.

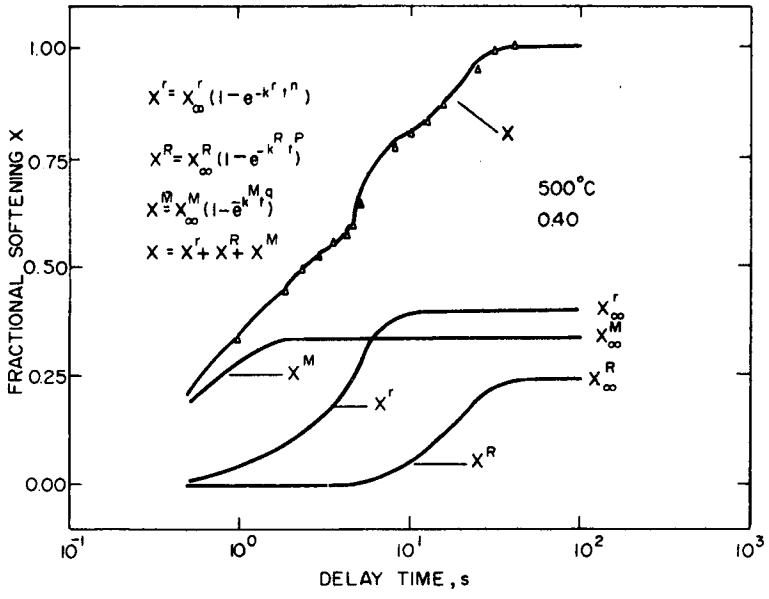

Fig. 10. The experimental data as fitted by the three softening curves based on equations (5), (8) and (9).

hand, integration of equation (13) yields an expression of the form of equation (5), but with a time exponent of $n = 1$, rather than $n = 1.33$, as observed. The excellent representation of the present data by equation (5) with $n > 1$ indicates that the *rate of recovery is zero at* $t = 0$, *increases to a maximum, and then decreases.* Such a sigmoidal softening curve (on a *linear* time axis) is equivalent to a two-stage or sequential process, in which the second mechanism cannot operate until the first one has taken place.

The above sequence of events includes the situation where there is an incubation or delay time τ associated with the characteristic time of the first mechanism†. Under such conditions, the two integral forms of equation (13) are,

$$\left(\frac{\sigma_r - \sigma_\infty}{\sigma_m - \sigma_\infty}\right) = [1 - x_r] = \exp[-k(t - \tau)] \quad (14)$$

and

$$\left(\frac{\sigma_r - \sigma_\infty}{\sigma_m - \sigma_\infty}\right)^{1-m} = [1 - x_r]^{1-m} = 1 + k''(t - \tau) \quad (15)$$

where

$$k'' = k(m - 1)(\sigma_m - \sigma_\infty)^{m-1}$$

The recovery data determined at 500°C are displayed in Fig. 11, plotted in terms of equation (14). It is clearly evident that immediately after each of the four prestrains, the recovery rate is zero or low. It

† Note also that if $\log (t - \tau)$ is used instead of $\log t$ as the abscissa of Fig. 2, the time exponent n is reduced by an amount that depends on the value of τ.

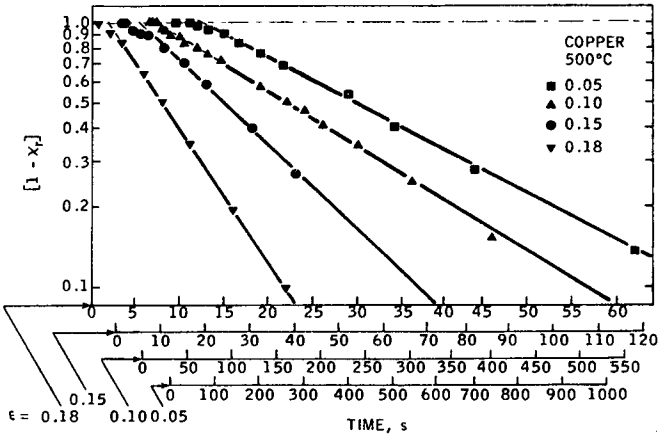

Fig. 11. Dependence of the logarithm of the normalized retained work hardening $[1 - X_r]$ on the time of recovery. The evidence for the incubation time associated with the first stage of recovery can clearly be seen, as can the degree to which the second stage obeys the linear kinetics of equations (12) and (15).

Table 2. Critical times determined for the recovery processes

	450°C		500°C		540°C	
Prestrain	τ, s	$(t_{0.5} - \tau)$, s	τ, s	$(t_{0.5} - \tau)$, s	τ, s	$(t_{0.5} - \tau)$, s
0.05	2500	21500	70	340	18	232
0.10	1000	16200	18	134	2.5	66.5
0.15	109	1920	4.5	19.5	0.65	3.2
0.18	—	—	2.0	6.0	—	—

then increases to a maximum, after which the rate of decrease in yield strength follows the linear kinetics specified by equation (14). A similar dependence of yield strength on recovery time was observed at 450°C and 540°C. The delay times τ associated with the first mechanism were determined by back-extrapolating the linear fit to the data in the region of the second mechanism as shown in Fig. 11. These delay times, as well as those calculated at 450° and 540°C are given in Table 2. They were used to evaluate the activation energy associated with the first mechanism (see Fig. 12a), from which a value of 286 kJ/mole was obtained.

3.2 Physical interpretation of the empirical recovery kinetics

To the extent that a relation of the form of equation [14] describes the recovery process, it is necessary to inquire into the nature of the events that lead to an apparent incubation period. At the start of recovery, the driving force for the process, the internal stress, is at a maximum so that, if recovery involves only one type of thermally activated event, such as network node unpinning or climb into the subboundaries, the rate of recovery should be initially at a maximum. This is evidently not the case. Before conventional "recovery" can take place, however, the dislocations must obviously contact the recovery obstacles. These are not necessarily the same as the barriers resisting forward flow (the *dynamic* recovery obstacles). It can therefore be hypothesized that, on unloading, the dislocations travel backwards to the rearward (*static* recovery) obstacles. This motion is driven by the line tension of the dislocations and by the local internal stress†. Once the rearward barriers are reached, thermally assisted unpinning or some diffusion-related event takes place, leading eventually to dislocation annihilation. In this model, the incubation period τ involves the time required for the network dislocations to travel from the forward to the backward obstacles.

The first mechanism can also be associated with the anelastic or recoverable strain [22] and therefore with the unbowing, reverse bowing and thermally activated unpinning and backward glide of the dislocation network [23]. This interpretation is supported by the observation that, on reloading after the first stage of recovery, the flow curve rapidly regains the level of the interrupted curve [1], because only a small forward strain must be imposed during loading to restore the dislocation configuration to approximately that of the moment of unloading. The second mechanism may also involve a component of rearward strain, but is distinguished from the first by the greater degree of dislocation annihilation it produces, leading to an appreciable drop in σ_r on reloading. It is significant that, even after the second recovery mechanism has gone to completion, the reloading flow curve still displays a limited transient (longer than the transient associated with the first recovery mechanism), after which it returns again to the stress level and work hardening rate of the continuous (uninterrupted) curve [1]. Such recovery reloading curves differ markedly from the flow curves observed after static recrystallization, which are characterized by 'normal' workhardening. The longer transient, as well as the results of a concurrent electron microscopic investigation of the substructures of the present materials [24], suggest that the second process pri-

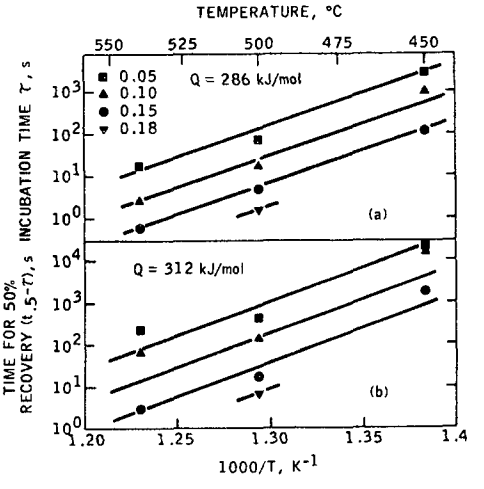

Fig. 12. (a) Arrhenius plot of incubation time τ versus $1/T$ for the first component of static recovery, associated here with network recovery. (b) Arrhenius plot of $[t_{0.5} - \tau]$ versus $1/T$ for the second component of static recovery associated here with recovery within the subboundaries.

† Note that the forward (dynamic recovery) and backward (static recovery) barriers can be of the same class (e.g. dislocation nodes), but are spatially separated by the reverse glide distance.

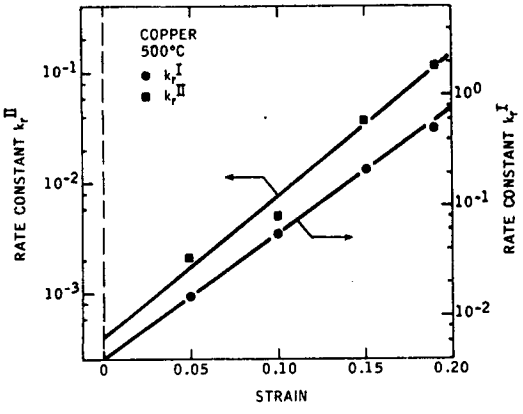

Fig. 13. The strain dependence of the rate constants for recovery: Stage I recovery, $k_r^I = 1/\tau$. Stage II recovery, k_r^{II}, the negative of the slopes of the linear portions of the curves Fig. 11.

marily involves the loss of redundant dislocations in the sub-boundaries.

It is apparent from the experimental results that the recovery rate associated with the first mechanism is not only temperature dependent (Fig. 12a), but also depends on the level of accumulated work hardening, and therefore on the substructure density ρ. The temperature dependence associated with the second mechanism is shown in Fig. 12b, where the time for 50% recovery is plotted against inverse temperature for different amounts of prestrain. Since prestraining in the present experiments was carried out at the same temperature—corrected strain rate, the starting structure and internal stress were nominally the same for a given prestrain at the three temperatures. Although more scatter is present in this case, it is evident that the activation energy for the second recovery mechanism is approximately equal to that for the first mechanism. It therefore appears likely that the same type of thermally activated event is rate controlling with respect to the static recovery of the sub-boundary dislocations as is involved in the first mechanism. The activation energies determined for both processes are about 20% higher than that of self-diffusion in copper. Similar observations were made for recovery after creep in aluminum [25]. This effect could be attributed to the influence of impurities on the rearrangement of dislocations during the two recovery processes.

The 'structure dependence' of the recovery rate constants k_r^I and k_r^{II} is shown in more detail in Fig. 13. From the diagram it is evident that the rate constants increase with prestrain, and therefore with the dislocation density ρ present at the moment of unloading. Thus the rate of recovery $d(\sigma_r - \sigma_\infty)/dt$ depends not only on the current level of the internal stress ($\sigma_i \propto [\sigma_r - \sigma_\infty]$, Fig. 11), *but also on the starting structure.* This result underlines the physical distinction that must be drawn between the internal stress σ_i and the 'hardness state' $\sigma^* \propto \sqrt{\rho}$ [26]. During static recovery, σ_i is generally reduced from its starting level to a small or negligible value. The hardness state σ^*, on the other hand, decreases only slightly, from the level associated with σ_m to that associated with σ_r (see Fig. 14).†

3.3 *Relevance of* σ_i and σ^* *to rolling loads*

The difference between σ_i and σ^* is particularly relevant to rolling load calculations. It has long been known in the rolling industry that static recovery between mill passes has only a small influence on the rolling load in the next pass, whereas static recrystallization has a much larger effect. This seeming paradox can be given a ready interpretation in terms of the present results [1], as shown in Fig. 14. When recovery annealing is carried to completion, there is a large drop in σ_i, and therefore in the density of 'high energy' or mobile dislocations, ρ_m. The loss of ρ_m during recovery leads in turn to a drop in the reloading yield stress σ_r.‡ There is also a small drop in the density of the "lower energy" fixed dislocations ρ_f and therefore in σ^*. On reloading and straining beyond σ_r, there is a transient (shown dotted) associated with the return of ρ_m to the level associated with ρ_f and therefore σ^*. Once ρ_m and ρ_f reassume their

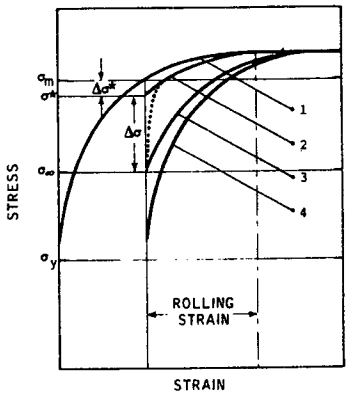

Fig. 14. Schematic representation of an interrupted compression test performed at the "reference" strain rate $\dot{\epsilon}_s$. Curve 1 is the continuous curve; curve 2 shows the evolution of the hardness state σ^* after an interruption; curve 3 is the flow curve expected from the value of $\sigma_r = \sigma_\infty$ and the work hardening behavior of curve 1 beyond this stress; curve 4 is the flow curve produced after full recrystallization and is parallel to curve 1; the dotted curve represents the transient behavior of the flow stress σ between σ_r and curve 2. For simplicity the hardness state σ^* is here defined as the transient-free flow stress at the reference strain rate $\dot{\epsilon}_s$.

† For purposes of illustration, the "hardness state", σ^*, is defined as the transient-free value of the flow stress at the standard strain rate $\dot{\epsilon}_s$ (27).

‡ This is because, under 'transient' conditions (i.e. when ρ_m is changing rapidly), a component of the reloading strain rate is provided by $\rho_m b\bar{L}$ (where $\bar{L}$ is the mean free path of the freshly generated dislocations, so that the non-multiplication component of the strain-rate $\rho_m b\bar{v}(\sigma)$ is significantly reduced, as is the associated flow stress σ_r.

'normal' proportions, the rate of work-hardening re-attains its normal value appropriate to the current magnitudes of σ and $\dot{\epsilon}$. During this transient, the flow stress rapidly increases to the σ^*-appropriate and $\dot{\epsilon}$-appropriate level. Thus the rolling load is close to that obtained by integrating either the continuous curve (curve 1) or the transient-free interrupted curve (curve 2), but differs considerably from that expected from an integration of an estimated flow curve based on σ_r and on the rate of work hardening associated with σ_r as anticipated from the continuous curve (curve 3). From the above, it is readily apparent that the yield stress σ_r under transient conditions is not at all closely linked to the hardness state σ^*. It also suggests that the internal stress σ_i, as defined above, may be a useful state variable for the description of the type of short term transient encountered here.

3.4 *Interpretation of recrystallization kinetics*

The current experiments indicate that two forms of recrystallization, metadynamic and classical, can take place in hot worked materials. These two processes are distinguished from each other by their time exponents and rate constants. It is a feature of their kinetics that the metadynamic process goes to completion before classical recrystallization begins†. The time exponents in transformation reactions described by equation (1) have commonly been associated with the preferred sites on which growth of the new phase is centered (28–30). In general, recrystallization nuclei are not expected to be uniformly distributed (homogeneous), but rather to be associated with grain corners, edges or faces. These potential sites are listed in order of increasing 'dimensionality'. As the dimensionality of the site increases, the time exponent in the rate equation has been shown to decrease as long as all the nucleation sites are saturated very early in the process [29]. According to this view, metadynamic nuclei which are fully "site saturated" *ab initio*, are predominantly located at grain boundary *faces*, and so are associated with a time exponent of 1. The nuclei for classical recrystallization are also likely to be located principally at the boundary faces. In this case, however, nucleation probably continues during recrystallization, i.e. the sites are *not* saturated at $t \simeq 0$. This latter picture is in keeping with the present kinetic results since recovery continues in the unrecrystallized material until 80–90% of the recrystallization process is complete, and is therefore likely to continue to produce new nuclei until this stage of the restoration process is reached.

† An unexplained, but intriguing feature of the present results is the inability of metadynamic recrystallization to produce full softening, and therefore to eliminate entirely the need for classical recrystallization. This is probably related to the inhomogeneous distribution of metadynamic nuclei, and therefore the remoteness of certain partially worked regions from metadynamic recrystallization fronts.

SUMMARY

In the present paper, a three component model has been used as the basis for analysis of the complex restoration curves obtained during the isothermal annealing of hot worked copper (1). The analysis of experimental data was made possible by the availability of quantitative metallographic data as well as mechanical softening results. According to the model, overall softening arises from the linear combination of three elements due to static recovery, classical recrystallization and metadynamic recrystallization. The recrystallization components are described by a general rate law of the form

$$x = 1 - \exp(-kt^n)$$

where x is the fraction of the process completed at a given time t and k and n are constants. The analysis shows that, for the present material and test conditions, the time exponent for classical recrystallization is 2.2 and for metadynamic recrystallization it is approximately 1. The exponents are independent of the amount of prestrain and temperature. The rate constants for static recovery and classical recrystallization on the other hand, increase rapidly with temperature and with the amount of strain up to a critical value (0.225) associated with the onset of dynamic recrystallization.

The empirical kinetics associated with metadynamic recrystallization are consistent with a concept of the process as one in which all nuclei are formed during the prestrain. Furthermore, support is given to the notion that the metadynamic nuclei are located preferentially at the grain boundary faces. As the nucleation sites for classical recrystallization are expected to be the same, the time exponent of 2.2 for the process can be attributed to the occurrence of continued recovery ahead of the advancing recrystallization front.

The experimental data indicate that the recovery process is comprised of *two* sequential mechanisms, the first of which leads to a smaller degree of dislocation annihilation than the second. The former component is attributed to the retreat of dislocations from the forward (dynamic recovery) to the rearward (static recovery) obstacles, and the observed incubation or delay time τ associated with this anelastic process is identified with the time required for the high energy network dislocations to reach the vicinity of the sub-boundaries. The second component is likely to involve thermally activated unpinning or some diffusion-related event, in the neighborhood of the sub-boundaries, leading to dislocation annihilation. Although the two sequential recovery mechanisms have similar activation energies ($\sim$300 kJ/mole), it is only the second mechanism which leads to significant recovery of flow stress and for which the recovery rate is first order in stress.

Acknowledgements—The authors are indebted to the National Research Council of Canada for their financial

support and to the McConnell Foundation for the award of a Research Fellowship (RAP). They would also like to express their thanks to Dr R. H. Doherty with respect to the revision of this paper.

REFERENCES

1. R. A. Petković, M. J. Luton and J. J. Jonas, *Acta metall.*, **27**, 1633 (1979).
2. R. A. Petković-Djaić and J. J. Jonas, *J. Iron & Steel Inst.* **210**, 256 (1972).
3. R. A. Petković-Djaić and J. J. Jonas, *Metall. Trans.* **4**, 621 (1973).
4. R. A. Petković, M. J. Luton and J. J. Jonas, *Can. Metall. Q.* **14**, 137 (1975).
5. M. Avrami, *J. chem. Phys.* **7**, 1103 (1939).
6. M. Avrami, *J. chem. Phys.* **8**, 212 (1940); **9**, 177 (1941).
7. M. Schweizer and W. Form, *J. Inst. Metals* **101**, 24 (1973).
8. W. A. Johnson and R. F. Mehl, *Trans. AIME* **135**, 416 (1939).
9. W. A. Anderson and R. F. Mehl, *Trans. AIME* **161**, 140 (1945).
10. J. E. Burke and D. Turnbull, *Prog. Metal Phys.* **3**, 226 (1952).
11. J. E. Bailey and P. B. Hirsch, *Proc. R. Soc.* (Lond), **A267**, 11 (1962).
12. D. Kuhlman, *Z. Phys.* **124**, 468 (1947).
13. R. Drouard, J. Washburn and E. G. Parker, *Trans. AIME* **197**, 1226 (1953).
14. J. T. Michalak and H. W. Paxton, *Trans AIME*, **221**, 850 (1961).
15. T. E. Tietz, C. L. Meyers and J. L. Lytton, *Trans. AIME* **224**, 339 (1962).
16. J. L. Lytton, C. L. Meyers and T. E. Tietz, *Trans. AIME* **224**, 1250 (1962).
17. R. A. Petković, M. J. Luton and J. J. Jonas, *Metal Science*, **13**, 569 (1979).
18. C. Rossard, *3rd Int. Conf. on Strength of Metals and Alloys*, Inst. Metals. Iron Steel Inst. London, Vol. 2, 175–203 (1973).
19. R. A. Petković, Ph.D. Thesis, McGill University, Montreal Canada (1975).
20. J. C. M. Li, in *Recrystallization, Grain Growth and Textures*, Am. Soc. Metals, Ohio, p. 45 (1966).
21. J. Friedel, *Dislocations*, Pergamon Press, Addison-Wesley Pub. Co., Reading, Mass, p. 276 (1964).
22. N. Nir, E. W. Hart and C-Y. Li, *Scripta Met.* **10**, 189 (1976).
23. M. Pahutová, J. Čadek and P. Ryš, *Scripta Met.* **11**, 1061 (1977).
24. L. Fritzemeier and M. J. Luton, unpublished research, Columbia University (1979).
25. L. Raymond and J. E. Dorn, *Trans. AIME* **230**, 560 (1964).
26. E. W. Hart, *Acta metall.* **18**, 599 (1970).
27. U. F. Kocks, A. S. Argon and M. F. Ashby, Thermodynamics and Kinetics of Slip, *Prog. Mater. Sci.* **19**, 87 (1975).
28. P. J. Clem and J. C. Fisher, *Acta metall.* **3**, 70–73 (1955).
29. J. W. Cahn, *Acta metall.* **4**, 449 (1956).
30. J. W. Christian, *The Theory of Transformations in Metals and Alloys*, Part 1, Pergamon Press, Oxford, p. 476 (1975).

Grain size and high-temperature yield strength of polycrystalline copper

R. A. Petkovic, M. J. Luton, and J. J. Jonas

Polycrystalline, electrolytic tough pitch copper was prepared in a series of stable grain structures by deforming at 540 and 600°C at strain rates from $7{\cdot}5 \times 10^{-4}$ to 8×10^{-2} s^{-1}. By applying a prestrain of 0·4 and annealing isothermally, grain sizes ranging from 0·056 to 0·810 mm were produced. The prepared grain sizes decreased with the amount and strain rate of the prestrain, and increased with the prestraining and annealing temperature. After working and sufficient annealing to permit full recrystallization, the yield strengths were determined at 540°C ($0{\cdot}6T_m$) and at four strain rates ranging from $7{\cdot}5 \times 10^{-4}$ to 8×10^{-2} s^{-1}. The high-temperature yield strength increased linearly with the inverse square root of the grain size, as it does at room temperature. However, the grain boundary strength coefficient (slope of the Hall–Petch plot) increased with strain rate, indicating that the grain boundaries serve as both local and long-range obstacles to flow at elevated temperatures.

Manuscript received 2 October 1978; in final form 3 April 1979.
R. A. Petkovic, DipIng, MEng, PhD, is with Exxon Research and Engineering Co, Linden, New Jersey, U.S.A. M. J. Luton, BMet, MMet, PhD, is at Columbia University, New York, U.S.A. J. J. Jonas, BEng, PhD, is at McGill University, Montreal, Canada.

The presence of grain boundaries is generally considered to lead to weakening at high temperatures. Thus, above the 'equicohesive temperature'[1] a coarse-grained material is expected to be stronger than a fine-grained one. This is, of course, because of the ease of grain boundary and phase boundary sliding at elevated temperatures and low to moderate strain rates.[2] Less well understood is the contribution of grain boundaries to strengthening at elevated temperatures; this lack of information is directly attributable to experimental difficulties inherent in investigation in this range.[3–6] Such problems as the reliable determination of the yield strength at high temperatures are compounded by the high rate dependence of the flow stress under these conditions as well as by the difficulties involved in producing a range of stable grain sizes.

The aim of the present investigation was twofold. The first objective was to use the principles of metal processing at high temperatures to prepare grain structures which are stable at these temperatures. The manner in which this was accomplished is described below. The second objective was to determine the influence of the microstructures produced on the high-temperature flow stress. The results obtained from this part of the investigation are also presented below and are used to assess the extent to which strengthening relations of the Hall–Petch type[7,8] are applicable at elevated temperatures.

MATERIAL PREPARATION

The present study was based on the use of annealed electrolytic tough pitch (ETP) copper*[9] and of a prior heat treatment which produces both coherent and incoherent β (Cu_2O) and γ (CuO) precipitates. The presence of these particles helps to stabilize the grain boundaries,[10,11] and thus aids in the maintenance of a given grain size during the course of an experiment.

The test samples were all prepared from one 6 m length of cold drawn, 9 mm diameter round bar. The compression samples were machined from these rods into right cylinders 11·4 mm in height and 7·6 mm in diameter. The dimensions selected were based on the load capacity and crosshead speed range of the available Instron testing machine and previous experience with the equipment.[12,13] The end faces of the samples were grooved[12–17] in order to retain the glass lubricants used in high-temperature deformation. A flat-bottomed groove geometry was used such that the grooves were wider at their bases than were the ridges between them. These were machined with the aid of a modified 2 tooth/mm thread chaser.

In order to minimize differences in the initial structure of the samples, all specimens were strain annealed. The samples were prestrained 0·02 in compression between two polished platens. Prior to compression, Teflon tape was placed on the specimen ends to act as a lubricant and to help prevent collapse of the grooves. The strained samples were subsequently annealed for 16 h at 900°C in dry argon.[18] This treatment produced a stable recrystallized grain size of 0·56 mm.

EXPERIMENTAL METHOD

The mechanical tests described below were carried out on an Instron machine modified for constant true strain rate compression at elevated temperatures.[19] The tests were controlled and the data acquired with the aid of a GE4020 process control computer. The experimental procedure consisted of prestraining the strain-annealed samples to a strain of 0·4 at 540 or 600°C and at constant true strain rates of 8×10^{-2}, $1{\cdot}8 \times 10^{-2}$, $3{\cdot}7 \times 10^{-3}$, and $7{\cdot}5 \times 10^{-4}$ s^{-1}. After holding for sufficient time to allow complete recrystallization to take place[20–22] the samples treated at 540°C were quenched to room temperature to permit grain size measurement. The second temperature of 600°C was selected so that larger grain sizes than were obtained at

* Electrolytic tough pitch copper (wt-%): 0·09Pb; <0·05Ni; $0{\cdot}015O_2$; <0·005Ag; <0·04Bi; <3 ppm As.

540°C could be produced. These samples were cooled to 540°C and held for 30 min before quenching to room temperature. The latter treatment was applied because the yield stress measurements were all performed at 540°C and it was desired to equilibrate the distribution of Cu_2O and CuO at this temperature. In this way, it was possible to produce different stable grain sizes in the range 0·056 to 0·81 mm.

Another series of samples was given an identical prestraining and recrystallization treatment but, instead of being quenched to room temperature, was reloaded at 540°C to determine the yield stress as a function of grain size at the various strain rates. The yield stresses were determined by plotting the true stress/true strain data on an expanded strain scale. In this way the stress at a 0·01 offset could be determined in a consistent manner.[23]

Grain size measurements were carried out on two sections cut transversely to the compression axis on each of the samples. One section was taken close to the mid-height and the other near one of the ends. This procedure was adopted in order to minimize the effect of strain localization on the observed microstructures. The sections were ground and polished and etched lightly to reveal the grain boundaries.* Mean linear intercept grain sizes were determined by the standard technique and in excess of 400 intercepts were counted on each sample.

During the grain size measurements great care was taken not to include twin boundaries in the boundary count. However, it was observed qualitatively that the frequency of twins per grain was similar in all the microstructures examined. So that any effect of twin density is automatically included in the grain size measurement.

RESULTS AND DISCUSSION

Dependence of recrystallized grain size on experimental parameters

Grain size and strain

Experiments dealing with the effect of strain on the grain size were carried out at 500°C and $1{\cdot}8 \times 10^{-2}$ s^{-1}, leading to the results shown in Fig. 1. The grain size was determined after prestrains of 0·05, 0·10, 0·15, 0·18, 0·30, 0·40, 0·52, and 0·64, as indicated on the flow curve.

The grain sizes of the samples subjected to strains of 0·05 and 0·10, which are below the critical strain for static recrystallization,[21,22] were the same as the initial grain size but contained subgrains as revealed by etch-pitting. These data are not shown in Fig. 1. When the high-temperature prestrain exceeded the critical strain for static recrystallization the grain size decreased with increasing strain, as it does for cold working. At large strains, however, a steady state was reached where the grain size remained constant with further strain.

Grain size, strain rate, and temperature

The data shown in Fig. 2 were determined at two temperatures, 540 and 600°C, and over a range of strain rates covering about two orders of magnitude ($\sim 10^{-1}$ to 10^{-3} s^{-1}). It is evident that when the strain rate is increased, the grain size decreases. This effect is more pronounced at the higher temperature (600°C), which is reasonable when it is recalled that both the dislocation density and the mechanical properties in general are more rate sensitive at higher temperatures. The effect of temperature is also displayed in Fig. 2. The results indicate that the grain size increases with temperature and that the grain size difference Δd is larger at lower strain rates, i.e. $\Delta d = 0{\cdot}31$ mm at $7{\cdot}5 \times 10^{-4}$ s^{-1}, and decreases to $\Delta d = 0{\cdot}12$ mm at 8×10^{-2} s^{-1}.

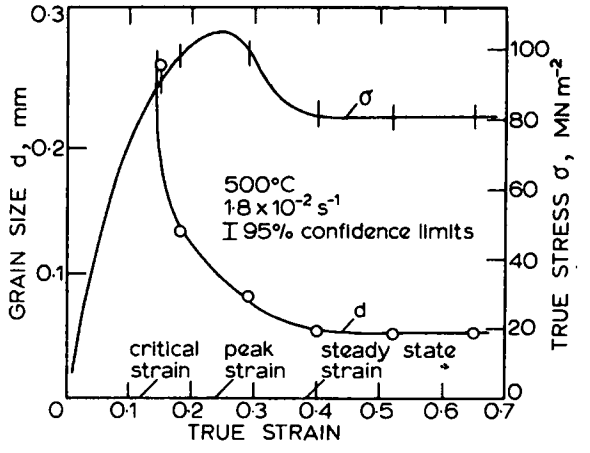

1 Effect of strain on grain size of electrolytic tough pitch copper.

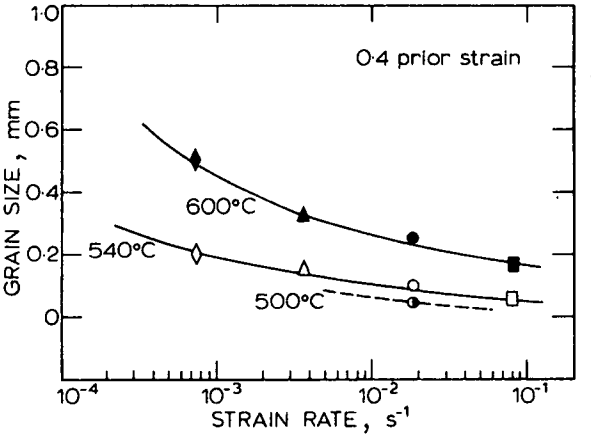

2 Effect of strain rate and temperature on grain size.

Effect of grain size on high-temperature yield stress

The experiments dealing with the effect of grain size on the high-temperature yield stress were carried out at various combinations of strain rate and temperature selected to produce the largest possible variation in recrystallized grain size. The results shown in Fig. 3 represent four of the combinations of strain rate and temperature at which prestraining was performed resulting in recrystallized grain sizes of 0·056 to 0·2. The reloading strain rate for this set of experiments was the same, 8×10^{-2} s^{-1}.* The resulting yield stresses on reloading varied with the prestraining strain rate and therefore with the recrystallized grain size.

* Electropolishing; 133 ml glacial acetic acid, 25 g chromium trioxide, 7 ml H_2O at 8·5 V and 18°C. Etching; 65 ml concentrated H_2SO_4, 16 g potassium dichromate, 3 g sodium chloride, 800 ml H_2O.

* In Fig. 3, the flow curves appear to diverge from a common point. This arises because of the large strain axis used in the diagram. On the expanded strain scale, used for the determination of the yield stresses, the variation in the 0·2% proof stress is more clearly evident, and it is these values that are used in the following analysis.

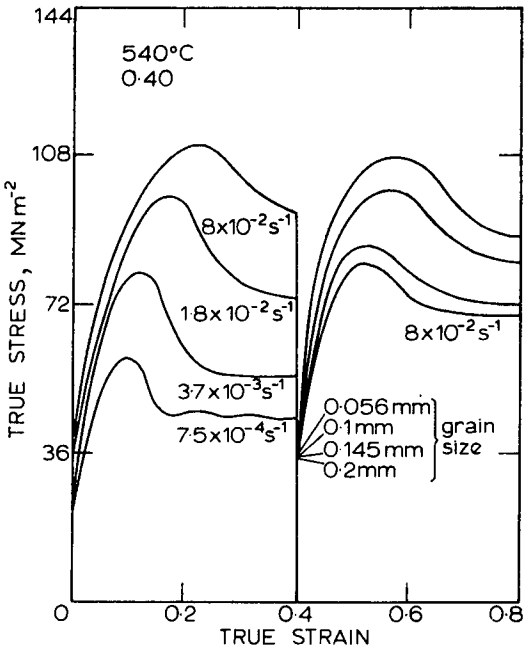

3 Example of flow curves obtained by interrupted compression at four different strain rates where, following a delay, reloading was carried out at a new strain rate. Grain sizes produced are indicated under the appropriate flow curve. On retesting at $8\times10^{-2}\ s^{-1}$ the yield stress and the shape of the flow curve were observed to be grain size dependent.

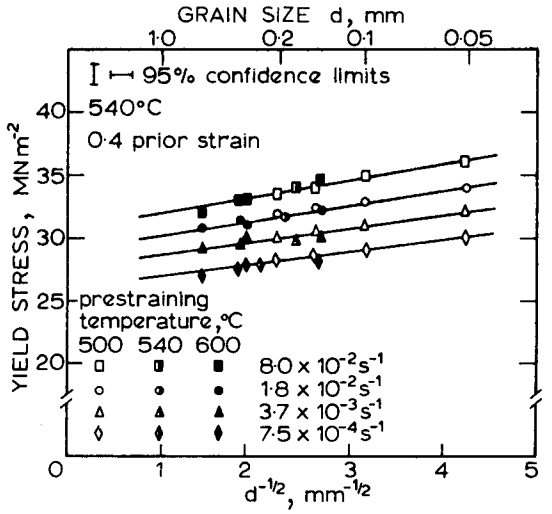

4 Effect of grain size on high-temperature yield stress of electrolytic tough pitch copper. Different shaped symbols define the reloading strain rate at 540°C as indicated. Shading of symbols represents prestraining temperature; open symbols—500°C, half closed—540°C, closed—600°C.

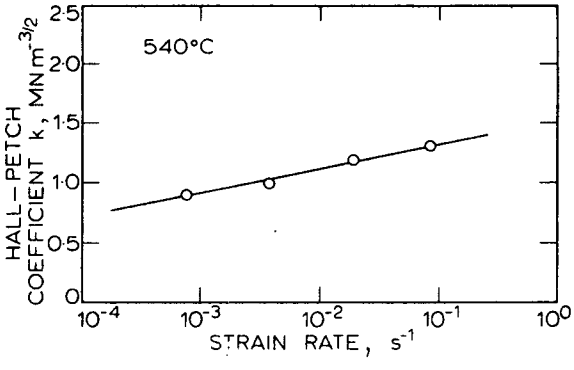

5 Strain-rate dependence of grain boundary strengthening coefficient k.

From this type of data, the dependence of the yield stress on grain size was plotted in a Hall–Petch manner, as shown in Fig. 4. It is evident that under the present experimental conditions, the high-temperature yield stress increases linearly with the inverse square root of the grain size. Note that the data of Fig. 3 are represented by open symbols on the uppermost curve of Fig. 4. It is evident that annealed copper exhibits classical grain size strengthening even at elevated temperatures. The rationalization of the effect of grain size on the flow stress of metals has been based on two alternative concepts. Hall[24] and Petch[25] based their models on dislocation pile-ups, while Conrad,[26,27] Meakin and Petch,[28] and Li[29] have advocated work-hardening models. Since dislocation pile-ups are seldom observed in hot-worked materials, it is apparent that the work-hardening approach is more appropriate to the interpretation of high-temperature yield measurements, such as the ones described here. This approach is based on the observation[26] that the dislocation density for a given strain is proportional to the inverse grain size, and occurs when the principal effect of grain size is through the mean slip distance.

The strain-rate dependence of the grain boundary strengthening coefficient k is shown in Fig. 5. It is of interest that the value of k gradually decreases with decreasing rate of deformation. It is therefore possible that in the creep range of strain rates ($<10^{-4}\ s^{-1}$), the value of k becomes rather small (i.e. $<0{\cdot}8\ MN\ m^{-3/2}$), which would explain the deductions concerning the invalidity of the Hall–Petch relation that are often made in high temperature creep studies. In a similar way, an increase in the temperature may also lead to a decrease in k because its effect on thermally activated processes is analogous to that of a decrease in strain rate.

According to Fig. 5, the Hall–Petch relation can be written in the form:

$$\sigma_y = \sigma_0(T,\dot{\varepsilon}) + (a[T] + b[T]\log\dot{\varepsilon})d^{-1/2}. \quad . \quad . \quad . \quad . \quad (1)$$

Here the first term on the right-hand side of the equation represents the yield stress of a single crystal and the grain boundary strengthening coefficient k is expressed as $(a+b\log\dot{\varepsilon})$, signifying that it includes both athermal and strain-rate dependent components. The terms a and b are temperature dependent through the shear modulus and take the values 1·5 and 0·2 at 540°C in the units used here. The presence of both athermal and thermal components of grain boundary strengthening is worthy of note in that it suggests that the boundaries can serve as both local and long-range obstacles at elevated temperatures.

CONCLUSIONS

As a result of this study, the following general conclusions were drawn.

1. When the high-temperature prestrain exceeds the critical strain for static recrystallization (about 12% for ETP copper under the current conditions), the grain size decreases with increasing strain. At large strains, a steady

state is reached where the grain size remains constant with further strain.

2. The recrystallized grain size of ETP copper decreases with an increase in strain rate. This effect becomes more pronounced when the temperature is increased. The results also indicate that the recrystallized grain size increases with working temperature.

3. A plot of the high-temperature yield stress versus grain size drawn up in the Hall–Petch manner shows that, in ETP copper, the yield stress increases linearly with the inverse square root of the grain size. Thus, grain boundaries can be a source of strengthening at elevated temperatures (at least as long as the strain rate is greater than 10^{-4} s^{-1} and the grain size is coarser than about 40 μm).

4. At 540°C, the Hall–Petch coefficient k for ETP copper can be written as the sum of two terms:

$$k = 1{\cdot}5 + 0{\cdot}2 \log \dot{\varepsilon}$$

Since both terms are positive, grain boundaries always provide strengthening (at least in the temperature, strain rate, and grain size regime under investigation). The presence of athermal and thermal components in the grain boundary strengthening coefficient suggests that grain boundaries act both as long-range and short-range obstacles to dislocation motion at elevated temperatures.

REFERENCES

1. P. SHAHINIAN and J. R. LANE: *Trans. ASM*, 1953, **45**, 177.
2. B. BANDELET: Fourth Int. Conf. on the Strength of Metals and Alloys, edited by ESNMIM–INPL, Nancy, France, September 1976, vol. 1, pp. 2–25.
3. O. D. SHERBY, M. J. HARRINGTON, L. CHAMPAGNE, and C. SAUVE: *Trans. ASM*, 1969, **62**, 575.
4. C. M. YOUNG and O. D. SHERBY: *J. Iron Steel Inst.*, 1973, **211**, 640.
5. C. M. YOUNG, B. WLASER, E. P. ABRAHAMSON, and O. D. SHERBY: *Scr. Metall.*, 1975, **9**, 35.
6. E. DiRUSSO, M. COUSERVA, M. BURATT, and F. GATTO: *Mater. Sci. Eng.*, 1974, **14**, 23.
7. R. W. ARMSTRONG: 'Ultrafine grain metals', Proc. 16th Sagamore Army Mater. Res. Conf. (ed. by J. J. Burke and V. Weiss), pp. 1–28. **1970**: Syracuse, New York (Syracuse University Press).
8. P. J. WRAY and M. F. HOLMES: *Metall. Trans.*, 1975, **6A**, 1189.
9. S. MURPHY and C. J. BALL: *J. Inst. Met.*, 1972, **100**, 225.
10. P. K. SENGUPTA, B. CHATERJEE, and J. REZEK: *Can. Met. Q.*, 1972, **11**, 601.
11. J. REZEK: *ibid.*, 1974, **13**, 545.
12. R. A. PETKOVIC-DJAIC and J. J. JONAS: *J. Iron Steel Inst.*, 1972, **210**, 256.
13. M. J. LUTQN and J. J. JONAS: *Can. Met. Q.*, 1972, **11**, 79.
14. J. F. ALDER and V. A. PHILLIPS: *J. Inst. Met.*, 1954–55, **83**, 80.
15. A. T. ENGLISH and W. A. BACKOFEN: *Trans. TMS–AIME*, 1964, **230**, 396.
16. J. E. HOCKETT: *Proc. ASTM*, 1959, **59**, 1309.
17. J. E. HOCKETT: *Trans. TMS–AIME*, 1967, **239**, 969.
18. E. SHAPIRO: private communication.
19. M. J. LUTON, J-P. A. IMMARIGEON, and J. J. JONAS: *J. Phys. E, Sci. Instr.*, 1974, **7**, 862.
20. R. A. PETKOVIC: PhD thesis, McGill University, Montreal, 1975.
21. R. A. PETKOVIC, M. J. LUTON, and J. J. JONAS: *Acta Metall.*, 1979, in press.
22. M. J. LUTON, R. A. PETKOVIC, and J. J. JONAS: to be published.
23. M. J. LUTON and J. J. JONAS: Proc. Second Int. Conf. Strength of Metals and Alloys, Asilomar, California, August 31, 1970.
24. E. O. HALL: *Proc. Phys. Soc. (London)*, 1951, **B64**, 747.
25. N. J. PETCH: *J. Iron Steel Inst.*, 1953, **174**, 25.
26. H. CONRAD: 'Electron microscopy and strength of crystals', p. 299. **1961**: New York (Interscience).
27. H. CONRAD: *Acta Metall.*, 1963, **11**, 75.
28. J. MEAKIN and N. PETCH: Symp. on the Role of Substructure in the Mechanical Behavior of Metals, Orlando, Fla. ASD-7DR-63-324, p. 243, 1963.
29. J. C. M. LI: AIME Fall Meeting, Detroit, Michigan, 1968.

Effect of precipitation on recrystallization in microalloyed steels

J. J. Jonas and I. Weiss

The progress of precipitation in undeformed austenite containing 0·018%Nb was determined by means of a mechanical testing technique. This technique is based on the influence of dynamic precipitation on the strain to the peak in the flow stress observed during isothermal compression testing at a constant true strain rate. The results obtained over the temperature range 875 to 1025°C lead to precipitation kinetics which are somewhat faster than those reported previously. A modification of this method was used to measure the precipitation rate in austenite containing 0·035%Nb which was given a prestrain of 5% in the temperature range 885 to 925°C. These results indicate that precipitation in deformed austenite is at least one order of magnitude faster than precipitation in undeformed austenite. A related method was employed to determine the rate of precipitation during deformation. This was observed to be a further order of magnitude faster than precipitation in deformed austenite. The retarding effect of Nb addition on the rates of both static recovery and static recrystallization is discussed, and it is concluded that a significant part of the retardation is due to the presence of Nb in solution. Furthermore, the results indicate that the occurrence of carbide precipitation can retard static recrystallization only when recrystallization is already sufficiently retarded by the solute additions to prevent its initiation prior to the beginning of the precipitation process.

J. J. Jonas, BEng, PhD, and I. Weiss, BSc, MSc, PhD, are in the Department of Mining and Metallurgical Engineering, McGill University, Montreal, Canada.

The influence of the precipitation process on recrystallization and grain growth in microalloyed steels has been the subject of numerous studies.[1-7] In general, fine particles (≃5 nm dia.) deposited on dislocations, even when present in very small volume fractions (≃0·03%), can retard recrystallization significantly, while coarser precipitates (>30 nm dia.) have less effect. Less clear has been the influence on the recrystallization process of the microalloying elements which are in solution prior to the onset of precipitation. On the basis of the absence of both precipitation and recrystallization under certain conditions, some workers[8-12] have even suggested that precipitation is not a necessary condition for the retardation of recrystallization, and that the delay introduced by the addition of Nb, for example, is caused by a solid solution or pre-precipitation phenomenon which acts before the onset of precipitation itself.

In a recent paper,[13] the present authors introduced some data regarding precipitation rates in an 0·035%Nb steel which were determined by a new mechanical technique. The results indicated that, in the neighbourhood of 900°C, the presence of Nb in solution retarded recrystallization until precipitation could begin, and that the overall delay in softening was attributable to significant contributions from both solute and precipitate effects. In the present paper, some new data are reported on the 0·035%Nb steel and on an additional material, an 0·018%Nb steel, and further details are given of the experimental procedure used. By means of this method, the rate of precipitation has been measured in high-temperature austenite in three 'states' or conditions:

(i) undeformed austenite,
(ii) deformed austenite,
(iii) deforming austenite (undergoing deformation).

The effects of the solutes present and of both static and dynamic precipitation on the occurrence of static and dynamic recrystallization, as well as on the retardation of static recovery, are then examined in the present and the previous materials.

MATERIALS AND PROCEDURE

The experiments were carried out on an Instron testing machine modified for hot-compression at constant true strain rate.[14] The compression tools and the testing system are described elsewhere.[15] Three materials were used, a plain-carbon steel and two microalloyed steels, with the compositions shown in Table I.

The steels were received in the form of 25 mm thick plate, which was then machined into compression specimens, 13·06 mm high and 8·71 mm in diameter, with the axis of the compression specimens aligned in the rolling direction. Prior to testing, the Nb-modified steels were solution-treated at 1100°C under argon for 30 min. The plain-carbon steel was austenitized for 30 min at 1030°C, with the aim of producing the same grain size as in the two HSLA steels. After austenitizing, all the steels were cooled to the testing temperature at a rate of 1°C s^{-1}.

Three types of experiments were performed. In the first type, after solution treatment, cooling to the test temperature, and ageing for periods up to 2×10^5 s, the

Table 1 Chemical composition of materials tested, wt-%

Materials	C	Mn	S	P	Al	Cu	Si	N	Nb
Niobium-bearing steels	0·05	0·42	0·009	0·002	0·057	0·006	0·045	0·004	0·035
	0·06	0·42	0·009	0·002	0·051	0·006	0·014	0·004	0·018
0·05%C low-carbon steel	0·05	0·33	0·21	0·004	0·090	---	0·007	0·004	·

specimens were deformed without interruption to a strain of about 80%. In the second series, after solution treatment and cooling to the test temperature, the specimens were prestrained at a strain rate of $0{\cdot}14\ s^{-1}$ and then unloaded. The prestrained specimens were aged for various times up to $7{\cdot}2 \times 10^3$ s and then reloaded at (generally) the same strain rate of $0{\cdot}14\ s^{-1}$. In the third series of experiments, the samples were deformed at strain rates between $10^{-5}\ s^{-1}$ and $1\ s^{-1}$ immediately after cooling to the test temperature, which ranged from 875 to 1025°C.

RESULTS

Precipitation in undeformed austenite

In the early stages of this investigation an attempt was made to follow the progress of precipitation through its effect on the high-temperature yield strength. This procedure is the isothermal equivalent of using hardness measurements or yield strength determinations at room temperature after periods of ageing or tempering at elevated temperatures. It is of interest that, over the temperature range 875 to 1025°C, the high-temperature yield strength did not change appreciably over the ageing interval from 90 to 2×10^5 s shown in Fig. 1. As will be seen below, this ageing interval includes the entire precipitation period, leading to the conclusion that the yield stress is not sensitive to the state of precipitation. This deduction is supported by the observation that the mean particle size produced during precipitation in undeformed austenite at 900°C is in the range from 40 to 60 nm,[16] so that, on the basis of a volume fraction of 0·032% of precipitate and an interparticle spacing of about 2300 nm, no significant particle or Orowan strengthening can be expected.

The unsuitability of isothermal yield strength measurements for following the progress of precipitation in undeformed austenite led to the development of an alternative technique based on the strain to the peak stress ε_p. Three of the flow curves obtained in the 0·018%Nb steel after successively longer ageing times are shown in Fig. 2. By increasing the holding time before deformation, a distinct change in ε_p can be observed. The highest curve, which exhibits the highest work-hardening rate and peak strain, represents the behaviour of material that was aged for 210 s prior to testing. The middle curve, for material aged 3400 s prior to testing, exhibits an intermediate value of peak strain, and the lowest curve, for material aged 65 000 s, exhibits the smallest peak strain. This change is associated with the occurrence of increasing amounts of static precipitation during the holding period, and therefore of decreasing amounts of dynamic precipitation during the work-hardening interval. A decrease in the amount of dynamic precipitation in turn decreases the amount of retardation of dynamic recrystallization, and therefore the peak strain. The decrease in ε_p with ageing time observed in the current series of experiments is displayed in more detail in Fig. 3. In the absence of precipitation before deformation, a constant and maximum ε_p is obtained; this is associated with the maximum volume fraction of carbonitride available for inhibiting the nucleation of dynamic recrystallization during the rising portion of the flow curve. Increasing the amount of static precipitation prior to straining leads to a decrease in the potential for dynamic precipitation, and

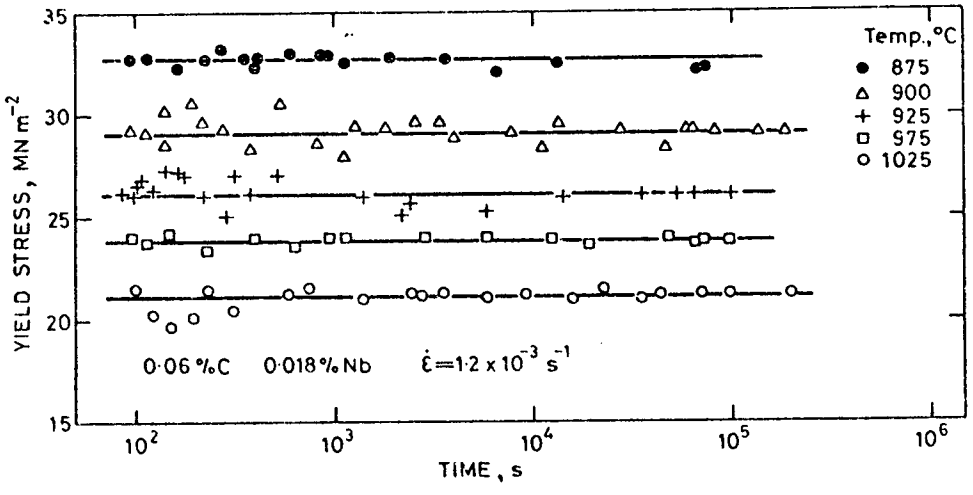

1 Yield stress 0·018%Nb steel at strain rate of $1{\cdot}2 \times 10^{-3}\ s^{-1}$. Samples solution-treated at 1100°C, cooled to test temperature, and aged for 90 to 2×10^5 s.

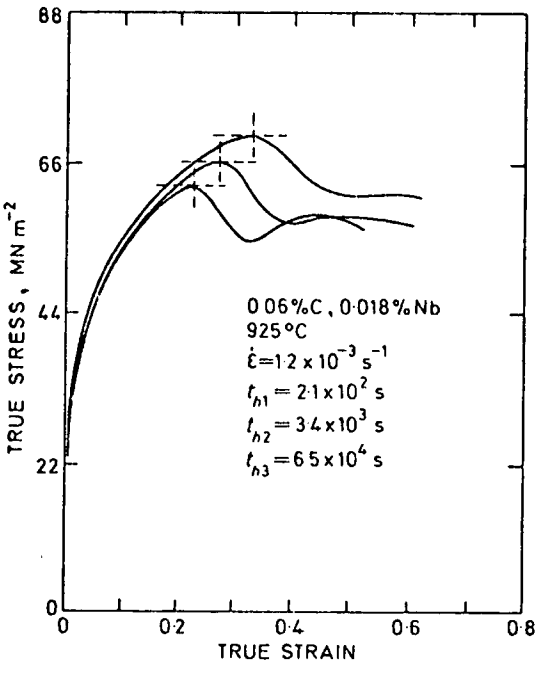

2 Flow curves for 0·018%Nb steel determined in compression at 925°C and at strain rate of $1{\cdot}2\times10^{-3}\ s^{-1}$.

therefore to a decrease in ε_p. Once all the available Nb has been precipitated prior to deformation, on further ageing, no further change in ε_p can be observed. Thus the end of the first plateau and the beginning of the second are equivalent, respectively, to the 'start' P_s and 'finish' P_f of precipitation in undeformed austenite.†

The PTT diagram obtained in this way for the 0·018%Nb steel is shown in Fig. 4, in which it is compared with the one determined previously[13] for the 0·035%Nb steel. For both curves, the nose is observed at around 960°C, and the P_s time can be seen to be accelerated slightly, e.g. from about 100 to 90 s at the nose, as a result of increasing the Nb level from 0·018 to 0·035%Nb. The P_f time is affected more noticeably by the change in Nb level; the increase in Nb concentration prolongs the precipitation process by more than 1000 s. A P_s time of about 100 s at 960°C typifies the present compositions of the austenite in the undeformed state.

Precipitation after deformation

In order to determine the effect of an appreciable density of dislocations on the precipitation kinetics, in the second series of tests a prestrain of 5% was applied to specimens of the 0·035%Nb material at a constant strain rate of 0·14 s^{-1}. This was followed by ageing intervals of increasing length,

† On the basis of electron microscopic evidence,[16] P_s and P_f are estimated to correspond to about 10% and 90% completion of precipitation.

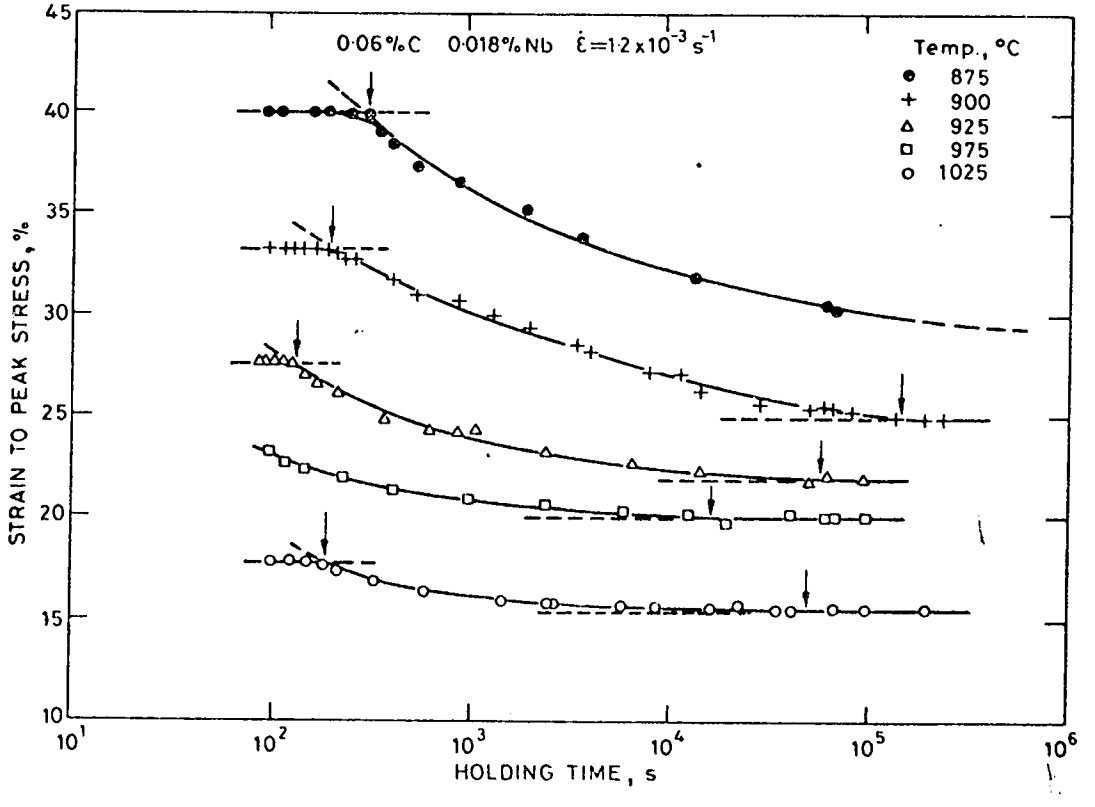

3 Dependence of peak strain on holding time in 0·018%Nb steel. Samples solution-treated at 1100°C, cooled to test temperature, aged in undeformed condition, and tested at strain rate of $1{\cdot}2\times10^{-3}\ s^{-1}$. P_s times identified by vertical arrows at left-hand extremities of curves and P_f times by arrows at right-hand extremities.

and then by continued deformation at the prestraining strain rate to a total strain of about 80%. The amount of prior strain was chosen to be less than the critical strain for static recrystallization under these conditions so as to eliminate the possibility that the dislocations introduced by prestraining are eliminated before they can affect the precipitation process. It should be noted that the prestraining strain rate was 0·14 s^{-1} in this series of tests, whereas it was 5×10^{-2} s^{-1}, and therefore a factor of about 3 lower, in the earlier experiments.[13] A further difference is that the current reloading strain rate was the same as the preloading strain rate (0·14 s^{-1}), whereas it was two orders of magnitude slower ($1{\cdot}2 \times 10^{-3}$ s^{-1}) in the work reported earlier.[13] Thus the effect of dynamic precipitation and of precipitate coarsening can be expected to be much less in the present than in the previous experiments.

In Fig. 5, three of the interrupted tests carried out in this way can be seen, corresponding to three selected ageing times following prestraining. Increasing the hold time increases ε_p by increasing the amount of *static* precipitation taking place after unloading the specimen and prior to reloading. In these experiments, unlike those reported previously,[13] the influence of *dynamic* precipitation is negligible because of the relatively fast strain rate used. The general levels of the flow curves are a reflection of the amount of static recovery (see Fig. 13) taking place during the ageing interval.

The dependence of the peak strain (including the 5% prestrain) on holding time at 885 and 900°C is depicted in more detail in Fig. 6. Here the *increase* in ε_p with holding time can be seen more clearly than in Fig. 5. This is in sharp contrast to the *decrease* in ε_p with holding time reported previously.[13] In the earlier experiments, as a result of the relatively low reloading strain rate, dynamic precipitation was more important than static precipitation, so that an increase in holding time (and therefore in static precipitation) *decreased* the potential for dynamic precipitation (and therefore for the retardation of dynamic recrystallization). In the current experiments, as a result of the relatively high reloading strain rate, static precipitation is more important than dynamic precipitation, so that an increase in holding time increases the density of static precipitates. These do not have time for much coarsening during reloading, so that ε_p *increases* with holding time in this case.

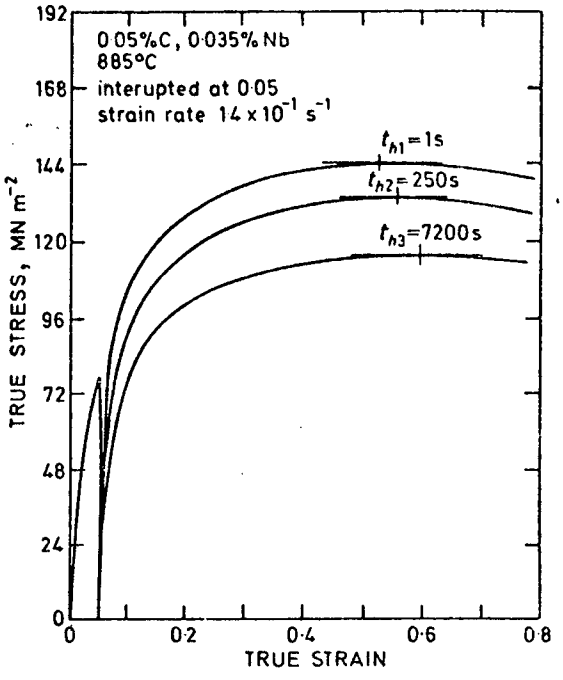

5 Selected interrupted flow curves determined at 885°C on 0·035%Nb steel. Samples were solution-treated at 1100°C, cooled to testing temperature at about 1°C s^{-1}, an initial strain of 5% applied followed by unloading and holding for times indicated before testing resumed.

As before, the transition from constant ε_p to a change in ε_p with time was used to define P_s on the basis that no static precipitation takes place before this event. In a similar way, the subsequent return to constant ε_p with time was employed to define P_f on the related assumption that, after this point in time, no further Nb is available for precipitation. The PTT diagram determined in this way is shown in Fig. 7, together with the results obtained on the same material by means of the previous 'low-strain-rate' technique. The PTT curves are both C-shaped with a nose at around 900°C. By comparison with Fig. 4, precipitation

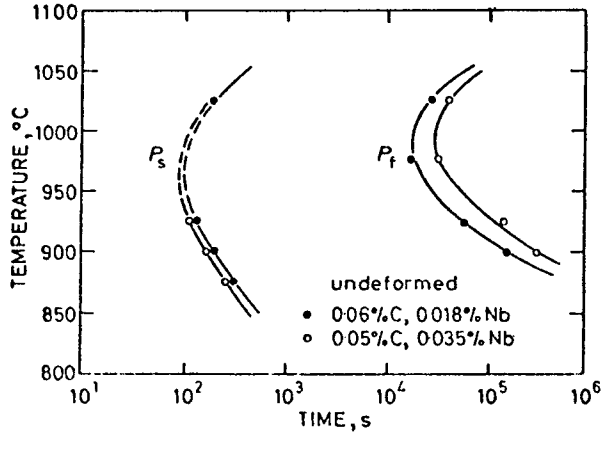

4 PTT diagrams for present 0·018%Nb steel and for 0·035%Nb steel.[13] Precipitation begins slightly earlier for 0·035%Nb steel and ends somewhat later.

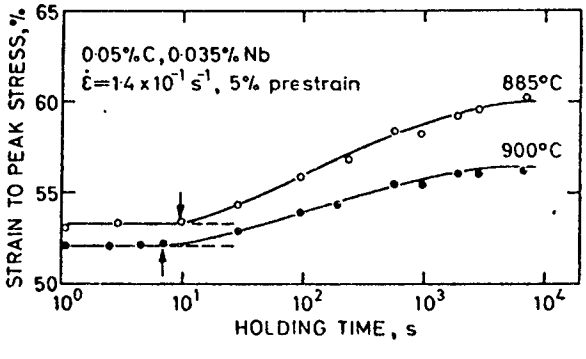

6 Dependence of peak strain on holding time in 0·035%Nb steel after 5% prestrain. P_s times are indicated by arrows.

can be seen to be about an order of magnitude faster when the material contains prestrain dislocations, than when these are absent. Furthermore, a more rapid preloading strain rate (0·14 rather than 0·05 s^{-1}), leads to slightly more rapid precipitation (9 s at the nose as opposed to 11 s), presumably because the dislocation density at a prestrain of 5% is slightly higher when the material is deformed at the higher strain rate.

Precipitation during deformation

In the absence of precipitation effects, the strain to the peak stress ε_p (and the critical strain to initiate dynamic recrystallization) increase monotonically with an increase in strain rate, as long as the experimental temperature and initial grain size are held constant. The 'normal' dependence of ε_p on strain rate is typified by the lower curve in Fig. 8(*a*) for an 0·05%C plain-carbon steel. By contrast, the 0·035%Nb steel of Fig. 8(*a*), despite heat-treatment to ensure the same grain size, gives evidence of distinctly different behaviour associated with the occurrence of precipitation *during* straining. It shows a 'normal' dependence only at relatively high (see Ref. 13) and relatively low strain rates with the greatest difference in peak strains at intermediate strain rates. The retardation in dynamic recrystallization observed in the high strain rate region (excess in ε_p for the Nb steel over ε_p for the plain-carbon steel), can be attributed to the effect of Nb in solution[13] since precipitation does not begin in the fractions of a second required to attain the peak strain at these strain rates. In a similar way, at very low strain rates, precipitation is completed at very small strains, and dynamic coarsening subsequently increases the mean particle size,[16] thus rendering the particles less effective in retarding recrystallization. Thus the excess in ε_p for the Nb steel over the plain-carbon steel in this strain-rate range can be attributed to the presence of coarse precipitates in the former material, and is considerably less than that produced by the fine precipitates of the intermediate strain rate range, in which there is insufficient time for coarsening to occur.

As suggested earlier,[17] this difference in behaviour between precipitate-forming and non-precipitate-forming

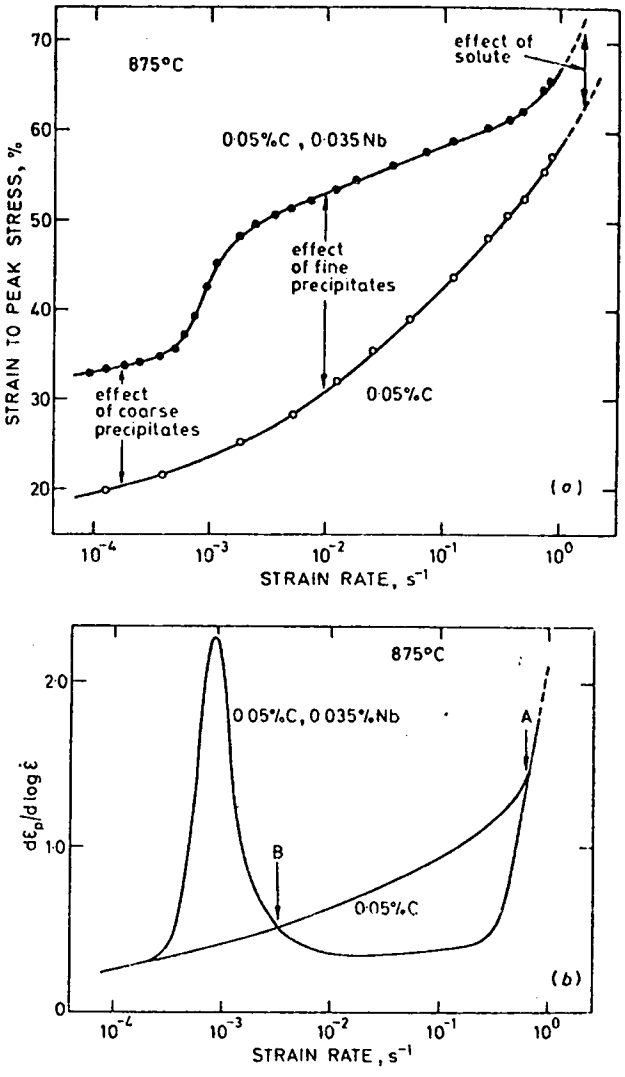

8(*a*) Dependence of peak strain on strain rate at 875°C in 0·05%C plain-carbon steel and 0·035%Nb modified steel.

(*b*) Dependence of slopes of curves in (*a*) on strain rate. Points A and B refer to strain rates above which no dynamic precipitation takes place prior to peak strain and below which dynamic precipitation is completed before peak strain, respectively.

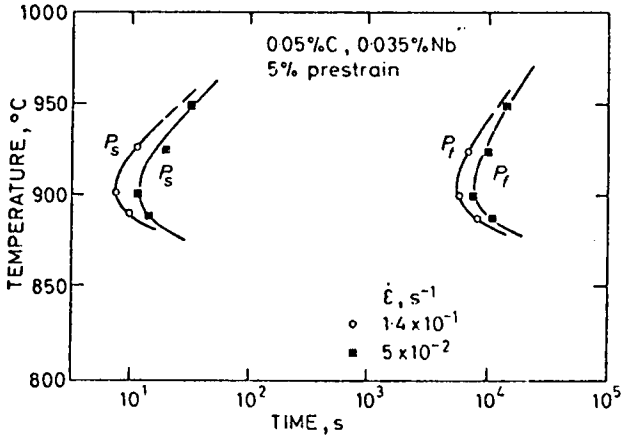

7 PTT diagrams for 0·035%Nb steel determined using high strain rate technique (open symbols) compared with those obtained previously[13] using low strain rate technique (closed symbols).

materials can be used to determine P_s and P_f times for dynamic precipitation. The technique required is depicted in Fig. 8(*b*) in which the slopes of the two curves of Fig. 8(*a*) are plotted against strain rate. It can be seen that, as the strain rate is decreased from the right-hand side of the diagram, a deviation from 'normal' behaviour is first observed at a critical strain rate of about 0·7 s^{-1} (at 875 °C), that is, at Point *A*. The critical strain rate associated with *A* corresponds to the strain rate for which dynamic precipitation in the Nb steel begins just before the peak strain, so that its occurrence perturbs just perceptibly the dependence of ε_p on strain rate from that observed in the absence of precipitation.

The difference in slope at strain rates below 0·7 s^{-1} leads to a continuous divergence in ε_p for the Nb and plain-carbon steels as the strain rate is decreased, until Point *B*

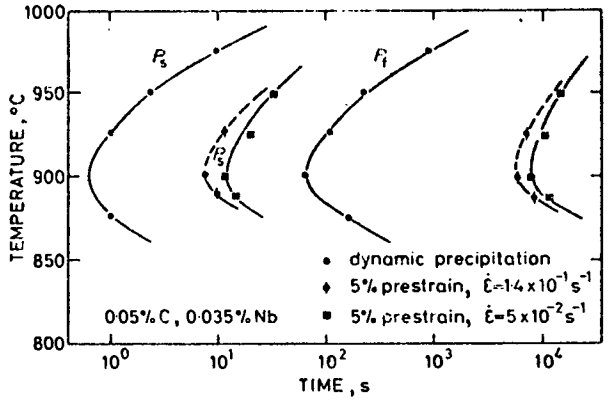

9 PTT diagram for dynamic precipitation in 0·035%Nb steel compared with present ($\dot{\epsilon}=1{\cdot}4\times10^{-1}\ s^{-1}$) and previous ($\dot{\epsilon}=5\times10^{-2}\ s^{-1}$) results for precipitation in predeformed austenite (5% strain).

(Fig. 8(*b*)) is reached. At this strain rate ($3{\cdot}5\times10^{-3}\ s^{-1}$ at 875°C), the two curves of Fig. 8(*a*) are parallel (the difference in ε_p is at a maximum), and dynamic precipitation has the largest relative effect in retarding recrystallization. At strain rates below that pertaining to *B* in Fig. 8(*b*), dynamic precipitation begins at lower and lower strains, and goes to completion earlier and earlier in the flow curve; coarsening of the dynamic precipitates sets in,[16] and the carbonitrides become less and less effective in retarding the initiation of dynamic recrystallization. Finally, at the low strain rates corresponding to the left-hand side of Fig. 8(*a*), dynamic precipitation is completed and coarsening has taken place so early in the strain cycle that the dependence of ε_p on strain rate once again parallels that of plain-carbon steel.

By means of a series of constructions similar to Fig. 8(*b*), the points '*A*' and '*B*' were determined at each of five temperatures in the range 875 to 975°C. Point *A* was assumed to be associated with the P_s time t_s, and Point *B* with the P_f time t_f. These were then calculated from the relations[13,17]

$$t_s = \varepsilon_p^s/\dot{\varepsilon}_s$$
$$t_f = \varepsilon_p^f/\dot{\varepsilon}_f$$

where $\dot{\varepsilon}_s$ and $\dot{\varepsilon}_f$ are the strain rates corresponding to *A* and *B*, respectively, and ε_p^s and ε_p^f are the respective peak strains. The PTT diagram for dynamic precipitation determined in this way is presented in Fig. 9, together with the precipitation kinetics for the prestrained austenite. It can be seen that concurrent straining advances the start of precipitation by about *one* order of magnitude in time and the finish of precipitation by about *two* orders of magnitude in time. A minimum start time of 0·6 s can be observed around 900 C, indicating that the rate of dynamic precipitation is considerably faster than the two static rates. This significant increase in precipitation rate is attributed to: (*a*) the higher densities of dislocations, and therefore of nucleation sites, present under dynamic conditions; and (*b*) the higher densities of vacancies induced by straining, which lead in turn to higher Nb diffusion rates. Given the effect of predeformation strain rate on the kinetics of *static* precipitation (Fig. 7), the *dynamic* PTT curves are of particular interest inasmuch as they can be considered to represent an 'upper bound' that applies to prestrained γ when the latter is deformed to strains larger than the present 5% and at considerably higher strain rates, such as those corresponding to industrial rolling.

DISCUSSION

The P_s curves for the three different states of austenite are collected in Fig. 10, together with the results obtained by other workers using a variety of techniques. It can be seen that the precipitation kinetics obtained by the present mechanical method tend to be somewhat faster than the kinetics deduced from the other techniques. For example, for the undeformed austenite at equivalent Nb concentrations, the microhardness data of LeBon *et al.*[9] and the electrical resistivity measurements of Simoneau *et al.*[18] both indicate slower kinetics. Although the observations of Watanabe *et al.*[19] obtained by electrochemical extraction lead to faster precipitation rates, the difference can probably be accounted for by their appreciably higher Nb levels (0·08 vs. 0·035%). When the data for the prestrained austenite are compared, the present method appears to give the slowest kinetics. However, the prestrain of 5% used here is considerably lower than the 30% applied by Watanabe *et al.*[19] and is even further from the 'maximum work-hardening without recrystallization' applied by LeBon *et al.*[20] Thus the general trend observed for the undeformed γ is likely to apply to the deformed γ as well. This conclusion is further supported by the features of the P_s line for dynamic precipitation. This curve, like the static ones, is C-shaped, and its location well to the left of the others suggests that it does indeed represent the limiting case for the static process when large prestrains are applied at high strain rates.[13]

Effect of Nb in solution on static recovery

In order to determine the influence of Nb addition on the rate of static recovery, softening rates were measured at 900°C for the plain-carbon and 0·035%Nb steels. The amount of softening produced by recovery was measured in

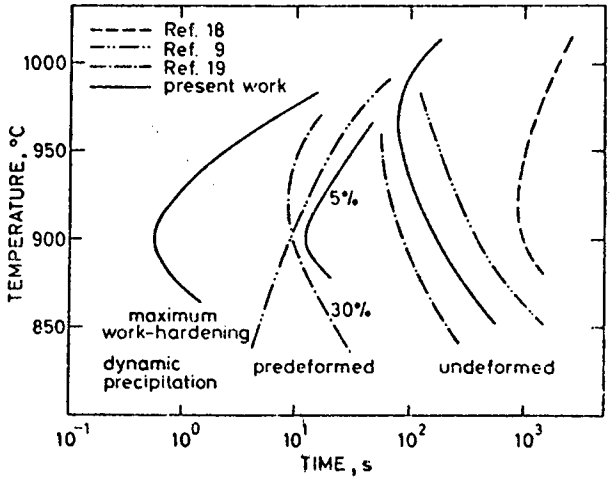

10 Precipitation start P_s times for undeformed, predeformed, and deforming austenite compared with results of other workers.

terms of the yield stress on reloading of a prestrained sample held at the test temperature for increasing intervals of time before reloading. The amount of static softening was expressed in terms of the relative softening X, given by

$$X = [1-(\sigma_2-\sigma_1)/(\sigma_m-\sigma_1)] \times 100$$

Here σ_2 is the yield stress on reloading, σ_1 is the initial yield stress, and σ_m is the flow stress immediately prior to unloading.

The softening curve for the plain-carbon steel illustrated in Fig. 11 indicates that static recovery is initiated in less than 1 s at 900°C and is completed in less than 10 s with about 50% of the work hardening being removed by the recovery process. By contrast, in the Nb steel, the absence of recovery prior to P_s testifies to the retarding effect of Nb as solute. After P_s, during the period of static precipitation, recovery is further delayed, but is not prevented from eventual initiation at about 100 s and completion after about 4000 s, with only some 35% of the work hardening introduced by straining being recovered.

Comparison of the two sets of softening curves shows that the addition of 0·035%Nb retards the initiation of static recovery by two decades of time, and also reduces the *rate* of recovery. The start and finish times for precipitation under these conditions (Fig. 7) indicate that a solute effect is responsible for the retardation of static recovery in the early stages of the delay period. This is analogous to the retardation of static recrystallization by Nb in solution discussed earlier.[13] A further and larger retardation can be associated with the occurrence of static precipitation, which does not, however, prevent the eventual initiation of static recovery.

Interaction between Nb as solute, Nb as precipitate-former, and recrystallization

One of the aims of the present investigation was to interpret the large retardation in the rate of static recrystallization produced by the addition of small amounts of Nb to plain-carbon steel. Some typical results of this type are reproduced in Fig. 12(*a*) taken from the work of LeBon *et al.*[9] The temperature-dependent reverse-knee they detected in the Nb steel indicated that the addition of Nb had its greatest effect in the vicinity of 900°C. Given the C-shape and location of the PTT curves presented above (see Fig. 9), it is evident that the retardation of dynamic recrystallization observed in Fig. 12(*a*) at high temperatures (950–1000°C) and at low temperatures (800–825°C) cannot be ascribed to the precipitation of niobium carbonitride, as this does not take place during the time interval between R_s (recrystallization start) for the plain-carbon and Nb-modified steels. It can be associated instead with the presence of Nb in solution, as has already been suggested by others.[11,20] The retarding influence of the solute on the rate of recrystallization deduced in this way[13] is shown in Fig. 12(*b*) and can be seen to increase as the temperature is decreased.† Experiments of this type can be performed by giving the Nb-

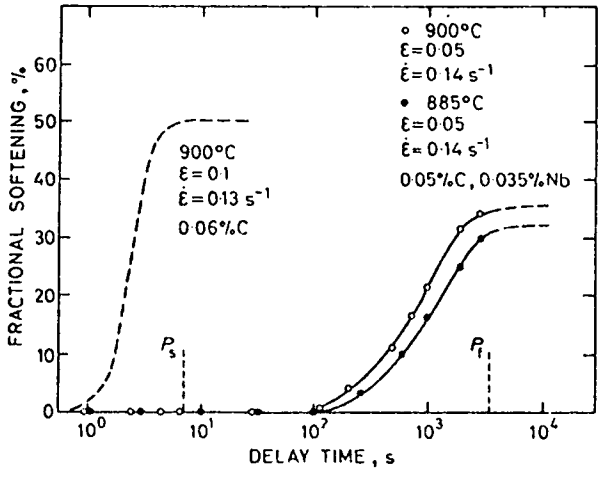

11 Effect of Nb as solute and as static precipitate on rate of static recovery. Broken line at left describes progress of recovery in 0·06%C plain-carbon steel.

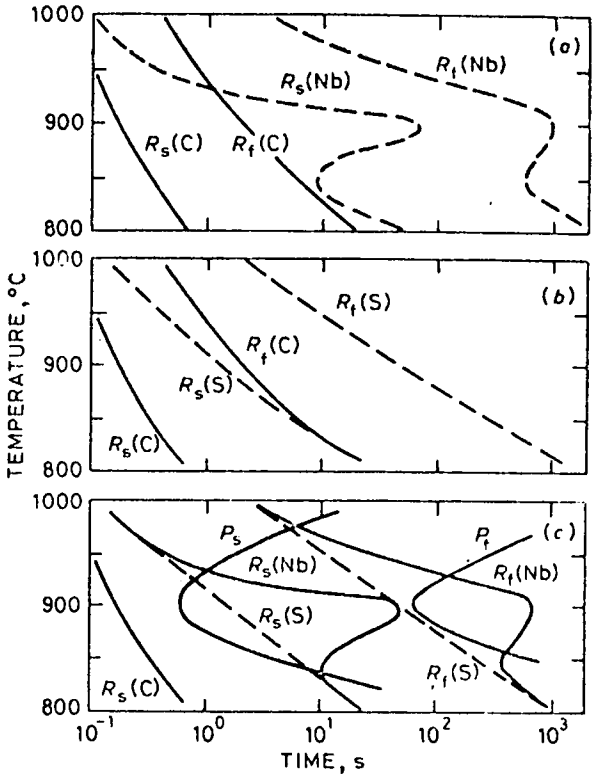

12(*a*) Comparison of recrystallization kinetics of plain-carbon (C) and Nb-modified (Nb) steel reported by LeBon *et al.*[9]
(*b*) Derived effect of Nb as solute (S) on recrystallization kinetics of Nb-modified steel of (*a*).[13]
(*c*) Superposition of PTT diagram for dynamic precipitation (Fig. 10) and derived RTT diagram of (*b*) for rate of solute-modified recrystallization.

† This interpretation is supported by the more recent results of Owen and White[21] on two vanadium steels. They determined the recrystallization rates of these steels above the solution temperature of the vanadium carbonitrides and compared them with that observed in a reference plain carbon steel. The markedly slower kinetics of the vanadium steels indicates that this element has a retarding effect on recrystallization even when it is fully in solution. The solute effect is of course less than the combined effect of solute and precipitate.

modified steel an appropriate decarburizing and denitriding heat treatment.[21]

The reverse-knee of Fig. 12(*a*) can now be rationalized in terms of the RTT curves of Fig. 12(*b*) and the PTT results for dynamic precipitation presented in Fig. 9. As indicated in Fig. 12(*c*), when the P_s time is longer than the solute-modified R_s time, the observed RTT curve has the normal dependence on temperature. This is the case at high and at low temperatures. When the P_s time is shorter than the solute-modified R_s time, the nucleation and growth of new grains are severely retarded. The construction suggests, therefore, that the reverse-knee of Fig. 12(*a*) is attributable to the combined effect of Nb as solute and as precipitate-former on the rate of recrystallization.[13] In the absence of the retardation due to Nb as solute, recrystallization of the Nb-modified austenite would begin before the onset of precipitation. This model also suggests that, in problematic cases, recrystallization can be prevented during controlled rolling by the addition of a quantity of a soluble microalloying element sufficient to delay recrystallization until the precipitate-forming microalloying elements begin to be rejected from solution.

ACKNOWLEDGEMENTS

Financial support from the Department of Energy, Mines, and Resources, Ottawa, the National Research Council of Canada, and the Quebec Ministry of Education (FCAC program) is gratefully acknowledged. The authors are also indebted to Dr Murray Stewart (CANMET-EMR) for his encouragement and support, to Malcolm Gray, Brian Rothwell, and Hugh McQueen for their stimulating suggestions and comments, and to the Algoma Steel Corporation for providing the experimental materials.

REFERENCES

1. B. L. PHILIPPO and F. A. A. CRANE: *J. Iron Steel Inst.*, 1973, **211**, 653.
2. T. GREDAY and M. LAMBERIGTS: 'Processing and properties of low-carbon steel', p. 75. 1973: New York (Metall. Soc. AIME).
3. A. LeBON, J. ROFES-VERNIS, and C. ROSSARD. *Mém. Sci. Rev. Métall.*, 1973, **70**, 577.
4. A. B. ROTHWELL: *ibid.*, 1972, **69**, 413.
5. K. J. IRVINE, T. GLADMAN, J. ORR, and F. B. PICKERING: *J. Iron Steel Inst.*, 1970, **208**, 717.
6. T. GLADMAN and F. B. PICKERING: *ibid.*, 1967, **205**, 653.
7. R. PHILLIPS and J. A. CHAPMAN: *ibid.*, 1966, **204**, 615.
8. T. GLADMAN, I. D. McIVOR, and F. B. PICKERING: *ibid.*, 1971, **209**, 380.
9. A. LeBON, J. ROFES-VERNIS, and C. ROSSARD: *Met. Sci.*, 1975, **9**, 36.
10. R. G. HOOK and H. NYO: *Metall. Trans.*, 1975, **6A**, 1443.
11. R. COLADAS, J. MASOUNAVE, and J. P. BAÏLON: 'The hot deformation of austenite' (ed. J. B. Ballance), p. 341. 1977: New York (AIME).
12. M. A. PACINA: PhD thesis, University of Sheffield, 1975.
13. I. WEISS and J. J. JONAS: Proc. ASM/AIME Conf. on Recovery, Recrystallization, and Grain Growth in Materials, Chicago, October 1977, *Metall. Trans.*, 1979, **10A**, in press.
14. M. J. LUTON, J. P. IMMARIGEON, and J. J. JONAS: *J. Phys. E. (Sci. Instrumen.)* 1974, **7**, 862.
15. I. WEISS: PhD thesis, McGill University, Montreal, 1978.
16. I. WEISS and J. J. JONAS: Proc. AIME Symp. on Precipitation Effects in HSLA Steels, Denver, Colorado, February 1978. *Metall. Trans.*, 1979, **10A**, in press.
17. J. J. JONAS: Proc. 4th Int. Conf. on the Strength of Metals and Alloys (ed. ENSMIM–INPL), vol. III, pp. 976–1002. 1976: Nancy (editor).
18. R. SIMONEAU, G. BÉGIN, and A. H. MARQUIS: *Met. Sci.*, 1978, **12**, 8.
19. H. WATANABE, Y. E. SMITH, and R. D. PEHLKE: Ref. 11, p. 140.
20. A. LeBON, J. ROFES-VERNIS, and C. ROSSARD: IRSID Publication, M.P. 1429 JRV/CC, November 1975.
21. W. S. OWEN and M. J. WHITE: paper presented at the Fall Meeting of ASM/AIME, St. Louis, Missouri, October 1978.

Dynamic Precipitation and Coarsening of Niobium Carbonitrides During the Hot Compression of HSLA Steels

I. WEISS AND J. J. JONAS

The size distribution of the static precipitates produced in unstrained austenite was determined at 900°C by the method of extraction replication. The effect of deformation on the rate of coarsening of the particles was established up to a true strain of 0.75. Size distributions were also measured in materials containing static precipitates which were undergoing dynamic precipitation at 900°C. The mean size in these materials decreased while dynamic precipitation was occurring and then increased due to dynamic coarsening. The rate of increase during *dynamic* ripening was two to three orders of magnitude higher than the rate of *static* Ostwald ripening reported in the literature. The effect of particle size on the initiation of dynamic recrystallization was also evaluated. The results confirm the general rule that fine particles (d ≃ 6 nm) are more effective than coarser ones (*e.g.* d ≃ 20 nm) with respect to the retardation of dynamic recrystallization. The necessary fine particles can be nucleated homogeneously in the alpha phase or heterogeneously on gamma phase dislocations.

THE recovery and recrystallization processes taking place during and after the hot working of HSLA steels are significantly retarded by the presence of the niobium (columbium) and other carbonitrides. The two particle distribution parameters which have the greatest influence on the degree of retardation are the volume fraction and mean particle size. The volume fraction has been observed to increase more rapidly following high temperature deformation than it does in undeformed materials. This is because straining accelerates the rate of carbonitride precipitation in materials cooled from the solution temperature.[1-3] Less well-known is the dependence of the particle *size* on straining, and the relation between coarsening and deformation more generally.

The aim of the present work was therefore to throw some light on the effect of high temperature deformation on the size distribution and coarsening behavior of Nb(CN). To this end, size distributions were determined in deformed specimens held for 6, 34 and 760 min prior to straining. Strains of 0.11 to 0.75 were then applied, followed by quenching. In addition, some specimens were quenched after aging but without straining so as to establish the distribution in the undeformed condition. The effect of particle size on the initiation of dynamic recrystallization was also evaluated.

MATERIALS AND PROCEDURE

The deformation experiments were carried out on an Instron testing machine modified for constant true strain rate hot compression. The compression tools and the testing system are described elsewhere.[4] The materials investigated were two microalloyed steels with the compositions shown in Table I. The steel was received in the form of 25 mm thick plate, which was cut lengthwise into square bars, and then machined into compression specimens 13 mm high and 8.7 mm in diam. In this way, the axes of the compression specimens were aligned in the rolling direction. Prior to testing, the Nb-modified steel was solution treated at 1100°C for 30 min. After austenitizing, the steel was cooled to the test temperature at a rate of 1°C/s.

In order to establish the size distributions, a carbon extraction replica method was used. The specimens were cross-sectioned perpendicular to the deformation axis, and then mechanically ground and polished. To prepare the surfaces for extraction replication, the sectioned samples were electropolished in a solution containing 7 pct perchloric acid + 93 pct ethylene glycol monobutyl ether under the following conditions: 0°C, 11 v, 15 min, and then etched lightly in 1 pct nital. A film of carbon was deposited on the etched surface, which was then cut up into 3 × 3 mm squares. The extraction replicas were removed from the specimen surfaces with the aid of a solution of 2 pct nital + 5 pct HCl in water. These were placed on copper grids in the usual way and examined in a Philips EM 300 electron microscope.

The electron micrographs of such replicas represent projections of the precipitates on a single plane. However, the desired parameter is the number of precipitates per unit volume of the matrix Nv_i. This number (Nv_i) can only be calculated from the number of particles per unit surface (Ns_i) (the parameter obtained directly from the electron micrograph) with the aid of a further assumption. In the present work, it was assumed that precipitates having a given diameter, *e.g.* d_i, are extracted by the carbon replica from a layer of matrix which is d_i thick.[5] Then Nv_i can be expressed in terms of Ns_i by the following equation:

$$Nv_i = Ns_i/d_i \qquad [1]$$

Through the use of this expression for each size

I. WEISS and J. J. JONAS are Research Associate and Professor, respectively, with the Department of Metallurgical Engineering, McGill University, 3450 University St., Montreal H3A-2A7, Canada.

This paper is based on a presentation made at a symposium on "Precipitation Processes in Structural Steels" held at the annual meeting of the AIME, Denver, Colorado, February 27 to 28, 1978, under the sponsorship of the Ferrous Metallurgy Committee of The Metallurgical Society of AIME.

ISSN 0360-2133/80/0311-0403$00.75/0

Table I. Chemical Composition in Wt Pct of the Materials Tested

Materials	C	Mn	S	P	Al	Cu	Si	N	Nb
Niobium Bearing Steels	0.05	0.42	0.009	0.002	0.057	0.006	0.045	0.004	0.035
	0.06	0.42	0.009	0.002	0.051	0.006	0.014	0.004	0.018

group of precipitates, as characterized by its diameter d_i, the distribution of precipitates per unit volume of matrix was estimated. The mean diameter D of the distribution was also calculated by means of the classical formula:

$$D = \left\{ \sum_i N v_i d_i^3 / \sum_i N v_i \right\}^{1/3} \quad [2]$$

Here D is the diameter of the sphere having the average volume of the distribution. In the present work, the precipitate density $Nv_i = f(d_i)$ and the mean precipitate size D were determined for the following aging and deformation conditions:

(i) aged for 6 min in the recrystallized state and deformed to 0.11 strain;

(ii) aged for 34 min before deformation and then deformed for 0, 0.11, 0.36 and 0.45 strain;

(iii) aged for 760 min before deformation and then deformed to 0, 0.15, 0.43 and 0.75 strain.

On the basis of the kinetics of static precipitation determined earlier in the present investigation,[1,6] these aging times correspond to around 10, 20 and 90 pct precipitation respectively.

RESULTS

The true stress-true strain curves of Fig. 1 show the effect of prior aging on the flow behavior of the present microalloyed steel deformed at a constant true strain rate of $1.2 \times 10^{-3}s^{-1}$. The intervals of strain after which the specimens were quenched are also indicated on this diagram. After 6 min of aging before deformation, the flow curve (t_{h_1}) exhibits the highest stress level and the greatest peak strain. This is because the potential for dynamic precipitation is greater after 6 min of aging than after either 34 min (curve t_{h_2}) or 760 min (curve t_{h_3}).[1,6]

Under these conditions, the size distribution was measured only during the work hardening period (ϵ_1). When the aging time before deformation was increased, less dynamic precipitation occurred, and the particle size distribution was also established for strains beyond the critical strain to initiate dynamic recrystallization (ϵ_3, ϵ_4 for t_{h_2}; ϵ_6, ϵ_7 for t_{h_3}).

Size Distribution After 6 Min of Aging

The size distribution of the Nb(CN) precipitates was measured after a strain of 0.11 in order to evaluate the effect of deformation at 900°C on the morphology of the particles (see Fig. 2). Here the spread of particle sizes after 6 min of aging followed by deformation at a constant strain rate of $1.2 \times 10^{-3}s^{-1}$ can be seen. This delay is short enough to enable a large number of dynamic precipitates to be formed.[1] Precipitates in the overall range of 3 to 20 nm were

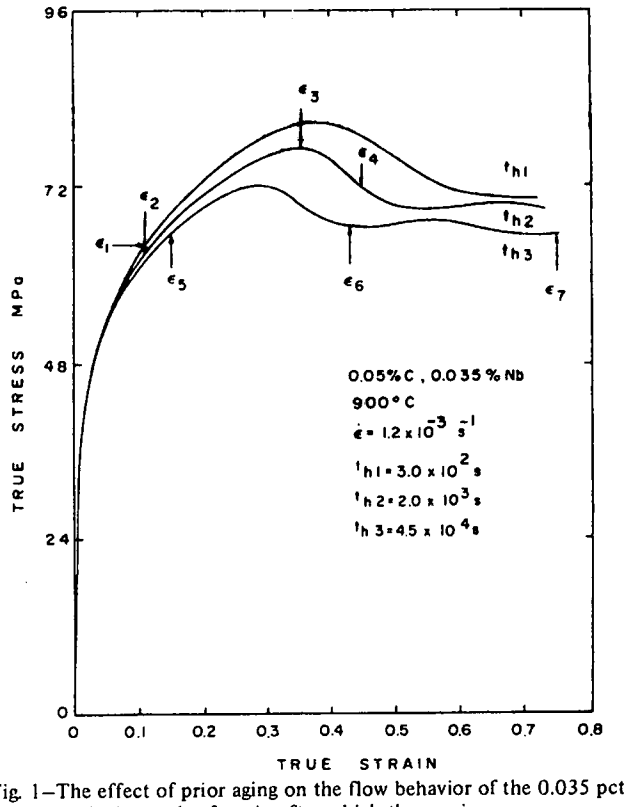

Fig. 1—The effect of prior aging on the flow behavior of the 0.035 pct Nb steel. The intervals of strain after which the specimens were quenched are also indicated.

observed with a mean particle size of 8 nm. However, the *dynamic* precipitates can be considered[22] to fall in the range 3 to 10 nm, so that, according to the cumulative frequency plot, 80 pct of the precipitates were produced dynamically and only 20 pct statically. The high degree of size homogeneity of the particles precipitated during deformation should also be noted.

The present mean size agrees quite well with the results of Greday and Lamberigts[7] who reported mean diameter between 3 and 5 nm after two rolling passes equivalent to a total true strain of 0.50. The present observations are also consistent with the work of Davenport *et al*,[8] who determined the mean precipitate size to be between 5 and 12 nm following a hot reduction of 0.50. The mean particle size measured in this work is larger, however, than the mean particle sizes observed for strain induced (dynamic) precipitation alone, for which values around 5 nm have been reported.[2] The larger value observed here can be attributed to the large particles (10 to 20 nm) which were precipitated statically (around 10 pct by volume of all the particles precipitated, both statically and dynamically, at this temperature).

Size Distributions After 34 Min of Aging

In this case, the size distributions were also measured after increasing amounts of strain, so that the progressive effect of high temperature deformation could be evaluated. The conditions were chosen so that some supersaturated Nb* was still available for

*About 80 pct of the Nb available for precipitation at 900°C after solution treatment at 1100°C can be estimated to be still in solution after 34 min of aging of the undeformed austenite.[1,6]

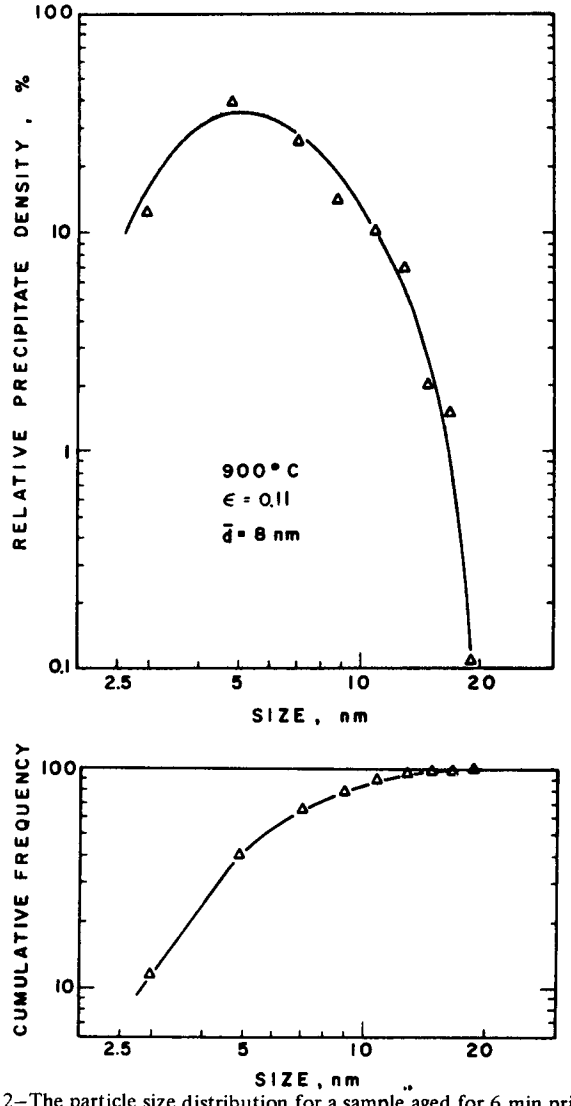

Fig. 2–The particle size distribution for a sample aged for 6 min prior to deformation and given a strain of 0.11 at 900°C.

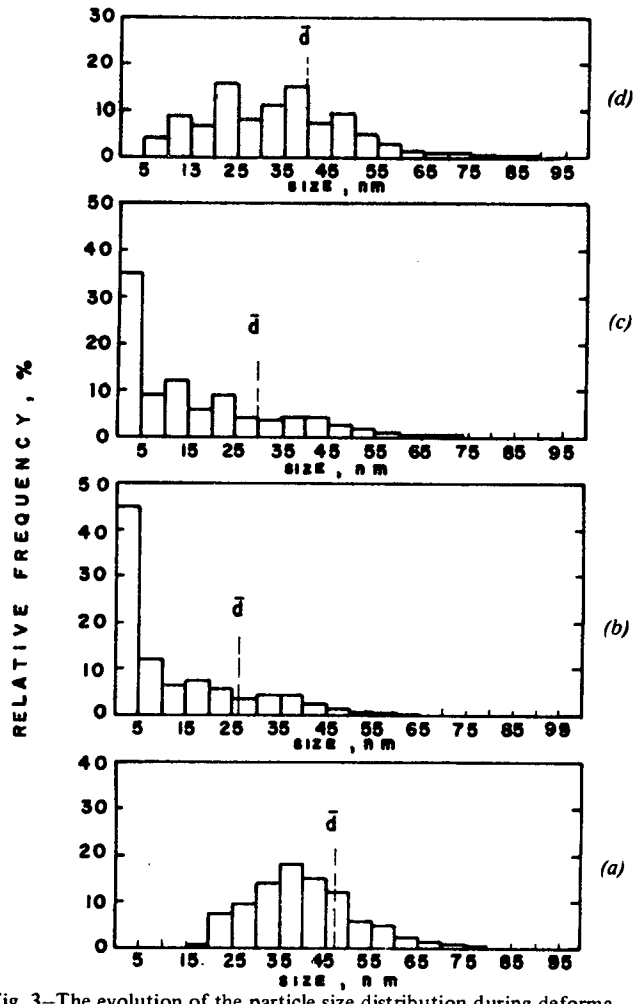

Fig. 3–The evolution of the particle size distribution during deformation at 900°C after aging for 34 min (relative frequency scale). (*a*) 900°C, t_h = 34 min, d = 47 nm, and ϵ = 0; (*b*) 900°C, t_h = 34 min, d = 27 nm, ϵ = 0.11; (*c*) 900°C, t_h = 34 min, d = 30 nm, and ϵ = 0.36; (*d*) 900°C, t_h = 34 min, d = 40 nm, and ϵ = 0.45.

precipitation during the experiment. Aging for 34 min following the solution treatment and cooling to 900°C produced the size distribution shown in Fig. 3(*a*). Particle sizes in the range 15 to 80 nm were observed, with a mean of 47 nm. The degree of homogeneity is lower than in the previous case (Fig. 2). This particle size range is in agreement with the results of Gray[9] on precipitation from ferrite at equivalent diffusion temperatures, who reported diameter of 10 to 60 nm. The particle sizes measured in this work also overlap those of Gladman and Pickering,[10] who determined sizes of 15 to 40 nm after aging for 1 h at 900°C.

The size distribution after 0.11 strain at 900°C is shown in Fig. 3(*b*). Particles in the range 5 to 70 nm were counted, with a mean of 27 nm. In this case the relative frequency plot indicates that 50 pct of the particles precipitated were less than 5 nm in diam. This result can be attributed to the fine dynamic particles (< 5 nm) which precipitate on dislocations during deformation. When the strain is increased to 0.36, the size distribution is modified to the one shown in Fig. 3(*c*). Under these conditions, the particles cover the range 5 to 75 nm, with a mean of 30 nm. Thus it is evident that, during deformation, there is an increase in the mean size, even though the size range remains almost the same. The size distribution obtained after 0.45 strain is illustrated in Fig. 3(*d*), which covers the range 7 to 85 nm. In this case the mean is 40 nm. The degree of homogeneity is the lowest after the highest strain.

In order to follow the evolution of the precipitation and coarsening processes during deformation more closely, the particle size distributions were replotted on an absolute scale, as shown in Fig. 4. It is evident that the original static precipitates (Fig. 4(*a*)) are coarsened slightly during deformation, and that large amounts of dynamic precipitates are formed in the early stages of straining (Figs. 4(*b*) and 4(*c*)). Once dynamic precipitation is complete (Fig. 4(*d*)), both the static and dynamic particles coarsen simultaneously.

Size Distributions After 760 Min of Aging

In this series of experiments, the size distribution was measured after an aging interval of 760 min followed by increasing amounts of strain. This was with

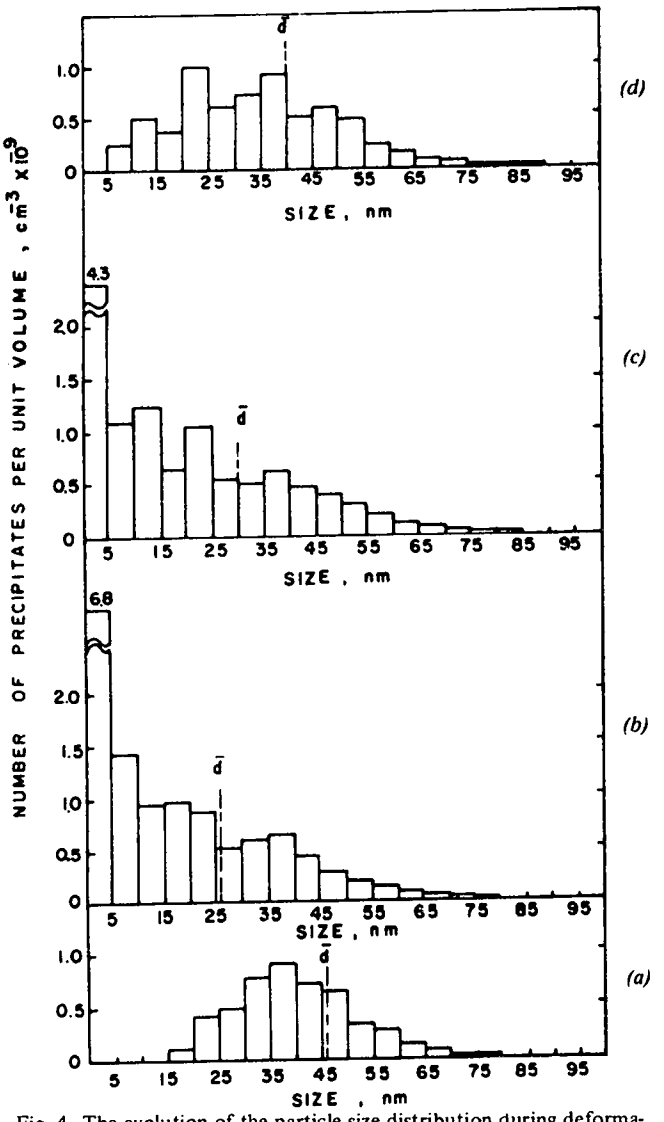

Fig. 4—The evolution of the particle size distribution during deformation at 900°C after aging for 34 min (number per unit volume scale). (*a*) 900°C, t_h = 34 min, d = 47 nm, and ϵ = 0; (*b*) 900°C, t_h = 34 min, d = 27 nm, and ϵ = 0.11; (*c*) 900°C, t_h = 34 min, d = 30 nm, and ϵ = 0.36; (*d*) 900°C, t_h = 34 min, d = 40 nm, and ϵ = 0.45.

the aim of determining the effect of progressive deformation on the pre-existing distribution of static particles. Following solution treatment and cooling to 900°C, the samples were aged for 760 min, producing the size distribution shown in Fig. 5(*a*). These particles fell in the range 15 to 110 nm, with a mean of 53 nm. The latter is in the upper range of the sizes detected by Gray[11] in ferrite with an equivalent diffusion temperature. The relative frequency plot indicates that the distribution has a low degree of homogeneity. The effect of 0.15 strain is illustrated in Fig. 5(*b*). Comparison with Fig. 5(*a*) reveals that particles with larger diam were produced (25 to 140 nm), with a mean of 78 nm. Further deformation to 0.43 continued the coarsening trend, as can be observed from Fig. 5(*c*). The mean particle size is 83 nm, with a range between 25 and 150 nm. The maximum size range produced was 35 to 200 nm after 0.75 strain (Fig. 5(*d*)). It appears that the larger the deformation at 900°C, the larger the mean particle size and the broader the distribution.

In Fig. 6, the appearance of the Nb(CN) particles precipitated under the present experimental conditions can be seen. The precipitates produced by aging for 760 min at 900°C and deforming to 0.75 strain are shown in Fig. 6(*a*). These particular precipitates were nucleated in the matrix in a cluster arrangement, and then coarsened during deformation on their original nucleation sites. A mean particle size of 100 nm was observed under these conditions. The Nb(CN) particles precipitated *during* deformation to 0.45 strain at 900°C show up as the finer precipitates in Fig. 6(*b*). The larger particles were precipitated during the aging prior to deformation.

Effect of Particle Size on the Initiation of Dynamic Recrystallization

The presence of second phase particles during or after high temperature deformation influences the process of substructure formation and modification as well as the rate of grain boundary migration. Several workers[12,13] have shown that particle size and volume fraction are the two most important parameters with respect to whether or not the retardation of *static* recrystallization occurs. In order to investigate the retardation of *dynamic* recrystallization in austenite, specimens containing a constant volume fraction of precipitate (0.0003) and with a variety of particle sizes were prepared in the following way. After solution treatment at 1100°C for 30 min, each specimen was quenched into the ferrite or ferrite plus austenite phase, and then aged for 24 h at different temperatures to produce a fine dispersion of Nb(CN) particles. Since the aging treatment performed in this work was similar to that carried out by Gray,[9] the mean particle sizes shown in Table II and reported by him were assumed to apply to the present experiments.* It should be noted that, although aging at different temperatures produces differences in the volume fraction precipitated, these are expected to be eliminated once the specimens are preheated to and held at the test temperature. The specimens were deformed at a strain rate of $1.2 \times 10^{-3} s^{-1}$ after a stabilization time of around 5 to 10 min, which also permitted the ferrite to transform to austenite.

*The mean sizes were not determined directly due to time limitations.

Figure 7 demonstrates the observed effect of initial particle size on the initiation of dynamic recrystallization at 1025°C. For this purpose ϵ_p, which is the peak strain, is defined to be the critical strain to initiate dynamic recrystallization. It can be seen that the largest peak strain was obtained for the smallest initial particle size (5 nm, Table II). Furthermore, as the particle size was *increased*, ϵ_p *decreased*. The fine dispersion produced at 650°C also promotes the retention of a finer grain size after transformation to austenite. This in turn tends to reduce the critical strain for dynamic recrystallization.[14,15] Furthermore, particle coarsening and partial dissolution take place to a greater degree during deformation at 1025°C after aging at 650°C than after aging at 800°C. These effects can also contribute to a reduction in ϵ_p for the lower aging temperatures. Thus, under conditions of constant austenite grain size, and in the relative absence of

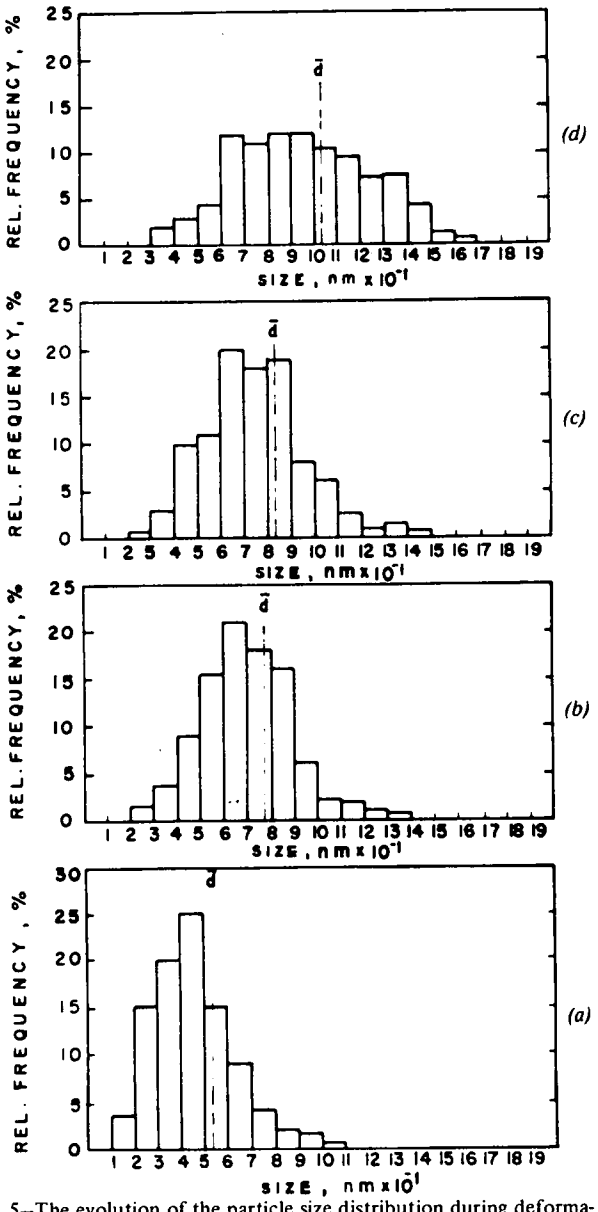

Fig. 5—The evolution of the particle size distribution during deformation at 900°C after aging for 760 min. (*a*) 900°C, t_h = 760 min, d = 53 nm, and ϵ = 0; (*b*) 900°C, t_h = 760 min, d = 78 nm, and ϵ = 0.15; (*c*) 900°C, t_h = 760 min, d = 83 nm, and ϵ = 0.43; (*d*) 900°C, t_h = 760 min, d = 102 nm, and ϵ = 0.75.

particle coarsening, the effect of initial particle size on peak strain can be expected to be still greater than that shown in Fig. 7.

DISCUSSION

The Influence of Deformation on Precipitation and Coarsening

The effect of deformation on the particle size distributions present after aging for 34 min was illustrated in Figs. 3 and 4. The above results are collected and plotted in terms of r^3 in Fig. 8. Thirty-four min of aging produced a mean particle size of 47 nm, with most of the Nb still in solid solution. Thus deformation led to the dynamic precipitation of fine particles, so that a strain of 0.11 produced a reduced mean of 27 nm. Further deformation to

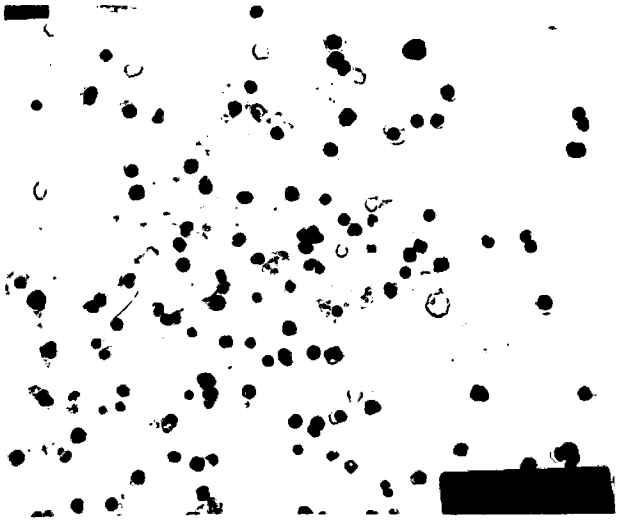

Fig. 6(*a*)—Nb(CN) precipitates produced by aging for 760 min at 900°C and deforming to a strain of 0.75 (carbon extraction replica). Magnification 18,000 times.

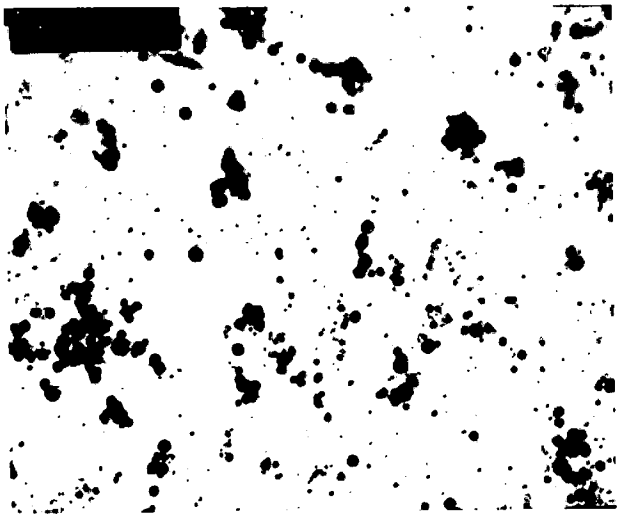

Fig. 6(*b*)—Nb(CN) particles precipitated during deformation to a strain of 0.45 at 900°C. The large particles were precipitated during aging for 34 min prior to deformation. Magnification 18,000 times.

strains of 0.36 and 0.45 increased the mean particle size to 30 and 40 nm respectively. The effect of the large volume fraction of fine precipitates formed during the early stages of straining can be seen in Fig. 8. The occurrence of dynamic precipitation causes a sharp drop in r^3 despite the concurrent coarsening of the large particles present before deformation. According to Fig. 8, precipitation during deformation comes to an end at a strain of about 0.17, which corresponds to a time of about 150 s. This value is in reasonable agreement with that obtained by the mechanical test method described earlier.[6] The finish time for precipitation determined by the mechanical technique was expected to correspond to about 95 pct precipitation. Thus the difference in the finish times observed utilizing electron microscopy and mechanical testing can be attributed in part to the time needed to reach completion of the precipitation process. Further deformation at constant temperature coarsens both the large

Table II. Mean Particle Size as a Function of Aging Temperature[9]

Aging Temperature, °C	Mean Particle Size, nm
600	3
650	5
700	9
750	15
800	20

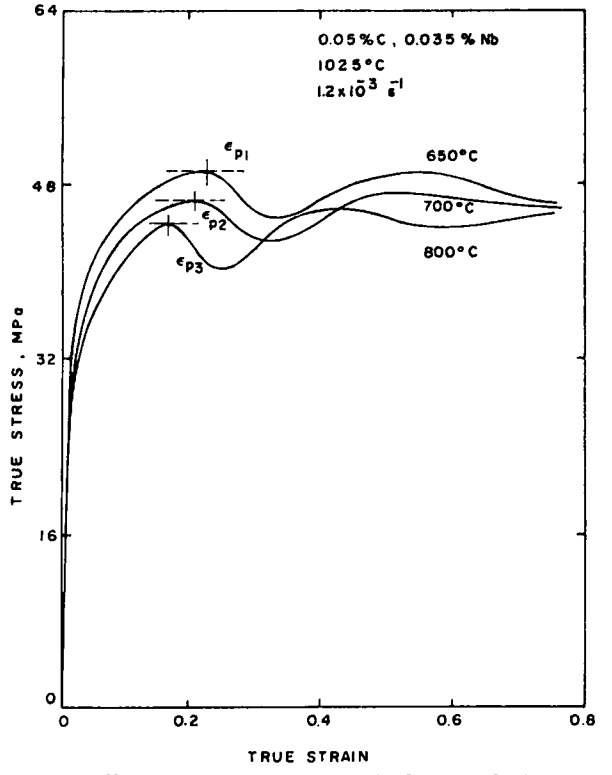

Fig. 7—The effect of aging temperature in the ferrite or ferrite + austenite range on the subsequent flow behavior at 1025°C in the austenite range.

and fine particles, resulting in an increase in the mean particle size. Finally, it should be noted that, despite dynamic coarsening, the mean particle size after a strain of 0.45 is still smaller than the one obtained after static aging for 34 min before deformation.

Particle Coarsening During Deformation

When the matrix is once again in equilibrium following the completion of precipitation, true coarsening unencumbered by concurrent precipitation can take place. The evolution of the particle size distribution during the progress of deformation after such an aging treatment was depicted in Fig. 5. It was seen above that the mean particle size increased continuously, and that a mean diam of 102 nm was attained after a strain of 0.75. It will now be of interest to re-examine these results in terms of the mean cube radius and the theory of Ostwald ripening.

According to Wagner's diffusion-controlled model[16,17] particle growth under Ostwald conditions

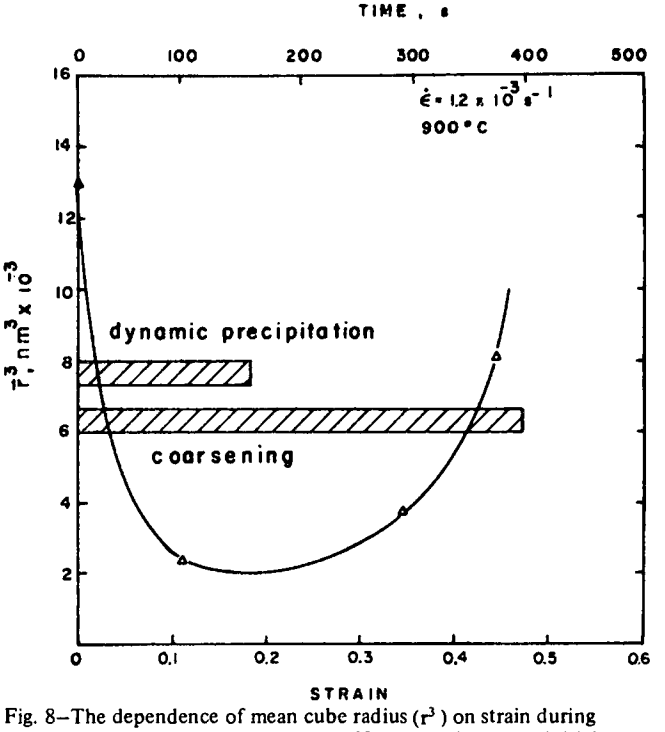

Fig. 8—The dependence of mean cube radius (r^3) on strain during dynamic precipitation and coarsening. Note that the coarse initial particle size of 47 nm (equivalent to $r^3 = 13 \times 10^3$ nm^3) was produced by *static precipitation* during the 34 min aging period. During the 150 s interval of *dynamic precipitation* (*i.e.*, up to a strain of 0.19), the mean particle size decreased to 13 nm (equivalent to $r^3 = 2000$ nm^3). Although *dynamic coarsening* takes place from the initiation of straining, its effect cannot be observed until after dynamic precipitation has come to an end through the exhaustion of the Nb in supersaturation.

can be described by:

$$\mathbf{r}_t^3 = \mathbf{r}_0^3 + Kt \qquad [3]$$

where

$$K = \frac{8\sigma_p D C_0 V_m}{9k} \qquad [4]$$

$\mathbf{r}_t$ is the average particle radius at time t, $\mathbf{r}_0$ is the average particle radius at time t_0, D is the diffusivity in austenite of the particle species, C_0 is the concentration of the particle species in the matrix, k is Boltzmann's constant, V_m is the particle molar volume, and σ_p is the surface energy between the particle and the matrix.

The present mean cube radius $\mathbf{r}^3$ values are shown plotted against time in Fig. 9. The results are in reasonable agreement with the linear relationship of Eq. [3], except that the slope for dynamic ripening is considerably higher than that given for static ripening by relation [4]. The latter can be evaluated using the following data:

$\sigma_p = 15 \times 10^{-7}$ J/cm^2
$C_0 = 5 \times 10^{-5}$
$V_m = 2 \times 10^2$ nm^3
$Q = 293$ KJ/mol
$D_0 = 5.3 \times 10^2$ cm^2/s

which leads to a K value for 'normal' Ostwald ripen-

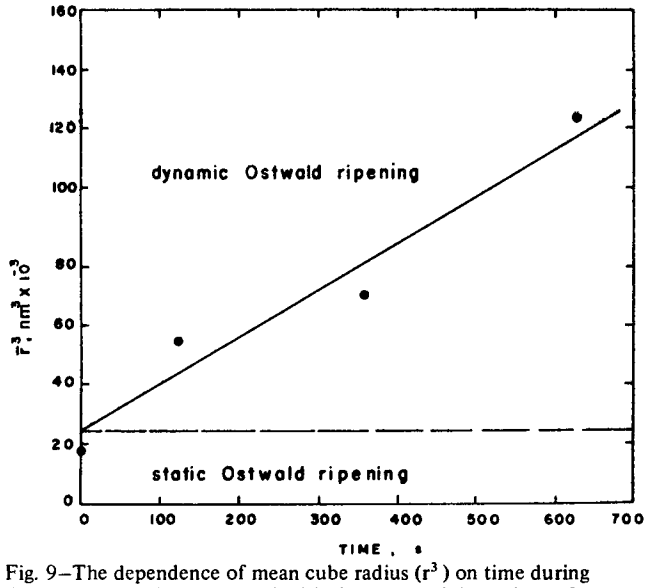

Fig. 9—The dependence of mean cube radius (r^3) on time during dynamic coarsening compared with the expected dependence for static coarsening.

ing of 3.8×10^{-2} nm^3/s. According to the present data, the 'dynamic' Ostwald process exhibits a value of $K = 140$ nm^3/s, so that deformation at 500°C appears to *accelerate* the rate of coarsening by about three orders of magnitude, as indicated by the ratio:

$$K_{dyn}/K_{nor} = 3.68 \times 10^3$$

Comparison of the Effect of Particles Formed in Ferrite and Austenite on the Initiation of Dynamic Recrystallization

As shown above, the finer the dispersion of the alpha precipitates, the larger the peak strain when the samples are subsequently deformed in the gamma phase. The influence of particle size on the γ peak strain may in fact be independent of whether the precipitates were formed in the ferrite or in the austenite phase. For example, in Figs. 10(*a*) and 10(*b*), we illustrate the effects of prior precipitation in α and γ iron on the initiation of dynamic recrystallization in γ iron subsequently deformed at 925°C. In both diagrams, the upper two curves were obtained after aging in ferrite, and in ferrite + austenite respectively; these samples were estimated[9] to contain particles 3(α) and 20(α + γ) nm in diam. Relatively large peak strains were observed under these conditions. The two lower curves in both figures were produced after aging in austenite. It can be seen that the larger peak strain is attained when no static precipitation occurs before deformation. Under these conditions, fine precipitates (< 5 nm) are deposited on the dislocations *during* deformation.

The two different modes of precipitation illustrate that large retardations are produced either when fine particles are present before deformation (as formed by aging at 600°C in α), or when precipitation occurs concurrently with deformation in the austenite phase. In the latter case, the larger austenite grain size also contributes to increasing the peak strain. For the *same* austenite grain size, the retardation can be expected to be greater when the fine particles are present *before* deformation.

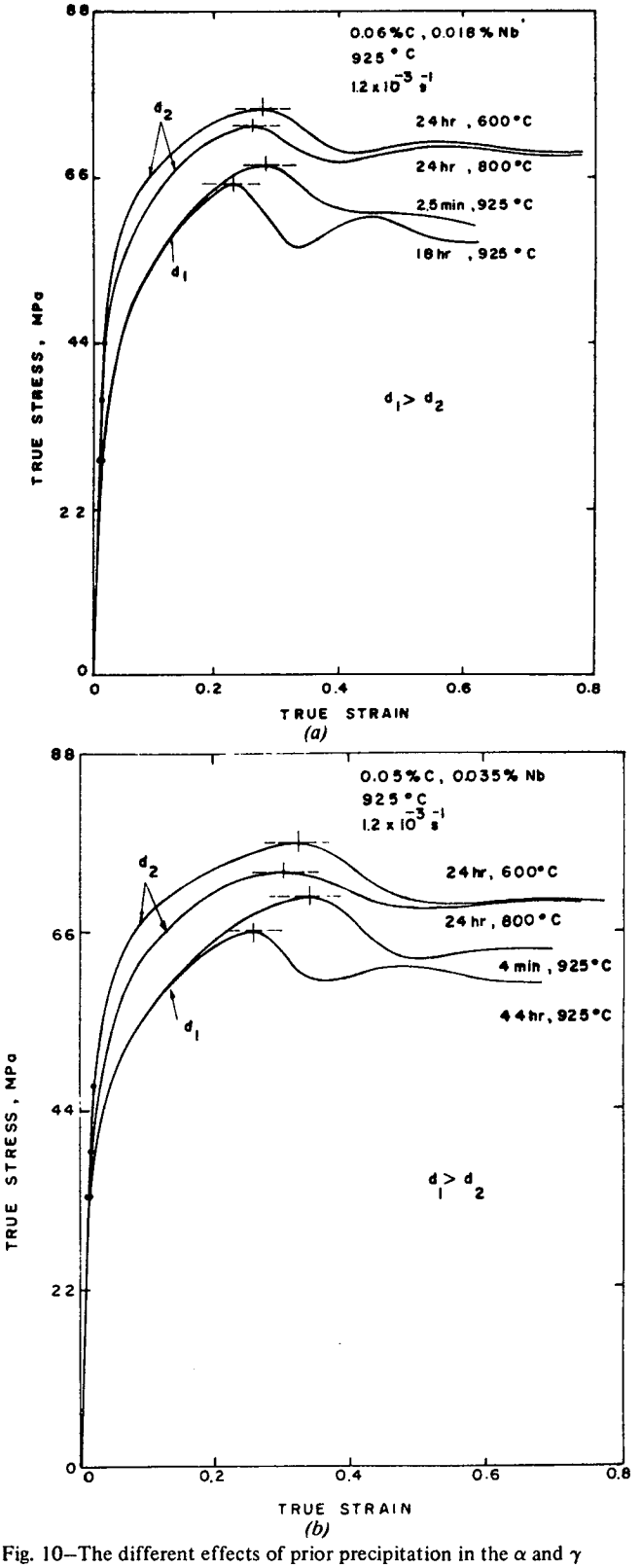

Fig. 10—The different effects of prior precipitation in the α and γ phases on the initiation of dynamic recrystallization in the γ phase: (*a*) 0.018 pct Nb steel, (*b*) 0.035 pct Nb steel. The circles indicate the 0.1 pct offset yield stress pertaining to each condition. The grain size in the austenite cooled from 1100 to 925°C ($d_1 \cong 150$ μm) is greater than that of the quenched samples reheated at 600 and 800°C prior to testing at 925°C ($d_2 \cong 50$ μm).

Figures 10(*a*) and 10(*b*) also indicate that higher yield stresses and work hardening rates are observed

when the samples contain prior precipitates. The higher yield stress can be attributed in part to the smaller grain size[18] and in part to the fine particles.[19–21] In a similar way, the higher work hardening rate can also be ascribed to an Orowan strengthening effect.

CONCLUSIONS

1. The dynamic precipitation of Nb(CN) at 900°C produces fine particles in the range 3 to 10 nm, with a mean diam of 6 nm. When static precipitation takes place *before* deformation, larger particles are formed; for example, aging for 6 min produces particles with a mean diam of 15 nm, whereas aging for 760 min leads to particle sizes of about 53 nm.
2. When 34 min of static precipitation at 900°C (leading to d = 47 nm) is followed by dynamic precipitation to a strain of 0.11, the mean size of the Nb(CN) particles decreases to 27 nm. This is because the dynamic precipitates ($d \simeq 6$ nm) are much finer than the static ones. If straining is continued when the dynamic precipitation comes to an end (*i.e.*, when all the supersaturated Nb has been exhausted), particle coarsening takes place. In this way, the mean particle size increases to 40 nm after a strain of 0.45 at 900°C.
3. Under dynamic coarsening conditions, the cube radius (r^3) increases linearly with time, and the Wagner coefficient K is 140 nm^3/s. This indicates that the coarsening rate is accelerated during straining by about three orders of magnitude when compared to the static rate of Ostwald ripening.
4. Fine particles ($d \simeq 5$ nm) precipitated in the ferrite phase are effective in retarding the initiation of dynamic recrystallization during subsequent deformation in the austenite phase. Similar retardations are observed when the maximum amount of dynamic precipitation occurs during the concurrent deformation of austenite. In the latter case, the mean particle size determined by extraction replication is about 6 nm, and the absence of particles at the commencement of straining is compensated by the continued production of fine particles at strains which lead to the coarsening of the ferrite precipitates.

ACKNOWLEDGMENTS

Financial support from the Department of Energy, Mines and Resources, Ottawa, the National Research Council of Canada, and the Quebec Ministry of Education (FCAC program) is gratefully acknowledged. The authors are also indebted to Murray Stewart (CANMET-EMR) for his encouragement and support, to Malcolm Gray for helpful suggestions relating to extraction replication, to Brian Rothwell for his stimulating suggestions and comments, and to the Algoma Steel Corporation for providing the experimental materials.

REFERENCES

1. I. Weiss and J. J. Jonas: *Met. Trans. A*, 1979, vol. 10A, pp. 831-40.
2. A. LeBon, J. Rofes-Vernis, and C. Rossard: *Met. Sci.*, 1975, vol. 9, p. 36.
3. H. Watanabe, Y. E. Smith, and R. D. Pehlke: *The Hot Deformation of Austenite*, J. B. Ballance, ed., p. 140, AIME, New York, NY, 1977.
4. M. J. Luton, J. P. Immarigeon, and J. J. Jonas: *J. Phys. E: Sci. Inst.*, 1974, vol. 7, p. 864.
5. M. F. Ashby and R. Ebeling: *Trans. TMS-AIME*, 1966, vol. 236, p. 1336.
6. J. J. Jonas and I. Weiss: *Met. Sci.*, 1979, vol. 13, p. 238.
7. T. Greday and M. Lamberigts: *Microalloying 75*, p. 172, Union Carbide Corporation, New York, NY, 1977.
8. A. T. Davenport, R. E. Miner, and R. A. Kot: Ref. 3, p. 186.
9. J. M. Gray: *Met. Trans.*, 1972, vol. 3, p. 1495.
10. T. Gladman and F. B. Pickering: *J. Iron Steel Inst.*, 1967, vol. 205, p. 653.
11. J. M. Gray: *Processing and Properties of Low Carbon Steel*, J. M. Gray, ed., p. 225, AIME Publication, NY, 1973.
12. C. Zener and C. S. Smith: *Trans. AIME*, 1949, vol. 175, p. 15.
13. T. Gladman: *Proc. Roy. Soc.*, 1966, vol. 294A, p. 298.
14. H. J. McQueen and S. Bergerson: *Met. Sci. J.*, 1972, vol. 6, p. 25.
15. J. P. Sah, G. J. Richardson, and C. M. Sellars: *Met. Sci.*, 1974, vol. 8, no. 10, p. 325.
16. I. M. Lifschitz and V. J. Slyozov: *J. Phys. Chem. Solids*, 1961, vol. 19, p. 35.
17. C. Wagner: *Zeit. Electrochem.*, 1961, vol. 65, nos. 7 and 8, p. 581.
18. A. Cracknell and N. J. Petch: *Acta Met.*, 1955, vol. 3, p. 186.
19. T. Gladman, D. Dulieu, and I. D. McIvor: Ref. 7, p. 32.
20. M. W. Lui and I. LeMay: Ref. 7, p. 55.
21. M. W. Lui and I. LeMay: *Met. Sci.*, 1974, vol. 8, p. 435.
22. I. Weiss: Ph.D. Thesis, McGill University, Montreal, Canada, 1978.

Prepared for inclusion in the
Commemorative Issue for Dr. R.C. Gifkins
Metals Forum, 4 (1981)

RETARDATION OF AUSTENITE RECRYSTALLIZATION BY SOLUTES: A CRITICAL APPRAISAL

John J. Jonas and Melek G. Akben

Department of
Metallurgical Engineering
McGill University
3450 University Street
Montreal, H3A 2A7, Canada

ABSTRACT

The start times for the recrystallization of austenite following high temperature deformation are reviewed for both plain carbon and microalloyed steels. These are shown to be about 0.1 to 1 and 10 to 100 s in the two types of materials, respectively, at 950°C. The precipitation start times in deformed HSLA steels are also surveyed and found to generally lie in the range 10 to 20 s. Thus carbonitride precipitation begins at times longer than R_s for plain C and shorter than R_s for microalloyed steels.

The role of precipitation in promoting 'pancaking' and preventing recrystallization during control rolling is examined critically. For this purpose, the recrystallization kinetics determined in a decarburized and denitrided Nb steel are considered, as are the dynamic recrystallization kinetics of a series of HSLA steels tested above the solubility temperatures of the respective carbonitrides. The retarding effect of solute elements on the rate of recovery is also investigated. It is concluded that solute effects lead to significant delays in both recovery and recrystallization during hot working and that carbonitride precipitation alone is insufficient to prevent austenite recrystallization during steel processing.

RETARDATION OF AUSTENITE RECRYSTALLIZATION BY SOLUTES: A CRITICAL APPRAISAL

It is a pleasure to participate in the preparation of a commemorative volume for Bob Gifkins, who has contributed so much to the study of both recrystallization as well as of the nature of high temperature flow. During his professional career, Bob has not shrunk from expressing his views on controversial topics, and we would like in a similar way to add some fuel to the current debate concerning the factors which prevent the recrystallization of austenite during the control rolling of steel. It is now generally acknowledged that the production of fine-grained ferrite in as-hot-rolled steels requires the suppression of recrystallization during the finishing passes (1-6). The temperature below which no recrystallization occurs at all after an increment of strain is known as the 'pancaking' temperature (2,7-10). Although such pancaking is usually accompanied by the precipitation of carbonitrides on dislocations (2,4,8-10), the role of the precipitate-forming process has been discounted by some (11-13), who have favoured an explanation based on solute drag, or on the formation of some kind of 'pre-precipitate'. Other researchers, alternatively, have concluded that solute effects are of incidental importance at best, and that the key to control rolling lies in the process of strain-induced precipitation (8,9,14-16). It is the purpose of the present brief review to examine these two hypotheses critically,

and to highlight a possible synthesis of these opposing points of view based on some recently published papers and reports.

Recrystallization Start Times in Plain Carbon Steels

In order to be able to appreciate the demands made on the microalloying additions with respect to the prevention of recrystallization, we must first ascertain the rapidity of the recrystallization process in plain carbon steel in the finish rolling temperature range. Such measurements have been made by several researchers, and an example is given in Fig. 1 from the work of LeBon, Rofès-Vernis and Rossard (12). The results obtained by others (13,14,17,18) are in good agreement with those of Fig. 1, and all indicate that recrystallization begins at approximately the following intervals after high temperature deformation:

1000°C - <0.1 s

950°C - $0.1 < t < 0.5$ s

900°C - 0.5 s $\leq t$

Thus, if a microalloying agent is to prevent all recrystallization after rolling at say 950°C, it must be able to act in 0.1 s or less. This general statement must nevertheless be qualified in that the rate of recrystallization increases with the prior strain and strain rate (and conversely it decreases if the pre-strain is small or the imposed strain rate low) (16,19). The times quoted above are for strains in the range 0.25 to 1.0 and strain rates of about 1 to 10 s^{-1}. The 'start' of recrystallization also refers to the beginning of detection by means of

optical microscopy. If electron microscopy were to be employed and if, furthermore, shorter quench times were experimentally available, shorter R_s times would be expected to apply.

Recrystallization Start Times in Microalloyed Steels

Recrystallization start times for the microalloyed steels are universally reported to be greater than for the plain C steels. Some data taken from the work of Hansen et al. (14) are presented in Fig. 2 to illustrate this trend. Here it can be seen that 5% recrystallization requires less than 0.1 s at 950°C in a 0.11 C - 1.30 Mn plain C steel, whereas the same stage of recrystallization is not attained until about 80 s have elapsed in a 0.11 C - 1.35 Mn - 0.031 Nb HSLA steel. When the Nb level was increased to 0.095% (and the Mn level was decreased to 1.24%), the R_s time increased slightly to about 100 s (14).

Somewhat similar R_s times have been reported by Petkovic et al. (17) and by Ouchi et al. (20). At 950°C, they observed that it took about 20 and 30 s for recrystallization to be initiated in a 0.07C - 1.18 Mn - 0.074 Nb and a 0.16C - 1.41 Mn - 0.031 Nb steel, respectively. As in the case of the plain C steels, these R_s times decrease with increasing temperature, and with increasing prestrain and strain rate. The recrystallization behaviour of the microalloyed steels differs in a further important respect from that of the reference plain C materials:

> As the temperature is decreased to the vicinity of 900°C and below, the start of recrystallization is delayed to 1000 s or more, so that

recrystallization is entirely prevented

under commercial rolling conditions.

In principle, these differences in recrystallization behaviour could be attributed entirely to a single process, i.e. either to precipitation acting alone (4,5,8,21), or to solute effects on their own (1,3,12,13,22), or possibly to a suitable combination of the two mechanisms (6,18,23-26). Before these alternatives are considered in detail, however, the precipitation start times commonly reported will first be reviewed.

Precipitation Start Times in Microalloyed Steels

The start of precipitation in high temperature austenite is notoriously difficult to detect experimentally. To date, numerous techniques have been tried, including electrical resistivity (27), microhardness measurement (12,20,28,29), chemical and electrochemical extraction (30,31), extraction replication (14,15,32-34), transmission electron microscopy (16), and high temperature torsion and interrupted compression testing (15,24-26,35-37). It is a common feature of all these methods that (with two exceptions*) the minimum precipitation

*The first exception pertains to the results of Ref.24 . These experiments were conducted on a 0.42 Mn - .035 Nb - .05 C steel and the nose for dynamic precipitation was located at less than 1 s at 900°C. However, it has recently been shown (26) that the kinetics of precipitation are very sensitive to Mn level,

start (P_s) time is 10 s or more in prestrained materials and that the nose of the PTT curve is situated between 900 and 950°C (see Fig. 3). Typical P_s times at 950°C range from 10 to 30 s and at 1000°C from 30 to 100 s. Thus the reported P_s times in microalloyed steels are greater than the R_s times in unmodified steels by the following ratios:

1000°C - 2-3 orders of magnitude

950°C - 1-2 orders of magnitude

900°C - 1 order of magnitude

On the basis of the differences between the R_s and P_s times described above, it would appear to be difficult to maintain that the initiation of strain induced precipitation can prevent recrystallization of the deformed matrix in the absence of other effects. However, it could be claimed that no experimental technique has yet been devised that is sensitive enough to detect the real start of precipitation. According to this view, precipitation could begin at say 50 ms at 900°C and at perhaps 100 ms at 950°C.

---

increasing in rate as the Mn concentration is reduced. Thus the PTT curve of Ref. 24 can be considered not to apply to typical HSLA steels containing 1.0% Mn or more. The second exception concerns the results of Hansen et al. (14) for the start of grain boundary precipitation (see Fig. 2). The nucleation time for this process appears to be somewhat shorter than for matrix precipitation. Thus, at 950°C, grain boundary precipitation began at 6 and less than 1 s, respectively, for the 0.031 Nb and 0.095 Nb steels investigated by these workers.

The simplest alternative is to consider that the precipitate forming elements play a role in retarding recrystallization while in supersaturated solid solution prior to precipitation (6,12,24-26). According to this view, certain elements can influence the temperature and rate of recrystallization by means of a solute drag or some other process, first by affecting the dislocations associated with the recovery and nucleation stages, and then by interacting with the grain boundaries involved in recrystallization. In α-iron, for example, it has been shown (38) that the recrystallization temperature after cold working can be increased by significant amounts (e.g. 50 to 100°C) by the addition of as little as 150 to 200 ppm (atomic) of solutes such as Ti, Hf, Zr, Nb, Ta, Mo and V. In the classical experiments of Aust and Rutter (39), additions of as little as 60 ppm of Sn decreased grain boundary mobility in Pb by a factor of about 1000.*

---

* A rationalization for the relative effects of different solutes in α-iron based on the electronic difference between the particular element and Fe was advanced by Abrahamson and Blakeney in 1960. Their order of importance appears to hold for γ-iron as well (26), but must be modified slightly to allow for the effects of atomic size and modulus difference with respect to Fe (26,35).

Pancaking Temperatures in Controlled Rolling

At roughing temperatures, i.e. in the range 1200 to 1050°C, plain carbon steels are able to recrystallize completely in about 100 ms, and microalloyed steels in about 1 s. These times are of course modified, as suggested above, by the strain rate and amount of the prestrain, decreasing somewhat as either of these (particularly the latter) is increased. Thus full recrystallization can take place during roughing, as the interpass time in a reversing mill is generally about 10 s (40,41). In the intermediate temperature range, extending for the present purpose from about 1050 to 900°C, recrystallization tends to be incomplete, particularly when the reduction in the previous pass is small, or the level of microalloying addition relatively large. Rolling in this temperature range is thus conducive to the introduction of mixed austenite grain sizes, which lead, on transformation, to mixed ferrite grain sizes (4,6,7,16,40,41).

Finally, in decreasing the temperature still further, a level is reached, called the 'pancaking temperature', at which no further recrystallization occurs. This has been reported as 960°C for a 0.05 C - 1.4 Mn - 0.04 Nb steel (8) and 950°C for a 0.1 C - 1.3 Mn - 0.03 Nb steel (14). As before, this temperature is sensitive to the prior pass strain (or to the accumulated strain since the last recrystallization), and is not a fixed quantity.* It is of interest that, when steels rolled in the pancaking range are quenched, some contain precipitates and others

---

*In Refs. (8) and (14), a single pass was employed to establish T_p. When multiple passes are used (40,41), a much lower (and somewhat variable) value of T_p is obtained.

do not* (8,14). Without further evidence or analysis, the presence or absence of particles can be taken to lend support to either school of interpretation, that is to retardation either by a solute effect or by strain-induced precipitation. These alternatives will now be examined more closely.

Effect of Decarburization and Denitriding

Some evidence which concerns the separate effects of solutes and precipitates and which will be introduced at this stage is from the work of Luton et al. (18). These authors compared the behaviour of three steels: a reference 0.055 C - 0.41 Mn plain C steel and two 0.92 Mn - 0.054 Nb steels. The first of the Nb steels contained 'normal' levels of 0.05 C and 0.005 N, whereas the second had been decarburized and denitrided (by heating in wet hydrogen at 1100°C for one week) so that the C and N levels were reduced to 14 and 10 ppm respectively. The three steels were austenitized at 1150°C for 30 min. and then compressed 25% at a strain rate of 1.3×10^{-1} s^{-1} at one of three temperatures: 1000, 950 and 900°C. After holding at temperature in the unloaded condition for increasing delay times, the samples were reloaded at the same strain rate to determine the amount of softening (decrease in flow stress) that took place during the delay.

Some of the results obtained at the three temperatures are presented in Fig. 4. The data determined at 1000°C (Fig. 4a)

---

*Within the detectability limits of electron microscopy; i.e. about 0.003% vol. pct. of carbonitride.

reveal two items of interest. First of all, it is apparent that the decarburized material displays the same recovery and recrystallization kinetics as does the material containing the normal commercial levels of C and N. The second conclusion is not as clearly established because it was not possible to follow the rapid progress of recrystallization in the plain C steel after a prestrain of 25% with the equipment available. The curve displayed is therefore estimated from the results of Luton et al. (18) for a prestrain of 10%, and by reference to the data of other workers (14). It is clear from the two curves for the Nb steels that the addition of Nb delays recovery and recrystallization to a considerable degree with reference to the usual kinetics observed for carbon steels. From the approximate R_f times, this retardation can be estimated to be about 1½ orders of magnitude in time. The retardation in this case is unlikely to be caused by precipitation because: (i) R_s and R_f are about 6 and 15 s, while P_s is about 20 s at 1000°C in the commercial material (18); and (ii) the low C and N levels in the decarburized material (14 and 10 ppm, respectively) indicate that the Nb(CN) is fully dissolved at this temperature (3,42-44).

The data determined at 950°C (Fig. 4b) are consistent with those of 1000°C in that softening in the decarburized alloy is about 1½ orders of magnitude slower than in the reference plain C material. At this temperature, both recovery and recrystallization are somewhat slower in the commercial than in the decarburized steel. This was shown by Luton et al. to be associated with

the occurrence of a small amount of both dynamic and static precipitation. However, the volume fraction of precipitate formed was too small (about 0.002 to 0.005%) to inhibit recrystallization entirely.

Finally, the data obtained at 900°C (Fig. 4c) show the combined effects of both solute and appreciable precipitate retardation. It is evident from the plain C and decarburized samples that the addition of Nb alone retards both the recovery and the recrystallization kinetics by about one order of magnitude. When the commercial and decarburized materials are compared, it can be seen that recovery is a further order of magnitude slower in the commercial material and that recrystallization is completely prevented from taking place. The retardation of recovery is attributed to the dynamic precipitation of about 0.01 vol. pct. of carbonitride during prestraining. This is followed during holding by the further formation of a similar or greater amount of static precipitate. It appears from this work that the presence of about 0.02 vol. pct. of precipitate or more completely suppresses recrystallization (18).

Effect of Solute Elements on the Kinetics of Static Recovery

The results of Luton et al. (18) for the decarburized Nb-modified steel reviewed above indicate that the rate of recovery can be retarded significantly by solute effects, and that there can be a further retardation due to dynamic or static precipitation, as long as the latter mechanisms are initiated early enough to produce a critical volume fraction (e.g. at

least 0.02 vol. pct.) of sufficiently fine precipitates (e.g. particles 5 to 20 nm in dia.). Some further light on the relation between solute additions and the rate of recovery is cast by the work of Ouchi and coworkers (45). These authors have constructed a computerized compression machine which is capable of unloading and reloading upset specimens in times as short as 0.1 s. In this way, the amount of softening occurring in the brief time interval before precipitation begins can be investigated with greater reliability than heretofore.

The above researchers have investigated the influence of most of the addition agents and impurities present in low alloy steels (46) and some typical results depicting the relative importance of Mn and Nb are illustrated in Fig. 5 (45). From the compression tests carried out at 1000 and 900°C in which a fixed prestrain of 25% was applied (Figs. 5a and 5b respectively), it is evident that an increase in the Mn level from 0.17 to 1.30 wt. pct. (and in the C level from 0.05 to 0.12 wt. pct.) leads to a decrease in the rate of recovery by <u>one order of magnitude</u>. (The break in the softening curve indicates the saturation of recovery and the start of static recrystallization (47)). In a similar way, the addition of 0.03 wt. pct. Nb produces a decrease in the recovery rate of <u>half</u> an order of magnitude with respect to the 0.12 C - 1.30 Mn plain C steel. This suggests that Nb is about 50 times as effective as Mn (on an atom fraction basis) in retarding static recovery, a conclusion that is in reasonable agreement with the factor of 40 reported by the present authors (26) for the relative effectiveness of these two solute elements

in retarding dynamic recovery.

Effect of Nb Addition to a Medium C Steel

Although microalloying additions are usually made to low carbon grades, some experiments carried out by Coladas et al. (13) on a series of 18 medium and high C Nb-modified steels are relevant to the present discussion and will now be reviewed briefly. The results these authors obtained by means of rolling, quenching and optical microscopy are presented in Fig. 6. The two steels being compared are a 0.40 C - 0.67 Mn reference material and a 0.41 C - 0.68 Mn - 0.064 Nb microalloyed grade. In the diagram, the start and finish of both recovery and recrystallization are indicated, as well as the approximate start time for precipitation. The reduction in this case was 25%, as in the work of Luton et al., but was only half that applied by Hansen et al. (14). It is evident from Fig. 6 that the addition of 0.064% Nb* delays the start of recovery by about 1½ orders of magnitude in time and that this delay is effected prior to the occurrence of any precipitation. Although no data were reported for the 0.064 Nb steel at the higher temperatures, the results suggest that above 1050°C, where precipitation is expected to be slower than recrystallization, there remains a clear difference between the recrystallization rates of the two steels. The

* From the data of Koyama et al (44), it can be estimated that about one quarter of this amount (i.e. 0.016% Nb) was dissolved at the austenitization temperature of 1200°C.

difference above 1050°C was attributed to a solute effect (13,22), whereas the much sharper difference below 900°C can be ascribed to the additional effect of static precipitation which, in the lower temperature range, begins before the recovery mechanism has run its course.

Recrystallization Kinetics Above the Carbonitride Solubility Temperature

It may have struck the reader by now that there is a critical experiment which could be performed to distinguish between the retardation of recrystallization by solute as opposed to precipitation effects. Such an investigation would involve the determination of the recrystallization rate in a reference plain C steel and in a comparable Nb- or V- modified microalloyed steel, where the experiment would have to be carried out above the solution temperature of the carbonitride.* Such an approach is suggested by the data of White and Owen (15) pertaining to softening in a 0.11 C - 1.38 Mn - 0.10 V microalloyed and a 0.11 C - 1.35 Mn plain C steel. Their results at 1000°C, estimated to be in the vicinity of the VN solution temperature (3,42,49), indicate that recrystallization in the V-modified

---

* The proposition that alloy additions in the range 0.03 to 0.3 wt. pct. can cause appreciable solute effects can also be verified by measuring the influence of elements such as Mo and Cr (48), which do not precipitate in austenite under the conditions of interest.

material is slower than in the unmodified grade, even though no precipitation was likely to have occurred in the former specimens under the conditions of the experiment.

An attempt was made by the present authors to extend such an approach to a series of HSLA steels containing Nb (50,51), but in which a testing temperature clearly above T_{sol} is employed. For experimental convenience, the investigation concerned the effect of the alloying elements on the peak strain produced in compression testing (and therefore on the dynamic recrystallization kinetics). The steels all contained 0.05 or 0.06 C, and the other elements that were present are listed in Table I, together with the estimated carbonitride solution temperatures. The R_s times for these materials are displayed as a function of temperature in Fig. 7. In this diagram, three trends are of interest:

(i) Compared to the plain C material, the addition of 0.115 V produces the least retardation, whereas the combination 0.040 Nb - 0.30 Mo produces the most, followed by the 0.035 Nb addition.

(ii) At temperatures (e.g. 900°C) and times (e.g. 20 s) that permit dynamic precipitation, the RTT curves break to the right, in keeping with the well-known phenomenon observed under conditions of static recrystallization.

(iii) Even at the highest testing temperature of 1150°C, which is well above T_{sol} for these materials, the order and relative spacing determined at lower temperatures remain valid.

It should be particularly noted that the RTT curves remain parallel from 1150 down to about 1000°C. Thus the degree of solute retardation (relative to the plain C steel) remains approximately constant from above the T_{sol} to the vicinity of the nose of the PTT curve.

The Importance of Grain Boundary Precipitation

Before terminating this discussion concerning the precise role of carbonitride precipitation in retarding austenite recrystallization, it is necessary to return to the topic of grain boundary precipitation, which was mentioned briefly above when the research of Hansen et al. (14) was reviewed. As can be seen from Fig. 2, the initiation of grain boundary precipitation preceded that of matrix precipitation by about half an order of magnitude in time (14). Both these processes began before the start of recrystallization in the temperature range of interest (850 to 950°C). These authors, and others, have accordingly concluded that grain boundary (rather than matrix) precipitation may be the process responsible for the inhibition of recrystallization, partly because recrystallization is normally nucleated at the grain boundaries, and partly because it has been acknowledged by several workers that matrix precipitation is frequently not initiated soon enough to prevent the nucleation of recrystallization.

Here, however, an alternative interpretation is presented and explored. First of all, it is considered that the relevant question is the following: 'Does grain boundary precipitation

begin before or after the start of recrystallization in an identical steel containing no Nb (i.e. in an equivalent plain C steel)?' It is evident from Fig. 2 that the answer to the above query is 'after R_s for the plain C steel.' That is, in the experiments of Ref. (14), g.b. precipitation was initiated well after recrystallization began in the plain C steel, and even later than the time for 50% recrystallization. Thus the occurrence of g.b. precipitation is unlikely to be effective in a given steel unless some other process, such as solute retardation, is acting so as to prevent recrystallization until precipitation is well under way.

Two further comments need be made at this point.

(a) When solutes such as Nb are added to a steel, not only is recrystallization retarded, but the rate of recovery is decreased as well (13,17,18). As it is not clear how g.b. nucleation can affect the rate of recovery, a further mechanism, such as solute retardation, seems to be necessary to explain the recovery results.

(b) It has been maintained by some researchers that the true start of precipitation may not be detected by the experimental methods currently available, and that it is the true start that precedes R_s in the unmodified material. This interpretation cannot be completely ruled out; however, in the detailed study of Luton et al. (18) referred to above, it was shown that a certain minimum volume fraction of precipitate (e.g. 0.02 vol. pct.) was necessary to arrest recrystallization.

Thus the view is taken here that the early, undetectable stages of precipitation are unlikely to be of importance in producing 'pancaking' and preventing recrystallization.

CONCLUSIONS

1. The R_s times for the static recrystallization of deformed microalloyed austenites fall in the range 10 to 100 s at 950°C. The P_s times for similar steels are about 10 to 20 s. Thus it is frequently concluded that, during control rolling at lower temperatures, recrystallization is prevented by the initiation of strain-induced precipitation.

2. The R_s times for the static recrystallization of deformed plain C steels fall in the range 0.1 to 1 s at 950°C. These are about 1½ orders of magnitude shorter than the P_s times for microalloyed steels. It is therefore evident that the process of precipitation in an otherwise unaffected plain C steel cannot act rapidly enough to prevent recrystallization, despite the more circumstantial evidence summarized in Conclusion 1 above.

3. The interrupted compression experiments of Luton et al. (18) on a conventional and a decarburized and denitrided HSLA steel give strong support to the view that the presence of about 0.05% Nb in solution retards both the recovery and the recrystallization kinetics by about 1½ orders of magnitude in time. This conclusion is based on: (i) the coincidence of the softening curves determined at 1000°C on the conventional and decarburized grades; and (ii) the much more rapid softening kinetics of their reference plain C steel.

4. Short-time interrupted compression tests carried out by Ouchi et al. (45) have permitted the reliable determination of the effect of several solute elements on the recovery rate of deformed austenite in the interval prior to the initiation of precipitation. These tests, in which the time in the unloaded condition was varied down to 0.1 s, show that typical additions of Mn or Nb retard the recovery rate by about an order of magnitude. For equivalent atom fractions, Nb is 40 to 50 times as effective as Mn. The other common alloying elements have solute effects which are also in reasonable agreement with the rationalizations of Abrahamson and Blakeney (38) and of Refs. (26) and (35).

5. The determination of RTT diagrams at temperatures above the particular solution temperatures of the respective carbonitrides permits an unequivocal estimate to be made of the solute retardation produced by the relevant microalloying addition. Such experiments (51) have shown that at temperatures above about 1000°C, where precipitation is no longer of importance, the presence of Mo and Nb in solution produces significant retardation, and that V makes a much smaller, but distinct, contribution.

6. Although grain boundary precipitates can influence the recrystallization process, they are unlikely to affect the progress of static recovery. Furthermore, P_s for g.b. precipitation has been observed to be greater than R_s for plain C steel. Thus, by an extension of Conclusion 2 above, g.b. precipitation is judged not to be the mechanism responsible for delaying recrystallization until matrix precipitation can play its particular role in the pancaking process.

ACKNOWLEDGEMENTS

The authors are indebted to the Physical Metallurgy Research Laboratory of the Department of Energy, Mines and Resources, Ottawa, the Natural Sciences and Engineering Research Council of Canada, and the Quebec Ministry of Education (FCAC program) for financial support.

REFERENCES

1. A.B. LeBon and L.N. de Saint-Martin: 'Microalloying 75', Union Carbide Corp., New York, N.Y. (1977), p. 90.

2. I. Kozasu, C. Ouchi and T. Okita: ibid., p. 121.

3. J.N. Cordea: Symposium on Low Alloy High Strength Steels, Nurnberg, B.R.D., May (1970), Metallurg Companies, p. 61.

4. J.D. Jones and A.E. Rothwell: 'Deformation Under Hot Working Conditions', Iron and Steel Institute Publication 108 (1968), p. 78.

5. W.B. Morrison and J.A. Chapman: Phil. Trans. Roy. Soc., Series A, 282 (1975), p. 289.

6. J.M. Gray: 'Heat Treatment '73', The Metals Society, London (1974), p. 19.

7. L.J. Cuddy: Met. Trans., 12A (1981), in press.

8. A.T. Davenport and D.R. DiMicco: Proc. Intl. Conf. on Steel Rolling, Iron and Steel Inst. of Japan (1980), p. 1236.

9. M. Cohen and S.S. Hansen: 'MiCon 80: Optimization of Processing, Properties and Service Performance Through Microstructural Control', ASTM STP 672 (1979), p. 34.

10. L.J. Cuddy, J.J. Bauwin and R.J. Ridley: Met. Trans., 11A (1980), p. 381.

11. M.A. Pacina: Ph.D. thesis, University of Sheffield (1975).

12. A. LeBon, J. Rofes-Vernis and C. Rossard: Met. Sci., 9 (1975), p. 36.

13. R. Coladas, J. Masounave and J.P. Bailon: 'Hot Deformation of Austenite', J.B. Ballance, ed., AIME, N.Y. (1977), p. 341.

14. S.S. Hansen, J.B. Van der Sande and M. Cohen: Met. Trans., 11A (1980), p. 387.

15. M.J. White and W. Owen: ibid., p. 597.

16. A.T. Davenport, R.E. Miner and R.A. Kot: 'Hot Deformation of Austenite', J.B. Ballance, ed., AIME, N.Y. (1977), p. 186.

17. R.A. Petkovic, M.J. Luton and J.J. Jonas: Can. Met. Quart., 14 (1975), p. 137.

18. M.J. Luton, R. Dorvel and R.A. Petkovic: Met. Trans., 11A (1980), p. 141.

19. R.A. Petkovic, M.J. Luton and J.J. Jonas: Acta. Met., 27 (1979), p. 1633.

20. C. Ouchi, T. Sampei, T. Okita and I. Kozasu: 'Hot Deformation of Austenite', J.B. Ballance, ed., AIME, N.Y. (1977), p. 316.

21. T. Gladman and D. Dulieu: Met. Sci., 8 (1974), p. 167.

22. J. Masounave: Ph.D. thesis, Ecole Polytechnique de Montréal, Montreal (1976).

23. L. Mayer, F. Heisterkamp and W. Mueschenborn: 'Microalloying 75', Union Carbide Corp., New York, N.Y. (1977), p. 153.

24. I. Weiss and J.J. Jonas: Met. Trans., 10A (1979), p. 831.

25. J.J. Jonas and I. Weiss: Met. Sci., 13 (1979), p. 238.

26. M.G. Akben, I. Weiss and J.J. Jonas: Acta Met., 29 (1981), p. 111.

27. R. Simoneau, G. Begin and A.H. Marquis: Met. Sci., 12 (1978), p. 381.

28 R.K. Amin, G. Butterworth and F.B. Pickering: 'Hot Working and Forming Processes', C.M. Sellars and G.J. Davies, eds., The Metals Society, London, (1980).

29. J. Jizaimaru, H. Kobayashi and T. Kosaka: Tetsu-to-Hagane, 60, No. 4 (1974), p. 177.

30. T.M. Hoogendorn and M.J. Spanraft: 'Microalloying 75', Union Carbide Corp., New York, N.Y. (1977), p. 75.

31. H. Watanabe, Y.E. Smith and R.D. Pehlke: 'The Hot Deformation of Austenite', J.B. Ballance, ed., AIME, N.Y. (1977), p. 140.

32. I. Weiss and J.J. Jonas: Met. Trans., 11A (1980), p. 405.

33. T. Chandra, I. Weiss and J.J. Jonas: Metal Science, 15 (1981), in press.

34. R. Phillipo and F.A.A. Crane: J. Iron and Steel Inst., 211 (1973), p. 653.

35. J.P. Michel and J.J. Jonas: Acta Met., 29 (1981), p. 513.

36. W. Roberts: Swedish Institute for Metals Research, Report No. I.M. 1211.

37. W. Roberts: Swedish Institute for Metals Research, Report no. I.M. 1333.

38. E.P. Abrahamson, II and B.S. Blakeney, Jr.: Trans. AIME, 218 (1960), p. 1101.

39. K.T. Aust and J.W. Rutter: Trans. AIME, 215 (1959), p. 119.

40. I. Weiss, J.J. Jonas, P.J. Hunt and G.E. Ruddle: Proc., Intl. Conf. on Steel Rolling, Iron and Steel Inst. of Japan (1980), p. 1225.

41. I. Weiss, J.J. Jonas and G.E. Ruddle: Proc. ASM Symposium on 'Process Modelling Tools', Cleveland, Oct., 1980, ASM, in press.

42. K.J. Irvine, F.B. Pickering and T. Gladman: J. Iron and Steel Inst., 205, part 2 (1967), p. 161.

43. H. Nordberg and B. Aronsson: ibid., 206 (1968), p. 1263.

44. S. Koyama, T. Ishii and K. Narita: Journal of the Japan Inst. of Metals, 35 (1971), p. 1089.

45. C. Ouchi, T. Okita, M. Okado and Y. Noma: Proc. Intl. Conf. on Steel Rolling, Iron and Steel Inst. of Japan (1980), p. 1272.

46. C. Ouchi, T. Okita, M. Okado and Y. Noma: Technical Research Center, Nippon Kokan K.K., Kawasaki-ku, Kawasaki, Japan, to be published.

47. R.A. Petkovic-Djaic and J.J. Jonas: Met. Trans., 4 (1973), p. 621.

48. B. Bacroix, M.G. Akben and J.J. Jonas: Proc. Symp. on the Thermomechanical Processing of Microalloyed Austenite, Pittsburgh, Aug. 17-18, 1981, AIME, to be published.

49. M.G. Frohberg and H. Graf: Stahl u. Eisen, 80 (1960), p. 539.

50. M.G. Akben: Ph.D. thesis, McGill University, Montreal (1980).

51. M.G. Akben and J.J. Jonas: McGill University, Montreal, unpublished work.

TABLE I

CHEMICAL COMPOSITIONS AND CARBONITRIDE SOLUTION TEMPERATURES FOR THE STEELS OF FIG. 7

Steel Type	CHEMICAL COMPOSITION, WT. %							SOLUTION TEMPERATURE (^{o}C)			
	C	Mn	Si	Al	Nb	V	Mo	T_{sol}^{a}	T_{sol}^{b}	T_{sol}^{c}	T_{sol} average
Plain C	0.06	1.43	0.24	0.025	-	-	-	-	-	-	-
V	0.05	1.20	0.25	0.030	-	0.115	-	985	965	1025*	990
Nb	0.05	1.25	0.27	0.030	0.035	-	-	1050	1090	995†	1045
Nb-Mo	0.06	1.33	0.21	0.025	0.040	-	0.30	1050 max.	1100 max.	995† max.	1050

N∿0.006

a) J.N. Cordea (3), for Nb(C,N)
b) Irvine et al. (42), for Nb(C,N)
c) Koyama et al. (44), for NbC only
* No oorrection for effect of Mn on N activity.
† Oorrected for effect of Mn on C activity.

FIGURE CAPTIONS

Fig. 1 RTT curve for a 0.17 C - 1.36 Mn plain C steel given the largest pre-deformation compatible with the absence of dynamic recrystallization (12).

Fig. 2 RTT curves for a 0.11 C - 1.3 Mn plain C and a 0.11 C - 1.35 Mn - 0.031 Nb microalloyed steel hot rolled 50% at 950°C (latter solutionized at 1250°C). PTT curves for both grain boundary and matrix precipitation (P_s only) for the Nb steel (after Hansen et al. (14)).

Fig. 3 Comparison of some of the start times for Nb(CN) precipitation reported in the literature. The numbers associated with the curves are the respective reference numbers listed in this paper.

Fig. 4 Normalized static softening curves for steels A, B and C prestrained 25% at a strain rate of $1.3 \times 10^{-1} s^{-1}$. The steel compositions are: A - 0.055 C - 0.41 Mn; B - 0.05 C - 0.92 Mn - 0.054 Nb - 0.005 N; C - 0.0014 C - 0.92 Mn - 0.054 Nb - 0.001 N (after Luton et al. (18)).

(a) 1000°C

(b) 950°C

(c) 900°C

Fig. 5 Effect of time in the unloaded condition and steel chemistry on the softening ratio. Samples were pre-strained 25% by hot compression. The steel compositions are: A - 0.05 C - 0.17 Mn; B - 0.13 C - 0.57 Mn; C - 0.12 C - 1.30 Mn; D - 0.13 C - 1.35 Mn - 0.03 Nb (45).

(a) 1000°C

(b) 900°C

Fig. 6 RTT curves for a 0.40 C - 0.67 Mn plain C and a 0.41 C - 0.68 Mn - 0.064 Nb microalloyed steel hot rolled 25% and held at each temperature (steels pre-heated for 1 hour at 1200°C) (13). The approximate start (r_s) and finish (r_f) times for static recovery are also shown, as is the start time (P_s) for static precipitation (22).

Fig. 7 RTT times for dynamic recrystallization for four steels tested at a strain rate of $5.6 \times 10^{-3} s^{-1}$. Note that for the Nb and V steels, respectively, the higher two and three temperatures are above the carbonitride solution temperatures (see Table I) (51).

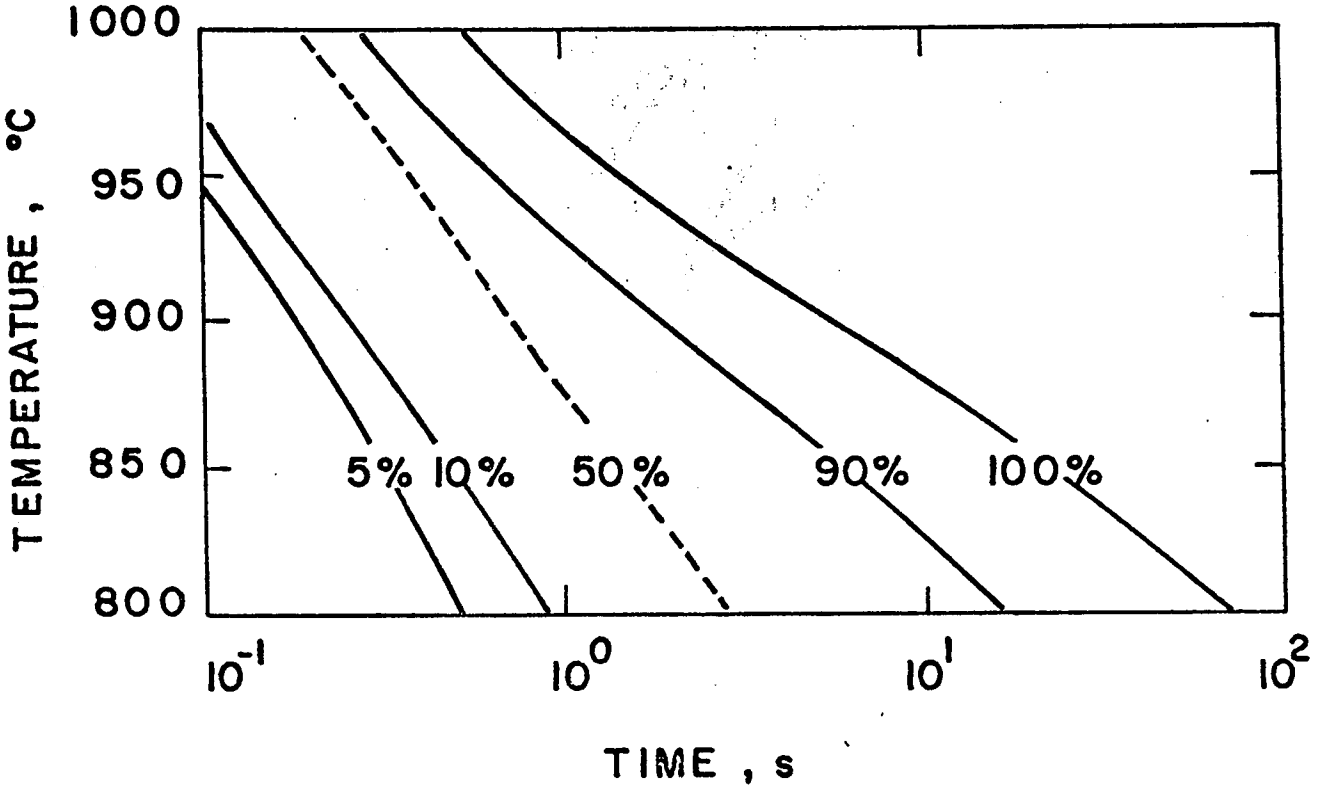
1000
950
900
850
800
TEMPERATURE , °C
5%
10%
50%
90%
100%
10^{-1}
10^{0}
10^{1}
10^{2}
TIME , s

FIG. 1

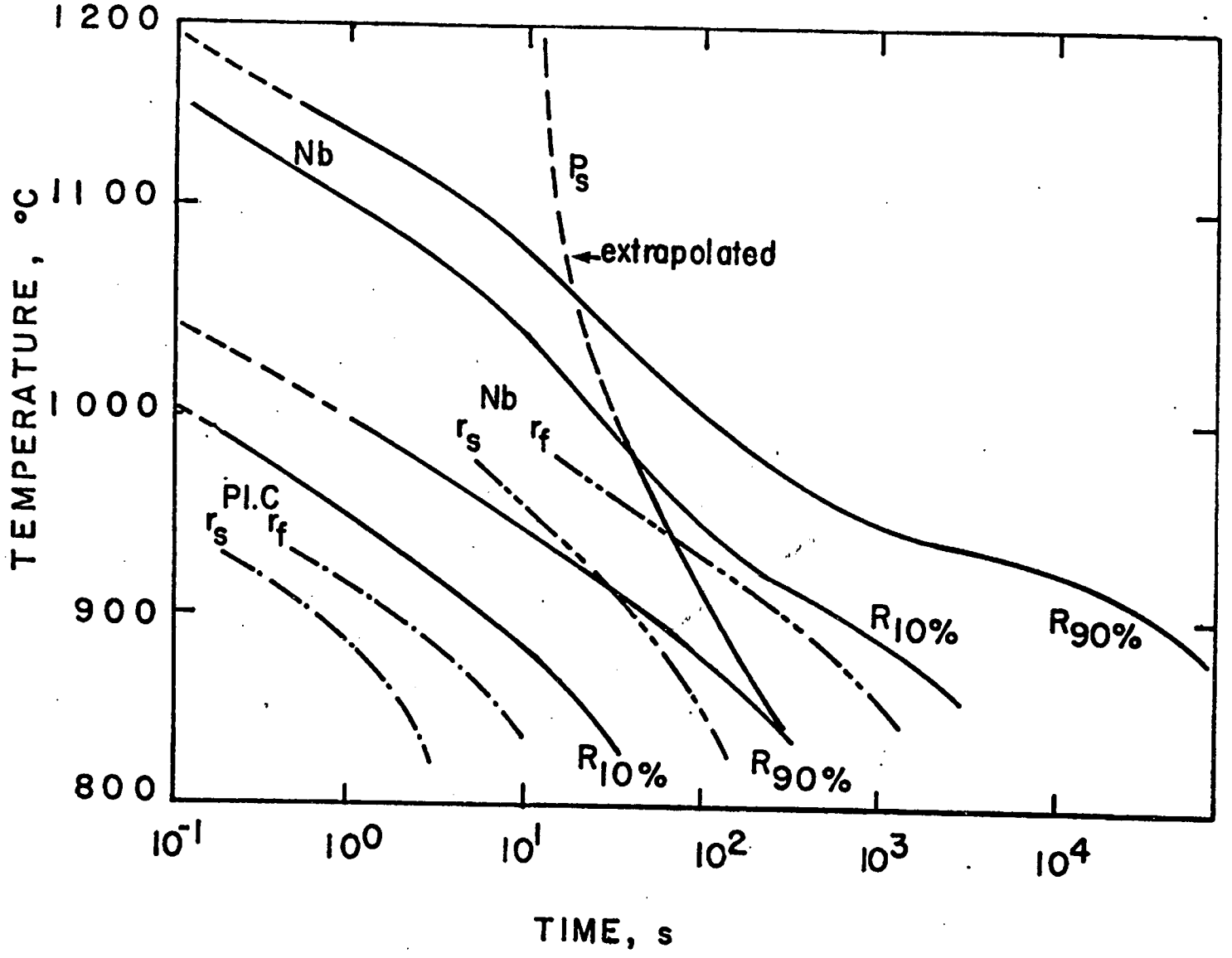
1200
1100
1000
900
800
TEMPERATURE, °C
Nb
P_s
extrapolated
Nb
r_s
r_f
Pl.C
r_s
r_f
$R_{10\%}$
$R_{90\%}$
$R_{10\%}$
$R_{90\%}$
10^{-1}
10^0
10^1
10^2
10^3
10^4
TIME, s

FIG. 2

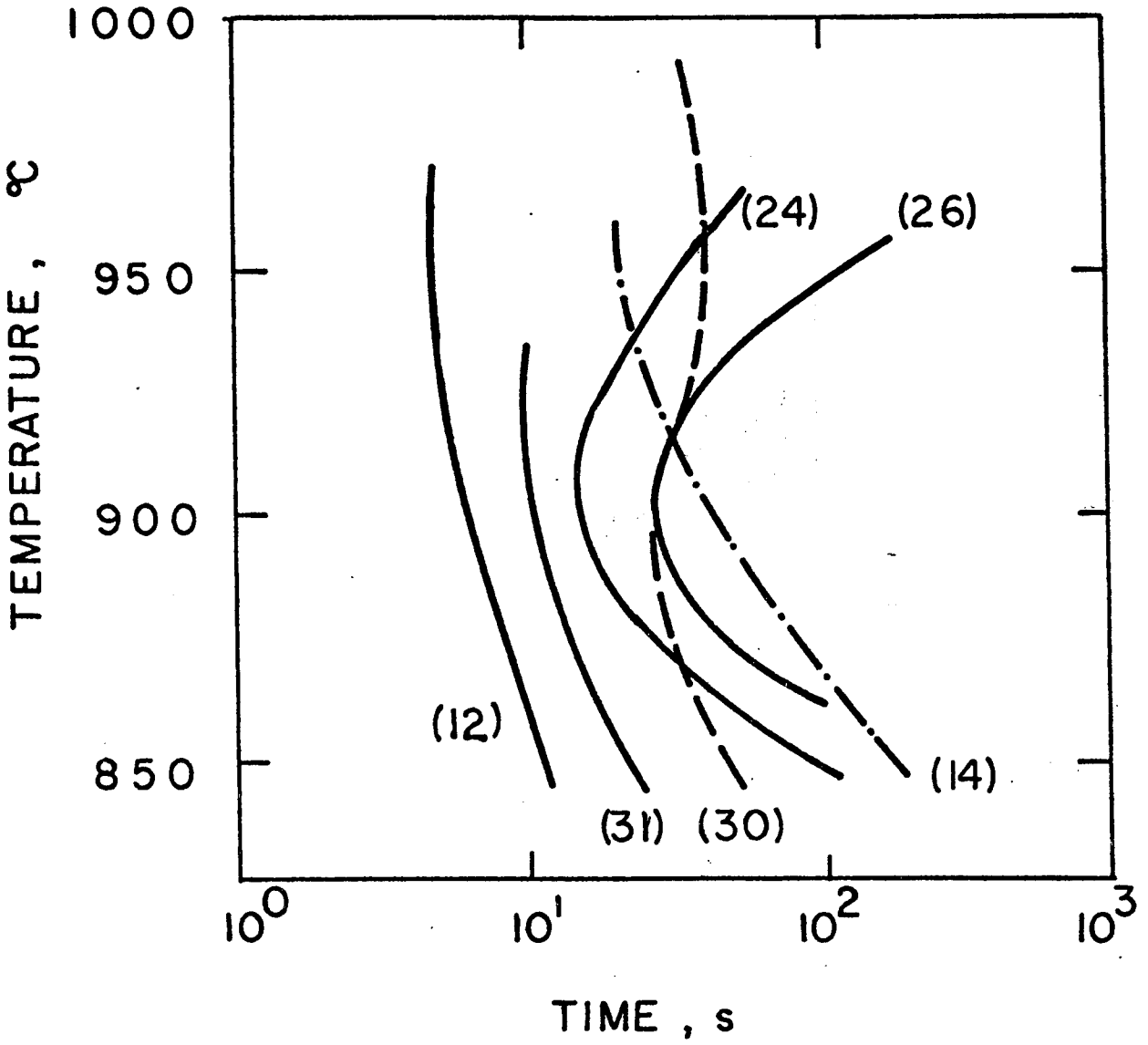
1000
950
900
850
TEMPERATURE, °C
(24)
(26)
(12)
(14)
(31)
(30)
10^0
10^1
10^2
10^3
TIME, s

FIG. 3

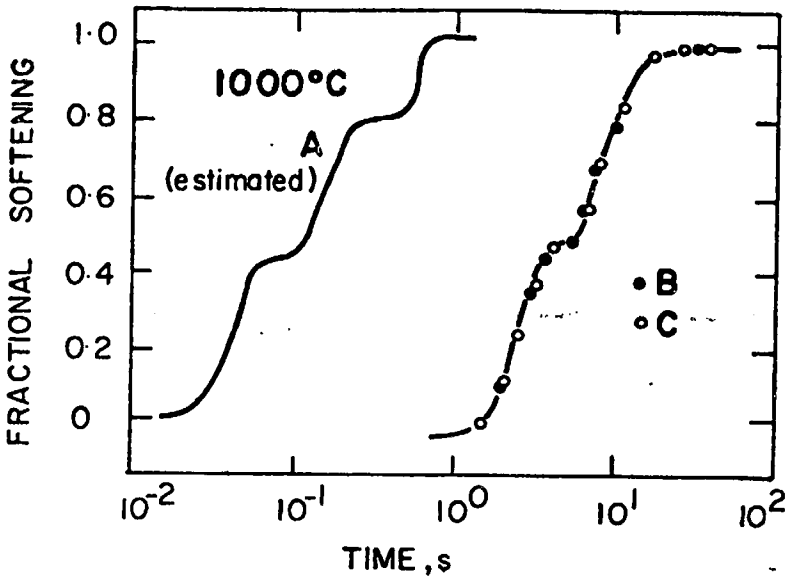

FIG. 4a

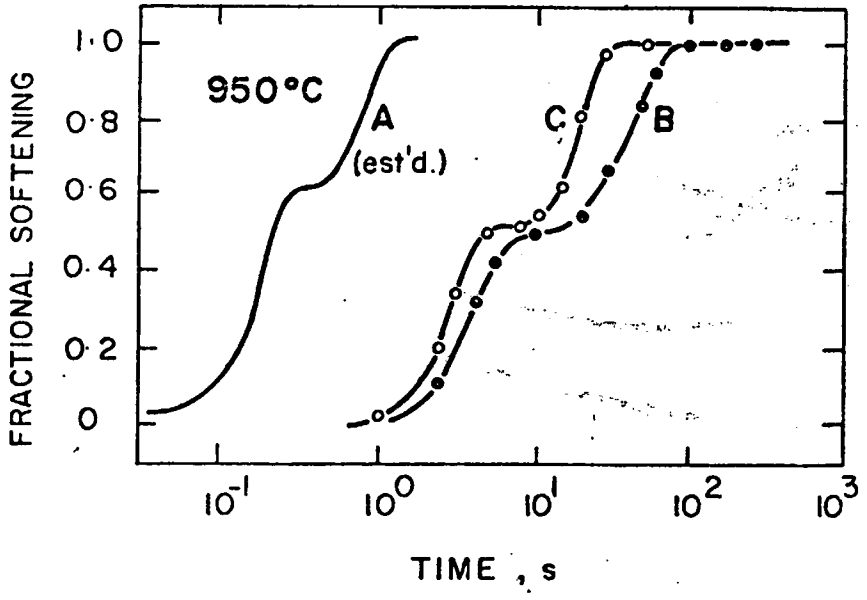

FIG. 4b

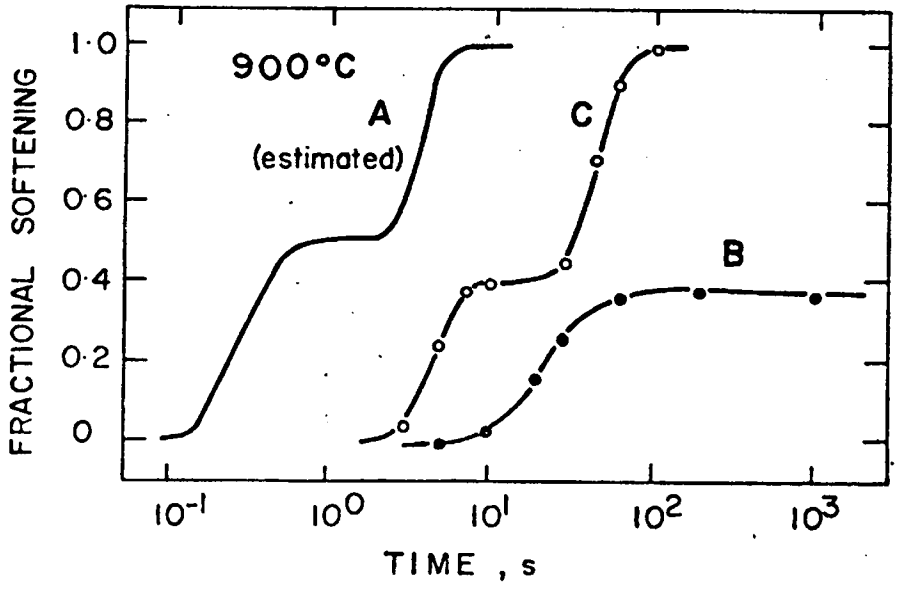

FIG. 4c

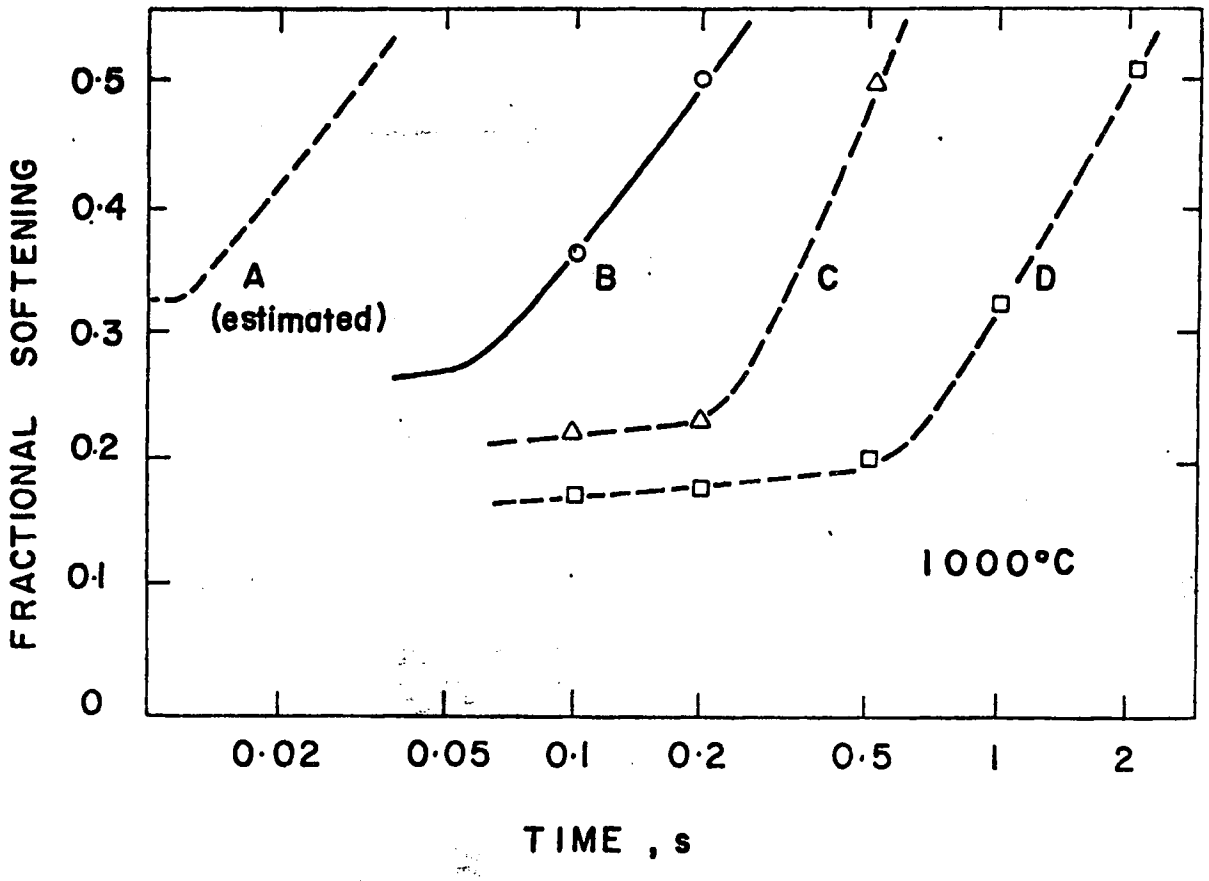
FRACTIONAL SOFTENING
0·5
0·4
0·3
0·2
0·1
0
A
(estimated)
B
C
D
1000°C
0·02
0·05
0·1
0·2
0·5
1
2
TIME , s

FIG. 5a

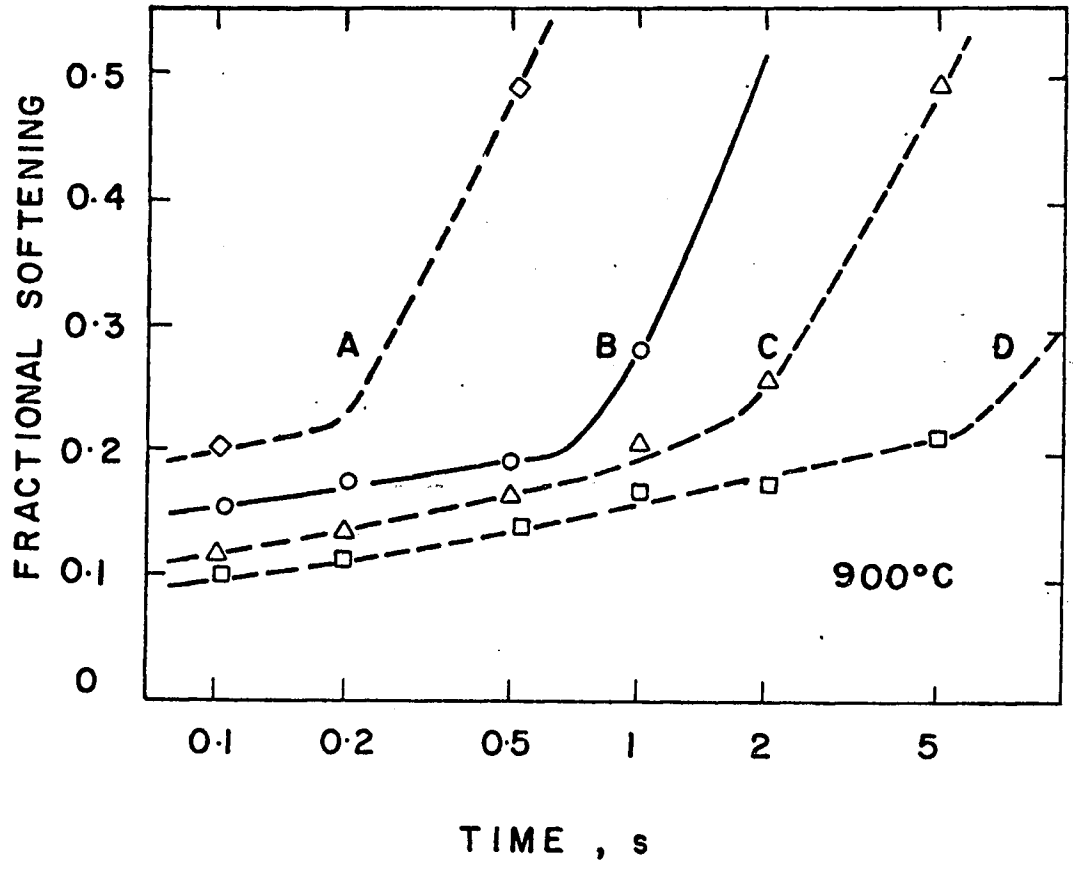
FRACTIONAL SOFTENING
0·5
0·4
0·3
0·2
0·1
0
A
B
C
D
900°C
0·1
0·2
0·5
1
2
5
TIME , s

FIG. 5b

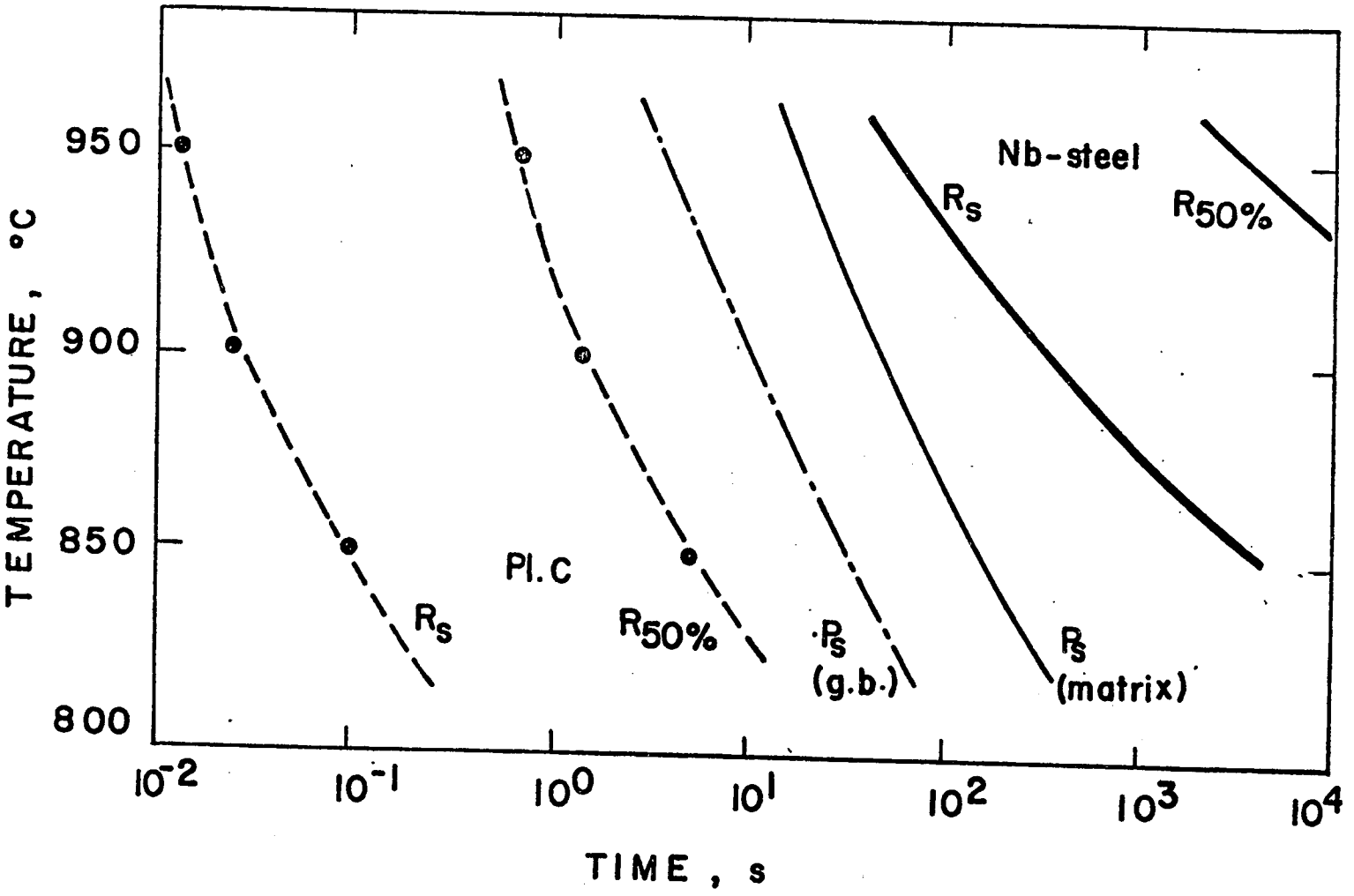
950
900
850
800
TEMPERATURE, °C
10^{-2}
10^{-1}
10^{0}
10^{1}
10^{2}
10^{3}
10^{4}
TIME, s
Nb-steel
R_s
$R_{50\%}$
Pl.C
R_s
$R_{50\%}$
R_s (g.b.)
R_s (matrix)

FIG. 6

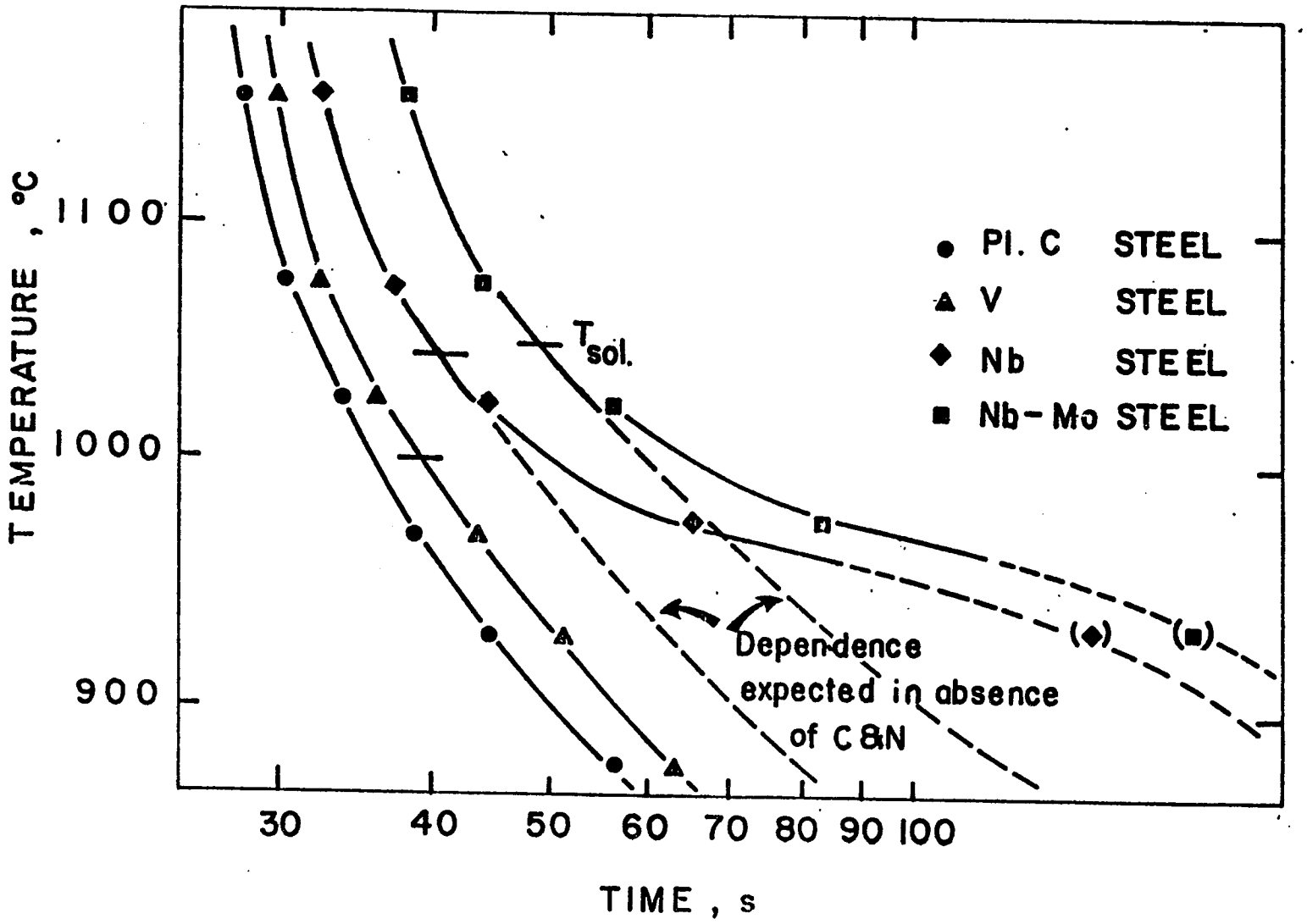
TEMPERATURE , °C
1100
1000
900
30
40
50
60
70
80
90
100
TIME , s
Pl. C STEEL
V STEEL
Nb STEEL
Nb-Mo STEEL
$T_{sol.}$
Dependence expected in absence of C&N
(◆)
(■)

FIG. 7

Acta Metallurgica Vol. 29, pp. 513 to 526

0001-6160/81/030513-14$02.00/0

PRECIPITATION KINETICS AND SOLUTE STRENGTHENING IN HIGH TEMPERATURE AUSTENITES CONTAINING Al AND N

J. P. MICHEL† and J. J. JONAS

Department of Mining and Metallurgical Engineering, McGill University, 3450 University St., Montreal, Canada H3A 2A7

(*Received* 23 *April*; *in revised form* 19 *August* 1980)

Abstract—Hot torsion tests were performed on 6 plain C steels containing increasing concentrations of Al and N to maxima of 0.084 and 0.028% by weight respectively. The experiments were carried out at 875, 900 and 925°C and at ten strain rates ranging from 6×10^{-4} to $0.6\,s^{-1}$. The dependence of the peak strain on strain rate and composition was established at each of the three temperatures; in this way, the kinetics for the dynamic precipitation of AlN were determined. At 875°C, precipitation was initiated after 6–11 s and was completed in 45–130 s. The rate of precipitation decreased with increasing temperature and increased with increasing Al concentration. No effect of N concentration or of off-stoichiometry was observed. The present rate of AlN precipitation is similar to that of Nb(CN) and of VN in deformed materials; the retarding influence of Al *in solution* on recrystallization is considerably less than that of Nb however. The presence of Al in solid solution in γ-Fe increases the flow stress by about 12 ± 5% per 0.1 at.%; by contrast, N in solid solution leads to a flow stress *decrease* of 9 ± 5% per 0.1 at.%. The hardening and softening effects of Al and N in γ-Fe are discussed in terms of lattice parameter, modulus and electronic effects.

Résumé—Nous avons effectué des essais de torsion à chaud dans six aciers au carbone contenant des concentrations croissantes en impuretés Al et N pouvant atteindre respectivement 0,084 et 0,028% en poids. Nos expériences ont été effectuées à 875, 900 et 925°C, pour dix vitesses de déformation différentes comprises entre 6×10^{-4} et $0{,}6\,s^{-1}$. Pour chacune des trois températures, nous avons mesuré la variation de la déformation au pic en fonction de la vitesse de déformation et de la composition; nous avons ainsi déterminé la cinétique de la précipitation dynamique d'AlN. A 875°C, la précipitation commençait aprés 6 à 11 secondes et elle était terminée au bout de 45 à 130 secondes. La vitesse de précipitation diminuait lorsqu'on augmentait la température et elle augmentait avec la teneur en Al. Nous n'avons pas observé d'effets de la teneur en N, ni de la non-stoechiométrie. La vitesse de précipitation d'AlN est semblable à celle de Nb(CN) et de VN dans les matériaux déformés; l'influence retardatrice de l'aluminium *en solution* sur la recristallisation est cependant considérablement inférieure à celle du niobium. La présence d'Al en solution solide dans le fer-γ augmente la contrainte d'écoulement d'environ 12 ± 5% par 0,1 at%. Nous discutons les effets de durcissement et d'adoucissement de l'aluminium et de l'azote dans le fer γ en fonction du paramètre réticulaire et des effets électroniques et de module.

Zusammenfassung—Hochtemperatur-Torsionsversuche wurden an sechs üblichen C-Stählen mit zunehmendem Al- und N-Gehalt bis zu maximal 0,084 bzw. 0,028 Gew.-% durchgeführt. Verformungstemperaturen waren 875, 900 und 925°C; zehn verschiedenen Verformungsgeschwindigkeiten im Bereich von 6×10^{-4} bis $0{,}6\,s^{-1}$ wurden verwendet. Die Abhängigkeit der Spitzendehnung von der Dehngeschwindigkeit und von der Zusammensetzung wurde bei allen drei Temperaturen bestimmt. So konnte die Kinetik für die dynamische Ausscheidung von AlN ermittelt werden. Bei 875°C beginnt Ausscheidung nach 6 bis 11 Sekunden und ist nach 45 bis 130 Sekunden beendet. Die Geschwindigkeit der Ausscheidung nahm mit ansteigender Temperatur ab und stieg mit zunehmendem Al-Gehalt an. Es wurde kein Einfluß durch die N-Konzentration oder durch Nichtstöchiometrie beobachtet. Die beobachtete Geschwindigkeit der AlN-Ausscheidung ist ähnlich der von Nb(CN) und VN in verformten Materialien; die verzögernde Wirkung des *gelösten* Al auf die Rekristallisation jedoch ist beträchtlich geringer als die des Nb. Anwesenheit von gelöstem Al in γ-Fe vergrößert die Fließspannung um 12 ± 5% pro 0,1 At.-%; dagegen verursacht gelöstes N eine Absenkung der Fließspannung um 9 ± 5% pro 0.1 At.-%. Ver- und Entfestigungswirkung von Al und N in γ-Fe werden anhand von Gitterparameter, Modul und elektronischen Effekten diskutiert.

INTRODUCTION

The approximate precipitation kinetics of AlN have been determined in several annealed, low carbon steels in the temperature range 500–1000°C. For example, Leslie and co-workers [1], Vodopivec [2, 3] and Ichiyama *et al.* [4], using the chemical extraction method of Beeghly [5], reported that the temperature of most rapid precipitation lay variously in the range 650–900°C. Somewhat similar results were obtained by Meyzaud [6], with the aid of an electrical resistivity technique. When the material is given a prior cold reduction of 60–70%, the rate of precipitation is increased [1, 6], as it is in the case of quenched, as opposed to annealed, samples [2, 7]. The influence of prior deformation at elevated temperatures is less well known. Nevertheless, Vodopivec [8] has shown, using

† On leave from Laboratoire de Physique du Solide, L.A. C.N.R.S. No. 155, Ecole des Mines, Parc de Saurupt, 54042 Nancy-Cedex, France.

the Beeghly technique, that a small torsional strain applied at 1100°C is sufficient to accelerate precipitation by about two orders of magnitude in time with respect to undeformed austenite. In a later study [9], he attributed changes in the shape of the torque vs (time)$^{\frac{1}{2}}$ curve to the initiation of dynamic precipitation. By this means he deduced that the incubation time for this type of precipitation was 6 and 10 s respectively at 1000 and 1100°C.

The formation of AlN can be of interest for a variety of reasons. When deposited on the austenite grain boundaries in massive form, it can lead to embrittlement [10–13] or to a decrease in hot workability [14–16]. By contrast, when it forms as fine particles on dislocations, it can play a possible role in retarding both the nucleation of new grains, as well as their subsequent growth, in a manner somewhat analogous to the effect of Nb(CN) and of VN in microalloyed steels. The study described below was therefore undertaken with the aim of exploring the extent to which AlN precipitation could be employed to retard austenite recrystallization during control rolling. Six Al-killed, plain C steels were prepared, with increasing Al and N concentrations to maxima of 0.084 and 0.028% by weight respectively. These were tested in the temperature range 875–925°C, and over the strain rate range 6×10^{-4} to $0.6\,s^{-1}$. The results obtained were used to define the start and finish times for dynamic precipitation in the low gamma phase region. The flow stresses determined also permitted an evaluation of the solute hardening contribution of the Al and the alloy softening effect of the N additions. These solute strengthening and weakening phenomena are discussed below in terms of the lattice parameter, modulus and electronic effects of Al and N addition.

EXPERIMENTAL METHOD AND PROCEDURE

The method used to determine the precipitation kinetics of AlN was the indirect one developed by Weiss and Jonas [17, 18], which is based on a mechanical testing technique. This procedure involves the determination of the strain to the peak in stress (peak strain) during constant strain rate testing, a strain associated with the initiation of dynamic recrystallization [19, 20]. The peak strain is sensitive to strain rate and temperature, and also to the occurrence of dynamic precipitation during deformation. Under fixed testing conditions, it is a maximum in a given material when precipitation begins soon after the initiation of flow and continues until the peak strain is attained. By determining the dependence of peak strain on strain rate and temperature, the precipitation start time can be detected more sensitively than by more conventional techniques, for which the minimum particle diameter for detection or extraction is larger. The present procedure differs from those reported earlier [17, 18, 21], however, in that it is based on torsion rather than on compression testing, and that it was addressed to the precipitation of Al, a non-transition element, rather than to that of a microalloying addition agent.

Six low carbon steels were studied, a reference material containing 0.06 C and 0.68 Mn, and five steels similar in their C and Mn levels, but containing increasing levels of Al and N. The compositions of these alloys are listed for reference in Table 1, together with the relevant Al/N ratios and solubility products. It should be noted that two of the steels (Nos 12 and 13) had similar N levels, but their Al concentrations differed by more than a ratio of 2:1. In an analogous way, two other steels (11 and 14) had similar Al levels, but with N concentrations differing by more than 2:1. As will be seen below, it was possible in this way to distinguish between the effects of dissolving Al and N in the reference material. The influence of non-stoichiometric proportions of Al and N on the precipitation kinetics was also determined in this way.

Prior to testing, the AlN was dissolved by holding the torsion specimens for 30 min at 50°C above the solution temperature predicted by Darken *et al.* [22] (the latter are listed in the first row of Table 2). For the reference steel, the preheat temperature was 1000°C. The Ar_3 temperatures for the present steels were determined by dilatometry [23] at cooling rates of 10^{-2}, 10^{-1}, 1, and $10\,°C\,s^{-1}$, and range from 800°C at the highest cooling rate to 870°C at the slowest cooling rate. As reported in more detail by Andrews [24] both the Ae_3 (see Table 2) and Ar_3 temperatures increase with the Al concentration. Thus the lowest testing temperature was just at the limit of the fully γ field for the higher Al alloys when tested isothermally.

Table 1. Chemical composition (in wt%) of the materials investigated

Steel series No.	C	Mn	P	S	Si	Al	N	[Al]·[N] $\times 10^5$	(Al/N) wt	(Al/N) at.
8	0.060	0.68	0.027	0.009	0.26	0.002	0.003	0.6	0.7	0.3
9	0.070	0.74	0.030	0.013	0.26	0.033	0.005	17	6.6	3.3
11	0.084	0.68	0.029	0.010	0.25	0.062	0.011	68	5.6	2.8
12	0.074	0.59	0.029	0.011	0.26	0.041	0.018	74	2.3	1.1
13	0.082	0.70	0.027	0.012	0.29	0.084	0.016	134	5.2	2.6
14	0.082	0.69	0.028	0.010	0.25	0.056	0.028	157	2.0	1.0

Table 2. AlN solution temperature [22], austenite grain size, and equilibrium γ–α transformation temperature [24] for the present materials

Steel series No.	8	9	11	12	13	14
AlN solution temperature [22] °C	760	1018	1173	1180	1262	1280
Austenite grain size μm	100	120	250	230	180	250
Equilibrium γ–α transformation temperature [24] °C	873	876	878	880	885	877

The present solution time is considerably higher than the 5 s reported as necessary by Pont *et al.* [25], and was therefore judged to be adequate. After solution treatment, one sample of each steel was quenched for determination of the austenite grain size. This led to the decoration of the austenite boundaries by a thin layer of ferrite and to the grain sizes also shown in Table 2.

Following solution treatment, the samples were cooled to the testing temperature and testing was begun within 4 min. This was selected as the standard cooling interval as it coincided with the time required to pass from the highest solution temperature (1330°C) to the lowest testing temperature (875°C). Such a limited holding time is also too short to initiate the static precipitation of AlN in *undeformed* austenite [3].

Testing was performed on a closed-loop hydraulic torsion machine of the MTS type, which has been described elsewhere [26]. Prior to the present investigation, the machine was interfaced with a PDP-11-04 minicomputer for data acquisition and plotting purposes. Specimens were machined out of 13 mm plate with their axes in the rolling direction. All the samples had gauge lengths of 25.4 mm and diameters of 6.35 mm. The samples were heated and tested in a radiation furnace, under an atmosphere of flowing argon, which was introduced to minimize oxidation and decarburization. Ten testing strain rates were used; these were evenly distributed within the range 6×10^{-4} to $0.6\,s^{-1}$.† All 6 steels were deformed at 875°C, whereas only steels 8, 9, 11 and 13 were tested at 900 and 925°C.

RESULTS

Some typical flow curves are presented in Fig. 1 for steel No. 13 (0.084 Al; 0.016 N) deformed at 900°C. Here the results are displayed in terms of effective or equivalent stress, strain and strain rate at the surface of each sample. The equivalent strain at the surface is defined as:

$$\epsilon_{eq} = \gamma/\sqrt{3} = R\theta/\sqrt{3}\,L \qquad (1)$$

where γ is the surface shear strain, R the specimen

† The strain rates referred to here apply to the external layer of the sample and are expressed in terms of the equivalent or effective strain rate (see below).

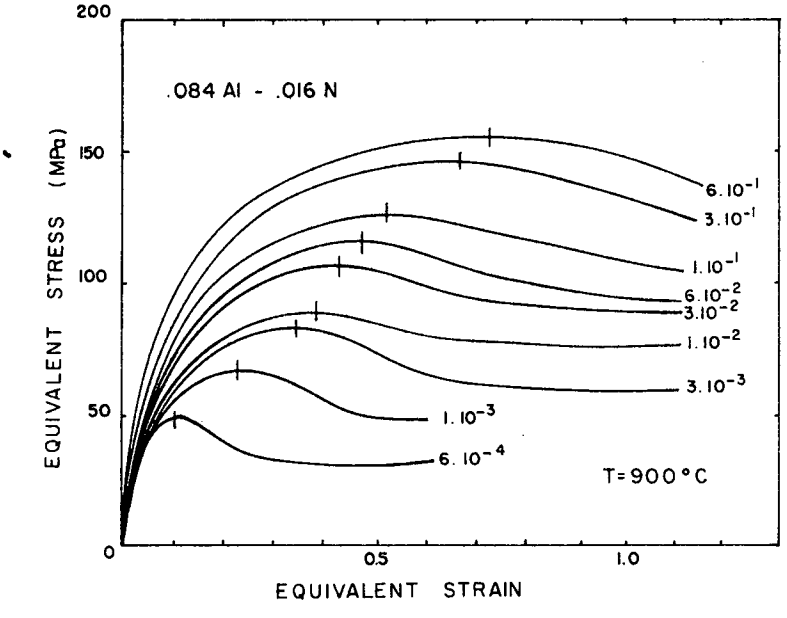

Fig. 1. Flow curves for steel No. 13 determined at 900°C at nine strain rates ranging from 6×10^{-4} to $0.6\,s^{-1}$. The results are displayed in terms of equivalent surface stress vs. equivalent surface strain.

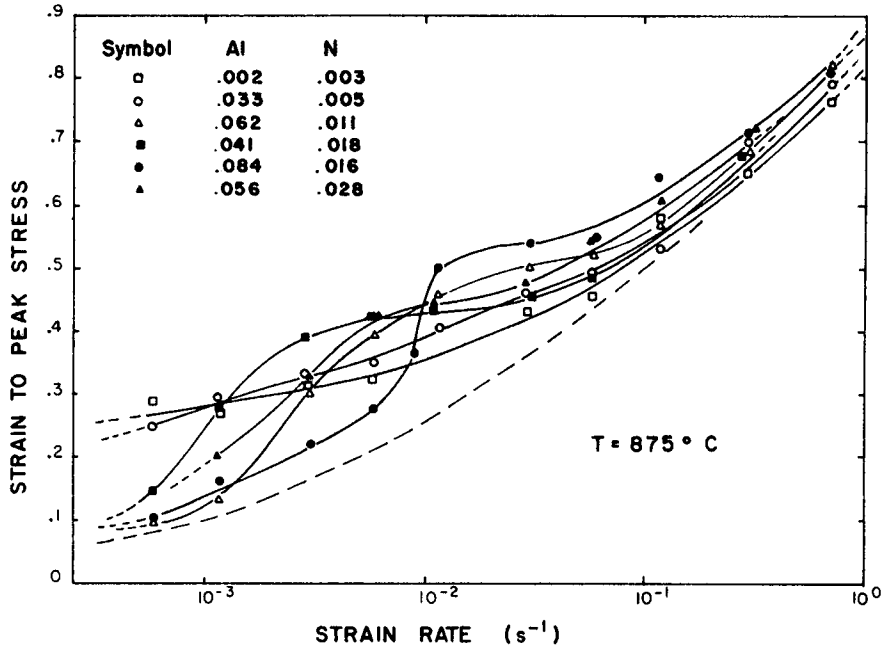

Fig. 2(a)

† Note that the contribution to the total torque of a given material element is a strong function of the element radius r, as given by

$$T = 2\pi \int_0^R \tau(r) \cdot r^2 \cdot dr.$$

Thus, during steady state flow, and on the assumption that $\tau(r) \propto \dot{\epsilon}^{0.15} \propto r^{0.15}$, for example, $T = (2\pi/3.15)\, R^3 \cdot \tau(R)$, so that the material in the interval say from 0.8 R to R provides some 50% of the total torque. On this basis, the occurrence of precipitation in the region $0.8\ R < r < R$ will have a marked effect on the torque, *whether or not precipitation is occurring* in the layers below $r = 0.8\ R$. (These contribute only 50% of the total torque.) Furthermore, within the region $0.8\ R < r < R$, the strain and strain rate vary by only $\pm 10\%$, so that the state of precipitation in these layers can be considered to be fairly uniform, to a first approximation. This is why it is possible, as will be demonstrated below, to determine precipitation kinetics by means of torsion testing, despite the large strain and strain rate gradients present within torsion samples. Nevertheless, both the strain and strain rate variation within the layer $r > 0.8\ R$, as well as the much larger differences between the values of these parameters above and below $r = 0.8\ R$ produce a variation in dislocation and precipitate density within the sample which is not present under compression testing conditions. Thus the present technique is less sensitive with regard to the determination of the peak strain and its dependence on the state of precipitation than is either axisymmetric or plane strain compression testing. In this respect it should be added that, in compression testing, because of the uniformity of flow, the rate sensitivity of the load $m = (\partial \ln F/\partial \ln \dot{\epsilon})_\epsilon$ is a true (local) material property, as is the work hardening exponent $n = (\partial \ln F/\partial \ln \epsilon)_{\dot{\epsilon}}$. By contrast, in torsion testing, because of the integration procedure for the torque discussed above, the equivalent exponents m and n are *mean* quantities. Because they are *not locally defined* material properties, they are termed *coefficients* rather than *sensitivities* in the present treatment.

radius, θ the angle of twist, and L the gauge length. Thus the equivalent strain rate is given by

The equivalent stress at the surface is in turn derived from [27]:

$$\dot{\epsilon}_{eq} = \dot{\gamma}/\sqrt{3} \tag{2}$$

$$\sigma_{eq} = \sqrt{3}\tau = \frac{\sqrt{3}T}{2\pi R^3}(3 + m + n) \tag{3}$$

where τ is the surface shear stress, T is the measured torque or couple, m is $(\partial \ln T/\partial \ln \dot{\theta})_\theta$, and $n = (\partial \ln T/\partial \ln \theta)_{\dot{\theta}}$.† The coefficients m and n were evaluated at strain intervals of approx. 0.02 from the raw data on the assumption that the torque depends only on the instantaneous values of the angle of twist and the twist rate [28]. Such an approach led to m values which increased with strain from 0.09 and 0.10 at $\epsilon_{eq} = 0.03$ and 0.06 to about 0.15 during steady state flow. The values of the work hardening coefficient n fell in the range $0.3 > n > -0.3$.

The flow curves for the other materials had the same general appearance, i.e. dependence on strain and strain rate, as shown in Fig. 1 for steel No. 13. In particular, they all displayed a peak in stress, indicative of dynamic recrystallization, and the peak strain increased with strain rate and decreasing temperature, from a minimum of about 0.12 at the lowest strain rate to a maximum of about 0.92 at the highest strain rate. The detailed dependence of the peak strain on strain rate, and on the Al and N levels is illustrated in Fig. 2 for the six materials. It is evident from this figure that at 875, 900 and 925°C, ϵ_p in the reference steel (No. 8) increases monotonically with strain rate,

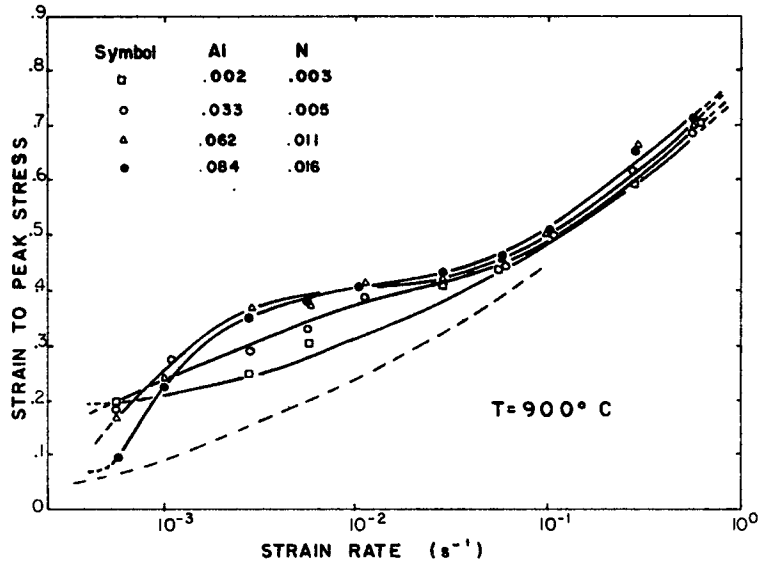

Fig. 2(b)

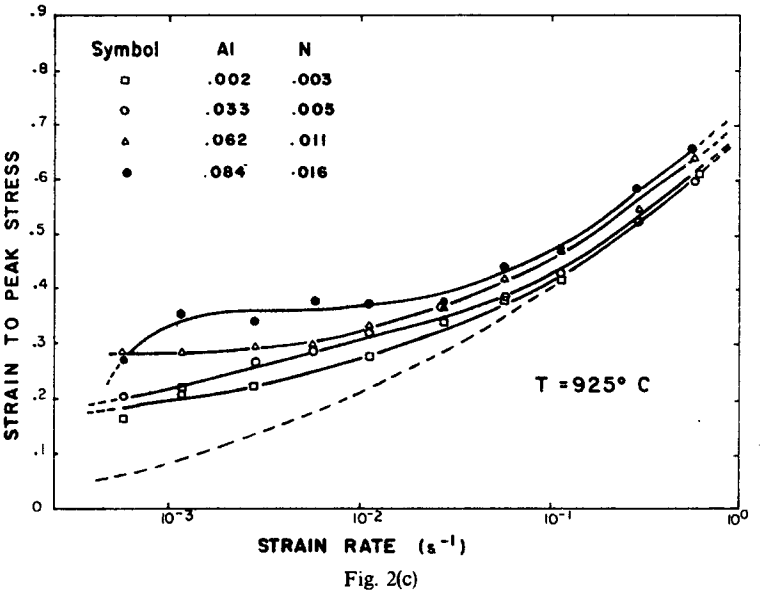

Fig. 2(c)

Fig. 2. Dependence of the peak strain ϵ_p on equivalent strain rate for the steels studied. (a) 875°C, (b) 900°C, (c) 925°C. In each case the broken curve represents the ϵ_p behaviour of a hypothetical reference steel containing coarse precipitates.

in the normal manner [17, 18, 21]. For the other steels, however, the bulge in the ϵ_p vs $\dot{\epsilon}$ relationship attributable to dynamic precipitation (as confirmed [29, 30] by extensive electron microscopy) is clearly evident. It is also apparent, by reference to Table 1, that the magnitude of the bulge increases with Al concentration; by contrast, it is not particularly sensitive to the N concentration, or to the solubility product [Al]·[N].

In Fig. 2, as in earlier studies of this kind [17, 18, 21], three different regions of ϵ_p vs. $\dot{\epsilon}$ dependence can be distinguished for the Al–N steels. At the highest strain rates (e.g. above about 10^{-1} s^{-1}, depending on composition and temperature) there is no dynamic precipitation during the 5 or so seconds required to attain the peak strain. Thus the initiation of dynamic recrystallization is not influenced by a possible interaction with precipitation. Instead, the differences in peak strain in this region are primarily a reflection of the amount of Al in solution in each steel prior to precipitation (see below); ϵ_p is also influenced by differences in the austenite grain size [31], and possibly in the N level.

In the intermediate strain rate region (about 3×10^{-3} to 10^{-1} s^{-1}, depending on composition and temperature), the occurrence of dynamic precipitation during the strain interval prior to the peak stress can lead to substantial increases in ϵ_p. This arises because

fine precipitates are deposited on the sub-boundaries that form during deformation in this strain rate interval, impeding first the nucleation of new grains and then their subsequent growth [29, 30]. The degree to which dynamic recrystallization is retarded in this region (with respect to the broken curve representing ϵ_p in the presence of coarse precipitates—see below) is proportional to the volume fraction of precipitate formed prior to attaining the peak strain. As noted above, this appears to increase with the atom fraction of Al present and is not related to the N concentration. A possible explanation of this observation is that the diffusion of Al (and not of N, an interstitial) is rate controlling with respect to the dynamic precipitation of AlN.

In the low strain rate region (below about $10^{-3}\,s^{-1}$, depending on composition and temperature), dynamic precipitation is initiated early in the test and is completed before the peak strain is attained† [17, 18]. Once dynamic precipitation is complete, the fine particles deposited on the dislocations coarsen rapidly with continued straining [29, 30], and so become too large to pin the sub-boundaries with any effectiveness [32]. It is worthy of note that in this strain rate interval, ϵ_p in the Al–N steels is significantly less than ϵ_p for the reference plain C steel. It is also appreciably less than the values of ϵ_p reported for plain C steels in earlier investigations [17, 18, 21]. The difference in ϵ_p is even greater when the Al steels are compared with the Nb microalloyed steels in this strain rate range. The unusually small peak strain in the Al–N steels containing coarse precipitates cannot be simply attributed to a grain size effect, as it would require a much *finer* grain size in the Al steels than in the Nb or plain C ones [31], and the opposite trend was observed (see Table 2). The present results suggest instead that dynamically ripened AlN has a higher mean particle diameter than dynamically ripened Nb(CN). The latter attains a mean size of about 0.1 μm at a strain of 0.75 (29, 30). If the coarsened AlN particles reach the size range of $\simeq 0.5\,\mu$m,‡ they can *aid* rather than retard recrystallization by inducing strain gradients in their vicinity during deformation, thus enhancing the nucleation of new grains [34]. It should be remarked that the steel with the highest atom fraction of dissolved Al (No. 13) is also the one that is susceptible to the most rapid coarsening. This is indicated by the rapidity of the drop in ϵ_p as the $\dot{\epsilon}$ is decreased from its value at the position of maximum deviation from the reference curve for material with coarse precipitate. Such a possible increased propensity to coarsening may lead to problems in the utilization of AlN precipitation for the prevention of recrystallization during thermomechanical processing.

PTT Curves for Dynamic Precipitation

The rate of *dynamic* precipitation appears to represent the upper limit to the rate of *static* precipitation in heavily deformed materials [17, 18]. It is therefore of special interest with respect to metal processing methods such as control rolling. The P_s and P_f times for AlN precipitation during deformation are presented in Fig. 3, and were deduced from the ϵ_p vs $\dot{\epsilon}$ curves of Fig. 2 according to the method of Refs [17] and [18]. Here $P_s = \epsilon_p^s/\dot{\epsilon}_s$, where ϵ_p^s is the peak strain at which the slope of the Al–N curve first deviates noticeably from the slope of the reference curve, and $\dot{\epsilon}_s$ is the relevant strain rate. At $\dot{\epsilon}_s$, dynamic precipitation is initiated just prior to ϵ_p^s. In a similar manner, $P_f = \epsilon_p^f/\dot{\epsilon}_f$, where ϵ_p^f is the peak strain at which the slopes of the Al–N and reference curves are again equal and $\dot{\epsilon}_f$ is the relevant strain rate. At $\dot{\epsilon}_f$, dynamic precipitation is terminated at ϵ_p^f. As the strain rate is decreased below $\dot{\epsilon}_f$, dynamic precipitation is completed at smaller and smaller strains and the amount of precipitate coarsening taking place during deformation to the peak stress increases, thus reducing the peak strain.

From Fig. 3 it can be seen that dynamic precipitation is most rapid at 875°C, beginning in about 6 to 11 s in the present materials. (The results for steel No. 9—0.033 Al and 0.005 N—have not been included here as the interaction between precipitation and recrystallization was considered to be too weak to permit the determination of P_s and P_f with confidence.) It is also apparent from the curves that, as already suggested above, the rate of precipitation increases with Al concentration. The finish time for precipitation, for example, decreases from about 130 to 45 s. as the Al level is increased from 0.041 to 0.084%. As the temperature is increased to 900 and 925°C, both P_s and P_f increase. The slope for the 0.084 Al material is higher than that for the 0.062 Al material, however, in keeping with the higher solubility temperature pertaining to the former steel. (Steels 12 and 14 were not tested at 900 and 925°C.) It should be noted that steels 13 and 14, which had the highest and similar solubility products (Table 1), but different Al/N ratios, had distinctly different P_f times at 875°C. Steels 11 and 13, on the other hand, with almost equal Al/N ratios of 2.8 and 2.6, respectively, had less differentiated P_f times, which were less than those of steels 12 and 14, with Al/N ratios of 1.1 and 1.0. These observations indicate that, for equal solubility products, off-stoichiometric compositions on the Al-rich side have faster kinetics than stoichiometric ones. As indicated earlier, this could be related, via the smaller mean free path, to the role of Al diffusion as the rate controlling process in precipitate growth.

† The validity of the above statement is restricted to 875 and 900°C (Figs 2a and 2b), temperatures at which precipitation is fairly rapid. At 925°C (Fig. 2c), because of the approach of the solution temperature, the time for the completion of precipitation (200–600 s) is so long that no appreciable precipitate coarsening is produced prior to the peak strain at the lowest strain rate ($3 \times 10^{-4}\,s^{-1}$) used in the present test series.

‡ The size distribution of the AlN particles, and its dependence on strain, strain rate, temperature, holding time, composition, etc., will form the subject of the future investigation [33].

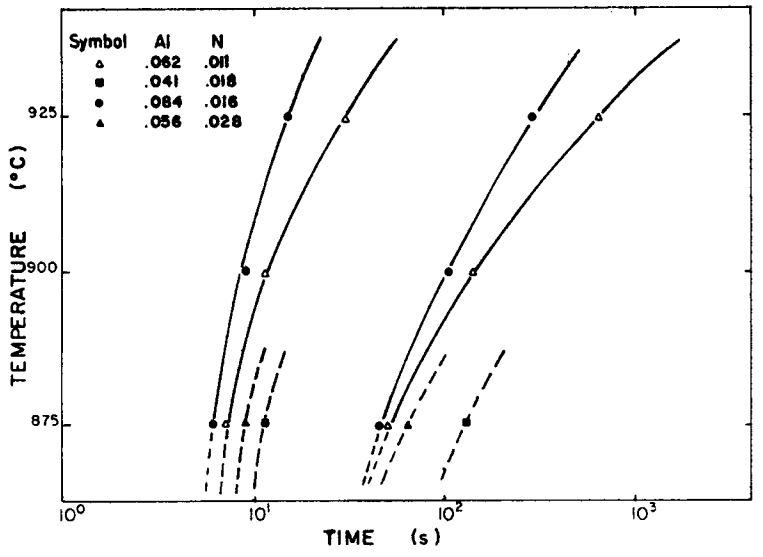

Fig. 3. PTT curves for the dynamic precipitation of AlN determined from the ϵ_p vs $\dot{\epsilon}$ data of Fig. 2.

Comparison of flow stresses

The flow stresses corresponding to an equivalent strain of 0.03 at 875°C are presented in Fig. 4 for the six materials. These are of interest in that they represent a level of strain which precedes the initiation of dynamic precipitation, so that essentially all of the metastable Al and N are still in solution. Although there is a fair amount of scatter, it is evident that the flow stress of the steels increases fairly regularly with Al concentration.

For the purpose of assessing the dependence of flow stress on composition more precisely, straight lines were fitted to the experimental points† by the method of least squares; this led to correlation coefficients of 0.95 or better. The relative strengthening was then assessed in terms of the expression:

$$\Delta\sigma_x(\%) = \frac{\sigma_x - \sigma_8}{\sigma_8} \times 100 \qquad (4)$$

Here σ_x is the flow stress of the Al–N steel under consideration and σ_8 is that of the reference plain C steel (No. 8). The relative strengthening calculated in this way for strains of 0.03 and 0.06 is collected and presented in Table 3. Here it can be seen that the flow stress increases in the order: steel Nos 8, 9, 14, 12, 11, and 13. This is in the order of increasing Al concentration, except for steel No. 14, which is out of

† The detailed dependence on strain rate has an upward curvature, of course.

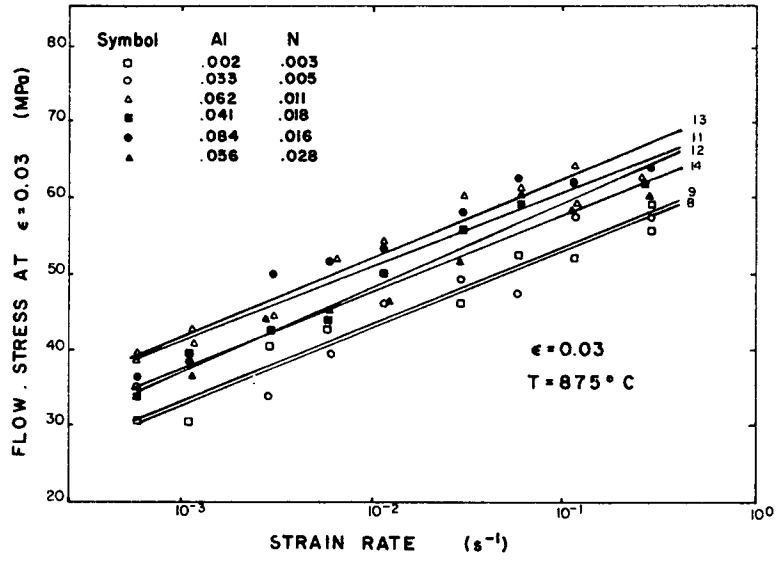

Fig. 4. Dependence of the flow stress at 875°C and an equivalent strain of 0.03 on strain rate for the six steels tested. The strengthening effect of increasing Al concentration is evident; the influence of N on flow stress can be discerned by comparing the fits for steel No. 11 (0.011 N) and steel No. 14 (0.028 N).

Table 3. Relative increase in flow stress (%), with respect to the reference material, attributable to high temperature solute strengthening

Temperature \ Strain*	Steel No. 9 ϵ_1	9 ϵ_2	11 ϵ_1	11 ϵ_2	12 ϵ_1	12 ϵ_2	13 ϵ_1	13 ϵ_2	14 ϵ_1	14 ϵ_2
875	1	3	20	20	15	15	21	22	10	11
900	16	13	28	28	—	—	36	34	—	—
925	8	15	24	22	—	—	27	26	—	—

*$\epsilon_1 = 0.03$ $\epsilon_2 = 0.06$.

sequence, but which contains the highest N level, namely 0.028%. A comparison of the fitted lines reveals that the dependence on Al concentration varies somewhat with temperature and strain rate, but falls in the overall range of about $12 \pm 5\%$ per 0.1 at.% Al addition over the complete range of the alloys. In a similar way, the *decrease* in flow stress with N concentration amounts to about $9 \pm 5\%$ per 0.1 at.% N addition. The reasons why N in solution can lead to a form of high temperature solute softening will be considered in more detail in the Discussion.

The dependence of the peak stress on strain rate and composition at 875°C is depicted in Fig. 5. These dependences incorporate both those of the yield stress shown previously and of the amount of work hardening accumulated between yielding and the attainment of the peak. It is evident from Fig. 5 that the peak stress increases with strain rate as well as Al concentration, in broad agreement with the dependence of Fig. 4. This indicates that the influence of Al and N addition on the amount of work hardening to the peak does not differ greatly from its influence on the yield stress. Such an observation is in turn consistent with the view that the macroscopic yield stress at high temperatures is controlled by a dynamic recovery mechanism, i.e. that 'yielding' corresponds to the beginning of stage III deformation [35]. According to this view, it is normal for the temperature and strain rate dependence of the yield stress to be closely similar to that of the peak or of the steady state stress. The increase in peak stress with Al concentration depicted in Fig. 5 corresponds approximately to 12% per 0.1 at.% of Al addition, but the scatter is too great to permit an estimate to be made of the effect of N addition.

DISCUSSION

Precipitation kinetics of AlN: comparison with previous workers

The present results are compared, in Fig. 6, with PTT curves deduced from data presented in the literature [1, 2, 8, 9] for temperatures above 800°C. For undeformed steels, two sets of results are shown. The first is the P_f relation reported by Leslie *et al.* [1] for a material containing 0.058% Al, 0.0058% N, and 0.35 Mn, following solution treatment at 1260°C. The second refers to curves for 10% and 90% completion of precipitation deduced from the observations published by Vodopivec [2] for a composition with 0.051% Al, 0.0073 N, and 0.36 Mn, following solution treatment at 1300°C. Comparison with the present data indicates that concurrent deformation accelerates the precipitation process by more than an order of magnitude in time. This effect can be attributed to the higher density of dislocations present in deformed steels which can serve as nucleation sites, as well as to the point defects introduced during straining which can, with the dislocations, accelerate the rate of diffusion. A similar dependence on temperature is displayed by both the static and dynamic data.

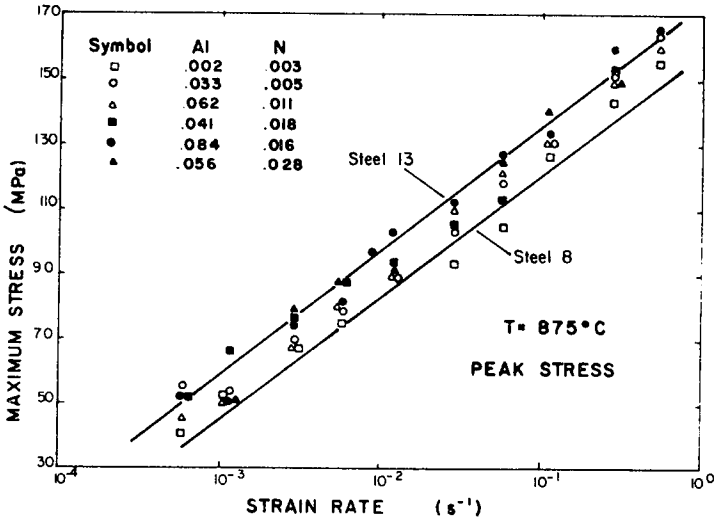

Fig. 5. Dependence of the peak stress at 875°C on equivalent strain rate. This stress also increases with Al concentration but has a higher rate sensitivity (0.19) than the flow stresses of Fig. 4 (0.09).

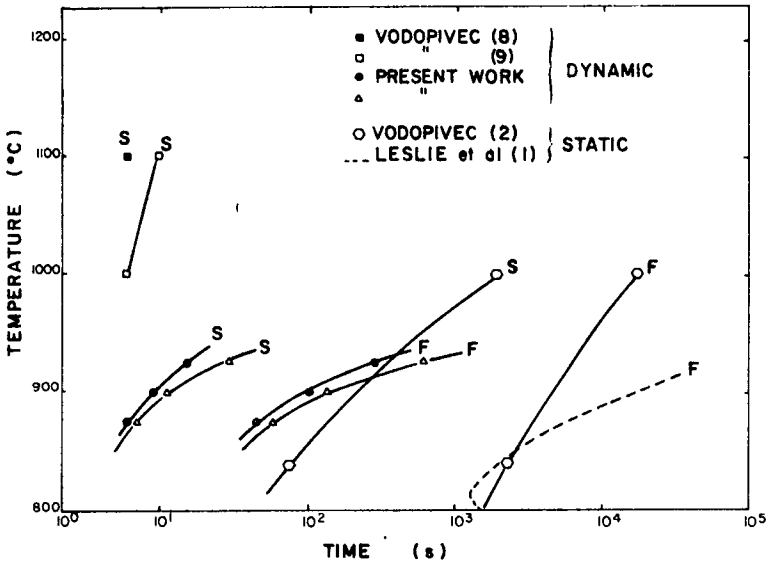

Fig. 6. Comparison of PTT curves for the static and dynamic precipitation of AlN. (S: precipitation start; F: precipitation finish).

With respect to the kinetics of *dynamic* precipitation, three points have been reported by Vodopivec [8, 9] as corresponding to the start of transformation for a steel containing 0.073% Al and 0.010% N. These results conflict to a certain extent with the present ones in that similar incubation times were observed for markedly higher deformation temperatures. A possible explanation for this divergence lies in the difference in Mn levels, 0.36% for Vodopivec and 0.7% in the current study. This element may have the same retarding effect on AlN precipitation as it does on that of Nb(CN) and of VN. For example, Akben *et al.* [21] have shown that an addition of 0.8% Mn can retard the kinetics of Nb(CN) precipitation by more than one order of magnitude. This was attributed to the decrease in C activity associated with Mn addition [36]. A similar dependence on Mn concentration has been noted by Woodhead [37] for VN precipitation in V microalloyed steels.

It is of interest that the start and finish times for AlN precipitation are closely similar to those establishd for the Nb(CN) and VN reactions [17, 18, 21] at similar temperatures and Mn levels. Such an observation suggests that the deposition of AlN on subboundary dislocations could be an effective agent for the retardation of static and dynamic recrystallization during steel rolling. Indeed, as evident from Fig. 7, the retardation of dynamic recrystallization produced by AlN precipitation (as measured by the increase in ϵ_p in the vicinity of the 'bulge'), is similar in magnitude in steels containing the three types of addition agents. The prevention of recrystallization, however, cannot be achieved by a precipitation reaction alone. Because of the rapidity of recrystallization in plain C steels in the vicinity of 900°C, e.g. recrystallization is complete in times of 1 s or less, the recrystallization process must be delayed by some other means for at least 10 s until the precipitation process itself can play a role. As indicated in Fig. 7 and discussed in more detail in Ref. [21], the influence of solutes on the retardation of recrystallization can be assessed from the position of the ϵ_p vs $\dot{\epsilon}$ curve at high strain rates; under these conditions, recrystallization *precedes* precipitation. It is evident from the figure that Nb in solution is particularly effective in retarding austenite recrystallization in this way. On an atom fraction basis, V is much less effective, so that an order of magnitude more is required for equal retardation. The presence of Al in solution appears to have a small and similar retarding effect on austenite recrystallization, per atom fraction, as that of V and distinctly less than that of Nb. This is somewhat surprising in that Al and Nb have similar atomic diameters (see Table 4) and the elastic moduli of Al differ from those of γ-Fe by at least as much as those of Nb. Some of the factors that make Al a less powerful solute in steel than Nb will be discussed in more detail below. For the moment, it is apparent that it is the much smaller retarding effect of Al *in solution* than Nb which makes the Al–N steels less suitable candidates for control rolling than the Nb–C–N steels, and not the difference in the kinetics of precipitation or in the amount of interaction between the precipitates and the deformation substructure.

Effect of Al and N in solid solution

The apparent hardening and softening effects of Al and N, respectively, were presented in Fig. 4 above. Although the conventional theories of solute hardening [38] are primarily addressed to lower temperatures, i.e. to the plateau stress and the low temperature thermally activated region, it will nevertheless be of interest to explore the possible contribution to the flow stress of γ-iron of the lattice parameter and,

Table 4. Solubility limit, strengthening, size, modulus and electronic effects in selected binary solutions in γ-Fe

Element ×	Solubility limit in γ-Fe at 1000°C at%†	Strengthening % per 0.1 at% at 900°C†	Effect of difference in atomic size: Relative difference in diameter (%) $\frac{d_x - d_{Fe}}{d_{Fe}} \times 100$ at 25°C† [44]	Effect of difference in atomic size: Relative increase in lattice parameter with concentration $\frac{1}{a}\cdot\frac{da}{dc} \times 100$	Effect of difference in modulus: Relative difference in Young's modulus $\frac{E_x - E_{Fe}}{E_{Fe}} \times 100$	Effect of difference in modulus: Relative increase in Young's modulus with concentration $\frac{1}{E}\cdot\frac{dE}{dc} \times 100$	Effect of difference in modulus: Relative increase in shear modulus with concentration $\frac{1}{\mu}\cdot\frac{d\mu}{dc} \times 100$	Effect of difference in modulus: Influence on modulus of electronic effeets [39] $\frac{1}{E}\left(\frac{dE}{dc}\right)_e \times 100$	Effect of difference in modulus: Influence on modulus of electronic effeets [39] $\frac{1}{\mu}\left(\frac{d\mu}{dc}\right)_e \times 100$
C*	6.5 [40]	−0.6 [41]	−28	+16.5 at 1200°C [45]† +16.4 at 1100°C [46]	—	−63 at 1000°C −102 at 1050°C [52]†	—	+75	+150
N*	0.10 [22]	−9 [present work]	−31	similar to C at 25°C [47]†	—	<0 [53] and similar to C [53]†	—	—	—
Al	1.5 [40]	+12 [present work]	+12	+6.2 [48] +6.3 [49]	−65 [51]	−125 [49]	−132 [49]	about zero	about zero
Si	2.5 [40]	+0.5 [41]	+3.5	+1.5† at 1050°C [50] −1.7 [59] −2.3 [49]	—	−130 [49]	−139 [49] −200 [54]	−130	−190
P	0.22 [40]	+8 [42]	+0.5	−7 [59]	—	—	—	—	—
S	0.023 [40]	+16 [43]	−0.3	—	—	—	—	—	—
V	1.2 [40]	+7 [21]	+6	+3.9 [49]	−33 [51]	about zero [49]	+12 [49]	+84	+86
Mn	62 [40]	+1.3 [21]	+2.3	−1.7 [59]	−19 [51]	−42 [39]	−29 [39]	about zero	about zero
Nb	0.6 [40]	+70 [21]	+15	—	−47 [51]	—	—	—	—

* Present as interstitials.
† For austenite. Ferrite in all other cases.

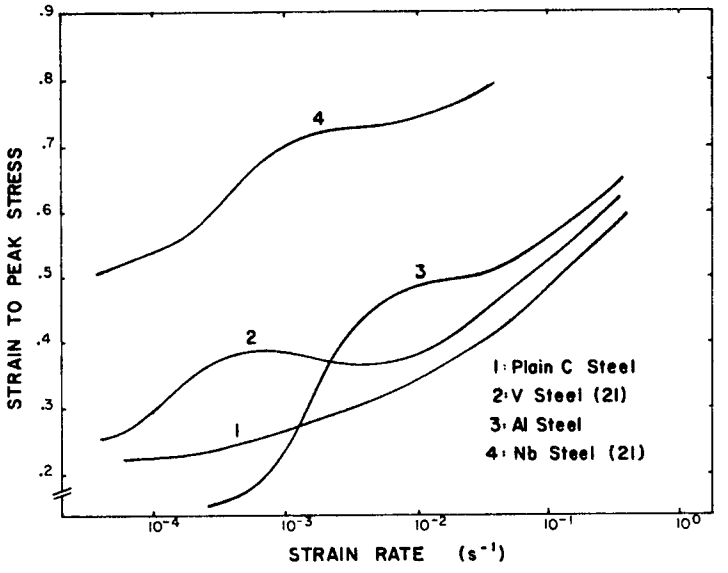

Fig. 7. Comparison of the peak strain vs. strain rate relationship expected for steels in which Nb(CN), VN or AlN is precipitating during testing. The curves are based on the present results and those of Refs 18 and 21, and have been adjusted to represent a fixed composition of 0.05 C and 1.25 Mn and a standardized method of testing by hot compression. It can be seen that the height of the 'hump' in the ϵ_p vs $\dot{\epsilon}$ curve with respect to the reference plain C steel is about the same for the three precipitating systems. By contrast, at high strain rates (prior to precipitation), Nb in solution has a much greater effect in retarding dynamic recrystallization than either V or Al.

modulus changes that attend the addition of Al and N to the iron lattice. Such a comparison must, by its nature, be a preliminary one, as the high temperature yield stress is controlled by dynamic recovery mechanisms and is below the plateau stress, and in any event the available data for lattice parameter and modulus changes in γ-Fe are scarce. For this purpose, some literature data concerning mean atomic diameter and modulus are collected and displayed in Table IV, not only for N and Al, but also for C, Si, P, S, V, Mn and Nb. The table includes the solubility limit at 1000°C (a rough measure of atomic size misfit and electronegativity difference), and the percent strengthening (per 0.1 at.% of solute) estimated from this investigation and from the literature. The lattice parameter data are presented both as the normalized difference in diameter between γ-Fe and the solute, as well as the atomic size misfit parameter $(1/a)(da/dc)\cdot 100$, when these data are available. In a similar way, the modulus data are quoted as normalized differences in modulus, and also as the modulus mismatch parameters $(1/E)(dE/dc)\cdot 100$ and $(1/\mu)(d\mu/dc)\cdot 100$, depending on availability.

Examination of Table 4 shows that, whereas the substitutional elements uniformly lead to hardening effects of varying magnitudes, the interstitials C and particularly N produce softening in austenite at about 900°C. Such softening has a ready interpretation in terms of the large increase in lattice parameter produced by the addition of interstitials. As the mean distance between atoms is increased (column 5), so the modulus decreases significantly (column 7). In addition to lattice dilation, there is an electronic component to the change in modulus. The magnitude of this component has not been reported in the literature for γ-Fe, but can be estimated for carbon addition to α-Fe from the work of Speich *et al.* [39] by subtracting the *observed* change in modulus from the modulus change expected *purely* on the basis of lattice dilatation or contraction. The value for the electronic component listed in Table 4 for C (column 10) is positive, thus offsetting in part the effect of lattice dilation. For N, no firm data are available, even for α-Fe, but as the diameter of the N atom is less than that of the C atom†, somewhat less dilation is expected. The smaller lattice dilation produced by N addition should lead in turn to a smaller degree of modulus decrease for N than for C addition. The admittedly scant information displayed in the table therefore suggests that the greater softening effect of N than C is probably associated with the greater electronic effect of N on the Fe lattice than C because N is further from Fe in the periodic table than is C (see Fig. 8).

Comparison of the effectiveness of the substitutional elements

A comparison of the strengthening effects of the substitutional elements reveals some interesting con-

† The following values of atomic radius, in Å, based on metallic bonding and a coordination number of 12, were used in the preparation of Table IV: Nb – 1.468; Al – 1.432; V – 1.346; Si – 1.319; Mn – 1.304; P – 1.28; Fe – 1.274; S – 1.27; C – 0.92; and N – 0.88 (44).

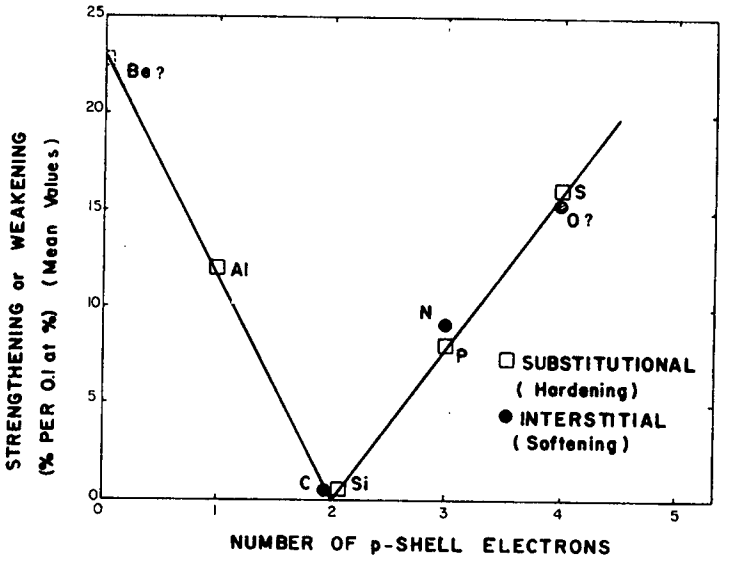

Fig. 8. Dependence of the strengthening or weakening effect of solute addition on the number of ground state p electrons of the solute. Only the *magnitude* and not the *sign* of the effect is represented, as in the diagrams of Abrahamson and co-workers [55–58]. Interstitial and substitutional elements produce softening and hardening respectively.

trasts. For example, all the elements of Table 4, with the possible exception of S, which has a marginally smaller atom than Fe (see previous footnote†), lead to lattice dilation in α-Fe. The lattice dilation, in turn, can be expected to produce a decrease in modulus in the cases of the remaining elements. Such a decrease is in fact observed experimentally for Al, Mn, and Si, but not for V, due apparently to an electronic interaction [39]. No data are available for Nb, although an even greater electronic effect is expected [21, 39], and the effects of P and S are not known.

The hardening attributable to the substitutional solutes in Table IV increases in the order: Si, Mn, V, P, Al, S and Nb. The considerations discussed above suggest that the modest hardening observed for Si and Mn is probably electronic in origin, as the size differences are small, and the addition of either element to Fe leads to a modulus decrease rather than an increase‡. The addition of V does not lead to a change in modulus, despite lattice dilation, again because of an electronic interaction [39], so that the strengthening reported can be attributed to a combination of size and electronic effects. With P and S, insufficient data are available to assess the importance of the modulus or electronic influences.

A clearer case, perhaps, is that of Al, the addition of which clearly *decreases* the modulus of α-Fe [49]. Nevertheless, hardening is observed (Table 4), and the modulus effect can be considered to be overcome by the size and electronic differences. With regard to the latter, it is relevant that Nb has essentially the same size difference with respect to Fe as Al, and thus a similar effect on lattice dilation and modulus change can be expected. The much larger hardening associated with Nb in solution therefore appears to be a purely electronic effect [21].

In summary then, the data available to date indicate that when the present substitutional solutes are added to α-Fe, only modulus *decreases* are observed. If these trends are followed in γ-Fe, the strengthening produced by these elements in austenite is likely to involve, in addition to size effects *per se*, appreciable electronic interactions. The significant role played by the latter may, in turn, be associated with the importance of dynamic recovery in this temperature region, rather than of the plateau hardening processes.

A possible rationalization for the strengthening effect of the non-transition elements in γ-Fe

Before dismissing the subject of the possible electronic effects of solutes in γ-Fe, it will be useful to re-examine the rationalization first introduced by Abrahamson and Grant in 1958 [55] to account for the influence of the non-transition '*p*-electron' elements on the fracture transition temperature of Cr. This approach has since been extended to the change in recrystallization temperature produced when various transition elements are added to host transition elements selected from groups IVa, Va, VIa and VIII of the periodic table. In the later investigations, the validity of the Abrahamson and Grant model was demonstrated for f.c.c. [56] and b.c.c. [57], as well as h.c.p. [58] lattices.

‡ We are concerned here particularly with the effect of substitutional solutes on the dynamic recovery mechanism at 900–1000°C. It is nevertheless possible that Si and Mn actually lead to softening *at 0 K*, as predicted from the modulus changes, and that the hardening observed at 1000°C is due to changes in the shape and density of the obstacles to flow [38]. It is unfortunately difficult to verify or reject this hypothesis because of the changeover to other rate controlling mechanisms as the experimental temperature is decreased.

The strengthening data obtained in this study are presented in Fig. 8 in terms of the number of ground state p electrons of the particular solute element. The results of the other workers referred to in Table 4 are also included. Although the number of data points is small, the V-pattern displayed by the observations, with a minimum at $p = 2$ for C and Si, follows exactly the overall pattern previously reported for Cr [55]. Whereas the *magnitude* of the effect varies with the number of p electrons, in the present case the *sign* of the interaction is negative for interstitials and positive for substitutionals. By contrast, Abrahamson [56–58] noted that individual substitutional elements could either accelerate or retard recrystallization with no pattern apparent for the sign of the interaction. Missing from the illustration are data points for the influence of Be and O in γ-Fe. This can be expected to be significant, even though the solubilities of these elements in γ-Fe are rather limited (about 3% at. Be as a substitutional at 1000°C and 0.02% at. O as an interstitial at 950°C [40]).

CONCLUSIONS

The hot deformation, by torsion, of a series of Fe–Al–N steels has permitted the determination of the flow characteristics and of the dynamic recrystallization behaviour of these materials. These tests, carried out at 875, 900 and 925°C, and at ten strain rates from 6×10^{-4} to $0.6\,s^{-1}$, have led to the following conclusions:

1. The kinetics for the dynamic precipitation of AlN, as determined from the dependence of the peak strain on strain rate, are more than an order of magnitude faster than the kinetics for static precipitation reported in the literature. The rate of precipitation decreases with temperature, indicating that the nose of the C-curve is below 875°C, i.e. below the γ–α transformation temperature. It increases with Al concentration, but is independent of N concentration, suggesting that the diffusion of Al is rate limiting.

2. The kinetics of AlN precipitation in plain C steels are similar to those of Nb(CN) and of VN in microalloyed steels. This suggests a possible application in metal processing. The much weaker effect of Al *in solution* than of Nb in retarding recrystallization, however, appears to be the primary reason why it is more difficult to use Al additions to prevent austenite recrystallization.

3. The precipitation of AlN on dislocations during deformation leads to a marked increase in peak strain, which is a measure of the effectiveness of a fine dispersion of such particles in retarding recrystallization. The rapid coarsening of these particles, after dynamic precipitation is complete, *promotes* rather than hinders recrystallization; this phenomena has not been observed in equivalent Nb or V microalloyed steels.

4. The presence of up to 0.084% Al in solid solution in γ-Fe at around 900°C increases the flow stress by $12 \pm 5\%$ per 0.1 at.% of addition. At high strain rates, where precipitation is absent, it increases the peak strain by about 8% per 0.1 at.%, indicating that Al in solution retards dynamic recrystallization to a modest degree. The presence of up to 0.028% N in solid solution in γ-Fe at around 900°C *decreases* the flow stress by $9 \pm 5\%$ per 0.1 at.% of addition. Due to the scatter in the results, the effect of N in solution on the ease of recrystallization could not be determined.

5. The presence of interstitial N, like that of C, dilates the lattice of γ-Fe and therefore *decreases* the elastic moduli. The softening produced by these elements in γ-Fe appears to be primarily a modulus effect, but the greater influence of N than of C probably involves an electronic component. The presence of Al in solution in γ-Fe, like that of N, dilates the lattice and decreases the elastic moduli. The hardening produced by Al addition is attributable partly to a size effect and partly to an electronic effect. The latter is much weaker for Al than for Nb, which has the same atomic diameter, but which produces significantly greater strengthening and retardation of recrystallization when in solution in γ-Fe.

Acknowledgements—The authors would like to express their gratitude to the following: to the US Steel Corp. Research Laboratory for preparing the six materials; to Dr L. J. Cuddy of the US Steel Corp. for providing the dilatometric results and for his many helpful comments and suggestions; to Dr P. J. Wray of the US Steel Corp. for permission to quote some of his results prior to publication, and to Professor Isaac Weiss of Wright State University for his assistance in the early stages of the investigation. One of the authors (J. P. Michel) thanks the E.N.S.-M.I.M. (Ecole Nationale Superieure de la Metallurgie et de l'Industrie des Mines de Nancy) for granting a period of sabbatical leave and the Ministry of Intergovernmental Affairs of Quebec for the provision of a postdoctoral fellowship.

REFERENCES

1. W. C. Leslie, R. L. Rickett, C. L. Dotson and C. S. Walton, *Trans. Am. Soc. Metals* **46**, 1470 (1954).
2. F. Vodopivec, *J. Iron Steel Inst.* **211**, 664 (1973).
3. F. Vodopivec, *Metals Technol.* **5**, 118 (1978).
4. T. Ichiyama, M. Koizumi, I. Yoshida, K. Watanabe and S. Nishiumi, *Trans. Iron Steel Inst. Japan* **10**, 429 (1970).
5. H. F. Beeghly, *Analytical Chem.* **21**, 1513 (1949).
6. Y. Meyzaud and P. Parniere, *Mém. scient. Revue Métall.* **71**, 423 (1974).
7. D. Thivellier, D. Rousseau and R. Tricot, *Mém. scient. Revue Métall.* **74**, 627 (1977).
8. F. Vodopivec, *Metals Technol.* **1**, 151 (1974).
9. F. Vodopivec, *J. Mater. Sci.* **10**, 1082 (1975).
10. B. C. Woodfine and A. G. Quarrell, *J. Iron Steel Inst.* **195**, 409 (1960).
11. L. A. Erasmus, *J. Iron Steel Inst.* **202**, 32 (1964).
12. M. Fukagawa, Y. Saiga and K. Tachimoto, *Trans. Iron Steel Inst. Japan*, Suppl. **11**, 1092 (1971).
13. M. T. Leger, *Fonderie* **354**, 107 (1976).
14. S. Hasebe, *Tetsu-to-Hogané* **3**, 200 (1963).
15. G. D. Funnell and R. J. Davies, *Metals Technol.* **5**, 150 (1978).

16. G. D. Funnell, Preprint from *Hot Working Int. Conf.*, Sheffield, **2**, 12.1 (1979).
17. J. J. Jonas and I. Weiss, *Metal Sci.* **13**, 238 (1979).
18. I. Weiss and J. J. Jonas, *Metall. Trans. A*, **10**, 831 (1979).
19. M. J. Luton and C. M. Sellars, *Acta metall.* **17**, 1033 (1969).
20. C. Rossard, *Metaux* **35**, 102, 140 and 190 (1960).
21. M. G. Akben, I. Weiss and J. J. Jonas, *Acta metall.* **29**, 111 (1981).
22. L. S. Darken, R. P. Smith and E. W. Filer, *Trans, Metall. Soc. AIME*, **191**, 1174 (1951).
23. L. J. Cuddy, U.S. Steel Corporation, Research Laboratory, Monroeville, PA., private communication.
24. K. W. Andrews, *J. Iron Steel Inst.* **203**, 721 (1965).
25. G. Pont, P. Maynier, J. Dollet and P. Bastien, *Proc. Conf. on Aciers de Construction Soudables a Dispersoides*, C.E.C.A., Luxembourg, p. 93, (1972).
26. S. Fulop, K. C. Cadien, M. J. Luton and H. J. McQueen, *J. Test. Eval.* **5**, 419 (1977).
27. D. S. Fields, Jr. and W. A. Backofen, *Proc. Am. Soc. Test. Mater.*, **57**, 1259 (1957).
28. G. Canova, M.Eng. Thesis, McGill University, Montreal, Canada (1979).
29. I. Weiss and J. J. Jonas, *Metall. Trans. A*, **11**, 403 (1980).
30. T. Chandra, I. Weiss and J. J. Jonas, submitted to *Metal Sci.*
31. J. P. Sah, G. J. Richardson and C. M. Sellars, *Metal Sci.* **8**, 325 (1974).
32. H. P. Stuwe, In *Recrystallization of Metallic Materials* (Edited by F. Haessner) p. 11, Riederer-Verlag GMBH Stuttgart (1978).
33. J. P. Michel and J. J. Jonas, to be published.
34. F. J. Humphreys, *Metal Sci.*, **13**, 136 (1979).
35. U. F. Kocks, Argonne National Laboratory, private communication.
36. S. Koyama, T. Ishii and K. Narita, *J. Japan Inst. Metals* **35**, 1089 (1971).
37. J. H. Woodhead, In *Vanadium in High Strength Steel*, Proc. Seminar in Chicago, November 1979, Published by VANITEC, London, 1980 pp. 3–10.
38. E. Pink and R. J. Arsenault, *Low Temperature Softening in Body-Centered Cubic Alloys, Progress in Materials Science*, Vol. 24, Pergamon Press, Oxford (1979).
39. G. R. Speich, A. J. Schwoeble and W. C. Leslie, *Metall. Trans.* **3**, 2031 (1972).
40. M. Hansen, *Constitution of Binary Alloys*, McGraw-Hill, New York (1958).
41. P. J. Wray, U.S. Steel Corporation, Research Laboratory, Monroeville, Pa., private communication.
42. S. S. Hansen and B. L. Bramfitt, Preprint from *21st Mechanical Working and Steel Processing Conference*, Cleveland, Ohio (1979).
43. J. P. Michel, Unpublished work.
44. W. B. Pearson, The Crystal Chemistry and Physics of Metals and Alloys, Wiley-Interscience, New York, p. 151 (1972).
45. N. Ridley and H. Stuart, *Metal Sci. J.* **4**, 219 (1970).
46. S. I. Veselova and Y. Z. Spektor, *Fizibci Metall.* **4**, 221 (1972).
47. K. H. Jack, *Proc. R. Soc. A*, **208**, 200 (1951).
48. A. Taylor and R. M. Jones, *Physics chem. Solids*, **6**, 16 (1958).
49. S. Takeuchi, *J. phys. Soc. Jap.*, **27**, 929 (1969).
50. G. H. Cockett and C. D. Davis, *J. Iron Steel Inst.*, **201**, 110 (1963).
51. R. E. Boltz and G. L. Tuve, *Handbook of Tables for Applied Engineering Science*, Chemical Rubber, Cleveland, Ohio, p. 94 (1970).
52. W. J. Arnoult and R. B. McLellan, *Acta metall.*, **23**, 51 (1975).
53. R. B. McLellan, William Marsh Rice University, Houston, Texas, private communication.
54. R. L. Routbort, C. N. Reid, E. S. Fisher and D. J. Denver, *Acta metall.*, **19**, 1307 (1971).
55. E. P. Abrahamson II and N. J. Grant, *Trans. Am. Soc. metals* **50**, 705 (1958).
56. E. P. Abrahamson II, *Trans. metall. Soc. AIME* **224**, 727 (1962).
57. E. P. Abrahamson II, *Trans. metall. Soc. AIME* **218**, 1101 (1960).
58. E. P. Abrahamson II, *Trans. metall. Soc. AIME* **221**, 1199 (1961).
59. W. C. Leslie, *Metall. Trans.* **3**, 5 (1972).

Acta Metallurgica Vol. 29, pp. 111 to 121

0001-6160/81/0101-0111$02.00/0

DYNAMIC PRECIPITATION AND SOLUTE HARDENING IN A V MICROALLOYED STEEL AND TWO Nb STEELS CONTAINING HIGH LEVELS OF Mn

M. G. AKBEN, I. WEISS and J. J. JONAS

Department of Mining and Metallurgical Engineering, McGill University, Montreal, Canada

(*Received* 21 *February* 1980; *in revised form* 26 *June* 1980)

Abstract—Constant strain rate hot compression tests were carried out on a 0.06% C–1.43% Mn reference steel, a 0.115% V–1.25% Mn microalloyed steel, and two Nb steels containing 0.035% Nb–1.25% Mn and 0.035% Nb–1.90% Mn, the latter steels all containing 0.05% C. Measurement of the peak strains at 875, 900 and 925°C over a range of strain rates permitted the determination of the PTT curves for dynamic precipitation, as well as the relative effectiveness of Nb and V in solution on retarding dynamic recrystallization. The results indicate that increasing the Mn level from 0.42 to 1.9% in the Nb-based steels shifts the nose of the C-curve to the right, decreasing the rate of precipitation by more than one order of magnitude. This change is associated with the increase in carbonitride solubility caused by Mn addition. The nose of the PTT curve for VN precipitation in deformed austenite is located at about 25 s, indicating a similarity in the precipitation kinetics of V and Nb at equivalent Mn levels. The greater effectiveness of Nb than V in promoting pancaking during control rolling at a given temperature is linked to the considerably greater influence of Nb *as solute* on the retardation of austenite recrystallization, rather than on differences in their precipitation behaviour. The difference in the effectiveness of these solutes is attributed primarily to the greater dissimilarity in electronic structure between Nb and Fe than between V and Fe, and secondarily to the greater atomic size discrepancy between Nb and Fe than between V and Fe. The yield strength of austenite was observed to increase by about 1.3, 7 and 70% respectively per 0.1 atomic % of Mn, V and Nb in solution. The magnitude of this effect follows the rank order for the differences in electronic structure and atomic diameter.

Résumé—Nous avons effectué des essais de compression à chaud et à vitesse de déformation constante sur un acier de référence 0,06% C–1,43% Mn, sur un acier microallié 0,115% V–1,25% Mn et sur deux aciers au niobium contenant respectivement 0,035% Nb–1,25% Mn et 0,035% Nb–1,90% Mn, ainsi que 0,05% C. La mesure des déformations maximals à 875, 900 et 925°C dans une large gamme de vitesses de déformation a permis de déterminer les courbes PTT de la précipitation dynamique, ainsi que l'efficacité relative du niobium et du vanadium en solution en ce qui concerne le retardement de la recristallisation dynamique. Nos résultats montrent qu'une augmentation de la teneur en manganèse de 0,42 à 1,9% dans les aciers à base de niobium déplace le nez de la courbe C vers la droite, abaissant ainsi la vitesse de précipitation de plus d'un ordre de grandeur. A ce changement est associée l'augmentation de la solubilité du carbonitrure produite par l'addition de Mn. Le nez de la courbe PTT de la précipitation de VN dans l'austénite déformée est située aux environs de 25 s, ce qui montre une certaine similitude entre les cinétiques de précipitation du V et du Nb pour des teneurs équivalentes en Mn. La plus grande efficacité du Nb, par rapport au V, à favoriser la structure en crêpes au cours du laminage de contrôle à une température donnée est liée à l'influence considérablement plus grande du niobium comme *soluté* pour retarder la recristallisation de l'austénite, plutôt qu'à des différences dans la précipitation. La différence d'efficacité de ces solutés est attribuée principalement à une plus grande différence de structure électronique entre Nb et Fe qu'entre V et Fe, et secondairement à la plus grande différence de taille atomique entre Nb et Fe qu'entre V et Fe. La limite élastique de l'austénite augmente respectivement d'environ 1,3; 7 et 70% par 0,1 at% de Mn, de V et de Nb en solution. La grandeur de cet effet suit le classement par ordre de grandeur des différences de structure électronique et de diamètre atomique.

Zusammenfassung—Druckversuche wurden mit konstanter Verformungsgeschwindigkeit bei hoher Temperatur an verschiedenen Stählen durchgeführt: an einem Referenzstahl 0.06% C–1,43% Mn, an einem mikrolegierten Stahl 0,115% V–1,25% Mn und an zwei Nb-Stählen mit 0,035% Nb–1,25% Mn und 0,035% Nb–1,90% Mn, die außerdem 0,05% C enthielten. Messungen der Spitzendehnungen bei 875, 900 und 925°C bei verschiedenen Verformungsgeschwindigkeiten erlaubten, die PTT-Kurven für die dynamische Ausscheidung und auch die relative Wirksamkeit des gelösten Niobs und des Vanadiums bei der Verzögerung der dynamischen Rekristallisation zu bestimmen. Die Ergebnisse zeigen, daß ein Anstieg des Mn-Gehaltes von 0.42 auf 1,9% in den Stählen auf Nb-Basis die Nase in den C-Kurven nach rechts verschiebt, wobei die Ausscheidungsrate um über eine Größenordnung verringert wird. Diese Änderung geht einher mit einer ansteigenden, durch die Mn-Zugabe erzeugten Carbonitrid-Löslichkeit. Die Nase der PTT-Kurve für VN-Ausscheidung im verformten Austenit liegt bei etwa 25 s, was auf ähnliche Ausscheidungskinetik von V und Nb bei gleichwertigen Mn-Gehalten hindeutet. Die größere Wirksamkeit von Nb gegenüber V, das testweise durchgefuhrte Herunterwalzen bei einer gegebenen Temperatur zu fördern, hängt mit dem beträchtlich größeren Einfluß des *gelösten* Nb auf die Verzöger-

ung der Austenit-Rekristallisation zusammen, also nicht mit Unterschieden im Ausscheideungsverhalten. Der Unterschied in der Wirksamkeit dieser Lösungsatome wird dem größeren Unterschied erstens in der elektronischen Struktur und zweitens im Atomdurchmesser bei Nb und Fe verglichen mit V und Fe zugeschrieben. Die Fließgrenze von Austenit stieg um 1,3%, 7% und 70% pro 0,1 At.% gelösten Mn, V und Nb. Die Größe dieses Effektes folgt der Rangordnung der Differenzen in elektonischer Struktur und im Atomdurchmesser.

INTRODUCTION

In an earlier investigation [1, 2], a new method was proposed for determining the kinetics of *dynamic* precipitation in microalloyed austenite. This technique was applied to two steels containing 0.018% and 0.035% Nb (as well as 0.05/0.06% C and 0.42% Mn) with the view of establishing the limiting kinetics for *static* precipitation in deformed austenite. In the analysis of the data, it was demonstrated that the retardation of static recrystallization in austenite is due to two distinct effects: the first is the retardation due to the presence of Nb *in solution* in the austenite; the second is the further retardation due to precipitation during the finishing stages of rolling. The essential function of the first phenomenon is to prevent recrystallization until the second process, which involves a delay time, can be initiated.

In the study described below, this technique was applied to a 0.035% Nb steel similar to the one investigated earlier, but with concentrations of Mn (1.25% and 1.90%) considerably higher than in the previous experiments. The object of this work was to determine the influence of Mn addition on the kinetics of precipitation of Nb(CN). In a second part of the investigation, the rate of dynamic precipitation of VN was measured in a 0.05 C–1.20 Mn–0.115 V–0.006 N steel, together with the effect of V *in solution* on the retardation of dynamic recrystallization. The results indicate that the considerably weaker influence of V addition (in the absence of Nb) on retarding austenite recrystallization during finish rolling can be attributed to the much smaller influence of V *as solute* when compared to Nb. The measurements also permit a comparison to be made between the flow stress increases caused by Nb, V and Mn addition. The much higher effect of Nb in solution is interpreted in terms of the differences between Fe and the relevant alloying element with respect to (i) electronic structure primarily, and (ii) atomic diameter secondarily.

EXPERIMENTAL MATERIALS & METHODS

With the purpose of investigating the effects of Nb, V and Mn singly and in combination on the dynamic recrystallization behaviour of austenite, a series of HSLA steels and a reference plain carbon steel were prepared in the Physical Metallurgy Research Laboratories of the Department of Energy, Mines and Resources, Ottawa. The chemical compositions of the four steels examined in this study are given in Table 1. The steels were prepared as follows: They were melted in an induction furnace in 230 kg heats and Al-killed. Each heat was cast into three 70 kg cylindrical ingots. Both ends were cropped and the ingots were cut into two cylindrical sections weighing roughly 23 kg each. They were soaked in an oil fired furnace for 2 h at 1200°C prior to being forged down to 67 mm thick slabs. These slabs were soaked for 2 h at 1250°C in an electric Globar furnace then hot rolled down to a final thickness of 13 mm in a reversing mill.

The samples were machined from the plates with the compression axis along the rolling direction. The ends of the samples were grooved to retain the glass lubricants used to minimize friction between the end faces of the sample and the test equipment.

Preliminary compression tests producted elliptical sample shapes as a result of the rolling texture. To eliminate this, the samples were vacuum annealed at 1000°C for 2 h and then water quenched. Immediately prior to testing, each sample was austenitized in the test chamber described below for half an hour in an argon atmosphere. The austenitizing temperatures were 1100°C for the two Nb steels, 1045°C for the V steel and 1030°C for the plain carbon steel. These temperatures were chosen to ensure the complete solution of the V and Nb carbonitrides and led to mean austenite grain sizes of 110, 100, 130 and 120 μm for the C, V, 1.25 Mn–Nb and 1.9 Mn–Nb steels respectively. A typical set of microstructures for these steel is shown in Fig. 1. After solutionizing, each sample was cooled to the test temperature at an average rate of 1°C/s.

Constant true strain rate compression tests were performed on a modified Instron testing machine, details of which have been given elsewhere [3]. The tests were carried out isothermally at 875, 900 and 925°C within an Inconel muffle, i.e. the test chamber,

Table 1. Chemical composition of materials tested, wt%

Steel type	C	Mn	S	P	Al	Si	Nb	V
Plain carbon	0.06	1.43	0.012	0.006	0.025	0.24	-	-
V-bearing	0.05	1.20	0.012	0.006	0.030	0.25	-	0.115
Nb-bearing	0.05	1.25	0.012	0.006	0.030	0.27	0.035	-
Nb-bearing (high Mn)	0.06	1.90	0.010	0.006	0.030	0.225	0.035	-
			$N \simeq 0.006$					

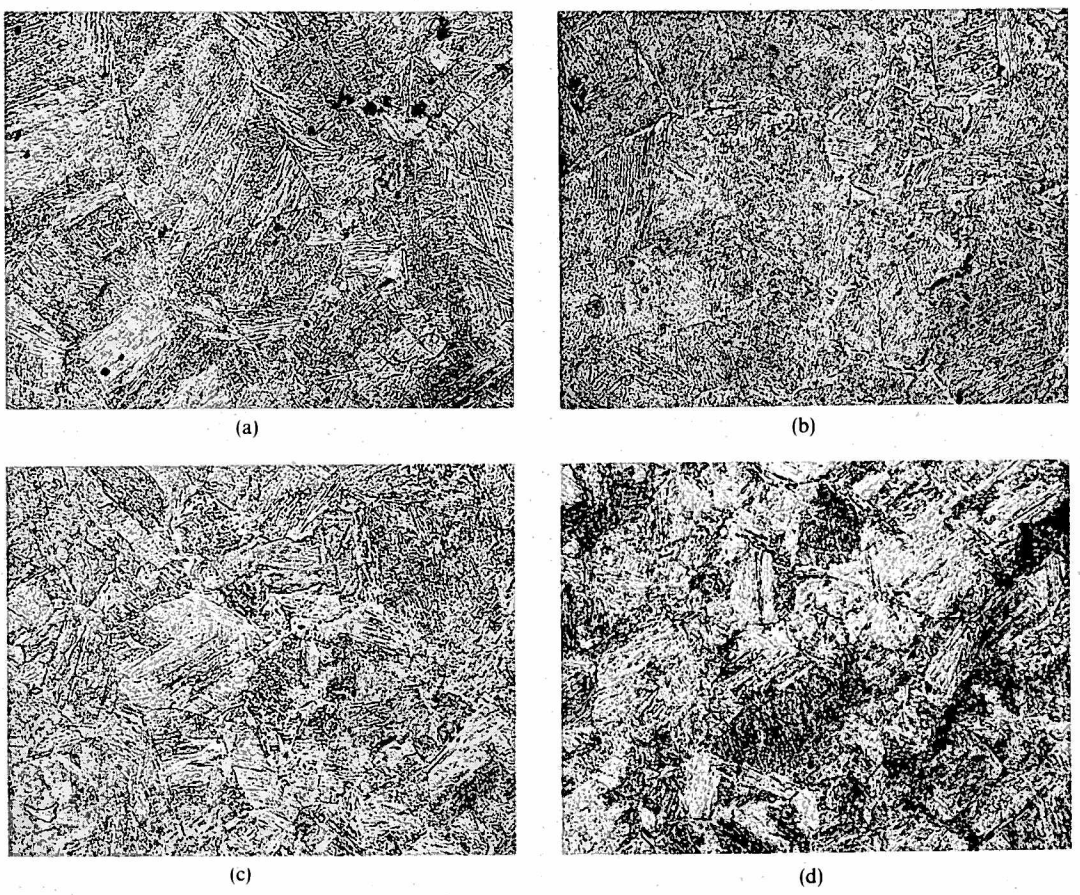

Fig. 1. Typical microstructure (×400) of each steel after ½ hour of austenitization: (a) plain C steel: 1030°C, (b) V steel: 1045°C, (c) 1.25% Mn–Nb Steel: 1100°C, (d) 1.90% Mn–Nb Steel: 1100°C.

under an argon atmosphere. The muffle was heated by a Satec split three-zone platinum resistance furnace with a capacity of 14.5 amp per zone. These tests were controlled with the aid of a Honeywell 4020 process control computer which was also used for data acquisition and plotting purposes. Thus, the true stress–true strain curves were available immediately after each experiment.

RESULTS

Two typical sets of flow curves for the four steels investigated are shown in Fig. 2. At a strain rate of $5 \times 10^{-4}\,s^{-1}$ (Fig. 2a), the early onset of dynamic recrystallization in the plain C steel is indicated by the relatively low values of peak strain ($\epsilon_p = 0.21$) and peak stress ($\sigma_p = 64$ MPa). By contrast, in the V steel, the peak strain ($\epsilon_p = 0.35$) is about 65% higher and in the two Nb steels ($\epsilon_p = 0.57$ and 0.64) they are between two and three times higher. As will be seen below, the difference between the V and C steels is essentially a *precipitate* effect†, whereas the greater difference between the Nb and C steels is largely a *solute* effect, with some assistance from precipitation.

These differences in the behaviours of the four steels can be seen to better effect in Fig. 2b, where the flow curves were determined at a strain rate of $3.5 \times 10^{-2}\,s^{-1}$, so that each test took only about 20 s to complete. Under these conditions (see Figs. 4 and 5 below), no dynamic precipitation took place in the Nb and V steels prior to the peak strain, so that the inequalities in the peak strains reflect differences in the solute rather than in the precipitate effects. It is evident from the figure that the peak strain for the V steel ($\epsilon_p = 0.39$) is only slightly greater than that for the C steel ($\epsilon_p = 0.36$), whereas the two Nb steels have peak strains 0.70 for the 1.25% Mn steel and 0.67 for the 1.90% Mn steel) roughly twice that of the plain C steel. These observations indicate that, at a strain rate of $3.5 \times 10^{-2}\,s^{-1}$, the presence of V in supersaturated solid solution retards dynamic recrystallization (increases the peak strain) to a much smaller extent than does the presence of 0.035% Nb.

The interpretation of Fig. 2 described above is based on the results obtained over a wider range of strain rates which are presented in Fig. 3. Here the

† At a strain rate of $5 \times 10^{-4}\,s^{-1}$, the tests depicted in Fig. 2a each took about 1600 s to perform. Thus the peak strain was reached in the V steel in about 700 s and, on the basis of the precipitation kinetics presented in Fig. 5 below, it is apparent that dynamic precipitation was taking place during most of this interval.

strain rate interval over which dynamic precipitation affects the peak strain can be seen more clearly from the presence of 'humps' on the otherwise smooth ϵ_p vs. $\dot{\epsilon}$ relationships for the Nb and V steels. At strain rates to the right of the humps, the peak strain is reached in times too short (e.g. 10 s) to permit significant precipitation during the work hardening interval. Thus the retardation of dynamic recrystallization with respect to the plain C steel is largely attributable to the presence in solution of 0.115% (0.126 atomic %) V and 0.035% (0.022 atomic %) Nb†. The much greater influence of the Nb per atom fraction on the peak strain is of considerable interest and will be examined more closely in the Discussion. The greatest retarding effect of Nb *as solute* on the nucleation of recrystallization extends to *static* as well as to *dynamic* conditions. Thus it has implications on the control rolling of microalloyed steels which will also be considered in more detail below.

At strain rates to the *left* of the hump, the peak strains are reached in times of 1000 s or more. Under these conditions, precipitation begins early during straining, is completed, and then followed by rapid coarsening [4, 5]. The coarse precipitates formed in this way are no longer able to pin the sub-boundaries and so to retard the nucleation of dynamic recrystallization. Thus the retardation of dynamic recrystallization in this range with respect to the plain C steel is due to the Nb and V remaining in solution (i.e. to the equilibrium solute), although a contribution from the coarse precipitates [1, 2] is also possible. In the present experiments, the amount of equilibrium solute after precipitation is about half that of the total solute present prior to precipitation [6], so that the solute effect can be expected to be somewhat less evident at the left as opposed to the right of the diagram. (Note that the strain rates used to establish the positions of the humps in Fig. 3 are in the range 5×10^{-4} to $5 \times 10^{-2}\,s^{-1}$ and are well removed from rolling mill strain rates. However, the laboratory strain rates are dictated by the kinetics of the precipitation process under study and even if, for example, a high speed cam plastometer were available, it would still, according to the present method, have to be employed in the above rate interval.)

DYNAMIC PRECIPITATION KINETICS

The PTT curves for the dynamic precipitation of Nb(C, N) were derived from Fig. 3, and from similar plots for 900 and 925°C, using the method developed by Weiss and Jonas [1, 2]. The results obtained for the two Nb steels are presented in Fig. 4, together

† Prior to dynamic precipitation at each experimental temperature, some of the Nb and V is present in the form of supersaturated solute and some in the form of equilibrium solute.

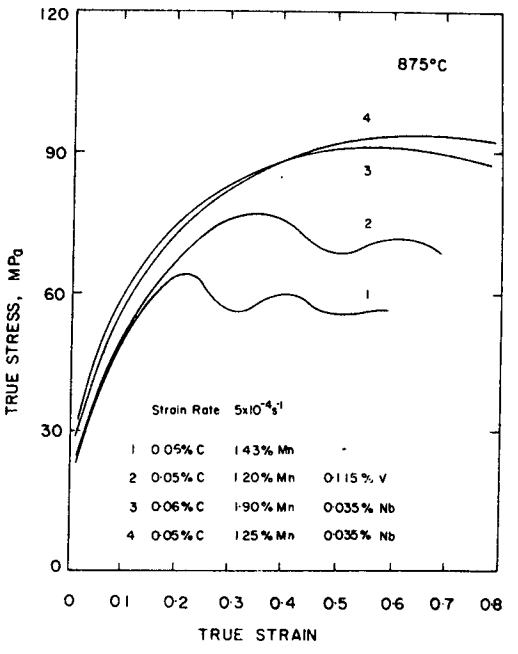

Fig. 2a. Flow curves for the four steels investigated determined at a strain rate of $5 \times 10^{-4}\,s^{-1}$. The greater peak strain in the V as opposed to the plain C steel is primarily due to dynamic precipitation in the former material during the test. The considerably higher peak strains in the Nb steels are due to the superposition of both precipitate and solute effects.

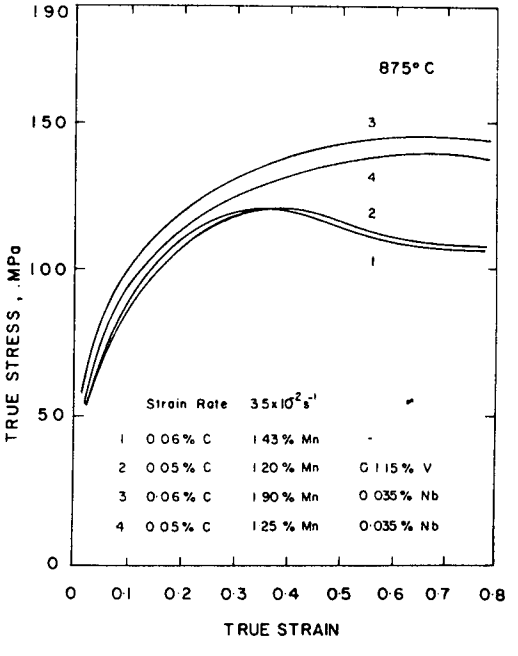

Fig. 2b. Flow curves for the present steels at a strain rate of $3.5 \times 10^{-2}\,s^{-1}$. No dynamic precipitation took place at these strain rates in the microalloyed steels. The high peak strains in the Nb steels are thus associated with significant solute effects. The similarity in the plain C and V flow curves is due to the small solute effect attributable to the latter element.

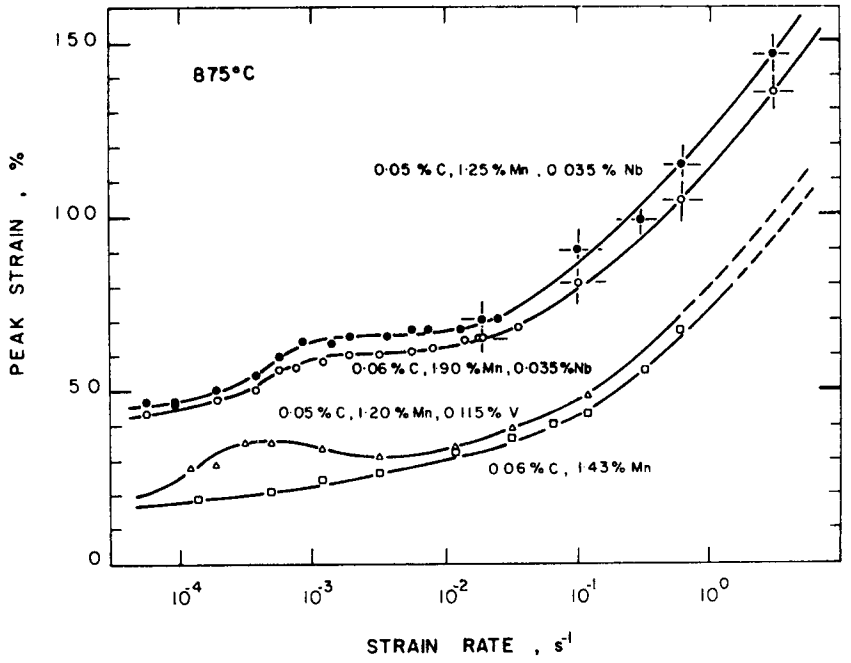

Fig. 3. Dependence of the peak strain on strain rate at 875°C for the four materials. Differences in the general levels of the curves are attributed to a solute effect. The 'humps' located in particular strain rate ranges are associated with the occurrence of dynamic precipitation during the test at these strain rates. (The peak strains at high strain rates for the Nb steels represented by ⊙ and ◆ were determined in torsion by the method of Ref [7]).

with the data for the 0.42% Mn steel† reported previously [1]. It can be seen that an increase in the Mn concentration from 0.42 to 1.9% moves the PTT curve sharply to the right, by more than one order of magnitude in time. That is, the addition of Mn *decreases* the rate of precipitation of Nb(C, N). The shape of the curves is also changed slightly, in a manner consistent with the observations of V. R. Golik *et al.* [9] that raising the Mn concentration from 0.75 to 1.28% increases the solubility of the carbides in steels of 0.16%C, with Nb concentrations of 0.08–0.29%. Note that the noses of these curves remain in the vicinity of 900°C, indicating that the addition of Mn not only decreases the nucleation rate, but also modifies the diffusion-controlled branch of the C-curve.

The PTT curve for the V steel is presented in Fig. 5, together with the curve of Fig. 4 for the Nb steel at the same level of Mn concentration. It can be seen that the nose of the VN curve is at a somewhat lower temperature (885 vs. 905°C) in keeping with the lower estimated solubility temperature of the VN (985 vs. 996°C). Of greater importance are the time coordinates of the noses of the curves, which are situated at about 16 and 26 s for the Nb and V-based materials, respectively, and are therefore fairly close. The present observations thus indicate that the rate of precipitation of VN *during deformation* (i.e. during compression tests which can last up to 1000 s or more) is approximately equal to the rate of dynamic precipitation of Nb(C, N). By analogy, the rate of static precipitation of VN *in the presence of dislocations* can be assumed about equal to the rate of precipitation of Nb(C, N) in pre-strained austenite (as determined, for example, by the method of Refs. [1] and [2]). The latter statement conflicts, however, with the common observation [6, 10–15] that, at a given temperature, V additions are less effective than Nb additions in promoting pancaking and in preventing austenite recrystallization during finish rolling. The resolution of this seeming paradox relies on the interaction between the effects of Nb and V as solutes on the one hand and as precipitate formers on the other. As will be shown below, it is the difference between the influence of Nb and V *in solution* as already suggested above (and not between their precipitate forming tendencies) that is primarily responsible for the higher effectiveness of Nb as an agent of γ and α grain refinement.

DISCUSSION

The roles of Nb and V as solutes in microalloyed austenite are not well understood. This is partly

† The 0.42% Mn steel tested previously contained 0.057% Al and 0.05% Si, whereas the present steels are based on 0.025% Al and 0.24% Si. These differences in Al and Si concentration are not considered to be significant for the purposes of the present discussion. This is because, while the two diameter ratios Nb/Fe and Al/Fe are similar at about 1.15 (see Table 2 below), as are the smaller ratios V/Fe and Si/Fe at about 1.05 (see Table 2), Al and Si not being transition elements, have much smaller electronic effects than Nb and V, respectively [7]. It is also evident that the electronic effects play a greater role in retarding austenite recrystallization and in raising the high temperature yield stress than the size effect [7, 8].

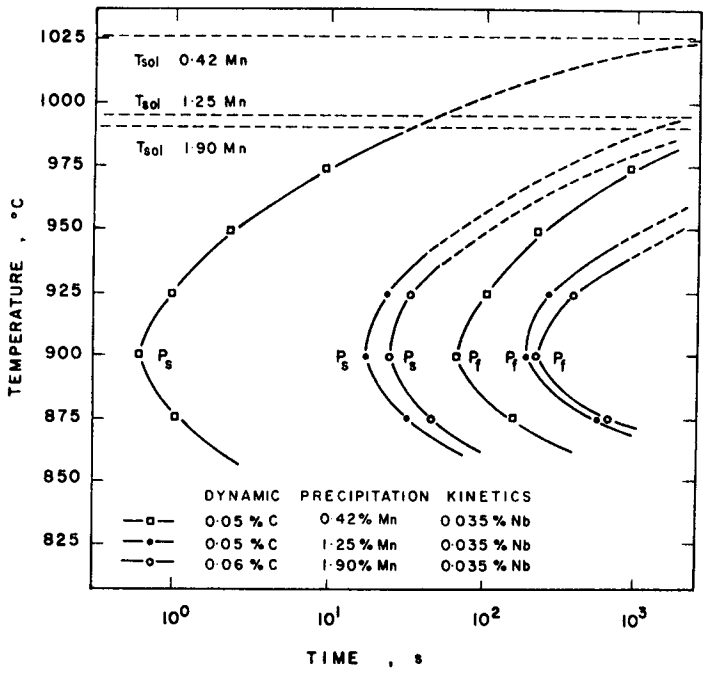

Fig. 4. PTT curves for the dynamic precipitation of Nb(CN) in the present Nb steels determined from Fig. 2 and from equivalent data for 900 and 925°C. The results obtained previously [1] on a low Mn steel are also included. It is evident that the addition of Mn *decreases* the rate of precipitation of Nb(CN).

because they are usually present at such low concentrations (e.g. 0.02 and 0.1 atomic percent, respectively in the present case, compared to C at about 0.25 atomic percent), that detectable effects are not generally expected. Nevertheless, there are both experimental and theoretical reasons for considering that the transition elements can have important solute effects in gamma iron. For example, the experiments of Luton *et al.* [16] on a decarburized and denitrided Nb steel have shown that Nb *in solution* retards both

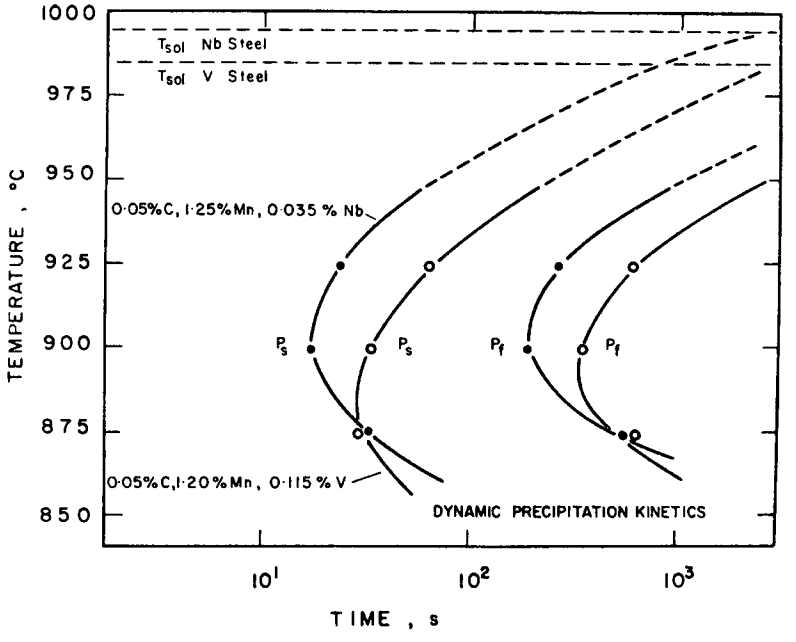

Fig. 5. PTT curve for the dynamic precipitation of VN in the present V steel determined from Fig. 2 and from the data for 900 and 925°C. The C-curve from Fig. 3 for the Nb steel at the same Mn level is also depicted, indicating that the kinetics of precipitation of Nb and V are similar in steel containing dislocations.

Table 2. Elements in decreasing order of atomic size difference with iron [18]

$a_x > a_{Fe}$	$a_x < a_{Fe}$
Y	C
Hf, Zr, Hg, U	B
Nb, Ta, Ti, Ag, Al	S
W, Mo, Se, Zn, Pd	P
Te, Pt, Ir, V	Be
Rh, Si, Mn	

Cr, Ni, Co ≃ Fe.

static recovery and static recrystallization by about one order of magnitude in time compared to an equivalent plain C steel. In a similar way, the work of White and Owen [14] on a V steel conducted above the solubility temperatures of VN and VC has demonstrated that V *in solution* retards the recrystallization of austenite with respect to a reference plain C steel. With regard to the retardation of *dynamic* recrystallization, the torsion data of Fig. 3 determined at $3\,s^{-1}$ and cam plastometer tests carried out at a strain rate of $55\,s^{-1}$ (and therefore in about 20 ms) indicate that the peak strains for V and Nb steels are higher than for C steels, even when there is insufficient time for dynamic precipitation [17].

If these observations are taken as reliable, they can be most readily interpreted in terms of the atomic size and electronic differences between Nb and V as solutes and Fe as solvent. For example, following Pearson [18], we can prepare the following Table 2 giving the ranking order for the size differences between gamma iron and the transition metals, as well as between iron and some of the other common alloying elements. It is apparent from this table that, at equal atom fractions in solution, Nb at a size difference of 15% is likely to have a stronger effect than V at 6%.

With regard to the electronic differences, we adopt here the basic approach proposed by Abrahamson *et al.* [8, 19, 20], according to which the effect of solute addition on the recrystallization behaviour of Fe depends primarily on the number of s and d electrons in the outer shells of the respective elements in the ground state. For convenience, Abrahamson's final plot is reproduced here as Fig. 6 with the addition of several elements (identified by crosses) which were not included in his investigation of 1960. The rank order is also summarized in Table 3†. From these results, it is evident that Nb has a considerably more powerful effect on the recrystallization kinetics of Fe than V.

† It should be noted that, even when elements have the same number of *s* and *d* electrons, it is still possible to rank their relative effects on the recrystallization temperature of alpha iron, as shown in Fig. 6. Here the influence of Hf, Zr and Ti is in the order just given, in keeping with their ranking in Table 2. From this observation it is also apparent that the number of free electrons has an appreciably stronger influence than the number of filled electron shells (atomic diameter).

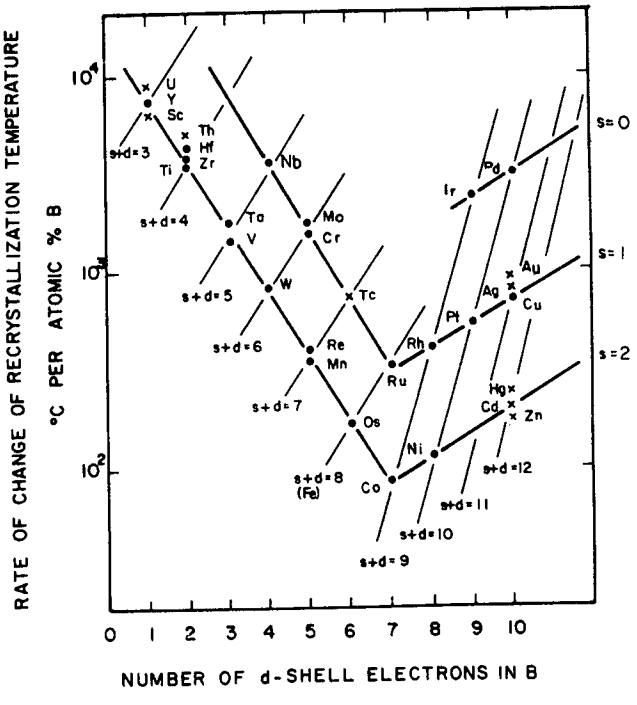

Fig. 6. Effect of the addition of transition elements on the recrystallization temperature of deformed alpha iron (after Abrahamson [8]). The elements identified by crosses were not investigated by Abrahamson, and are located here in the positions indicated by the periodic table. According to the diagram, the effectiveness of a given element in retarding recrystallization depends on the difference between the quantity $(2s + d)$ for Fe and for the element, where $s = 2$ and $d = 6$ for Fe.

Table 3. Transition elements in decreasing order of rate of change of recrystallization temperature

U, Y, Sc
Th, Hf, Zr, Ti, Nb
Ir, Pd
Ta, Mo, V, Cr
W, Tc
Au, Ag, Cu, Pt
Re, Mn, Rh, Ru
Os, Hg, Cd, Zn
Ni, Co

Before comparing Abrahamson's model to the present situation, however, two assumptions must be made. The first is that the ranking of Table 3 determined experimentally for *alpha* iron applies to *gamma* iron. This has not been demonstrated, but is reasonable in that (a) the phase transformation does not affect the electronic structure, and (b) the Abrahamson correlation has been demonstrated to be valid for f.c.c. [19] and h.c.p. [20], as well as b.c.c. [8] structures. The change in coordination number, on the other hand, implies that the *slope* in Fig. 6 does not apply to gamma iron, which will have a different proportionality factor. The second assumption concerns the conversion from isochronal to isothermal conditions, and stipulates that the *rate* of recrystallization at a *fixed temperature* follows the ranking given in Table 3 for the *temperature* of recrystallization at a *fixed time*, inasmuch as these are kinetically equivalent.

Superposition of solute and precipitate effects

We are now prepared to interpret the results of Figs 3–5 in more detail. In the first place, we can say that the much greater effect of Nb in solution, per atom fraction, evident in Fig. 3 is consistent with the position of Nb well above that of V in both Tables 2 and 3. For the time being, this justification remains qualitative, as a quantitative theory relating the number of filled electron shells and the number and type of free electrons to recovery and recrystallization rates is unfortunately lacking. Of continuing interest, however, is the possible quantitative determination of the relative influence of Zr, Ti, Ta, Mo, etc. as solutes in austenite along the lines proposed by Abrahamson for alpha iron.

We turn at this point to Figs 4 and 5 and the observation that the dynamic precipitation kinetics of Nb and V in austenite at about 900°C are closely similar, whereas their effectiveness in promoting pancaking during finish rolling is not [6, 10–14]. This apparent discrepancy can be reconciled with the aid of Fig. 7, which is based on Fig. 2, as well as on Tables 2 and 3. In Fig. 7a, the retarding effect of Nb in solution on austenite recrystallization is indicated by the shift to the right of the RTT diagram with respect to the one for the plain C steel. By means of this shift, the solute-modified RTT diagram intersects

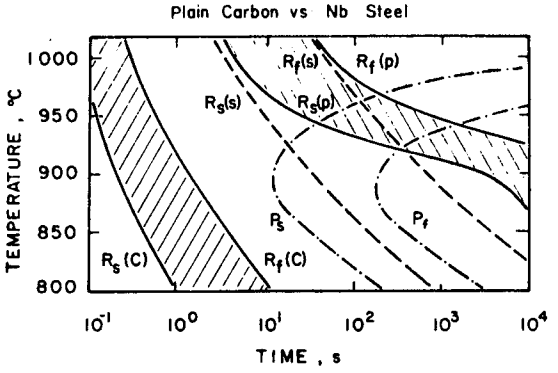

Fig. 7a. PTT diagram for the present 0.035 Nb–1.25 Mn steel shown in relation to RTT diagrams for typical plain C and Nb-modified steels. The basic RTT curve for the Nb steel has been shifted considerably to the right of the plain C curve (1, 2) by the solute effect depicted in Fig. 2. Note that precipitation does not begin in the Nb steel until *after recrystallization is complete* in the plain C steel.

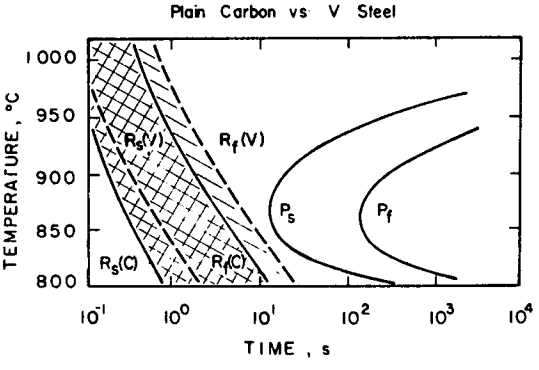

Fig. 7b. PTT diagram for the present 0.115 V–1.25 Mn steel shown in relation to RTT diagrams for typical plain C and V-modified steels. The basic RTT curve for the V steel has been shifted *only slightly* to the right, in keeping with the modest solute effect evident in Fig. 2. As a result, precipitation cannot begin soon enough to prevent recrystallization in the V steel.

the PTT diagram for deformed austenite so that, as long as recrystallization precedes precipitation, e.g. at 1000°C, the dislocations are eliminated, and the start of precipitation is delayed as given by the PTT curve for *undeformed* austenite [15, 21]. Conversely, if precipitation begins before the start of recrystallization indicated by the solute-modified RTT curve, e.g. at 900°C, then recrystallization is delayed for considerable periods [1, 2], leading to the pancaking of austenite during finish rolling. This sequence of events is modified in V steels that contain no Nb in the manner indicated in Fig. 7b. Here we see that the solute-modified RTT curve is displaced only a small distance to the right of the plain C curve, as suggested by Fig. 3 for dynamic recrystallization, and in keeping with the predicted effects of Tables 2 and 3. The small displacement of the RTT curve no longer permits it to intersect the PTT curve for the precipitation of VN in deformed austenite, so that recrystallization of the austenite will normally be followed much later if at all by precipitation in *undeformed* as opposed to

deformed gamma iron. In this way, the precipitation of vanadium nitride is effectively delayed by the removal of the dislocations and, once initiated, comes too late to prevent austenite recrystallization, even at 900°C. Three conclusions of relevance to industrial practice follow from this construction:

(i) In the absence of Nb, the precipitation of VN in austenite containing typical commercial quantities of V in solution will be much less common than that of Nb(CN) in austenite containing Nb, despite the similarities in the kinetics of dynamic precipitation for these two species.

(ii) The relative rarity of VN precipitation in deformed austenite (and the consequent diminished effectiveness of V addition as an agent for the retardation of austenite recrystallization) can be attributed to the much smaller retarding effect of V *in solution* on the rate of recrystallization, and not to any inherent sluggishness in the rate of precipitation of the nitride.

(iii) As a result of the above, for equal pancaking efficiency, lower finishing temperatures must be used with V as opposed to Nb microalloyed steels.

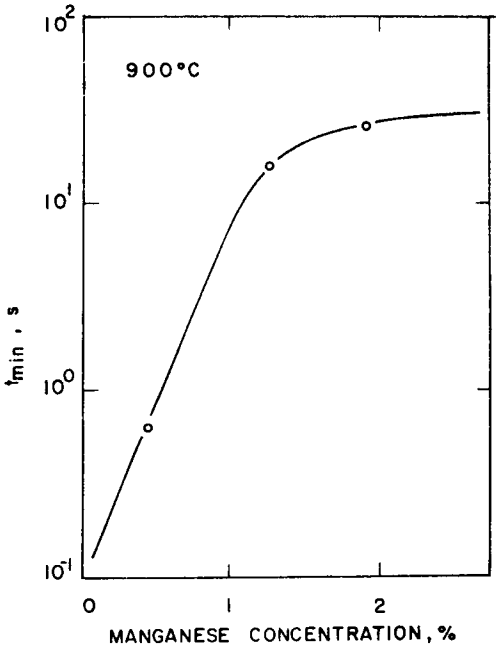

Fig. 8. The effect of Mn addition on the nose position of the Nb(CN) C-curves of Fig. 3.

Effect of Mn on the kinetics of Nb(CN) precipitation

The influence of Mn addition on the rate of precipitation of Nb(CN) can be deduced from the positions of the three C-curves of Fig. 4. This effect is illustrated in Fig. 8 in terms of the dependence of minimum precipitation time (nose of the C-curve) on Mn concentration. The time dependence can be linked to the increase in the solubility of niobium carbide that accompanies Mn addition which has been reported by both Russian [9] and Japanese [22] workers. The higher carbide solubility decreases the driving force for precipitation at a given temperature, which leads in turn to both a lower nucleation rate, as well as the steady rightwards displacement of the curves. In their more detailed investigation, Koyama *et al.* [22] showed that the addition of Mn leads to an *increase* in the activity coefficient of Nb in austenite. However, the *decrease* in the activity coefficient of C is greater in magnitude, and is responsible for the increase in the solubility of NbC. They reported that their observations can be represented by the equation:

$$\log[\%Nb][\%C] = -7970/T + 3.31 + (1371/T - 0.900)[\%Mn] - (75/T - 0.0504)[\%Mn]^2. \quad (1)$$

This relationship leads to solution temperatures of 1027, 996 and 991°C for the present 0.42, 1.25 and 1.90% Mn steels, as indicated on Fig. 4. It should be noted that, as only the V–Mn composition was available for the investigation described here, the possibility that Mn addition also decreases the precipitation rate and increases the solubility of VN could not be verified by the present technique. Woodhead [23], however, has recently considered this effect and reported results which are qualitatively similar to the ones discussed above for Nb.

Effect of Mn, Nb and V addition on the flow stress

The addition of Mn, Nb and V to carbon steels can affect the flow stress in three different ways. In the first place, there is the effect on the yield strength itself, which can be expected to follow the trends suggested in Tables 2 and 3 above, not only for Mn, Nb and V, but for the other transition metals as well. Then there is the direct effect of Nb and V as precipitate formers; thus when fine precipitates are present or being deposited, the work hardening rate can be predicted to rise above the normal level, leading to somewhat higher flow stresses. Finally there is the *indirect* effect of the precipitates, in terms of their prevention or retardation of static or dynamic recrystallization. In hot strip mills, it is the third effect which is normally considered to play the largest single role in determining the separating force.

The effects of Mn, Nb and V on the *yield* stress over the present strain rate range are presented in Fig. 9. It can be seen that V has a small effect, equivalent to about a 7% increase in flow stress over the plain C steel per 0.1 atomic percent addition. In keeping with Tables 2 and 3, Nb has a much larger effect (at approximately the same Mn level), which works out to an increase of about 70% over the plain C steel per 0.1 at.% addition. Finally, when the Mn concentration of the Nb steel is increased from 1.25 to 1.9%, a further increase in yield stress is produced, which is equivalent to about 1.3% per 0.1 atomic percent of Mn added. The smaller relative effect of Mn than of V is again consistent with the atomic size and electronic structure data presented above. It should be noted

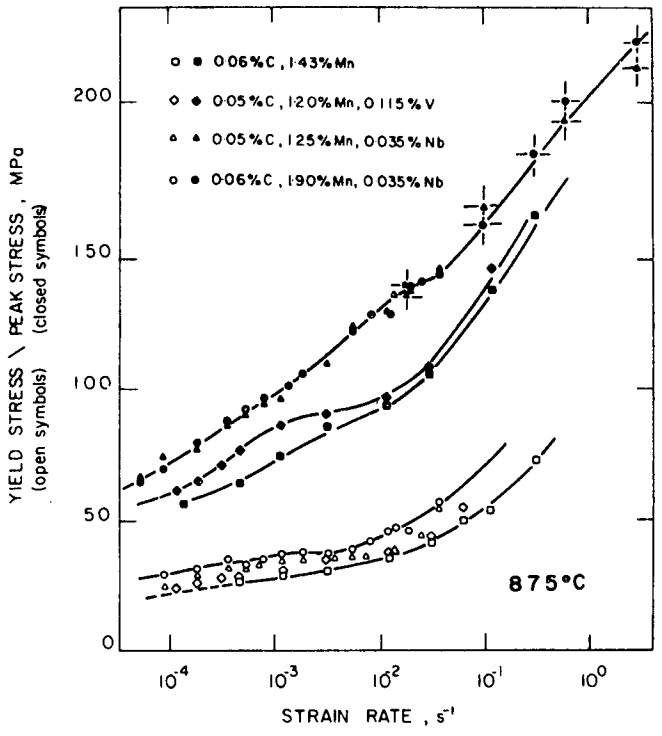

Fig. 9. Dependence of the yield stress (open symbols) and peak stress (closed symbols) on strain rate at 875°C for the four materials. The yield data demonstrate the relative strengthening effects of Nb, V and Mn addition. The peak stress data show similar trends, except that small 'humps' can be discerned over the strain rate ranges in which dynamic precipitation is occurring during a test. Note the large increase in the flow stress between generalized yielding and the peak. (The peak stresses at high strain rates for the Nb steel represented by -⧫- and -⧫- were determined in torsion by the method of Ref. [7]).

that, at the elevated temperatures under consideration, the yield stresses are 'recovery controlled' and thus significantly below the plateau stresses. This appears to be the reason why solutes affect the flow stress largely via *electronic* rather than through size or modulus interactions [7].

The *peak* stresses are also presented in Fig. 9, from which an indication can be obtained of the effect of Mn, Nb and V addition on the rate and extent of work hardening. Two conclusions can be drawn from these curves. First, the precipitation of the carbonitrides in the strain rate ranges defined in Fig. 3 only makes a barely perceptible difference to the peak stress. Thus the increase in the rate of work hardening associated with the presence or formation of fine precipitates is unlikely to be of practical importance. Second, the amount of work hardening in straining from the yield to the peak stress is large, representing an increase in flow stress by a factor of about 2.5, and is about equal for the four steels. (The somewhat smaller extent of work hardening prior to dynamic recrystallization in the 1.9 Mn steel is consistent with its slightly finer grain size after austenitization.) Thus the occurrence of complete recrystallization (or its absence) between mill passes will have a large and similar effect on the rolling load in subsequent passes for the four materials. However, the different *kinetics* of recrystallization displayed by these steels, as discussed above, will have different consequences during roughing and during finishing. During the early stages of roughing, all four steels will recrystallize in full between passes, so that the rolling load will not be affected by the work hardening increment produced by the previous pass, but will instead be sensitive to the effect of the alloying elements on the *yield* stress. During finishing, on the other hand, the work hardening increment will be preserved in the Nb steels, absent in the plain C steel, and partially present in the V steel. In this way, the microalloying elements affect the rolling load during finishing primarily indirectly, through retarding recrystallization, rather than by their direct influence on the yield strength, even though solution phenomena play large roles in both of these effects.

Finally, it should be noted that the present technique involves the measurement of the kinetics of *dynamic* precipitation and of the critical strain for *dynamic* recrystallization. Conclusions are then drawn regarding the interaction between precipitation and recrystallization during straining and the importance of solute effects. Under rolling conditions, however, most of the carbonitrides precipitate *statically* (on dislocations) and the principal recrystallization process is a *static* one. Thus it is legitimate to enquire into the extent to which the present model based on *dynamic* tests can be considered to apply under *static* con-

ditions. With regard to the relation between the kinetics for static and dynamic precipitation, it has been established [1, 2] that dynamic precipitation is somewhat faster than static precipitation in deformed materials and represents the limiting case of speed. No significant error is therefore likely to arise as far as the precipitation aspect of the model of Fig. 7 is concerned. With regard to the relation between the peak strain ϵ_p for dynamic recrystallization and the time, say, for 50% static recrystallization $t_{50\%}$, less is known. It is implicit in Fig. 7 that an increase in ϵ_p observed experimentally due to Nb, V, Mn, Mo or Al addition, for example, will lead to qualitatively similar increases in $t_{50\%}$. The conversion factor relating ϵ_p to $t_{50\%}$ has not, however, been measured quantitatively and should be determined before the present model can be considered to be fully justified.

CONCLUSIONS

The measurement of peak strain by means of hot compression in a reference plain C and three microalloyed steels has led to the following conclusions.

1. An increase in Mn level from 0.42 to 1.9% in a 0.05% C–0.035% Nb steel leads to a *decrease* in the rate of dynamic precipitation of the Nb(CN) by over one order of magnitude. This effect is associated with the decrease in the activity of the C and the increase in the solubility of the precipitate caused by the addition of Mn.

2. The rate of dynamic precipitation of VN in a 0.05% C–0.115% V steel is about equal to that of Nb(CN) in a 0.05% C–0.035% Nb steel containing the same amount (1.25%) of Mn.

3. With regard to the retardation of austenite recrystallization by *solute* effeets, 0.035% Nb has a much stronger influence than 0.115% V. Its more marked effectiveness is attributed primarily to the greater difference in electronic structure between Nb and Fe than between V and Fe, and secondarily to the appreciably greater atomic size difference between Nb and Fe than between V and Fe.

4. The lesser effectiveness of V than Nb in promoting the pancaking of austenite during control rolling at a given temperature is associated with the considerably smaller effect of V than Nb *as solute* on the retardation of austenite recrystallization.

5. The yield stress of austenite is increased by about 1.3, 7 and 70% respectively per 0.1 at.% of Mn, V and Nb in solution. The rank order of this effect depends, as does the retardation of recrystallization, first on the electronic differences and second on the atomic size differences with respect to Fe.

6. During roughing, when recrystallization goes to completion between passes in both plain C and microalloyed steels, the differences in rolling load are largely attributable to the *direct* influence of the alloying elements in solution on the yield and flow stresses. During finishing, the differences in rolling load are primarily attributable to differences in the recrystallization kinetics of the various steels. In this way, the alloying elements have only an *indirect* effect on separation force through their influence, both as solutes and as precipitate formers, on the rate of recrystallization.

Acknowledgements—This work was performed under contract for the Physical Metallurgy Research Laboratories of CANMET, Energy Mines and Resources, Canada. The authors are indebted to PMRL, CANMET for providing the experimental materials and for permission to publish this work. They also acknowledge the moral support received from Drs M. J. Stewart and G. E. Ruddle, PMRL, in the scientific administration of the contracts. They are grateful for the useful comments and suggestions received from Drs E. P. Abrahamson, II of the Portsmouth Naval Shipyard, J. M. Gray of Microalloying International, S. S. Hansen of the Bethlehem Steel Corporation, M. Korchynsky of the Union Carbide Corporation, and W. C. Leslie of the University of Michigan.

REFERENCES

1. I. Weiss and J. J. Jonas, *Metall. Trans.* A **10**, 831 (1979).
2. J. J. Jonas and I. Weiss, *Metals Sci.* **13**, 238 (1979).
3. M. J. Luton, J. P. Immarigeon and J. J. Jonas, *J. Phys. E.* **7**, 862 (1974).
4. I. Weiss and J. J. Jonas, *Metall. Trans.* A **11**, 403 (1980).
5. T. Chandra, I. Weiss and J. J. Jonas, *Metals Sci.* in press.
6. J. N. Cordea, *Symposium on Low Alloy High Strength Steels*, Nurnberg, BRD, May 1970. Metallurg Companies.
7. J. P. Michel and J. J. Jonas, submitted for Publication in *Acta metall.*
8. E. P. Abrahamson, II and B. S. Blakeney, Jr, *Trans. Metall. Soc. A.I.M.E.* **218**, 1101 (1960).
9. V. R. Golik, V. A. Dubrov, N. I. Sandler and V. M. Yunash, *Fizika Metall.* **14**, 555 (1962).
10. W. Roberts, Swedish Institute for Metals Research Report no. IM-1333, Nov. (1978).
11. J. R. Everett, A. Gittins, G. Glover and M. Toyama, *Preprint from Sheffield Int. Conf. on Hot Working and Forging Processes*, July (1979).
12. M. Cohen and S. S. Hansen, *MiCon 78: Optimization of Processing, Properties and Service Performance Through Microstructural Control.* ASTM STP **672**, 34 (1979).
13. K. J. Irvine, F. B. Pickering and T. Gladman, *J. Iron Steel Inst.* **205**, 161 (1967).
14. M. J. White and W. S. Owen, *Metall. Trans. A* **11**, 597 (1980).
15. S. S. Hansen, J. B. Vander Sande and M. Cohen, *Metall. Trans. A* **11**, 387 (1980).
16. M. J. Luton, R. Dorvel and R. A. P. Petkovic, *Metall. Trans.* **11**, 411 (1980).
17. M. J. Stewart, *Hot Deformation of Austenite* (Edited by J. B. Ballance) p. 47 and 233. AIME, New York (1977).
18. W. B. Pearson, *The Crystal Chemistry and Physics of Metals and Alloys* p. 151. Wiley, New York (1972).
19. E. P. Abrahamson, II, *Trans. Metall. Soc. A.I.M.E.* **224**, 727 (1962).
20. E. P. Abrahamson, II and J. A. Alexander, *Trans. Am. Soc. Metals* **56**, 377 (1963).
21. H. Kreye and E. Hornbogen, *J. Mater. Sci.* **5**, 89 (1970).
22. Shinji Koyama, Teruo Ishii and Kiichi Narita, *Nippon Kink. Gakk.* **35**, 1089 (1971).
23. J. H. Woodhead, *Preprint from Vanadium 1979*, Seminar held in Chicago, Ill., Vanadium International Technical Committee, Nov. 1979.

Proc. ASM Symposium on 'Process Modelling Tools', Cleveland, Ohio, October 1980, ASM, in press.

HOT STRENGTH AND STRUCTURE IN PLAIN C AND MICROALLOYED STEELS DURING THE SIMULATION OF PLATE ROLLING BY TORSION TESTING

I. Weiss,* J. J. Jonas† and G. E. Ruddle††

*Department of Engineering, Wright State University, Dayton, Ohio, U.S.A., 45435

†Department of Metallurgical Engineering, McGill University, Montreal, Canada, H3A 2A7

††Canada Center for Mineral And Energy Technology, Ottawa, Canada, K1A 0G1

ABSTRACT

The rolling of steel plate was simulated on a servo-controlled, hydraulic torsion machine interfaced with a PDP 1104 minicomputer. Three steels were studied: a 0.11C plain C and two microalloyed grades containing 0.10C-0.046Nb-0.05V and 0.13C-0.066Nb. Seventeen 'passes' were applied while the temperature was continuously decreased from 1250 to 765°C. Individual samples were quenched after each pass delay to permit observation of the changes in austenite grain size and shape during rolling. In this way, it was established whether full, partial, or no recrystallization followed a particular pass. The transformed ferrite structures were also investigated, and correlated with the state of the prior austenite and with the microalloying agents present.

The mean flow stresses pertaining to each 'pass' were determined from the measured torque/twist curves and employed in a Sims analysis. The predicted roll separation forces and torques are compared with the ones measured in the mill; reasonable agreement is observed, with the calculated forces being too low when the laboratory temperature was higher than the mill temperature, and vice versa. The torsion flow stresses were also used to verify, by means of a 'Softening Parameter', the amount of recrystallization occurring after the various rolling 'passes'.

INTRODUCTION

It is difficult to follow the evolution of the austenite grain structure during plate rolling. This is because the thickness of the slabs and plates does not permit the attainment of sufficiently rapid quench rates for martensite to be formed, and therefore for the γ grain boundaries to be revealed. This can be done instead by torsion testing, which is the laboratory test method best suited to the study of the progress of recrystallization during simulated rolling. By means of this technique, accumulated true strains of 4 or 5 can be readily achieved, and individual specimens can be quenched with ease after any given number of simulated 'passes' (1). In addition to the grain sizes and shapes, such simulations can also provide information about the flow stresses, and in this way permit the correlation of flow stress decreases with the occurrence of recrystallization.

The principal limitation of torsion testing arises from the differences that arise between the temperature/time profile observed in the mill and that experienced by the specimen during the simulation (1). For this reason, many previous workers have carried out their simulations by performing individual tests isothermally, and then repeating these tests on virgin specimens at other temperatures within the range of interest (2). The interpolation and superposition of such results, while useful as a first approximation, do not take into account the effect of the accumulating strain on both the structure and the flow stress.

The aim of the present work was to simulate plate rolling under conditions of continuously decreasing temperature. Both the structural changes taking place and the flow stresses developed were of interest. The study was carried out on a 0.11C-1.3Mn plain C steel, and two HSLA steels containing (i) 0.10C-0.046Nb-0.05V; and (ii) 0.13C-0.066Nb. Using the Sims analysis, the hot strength data from the investigation were employed to estimate the roll forces and torques expected in each pass. These were then compared with those measured on an industrial plate mill.

MATERIALS AND PROCEDURE

The plain carbon and microalloyed steels had the chemical compositions given in Table 1. They were hot rolled down to

a thickness of 25mm and were supplied in the form of 850mm wide plates. Torsion specimens with a gauge length of 26mm and a radius of 3.2mm were prepared from the plates with their axes aligned in the rolling direction. A servo-controlled, hydraulic torsion machine was employed for the torsion experiments; a description of this apparatus has been given elsewhere (3). This equipment has a maximum torque capacity of 100 N-m. For the present experiments, it was operated at 60 rpm; improvements carried out after the tests were completed now permit the running of simulations at 600 rpm, which corresponds to an equivalent strain rate of 5 s^{-1}.

Table 1. Chemical Compositions in wt %.

Steel	C	Mn	Si	Al	N	Nb	V
plain C	0.11	1.30	0.22	0.05	0.007	-	-
Nb-V	0.10	1.37	0.15	0.07	0.007	0.046	0.05
Nb	0.13	1.41	0.17	0.04	0.007	0.066	-

The torsion specimens were solution treated at 1250°C for 30 min before testing. The source of heat was a 4kW radiant furnace (R.I. dual elliptical radiant heater, model EZ-10WPA) mounted directly on the bed of the torsion machine. The purpose of each test was to apply a deformation-time-temperature sequence as close as possible to the one observed in the mill. The rolling schedule selected is displayed in Figure 1a. In each experiment, the most difficult part of the procedure was the accurate simulation of the temperature/time profile. The temperature profile actually achieved is shown in Figure 1b. This was obtained by shutting off the furnace and cooling each sample with a regulated stream of argon during the simulation. This practice, as can be seen from Figure 1b, led to temperatures higher than the mill temperature for the first few passes, and then lower than the mill temperature for the later passes. A flexible thermocouple fastened to the center of the gauge length and free to rotate during twisting was employed for determination of the specimen temperature. Further details of this procedure are reported elsewhere (1).

The torsion equipment was interfaced with a PDP-1104 minicomputer, which was employed for both data acquisition and control purposes. The minicomputer applied the required strain per pass, unloaded the sample for the required delay time between passes, and then continued the deformation sequence for a total of seventeen passes. Although the mean

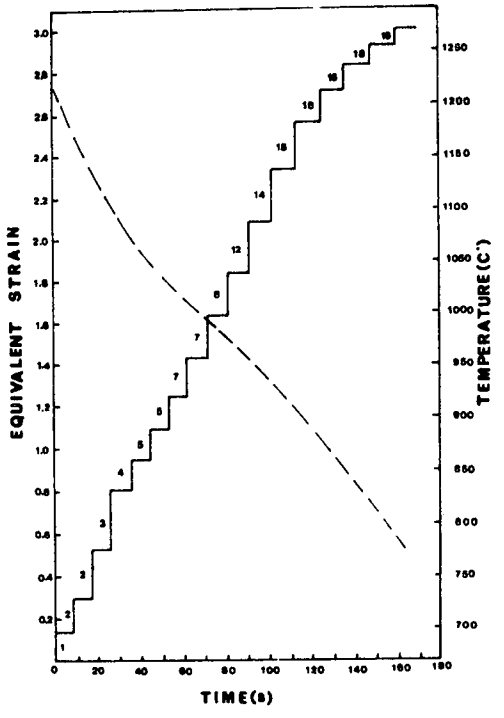

Fig. 1a - Deformation-temperature-time sequence followed in the mill during rolling. The mean strain rate is listed for each pass. The temperature profile is represented by the broken line.

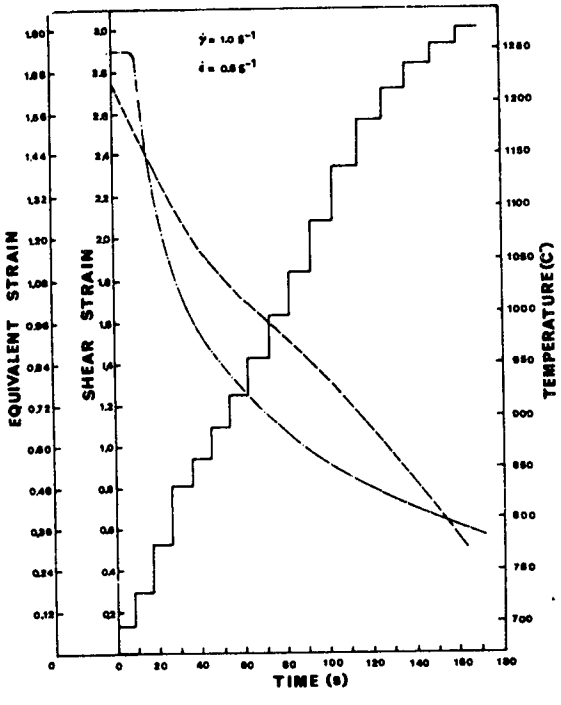

Fig. 1b - Deformation-temperature-time sequence achieved in the torsion machine. The temperature-time profile followed in the plate mill (---) is compared with that experienced by the sample in the torsion machine (-·-·-)

equivalent strain rate in the mill increases from about 1 s^{-1} during roughing to about 20 s^{-1} during finishing (see Figure 1a), during the course of these experiments, it was not possible to operate the control loop of the testing train reliably at such high speeds. Thus the tests were carried out at a constant strain rate of 0.6 s^{-1} (shear strain rate of 1 s^{-1}). To correct for the lower speed of rotation, the pass strains were also reduced by 60%, i.e. by the ratio of equivalent to shear strain. As the individual 'passes' were applied at the same fixed strain rate in the torsion machine, for the purposes of the Sims calculation, the mean flow stresses determined in torsion were increased to the levels appropriate to the actual mean strain rate of each pass by multiplying them by the ratio of the two strain rates raised to a power equal to the rate sensitivity.

For the microstructural part of this investigation, deformed samples were water quenched after each delay during the rolling schedule. In this way, 17 samples were required to reveal the grain structures associated with a 17 pass schedule. The prior austenite grain boundaries were revealed by etching the as-quenched samples in modified picric acid (4). The equivalent ferrite structures were prepared by air cooling the deformed test pieces to 200°C and then water cooling to room temperature. This required a further 17 specimens for a 17 pass rolling sequence.

The torque Γ and angle of twist θ were converted into equivalent stress σ_{eq} and equivalent strain ε_{eq} using the following relations:

$$\sigma_{eq} = \sqrt{3}\,\tau = \frac{\sqrt{3}\,\Gamma\,(3+m+n)}{2\pi r^3} \qquad (1)$$

and

$$\varepsilon_{eq} = \gamma/\sqrt{3} = r\theta/\sqrt{3}\,L \qquad (2)$$

Here τ and γ are the shear stress and shear strain at the specimen surface and r and L are the sample radius and gauge length, respectively. The coefficients m and n are the 'rate sensitivity' and 'work hardening' exponents of the torque, as given by $m = \partial \ln\Gamma/\partial \ln\dot{\theta}$ and $n = \partial \ln\Gamma/\partial \ln\theta$. Although both m and n varied with strain, for simplicity, constant values of $m = 0.17$ and $n = 0.13$ were employed to calculate σ_{eq}. In effect, the variations in m and n are two orders of magnitude smaller than the mean value of the multiplier $(3+m+n) = 3.3$.

RESULTS

The flow curves for the plain C and the two microalloyed steels are presented in Figures 2a, 2b and 2c. Also included in the diagrams is the mean temperature associated with each of the rolling 'passes'. It is evident that the temperature decreases from 1250°C during the first pass to 775°C during the last pass. It is also clear that, due largely to the dropping temperature, the flow stress increases rapidly in the course of each simulation. The mean effective stress was determined for each pass with the aid of an expanded stress/strain plot, using the method of graphical integration. By means of this technique, it was established that the mean stress increased from about 23 MPa during roughing to 152 MPa during finishing for the plain C steel. For the Nb-V and Nb steels, the equivalent quantities are 28 to 196 MPa and 32 to 208 MPa, respectively.

A closer examination of Figure 2a indicates that, for the plain C steel, austenite recrystallization was complete after each of the first five passes. By contrast, after passes 6 to 17, it was only partially complete. Note that less recrystallization was observed after the sixth pass due to the small strain applied, and after passes 14 to 17 due to the low finishing temperature. These qualitative observations are gleaned from the shapes of the individual loading curves in Figure 2a. Such tentative conclusions will now be compared with the metallographic observations. Later, in the discussion section of this paper, a method for the quantitative measure of the amount of recrystallization occurring after each pass will be presented and described.

Metallographic Results

The austenite structure of the plain C steel reheated to 1250°C for 30 min is displayed in Figure 3a. Large equiaxed grains are observed, with a mean grain size of around 250 μm. As indicated in Figure 3b, by the third pass, the grains are refined down to a size of about 160 μm. Further refinement (Figures 3c and 3d) takes place in subsequent passes, until, after the seventh pass, a mean size of 96 μm is produced. In the finishing passes, only partial recrystallization takes place, so that the grain structure is mixed, as is evident from Figure 3d.

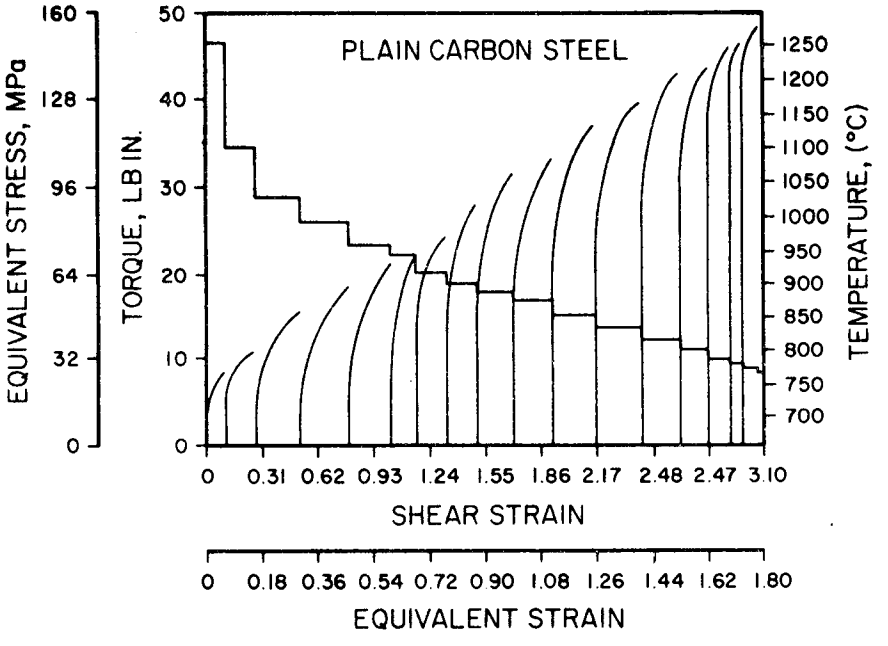

Fig. 2a

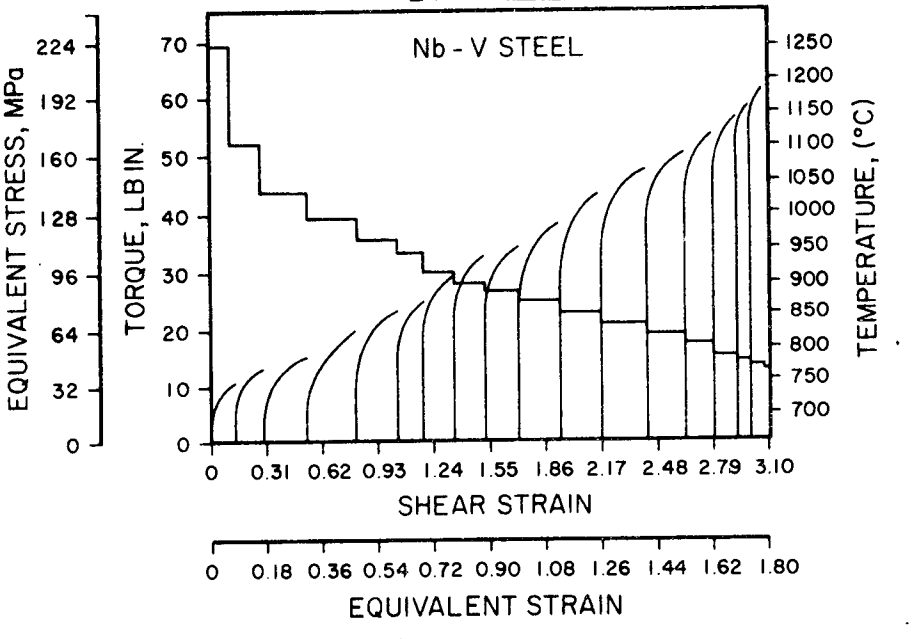

Fig. 2b

Fig. 2 - Stress-strain diagrams for the seventeen 'passes' applied to the steels in the torsion machine. The specimen temperatures are represented by the upper heavy line. a) plain C steel; b) Nb-V steel; c) Nb steel.

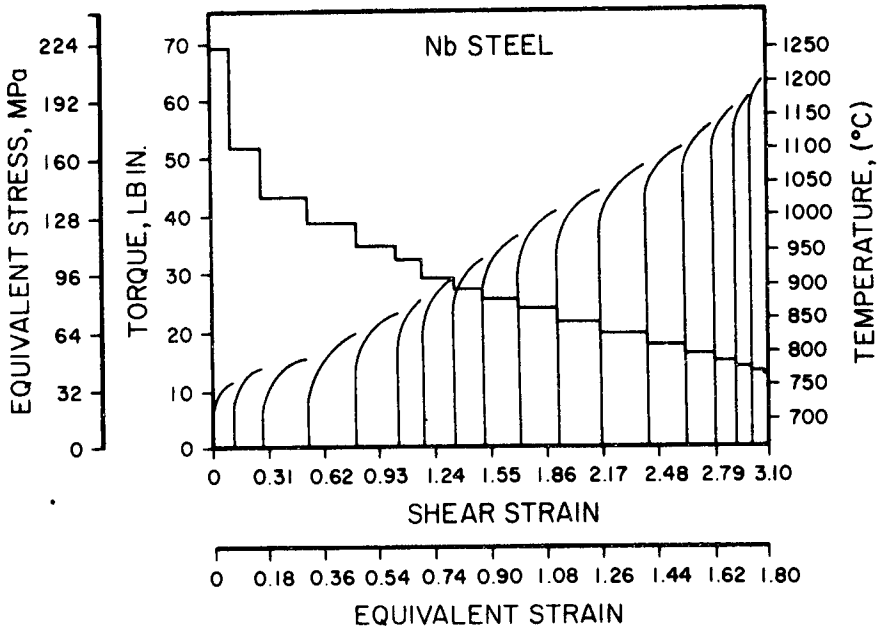

Fig. 2c

Figures 4a to 4d represent the development of the austenite structure during deformation of the Nb-V steel. A greater amount of grain refinement is observed during the first three passes than occurred in the plain C steel. Under these conditions, the mean grain size decreases from 270 to around 110 μm after the third pass. At these elevated temperatures, the difference is probably due to the solute drag effects of Nb and V in solution, which slow down the migration rates of the boundaries of the newly-recrystallized grains. In the last three passes, very little or no recrystallization occurs, and deformed elongated grains are observed, in which the degree of pancaking increases with increasing strain and decreasing temperature (see Figures 4c and 4d).

The changes in the grain structure taking place during the deformation sequence in the Nb steel are presented in Figures 5a to 5d. The transition from an equiaxed (Figure 5a), to a partially recrystallized structure (Figure 5b), and finally to an elongated grain structure (Figures 5c and 5d), is readily apparent. The refinement of the grain structure during the first passes is evident from Figure 5b. Thus the grain size decreases from 110 μm after the second pass to 22 μm after the seventeenth pass. Of importance in the present context is the presence, in the microalloyed steels, of deformation bands which are introduced during the finishing

Fig. 3a

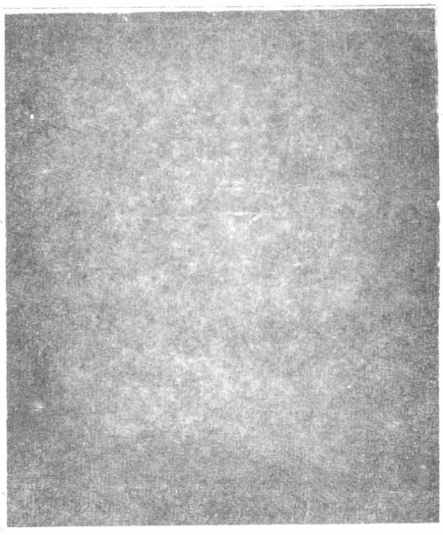

Fig. 3b

Fig. 3c

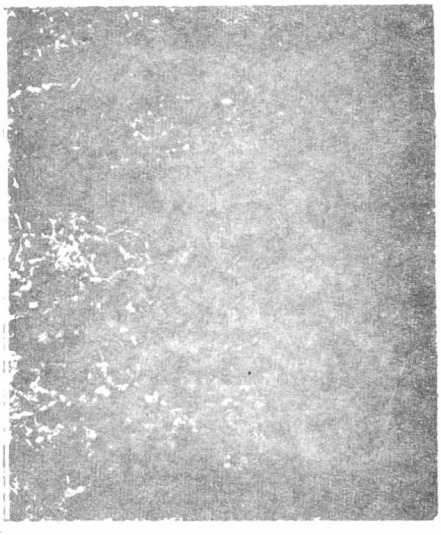

Fig. 3d

Fig. 3 - Austenite structure of the plain C steel:
a) reheated to 1250°C for 30 min; b) after 3 passes;
c) after 7 passes; d) after 14 passes.

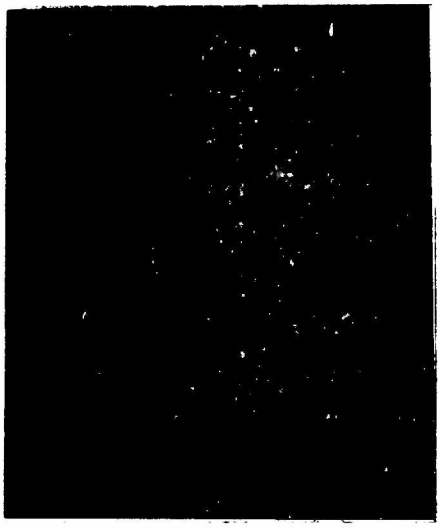

Fig. 4a

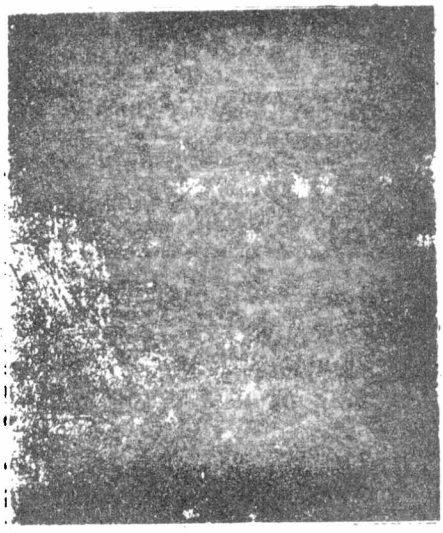

Fig. 4b

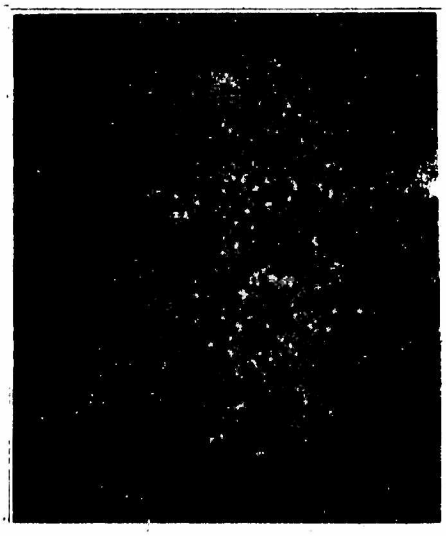

Fig. 4c

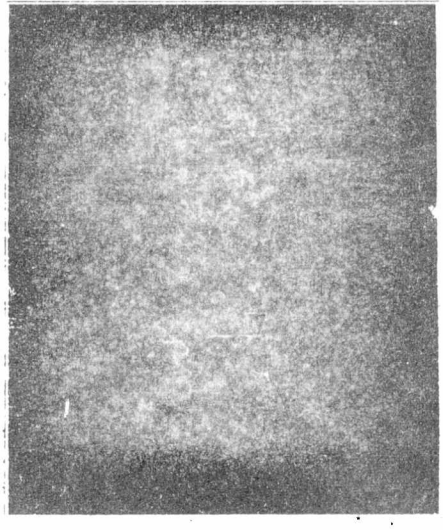

Fig. 4d

Fig. 4 - Austenite structure of the Nb-V steel:
a) reheated to 1250°C for 30 min; b) after 3 passes;
c) after 15 passes; d) after 17 passes.

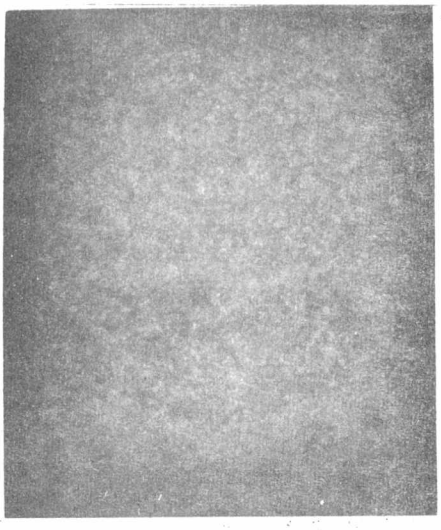

Fig. 5a

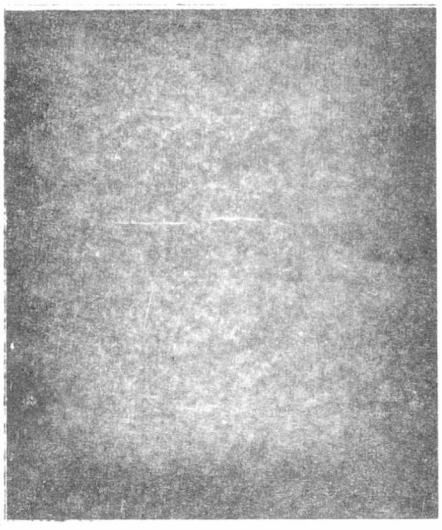

Fig. 5b

Fig. 5c

Fig. 5d

Austenite structure of the Nb steel:
a) after 2 passes; b) after 11 passes; c) after 13 passes;
d) after 14 passes.

passes. Due to the absence of recrystallization, these bands appear within the deformed grains and become more highly developed as the pass sequence proceeds (see Figures 5c and 5d). During the transformation to ferrite, these bands can be expected to act as nucleation sites (5), and thus add to the grain refining effect of austenite pancaking.

The changes in austenite grain size during the rolling simulation are illustrated in Figure 6 for the plain C and microalloyed steels, together with the temperature of each of the deformation passes. All the steels tested exhibit the same type of behaviour, namely that the austenite grain size decreases rapidly during the deformation sequence. Although it had the largest reheat grain size (260 μm), the Nb steel exhibits the smallest austenite grain size during deformation. By contrast, the plain C steel, which had the smallest reheat grain size (248 μm), exhibits the largest one during the remainder of the simulation. The higher degree of grain refinement produced in the Nb steel (and to a lesser extent in the Nb-V steel) during the first and second passes can be attributed, as suggested above, principally to the effect of Nb (and V) in solution on the recrystallization and growth processes. During the finishing passes, a contribution to grain refinement can also be expected from Nb(CN) precipitation, which will also act to reduce the growth rate of new grains. The final austenite grain size of 22 μm in the Nb steel is finer than that in the Nb-V and plain C steels (28 and 50 μm, respectively). This indicates, as suggested earlier (6), that the influence of the additional 0.02% Nb (in the Nb steel) is greater than that of the 0.05% V (in the Nb-V steel).

DISCUSSION

Microstructural Gradients in Samples Deformed in Torsion

The use of torsion testing to simulate plate rolling has the advantage that large strains can be accumulated without the onset of unstable flow. This advantage must be balanced against the effect of the strain gradients developed in the twisted samples, as a result of which the straining increases linearly from zero at the center to a maximum at the outer surface (7). As illustrated in Figure 7a for the Nb-V steel after 17 passes, the strain profile produces a gradient in the microstructure along a given radius. This micrograph depicts the austenite grain structure from a radius of 1.0mm (LHS of the micrograph) out to the maximum of 3.2mm (RHS

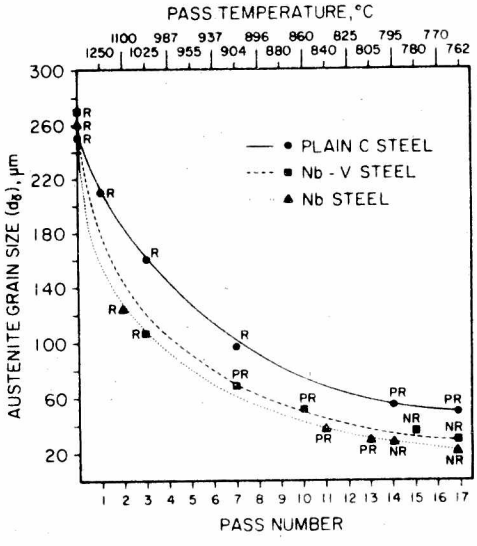

Fig. 6 - Reduction in austenite grain size produced by the rolling simulation in the plain C, Nb-V and Nb steels.

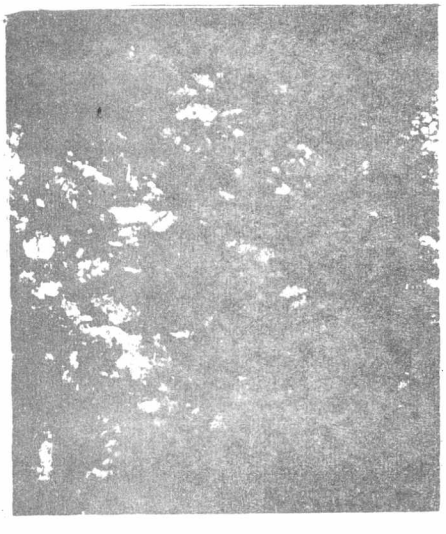

Fig. 7a - Austenite structure of the Nb-V steel after 17 passes (outer surface at right; axis of sample at left).

Fig. 7b - Ferrite structure of the Nb-V steel after 17 passes (outer surface at right; axis of sample at left).

Fig. 7c - Widmanstatten ferrite produced on transformation in the relatively undeformed central region of a Nb-V steel sample.

of the micrograph). It is evident that the outer third of the sample(right half of the photograph) contains the most highly deformed material. The intermediate third of the sample (left half) contains grains which have received less deformation, so that the austenite grains in this region are coarser and less deformed than those at the periphery. Finally, in the inner third of the sample, the material is only lightly deformed, so that the initial austenite grain structure is generally retained here. When this structure is transformed to ferrite, fine α grains are produced in the outer shell, as shown in Figure 7b. The ferrite grain size increases towards the center of the specimen due both to the gradient in austenite grain size, as well as to the gradient in strain. An example of the Widmanstatten ferrite produced on transformation in the lightly or relatively undeformed central region is presented in Figure 7c.

Effect of Microalloying on the Ferrite Grain Size

In order to study the evolution of the ferrite grain size (and morphology) during the pass sequence, individual specimens must be air cooled after each one has attained the required accumulated strain. In this way, a correlation with the evolution of the austenite grain structure (e.g. Figures

6 and 7) can be produced. In the current investigation, this would have required the testing of a further 51 (3 steels x 17 passes) specimens. Due to limitations of time and expense, this portion of the investigation was, unfortunately, curtailed. As an illustration of the technique, however, the ferrite structure after 17 passes is presented in Figures 8a, 8b and 8c for the plain C steel, Nb-V and Nb steels. Fairly large (25 μm) equiaxed grains are observed in the plain C steel. These can be attributed to the relatively large austenite grain size before transformation (Figure 6), as well as to the relative absence of deformation bands in this material. The smaller ferrite grain size (17 μm) in the Nb-V steel results from the presence of finer austenite grains in this material (Figure 6), and from the deformed nature of the γ grains (Figures 4c and 4d). The finest ferrite grain size (9 μm) was formed in the Nb steel, in which the austenite grains prior to transformation (Figure 5d) were the most highly deformed.

The dependence of the ferrite grain size on Nb concentration is illustrated in Figure 9. It is evident, as already suggested above, that the addition of 0.05% V to 0.046% Nb does not produce as much grain refinement as does the addition of 0.066% Nb (0.046 + 0.02) to the base steel.

Assessment of the Degree of Recrystallization between Passes

As indicated above, the occurrence of recrystallization can be determined metallographically. It also affects the shape of the flow curve, by making the latter resemble the one for the first pass. This effect can be employed for a quantitative assessment of the amount of recrystallization that occurs between passes. For this purpose we define the softening parameter S_p:

$$S_p(\%) = \frac{\sigma_m^{\,i} - \sigma_o^{\,i+1}}{\sigma_m^{\,i} - \sigma_o^{\,i}} \times 100 \qquad (3)$$

Here $\sigma_o^{\,i}$ and $\sigma_m^{\,i}$ are the initial (ε=1%) and unloading stresses for the ith pass, and $\sigma_o^{\,i+1}$ is the initial stress for the $(i+1)^{st}$ pass. The flow curves of Figures 2a, 2b and 2c were analyzed with the aid of this relation; it is in this way that the softening values illustrated in Figure 10 were obtained. Because of the increase in flow stress associated with the

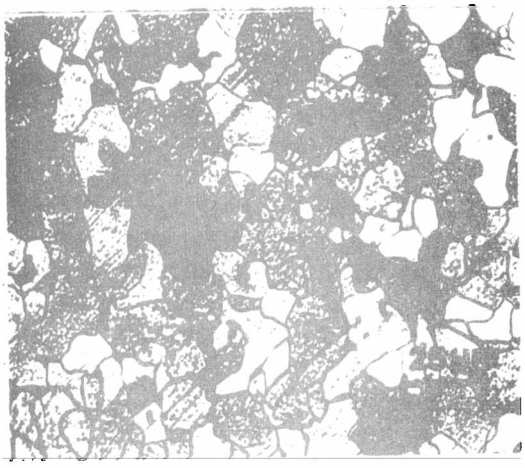

Fig. 8a - Ferrite structure of the plain C steel after 17 passes.

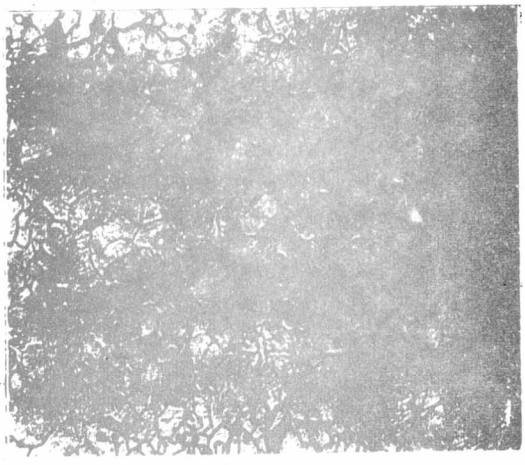

Fig. 8b - Ferrite structure of the Nb-V steel after 17 passes.

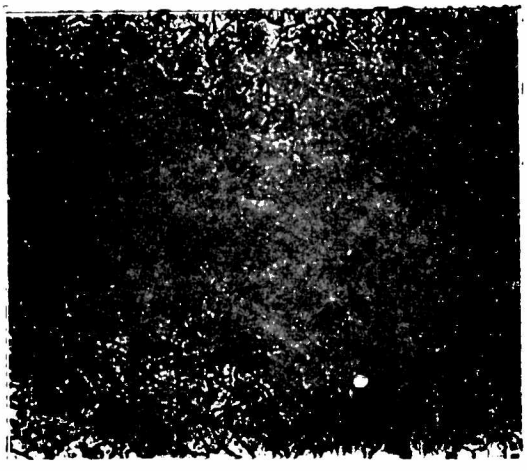

Fig. 8c - Ferrite structure of the Nb steel after 17 passes.

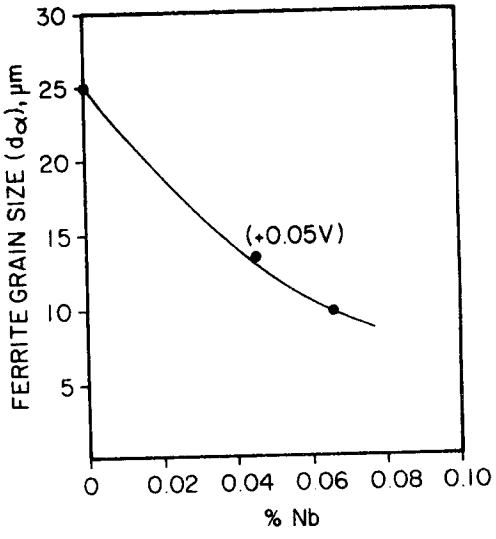

Fig. 9 - Dependence of the final ferrite grain size on Nb concentration.

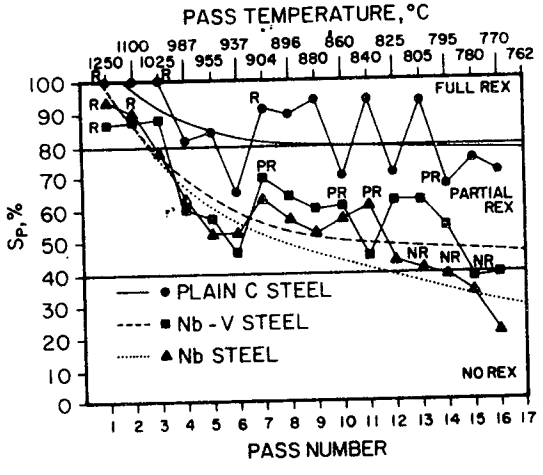

Fig. 10 - Dependence of the softening parameter S_p on pass number and type of steel.

continuous decrease in temperature (e.g. $\sigma_o^{i+1} - \sigma_o^{i} \neq 0$ for recrystallized material), full recrystallization corresponds to a softening parameter of about 80% (instead of 100%). In the absence of recrystallization and when recovery goes to saturation, about 50% softening is usually obtained in compression under isothermal conditions (8). For compression under continuous cooling conditions, S_p for full recovery can be expected to be reduced to about 45% (9). The equivalent figure for torsion testing must be modified to take into account that 'yielding' does not occur at a single instant in time, but extends over the interval during which the initiation of plastic flow is propagated from the surface to the axis of the specimen. Because of the effect this has on the flow curve following static recovery (10), the absence of recrystallization can be estimated to correspond to an S_p of 40% (and not 45%) during torsion under continuous cooling conditions (9). It is evident from the diagram that complete recrystallization occurred after the first three passes in all three steels. In the plain C steel, recrystallization was complete after passes 4 and 5 as well, but was incomplete after pass 6 because of the small pass strain involved. In a similar manner, between passes 9 and 14, recrystallization was complete only after alternate passes, as observed by Knudsen et al. (11) in isothermal deformation. In the present case, this is because more work hardening must be accumulated during the intermediate passes to offset the effect of the lower temperatures on the recrystallization kinetics. Finally, at the end of the pass sequence, even the work hardening accumulated from the last four passes was insufficient to provoke full recrystallization. In plant practice, the plain C steel is normally finish rolled at 875°C instead of at 775°C, as in the simulations described here. Thus there is much less partial recrystallization in this material under industrial conditions than is suggested by the present experiments.

In the Nb-V steel, partial recrystallization took place after passes 4 to 14, and very little or no recrystallization after passes 15, 16 and 17. In the Nb steel, partial recrystallization occurred after passes 4 to 12, and no recrystallization at all took place after passes 13 to 17. The absence of recrystallization after passes 15 to 17 in the Nb-V steel and passes 13 to 17 in the Nb steel is due in part to the small pass strains employed. A larger contribution is made by the low finishing temperature and by the effects of the microalloying elements, both in solution and as precipitate formers, on retarding recrystallization.

The Development of Mixed Ferrite Grain Sizes

In Figures 8a, 8b and 8c, examples are given of ferrite structures containing mixed grain sizes. In these cases, the ratio between the maximum and minimum grain size is around 10 for both the microalloyed and the plain C steels. This type of structure is associated with poor fracture properties at low temperatures. The observed mixed ferrite grain size is a result of a lack of uniformity in the austenite structure before the transformation to ferrite. Such inhomogeneities arise when partial recrystallization takes place after the last pass or when partial recrystallization occurs during pass intervals several passes prior to the final one. The occurrence of partial recrystallization in the last three passes is represented in terms of the softening parameter in Figure 10 for the plain C steel. In such materials, the simplest method of avoiding partial recrystallization is to finish roll at a temperature high enough for recrystallization to be complete (e.g. 850 to 900°C in Figure 10). The microalloyed steels, because of their slower recrystallization kinetics, are better suited to a different tactic. For these materials, it is preferable to cool (and not roll) through the temperature range that leads to partial recrystallization, and then to finish roll in the 'no-recrystallization' (pancaking) temperature range. If this scheme is followed closely enough, and if dynamic recrystallization is prevented during finish rolling (12), then both the austenite and ferrite grain size should be uniform.

In the present experiments (see Figure 10), partial recrystallization occurred in the Nb-V steel after passes 4 through 14. There was no recrystallization after passes 15 to 17. The considerable influence of partial recrystallization in the intermediate passes can readily be seen in Figure 8b. In the more heavily alloyed Nb steel, by contrast, partial recrystallization only occurred after passes 4 to 12, and there was no further recrystallization after passes 13 to 17. The improvement in the uniformity of the ferrite grain structure is evident when Figures 8b and 8c are compared.

It is unfortunate that partial recrystallization apparently occurs over such a large temperature range in HSLA steels (e.g. from 1025 to 825°C in Figure 10). The upper limit could, in principle, be reduced by applying larger pass strains (1) during roughing. It is also possible that a coil box (13) could be used to maintain the temperature in the

full recrystallization range during this part of the rolling schedule. It should, in a similar manner, be possible to raise the 'pancaking' temperature by employing smaller pass strains during this portion of the finishing sequence (1).

Effect of Microalloying on the Mean Stress

The mean stress per pass was determined graphically for the different steels tested and found to increase gradually from the first to the seventeenth pass. The lowest mean stress per pass of 22 MPa was observed for the first pass in the plain C steel. The mean stress increased almost linearly with pass number to its maximum value of 152 MPa in this material. Higher stress levels were established for the Nb-V steel: 28 MPa for the first pass and 196 MPa for the last pass. The highest mean stress (208 MPa) was detected for the Nb steel during the seventeenth pass.

In the initial passes, as there is full recrystallization in all the steels, the higher mean stresses associated with the microalloyed steels can be ascribed to the direct effect of Nb and V in solution on the yield stress and on the work hardening rate (6), see Figure 11. In the finishing passes, on the other hand, the higher stress levels determined for the microalloyed steels can be attributed to the indirect effect of Nb and V addition, both in solute and precipitate form, via the retardation of recrystallization. (There is also a direct effect of Nb and V on the yield stress in this temperature range, but this is smaller than the indirect effect of Nb and V on the flow stress due to the suppression of recrystallization.) It should be noted that the microalloyed steel containing 0.066% Nb exhibits higher mean stresses than the Nb-V steel with 0.046% Nb and 0.05% V. This is because the latter cannot compensate for the 'loss' of 0.02% Nb (6,14); this deficit affects not only the mean stress per pass, but also the rates of recovery and recrystallization. The higher mean stresses observed in the microalloyed steel lead directly to higher separation forces and torques during the rolling process. One method of predicting such forces and torques will now be described.

PREDICTION OF ROLL FORCES AND TORQUES FROM THE MEAN STRESSES

Roll separating forces and torques for an industrial plate mill were predicted from the mean stresses determined in the torsion simulation. The method of prediction was based

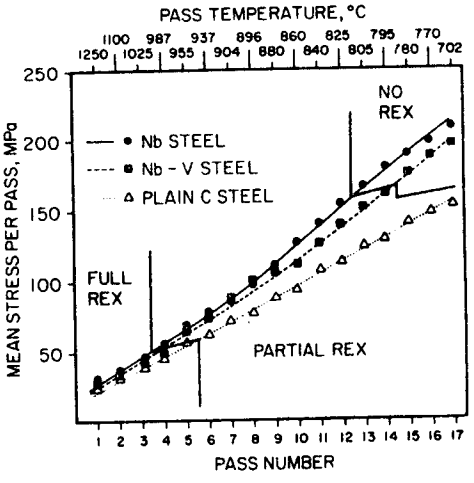

Fig. 11 - Dependence of the mean stress per pass on the pass number and type of steel.

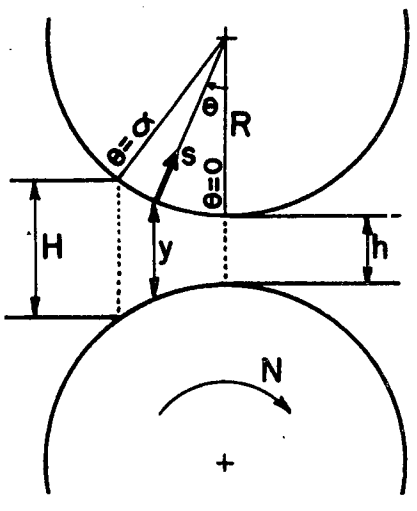

Fig. 12a - Roll geometry and notation for the Sims calculation

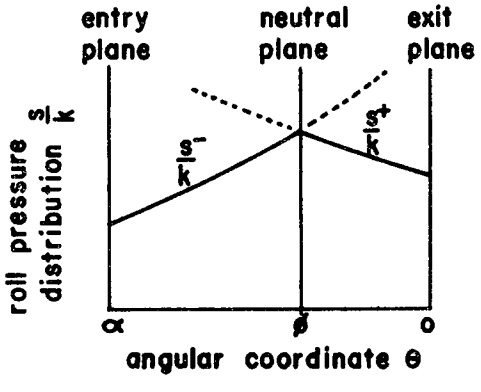

Fig. 12b - Distribution of roll pressure along the arc of contact (after Sims (15)).

on the Sims rolling analysis (15). The specific roll separating force can be determined by integrating the roll pressure over the arc of contact between the material and the roll, Figure 12a:

$$P = R \int_0^{\alpha} S d\theta \qquad (4)$$

Here R is the roll radius, s is the normal roll pressure and θ is the angular coordinate for the arc of contact. It is assumed that, when θ is small, the normal roll pressure and vertical roll pressure are nearly equal. In terms of the Sims pressure distribution functions s^+/k and s^-/k (Figure 12b), the integral becomes:

$$P = Rk\left[\int_0^{\phi} s^+/k \, d\theta + \int_{\phi}^{\alpha} s^-/k \, d\theta\right] \qquad (5)$$

where k is the mean flow stress of the material in plane strain compression, and is assumed constant over the arc of contact (i.e. it is assumed to be independent of strain and strain rate). When the plane strain flow stress is not known, as in the present case, uniaxial stress data are substituted for k, with the aid of the relation $k = 1.15\sigma$. The integration in equation (5) was computed by (a) subdividing the range of θ, $0 \leq \theta \leq \alpha$, into 99 increments, (b) determining the values of s^+/k and s^-/k for each increment, (c) finding the position of the neutral plane to the nearest increment, and (d) summing the s/k terms over the θ range as required. The specific roll torque was computed from the Sims relation:

$$G = 2RR'(1.15\sigma)(\alpha/2) - \theta) \qquad (6)$$

where R' is the radius of curvature of the elastically flattened roll, σ is the uniaxial mean stress and α and θ are the angles previously defined. For each rolling pass, numerical values were inserted for the entry thickness of the plate H, the exit thickness of the plate h, the width of the plate w, and for R and σ.

By means of this procedure (16), roll forces and torques were calculated, which can then be compared to the values determined in the mill. The measured roll forces for the Nb-V steel are compared with the calculated ones in Figure 13a.

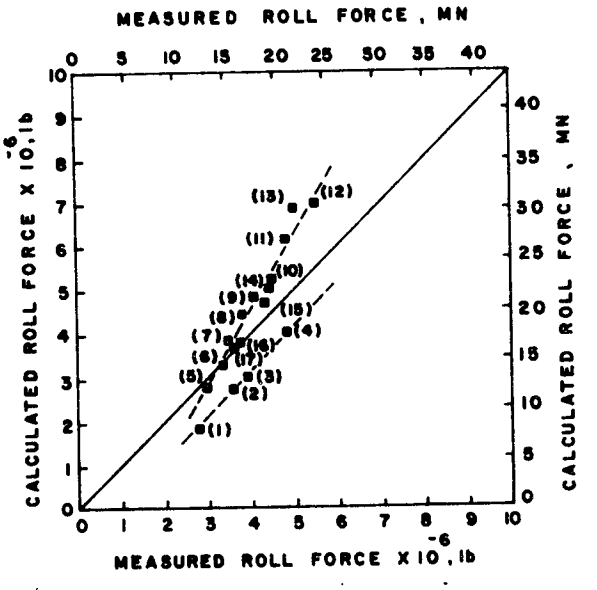

Fig. 13a - Comparison of the predicted and measured roll separation forces associated with rolling of the Nb-V steel. The pass number is shown beside each data point.

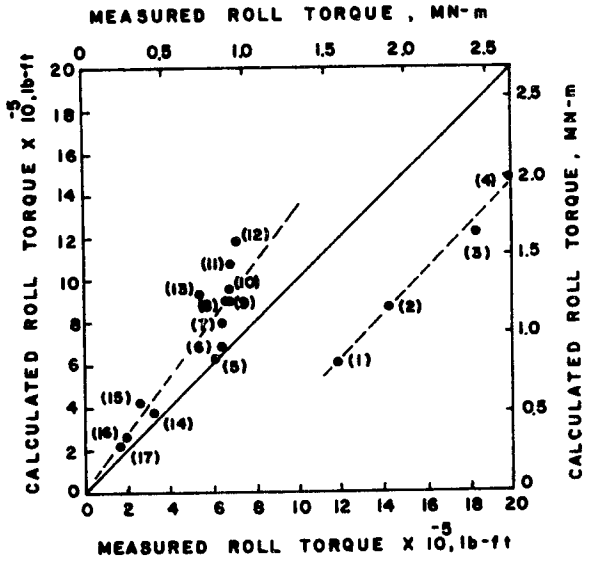

Fig. 13b - Comparison of the predicted and measured roll torques associated with rolling of the Nb-V steel.

The first four passes were rolled on a two-high roughing mill, for which the calculated values are lower than those observed in the mill. This is likely to have resulted from the higher deformation temperatures that prevailed during this portion of the torsion simulation (see Figure 1b). Passes 5 to 17 were carried out on a four-high finishing mill. In this case, the higher roll forces predicted for passes 9 to 15 are probably associated with the lower than desired deformation temperatures during the laboratory simulation. It is concluded from these experiments that the principal discrepancies between the predicted and measured forces are due to the differences between the laboratory and mill temperatures. Thus it is expected that, if the temperature differences can be largely eliminated, excellent correlations would be obtained.

The predicted and 'measured' roll torques are displayed in Figure 13b. Note that a good correspondence exists for the finishing passes (5 to 17), and that the differences in the laboratory and plant torques are generally consistent with the temperature discrepancies discussed above. By contrast, larger torques were 'measured' during the roughing passes (passes 1 to 4) than were predicted from the simulations. This is a result of the overestimation of the lever arm by the mill control algorithm (17). For the present purpose, neither the torques nor the currents were measured directly. The torque M was determined instead from the relation:

$$M = F \times a \qquad (7)$$

where F is the known separating force and the moment arm 'a' is estimated by the mill computer from a relation containing the roll radius and the entering and exiting slab heights (17). When the lever arms are corrected using the Larke method (18), the agreement between predicted and measured values is a reasonable one. (See addendum after references.)

Comparison of Simulated and Industrial Ferrite Microstructures. The ferrite microstructures obtained after transformation are displayed in Figures 14a and 14b for the torsion simulation and the rolled plate respectively. It is evident that there is a fairly good correspondence between the two morphologies. The two samples had mean grain sizes of around 15-20 μm, with some pearlite banding apparent in the rolled plate. It should be remarked that the torsion specimen was sectioned longitudinally. In order to check for pearlite

banding in the latter samples, they would have to be sectioned along planes inclined at an angle ϕ to a selected longitudinal plane (19), as given by:

$$\phi = [\pi - \tan^{-1}(2/\gamma)]/2. \qquad (8)$$

Here the shear strain $\gamma = r\theta/L$, as already defined above, and ϕ takes an initial value of $\pi/4$ and tends to $\pi/2$ during twisting. (Note that ϕ is always larger than the helix angle $\psi = \tan^{-1}\gamma$, and is in the same quadrant.)

ACKNOWLEDGEMENTS

The authors are indebted to Dr. M.J. Stewart of the Dominion Engineering Works Ltd. for developing the numerical method for integrating the roll pressure distribution; to B. Thomas, H. Baltussen and P.J. Hunt of the Algoma Steel Corp. for the measurement of roll forces and torques, and to Gilles Canova of McGill University for preparing the torsion testing program. They acknowledge with gratitude the financial support received from the Physical Metallurgy Research Laboratory of CANMET, Department of Energy, Mines and Resources, the Natural Sciences and Engineering Research Council of Canada, and the Quebec Ministry of Education (FCAC program).

REFERENCES

(1) I. Weiss, J. J. Jonas, P. J. Hunt and G. E. Ruddle, Proc., International Conference on Steel Rolling, Sept. 1980, Tokyo, Japan, pp. 1225-1236.

(2) A. Gittins, J. R. Everett and W. J. McG. Tegart, Metals Tech., 4, 1977, pp. 377-383.

(3) S. Fulop, K. C. Kadien, M. J. Luton and H. J. McQueen, Journal of Testing and Evaluation, 5, 1977, pp. 419-426.

(4) A. T. Davenport, R. E. Miner and R. A. Kot., The Hot Deformation of Austenite, J.B. Ballance, ed., p. 186, AIME, New York, N.Y. 1977.

(5) J. P. Sah, G. J. Richardson and C.M. Sellars, Metal Science, 8, 1974, pp. 325-331.

(6) M. G. Akben, I. Weiss and J. J. Jonas, Acta Met., 28, 1980, in press.

(7) D. S. Fields, Jr. and W. A. Backofen, Proc. Am. Soc. Test. Mater., 57, 1957, p. 1259.

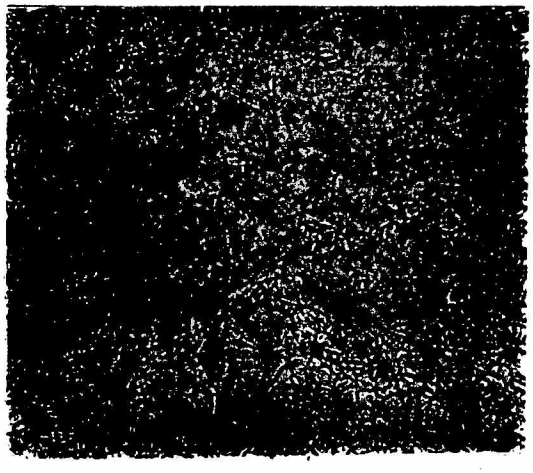

Fig. 14a - Ferrite structure produced in the Nb-V steel after the application of 17 rolling 'passes' in the torsion machine.

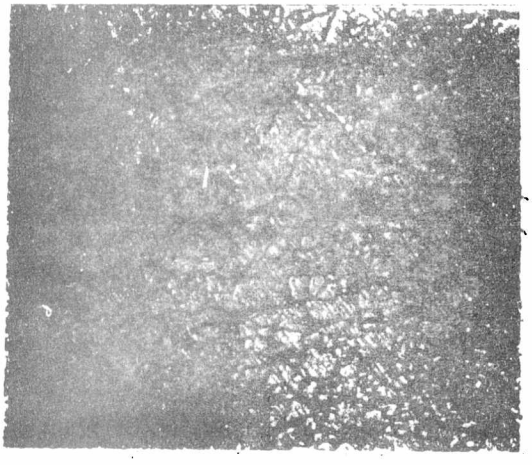

Fig. 14b - Ferrite structure obtained in the Nb-V steel after 17 passes of rolling in the plate mill.

(8) R. A. Petkovic, M. J. Luton and J. J. Jonas, Acta Met., 27, 1979, pp. 1633-1648.
(9) I. Weiss, unpublished work, McGill University, 1979.
(10) M. J. Luton, R. A. Petkovic and J. J. Jonas, Acta Met., 28, 1980, pp. 729-743.
(11) W. Knudsen, J. Sankar, H. J. McQueen, J. J. Jonas and D. Hawkins, Proc., Sheffield International Conference on Hot Working and Forming Processes, July 1979, Sheffield, U.K., The Metals Society, London, pp. 51-56.
(12) A. H. Ucisik, I. Weiss, H. J. McQueen and J. J. Jonas, Can. Met. Quart., in press.
(13) W. Smith, A. G. Watson and L. D. Newton, Ref. 1, pp. 497-508.
(14) J. R. Everett, A. Gittins, G. Glover and M. Toyama, Ref. 11, pp. 16-20.
(15) R. B. Sims, Proc., Inst. Mech. Eng., 168, 1954, 191-200.
(16) G. E. Ruddle and M. J. Stewart, 'Prediction of Roll Force and Torque from Yield Stress', Report MRP/PMRL 80-73(TR), Physical Metallurgy Research Laboratory, CANMET, Ottawa, Canada, 1980.
(17) P. J. Hunt, Algoma Steel Corp. Ltd., Sault Ste. Marie, Ontario, Canada, private communication.
(18) E. C. Larke, 'The Rolling of Strip, Sheet and Plate', Chapman & Hall, Ltd., London, 1957.
(19) G. Canova, M. Eng. thesis, McGill University, Montreal, Canada, 1979.

Addendum: The comparison between the predicted and measured roll forces and torques for the plain C and Nb steels is presented in Ref. 1.